

REPORT DOCUMENTATION PAGE

AFRL-SR-BL-TR-01-

Public reporting burden for this collection of information is estimated to average 1 hour per response, including the time for review data needed, and completing and reviewing this collection of information. Send comments regarding this burden estimate or any this burden to Department of Defense, Washington Headquarters Services, Directorate for Information Operations and Reports (C 4302. Respondents should be aware that notwithstanding any other provision of law, no person shall be subject to any penalty for valid OMB control number. PLEASE DO NOT RETURN YOUR FORM TO THE ABOVE ADDRESS.

ing the
educing
2202-
currently

0585

1. REPORT DATE (DD-MM-YYYY) 08312001		2. REPORT TYPE Final		3. DATES COVERED (From - To) 06/15/96 - 12/14/00	
4. TITLE AND SUBTITLE Environmentally Compliant Corrosion Resistant, & Electrically Conductive Inorganic Coatings for Aluminum Alloys				5a. CONTRACT NUMBER N/A	
				5b. GRANT NUMBER F49620-96-1-0305	
				5c. PROGRAM ELEMENT NUMBER N/A	
6. AUTHOR(S) Taylor, S. R.; Leggat, R. B.; Pehovaz, E.; Buchheit, R. G.; Zhang, W.; Babu, M.; Sehgal, A.				5d. PROJECT NUMBER N/A	
				5e. TASK NUMBER N/A	
				5f. WORK UNIT NUMBER N/A	
7. PERFORMING ORGANIZATION NAME(S) AND ADDRESS(ES) University of Virginia Office of Sponsored Programs P. O. Box 400195 Charlottesville, Virginia 22904-4195				8. PERFORMING ORGANIZATION REPORT NUMBER UVA/5-25849	
9. SPONSORING / MONITORING AGENCY NAME(S) AND ADDRESS(ES) Air Force Office of Scientific Research Defense Advanced Res. Proj. Agency 801 N. Randolph Street, Rm. 232 3701 N. Fairfax Drive Arlington, Virginia 22203-1977 Arlington, Virginia 22203-1714				10. SPONSOR/MONITOR'S ACRONYM(S) N/A	
				11. SPONSOR/MONITOR'S REPORT NUMBER(S)	
12. DISTRIBUTION / AVAILABILITY STATEMENT Approved for public release, distribution unlimited.					
13. SUPPLEMENTARY NOTES N/A					
14. ABSTRACT The objective of this project was to develop an environmentally compliant conversion coating on AA2024-T3. Hydrotalcite (HT) conversion coatings (CC) based on alkaline lithium salt chemistries were designed to replace chromate conversion coating processes in both mode of application (bath or spray applied) & function (stand-alone corrosion protection, adhesion to organic layers, self-healing, low electrical contact resistance). A Fractional Factorial Design (FFD) determined that temperature & the use of nitrate-based chemistries were critical processing variables. Use of an oxidant (e.g., persulfate) produced HT coatings (6 min.) that could withstand 168 hours of salt spray. Post-treatment of HT-CCs could revert the HT to aluminum oxide (chemical anodization). HT-CCs could be augmented to include rare earth cations (e.g., Ce) to develop self-healing characteristics. Self-healing was demonstrated by cerium-doped HT coatings. The Lewis-base nature of HTs makes them less able to be wet by the Lewis-base nature of epoxy. Wetting characteristics of HT were dramatically improved via cationic surfactants. Salt spray performance of full coating systems (HT + primer & HT + primer + topcoat) was not as good as CCC systems. These tests did not incorporate the appropriate surfactant determined in the previous adhesion studies. HT have demonstrated excellent & stand alone corrosion protection on AA2024.					
15. SUBJECT TERMS Environmentally compliant, conversion coating, hydrotalcite, corrosion resistant, adhesion					
16. SECURITY CLASSIFICATION OF:			17. LIMITATION OF ABSTRACT	18. NUMBER OF PAGES	19a. NAME OF RESPONSIBLE PERSON
a. REPORT Unclassified	b. ABSTRACT Unclassified	c. THIS PAGE Unclassified	UL	1	Taylor, S. R.
					19b. TELEPHONE NUMBER (include area code) 434-982-5788

20011126 084

AIR FORCE OFFICE OF SCIENTIFIC RESEARCH (AFOSR)
NOTICE OF TRANSMITTAL DTIC. THIS TECHNICAL REPORT
HAS BEEN REVIEWED AND IS APPROVED FOR PUBLIC RELEASE
LAW AFR 190-12. DISTRIBUTION IS UNLIMITED.

Performance Report

Grant F49620-96-1-0305

Environmentally Compliant Corrosion Resistant and Electrically Conductive Inorganic Coatings for Aluminum Alloys

Submitted by:

S. Ray Taylor, Robert B. Leggat, Emma Pehovaz, and Samuel A. Taylor
The Center for Electrochemical Science and Engineering
University of Virginia
Charlottesville, VA 22904

Rudy G. Buchheit, W. Zhang, M. Babu, and A. Sehgal
The Ohio State University
Columbus, OH

Submitted to:

Dr. Stephen Wax
Defense Advanced Research Projects Agency
3701 North Fairfax Drive
Arlington, VA 22203-1714

and

Lt. Col. Paul Trulove, Ph.D.
AFOSR/NL
801 North Randolph Street, Room 732
Arlington, VA 22203-1077

**Center for
Electrochemical
Science & Engineering**



University of Virginia
Department of Materials Science & Engineering
116 Engineer's Way
Charlottesville, Virginia 22904

EXECUTIVE SUMMARY

The objective of this project was to develop an environmentally compliant conversion coating for use on aerospace aluminum alloys (e.g., AA2024-T3). This conversion coating was to replace the current chromate conversion coating processes in both mode of application (bath or spray applied in the depot) and function (stand alone corrosion protection, adhesion to organic layers, self-healing, and low electrical contact resistance).

Hydrotalcite (HT) was developed within this program as a replacement to chromate conversion coatings. HT coatings are formed by exposure of aluminum and its alloys to alkaline lithium salt solutions. The coating chemistry used to form these conversion coatings has many processing variables (e.g., time, temperature, anion, etc.). A Fractional Factorial Design was used to determine that temperature was one the more critical processing variables. The FFD study also determined that HT coatings formed from nitrate-based chemistries had consistently better stand-alone corrosion protection properties. Through the use of additional oxidants within the coating bath, HT coatings with the ability to withstand 168 hours of salt spray could be formed in less than 6 min.

HT conversion coatings could also be post-treated (e.g., hydrothermally aged, surfactant) to revert the hydrotalcite to aluminum oxide, or augmented to include high valence-state rare earth cations (e.g., cerium). Hydrothermal aging allowed a procedure to chemically anodize aluminum, while incorporation of cerium into the molecular gallery of the hydrotalcite structure provided a means to develop self-healing characteristics, a highly sought property characteristic of chromate-based coatings. Self-healing was indeed demonstrated by the cerium doped HT coatings.

The adhesion of epoxy coatings to the hydrotalcite coating was studied in detail. The Lewis-base nature of HTs makes them intrinsically less able to be wet by the Lewis-base nature of epoxy. However, wetting characteristics of HT were dramatically improved through the use of cationic surfactants. The use of a surfactant allows the utilization of the tremendous mechanical advantage provided by the HT structure.

Salt spray performance of full coating systems (HT + primer and HT + primer + topcoat) was not as good as chromate conversion coated systems. These tests did not incorporate the appropriate surfactant determined in the previous adhesion studies.

Thus, while hydrotalcite conversion coatings have not been demonstrated as a complete drop-in replacement to chromate conversion coatings to serve as a pretreatment for a coating system on AA2024, they have demonstrated excellent adhesion and stand alone corrosion protection on this alloy system. This in combination with the ability to molecularly engineer self-healing capabilities makes hydrotalcite an extremely attractive, environmentally-compliant replacement of chromate.

TABLE OF CONTENTS

	Page
I. PROJECT OBJECTIVES	3
II. SUMMARY OF ACTIVITIES - STATUS OF EFFORT	4
III. ACCOMPLISHMENTS AND FINDINGS	4
A. Optimization of Processing	4
B. Hydrotalcite Coating Properties	9
C. Performance Bench-marking	13
IV. PERSONNEL SUPPORTED	15
V. PUBLICATIONS AND PRESENTATIONS	16
VI. INTERACTIONS/TRANSITIONS	16
VII. NEW DISCOVERIES, INVENTIONS, PATENT DISCLOSURES	19
VIII. AWARDS AND HONORS	19
IX. APPENDIX	20

I. PROJECT OBJECTIVE:

The goal of this research project was to develop a simple, low-cost, commercially applicable, chromate-free conversion coating process for the major aluminum alloys. This coating process will form coatings with properties that are consistent with general performance attributes of corrosion resistance, paint adhesion and electrical contact resistance established in MIL-C-81706 and MIL-C-5541. Processing methods that produce coatings with desirable electric and dielectric properties beyond contact resistance, and capacity for self-healing are also sought.

The coatings investigated are new variants of hydrothermal film growth from alkaline lithium salt solutions based on: (1) surface copper complexation, and (2) film doping with high valence state transition metal ions. It is intended that these processes be procedurally similar to methods used for chromate conversion. Attention was also given to performance issues related to self-healing, materials compatibility, de-painting, and field repair.

The objectives of the proposed research and development project were to:

- (1) Determine hydrothermal coating processing parameters which optimize corrosion resistance, electrical contact resistance, and paint adhesion according to MIL-C-81706 and MIL-C-5541E for the following aluminum alloys: 356 (cast), 2024-T3, 3003, 6061-T6, and 7075-T6.
- (2) Characterize and compare the corrosion resistance of hydrotalcite coated aluminum doped with various transition metal ions (e.g. Ce^{+3} , Ce^{+4} , Mn^{+n} , Ni^{+2} , Co^{+2} , Fe^{+3} , V^{+n} , W^{+n}) to conventional chromate conversion coatings in simulated conditions.
- (3) Characterize the contact resistance and intrinsic dielectric properties of variant hydrotalcite conversion coatings and compare to chromate conversion coatings after various periods of environmental exposure.
- (4) Investigate the relationship between coating defects and processing variables and the self-healing characteristics of the variant hydrotalcite films.
- (5) Investigate other application issues related to de-painting, field repair, and material compatibility.
- (6) Determine the causal link between processing variables and the physical and chemical structure of the film as well as film morphology.
- (7) Reduce to shop floor practice that process which optimizes the corrosion, electrical, and paint adhesion properties. Demonstrate at a DoD site.

This research and development project was performed through a four year collaboration between the Center for Electrochemical Science and Engineering at the University of Virginia, Ohio State University, and Clariant Corporation. The major results of this program will be delineated in a bulleted format. When applicable, further details for each conclusion will be provided in an attached manuscript. These manuscripts represent papers submitted to archival journals and are either in review, in press, or archival.

II. SUMMARY OF ACTIVITIES – STATUS OF EFFORT

The funding for this project was extended through the end of calendar year 2000 via a no cost-extension. The hydrotalcite effort continued via other funded programs. The technical momentum developed on certain subprojects associated with this DARPA program (e.g., adhesion studies) has propelled continued activities. This report will provide a state-of-the-art summary of the major findings and publications.

III. ACCOMPLISHMENTS AND FINDINGS

The accomplishments and findings of this project are be divided into the following scheme:

- A. Optimization of Processing
 - 1. Effects of anions
 - 2. Fractional Factorial Design (FFD) results
 - 3. The effects of oxidizers
 - 4. The control of copper
- B. Characterization of Properties
 - 1. Self-healing
 - 2. Adhesion
 - 3. Corrosion resistance
 - 4. Electrical contact resistance
- C. Performance Bench-marking
 - 1. Evaluation of field-applied chromate conversion coatings
 - 2. Evaluation of hydrotalcite conversion coatings within a coating system

This report describes the major results for each of the aforementioned sections in a bulleted format. When applicable, a reference will be provided to a manuscript for additional detail. These manuscripts are attached in the Appendix and represent, patents and papers that have been submitted to archival journals and are either in review, in press, or in print.

A. Optimization of Processing

Overview. As a class of materials, hydrotalcites possess broad chemical diversity. These materials are duplex metal hydroxides arranged in layers that are interleaved with hydrated anionic layers. Many different pairs of metals can be combined to make the duplex metal host structure, and many different anions can be accommodated in the anionic layer. In the processing of hydrotalcites as coatings for aluminum, there are some significant constraints that limit the range of compounds that make up the coating. Since the coatings are to be made by converting the Al substrate, one of the metals in the host structure must be Al. The other metal must be one that is a hydrotalcite former and one that is not reduced to its simple hydroxide in the presence of Al. Metals that meet this

requirement are Mg and Li. Mg-Al hydrotalcites are difficult to form as a coating on Al since the alkaline conditions required to activate the Al induce homogeneous precipitation of Mg as $\text{Mg}(\text{OH})_2$ or MgCO_3 . This precipitation interferes with coating formation. For this reason, all of the work in this study involved use of the $\text{Li}_2[\text{Al}_2(\text{OH})_6]^{2+}$ host structure.

Constraints on the anion type are less restrictive and much experimentation on the influence of anion type on hydrotalcite formation and properties was undertaken in this effort.

1. Fractional Factorial Design Results (ref. 1)

- A fractional factorial design (FFD) was used to investigate the importance of certain bath parameters on the corrosion resistance of the hydrotalcite (HT) coating. The parameters investigated included: temperature, immersion time, pH, lithium concentration, aluminate concentration, oxoanion concentration, and post-treatment in a cerium ion-containing bath. R_{corr} was used as a metric for the assessment of corrosion resistance. Four HT chemistry variants were examined based on four different anions (carbonate, nitrate, sulfate, and silicate) on three aluminum aerospace alloys (AA6061-T6, AA7075-T6, AA2024-T3).
- The FFD study indicated that temperature was the most important bath parameter with regards to impact on the corrosion resistance of HT coatings. Higher bath temperatures increased R_{corr} (improved corrosion resistance).
- Analysis of the replicate data for AA2024-T3 matrices indicated that contact time, pH, and lithium concentration were also significant factors.
- A bath chemistry based on lithium nitrate was down-selected for future study based on a combination of R_{corr} data and slat spray performance.

1. R.B. Leggat, N.P. Cella, C. Mastrenghelo, R.G. Buchheit, and S.R. Taylor, "Development of Hydrotalcite as Environmentally-Benign Conversion Coatings: Optimization by Fractional Factorial Design", submitted to *Corrosion Science*, (in review).

2. Effect of Anions (ref. 2-6)

- Synthesis of hydrotalcites with MoO_4^{2-} , and WO_4^{2-} anions was attempted during this project. However, direct synthesis of Al-Li-molybdate or Al-Li-tungstate coatings was not successful due to reduction of Mo^{6+} and W^{6+} on the very active Al surface during the earliest stages of coating formation. This resulted in non-protective metal hydroxide layers that interfered with proper hydrotalcite formation. Coatings of this type exhibited inferior properties.
- To avoid inadvertent reduction of high oxidation state metals a new processing strategy was explored. This process involves deposition of a hydrotalcite coating followed by exposure to an aqueous neutral or

acid metal salt solution. In the second steps the active agent could be either an anionic or cationic species. The first step formed a resistive layer that suppressed metal salt reduction. This second step sealed any latent porosity by precipitating metal oxide into pore spaces, but also left high oxidation state metal deposits on the film. This process is analogous to dichromate sealing of sulfuric acid anodized aluminum except that external electrolytic control is not required and the second sealing step can be completed in a very short periods of time. The corrosion resistance of a sealed hydrotalcite coating is not as effective as that of a sealed anodized coating, but it is good compared to chromate conversion coatings. This new process provided significant flexibility with respect to the types of metal chemistries that could be employed. These processes led to some of the most corrosion resistant coatings made in this study and was the foundation for building in self-healing characteristics to hydrotalcite coatings.

- The metal salts used in the second step of this coating process can be divided into two sets. The first set consisted of salts whose solubility minimum occurs under alkaline solution conditions. This included salts of Ce, Co, Ni, Fe, Mn and Mg. The second set consisted of metals, not included in the first class, but considered as potential inorganic sealants for oxide coatings. This includes salts of Mo, Bi, Al and Cr (Cr salts were used for reference only).
- This line of experimentation also led to a simple, non-electrolytic process for forming hydrated Al-oxide coatings with high corrosion resistance on aluminum. This process, called "reversion", is a derivative of the hydrotalcite coating process. In this process, hydrotalcite coatings are formed by "standard" methods, then immersed in boiling distilled water or a dilute sodium aluminate solution. This process transforms the hydrotalcite formed in the first stage of the process to a compact mass of bayerite crystals. In EIS corrosion testing, the coating corrosion resistance of reversion coated 6061-T6 approaches that for anodized coatings. To date, reversion coated samples have withstood 1500 hours of salt spray exposure without evidence of corrosion.

2. R.G. Buchheit, C.A. Drewien, M.A. Martinez, G.E. Stoner, "Chromate-Free Corrosion Resistant Conversion Coatings for Aluminum", in Advances in Coatings Technology for Corrosion and Wear Resistant Coatings, A.R. Srivatsa, C.R. Clayton, J.K. Hirvonen, Eds., p. 173 (TMS, Warrendale, PA: 1995).
3. R.G. Buchheit, M.A. Martinez, and C.B. Cooper, "Corrosion Resistant Coatings for Aluminum by Hydrothermal Film Formation in Alkaline Li-Salt Solutions," p. 273, in Aqueous Chemistry and Geochemistry of Oxides, Oxyhydroxides, and Related Materials, vol. 432, J. A. Voigt, T. E. Wood, B. C. Bunker, W. H. Casey, and L. J. Crossey, Eds. , Materials Research Society, Warrendale, PA (1996).
4. R.G. Buchheit, "Alkaline Oxide Conversion Coating for Aluminum Alloys", CORROSION/96, Paper No. 96625 (NACE, Houston, TX: 1996).

5. R.G. Buchheit, N. Cella, M.A. Martinez, L.P. Montes, G.E. Stoner, S.R. Taylor, "Non-Electrolytic Formation of Al-Oxide Surface Layers By Reversion of Hydrotalcite", CORROSION/98, Paper No. 98216 (NACE, Houston, TX:1998).
6. R.G. Buchheit, M.A. Martinez, "Corrosion Protective Coating for Metallic Materials", U.S. Patent 5 756 218, May 26, 1998.

3. The Effect of Oxidizers (ref. 7-8)

- The effects of bath oxidizing power on hydrotalcite coating formation and breakdown were examined. Overall, results indicated that increasing the oxidizing power of the coating bath shortened the immersion time required to form highly corrosion resistant coatings. Hydrotalcite conversion coatings were formed on 2024-T3 (Al-4.4Cu-2.5Mg-0.6Mn) panels by immersion in alkaline lithium salt solutions containing either carbonate, nitrate, or nitrate plus persulfate additions. The resulting coating structure was characterized by scanning electron microscopy. Corrosion resistance was characterized by EIS and salt spray exposure testing. (ref. 7)
- When nitrate and persulfate oxidizers were present in the bath, coating formation time and hydrogen evolution were sharply reduced, while coating weight was increased indicating an overall increase in coating efficiency. (ref. 7)
- A decrease in pinhole-type coating defects was attributed to early cessation of hydrogen evolution. (ref. 7)
- **Coatings with corrosion resistance high enough to withstand 168 hours of salt spray exposure without pitting were formed in 6 minutes or less of simple immersion.** These coatings were much more corrosion resistant than those formed in carbonate-only solutions. In EIS tests, coatings exhibited total impedances of 2 to 5 $M\Omega\text{cm}^2$ after 24 hours exposure to aerated 0.5M NaCl solution. It was also found that in EIS tests in chloride solution, the total impedance of coatings formed in oxidizing baths increased with increasing exposure time. This "healing" process is so far unique to hydrotalcite coatings formed in the presence of oxidizers and is thought to be associated with low temperature hydrothermal sealing of the coating. (ref. 7)
- It has been observed that film HT film quality diminishes with prolonged use of a given bath. An investigation was undertaken to analyze bath chemistry changes and the respective effect on R_{corr} of the resulting HT films. (ref. 8)
- As the number of runs in a bath increased, the open circuit potential (OCP) of the sample increased (as well as platinum) indicating an increase in oxidizing capacity of the bath. In contradiction to this, the quality of the HT film as assessed by R_{corr} decreased. (ref. 8)
- It was observed through capillary electrophoresis (CE) that the Al^{3+} ion concentration increased with run number, as did the ratio of nitrite

to nitrate ions ($\text{NO}_2^-/\text{NO}_3^-$). No correlation to R_{corr} was observed with other ionic species. (ref. 8)

- The relationship between the nitrite/nitrate ratio and the corrosion resistance was verified causal, however the counterintuitive relationship between the nitrite/nitrate ratio and the OCP remains unexplained. (ref. 8)
7. W. Zhang, R.G. Buchheit, "Hydrotalcite Coating Formation on Al-Cu-Mg Alloys from Oxidizing Bath Chemistries", *Corrosion*, (in review), April (2001).
 8. E.A. Pehovaz-Diez, R.B. Leggat, and S.R. Taylor, "Development of Hydrotalcite as an Environmentally Benign Conversion Coating: Effect of Bath Chemistry Evolution on Corrosion Resistance", *Corrosion Science* (in review).
- 4. Copper Control** (ref. 9)
- Rapid formation of hydrotalcite coatings requires the use of alkaline bath chemistries. In alkaline solutions Cu enrichment occurs during film formation on Cu-bearing Al alloys. This film of copper degrades coating corrosion resistance and adhesion characteristics of subsequent organic layers. A modification to the hydrotalcite coating process was made to mediate Cu surface enrichment. This modification involved use of a two-stage process involving exposure to a pH 11.5 Li-salt solution followed by exposure to a pH 13.5 solution that simultaneously eliminated Cu enrichment and formed a corrosion resistant coating.
 - Films formed by this process were free from Cu in excess of the concentration present in the alloy substrate matrix. Hydrotalcite films formed using this method exhibited total impedances greater than $10^6 \Omega\text{-cm}^2$ after 24 hours exposure to aerated 0.5 M NaCl and withstood 168 hours of salt spray exposure without pitting.
 - Cu appears to accumulate in oxide films formed during exposure to pH 11.5 Li-salt solutions, but was subsequently removed when samples are exposed to a pH 13.5 solution. Cu removal during the modified process has been rationalized using an argument based on the increase in Cu solubility that occurs in solutions with a pH greater than the solubility minimum for Cu (9.8), and the effect of Cu complexation by carbonate.
9. R.G. Buchheit, "Copper Removal During Formation of Corrosion Resistant Alkaline Oxide Coatings on Al-Cu-Mg Alloys", *J. Applied Electrochem.*, 28, 503 (1998).

B. Hydrotalcite Coating Properties

Overview. The primary performance attributes required of conversion coating are corrosion resistance and adhesion for subsequently applied paints. Chromate conversion

coatings are also reported to possess low electrical contact resistance and self-healing abilities. These four attributes were therefore a focus of our studies as described below.

1. Self-healing (ref. 10-11)

- Chromate conversion coatings are noteworthy because of their ability to self-heal if mechanical or chemical damage occurs, provided the damage is not too severe. Self-healing, or active corrosion protection (ACP), involves several discrete processes: release of chromate from the coating, its transport through solution, and its action at the site of damage; typically pits. A simple exposure cell, named the "simulated scratch cell", was recently devised to reproducibly examine chromate conversion coatings for evidence of these processes. This cell consists of two aluminum alloy surfaces, one coated and one bare, separated by a gap several millimeters in width filled with an aggressive solution. If a coating exhibits ACP, the inhibiting agent will be released into solution, interact with the bare surface, and stifle corrosion. Each of these processes can be readily tested and examined by standard laboratory and analytical methods. These techniques were used to study a Ce-bearing conversion coatings for evidence of ACP. Candidate coatings were formed on AA 2024-T3 substrates by modifying hydrotalcite coatings with Ce^{4+} compounds. Results of experiments conducted with the simulated scratch cell show that when Ce^{4+} is introduced into hydrotalcite, a classic ACP response is observed.
- ACP occurs because Ce is introduced into the hydrotalcite as a soluble high oxidation state species. When solution contacts the coating, tetravalent Ce compounds dissolve and Ce^{4+} ions migrate through solution, and are reduced and precipitated as low solubility Ce^{3+} compounds at exposed Al surface sites. Since Ce is much less soluble in reduced form, it then precipitates on the bare surfaces and slows corrosion by stifling cathodic and possibly anodic kinetics.
- Similar experiments conducted with La-modified hydrotalcite do not show evidence of ACP. La exists only in a low solubility trivalent form. Once it is introduced to the hydrotalcite coating, it is not released and cannot participate in the subsequent events that lead to Ce-like ACP.
- Permanganate-modified hydrotalcite coatings have also been examined for evidence of self-healing. In this case, we seek to induce self-healing due to leaching of Mn^{7+} , transport through solution and reduction to an insoluble form of Mn, either MnO_2 -type, or MnO -type at defects (local cathodes). Results from simulated scratch cell experiments with permanganate modified hydrotalcite coatings were mixed and a clear indication of self-healing in these systems has not been observed.

10. R.G. Buchheit, S.B. Mamidipally, P. Schmutz, H. Guan, "Active Corrosion Protection in Chromate and Chromate-Free Conversion Coatings," p. 67-92, in Surface Conversion for Aluminum and Ferrous Alloys, NACE International, Houston, TX (2000).
11. R.G. Buchheit, S.B. Mamidipally, P. Schmutz, H. Guan, "Active Corrosion Protection in Ce-modified Hydrotalcite Conversion Coatings", *Corrosion*, accepted, July (2001).

2. Adhesion (ref. 12-13)

- Adhesion of subsequent organic layers is a requisite property of any conversion coating system. While the lathe (or blade-like) crystalline morphology typical of a HT is predictive of excellent mechanical interlocking, and thus excellent practical adhesion, it can not be assumed that the surface chemistry of HT's is optimal for wetting. This investigation examines the relationship between the interlayer oxoanion in the HT structure and the surface chemistry, and their subsequent effect on adhesion of organic coatings. (ref. 12)
- The interlayer ions examined included nitrate, carbonate, and persulfate. (ref. 12)
- Dry- and wet-state adhesion of 25-75 μm thick epoxy films were measured by the pull-off tensile strength. (ref. 12)
- The results were compared to surface energy and isoelectric point measurements using respectively, the rising height method and electrophoresis of HT powders. The Lifshitz-van der Waal (LVW)/Lewis acid-base approach was employed for analysis of contact angle data. (ref. 12)
- The HTs having increased LVW had better wet-state adhesion, while a reciprocal relation was observed between dry-state adhesion and the isoelectric point. (ref. 12)
- The dry-state adhesion is controlled by repulsive interactions between the basic conversion coatings and the epoxy. (ref. 12)
- The wet-state is controlled by polar interactions that can be disrupted by water, thus allowing dispersive interactions to dominate.
- Results indicate that epoxy adhesion to HT can be increased by modification of the wettability or electrostatic characteristics of the HT. (ref. 12)
- The effect of ionic surfactants (trialkyl ammonium (TAS), sodium lauryl sulfate (SLS), cetyltrimethylammonium bromide (CTAB)) was examined. Treatment of a nitrate-based HT with TAS increased the pull-off tensile strength (POTS) by 55%. Treatment with either SLS, CTAB or a divalent cation (Ca^{2+}) had no effect on the POTS of epoxy. (ref. 13)
- Electrophoresis and the rising height method were employed to respectively examine the effect of these surfactants on electrostatic interactions and interfacial tension. TAS decreased the isoelectric

point of NO₃-HT powders from 11.3 to 10.5. This was attributed to a shift in the Outer Helmholtz Plane by the STS. (ref. 13)

- A model epoxy molecule, N-methylethylanolamine (NMEA), was used for contact angle measurements of conversion coating powders using the rising height method. (ref. 13)
- The contact angle was found to correlate with the epoxy dry adhesion rankings. TAS adsorption on NO₃-HT powders decreased the NMEA contact angle from 68° to 24°. (ref. 13)
- FTIR spectroscopy did not indicate primary bonding between NO₃-HT and STS, nor with NMEA. (ref. 13)
- The improvement of epoxy adhesion to NO₃-HT by STS is proposed to result from the increased wettability (as determined by NMEA) of the HT caused by the reduction in the isoelectric point. (ref. 13)

12. R.B. Leggat, S.A. Taylor, and S.R. Taylor, "Adhesion of Epoxy to Hytrotalcite Conversion Coatings: I. Correlation with Wettability and Electrokinetic Measurements", *Colloids and Surfaces A: Physicochemical and Engineering Aspects*, (in review).

13. R.B. Leggat, S.A. Taylor, and S.R. Taylor, "Adhesion of Epoxy to Hytrotalcite Conversion Coatings: I. Surface Modification with Ionic Surfactants", *Colloids and Surfaces A: Physicochemical and Engineering Aspects*, (in review).

3. Corrosion Resistance (ref. 14-16)

- A great deal of effort was dedicated to optimizing stand-alone corrosion resistance. The primary objective of this activity was to develop a coating that could be deposited in a matter of seconds to minutes, then withstand 168 hours of salt spray corrosion resistance on 2024-T3 substrates. This goal was achieved with Li-Al-nitrate coating chemistries, and with Ce-sealed coatings. The influence of other bath variables on corrosion resistance already reported include bath pH, concentration, temperature.
- It should be noted that to facilitate coating chemistry optimization studies a rapid coating corrosion resistance test was needed. For this, we turned to electrochemical impedance spectroscopy. A standard method for determining the coating resistance, R_c (equivalent to R_{corr}), after a 24 hour immersion in 0.5 M NaCl solution was used throughout this study. R_c is easily determined from EIS data and is essentially equivalent to the DC limit of the impedance. The methodology used throughout this study is derived directly from the original research of Kendig and Mansfeld indicated in the citations listed below.

14. C.A. Drewien, M.O. Eatough, D.R. Tallant, C.R. Hills, R.G. Buchheit, "Lithium-Aluminum-Carbonate-Hydroxide Hydrate Coatings on Aluminum Alloys: Composition, Structure and Processing Bath Chemistry", *J. Materials Res.*, **11**, 1507 (1996).

15. R.G. Buchheit, M. Cunningham, H. Jensen, M.W. Kendig, M.A. Martinez, "Rapid Electrochemical Corrosion Testing of Chemically Passivated Aluminum Alloys", CORROSION/98, Paper No. 98740 (NACE, Houston, TX:1998).
16. R.G. Buchheit, Jr., G.E. Stoner, "Method for Increasing the Corrosion Resistance of Aluminum and Aluminum Alloys", U.S. Patent granted, Nov. 13, 1996.

4. Electrical Contact Resistance (ref. 17)

- Many military applications require that conversion coatings for aluminum alloys provide high corrosion resistance while retaining low electrical contact resistance. In this paper, the performance requirements for Class 1A and Class 3 conversion coatings established in Military Specifications MIL-C-81706 and MIL-C-5541E are summarized. The corrosion resistance and electrical contact resistance of actual Class 1A and Class 3 coatings are presented.
 - Results show that the required levels of performance are usually achieved on wrought alloys, but not on cast alloys. The corrosion resistance and electrical contact resistance of Cr-free conversion coatings have also been examined. Results indicate that the required performance levels are rarely achieved on any type of alloy substrate.
 - Last, corrosion and electrical properties of coatings formed using methods based on low-toxicity alkaline oxide coatings procedures are described. Results from initial attempts to produce highly corrosion resistant coatings with low electrical resistance are presented.
 - In some applications, conversion coatings for Al alloys must provide high corrosion resistance and low electrical contact resistance. Achieving this mix is difficult because a conductive coating can facilitate galvanic corrosion action, which lowers corrosion resistance. Nevertheless, traditional chromate conversion coatings provide these attributes. A survey of Cr-free conversion coatings shows that very few provide a mix of high corrosion resistance and low electrical contact resistance that chromate conversion coatings do. This severely limits choices in procurement of Cr-free conversion coatings for military applications, and defines an area where development work could be focused.
 - Last, Cr-free hydrotalcite coatings normally exhibit high electrical contact resistance. However, initial studies show that appropriate types of post treatment can increase corrosion resistance and decrease electrical contact resistance.
17. R.G. Buchheit, M.A. Martinez, L.P. Montes, N. Cella, G.E. Stoner, S.R. Taylor, "Inorganic Cr-Free Conversion Coatings for High Corrosion Resistance and Low Electrical Contact Resistance", CORROSION/98, Paper No. 98212 (NACE, Houston, TX:1998).

C. Performance Bench-marking

Overview. Performance benchmarks for new conversion coatings are not standardized. This is due to the fact that these coatings are used in many different applications for many different reasons. In some cases conversion coatings are the primary means of corrosion protection; in others the primary function of a conversion coating is to serve as a foundation layer for subsequently applied paints.

In this phase of investigation we used performance benchmarks applicable for the use of stand-alone and foundation layer conversion coatings used in aerospace applications. The primary performance attributes were corrosion resistance, paint adhesion and electrical contact resistance. Initially, performance benchmarks were derived from MIL-C-5541E and MIL-C-87106, which establish the performance basis for conversion coatings for nearly all DoD applications. However, as the project progressed it became clear that even the best chromate conversion coatings could not meet these lofty standards. As a result we sought to define the performance attributes of chromate conversion coatings as they were applied in Air Force depots.

1. **Evaluation of field-applied chromate conversion coatings** (ref. 18)
 - Alternatives conversion coatings are commonly benchmarked against the corrosion properties of laboratory prepared CCCs. This study sought to determine the stand-alone corrosion resistance of field-applied CCCs in order to establish a more realistic benchmark for alternative conversion coatings since conversion coatings applied at the depot provide adequate performance.
 - Salt-spray exposure, wet tape adhesion tests and measurement of electrical contact resistance were performed according to military specifications for conversion coating acceptance. EIS and Auger depth profiling of the CCCs were also employed.
 - In an initial series, all of the field-applied (depot-applied) CCCs on AA2024, AA6061, and AA7075 displayed significant pitting after 168 hours salt spray exposure.
 - Attention to precleaning the surface (e.g., Scotchbrite + deoxidizing) was found to increase the corrosion resistance of the CCC.
 - A second series of experiments was initiated to examine the effects of coating time and application method (spray vs. immersion) on the corrosion resistance and paint adhesion. The CCCs were applied in a facility specifically designed to simulate the conditions at an aircraft maintenance depot.
 - It was determined that spray and immersion application produced coatings with equivalent performance. Regardless of application method, five-minutes of continuous exposure to CCC solution was required to obtain consistently adequate coating weight.
 - The present military specifications for conversion coatings require a level of performance in salt spray, that not even field-applied CCCs can meet. Yet we know from experience that field-applied CCCs do

indeed provide an excellent substrate for painting, and that these same field-applied CCCs **do** pass military specifications when tested within a coating system (i.e., conversion coating, primer, and topcoat). Thus, present military specifications may set unreasonable requirements for emerging environmentally benign conversion coatings that would eventually be used in a coating system because they are screened out due to poor stand alone salt spray performance.

18. R.B. Leggat, S.R. Taylor, W. Zhang, and R.G. Buchheit, "Corrosion Performance of Field-Applied Chromate Conversion Coatings", *Corrosion* (in press).

2. Evaluation of hydrotalcite conversion coatings within a coating system (ref. 19)

- Relevant to the acceptance of HT as an alternative to chromate conversion coatings is the ability of these coatings to provide: stand alone corrosion protection, suitable adhesion with organic layers, and overall corrosion protection when used within a coating system. This study examines the salt spray performance of nine different hydrotalcite treatments on AA2024 as stand alone conversion coatings and as a substrate for an epoxy primer. In addition, the adhesion of epoxy to the HT and the corrosion characteristics of the HT as assessed by EIS were determined. Salt spray testing was done under pertinent military specifications and used laboratory applied CCC as the benchmark. Two epoxy primers were evaluated: one with a chromate-bearing inhibitive pigment (Class-C) and one with non-chromate inhibitive pigment (Class-N).
- In stand alone salt spray tests, HT did not perform as well as the CCC, but most treatments showed favorable performance relative to bare AA2024. A correlation between salt spray results and EIS data was observed.
- For primed samples, the CCC and bare AA2024 performed better than the HT coated samples.
- No correlation was observed between the wet and dry POTS rankings and the salt spray performance of primer coated samples.
- No correlation was observed between the primer-coated salt spray performance and the stand alone corrosion resistance whether gauged by EIS or by salt spray.
- Current HT coating chemistries have been optimized for stand alone corrosion resistance.
- Neither the stand alone corrosion resistance nor epoxy adhesion data could explain the salt spray performance of the epoxy-primed samples. **This supports the need for total system testing when developing a coating component to be used within a coating system.**

19. R.B. Leggat, W. Zhang, R.G. Buchheit, and S.R. Taylor, "Performance of Hydrotalcite Conversion Treatments on AA2024-T3 When Used within a Coating System", *Corrosion*, (in press).

IV. PERSONNEL SUPPORTED

S.R. Taylor, Principal Investigator, University of Virginia, 20%
R.B. Leggat, Graduate Research Assistant, University of Virginia 50%
E. Perhovaz, Undergraduate Research Assistant, University of Virginia, 50%
J. Genthener, Undergraduate Research Assistant, University of Virginia, 0%
G.E. Stoner, Co-Principal Investigator, University of Virginia, 0%
R.G. Buchheit, Co-Principal Investigator, The Ohio State University, 20%
W. Zhang, Graduate Research Assistant, The Ohio State University, 100%
S. Mamidipally, Graduate Research Assistant, The Ohio State University, 100%
D. Devecchio, Graduate Research Assistant, The Ohio State University, 25%
L. Flores, Technician, The Ohio State University, 25%
V. Laget, Post-doctoral Researcher, 50%, The Ohio State University
J. Wisecup, Undergraduate Research Assistant, The Ohio State University, 100%
T. Gaddy, Technician, Clariant Corporation, 80%

V. PUBLICATIONS

See Appendix

Not in Appendix

- S.R. Taylor, "Coatings for Corrosion Protection: Non-Metallic", Encyclopedia of Materials: Science and Technology, Ed. by K.H.J. Buschow, R.W. Cahn, M.C. Fleming, B. Ilschner, E.J. Kramer, and S. Mahajan, Pergamon, London (in press) (3500 words).
- R.B. Leggat, E.A. Pehovaz-Diez, N.P. Cella, and S.R. Taylor, "Optimization of Bath Chemistry for Hydrotalcite-Based Conversion Coatings on Aerospace Aluminum Alloys", in *Corrosion and Corrosion Prevention of Low Density Metals and Alloys*, Ed. by B.A. Shaw, R.G. Buchheit, and J.P. Moran, The Electrochemical Society, Pennington, NJ, **PV 2000-23**, pp.124-135 (2001).

VI. INTERACTIONS/TRANSITIONS

S.R. Taylor

A. Participation, Presentations at Meetings, Conferences, Seminars, etc.

- Attended Gordon Research Conference on "Coatings and Thin Films", July 2001
- R.B. Leggat and S.R. Taylor, "Correlation of Epoxy Adhesion to Hydrotalcite with Contact Angle and Electrokinetic Measurements", to be presented at Fall ECS Meeting, San Francisco, CA (2001).

- S.R. Taylor, R.B. Leggat, R.G. Buchheit, et al., "Environmentally Compliant Corrosion Resistant and Electrically Conductive Inorganic Coatings", 2001 AFOSR Corrosion Review, Duck Key, FL (2001).

B. Advisory Functions

None

C. Transitions

Met with David Katila from Metal Coatings Intl. (Chardon, OH). They were possibly interested in acquiring a license for the HT process. Samples of Al, Mg, and steel were received from this company. Samples were sent to OSU for preparation. Communications licensing etc. were subsequently conducted by R.G. Buchheit (OSU) and Metal Conainers.

R.G. Buchheit

C. Transitions

1996

- DoD demonstration sites are in discussion with Warner Robbins AFB (Dick Kinsey), Tinker AFB (Don Neiser), and WPAFB (Mike Donley).
- Lockheed-Martin, Fort-Worth, TX: POC Tom Woodrow. Samples were prepared for joint evaluation. Lockheed-Martin's interests are in Cr-free conversion coatings for low electrical contact resistance and corrosion resistance for military aircraft applications.
- Agency: Technology Management Associates, Denver, CO,
POC: M. MacIntosh, P. Pickell, J. Johnson.
Activity: Discussions on commercialization and licensing new intellectual property.
- Agency: AMMPEC, Albuquerque, NM,
POC: J. Bullington.
Activity: Discussions on commercialization and licensing new intellectual property.
- Agency: Ashurst Government Services, Inc., Baltimore, MD,
POC: T. Langan.
Activity: Discussions on commercialization and licensing new intellectual property.

1997

- Agency: Dow Chemical Co., MI
POC: B. Larkin
Activity: Non-proprietary information exchange. Hosted Visit to Ohio State.
- Agency: Lockheed-Martin, Fort Worth, TX.
POC: M. Wossene.
Activity: Prepared coatings for evaluations on armor alloy samples for chemical agent resistant coatings (CARC).
- Agency: Lockheed-Martin, Michoud, LA.
POC: L. Knauer

- Activity: Non-proprietary information exchange, hosted visit at Ohio State.
- Agency: Henkel-Parker Amchem
POC: S. Dolan.
Activity: Non-proprietary information exchange. On-going, Henkel offers products that compete with hydrotalcite technology.
- Agency: Horton Emergency Vehicles, Inc.
POC: M. Riley.
Activity: Conducted Cr-free coating process evaluation in support of manufacturing operations involving priming and painting of aluminum automotive products.
- Agency: Lockheed-Martin, Fort Worth TX:
POC T. Woodrow,
Activity: Samples prepared for joint evaluation. Lockheed Martin's interests were Cr-free conversion coatings for low electrical contact resistance and high corrosion resistance for military aircraft applications.
- Agency: DuPont Company, Chambers Works, Deepwater, NJ.
POC: C. Seastrom.
Activity: Prepared coatings on flame sprayed aluminum vessels.

1998

- Agency: Dow Chemical Co., MI
POC: B. Larkin
Activity: Non-proprietary information exchange. Testing of samples. Hosted Visit to Ohio State.
- Agency: Lockheed-Martin, TX.
POC: M. Wossene.
Activity: Prepare coatings for evaluations on armor alloy samples for chemical agent resistant coatings (CARC).
- Agency: Lockheed-Martin, LA.
POC: L. Knauer
Activity: Non-proprietary information exchange, hosted visit at Ohio State.
- Agency: Henkel-Parker Amchem
POC: S. Dolan.
Activity: Non-proprietary information exchange.
- Agency: Horton Emergency Vehicles, Inc.
POC: M. Riley.
Activity: Conducting research and testing in support of manufacturing operations involving priming and painting of aluminum automotive products.
- Agency : Natural Coating Systems, Inc.
POC. C. Tomlinson
Activity: Coating development and process exploration using hydrotalcite coatings and Natural Coating System's sealant technology.

1999

- Agency: Morton Industrial Coatings, Columbus Laboratory
POC: Wendy Holtmann, Jeff Soltwedel
Activity: Technical discussions on potential joint projects, visit and tour at OSU.
- Agency: GM/Delphi
POC: K. Kumar

- Activity: Technical discussions on potential joint projects on coating test methods.
- Agency: Lorin Industries
POC: J. Kessler, G. Marczak
Activity: Technical discussions on potential joint projects, visit and tour at OSU.

VII. NEW DISCOVERIES, INVENTIONS, PATENT DISCLOSURES

None

VIII. AWARDS AND HONORS

None

APPENDIX

Publications and Patents

Submitted to *Corrosion Science* (in review)

This work was presented in the "Corrosion and Corrosion Prevention of Low Density Metals and Alloys" symposium of the 198th Meeting - Phoenix, Arizona

**Development of Hydrotalcite as an Environmentally-Benign Conversion Coating:
I. Optimization by Fractional Factorial Design**

R. B. Leggat*, N.P. Cella*, C. Mastrangelo**, R.G. Buchheit***, S. R. Taylor*

*Department of Materials Science and Engineering
University of Virginia
Charlottesville, VA 22904

**Department of Systems Engineering
University of Virginia
Charlottesville, VA 22904

*** Department of Materials Science and Engineering
The Ohio State University
Columbus, OH 43210

Introduction

Conversion coatings based on a naturally occurring compound, hydrotalcite, are being developed as an environmentally benign alternative to chromate conversion coatings (CCC)¹. In order to be a viable technology, hydrotalcite-based conversion coatings (HT) should provide functionality similar to CCC including high corrosion resistance, active corrosion protection (i.e. "self-healing"), and good adhesion with subsequent organic layers. The large number of processing options for HT coatings provides a range of structures and properties that require optimization.

HT coatings are formed by the immersion of aluminum alloys in alkaline lithium salt solutions. Although hydrotalcite is a general mineral class, the specific hydrotalcite compound present in the coatings, hydrolithisite, has the general composition $\text{Li}_2[\text{Al}_2(\text{OH})_6]_2 \cdot \text{XO}_n \cdot n\text{H}_2\text{O}$ where XO_n is an oxoanion such as carbonate or nitrate². Figure 1 shows the lithisite atomic structure that consists of an oxoanion and water intercalated between lithium-aluminum hydroxide layers³. A range of oxoanions can be used to tailor the properties of the coatings. In addition, a number of post-treatments are possible including hydrothermal reversion and transition metal sealing^{4,5}.

Based on the numerous processing options and bath variables, A multi-stage approach has been used in the optimization of HT coating production. The first stage employed a fractional factorial design (FFD) to determine which parameters were the most important in producing corrosion resistant coatings. Once the initial parameters had been optimized, the effect of bath chemistry evolution on the corrosion resistance of the HT films was investigated in the final stage⁶. The first stage is discussed here.

The objective of this study was to define the optimum combination of process variables that produce corrosion resistant conversion coatings in the minimum number of experiments. Based upon the large number of potentially relevant variables (e.g. temperature, immersion time, pH, and component concentrations), the effects of initial bath conditions were analyzed using a FFD to optimize the corrosion resistance of HT coatings. FFD allows the experimental matrix to be compressed so that more variables (factors) can be measured in fewer runs than is possible with a full factorial design⁷. This is achieved by limiting the levels of the factors to a high and low value and by pairing main effects with higher order effects in the runs (aliasing). The effects of the different factors were compared by analysis of variance (ANOVA). A linear mathematical model was used to relate the response level (corrosion resistance) to the factors that were found to be significant by ANOVA. Therefore the significance of the factors on the response and the goodness of fit of the model were of interest.

Statistical experimental designs have been successfully employed in previous studies of conversion coating optimization⁸⁻¹¹. Although the specific experimental designs differed, the approaches are similar in that the effects of process variables on the response were monitored. In one study that is particularly relevant to the present work, Meldrum and Lin used electrochemical impedance spectroscopy (EIS) and a full factorial design to investigate the barrier properties, hardness and exudation of a single-step phosphate / paint system¹¹.

Experimental

A three-bath process was used to produce the samples. After degreasing and deoxidizing baths, panels were coated by immersion in a third alkaline lithium salt bath. Bath parameters were examined via a two-level FFD. The coatings were evaluated by

The corrosion resistance of the coatings formed on the different alloys by the different oxoanion chemistries could be assessed by the average response for all the baths within a given matrix (Table 3). The different oxoanions could be compared within an alloy type. Based on the average response, the nitrate and sulfate chemistries appear to be the most promising candidates. However, the variance within the response was too high to assign statistical significance to the average response. The EIS data alone was not sufficient to determine the best chemistry. The additional information provided by salt spray and SEM were used to decide which chemistry should be further developed.

Analysis of Variance (ANOVA) was used to determine which factors were responsible for the observed responses. After analysis of the initial model, factors were removed to decrease the variance estimates and remove irrelevant factors. It was often necessary to transform the data to detect significant effects because the R_{corr} response ranged over several orders of magnitude. Data transformation minimized the leveraging effect of large values and allowed certain modeling assumptions, such as homogenous variance, to be met. For each alloy-anion matrix, a model was developed to relate the response value to the factors. The significant factors for each matrix and their p-values are listed in Table 4. The p-value is the observed significance level with values less than 0.05 generally considered significant. In addition, the goodness of fit (R^2) for each model is included. Though the model-adequacy assumptions used in the model development were checked, the results are not presented here.

As seen in Table 4, temperature was a significant factor for the unreplicated data. It was a significant factor for all the oxoanion chemistries on AA 7075, the AA 6061 carbonate and silicate matrices as well as the AA2024 nitrate. It should be noted that the goodness of fit for many of the models was low indicating that there were factors contributing to the response other than those included in the model.

In many instances, none of the factors was found to account for the unreplicated response. This may be due to several causes including:

1. Interactions between the factors were assumed negligible. In fact, the interaction between temperature and oxoanion concentration was observed to be significant for the nitrate chemistry on AA 7075. That effect was observable because six factors were examined in eight runs leaving an extra degree of freedom in the analysis. This would not have been possible with the matrix used for the AA2024, which had seven factors in eight runs.
2. The factors that effected the response were not controlled within the experimental design. If the dominating factor was not one of the seven controlled, its effect would be observed as random error.
3. The values for the high and low levels may have been poorly chosen. For instance, the optimum aluminate concentration was found to be 600 ppm in another study¹⁴. This concentration was not within the range defined by the high and low levels in this study.
4. Experimental, analytical, and random error may have contributed significantly to the response. The experimental variance for the unreplicated data was considerable and most likely contributed significantly to the total variance. The variance due to random error can be partitioned by replication as was done for the AA2024 matrices. In addition the experimental matrix was repeated at another laboratory for the AA7075 nitrate chemistry. The data for the AA7075 was used in development of the model and treated as a blocked experiment.

Analysis of the replicated AA2024 matrices allowed for a better fit of many of the parameters (Table 5). Temperature, time, pH and lithium concentration were significant

factors for three of the four HT oxoanion variants. These results indicate the importance of replicated measurements.

The AA7075 matrices from the second laboratory were treated as a block design. Blocking is frequently used when it is impossible to conduct the experiment under homogeneous conditions. In this case the second lab was a potential source of additional variation, therefore the data from the two labs was blocked. This allowed the data sets to be analyzed in aggregate despite the effect of the two laboratories. The effect of the different laboratory was determined to be insignificant. The model developed from the blocked data yielded the same significant factors (temperature, oxoanion concentration, and temperature-oxoanion interaction) as the data from the single lab. These results verify the analysis of the unreplicated data previously discussed.

SEM Imaging and Salt Spray Testing. Scanning electron micrographs were made of each sample. In general, no correlation was observed between the general morphology and the corrosion performance. SEM images of the HT coatings on AA6061 (run #4) show considerable difference between surface morphology produced by the different oxoanion chemistries (Figure 3). A lathe or blade-like structure is created in the carbonate and nitrate baths, but not in the sulfate or silicate baths. The sulfate bath produced HT structures that were more coral-like with curvature in the HT ligaments of the porous layer, while the silicate bath produced HT coatings that did not show any distinctive surface texture. The silicate chemistry was not considered for future development because of its predominantly low R_{corr} values and the absence of the characteristic HT structure.

Samples were examined after 24h exposure to salt spray for the AA6061 and the AA7075 matrices. None of these samples passed the corrosion resistance requirement of less than 5 pits per panel after 168 hours required by the military specification¹⁵. As a qualitative ranking, the area fraction that was uncorroded was recorded. The salt spray rankings of carbonate, nitrate, and sulfate coatings on AA7075 and AA6061 are shown in Figure 4 and 5, respectively. The high and low temperature runs are grouped to show the effect of temperature. In general, the nitrate chemistry produced the most corrosion resistant coatings based on salt spray performance. Based on the performance of the AA7075 and AA6061 in the salt spray, it was believed that coatings on AA2024 would not pass. Therefore the salt spray testing was limited to nitrate-based coatings. In addition, all runs received the cerium post-treatment. Three of the runs produced coatings that survived 168 hours salt spray per the military specification. The rankings are shown in Figure 6.

The nitrate chemistry was chosen as the chemistry for future evaluation. In addition to consistently having the second best R_{corr} values, it also showed the best salt spray performance. In subsequent RSM studies, the temperature, contact time, and pH were further optimized.

Conclusions

- The FFD study indicated that temperature was the most important bath parameter in effecting the corrosion resistance of HT coatings.
- Analysis of the replicate data for the AA2024 matrices indicated that contact time, pH, and lithium concentration were also significant factors.
- The nitrate chemistry was selected for future studies based on EIS and salt spray performance.

Acknowledgements

This work is sponsored by DARPA (Contract # F49620-96-1-0305) under the direction of Dr. Stephen Wax and Maj. Paul Trulove (AFOSR). The authors thank L. Montes (Sandia) and M. Martinez (Sandia) for salt spray testing.

References

1. R.G. Buchheit, M.D. Bode, and G.E. Stoner. *Corrosion*, **50**, 205 (1994).
2. C.J. Serna, J.L. Rendon, and J.E. Iglesias. *Clays and Clay Minerals*, **30**, 180 (1982).
3. G. Marcelin, *The Behavior of Interlayered Water in Open-Hydroxide Layered Lattices, Final Report to GRI*. Rpt. No. GRI92/0212, Gas Research Institute, Chicago, IL (1992).
4. R.G. Buchheit, et al. Paper 216, Corrosion 98. NACE, Houston Texas
5. R.G. Buchheit and M.A. Martinez, U.S. Patent 5,756,218: *Corrosion protective coating for metallic materials* (1998).
6. R.B. Leggat, E.A. Pehovaz-Diez, S.R. Taylor, *JECS*, submitted.
7. G.E.P. Box, W.G. Hunter, J.S. Hunter. *An Introduction to Design, Data Analysis, and Model Building*, p.374, Wiley Interscience, New York (1978).
8. S. El Hajjaji, M. T. Maurette, E. Puench-Costes, A Ben Bachir, and L. Aries, *British Corrosion Journal*, **34**, 273 (1999).
9. M. P. Gigandet, H. Maillard, M. Tachez, *Plating and Surface Finishing*, **86**, 71 (1999).
10. S.-H. Lin, T.-C. Wen, *Plating and Surface Finishing*, **81**, 59 (1994).
11. D. A. Meldrum, C.-T. Lin, *J. Coatings Technology*, **65**, 47 (1993)
12. ASTM-B117 "Standard Test Method of Salt Spray (Fog) Testing", ASTM, West Conshohocken, PA.
13. R.G. Buchheit, M. Cunningham, H. Jensen, M.W. Kendig, and M.A. Martinez, *Corrosion* **54**, 61 (1998).
14. L. Montes. *Effects of Solution Chemistry on the Electrochemical Response of Talc Coatings*, MS Thesis, University of Virginia (1997).
15. MIL-C-5541E. *Military Specification Chemical Conversion Coatings on Aluminum and Aluminum Alloys*. (1990)

Tables

Table 1.

Run	Factor						
	1 (Temp)	2 (time)	3 (pH)	4 [AlO ₂]	5 [Li ⁺]	6 [XO]	7 (Ce)
1	-	-	-	+	+	+	-
2	+	-	-	-	-	+	+
3	-	+	-	-	+	-	+
4	+	+	-	+	-	-	-
5	-	-	+	+	-	-	+
6	+	-	+	-	+	-	-
7	-	+	+	-	-	+	-
8	+	+	+	+	+	+	+

Table 2 .

AA 7075					Factor	(+)	(-)
Effects	Li ₂ CO ₃	LiNO ₃	Li ₂ SO ₄	LiSiO ₃	1. Temp	Boiling	RT
1+24+35	57	149	251	38	2. time	60 min	10 min
2+14+36	34	-11	216	7	3. pH	14	12
3+15+26	4	-1	176	0	4. [AlO ₂]	200 ppm	20 ppm
4+12+56	20	-10	216	-10	5. [Li ⁺]	90% solubility	9% solubility
5+13+46	-14	5	178	18	6. [XO]	90% solubility	9% solubility
6+23+45	19	-126	144	9	7. Ce bath	yes	no

AA6061	CO ₃	NO ₃	SO ₄	SiO ₃	AA2024	CO ₃	NO ₃	SO ₄	SiO ₃
1+24+35	35	652	169	1218	1+24+35+67	64	43	33	31
2+14+36	4	639	137	1202	2+14+36+57	62	36	121	-12
3+15+26	-15	-659	-165	-1178	3+15+26+47	-61	-27	-125	-30
4+12+56	-16	595	139	1204	4+12+56+37	61	7	30	-30
5+13+46	-32	-631	-139	-1174	5+13+46+27	-55	9	11	-46
6+23+45	13	-637	-168	-1186	6+23+45+17	-46	7	-88	36
					7+34+25+16	-47	14	13	32

Table 3.

	Carbonate	Nitrate	Sulfate	Silicate
AA7075	44.6 +/- 39.0	84.8 +/- 124.0	135.4 +/- 273	37.4 +/- 27.1
AA6061	50.0 +/- 28.9	375.8 +/- 899.5	115.5 +/- 217.5	628.1 +/- 1686
AA2024	55.5 +/-80.6	73.7 +/- 34.7	106.6 +/- 107.1	42.8 +/- 45.6

Table 4.

AA7075				
Oxoanion	transform	R ²	Factor(s)	p-value
Carbonate	ln (Rcorr)	0.66	Temp	0.015
Nitrate	none	0.99	Temp	< 0.0001
			[XO ⁻]	< 0.0001
			Temp / XO ⁻	< 0.0001
Sulfate	(Rcorr) ^{-1/2}	0.69	Temp	0.011
Silicate	none	0.57	Temp	0.031
AA6061				
Oxoanion		R ²	Factor	p-value
Carbonate	ln (Rcorr)	0.83	Temp	0.012
			[Li ⁺]	0.030
Nitrate	(Rcorr) ^{-1/2}	-	-	
Sulfate	(Rcorr) ^{-1/2}	-	-	
Silicate	(Rcorr) ⁻¹	0.64	Temp	0.018
AA2024				
Oxoanion		R ²	Factor	p-value
Carbonate	(Rcorr) ⁻¹	-	-	
Nitrate	none	-	Temp	0.076
Sulfate	(Rcorr) ⁻¹	-	-	
Silicate	ln (Rcorr)	-	-	

Table and Figure Captions

Table 1. Fractional factorial design. Factor 7 included only for AA2024. (-) indicates low level and (+) indicates high level.

Table 2 . Effect estimates for all HT anion chemistries on AA 7075(top, right), AA 6061 (bottom, left), AA2024 (bottom, right). R_{corr} units are ($k\Omega\text{ cm}^2$). Factor interactions aliased with main effects are listed. The factors and their level values are listed (top, left)

Table 3. Average R_{corr} +/- standard deviation ($k\Omega\text{ cm}^2$) for all runs for each alloy-oxoanion matrix.

Table 4. ANOVA for factor effects on unreplicated R_{corr} response for AA7075, AA6061, AA2024. A linear model was developed for each alloy-anion combination. The transformation of the data used for that model and the model goodness of fit (R^2) listed. The factors found to be significant by ANOVA and their p-values listed as well.

Table 5. Analysis of variance for effect of factors on replicated R_{corr} for AA2024.

Figure 1. Atomic structure of hydrolithisite showing anion layer intercalated between lithium-aluminum hydroxide layers (reference 3).

Figure 2. R_{corr} measured by EIS for runs from all alloy-oxoanion combinations. R_{corr} units ($k\Omega\text{ cm}^2$)

Figure 3. SEM of surface morphologies created on aluminum alloy 6061-T6 in (a) carbonate, (b) nitrate, (c) sulfate, and (d) silicate. Scale indicated by micron maker.

Figure 4. Salt spray results of carbonate, nitrate, and sulfate chemistries on AA7075. High and low temperature runs grouped to show effect of temperature

Figure 5. Salt spray results of carbonate, nitrate, and sulfate chemistries on AA6061. High and low temperature runs grouped to show effect of temperature

Figure 6. Salt spray results of nitrate chemistry on AA2024. High and low temperature runs grouped to show effect of temperature.

Figures

Figure 1

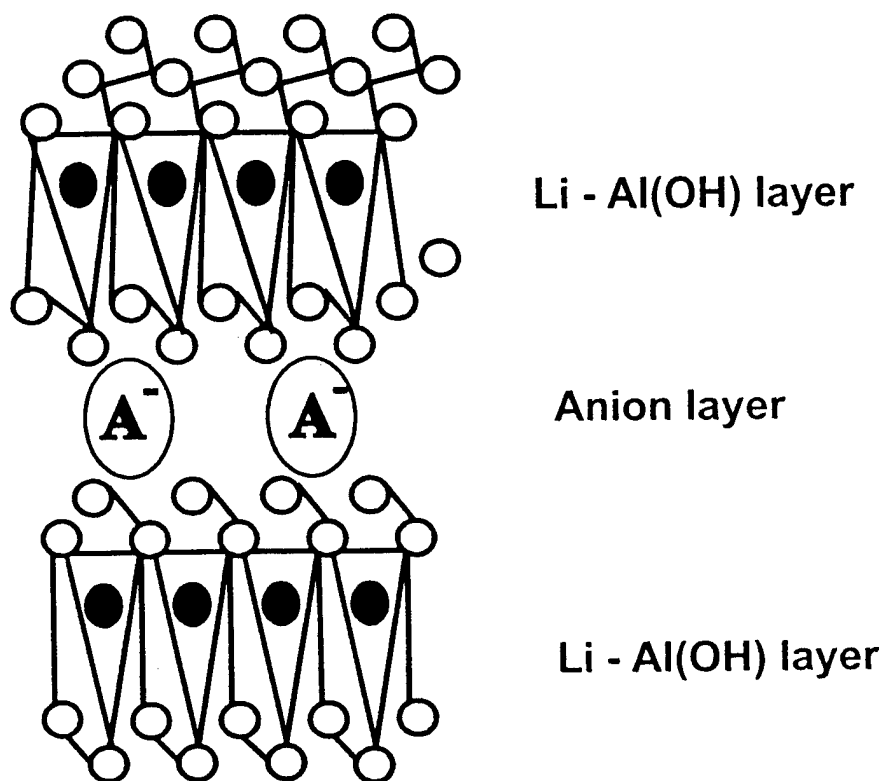


Figure 2

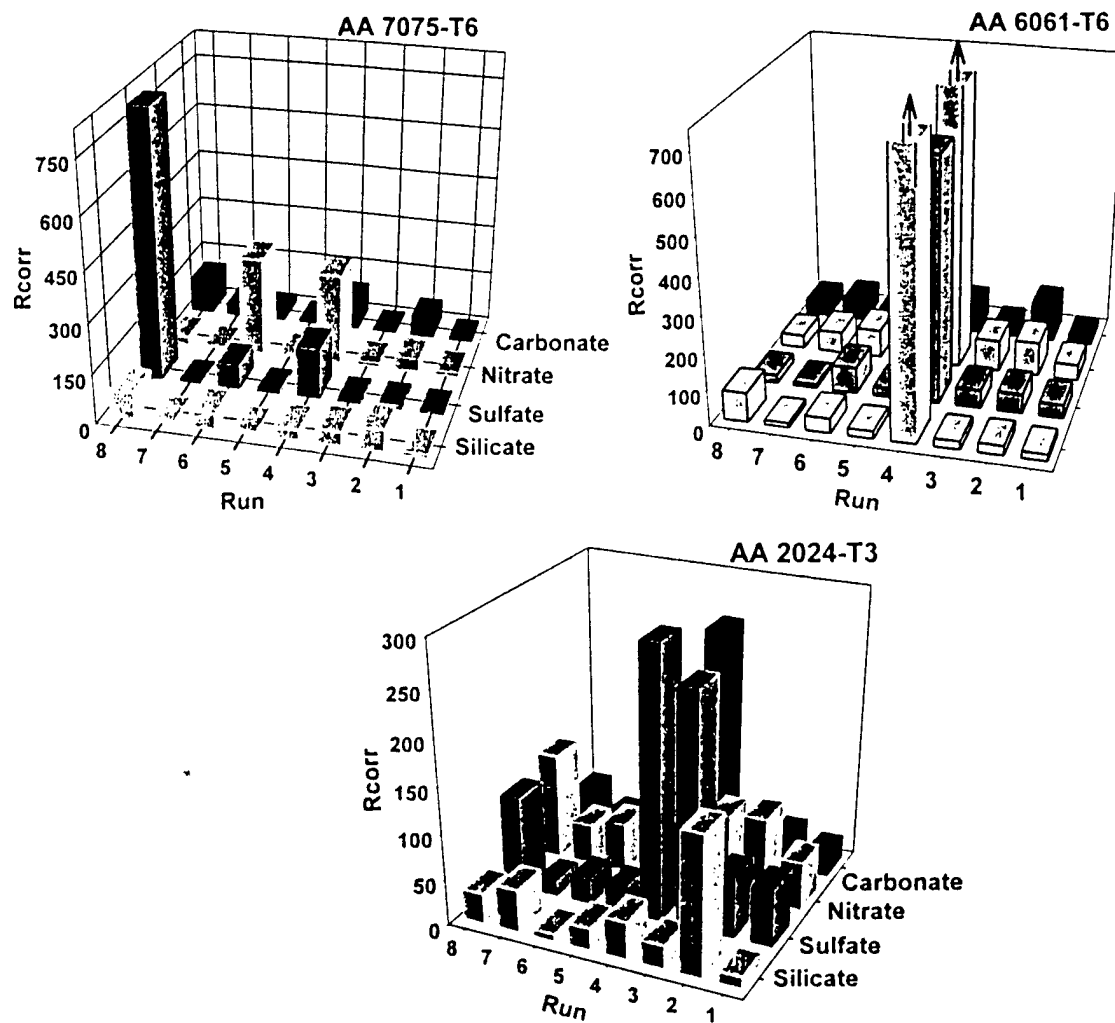
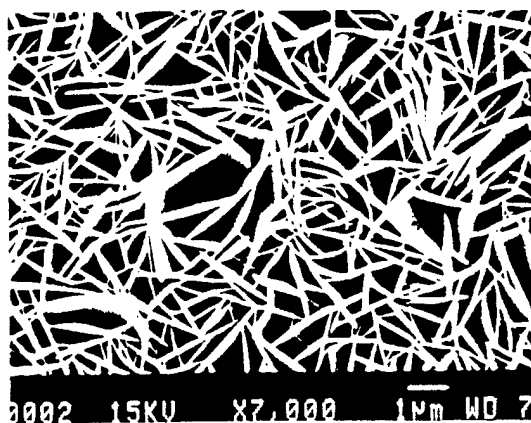
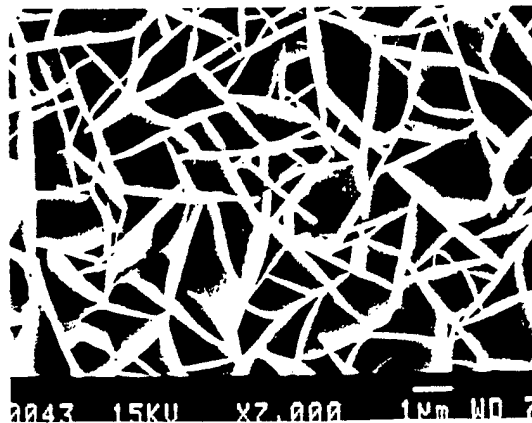


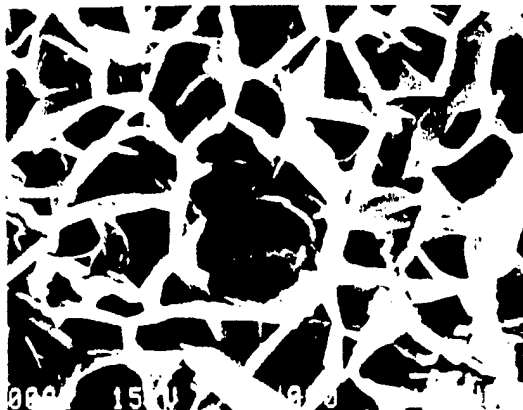
Figure 3



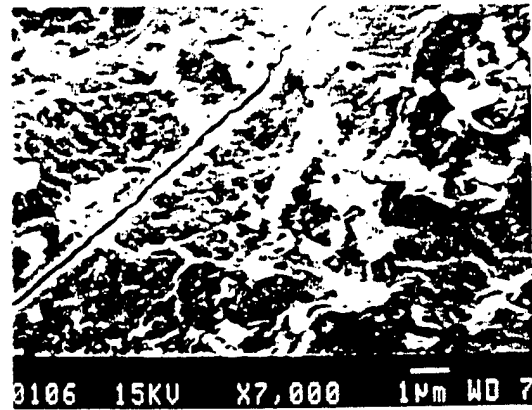
(a)



(b)



(c)



(d)

Figure 4.

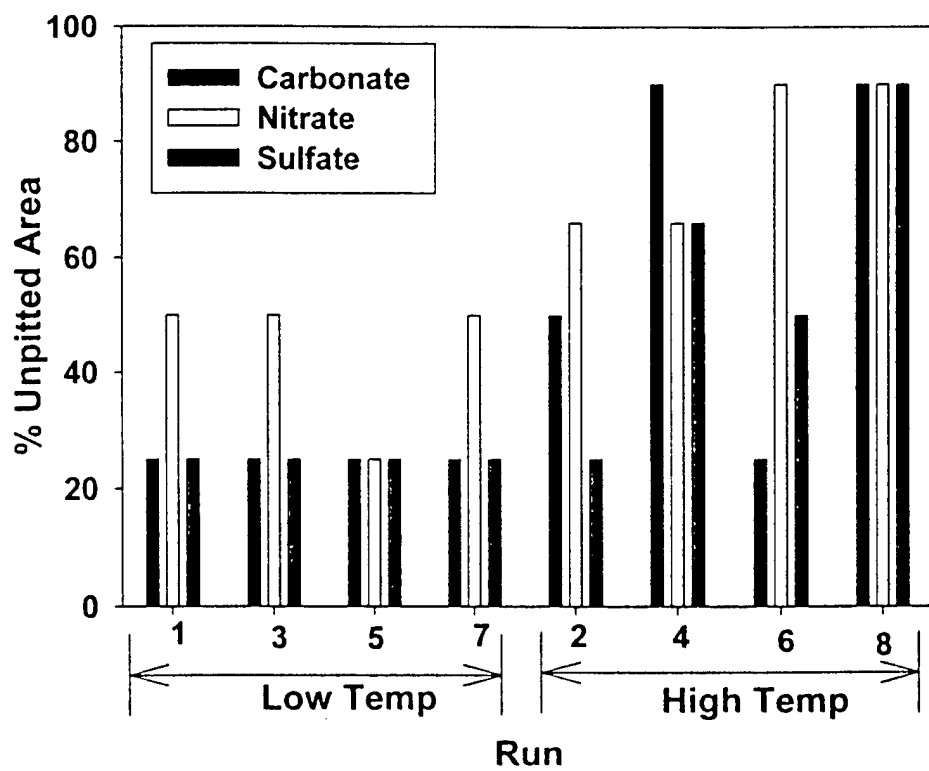


Figure 5.

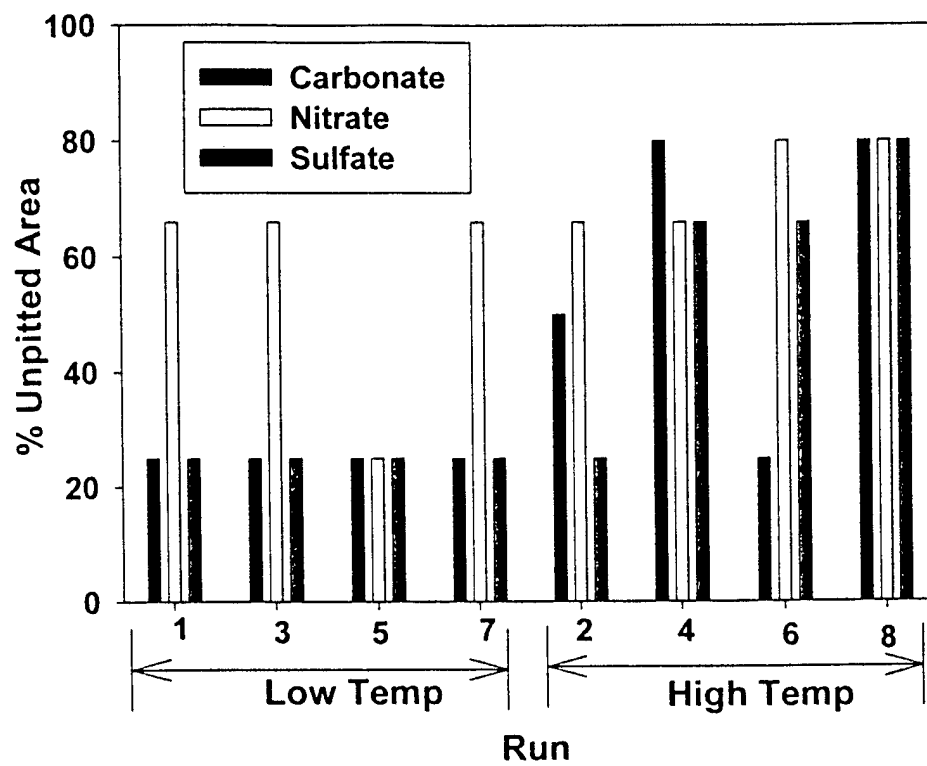
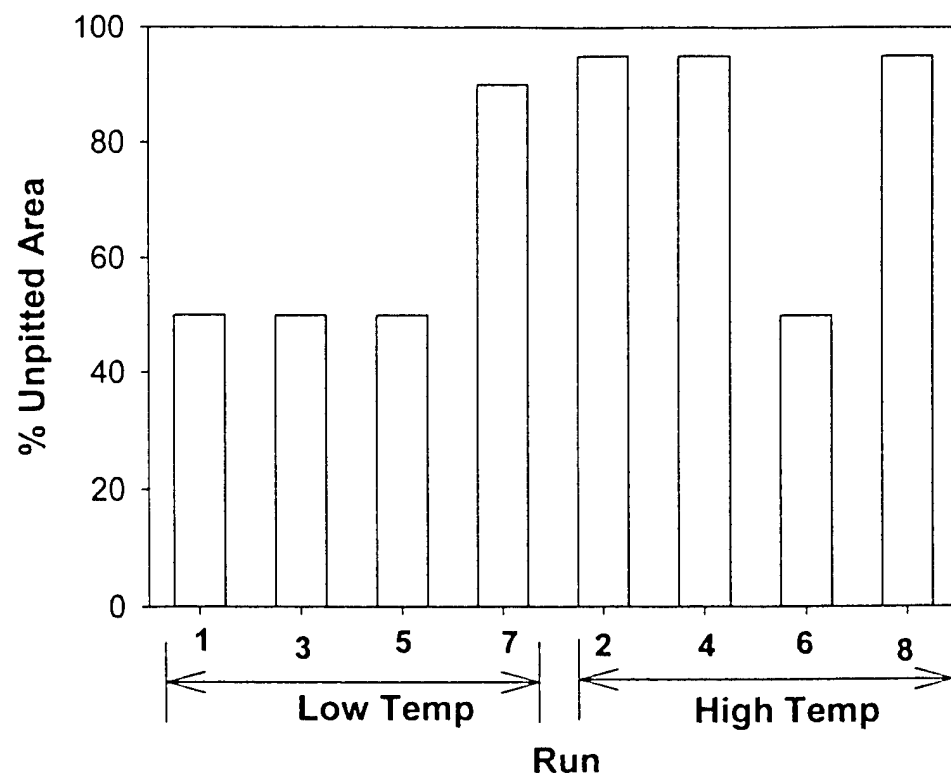


Figure 6.



R.G. Buchheit, C.A. Drewien, M.A. Martinez, "Chromate-Free Corrosion Resistant Conversion Coatings for aluminum Alloys", p. 173, Advances in coatings Technologies for Corrosion and Wear Resistant Coatings, A.R. Srivatsa, C. R. Calyton, J. K. Hirvonen, Eds., TMS, Warrendale, PA (1995).

CHROMATE-FREE CORROSION RESISTANT CONVERSION

COATINGS FOR ALUMINUM ALLOYS

R.G. Buchheit, C.A. Drewien, M.A. Martinez
Sandia National Laboratories
P.O. Box 5800
Albuquerque, NM 87185

G.E. Stoner
Dept. of Materials Science
University of Virginia
Charlottesville, Virginia 22903

Abstract

Inorganic polycrystalline hydrotalcite, $\text{Li}_2[\text{Al}_2(\text{OH})_6]_2 \cdot \text{CO}_3 \cdot 3\text{H}_2\text{O}$, coatings can be formed on aluminum and aluminum alloys by exposure to alkaline lithium carbonate solutions. This process is conducted using methods similar to traditional chromate conversion coating procedures, but does not use or produce toxic chemicals. The coating provides anodic protection and delays the onset of pitting during anodic polarization. Cathodic reactions are also inhibited which may also contribute to corrosion protection. Recent studies have shown that corrosion resistance can be increased by sealing hydrotalcite coated surfaces to transition metal salt solutions including $\text{Ce}(\text{NO}_3)_3$, KMnO_4 and Li_2MoO_4 . Results from these studies are also reported.

Introduction

Thickening of aluminum oxides films by hydrothermal exposure is well known (1-3) and is exploited in methods for promoting corrosion resistance of aluminum alloys (1,4-6). Oxide film formation by hydrothermal exposure is common to many of the procedurally simple, environmentally friendly coating methods under development. When required, additional corrosion resistance is obtained by sealing hydrothermal coatings to fill pore spaces intrinsic to hydrothermal oxide layers, or to reinforce the coating imperfections that occur at intermetallic particles in the alloy surface.

Inorganic polycrystalline hydrotalcite (hereafter referred to as 'talc') $\text{Li}_2[\text{Al}_2(\text{OH})_6]_2\cdot\text{CO}_3\cdot 3\text{H}_2\text{O}$, coatings can be formed rapidly by precipitation on aluminum alloy surfaces during immersion in alkaline lithium salt solutions at temperatures up to 100° C. Since the coating forms by precipitation under conditions where aluminum is normally quite soluble, the process is essentially a chemically stimulated method of forming a complex hydrothermal oxide. The coatings offer desirable properties including enhanced corrosion resistance, low electrical contact resistance and good paint adhesion (7). Additionally, lithium salts are low toxicity non-carcinogens and are not subject to strict environmental regulations.

In this paper, methods for depositing hydrothermal talc coatings are described. A summary of coating characteristics and properties is also provided. The mechanism of corrosion protection offered by the talc coating is addressed, and results from recent work aimed at enhancing corrosion resistance by sealing talc coatings using transition metal salt solutions are reported.

Experimental Procedures

Coating Methods

Talc Coatings. Talc coatings were formed on aluminum alloy coupons prepared from 1100 (Al-1.0(Fe,Cu,Si)), 2024-T3 (Al-4.4Cu-1.5Mg-0.6Mn), 5052 (Al-2.5Mg-0.25Cr), 6061-T6 (Al-1.0Mg-0.6Si), and 7075-T6 (Al-5.6Zn-2.5Mg-1.6Cu) sheet stock. Panels were prepared for coating by manually washing using a water-soluble alkaline detergent, degreasing with an alkaline non-etching solution and deoxidizing with an acid HNO_3/NaBr bath. Rinsing in flowing distilled water was performed in between each step. Coating was performed by immersion in an aqueous lithium salt solution with a pH of 11.2 to 11.5 at ambient temperatures or at a temperature controlled to $55\pm 3^\circ\text{C}$. Because the coating forms by a co-precipitation reaction involving aluminate ($\text{Al}(\text{OH})_4^-$), the bath was conditioned by adding 200 ppm aluminate as sodium aluminate ($\text{NaO}\cdot\text{AlO}$) or potassium aluminate ($\text{KAO}\cdot\text{AlO}$) upon make-up of new bath solution. Once prepared, coupons were immersed for a minimum of 5 minutes to form the coating, removed, rinsed and allowed to air dry. Coupons were allowed to age undisturbed for a minimum of 24 hours prior to any further handling.

For sealing experiments, 2024-T3 and 6061-T6 mill finish panels were immersed in an alkaline lithium salt solution to form the hydrotalcite coating as described above. The panels were allowed to air dry for at least 24 hours prior to exposure to the transition metal salt baths. One tenth molar (0.1 M) salt solutions were prepared by adding the metal salt to a 0.1 M LiNO_3 base solution. The use of LiNO_3 was intended to minimize any hydrotalcite coating dissolution during the sealing step. Sealing baths were held at $50\pm 5^\circ\text{C}$ for the duration of the sealing process. Sealing times, metals salts and bath pH values are reported in Table I. Identical procedures were used for 2024-T3 and 6061-T6 samples.

Electrochemical Corrosion Testing

Potentiodynamic Polarization. Anodic and cathodic polarization curves were determined for coated and uncoated samples in 0.5M NaCl solutions. Curves were acquired potentiodynamically using a PAR Model 173 Potentiostat/Galvanostat controlled by an electrochemical experiment software package installed on a personal computer (8).

Table I. Details of the sealing baths for hydrotalcite coated samples.

Metal	Compound	Bath pH	Immersion Time (sec)
Cerium	Ce(NO ₃) ₃	4.5	800
Manganese	NaMnO ₄	7.0	600
Molybdenum	Li ₂ MoO ₄	6.5	800

A standard three electrode configuration was used in a 300 cm³ cylindrical Plexiglas flat cell with a 1.0 cm² port for exposing the test electrode surface. A scan rate of 0.2 mV/sec was used for acquiring all potentiodynamic scans. Potentials were referenced versus the saturated calomel electrode (see). Scans for anodic polarization curves were initiated 0.04 to 0.1 V negative of the corrosion potential (E_{corr}) and continued to an arbitrary potential slightly positive of the breakaway potential (E_{br}). Scans for cathodic curves were initiated 0.05 V positive to E_{corr} and continued to -2.5 V_{sce}.

Electrochemical Impedance Spectroscopy (EIS). The barrier properties of talc coatings were evaluated in 0.5 M NaCl solutions under free corrosion conditions using EIS. Measurements were carried out in a flat cell modified to accommodate a specimen with a 1.0, 16 or 20 cm² exposed area. Data were collected using either a PAR 273 potentiostat/Solartron 1255 frequency response analyzer (FRA) combination, or a Solartron 1286 electrochemical interface/1250 FRA combination. Each system was controlled by an impedance software package installed on a personal computer (9). Typically, measurements were made at frequencies ranging from 65 kHz to 5 mHz by sampling at 10 points per decade frequency using either a 10 or 20 mV sinusoidal voltage perturbation. Total resistances were determined either by circle fitting the data plotted in the complex plane, or by using a partial Kramers-Kronig transformation method (10). Total capacitances were determined from the slope of the $Y''(\omega)$ vs. ω plot.

Results

Talc Coating Characterization

Grazing incident angle X-ray diffraction of talc coated surfaces show that the predominant compound in the coating is hydrotalcite. The carbonate anion in the hydrotalcite structure can be replaced by hydroxyl or chloride without a detectable change in diffraction patterns collected under standard conditions. As a result, the presence of isomorphous hydrotalcite variants can not be ruled out. Figure 1 is a plan view scanning electron micrograph that shows the typical morphology of the talc coating. The coating is comprised of intersecting crystallites that form a continuous layer across the aluminum alloy surface. Breaks are occasionally observed at large intermetallic inclusions particularly in Al-Cu-Mg-Mn alloys. Transmission electron microscopy of a coating cross section in Figure 2 shows that the intercrystalline spaces observed in Figure 1 do not penetrate to the coating-metal interface.

Coated surfaces typically exhibit a uniform matte finish, and the presence of a white translucent coating is apparent. Talc coating thicknesses range from 0.5 to 10+ μm and have been observed to depend on alloy composition (11), coating bath composition and age (12), and immersion time (12). For 1100 Al and 6061-T6, typical coating thicknesses range from 1 to 3 μm for immersion times of 15 minutes. Coating thicknesses in excess of 10 μm have been observed for immersion times of 3 to 5 hours.

Corrosion Resistance of Hydrothermal Talc Coatings

Electrochemical Testing. Figure 3 shows anodic polarization curves for uncoated and talc coated 1100 Al in aerated 0.5 M NaCl solution. The curve for uncoated Al exhibits no passive

region at potentials positive to E_{corr} (at -0.700 V) indicating that the E_{corr} is at or positive to E_{br} . E_{corr} for talc coated Al is shifted in the negative direction and passive behavior is observed up to a potential of about -0.580 V. This comparison shows that the talc coating promotes corrosion resistance in chloride solutions by inhibiting the anodic portion of the corrosion process.

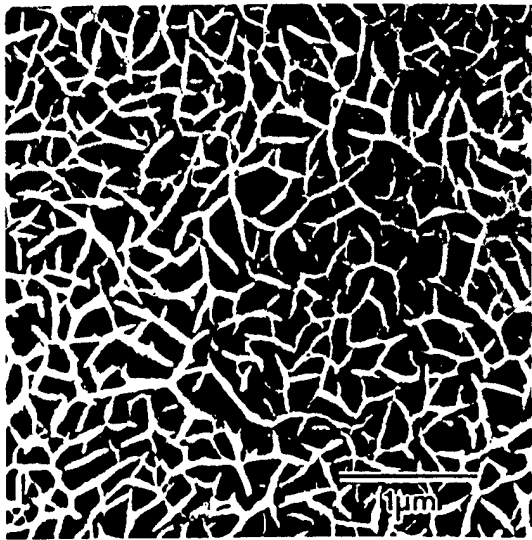


Figure 1. Plan view scanning electron micrograph of talc coated 1100 Al.



Figure 2. Cross sectional view transmission electron micrograph of talc coated 1100 Al.

Figure 4 shows cathodic polarization curves for uncoated and talc coated 1100 Al in aerated 0.5 M NaCl solution. Overall, the kinetics of reduction reactions are slower than on uncoated Al as evidenced by lower cathodic current densities observed at all but the most negative applied potentials. Under free corrosion conditions, cathodic current supporting localized anodic dissolution must be provided by reduction reactions occurring elsewhere. Since reduction reactions are suppressed on talc-coated Al surfaces, the corrosion process may be cathodically limited under the proper conditions.

0.5 M NaCl solution.

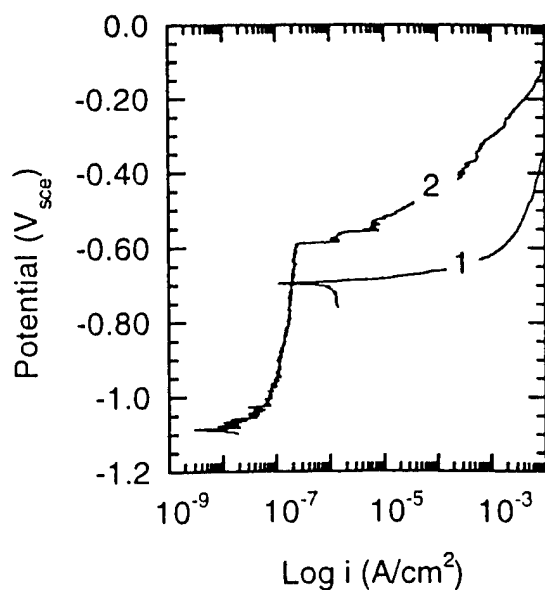


Figure 3. Anodic polarization curves for (1) uncoated Al, and (2) talc-coated Al in aerated

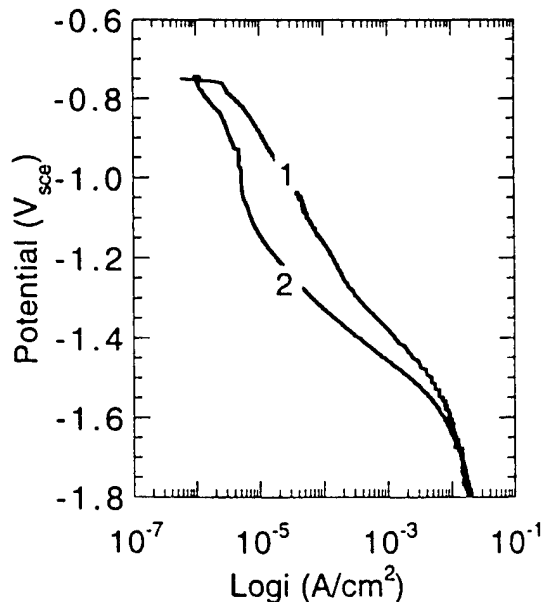


Figure 4. Cathodic polarization curves for

(1) uncoated Al and (2) talc-coated Al in aerated 0.5 M NaCl solution.

Figure 5 shows representative Bode plots for uncoated and talc coated 1100 Al after 72 hours exposure to aerated 0.5 M NaCl solution. The talc coated sample exhibits a capacitive response over a much broader frequency range than the uncoated sample due to the corrosion protection provided by the talc coating. The talc coated sample shown here exhibited a total resistance of 7×10^5 ohms-cm² as determined using the partial Kramers-Kronig method. This was more than two orders of magnitude greater than that for the uncoated sample.

Long term exposure of talc-coated 1100 Al to aerated 0.5 M NaCl solution shows that barrier properties of the coating are retained for approximately 80 hours. Figure 7 shows E_{corr} , total resistance (R_t), and total capacitance (C_t) as a function of exposure time up to 425 hours (17.7 days). After 80 hours exposure E_{corr} falls from -0.750 V_{sce} to -0.975 V_{sce} while the C_t increases from 5.5 $\mu\text{F}/\text{cm}^2$ to a peak of about 10 $\mu\text{F}/\text{cm}^2$. R_t exhibits a sharp decline between 50 and 125 hours. The decrease in corrosion potential, increase in total capacitance and decrease in total resistance indicate failure of coating by pitting at about 80 hours. The slight increase in R_t after 125 hours is attributed to the formation of a hydrated aluminum gel that was observed at the specimen surface. Examination of the exposed surface after testing confirmed that pitting had occurred during the test.

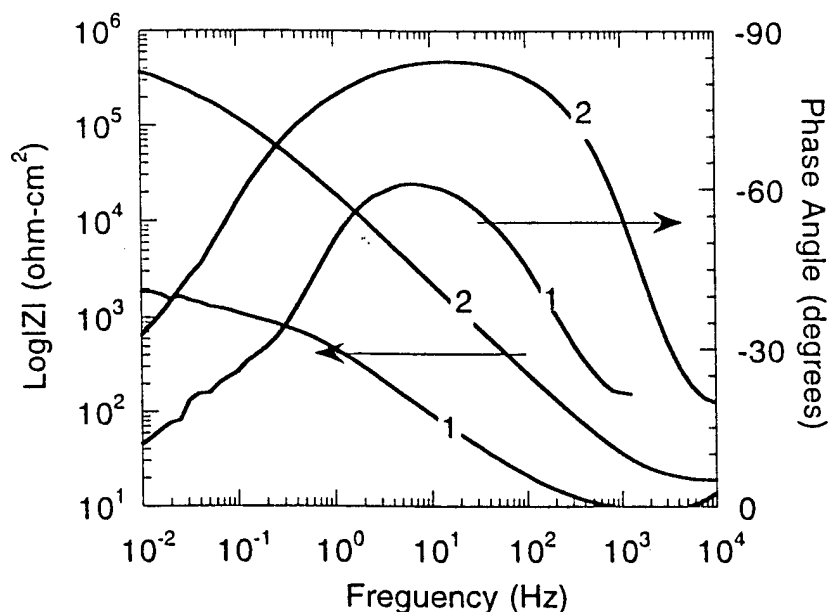


Figure 5. Bode magnitude and phase angle plots for (1) uncoated aluminum, and (2) talc-coated 1100 Al in aerated 0.5 M NaCl solution.

Corrosion Resistance in Salt Spray Exposure. The coating industry standard test for corrosion resistance of inorganic coatings on aluminum is an exposure test carried out at 95° F (35° C) using a fog or spray generated from a 5% salt solution (14). Aluminum alloys with properly formed chromate conversion coatings regularly survive this exposure test without any visible signs of corrosion. Table II summarizes salt spray test data for the range of alloys studied. This table reports the minimum coating time used to achieve a passing rank, and indicates the maximum exposure time used to test that particular alloy. Thicker coatings are required to protect alloys with higher copper contents. Coatings can be grown sufficiently thick to protect 7075-T6 (estimated to be 10 μm), but can not yet protect 2024-T3 sufficiently to pass salt spray testing.

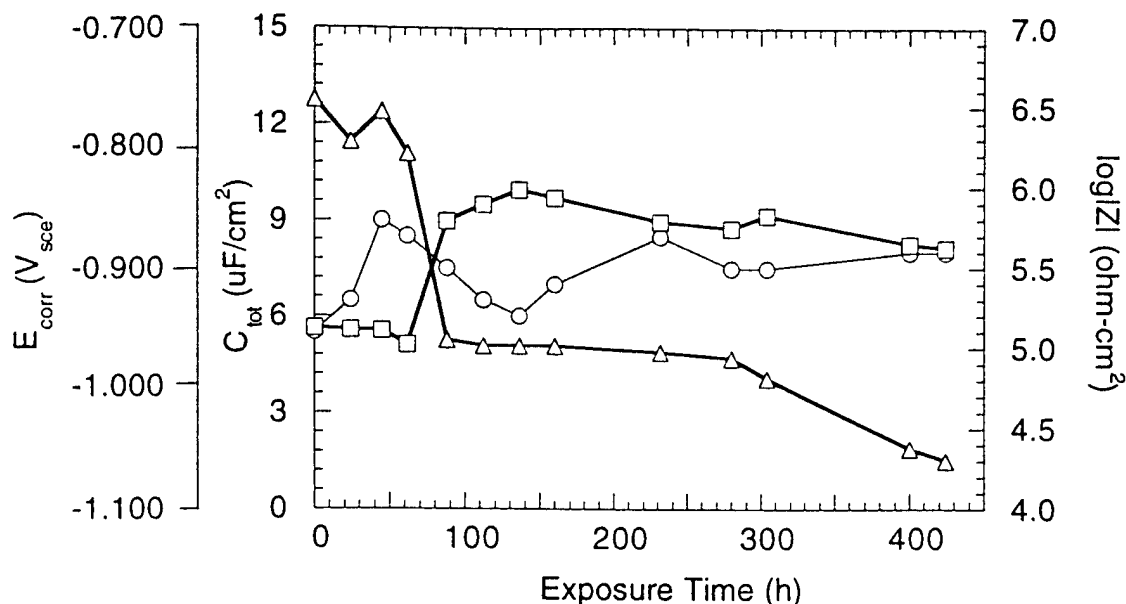


Figure 6. E_{corr} (triangles), R_t (circles), and C_t (squares) versus time for talc-coated 1100 Al in aerated 0.5 M NaCl solution.

Table II. Summary of salt spray test results.

Alloy	Cu	Mg	Zn	Si	Coating Time (minutes)	Salt Spray Result	Maximum Time Tested (hours)
5052	...	2.5	< 5	pass	168
1100	0.12	5	pass	336
6061-T6	...	1.0	...	0.6	10	pass	336
7075-T6	1.6	2.5	5.6	1.6	300	pass	168
2024-T3	4.4	1.5	900	fail	168

Corrosion Resistance of Sealed Hydrothermal Talc Coatings

Recently, studies have been conducted to determine if the protective properties of talc coatings can be enhanced by filling intercrystalline spaces or by reinforcing the coating at intermetallic particles by exposing hydrotalcite coated aluminum alloys to aqueous transition metal salt solutions known to improve the protective properties of other inorganic coatings on aluminum. Two widely studied oxy-anion analogs to chromate were selected for this study: permanganate (MnO_4^-) and molybdate (MoO_4^{2-}) (15). Ce(III) (as $\text{Ce}(\text{NO}_3)_3$) was also selected because of its tendency to preferentially precipitate as an oxide or hydroxide at defect sites in oxide coatings (16).

Figure 7 is a complex plane plot of hydrotalcite coated 6061-T6 sealed in each of the three metal salt solutions. In these tests corrosion resistance increases in the order:

$$\text{Ce(III)} < \text{MoO}_4^{2-} < \text{MnO}_4^-.$$

The total resistance ranged from 150 to 350 $\text{k}\Omega\text{-cm}^2$ which is not substantially greater than the total resistance that is achieved with unsealed talc coatings (17). A control experiment was conducted by exposing a 6061-T6 panel with no hydrotalcite coating to the MoO_4^{2-} sealing solution. The total impedance at 10 mHz was 6 $\text{k}\Omega\text{-cm}^2$ indicating that the sealing alone could not be capable of substantially improving corrosion resistance. The EIS response indicated a

single relaxation at intermediate frequencies due to the coating, and a transmission line response at low frequencies suggesting localized corrosion. Visual inspection after testing showed that localized attack occurred as crevice corrosion at the specimen-cell gasket interface.

Figure 8 is a complex plane plot of hydrotalcite coated 2024-T3 sealed in the three metal salt solutions. Here corrosion resistance increases in the order:



which is opposite for the trend observed for talc coated 6061-T6. In this case, sealing does result in an improvement in the protective properties compared to unsealed talc coatings. The relative contributions to protection are shown in Figures 9 and 10 which show Bode magnitude and Bode phase angle plots for the hydrotalcite coated, Ce(III) sealed-only, and hydrotalcite-coated and Ce(III) sealed 2024-T3 surfaces. Use of the sealing step alone improves corrosion resistance, but sealing combined with hydrotalcite coating offers a further factor of 3 improvement in corrosion resistance.

The Bode phase angle plot in Figure 10 shows that a second time constant is present at intermediate frequencies (~ 1 Hz), that is not observed in the sealed-only or talc coated-only samples. The two time constant behavior is consistent with the response expected from a hydrotalcite coated surface with coating defect sites that have been partially blocked by precipitation of cerium oxides or hydroxides.

Ce(III) sealed hydrotalcite coated 2024-T3 samples prepared as described above pit under salt spray exposure conditions, but suffer far less damage than unsealed samples. Efforts to further exploit the beneficial effects of Ce(III) sealing of hydrotalcite coated 2024-T3 are currently underway.

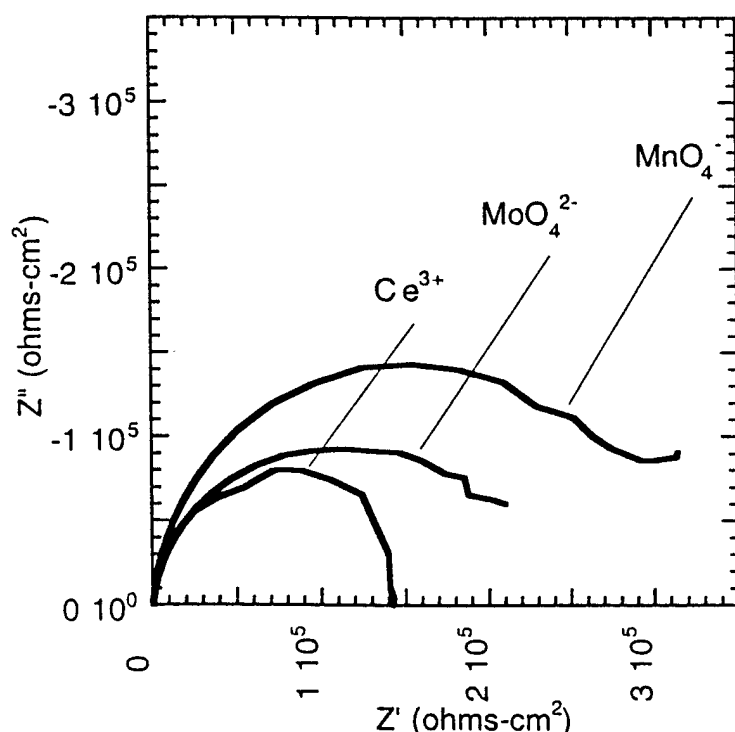


Figure 7. Complex plane plots for hydrotalcite coated 6061-T6 sealed in the three metal salt solutions.

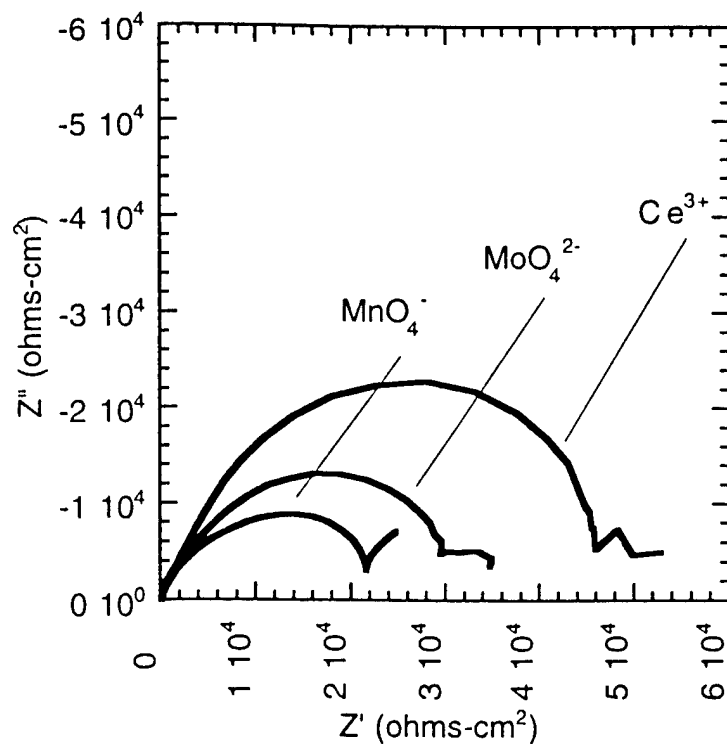


Figure 8. Complex plane plots for hydroxalcalite coated 2024-T3 sealed in the three metal salt solutions.

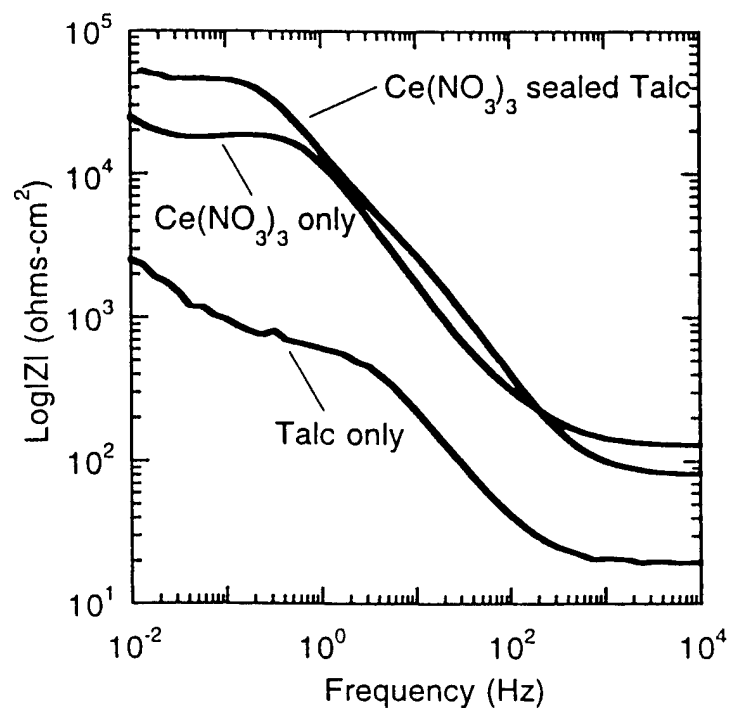


Figure 9. Bode magnitude plots for 2024-T3 with various treatments relevant to Ce(III) sealing. Differences in Log|Z| are due to specimen area normalization.

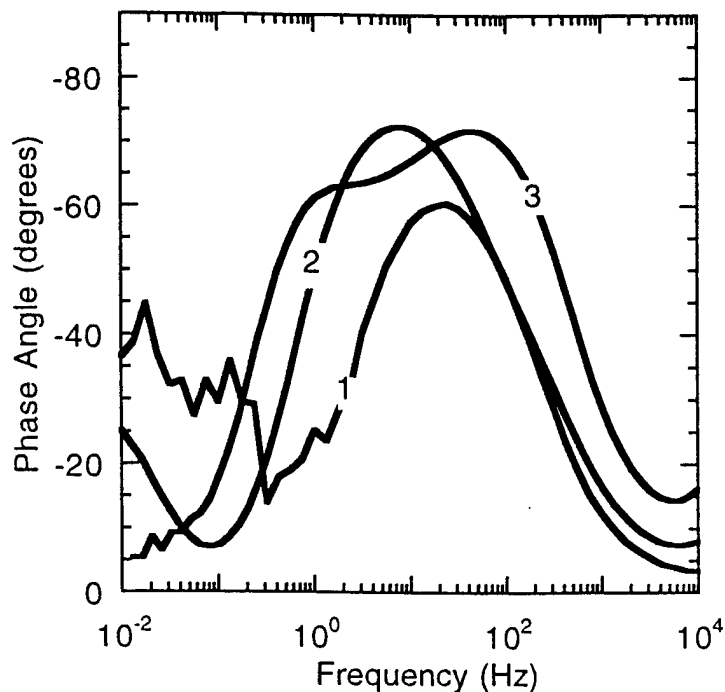


Figure 10. Bode phase angle plots for 2024-T3 with various treatments relevant to Ce(III) sealing. (1) Talc coated only, (2) $\text{Ce}(\text{NO}_3)_3$ sealed only, (3) Talc coated and $\text{Ce}(\text{NO}_3)_3$ sealed.

Summary

Polycrystalline hydrothermal oxide coatings may be deposited on aluminum and aluminum alloys from an alkaline lithium salt solution. This coating method is procedurally similar to traditional coating processes but does not use toxic or hazardous chemicals. The coating promotes corrosion resistance by inhibiting both anodic and cathodic reactions involved in the localized corrosion process. Corrosion protection of talc coatings is sufficient to inhibit pitting on 1100 Al and 6061-T6 (Al-Si-Mg) during salt spray exposure testing. Electrochemical testing shows that sealing hydrothermal talc coatings can enhance corrosion resistance, particularly on aluminum alloys with high copper contents.

Acknowledgments

The authors wish to thank M. Bode and J. Finch for sample preparation and electrochemical testing. B. McKenzie and C. Hills are thanked for conducting electron microscopy. Virginia's Center for Innovative Technology is also thanked for their continuing support.

References

- 1.) J.E. Hatch, ed., Aluminum: Properties and Physical Metallurgy, (Metals Park, OH, ASM, 1984), 307-309.
- 2.) K. Wefers and G.M. Bell, Oxides and Hydroxides of Aluminum, (Technical Paper No. 19, Alcoa Research Laboratories, 1972).
- 3.) M. Textor, and R. Grauer, A Photoelectron and Secondary Ion Mass Spectrometric Study of the Chemical Composition of Thermal Oxide Layers on Technically Pure Aluminium", Corrosion Science, 23 (1) (1983), 41-53.
- 4.) F.B. Mansfeld, H. Shih and Y. Wang, "Method for Creating a Corrosion Resistant Aluminum Surface" (U.S. Patent No. 5 194 138, March, 1992).

- 5.) H. Shih, Y. Wang and F. Mansfeld, "DC and AC Passivation of Aluminum Alloys", (CORROSION/91, paper no. 136, NACE, Houston, TX, 1991).
- 6.) R. Rungta, "Coating Process for Aluminum Alloys" (U.S. Patent No. 5 362 335, November, 1994).
- 7.) R.G. Buchheit, C.A. Drewien, J.L. Finch and G.E. Stoner, "Non-Chromate Talc Conversion Coatings for Aluminum" (CORROSION/94, paper no. 542, NACE, Houston, TX, 1994).
- 8.) Corrware, v. 2.1 (Scribner&Associates, Charlottesville, VA, 1993).
- 9.) ZPLOT, v. 1.65 (Scribner&Associates, Charlottesville, VA, 1993).
- 10.) M.W. Kendig and F. Mansfeld, Corrosion Rates From Impedance Measurements: An Improved Approach for Rapid Automatic Analysis", Corrosion, 39 (1983) 466.
- 11.) C.A. Drewien, R.G. Buchheit, K.R. Zavadil and T.E. Neil, "Microstructural Characterization of a Corrosion Resistant Hydrotalcite Coating on Aluminum" (Proceedings of the Microscopy Society of America, 51st Annual Meeting, Cincinnati, OH, Aug. 1-6, 1993).
- 12.) C.A. Drewien and R.G. Buchheit, "Issues for Conversion Coating of Aluminum Alloys with Hydrotalcite" (CORROSION/94, paper no. 542, NACE, Houston, TX, 1994).
- 13.) Product Information, Alodine 1200S (Parker+Amchem, Henkel Corporation, Madison Heights, MI, 1991).
- 14.) ASTM B117, "Standard Method of Salt Spray (Fog) Testing" (ASTM, Philadelphia, PA, 1990).
- 15.) B.R.W. Hinton, Metal Finishing, Sept. (1991), 55
- 16.) D.R. Arnott, B.W.R. Hinton and N.E. Ryan, "Cationic-Film-Forming Inhibitors for the Protection of the AA 7075 Aluminum Alloy Against Corrosion in Aqueous Chloride Solution", Corrosion, 45 (1989), 12.
- 17.) R.G. Buchheit, M.D. Bode and G.E. Stoner, "Chromate Free Talc Coatings for Aluminum", Corrosion, 50 (1994), 205.

Paper No.
625

CORROSION96

The NACE International Annual Conference and Exposition

ALKALINE OXIDE CONVERSION COATINGS FOR ALUMINUM ALLOYS*

R.G. Buchheit
Sandia National Laboratories
Albuquerque, New Mexico 87185

ABSTRACT

Three related conversion coating methods are described that are based on film formation which occurs when aluminum alloys are exposed to alkaline Li salt solutions. Representative examples of the processing methods, resulting coating structure, composition and morphology are presented. The corrosion resistance of these coatings to aerated 0.5 M NaCl solution has been evaluated as a function of total processing time using electrochemical impedance spectroscopy (EIS). This evaluation shows that excellent corrosion resistance can be uniformly achieved using no more than 20 minutes of process time for 6061-T6. Using current methods a minimum of 80 minutes of process time is required to get marginally acceptable corrosion resistance for 2024-T3. Longer processing times are required to achieve uniformly good corrosion resistance.

Keywords: hydrotalcite, conversion coating, corrosion resistance, aluminum alloys, electrochemical impedance spectroscopy.

**This work was performed at Sandia National Laboratories under contract DE-AC04-94AL85000.*

Copyright

©1996 by NACE International. Requests for permission to publish this manuscript in any form, in part or in whole must be made in writing to NACE International, Conferences Division, P.O. Box 218340, Houston, Texas 77218-8340. The material presented and the views expressed in this paper are solely those of the author(s) and are not necessarily endorsed by the Association. Printed in the U.S.A.

INTRODUCTION

Commercial chromate/chromic acid conversion coating processes were first introduced in 1945¹ as a method to improve the corrosion resistance and paint adhesion of many metal alloy systems. These processes are now regarded as technologically mature. These processes are trusted and used widely in automotive, aerospace, architectural and consumer durables applications.

In 1993, approximately 45,000 tons of Cr were used in metal finishing operations². The total value of Cr-based finishing chemicals used was \$250 million. These chemicals are critical to providing corrosion protection for fabricated aluminum components whose 1993 annual value was estimated to exceed \$22 billion³.

Chromate and chromic acid contain chromium in its hexavalent oxidation state, Cr^{6+} . Hexavalent chromium is a potent human carcinogen and is identified as a hazardous substance in federal legislation including the Clean Water Act, Clean Air Act and the Comprehensive Environmental Recovery Compensation and Liability Act.

Strict regulation of chromates was anticipated by the chromium chemical supplier and user communities. Efforts have been underway for over 25 years to identify and develop replacement processes for chromate conversion. In spite of these efforts, widespread acceptance of replacement technologies has not occurred. This situation exists for several reasons. First, performance of new coatings do not yet equal those of chromate conversion coatings. This is particularly true for conversion coatings applied to aluminum alloys with high Cu or Si contents. Second, some of the new coatings are not applicable to a wide range of alloy substrates. Third, most of the new processes require multiple processing steps or application of heat ($> 100^\circ \text{C}$) electrical potential, or current. This forces changes in plant processing equipment or process time that can not be easily accommodated on an industrial scale. Fourth, new coatings do not yet have a record of performance in service.

This paper describes the fundamental aspects of several related conversion coating methods that are potentially simple and low-cost. These methods are based on film formation that occurs when aluminum alloys are exposed to alkaline lithium salt solutions. These methods have the potential to be procedurally similar to traditional chromate conversion processes without the toxic hazard. The basic principles of film formation and general methods used to form the coatings are given. The resulting coating morphology, structure and composition are described. Finally, the corrosion resistance determined by electrochemical testing in aggressive chloride solutions is presented.

THE BASIC COATING FORMATION PROCESS

The basis of inhibited alkaline solution conversion coating is the reaction of aluminum with water at elevated temperatures (25° to 100°C). Experimental studies indicate that there are three primary steps in the reaction process which results in film growth on aluminum^{4,5}. These are the formation of an amorphous oxide, dissolution of this oxide to a soluble aluminum species, and precipitation of these species as a hydrous oxide. At temperatures less than boiling and with sufficient time, the reaction process results in a duplex film with a poorly crystalline boehmite (AlOOH) or pseudoboehmite inner layer and a crystallized bayerite ($\text{Al}(\text{OH})_3$) outer layer. This particular film structure is obtained due to the formation kinetics of the phases involved in the process: amorphous pseudoboehmite forms rapidly but does not readily crystallize; dissolution of this compound liberates sufficient aluminum ion to enable precipitation of crystalline boehmite, and at longer times bayerite forms.

In alkaline solutions, aluminum oxides are very soluble and the film dissolution-precipitation process proceeds rapidly and for long times before the aluminate ion concentration in solution attains the solubility limit which enables precipitation. As a result, the metal substrate experiences severe etching and corrosion. Additionally, the film that finally forms is more porous, hence less corrosion resistant

than one that forms at lower pH. The presence of lithium in alkaline solutions does not appear to alter the basic aluminum-water reaction sequence but it does alter the phases formed, increases the kinetics of film formation to suppress unwanted etching, and results in formation of a more corrosion resistant film.

Figure 1 is a scanning-transmission electron micrograph of the duplex film formed on aluminum during a 15 minute exposure to a mixed lithium carbonate-sodium aluminate solution at pH 11.5. This two layer film is structurally similar to that described above. However, the film is quite thick for the small reaction times used, and the phases formed are different than those normally formed by the reaction of aluminum with water. Figure 2 shows a grazing incidence angle X-ray diffraction pattern for the surface coating shown in Figure 1. This pattern indicates the presence of $\text{Li}_2[\text{Al}_2(\text{OH})_6]_2 \cdot \text{CO}_3 \cdot 3\text{H}_2\text{O}$ which belongs to the hydroxalite mineral family⁶. Electron diffraction of the inner layer indicates poor crystallinity similar to observations for hydrous aluminum oxide films⁷. Secondary ion mass spectroscopy of films formed on commercially pure aluminum under similar conditions indicates that this inner layer contains lithium and is therefore compositionally different than conventional hydrous aluminum oxide films. It has not been determined if this compositional difference results in a change in transport properties of this layer.

In alkaline solutions, hydroxalite is less soluble than bayerite which may contribute to the increased film formation rate. Figure 3 is a plot of bayerite and hydroxalite solubility as a function of solution pH⁷. Between pH 10 and 13, hydroxalite is less soluble than bayerite and would therefore be expected to form preferentially. The notion that hydroxalite is formed in preference to bayerite is substantiated by X-ray diffraction studies that indicate that the predominant compound formed under these conditions is hydroxalite.

Among Group IA and IIA cation salts only lithium salts appear to be suitable for use in coating formation for practical purposes. Additions of lithium, magnesium and calcium salts to alkaline solutions have been observed to promote film formation and passivation of aluminum alloys⁸⁻¹⁷. Magnesium, calcium and strontium are potent hydroxalite formers but their solubility in alkaline solutions is low and hydroxalite formation is sluggish. Sodium, potassium, rubidium and cesium salts are all highly soluble in alkaline solutions, but none form hydroxalites. As the lowest atomic number element in its group (neglecting hydrogen), lithium shares chemical properties of both Group IA and Group IIA. Therefore only lithium salts exhibit requisite solubility and capacity for hydroxalite formation that enable passive film formation in short periods of time. The salt anion appears to be less critical in determining passive film formation. Passivating hydroxalite films have been formed from alkaline lithium salt solutions including lithium hydroxide, sulfate, bromide, chloride and borate.

Aluminum ion, speciated as aluminate AlO_2^- , or equivalently $\text{Al}(\text{OH})_4^-$, is also critical to formation of passivating hydroxalite films. Figure 4 shows the open circuit potential (OCP) of 99.999 Al in a 7.4 g/L Li_2CO_3 plus 200 ppm AlO_2^- solution at pH 11.5 as a function of time. During this exposure the potential shifts in the positive direction by more than 1.0 V due to passive film formation. To demonstrate the role of aluminum in the film formation process, anodic polarization curves were collected before and after passivation was complete. Figure 5 shows an anodic polarization curve collected after 650 seconds of OCP exposure. At this point, the surface is incompletely passivated and the aluminum sample experiences an active to passive transition as sufficient aluminate ion is generated by dissolution to enable film formation. The contrasting situation is shown by the polarization curve collected after 52000 seconds of OCP exposure. In this case, the Al surface exhibits passive behavior only. Passivity is observed because sufficient aluminate ion was generated by dissolution under OCP conditions over the long exposure duration to enable complete film formation.

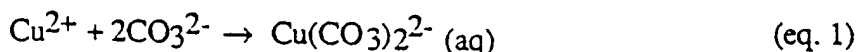
Based on these types of experiments, the requisite ingredients for hydroxalite film formation on a short time scale are: a lithium salt, an aluminum salt (or an equivalent source for aluminate) and an alkaline pH. Coating formation will occur at ambient temperatures, but elevating the solution temperature promotes rapid film formation. Coatings with desirable properties can be formed on Al, Al-Mg, and Al-Mg-Si alloys by exposure to alkaline lithium-aluminum salt solutions for times as short as 5 minutes.

A MODIFIED PROCESS FOR ALUMINUM ALLOYS CONTAINING COPPER

In many aqueous surface finishing procedures including degreasing, deoxidizing and conversion coating, the presence of copper in the alloy substrate is problematic. During these processes, the surfaces of work pieces become enriched with a variety of copper compounds, occasionally including metallic Cu, that are collectively referred to as "smut". Cu smut forms in etching alkaline degreasing solutions where Cu solubility is low¹⁸. Less frequently, it is observed to accumulate on surfaces during deoxidation where aggressive chemical action intended to remove surface oxides attacks the underlying alloy substrate⁷. Metallic copper deposits form because the open circuit potential for the alloy substrate is negative to the reduction potential for Cu. Cu smut interferes with conversion coating formation¹⁹, anodization²⁰ and with bonding of subsequently applied adhesives and paints^{19,21,22}. It is also suspected to contribute to increased susceptibility to corrosion during service due to galvanic coupling with Cu-rich surface regions.

A possible remedy to this situation has been identified for conversion coating processes using alkaline Li salt solutions. A modification to the basic process enables simultaneous coating formation and Cu removal. This process modification is based on the fact that it is thermodynamically possible to use complexing reactions to extract and retain Cu in aqueous solution, and that Cu solubility increases appreciably in very alkaline solutions. Coatings formed using the modified coating process offer good corrosion resistance on 2024-T3 (Al-4.4Cu-2.5Mg-0.6Mn) in both electrochemical and exposure corrosion testing (salt spray).

High corrosion resistance is due in part to removal of Cu compounds from the coating. The removal of Cu from the surface film can be explained by copper solubility in alkaline solutions and by copper complex formation by carbonate. The solubility minimum for Cu occurs at pH 9.8. At pH 11.5, the pH of the first stage coating bath, Cu solubility is less than 10^{-8} M. Cu enrichment in the surface film during exposure to this solution is therefore expected. At pH 13.5, Cu solubility increases to approximately 5×10^{-4} M. Since hydrotalcite formation is still possible at this pH, a Cu-free film forms. Removal of Cu is assisted by Cu complex formation which further increases the total solubility for Cu^{2+} . At pH 13.5 the following complex formation process is possible:



$$K_{\text{form}} = 9.83 \pm 0.04.$$

To illustrate how this modification to the process works, it is helpful to compare it to the more mature variant that offers good corrosion resistance on Al, Al-Mg and Al-Mg-Si alloys, but does not perform well on Al-Cu-Mg alloys. This process, which will be referred to as the "basic" process, is formed in a solution containing 7.4 g/L Li_2CO_3 plus 200 to 400 ppm $\text{Na}_2\text{Al}_2\text{O}_4$ with a pH of 11.2 to 11.8 at $50 \pm 5^\circ$ C for 15 minutes. In the modified process, the basic process is carried out followed immediately by a second immersion step carried out in a solution containing 7.4 g/L Li_2CO_3 , 7.2 g/L LiOH and 11.1 g/L $\text{Na}_2\text{Al}_2\text{O}_4$ with a pH of 13.5. This solution is also operated at a temperature of $50 \pm 5^\circ$ C and immersion times range from 15 to 180 minutes. The modified process has been used to generate highly corrosion resistant coatings on 2024-T3.

Figure 6 is a scanning electron micrograph (SEM) of a surface of a 2024-T3 sample after hydrotalcite coating with the basic process. The surface is featureless except for cracks that formed by shrinkage as the film dried. Figure 7 shows the surface morphology after coating according to the modified process. In this case, the distinctive surface morphology associated with hydrotalcite coatings is observed²³. Grazing incidence angle x-ray diffraction of the coating formed by the basic process shows that the primary compound in the coating is bayerite, $\text{Al}(\text{OH})_3$. However, coating formed using the modified process contains hydrotalcite with no detectable amounts of bayerite.

Figures 8 and 9 show oxygen, copper and aluminum sputter depth profiles determined by auger electron spectroscopy (AES) for the surface of 2024-T3 coated using the basic and modified processes respectively. The surface film and substrate regions can be clearly distinguished by the sharp decrease in the oxygen signal and the corresponding increase in the Al signal after 3500 seconds of sputtering time. In Figure 8, the Cu profile exhibits a broad maximum with a peak concentration that is approximately 4 times the concentration present in the alloy substrate. In Figure 9, the profile shows that use of the modified process results in no enrichment of the coating above levels that are present in the alloy substrate. As in Figure 8, the oxide-metal interface is reached after approximately 2000 seconds of sputtering time indicating no net change in film thickness assuming similar sputter rates for each film.

METAL OXIDE MODIFIED COATINGS

A third process variant has been identified for less corrosion resistant substrates including 2024-T3 and 7075-T6. This process involves deposition of a hydrotalcite coating followed by exposure to an aqueous neutral or acid metal salt solution. This second step is intended to seal any latent porosity by precipitating metal oxide into pore spaces. This process is analogous to dichromate sealing of sulfuric acid anodized aluminum except that external electrolytic control is not required and the second sealing step can be completed in a very short period of time. The corrosion resistance of a sealed hydrotalcite coating is not as effective as that of a sealed anodized coating, but it is good compared to chromate conversion coatings.

The metal salts used in the second step of this coating process can be divided into two sets. The first set consists of salts whose solubility minimum occurs under alkaline solution conditions. This includes salts of Ce, Co, Ni, Fe, Mn and Mg. The second set consists of metals, not included in the first class, but considered as potential inorganic sealants for oxide coatings. This includes salts of Mo, Bi, Al and Cr (Cr salts were used for reference only).

In these processes, hydrotalcite coatings are formed using one or the other of the two processes described in the earlier sections. The workpieces are then immediately immersed in the metal salt solution for a period of time ranging from seconds to tens of minutes.

During exposure to a transition metal salt solutions, the coating morphology, structure and composition of the original hydrotalcite coating change. The case of sealing with Ni-acetate (Ni-Ac) is given as a representative example. Figures 10 and 11 are scanning electron micrographs of a hydrotalcite coated 6061-T6 surface before and after 5 and 30 minutes exposure to a pH 6.5 Ni acetate solution respectively. The distinct hydrotalcite coating morphology is retained after 5 minutes exposure but not after the 30 minutes exposure. Grazing incidence angle X-ray diffraction (GIXRD) detected the major reflections for the hydrotalcite compound in the coating formed by the 30 minute exposure, but some of the minor peaks are absent. Peaks due to formation of other compounds including $\text{Ni}(\text{OH})_2$ were not detected. This suggests degradation of the hydrotalcite compound with possible replacement by an amorphous hydroxide compound during extended exposure. Figures 12 and 13 show sputter depth profiles of a hydrotalcite surface exposed to Ni-Ac solution for 5 and 30 minutes. After 5 minutes, Ni is detected in the outer portion of the coating. As exposure time increases the total coating thickness increases and the total amount of Ni in the coating increases. These data suggest degradation or replacement of hydrotalcite with a Ni-based compound after long exposures to the Ni-Ac solution.

COMPARISON OF COATING CORROSION RESISTANCE

Corrosion resistance was evaluated using electrochemical impedance spectroscopy (EIS). EIS spectra were collected from conversion coated samples after 24 hours exposure to a 0.5 M NaCl solution. The total exposed area of coated surface to solution was 16 cm^2 . Data were collected from 10 kHz to 10 mHz using a 10 mV sinusoidal voltage perturbation. A minimum sampling rate of 7 points

per decade frequency was used. Spectra for these samples usually exhibited a capacitive, though slightly lossy response from 1 kHz to 100 mHz. In some cases, at the lowest measured frequencies a DC limit or transmission line response was detected indicating corrosion by pitting. A representative Bode impedance magnitude plot for 2024-T3 coated using each of the three processing variants described is shown in Figure 14.

EIS spectra were analyzed by equivalent circuit modeling. Spectra were fit to a model using complex non-linear least square (CNLS) method²⁴. The models used for fitting were derived from the model proposed by Hitzig et. al. for the EIS response for aluminum covered by a damaged oxide film²⁵. In some cases distributed elements were substituted for the discrete elements in Hitzig's model, and whenever possible, simplified versions of the model were used to fit data. Most of the spectra were fit using the simplified model shown in Figure 15. This model consists of a solution resistance in series with a parallel resistor-constant phase element (CPE) combination. The use of a CPE rather than a discrete capacitor enables fitting of these inherently lossy coatings. The admittance of the CPE is given by:

$$Y(\omega) = (j\omega\tau)^\phi \quad (\text{eq. 2})$$

where j is $\sqrt{-1}$, ω is the frequencies in radians, τ is a time constant, and ϕ is an exponent whose value ranges from 0 to 1. The primary figure of merit derived from equivalent circuit modeling is the magnitude of the resistance due to the corrosion process, R_{cor} . For highly corrosion resistant chromate conversion coatings, an R_{cor} value of 1 to 2 $\text{M}\Omega\text{-cm}^2$ can be expected for the exposure regimen used here. This value can be used as a benchmark in evaluating the corrosion performance data for coated samples shown in Figures 16 and 17.

Figure 16 shows R_{cor} values for coatings applied to 6061-T6. This plot summarizes data from each of the three types of processes described and plots R_{cor} versus cumulative process time (excluding degreasing and deoxidation). Groups of data occur at certain discrete process times. The range in the R_{cor} values in a given group represent coatings prepared using different processes (e.g. different sealing baths operated for the same length of time) and do not represent scatter for a single process. Assignment of individual coating processes to individual data points will be made at a later time. The closed symbols indicate R_{cor} values for the basic process and the open symbols indicate R_{cor} values for the modified processes. The solid lines bound the majority of the data set. The data in this plot suggest that the metal oxide modification to the basic coating process can produce useful gains in corrosion resistance without adding a large amount of time to the coating process. For example, using a 5 minute transition metal sealing step after depositing a hydrotalcite coating can increase R_{cor} by an order of magnitude. Sealing a hydrotalcite coating for times longer than 5 minutes does not appear to provide much additional corrosion resistance. In some cases corrosion resistance is worse than for the basic process.

Figure 17 shows an R_{cor} versus process time plot for coated 2024-T3. This plot was constructed in a manner identical to that for Figure 16. Again the R_{cor} values for the basic process are shown by the closed symbols and R_{cor} for the modified processes are shown with open symbols. Two items are immediately obvious in comparison with the 6061-T6 data. First, for any given process time, R_{cor} for 2024-T3 is less than that for 6061-T6. This is probably a reflection of the low intrinsic corrosion resistance of Al-Cu-Mg alloys. Second, R_{cor} values improve continuously with increased process time. This somewhat unfortunate response indicates that using current methods, high corrosion resistance can not be attained in less than 80 minutes of process time. However, past experimentation with these processing methods has generally resulted in identification of means for improving corrosion resistance and decreasing total process time. To date, no information has been collected that suggests a change in these trends.

Empirical evidence collected from tests conducted in our laboratories and others²⁶ suggests that for 6061-T6 when an R_{cor} value greater than 10^5 ohm-cm^2 is measured a coated sample can be expected to withstand 168 hours of salt spray exposure testing without pitting. For 2024-T3 an R_{cor} value greater

than 10^6 ohm-cm² usually indicates that a coated sample will perform well in salt spray exposure. The data in Figure 16 show that coatings formed using the basic process can be expected to perform well in salt spray exposure testing. This has been observed to be the case²⁷. Using the metal oxide modified process, which adds 5 minutes of processing time, coatings can be formed that almost always exceed the 10^5 ohm-cm² threshold. Performance of these coatings in salt spray exposure testing is uniformly good suggesting that the metal oxide modification is the process of choice for high corrosion resistance. Forming a coating on 2024-T3 with good corrosion resistance requires considerably more processing time. The data from this study indicate a minimum of 80 minutes to achieve the 10^6 ohm-cm² R_{cor} threshold. Panels produced using these methods demonstrate significantly improved corrosion resistance over those formed using the basic process. However, unacceptable amounts of pitting are sometimes observed after 168 hours of salt spray exposure. The current situation is that uniformly acceptable salt spray performance is only observed for coatings formed using the longest coating processes. In this case, further process development is required to shorten process time and increase corrosion performance.

SUMMARY

Exposure of aluminum alloys to alkaline lithium salt solutions containing aluminate results in formation of a duplex surface film whose primary component is a hydrotalcite compound. This film is continuous across the surface and provides good corrosion resistance for Al, Al-Mg and Al-Mg-Si alloy substrates. To form corrosion resistant coatings on less corrosion resistant substrates like Al-Cu-Mg alloys, modifications to the basic process must be made. A modified process has been devised that can extract Cu compounds from the coating that may degrade its protective capacity. This process exploits Cu solubility at high pH and Cu complexing to produce Cu-free coatings. Corrosion resistant coatings can also be made by reinforcing a hydrotalcite coating with other metal oxides. These oxides are deposited in or on the coating using a second processing step. Each of these process variants improves the corrosion resistance over the basic process while retaining the simplicity and procedural similarity to traditional conversion coating operations.

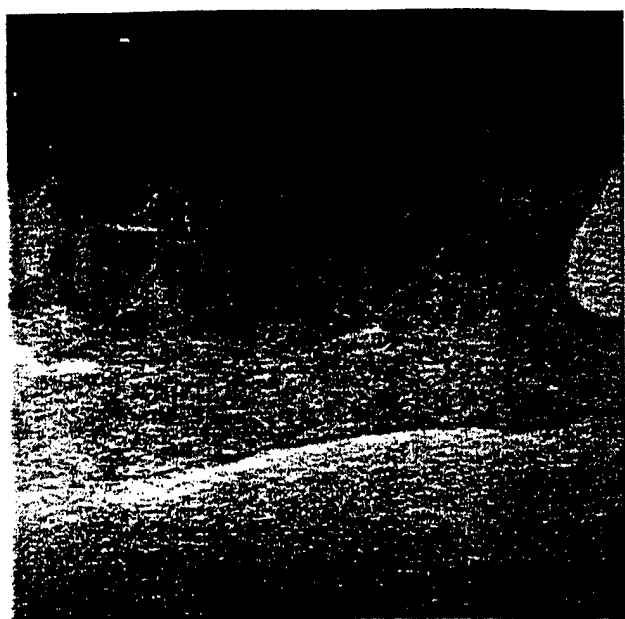
ACKNOWLEDGMENTS

The author wishes to thank M. Martinez sample preparation and electrochemical corrosion testing. W. Buttry and B. McKenzie for surface analysis and scanning electron microscopy.

REFERENCES

- 1.) J. Spruance, American Chemical Paint Co., U.S. Patent 2 438 887 (1948).
- 2.) Chemical Marketing Rep., 238, 1, p. 222 (1990).
- 3.) The Aluminum Industry WWW Server, <http://www.euro.net:80/concepts/industry.html>, Integrated Concepts, Inc. WWW Development, European Multimedia Engineering, B.V., Oud Beijerland, Netherlands (1995).
- 4.) W. Vedder, D.A. Vermilyea, Trans. Faraday Soc., 65, p. 561 (1969).
- 5.) R.S. Alwitt, J. Electrochem. Soc., 121, p. 1322 (1974).
- 6.) C.J. Serna, J.L. Rendon, J.E. Iglesias, Clays and Clay Minerals, 30, p. 180 (1982).

- 7.) C.A. Drewien, R.G. Buchheit, "Issues for Conversion Coating of Aluminum Alloys with Hydrotalcite", CORROSION/94. paper no. 622 (Houston, TX: NACE International, 1994).
- 8.) R. B. Mears, L. J. Benson, Ind. & Eng. Chem., 32, p. 1343 (1940).
- 9.) M. Mushiro, K. Shigoka, Met. Fin. Jpn., 23, p. 370 (1972).
- 10.) T. Uchiyama, T. Abe, Jpn Inst. Light Met.32, p. 202 (1982).
- 11.) V.V. Sysoeva, E.D. Artyugina, V.G. Gorodilova E.A. Berkman, Z. Prikladnoi Khim., 58, p. 921 (1985).
- 12.) T. Uchiyama, M. Hasegawa, H. Matsumoto, Met. Fin. Jpn., 37, p. 178 (1986).
- 13.) J. Gui, T.M. Devine, Scripta Met., 21, p. 853 (1987)
- 14.) J. Craig, R.C. Newman, M.R. Jarrett, N.J.H. Holroyd, J. Phys., 48, p. 825 (1987).
- 15.) Y. Isobe, S. Tanaka, M. Masaki, F. Hine, Boshoku Gijutsu, 38, p. 161 (1989).
- 16.) S. Tanaka, Y. Isobe, F. Hine, Boshoku Gijutsu, 39, p. 425 (1990).
- 17.) C.M. Rangel, M.A. Travassos, Corros. Sci., 33, p. 327 (1992).
- 18.) M. Pourbaix, *Atlas of Electrochemical Equilibria in Aqueous Solutions*, p. 389 (Houston, TX, NACE, 1974).
- 19.) N. Fin, H. Dodink, A.E. Yaniv, L. Drori, *Applied Surface Science*, 28, p. 11 (1987).
- 20.) J.S. Solomon, N.T. McDevitt, *Thin Solid Films*, 84, p. 155 (1981).
- 21.) A.V. Pocius, T.H. Wilson, Jr., S.H. Lundquist, S. Sugii, in *Progress in Advanced Materials and Processes: Durability, Reliability and Quality Control*, G. Bartelds, R.J. Schekelmann, Eds., p. 71 (Amsterdam: Elsevier Science Publishers B.V., 1985).
- 22.) T.S. Sun, J.M. Chen, J.D. Venables, *Applications of Surface Science*, 1, p. 202 (1978).
- 23.) R.G. Buchheit, M.D. Bode. G.E. Stoner, *Corrosion*, 50, p. 205 (1994).
- 24.) ZSIM for Windows, Scribner and Associates, Charlottesville, VA.
- 25.) J. Hitzig, K. Juttner, W.J. Lorenz, J. Electrochem. Soc., 133, p. 897 (1986).
26. M.W. Kendig, private communication, 1995.
- 27.) R.G. Buchheit, C.A. Drewien, J.L. Finch, G.E. Stoner, "Non-Chromate Conversion Coatings for Aluminum", CORROSION/94, paper no. 542, (Houston, TX:NACE International, 1994).



1 μm

Figure 1. Scanning transmission electron micrograph of the duplex film formed by reaction of aluminum with an alkaline lithium aluminum salt solution.

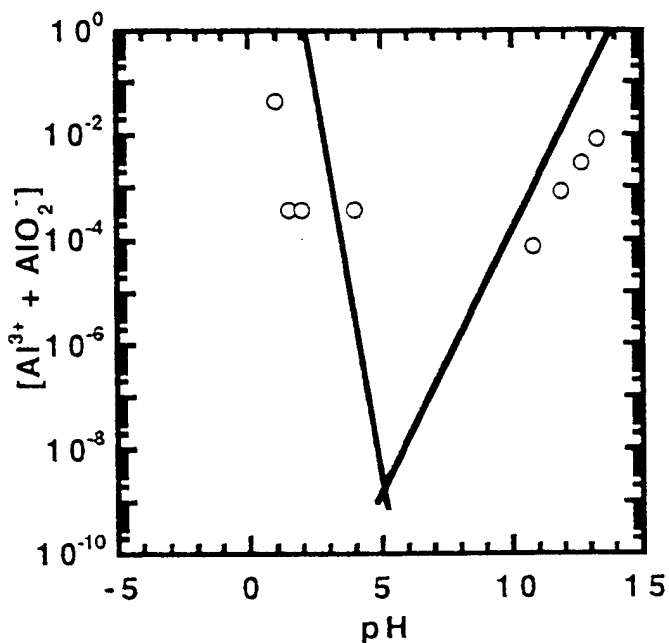


Figure 3. Bayerite and hydrotalcite solubility plotted as a function of solution pH. Bayerite is indicated by the solid lines, hydrotalcite by the data points.

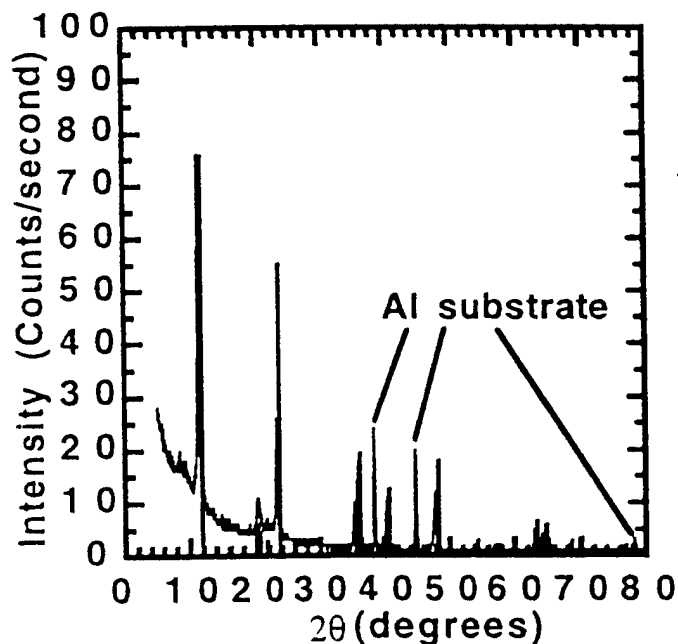


Figure 2. GIXRD pattern from the coated Al surface shown in Figure 1. The dominant compound identified is hydrotalcite. Vertical lines indicate the reference pattern.

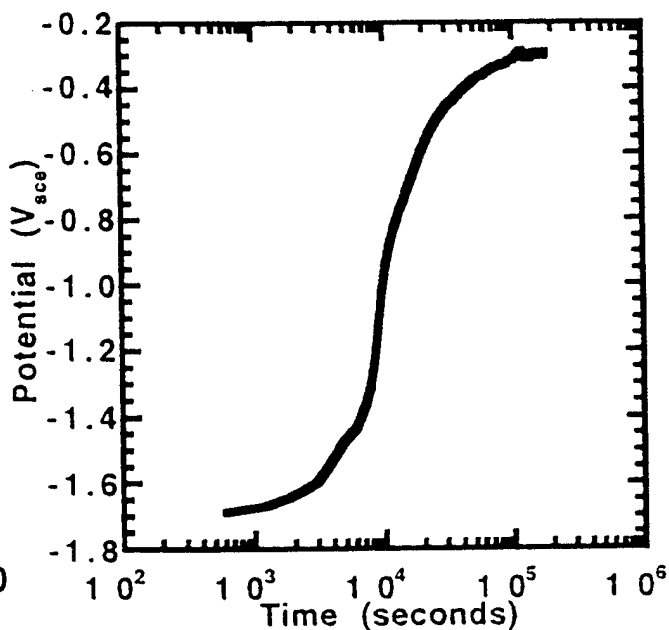


Figure 4. Open circuit potential of 99.999Al in 7.4 g/L Li_2CO_3 plus 200 ppm AlO_2^- pH 11.5 as a function of time.

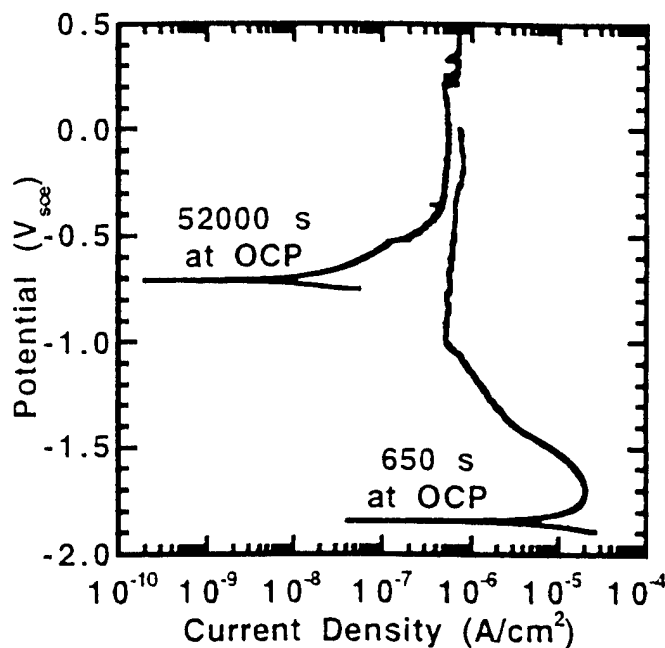
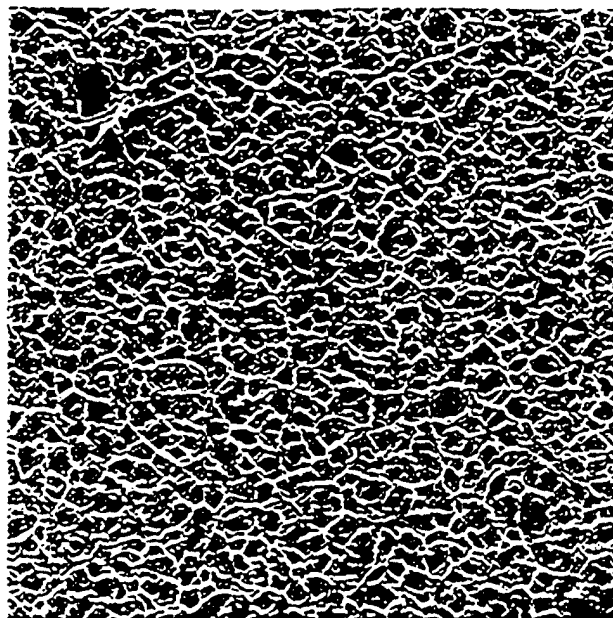
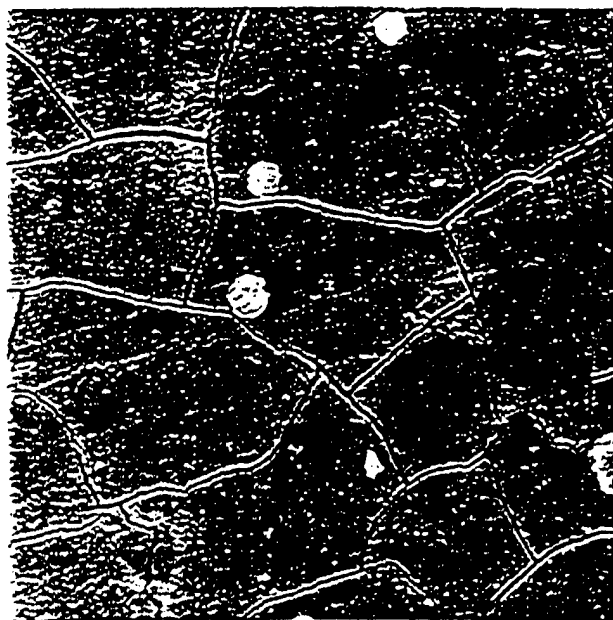


Figure 5. Anodic polarization curves for 99.999 Al in 7.4 g/L Li_2CO_3 plus 200 ppm AlO_2^- after different lengths of exposure time at OCP.



10 μm

Figure 7. Scanning electron micrograph of the coating formed on 2024-T3 using the modified coating process.



10 μm

Figure 6. Scanning electron micrograph of the coating formed on 2024-T3 using the control coating process.

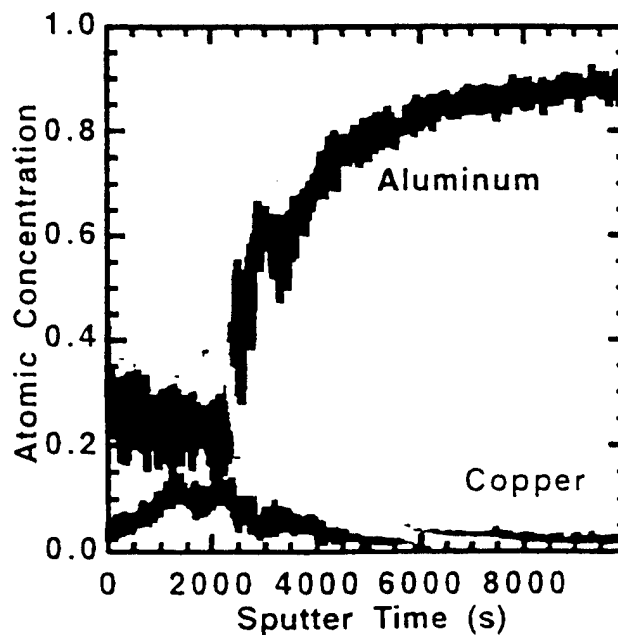


Figure 8. Auger electron spectroscopy sputter depth profiles for Al, Cu and O on 2024-T3 coated using the control process.

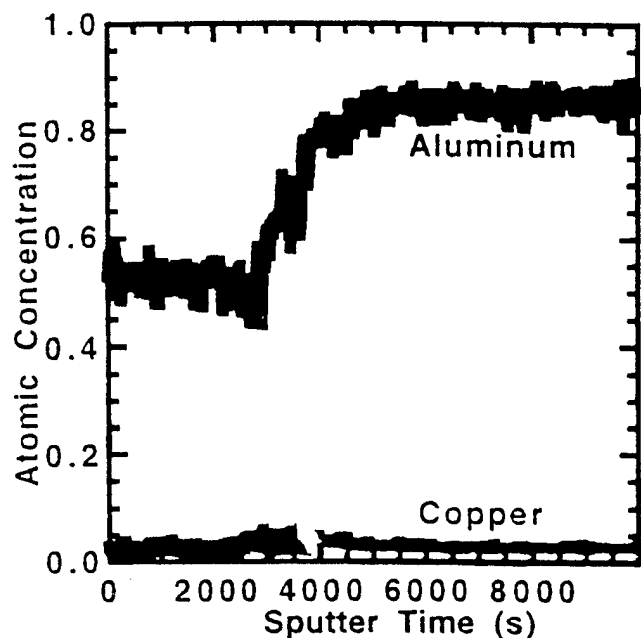
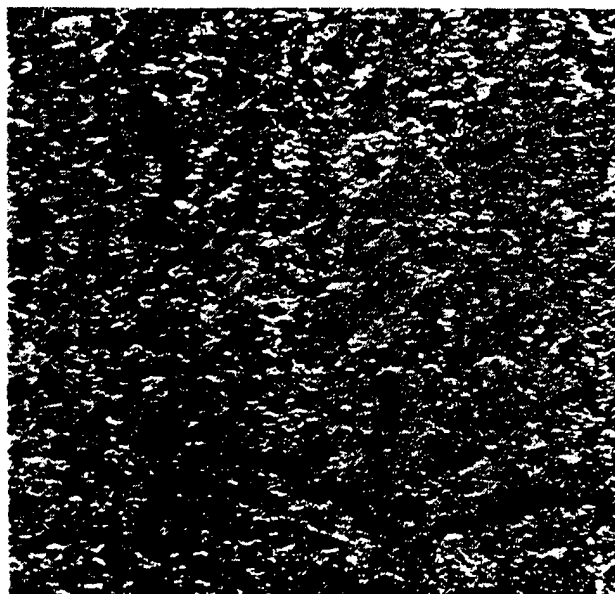
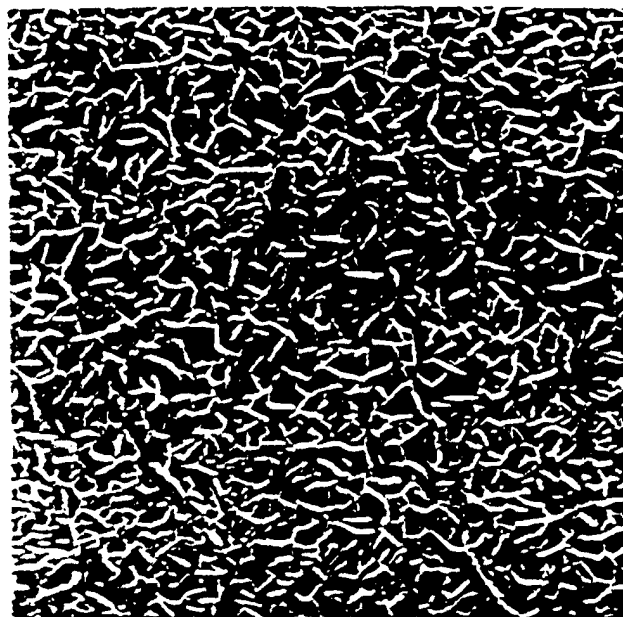


Figure 9. Auger electron spectroscopy sputter depth profiles for Al, Cu and O on 2024-T3 coated using the modified process.



1.0 μm

Figure 11. Scanning electron micrograph of a hydrotalcite coated 6061-T6 surface after exposure to a Ni-Ac solution for 30 minutes.



1.0 μm

Figure 10. Scanning electron micrograph of a hydrotalcite coated 6061-T6 surface after exposure to a Ni-Ac solution for 5 minutes.

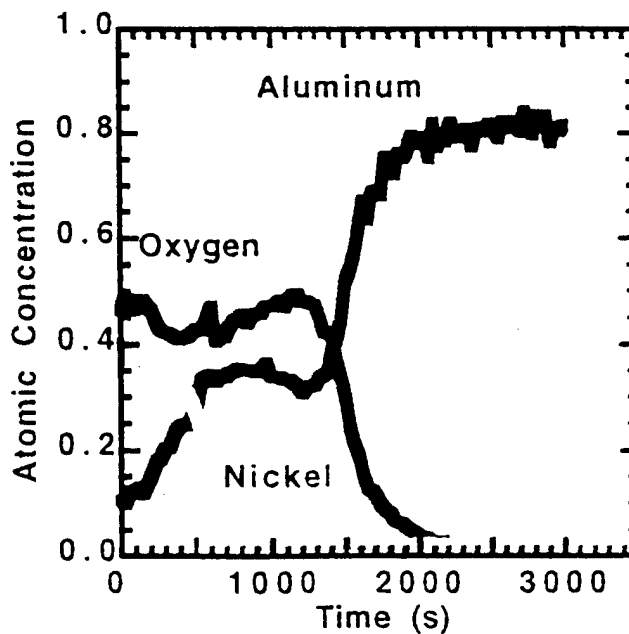


Figure 12. Auger electron spectroscopy sputter depth profiles for Al, O and Ni on 6061-T6 coated and exposed to a Ni-Ac solution for 5 minutes.

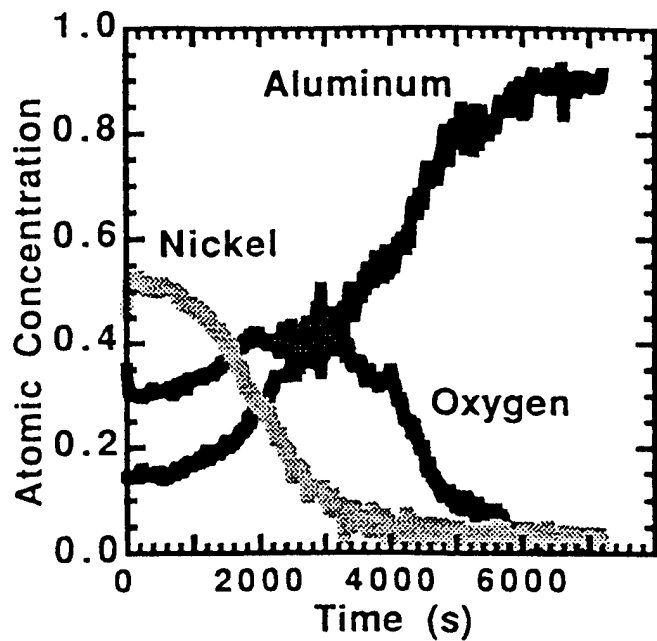


Figure 13. Auger electron spectroscopy sputter depth profiles for Al, O and Ni on 6061-T6 coated and exposed to a Ni-Ac solution for 30 minutes.

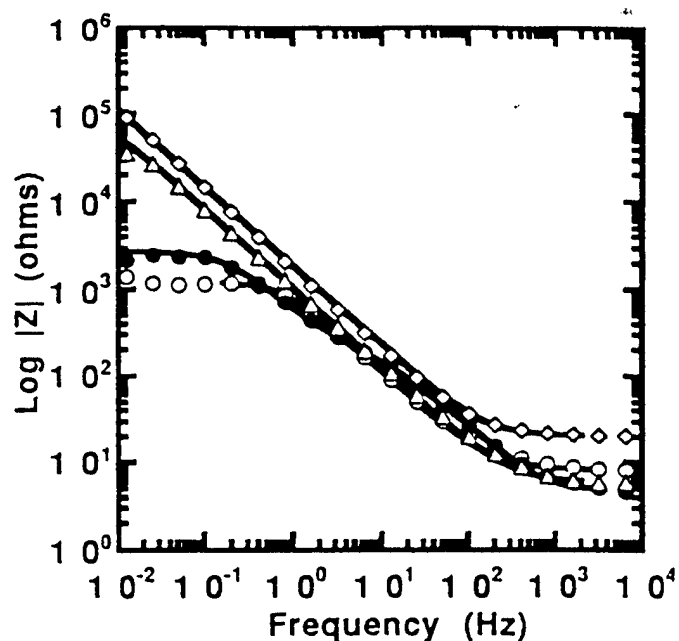


Figure 14. Bode impedance magnitude plots for bare 2024-T3 (o), coated using the original process (•), coated using the modified process (Δ), and coated using the Ce oxide modified process (◊). The symbols represent EIS data and the solid line represent the CNLS fit.

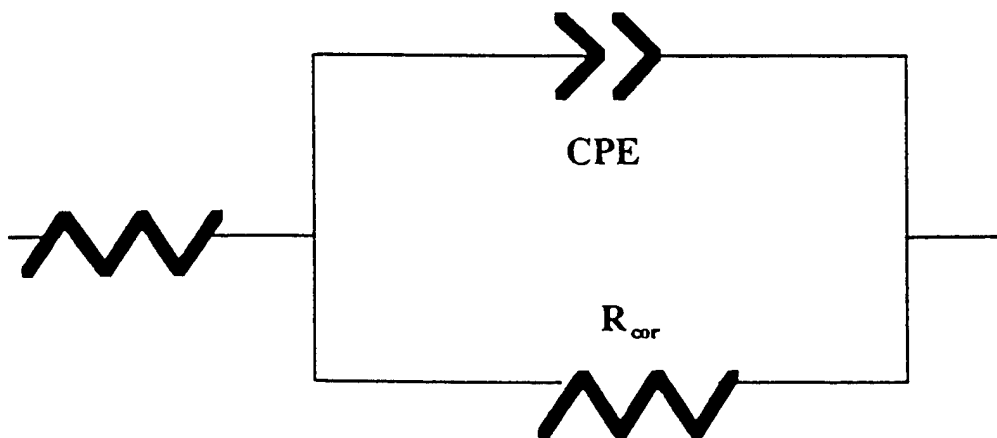


Figure 15. Schematic illustration of the equivalent circuit model used to fit most of the EIS data.

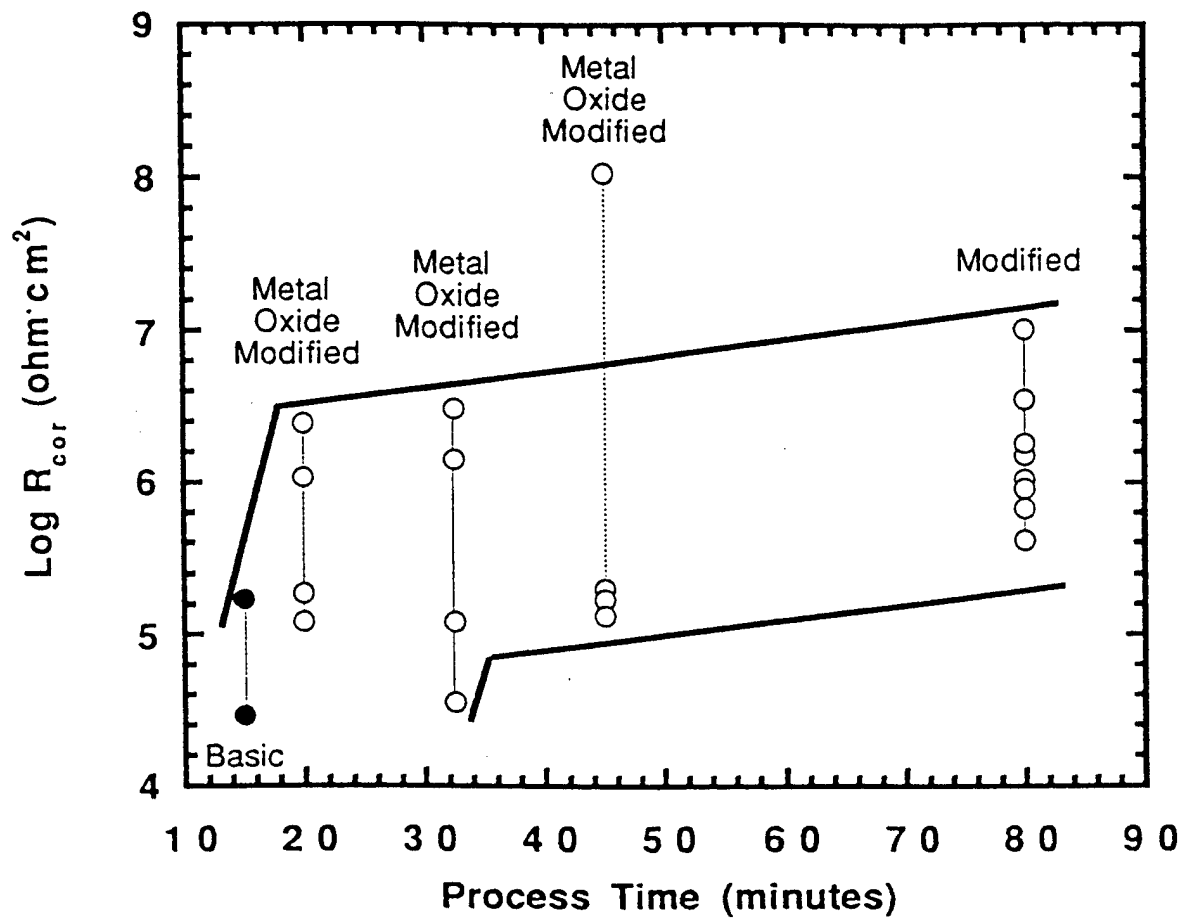


Figure 16. R_{cor} versus total process time for coated 6061-T6. The vertical lines indicate R_{cor} data from related, though not identical, coating processes.

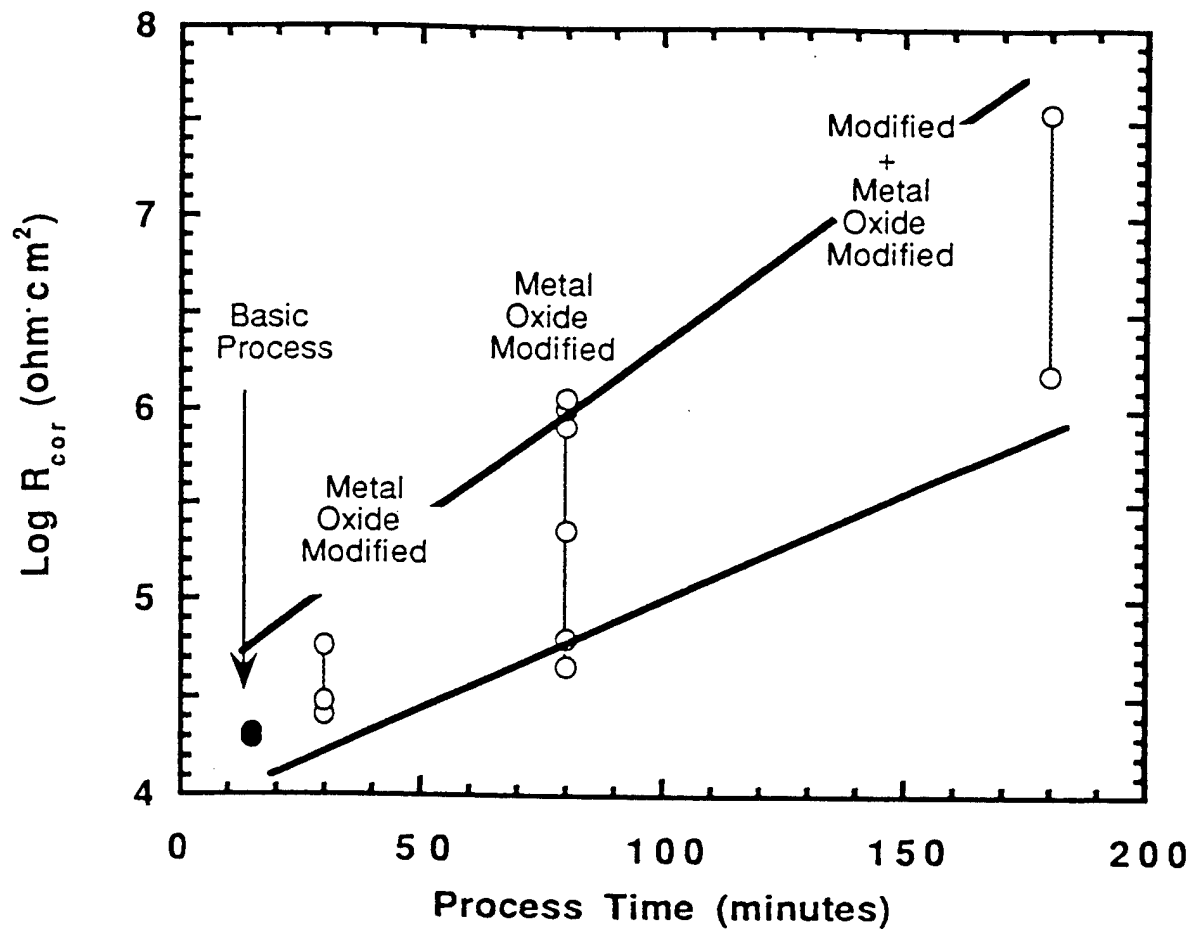


Figure 17. R_{cor} versus total process time for coated 2024-T3. The vertical lines indicate R_{cor} data from related, though not identical, coating processes.

Paper No.
216

CORROSION 98

NON-ELECTROLYTIC FORMATION OF AL-OXIDE SURFACE LAYERS BY REVERSION OF HYDROTALCITE

R.G. Buchheit
Department of Materials Science and Engineering
The Ohio State University
Columbus, OH 43210

M.A. Martinez, L.P. Montes
Materials Aging and Reliability Department
Sandia National Laboratories
Albuquerque, NM 87185

N.P. Cella, S.R. Taylor, G.E. Stoner
Department of Materials Science and Engineering
University of Virginia
Charlottesville, VA 22903

ABSTRACT

Polycrystalline hydrated aluminum oxide coatings with high corrosion resistance have been produced on Al alloys using non-toxic, non-electrolytic methods. These coatings are formed by a two stage process consisting of immersion in an alkaline Li-salt solution to form a hydrotalcite coating followed by immersion in boiling distilled water. Immersion in boiling water transforms the hydrotalcite to hydrated aluminum oxide (bayerite). This process has been termed "reversion". Reversion coatings can be formed in 30 minutes or less and exhibit corrosion resistances near that of anodized coatings. Reversion coating morphology, structure and composition are presented. The corrosion resistance of reversion coatings is compared to the corrosion resistance of coatings produced by chromate conversion and electrolytic anodization.

INTRODUCTION

Anodization is a common means of improving the corrosion resistance, paintability and appearance of aluminum alloys. Generally, anodization involves applying large voltages to a workpiece while it is immersed in an acid solution. Over the course of 30 to 60 minutes, this treatment produces a protective Al oxide coating. Coating thicknesses range from 0.5 to 1.0 mil (13 to 25 μm) depending on anodization time and bath chemistry. The coatings consist of a poorly crystalline inner layer that is an excellent barrier against corrosion, and a porous outer layer that is usually crystalline in nature. These coatings are highly corrosion resistant and provide an excellent base for paints and adhesives.

Copyright

©1998 by NACE International. Requests for permission to publish this manuscript in any form, in part or in whole must be made in writing to NACE International, Conferences Division, P.O. Box 218340, Houston, Texas 77218-8340. The material presented and the views expressed in this paper are solely those of the author(s) and are not necessarily endorsed by the Association. Printed in the U.S.A.

Anodization imparts excellent corrosion resistance to aluminum. However, it is an electrolytic process and is subject to certain processing limitations. The main limitation is in developing a uniform coating on complicated three dimensional parts. This is not always possible because of non-uniformities in the potential (hence current) distributions which affect the rate of film formation.

It has been found that a simple modification to the hydrotalcite coating process¹ generates hydrated aluminum oxide coatings with corrosion resistances approaching that of anodized coatings in electrochemical impedance and salt spray exposure. This process can be completed in times as short as 30 minutes. The process is non-electrolytic and avoids a main limitation associated with anodization.

EXPERIMENTAL PROCEDURES

Materials. Hydrotalcite and reversion coatings were formed on 4 x 5 inch (100 x 125 mm) 6061-T6 (Al-1.0Mg-0.6Si-0.3Cu) and 6063-T6 (Al-0.7Mg-0.4Si) alloy substrates. The 6061-T6 samples were prepared from 0.080 inch (2.0 mm) thick sheet stock. The 6063-T6 samples were cut in 0.125 inch (3.0 mm) thicknesses from extrusions. Alloy 6061-T6 is a medium strength, general purpose Al alloy available in a variety of commercial forms. Alloy 6063-T6 is almost always supplied in extruded form and has a composition very similar to that of 6061. It is mainly used in architectural applications.

Coatings. In preparation for coating, sample substrates were degreased using a detergent to remove bulk organic contamination. Samples were then immersed in an alkaline sodium silicate-sodium carbonate solution to remove molecular organic compounds. Next, samples were deoxidized by immersion in a commercial deoxidizing solution consisting of nitric acid and sodium bromate.

Coatings were formed non-electrolytically in a two stage, simple-immersion process. Processing parameter ranges are given in Table 1. A wide range of processing parameters have been examined in the course of this study. The table lists the range used for that variable and a value that is typical for producing coatings with high corrosion resistance.

Corrosion Testing. Coating corrosion resistance was tested by salt spray exposure as described in ASTM B117². During exposure, samples were periodically examined for evidence of pitting corrosion damage.

Corrosion resistance was also measured using electrochemical impedance spectroscopy (EIS). Coated panels were mounted in gasketed electrochemical test cells designed to expose well-calibrated surface areas of 24 or 32 cm². The test electrolyte was naturally aerated 0.5 M NaCl. This cell also contained either Pt or Ni counter electrode and a saturated calomel reference electrode (SCE) in a Luggin tube. After 24±1 h exposure of the panel in this apparatus, the electrochemical impedance across the surface of the panel was measured at the open circuit potential. The impedance measurement was made as a function of frequency between 10 kHz and 10 mHz using a sinusoidal voltage modulation not in excess of 10 mV. At least seven points per decade frequency were collected. All measurements were made under ambient laboratory conditions (23±3°C). The experiments were conducted using a PAR 273 potentiostat with a Solartron 1255 frequency response analyzer. Typically, two impedance spectra were collected from separate locations on each panel.

Electron microscopy and x-ray diffraction. The morphology of sample surfaces was examined using scanning electron microscopy (SEM) carried out on an Amray 1645 scanning electron microscope. Grazing incidence angle X-ray diffraction (GIXRD) was used to identify compounds present in the coatings formed during exposure. Samples were examined using a Siemens D500 diffractometer at a

grazing incidence angle of 4 degrees. At this angle, the target sampling depth was approximately 1.0 micrometer. Auger electron spectroscopy (AES) and ion etching were used to generate sputter depth composition profiles for elements of interest. AES was conducted using a Physical Electronics PHI 660 scanning auger microprobe. Sputtering was conducted using a rastered 3 kV Xe^+ ion beam. Individual element signals were corrected using the appropriate sensitivity factors to generate semi-quantitative composition versus depth profiles.

RESULTS

Freshly formed hydrotalcite coatings. Prior studies have shown that aluminum alloys exposed to alkaline Li-salt solutions passivate due to the formation of a polycrystalline coating¹. A scanning-transmission electron micrograph shows structure of this coating in cross section in Figure 1. The coating exhibits a duplex structure which consists of a porous, crystalline outer layer and a compact, non-crystalline inner layer. This duplex structure is characteristic of the reaction of Al with water at temperatures between 40° and 100°C. The coating shown was formed on 1100 Al (Al-1.0(Fe,Cu,Si)), however duplex coatings form on all alloys. Grazing incidence x-ray diffraction of the coating indicates that outer portions of the coating are porous and consist of hydrotalcite $\text{Li}_2[\text{Al}_2(\text{OH})_6]_2\text{CO}_3\cdot 3\text{H}_2\text{O}$ crystallites. The inner layer is not crystalline, but appears to consist of a lithiated aluminum oxide hydrate. Normally, the Al- H_2O reaction produces hydrated Al oxide films in reaction times on the order of tens of hours under simple-immersion conditions. The coating shown in Figure 1 forms a 1.5 μm thick layer in 15 minutes on Al, Al-Mg, and Al-Mg-Si alloys.

The coating shown in Figure 1 offers considerable corrosion resistance during exposure to salt spray testing and during immersion in aerated chloride solutions. Such coatings will resist pitting after 168 hours of ASTM B117² salt spray exposure and exhibit coating impedances of 1 to $5 \times 10^5 \Omega\text{-cm}^2$ after 24 hours of exposure to aerated 0.5 M NaCl solution. The coating also makes aluminum alloy surface paintable³.

Reversion coatings. When freshly formed hydrotalcite coatings are exposed to boiling distilled water, significant transformations occur. Figure 2 shows the morphology of a freshly formed hydrotalcite coating that was subjected to boiling water for 15 minutes. The blade-like crystallites of the hydrotalcite coating are replaced by trigonal somatoids. The somatoids form a compact layer on the alloy surface. There are no obvious voids or pores that extend into the coating as there are with the hydrotalcite. On a qualitative basis, this coating is much harder than the hydrotalcite precursor. The surfaces are much more resistant to scuffing and abrasion damage. This transformation has been termed "reversion".

X-ray diffraction (XRD) shows that boiling water exposure transforms the coating from hydrotalcite to bayerite. Figure 3 shows XRD patterns for a hydrotalcite coating and a reversion coating. A comparison of the data to reference patterns for hydrotalcite and bayerite clearly shows hydrotalcite in the coating formed by exposure to alkaline Li-salt solutions, and bayerite after the hydrotalcite coating is exposed to boiling water.

Reversion removes the CO_3^{2-} from the hydrotalcite coating. Figure 4 shows composition depth profiles for a hydrotalcite coating and a reversion coating determined by Auger electron spectroscopy sputter depth profiling. Analysis was conducted for Al, O, and C. Carbon from carbonate is detected through the entire thickness of the hydrotalcite coating as shown in Fig. 4a. However no C is detected in the reversion coating indicating that it has been extracted. Reversion probably removes Li^+ from the coating, but signal detection for Li was judged to be too inaccurate for reliable analysis. A greater length of

time is required to sputter through the coating for the reversion coating compared to the conversion coating. This indicates that the coating is either thicker (if the sputter rates for the two coatings are the same, or of the sputter rate for the reversion coating is greater), or more resistant to sputtering (if the sputter rate for the reversion coating is lower).

Hydrotalcite reversion by exposure to boiling water has been conducted for times ranging from 5 to 30 minutes. Based on SEM, XRD, and corrosion testing, reversion appears to be complete within 15 minutes, but the kinetics of the process are not very well characterized. It is not known if the morphology shown in Figure 2c represents a terminal morphology, structure or composition. However, it does not appear that there is any loss in performance (corrosion resistance) associated with partial or incomplete reversion. In practical terms: the corrosion resistance is improved by any length of exposure to boiling water and there is no performance penalty for incomplete reversion--at least for corrosion resistance.

Corrosion resistance. Corrosion resistance of reverted samples has been measured using electrochemical impedance spectroscopy (EIS) and salt spray testing. Figure 5 shows representative Bode magnitude and phase angle plots for bare, hydrotalcite coated and reversion coated 6061-T6 samples exposed to aerated 0.5 M NaCl solution for 24 hours at 23°C. The bare sample exhibits a DC limit of about 2000 ohm-cm² and a low frequency relaxation that is commonly observed with pitting. Inspection of the sample surface after testing confirmed the presence of large pits. The hydrotalcite coated sample exhibited an increase in the DC limit of about one order of magnitude, but still showed evidence of a low frequency relaxation due to pitting. Visual inspection after testing showed that a lesser degree of pitting had occurred. The reversion coated sample exhibited a nearly capacitive response indicating that the Al oxide film resisted any significant pitting. No pits were visible on this sample after exposure.

The corrosion resistance of 6061-T6 and 6063-T6 both coated and uncoated has been found to be nearly identical and it is reasonable to consider their behavior to be identical. EIS data from bare and coated samples has been analyzed by equivalent circuit modeling. The model used to fit consists of a solution resistance in series with a parallel combination of a resistor, representing coating resistance, and a capacitor (with some frequency dispersion), representing the coating reactance. Details of this model have been presented elsewhere⁴. Typically, the coating resistance, R_c , determined in this analysis can be used as a figure of merit to judge performance of the coating. Coating resistances ranging from 5×10^5 to 10^8 ohm-cm² have been measured for reversion coated 6061-T6 and 6063-T6 substrates.

For comparison, Table 2 also gives R_c values for bare alloys and for coatings prepared using other common surface treatments. R_c values determined by the same test for chromate conversion coated 6061-T6 range from 5×10^5 ohm-cm² to 4×10^6 ohm-cm². Sulfuric acid anodized coatings on 6061-T6 are so corrosion resistant that R_c cannot be determined reliably by this EIS protocol⁵. Nevertheless, R_c for anodized coatings is certainly not lower than 10^8 ohm-cm², and Table 2 data show that reversion coatings exhibit coating resistance values that are as high as the best chromate conversion coatings and approach the corrosion resistance of anodized coatings.

In salt spray testing, reversion coatings on both 6061-T6 and 6063-T6 regularly pass 336 hours of salt spray exposure with no evidence of corrosion whatsoever. To date, reversion coatings on 6063-T6 have survived 1500 hours of salt spray exposure without evidence of corrosion. This level of performance is equivalent to the performance of anodized coatings.

SUMMARY

A simple, non-electrolytic process has been devised to form hydrated Al-oxide coatings with high corrosion resistance on aluminum. This process, called "reversion", is a derivative of the hydrotalcite coating process. Coatings produced by this process are comprised primarily of a compact mass of bayerite crystals. In EIS corrosion testing, the coating corrosion resistance of reversion coated 6061-T6 approaches that for anodized coatings. To date, reversion coated samples have withstood 1500 hours of salt spray exposure without evidence of corrosion.

ACKNOWLEDGMENTS

This work was supported by a grant from the Defense Advanced Research Projects Agency and Sandia National Laboratories. Sandia is a multiprogram laboratory operated by Sandia Corporation, a Lockheed Martin Company, for the United States Department of Energy under contract DE-AC04-94AL85000.

REFERENCES

- 1) R.G. Buchheit, M.D. Bode, G.E. Stoner, Corrosion, 50 (1994): p. 205.
- 2) ASTM B117, "Standard Test Method of Salt Spray (Fog) Testing", Annual Book of ASTM Standards, ASTM, Philadelphia, PA, 1993.
- 3) R.G. Buchheit, C.A. Drewien, J.L. Finch, CORROSION/94, Paper No. 94542 (NACE, Houston, TX: 1994).
- 4) R.G. Buchheit, M. Cunningham, H. Jensen, M.W. Kendig, M.A. Martinez, Corrosion, 54 (1998): in press.
- 5) F. Mansfeld, M.W. Kendig, Corrosion, 41(1985): p. 490.

Table 1. Processing parameters for the coatings formed in this study.

Process Variable	Range	Typical
Stage I		
Lithium salt	Li_2CO_3 or LiNO_3	---
Li salt concentration (M)	0.1 to 0.9	0.5
Temperature ($^{\circ}\text{C}$)	55 - 92	92
pH	11 - 13	11.5
AlO_2^- (ppm)	20 - 400	200
Time	5 - 30	15
Stage II		
Time in Boiling distilled H_2O	5 - 30	15

Table 2. Summary of R_c values for various surface treatments determined from corrosion testing by EIS.

Surface Treatment	R_c (ohm-cm ²)
Bare	$10^3 - 10^4$
Hydrotalcite	$10^4 - 5 \times 10^5$
Reversion	$10^6 - 10^8$
Chromate Conversion	$2 \times 10^5 - 4 \times 10^6$
Sulfuric Acid Anodize	$>10^8$



Figure 1. Scanning transmission electron micrograph of a hydrotalcite coating formed on 1100 (Al-1.0 Fe, Cu, Si) Al showing its duplex structure.

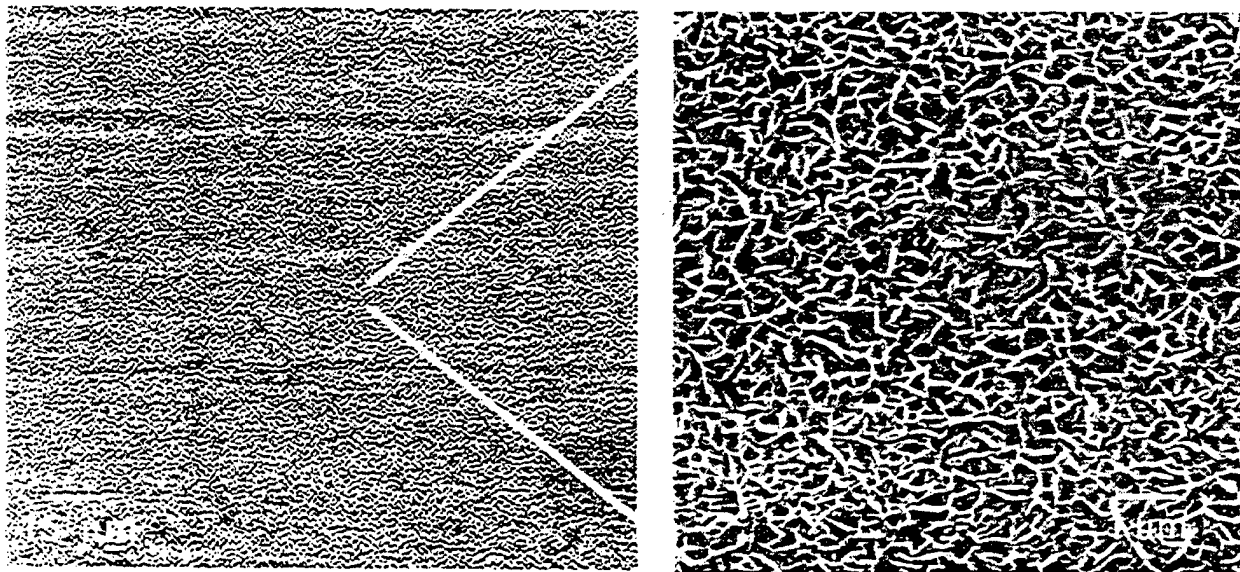


Figure 2a. Scanning electron micrographs showing the characteristic morphology of hydrotalcite coatings. This coating was formed on 6061-T6 in accordance with the general methods described in Table 1 (not including exposure to boiling water).

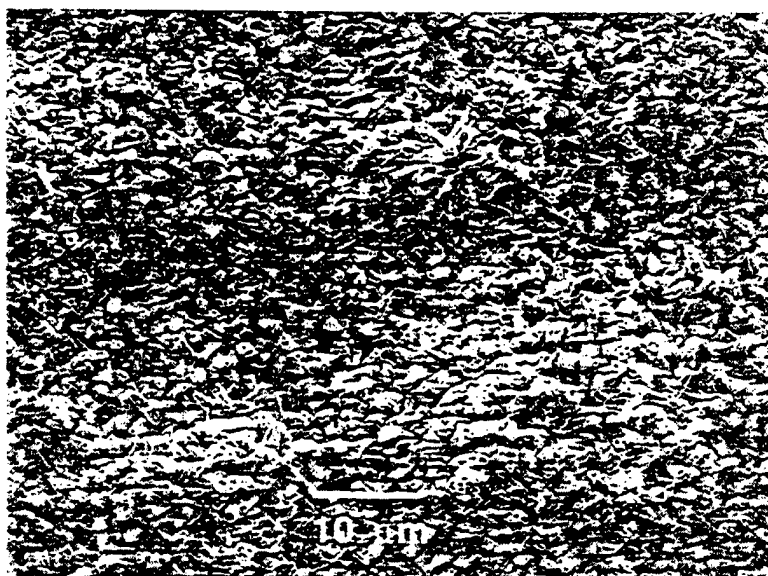


Figure 2b. Scanning electron micrograph showing the morphology of a reversion coating on 6061-T6.

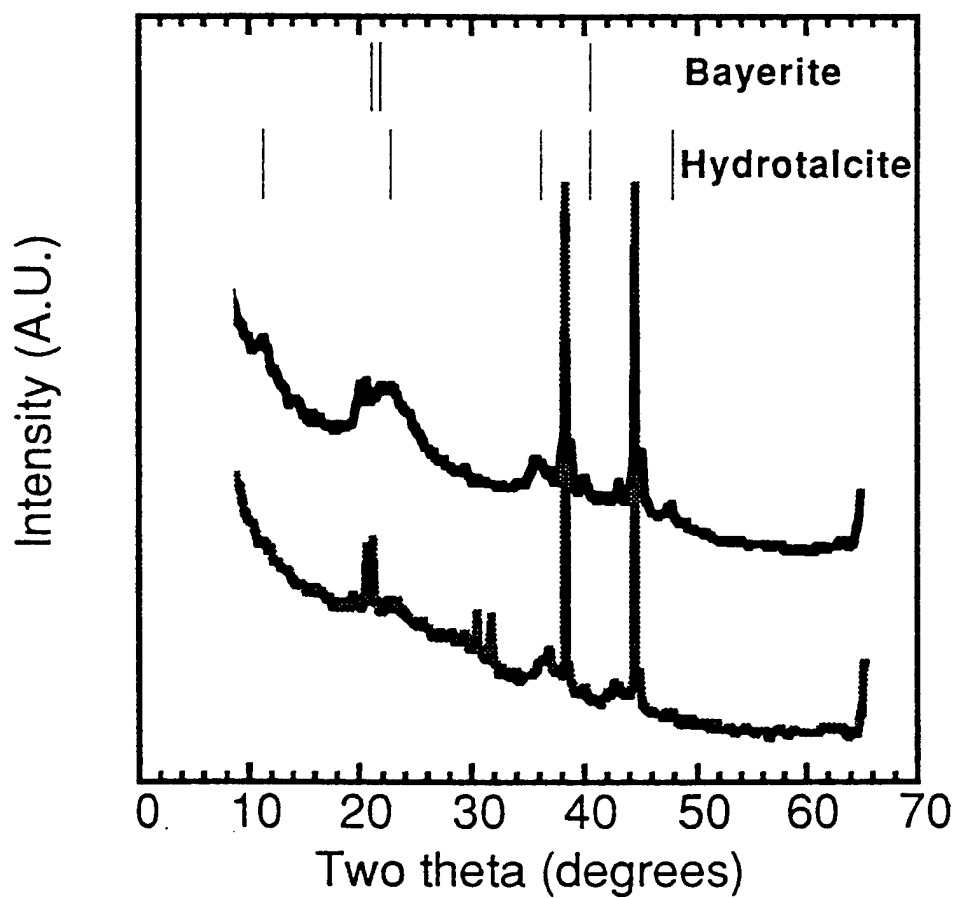


Figure 3. Grazing incidence angle x-ray diffraction patterns from coatings like that shown in Figs. 2a (upper pattern) and 2b (lower pattern). Positions for strong x-ray reflections for bayerite and hydrotalcite are given for reference.

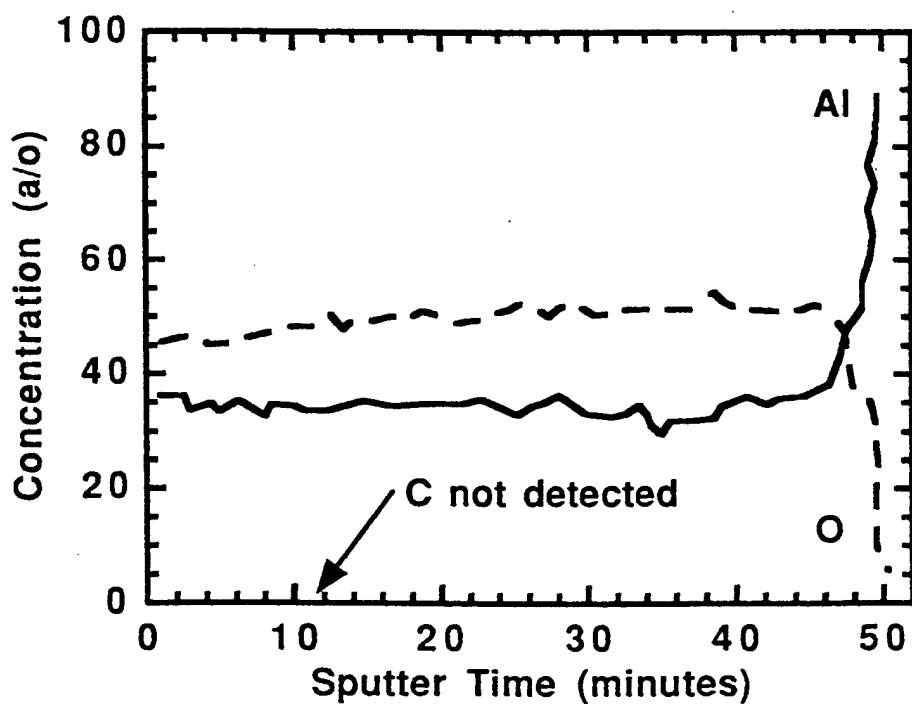
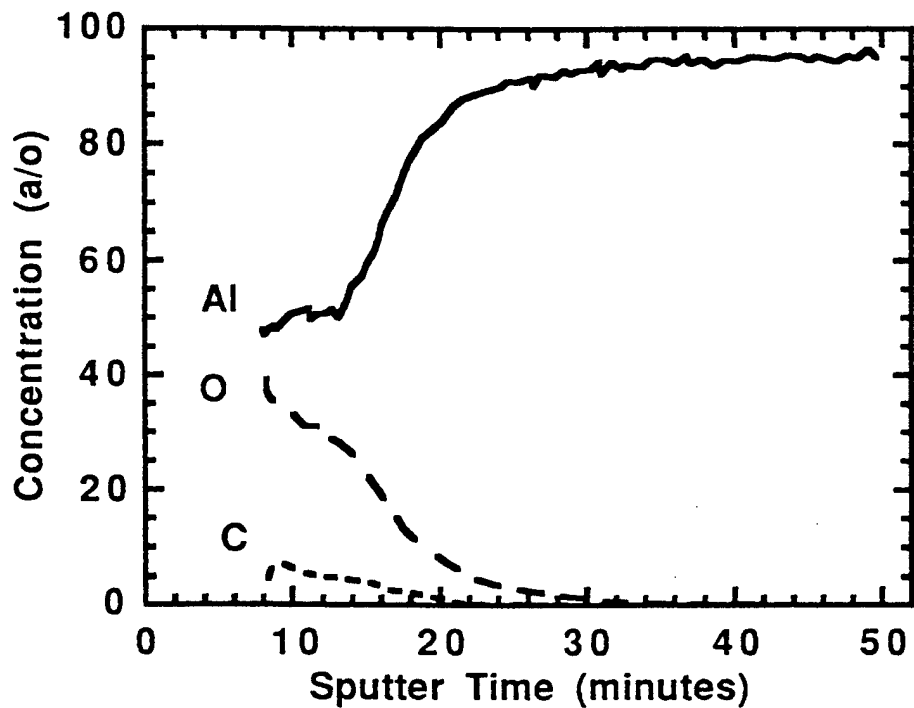


Figure 4. Auger electron spectroscopy sputter depth profiles for coated 6061-T6. The depth profile for a hydrotalcite coated sample reveals the presence of carbon from carbonate in the hydrotalcite compound (upper). No carbon is detected in the depth profile for the reversion coated sample (lower).

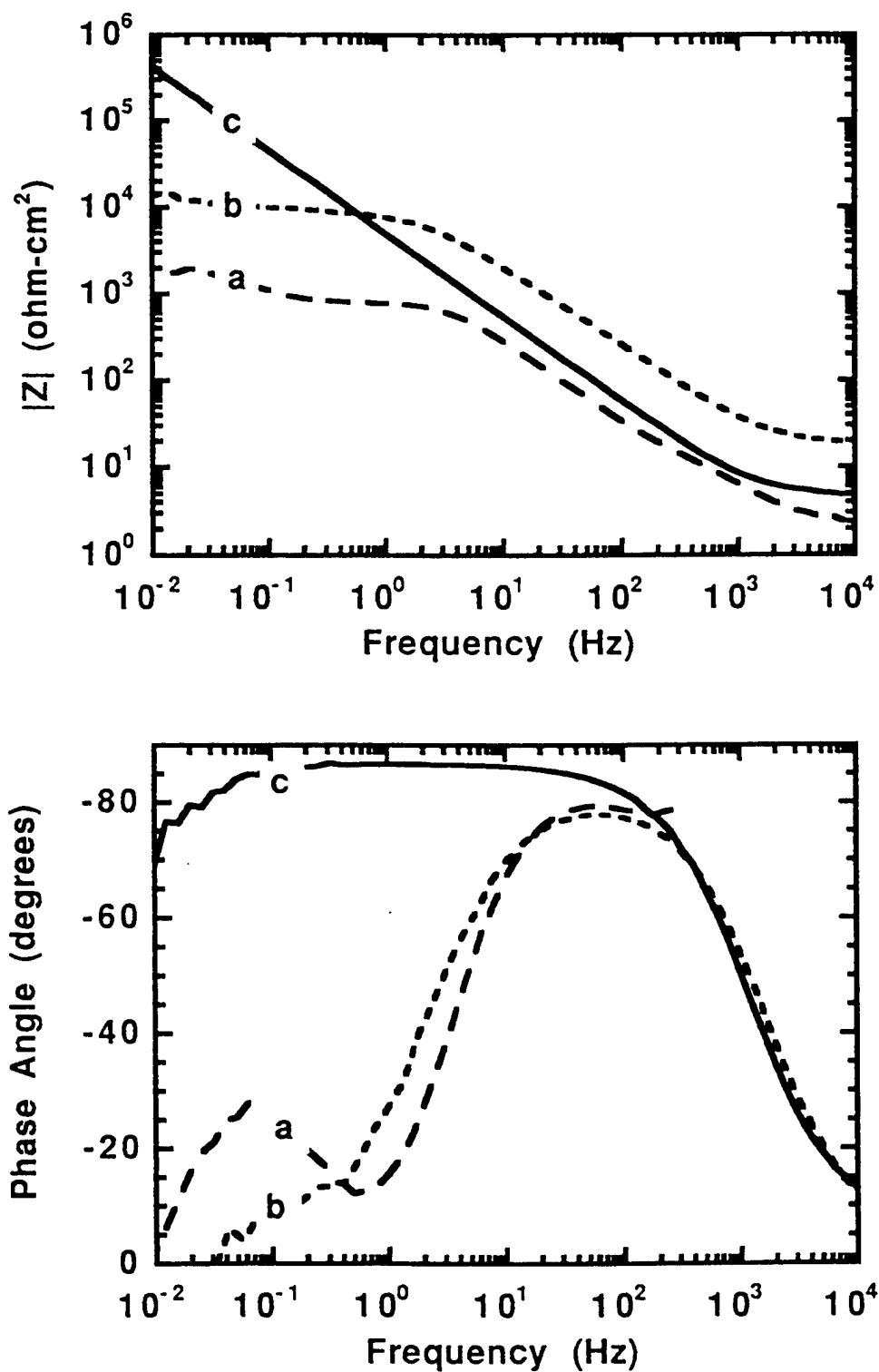


Figure 5. EIS data from 6061-T6 samples after exposure to aerated 0.5 M NaCl solution for 24 hours. The upper plot shows the magnitude of the impedance, the lower plot shows the phase angle as a function of measurement frequency. Curve (a) uncoated, (b) hydrotalcite coated, (c) reversion coated.

US PATENT & TRADEMARK OFFICE

PATENT FULL TEXT AND IMAGE DATABASE

[Home](#)[Boolean](#)[Manual](#)[Number](#)[Help](#)[\[HIT_LIST\]](#)[Bottom](#)[View Shopping Cart](#)[\[Add to Shopping Cart\]](#)[Images](#)

(1 of 1)

United States Patent

5,756,218

Buchheit, et al.

May 26, 1998

Corrosion protective coating for metallic materials

Abstract

Corrosion protective coatings for metallic materials, particularly aluminum and aluminum alloys, produced with simple, low-cost equipment and materials other than toxic metals or metal salts, or metal cyanides. The metallic material is cleaned, degreased, and deoxidized, the surface is converted to a substantially alkaline condition, and the surface is chemically sealed with inorganic metal compounds.

Inventors: **Buchheit; Rudolph G.** (Albuquerque, NM); **Martinez; Michael A.** (Albuquerque, NM)Assignee: **Sandia Corporation** (Albuquerque, NM)Appl. No.: **781784**Filed: **January 9, 1997**

Current U.S. Class:

428/469; 427/327; 427/328; 427/383.7; 427/419.8; 427/421; 427/429; 427/435; 428/457

Intern'l Class:

B32B 015/00; B05D 003/10; B05D 001/02; B05D 001/38

Field of Search:

427/299,327,328,329,320,321,383.7,436,438,435,429,421,419.8 428/469,457

References Cited [Referenced By]

U.S. Patent Documents

3864230	Feb., 1975	Springer et al.	204/181.
3964936	Jun., 1976	Das	148/6.
3985585	Oct., 1976	Tuttle et al.	148/6.
4004951	Jan., 1977	Dorey, Jr.	428/470.
4054466	Oct., 1977	King et al.	148/247.
4063969	Dec., 1977	Howell, Jr.	148/274.
5266356	Nov., 1993	Buchheit, Jr. et al.	427/372.
5346560	Sep., 1994	Mournet et al.	148/217.
5401337	Mar., 1995	Carlsn et al.	148/257.
5551994	Sep., 1996	Schriever	148/273.

Other References

A. Csanady, T. Turmezey, I. Imre-Baan, A. Briger, D. Marton, L. Fodor and L. Vitalis, The Relationship Between the Corrosion Resistance and Impurity Content of Aluminum Oxide Layers, Corrosion Science, vol. 24, No. 3, pp. 237-248, 1984.

Primary Examiner: Beck; Shrive

Assistant Examiner: Barr; Michael

Attorney, Agent or Firm: Klavetter; Elmer A.

Government Interests

This invention was made with Government support under Contract No. DE-AC04-94AL85000 awarded by the United States Department of Energy. The Government has certain rights in the invention.

Claims

What is claimed is:

1. A process for the corrosion protection of the surface of a metallic material comprising:

cleaning the metal surface;

- forming a coating by chemically treating the metal surface with a first alkaline aqueous solution so that the surface and resulting coating are in a substantially alkaline condition; and sealing the coating without an intermediate rinsing step by contacting the coating with an aqueous solution consisting essentially of at least one soluble metal salt to cause chemical deposition of the at least one soluble metal salt on the coating.
2. The process of claim 1 wherein cleaning comprises removing bulk and molecular organic contaminants, deoxidizing the surface by immersion in an acid solution, and rinsing in water.
 3. The process of claim 1 wherein the metallic material is selected from the group consisting of aluminum, aluminum alloys, magnesium, and magnesium alloys.
 4. The process of claim 1 wherein the substantially alkaline condition results from the presence of a solid film containing hydrotalcite compounds.
 5. The process of claim 1 wherein the substantially alkaline condition results from the presence of a liquid, alkaline film.
 6. The process of claim 4 wherein the step of forming a coating by chemically treating the metal surface so that it is in a substantially alkaline condition comprises immersing the metal surface in an alkaline aqueous solution of a soluble metal compound or compounds for about 6-180 min.
 7. The process of claim 4 wherein the step of forming a coating by chemically treating the metal surface so that it is in a substantially alkaline condition comprises spraying an alkaline aqueous solution of a soluble metal compound or compounds onto the surface for about 1-30 min.
 8. The process of claim 4 wherein the step of forming a coating by chemically treating the metal surface so that it is in a substantially alkaline condition comprises brushing an alkaline aqueous solution of a soluble metal compound or compounds onto the surface for about 1-15 min.
 9. The process of claim 4 wherein the step of forming a coating by chemically treating the metal surface so that it is in a substantially alkaline condition comprises rolling an alkaline aqueous solution of a soluble metal compound or compounds onto the surface for about 1-5 min.
 10. The process of claim 5 wherein the step of forming a coating by chemically treating the metal surface so that it is in a substantially alkaline condition comprises immersing the metal surface in an alkaline aqueous solution of a soluble metal compound or compounds for about 60-180 min.
 11. The process of claim 5 wherein the step of forming a coating by chemically treating the metal surface so that it is in a substantially alkaline condition comprises spraying an alkaline aqueous solution of a soluble metal compound or compounds onto the surface for about 1-30 min.
 12. The process of claim 5 wherein the step of forming a coating by chemically treating the metal surface so that it is in a substantially alkaline condition comprises brushing an alkaline aqueous solution of a soluble metal compound or compounds onto the surface for about 1-15 min.
 13. The process of claim 5 wherein the step of forming a coating by chemically treating the metal surface so that it is in a substantially alkaline condition comprises rolling an alkaline aqueous solution of a soluble metal compound or compounds onto the surface for about 1-5 min.
 14. The process of claim 1 wherein the soluble metal salt comprises a compound containing one or more cations selected from the group consisting of Al, Mg, Ca, Sr, Ti, Mo, Ce, Pr, Nd, Sm, Eu, Gd, Tb, Dy, Ho, Er, Tm, Yb, Lu, Mn, Fe, Co, Ni, and Bi.
 15. The process of claim 1 wherein the surface is unrinsed and wet before sealing.
 16. The process of claim 1 wherein the surface is unrinsed and dried before sealing.
 17. The process of claim 1 wherein the step of sealing the coating by contacting the coating in an aqueous solution comprises immersing the coating for about 0.1-15 min, the temperature of the solution is about 20.degree.-100.degree. C., and the surface is permitted to dry without rinsing.
 18. The process of claim 1 wherein the step of sealing the coating by contacting the coating in an aqueous solution comprises spraying for about 5-60 sec, the temperature of the solution is about 20.degree.-100.degree. C., and the surface is permitted to dry without rinsing.
 19. The process of claim 1 wherein the step of sealing the coating by contacting the coating in an aqueous solution comprises brushing for about 1-5 min, the temperature of the solution is about 20.degree.-100.degree. C., and the surface is permitted to dry without rinsing.
 20. The process of claim 1 wherein the step of sealing the coating by contacting the coating in an aqueous solution comprises rolling for about 5-300 sec, the temperature of the solution is about 20.degree.-100.degree. C., and the surface is permitted to dry without rinsing.
 21. The process of claim 1 wherein the step of sealing the coating by contacting the coating in an aqueous solution comprises immersing the coating for about 0.1-15 min, the temperature of the solution is about 20.degree.-100.degree. C., and the surface is rinsed with deionized water.
 22. The process of claim 1 wherein the step of sealing the coating by contacting the coating in an aqueous solution comprises spraying for about 5-60 sec, the temperature of the solution is about 20.degree.-100.degree. C., and the surface is rinsed with deionized water.
 23. The process of claim 1 wherein the step of sealing the coating by contacting the coating in an aqueous solution comprises brushing for about 1-5 min, the temperature of the solution is about 20.degree.-100.degree. C., and the surface is rinsed with deionized water.
 24. The process of claim 1 wherein the step of sealing the coating by contacting the coating in an aqueous solution comprises rolling for about 5-300 sec, the temperature of the solution is about 20.degree.-100.degree. C., and the surface is rinsed with deionized water.
 25. The process of claim 14 comprising the additional step of adding an oxidizing agent to the aqueous solution in sufficient quantity to oxidize solution cations to a higher valence state.
 26. The process of claim 25 wherein the oxidizing agent is hydrogen peroxide at a concentration of 5000 ppm by volume in the aqueous solution.
 27. The process of claim 1 further comprising the step of heat treating the metallic material at about 30.degree.-200.degree. C. for about 5-240 min between the steps of chemically treating and sealing the surface.
 28. The process of claim 1 further comprising the step of heat treating the metallic material at about 30.degree.-200.degree. C. for about 5-240 min after the step of sealing the surface.
 29. The product produced by the process of claim 1.
 30. The product produced by the process of claim 25.
 31. The product produced by the process of claim 27.
 32. The product produced by the process of claim 28.
 33. A process for the corrosion protection of the surface of a metallic material comprising:
cleaning the metal surface;

forming a coating by contacting the metal surface with an alkaline aqueous solution containing a soluble lithium salt so that the surface and resulting coating are in a substantially alkaline condition; and

sealing the coating without an intermediate rinsing step by contacting the coating with an aqueous solution consisting essentially of at least one soluble metal salt, wherein said metal salt comprises a metal salt containing one or more cations selected from the group consisting of Al, Mg, Ca, Sr, Ti, Mo, Ce, Pr, Nd, Sm, Eu, Gd, Tb, Dy, Ho, Er, Tm, Yb, Lu, Mn, Fe, Co, Ni, and Bi.

Description

BACKGROUND OF THE INVENTION

This invention relates generally to the application to the surfaces of metals and alloys, particularly aluminum and aluminum alloys, coatings with desirable properties using simple, low-cost equipment and materials other than toxic metals, metal salts, or metal cyanides.

Metallic surfaces are often protected from corrosion by the application of a barrier coating. A first type of barrier coating is anodic oxides usually formed by an electrochemical means (anodizing) while the metal is immersed in an inorganic acid such as H.sub.2 SO.sub.4 or H.sub.3 PO.sub.4. Anodic oxides have a wide range of thicknesses and porosities. Porous coatings can be sealed in steam, boiling water, or various salt solutions. A second type is ceramics, usually special cements applied to a metal to prevent corrosion. A common example of a ceramic coating is porcelain enamel. A third type is molecular barriers formed by the addition of organic molecules to solution. Effective inhibitors are transported to the metal-solution interface and have a reactive group attached to a hydrocarbon. The reactive group interacts with the metal surface while the hydrocarbon group is exposed to the environment. As the molecules form the molecular barrier coating, corrosion reactions are slowed. A fourth type is organic material generally intended to prevent interaction of an aggressive environment with the metal surface. Organic coatings are the most widely used barrier coatings for metals, and paint is a typical example. A fifth type is the conversion coating made by converting some of the base metal into a protective oxide. Chromate and phosphate coatings are the two most common kinds of conversion coatings.

Chromate and phosphate conversion coatings can be formed by chemical and electrochemical treatment of a metal or alloy material during immersion in a solution containing hexavalent chromium (Cr.sup.+6), phosphorous as a phosphate anion, and usually other components. Literally hundreds of subtly different, proprietary chromate-conversion coating formulas exist. For aluminum and aluminum alloys, the primary active ingredient in the bath is usually a chromate, dichromate (CrO.sub.4 sup.-2 or Cr.sub.2 O.sub.7 sup.-2), or phosphate (PO.sub.4 sup.-3). The pH of the solution is usually in the range of 1.3-2.5, but a few alkaline bath formulas are known. The process results in the formation of a protective, amorphous coating comprised of oxides of the substrate, complex chromium or phosphorous compounds, and other components of the processing solution. Only a small number of coatings and chromating processes have been characterized by surface analysis techniques, but in coating systems that have been studied the following compounds have been reported: substrate oxides and hydroxides such as Al.sub.2 O.sub.3 and Al(OH).sub.3, chromium oxides and hydroxides such as Cr.sub.2 O.sub.3, CrOOH, Cr(OH).sub.3, and Cr.sub.2 O.sub.3 .diamond-solid.sub.psi. H.sub.2 O, and phosphates such as AlPO.sub.4. These coatings enhance corrosion resistance of bare and painted surfaces, improve adhesion of paint or other organic finishes, or provide the surface with a decorative finish.

Chromate conversion coatings are applied by contacting the processed surfaces with a sequence of solutions. The basic processing sequence typically comprises the following six steps: cleaning the metal surface, rinsing, creating the conversion coating on the metal surface, rinsing, post-treatment rinsing, and drying. The cleaning, rinsing, and drying steps are standard procedures throughout the industry. The chief variant among the processes used is the composition of the chromate conversion solution. The compositions of these solutions depends on the metal to be treated and the specific requirements of the final product. The chief disadvantage of chromate-conversion coating processes is that they involve the use of hazardous substances.

Because of the environmental problems with chromates, much work has been done to develop protective coatings which do not employ such compounds. For example, U.S. Pat. No. 4,004,951 (Dorsey) discloses applying a hydrophobic coating to an aluminum surface by treatment with a long-chain carboxylic acid and an equivalent alkali metal salt of the carboxylic acid; U.S. Pat. No. 4,054,466 (King et al.) discloses a process for the treatment of aluminum in which vegetable tannin is applied to the surface of the aluminum; and U.S. Pat. No. 4,063,969 (Howell et al.) discloses treating aluminum with a combination of tannin and lithium hydroxide. In each of the above patents, the primary protective ingredient is the complex organic compound, the treatment solution is applied at slightly elevated temperatures (90.degree.-125.degree. F.), and the treatment solution is kept at a mid-level pH (4-8 in King et al. and Howell et al., and 8-10 in Dorsey).

Csanady et al. in Corrosion Science, 24, 3, 237-248 (1984) shows that alkali and alkali earth metals stimulated Al(OH).sub.3 growth on aluminum alloys. However, Csanady et al. reports that the incorporation of Li.sup.+ or Mg.sup.+ into a growing oxide film degrades corrosion resistance.

U.S. Pat. No. 5,266,356 (Buchheit et al.) discloses the corrosion protection of aluminum and aluminum alloys by immersion in an alkaline lithium or alkaline magnesium salt solution causing the formation of a protective film on the surface which includes hydrotalcite compounds. Only alkaline lithium or magnesium salt solutions are disclosed, and no beneficial sealing of the protective film by means of a sealing solution, with or without an oxidizing agent, is disclosed.

SUMMARY OF THE INVENTION

It is an object of this invention to provide a process for forming a corrosion resistant oxide coating on metals and alloys, particularly aluminum and aluminum alloys, using simple, low-cost equipment, and no toxic materials such as chromium, chromium salts, or metal cyanides.

It is a further object of this invention to treat metals and alloys to place their surfaces in a substantially alkaline condition, and then seal their surfaces by contact with an aqueous solution containing one or more soluble metal compounds.

It is a still further object of this invention to precipitate a metal compound or compounds from an aqueous solution, containing one or more soluble metal compounds, that has a neutral or slightly acidic pH onto, and into, the metallic surface to provide corrosion resistance.

It is a still further object of this invention to add an oxidizing agent to the seal-forming aqueous solution, containing one or more soluble metal compounds, in sufficient quantity to oxidize the solution cation or cations to a higher valence state.

BRIEF DESCRIPTION OF THE DRAWING

The drawing shows in sequence the three basic steps of the process whereby a corrosion-protective coating is applied to the surface of a metallic material.

DETAILED DESCRIPTION OF THE INVENTION

The present invention provides a process for the formation of coatings with desirable properties on surfaces of metals or alloys, particularly aluminum or aluminum alloys, using simple, low-cost equipment, and no toxic materials such as chromium, chromium salts, or metal cyanides. This method exploits formation of a substantially alkaline condition on the metal or alloy surface, followed by precipitation of insoluble metal oxides and hydroxides into and onto the film.

For example, corrosion-resistant films can be formed on aluminum and aluminum alloys using a multi-step process involving immersion in an alkaline lithium-salt solution. Corrosion resistance may be enhanced by a subsequent heat treatment and room-temperature aging process.

Components to be coated are first degreased with hexane or other suitable degreasing agent. The components are then cleaned in an alkaline bath, the residue from the cleaning process is removed in a deoxidizing acid bath, and the components are rinsed in water.

The components are then immediately immersed in an alkaline lithium-salt solution. For example, the solution may be about 0.01-0.6M Li.sub.2 CO.sub.3. The best results have been achieved with alkaline lithium-salt solutions with concentrations ranging about 0.05-0.1M. The pH of the solution must be greater than 8, preferably about 11-12. The components remain in the alkaline lithium-salt solution about 5-60 minutes, or longer for thicker coatings. The solution may be maintained at room temperature during immersion, after which the components are removed and dried. The components may then be heat treated, or after a subsequent sealing process. For example, heating in air at about 30.degree.-200.degree. C. for about 5-240 min yields desirable results. Coatings formed by this process are thin and translucent. The appearance of these coatings is similar to that produced by some conversion coatings, and the corrosion resistance is comparable to some chromate-conversion coatings in accelerated testing.

The hydrothermal species formed on an aluminum surface during immersion has a structure comprised of layers of hydroxide ions separated by alternating layers of Al and Li cations, or Al and Mg cations, and anions of the salt in solution. The species belongs to a class of clays known as hydrotalcites which can, without further processing, impart corrosion resistance to the aluminum. However, the protective properties of the hydrotalcite film may degrade in acid and neutral solutions. Therefore, a post-film formation heat treatment has been found to be beneficial in improving corrosion resistance. Heat treatment is believed to liberate water and volatile anions bound in the hydrotalcite structure to create a more corrosion-resistant film. Titanium salts, hydrofluoric acid, phosphoric acid, and sodium hydroxide may be advantageously added to the alkaline lithium-salt solution to improve the characteristics of the resulting corrosion resistant film.

Hydrotalcite compounds are detectable on aluminum and aluminum alloys after immersion in solutions with a pH as low as about 8. However, increasing amounts of the hydrotalcite compounds results when the solution has a higher pH. Increased corrosion resistance has been observed in the presence of several solutions of lithium salts including LiCl, LiBr, Li.sub.2 CO.sub.3, and Li.sub.2 SO.sub.4, as well as LiOH. Other lithium salts and compounds should also be suitable for hydrotalcite-compound formation.

Hydrotalcite films are formed in solution at room temperature. Increasing the lithium-salt solution temperature causes species like carbonates and sulfates to escape through the formation of carbon dioxide and sulfur dioxide, thereby inhibiting hydrotalcite formation. Aluminum alloys which contain lithium at a level ranging from about 0.5-10 wt % would need only be exposed to aqueous alkaline salts having anions such as, but not limited to, CO.sub.3.sup.-2, SO.sub.4.sup.-2, Cl.sup.-1, Br.sup.-1, and OH.sup.-1 since the lithium in the alloy could react with the immersion solution. The immersion time required to form the hydrotalcite compounds in the protective film depends on the alloy type, compound concentration and type, and bath pH.

For less corrosion-resistant substrates, including 2024-T3 and 7075-T6 aluminum alloys, the hydrotalcite coating should be exposed to an aqueous neutral or acid metal-salt solution. This seals any latent porosity in the coating by precipitating metal oxide into the pores. This process is analogous to dichromate sealing of sulfuric-acid anodized aluminum, except that external electrolytic control is not required, and the sealing can be done in a very short time. The corrosion resistance of such a sealed hydrotalcite coating is comparable to that of chromate-conversion coatings.

The metal salts used in the sealing process can be divided into two sets. The first comprises salts whose solubility minimum occurs under alkaline-solution conditions; this includes salts of Ce, Co, Ni, Fe, Mn, and Mg. The second set comprises salts that are potential inorganic sealants for oxide coatings; this includes salts of Mo, Bi, Al, and Cr.

A preferred embodiment of the invention comprises:

- a) cleaning the metal or alloy surface in an aqueous detergent solution, rinsing in deionized water, degreasing the surface in an alkaline silicate/carbonate solution held at elevated temperature, rinsing in deionized water, deoxidizing the surface by immersion in an acid solution typically containing nitric and/or hydrofluoric acid, and rinsing again in deionized water;
- b) growing a hydrothermal coating, by chemical treatment, on the metal or alloy by immersion for about 60-180 min in an aqueous solution that contains a soluble lithium salt together with: 1) a soluble aluminum salt if aluminum or an aluminum alloy is to be protected; or 2) a soluble magnesium salt if magnesium or a magnesium alloy is to be protected. Examples of suitable lithium salts are lithium nitrate, lithium carbonate, lithium chloride, as well as lithium hydroxide. Examples of suitable aluminum salts are sodium aluminate, potassium aluminate, aluminum chloride, and aluminum nitrate. The lithium-salt concentration is in the range of about 100 ppm by weight to the solubility limit of the particular compound, typically about 0.1-1.0M. An aluminum-salt concentration is typically in the range of about 10 ppm by weight to about 0.3M. The solution pH is about 8-14, and the temperature of the solution ranges from about 20.degree.-100.degree. C.; or
- c) as an alternative to immersion in part (b), growing the hydrothermal coating by spraying (where the contact time is about 1-30 min), brushing (where the contact time is about 1-15 min), or rolling (where the contact time is about 1-5 min) the aqueous salt solution onto the metal or alloy surface;
- d) sealing the unrinsed hydrothermal coating by immersion in an aqueous solution of a soluble metal compound or compounds comprised primarily, though not exclusively, of metal compounds that have low solubility under alkaline conditions. The cations of the metal salts may include one or more of the group consisting of: Al, Mg, Ca, Sr, Ti, Mo, Ce, Pr, Nd, Sm, Eu, Gd, Tb, Dy, Ho, Er, Tm, Yb, Lu, Mn, Fe, Co, Ni, and Bi. The temperature of the bath is about 20.degree.-100.degree. C. Immersion is followed by rinsing with deionized water; or
- e) as alternatives to immersion in part (d), sealing the unrinsed hydrothermal coating by spraying, brushing, or rolling (where the contact times are about 1-5 min) the aqueous solution of a soluble metal compound or compounds onto the coated metal or alloy surface, and rinsing with deionized water; or
- f) allowing the unrinsed hydrothermal coating to dry first, and then sealing it by the method of (d), except that the immersion time is about 1-15 min followed by rinsing with deionized water; or
- g) as an alternative to immersion in (f), allowing the unrinsed hydrothermal coating to dry first, and then sealing it by spraying (where the contact time is about 5-60 sec), brushing (where the contact time is about 0.1-5 min), or rolling (where the contact time is about 5-300 sec) the aqueous solution of a soluble metal compound or compounds onto the coated metal or alloy surface, and rinsing with deionized water; and
- h) optionally, adding an oxidizing agent such as hydrogen peroxide to the aqueous metal-salt sealing solutions of (d), (e), (f), and (g) in sufficient quantity to oxidize the solution cation to a higher valence state. An example is the addition of about 5 ml of hydrogen peroxide to 1 liter of sealing solution.

Tables 1 and 2 show the respective corrosion resistances of 6061-T6 and 2024-T3 aluminum alloys coated with a hydrothermal lithium-aluminum coating and sealed by exposure to different metal-salt solutions. The coated and sealed samples were exposed to an aerated 0.5M NaCl solution for 24.+-1 h under free corrosion conditions. An electrochemical impedance spectroscopy test was then conducted by applying a 10-mV sinusoidal voltage perturbation at frequencies ranging about 10 kHz-10 mHz. The data obtained were then analyzed by complex, non-linear, least-squares regression to an equivalent circuit model consisting of a constant-phase element in parallel with a resistance. This parallel-circuit element combination is in series with a solution resistance. The values shown in Tables 1 and 2 are the values of the polarization resistance obtained thereby. The polarization resistance has been shown to be an accurate measure of corrosion protection provided by chemically passivated aluminum alloys--the larger the resistance, the greater the protection. For comparison, uncoated aluminum alloys subjected to this test typically yield polarization resistances of about 1.times.10.sup.3 -5.times.10.sup.3 ohm-cm.sup.2.

TABLE 1

Metal Type of Oxide Sealant	Polarization Resistance (ohm-cm.sup.2)
Bi	4.17 .times. 10.sup.5
Ce	6.83 .times. 10.sup.5
Ni	9.12 .times. 10.sup.5
Mo	1.05 .times. 10.sup.6
Al	1.50 .times. 10.sup.6 -1 .times. 10.sup.8
Mg	1.51 .times. 10.sup.8
Mn	1.82 .times. 10.sup.6
Co	3.55 .times. 10.sup.6

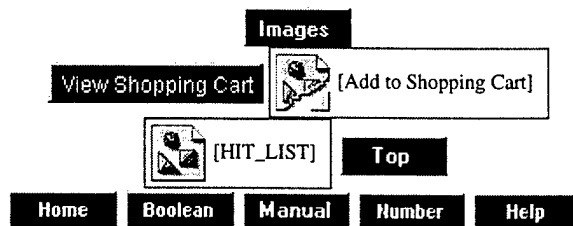
TABLE 2

Metal Type of Oxide Sealant	Polarization Resistance (ohm-cm.sup.2)
Mo	4.50 .times. 10.sup.4
Mg	4.57 .times. 10.sup.4
Bi	6.31 .times. 10.sup.4
Mn	2.29 .times. 10.sup.5
Ce	8.13 .times. 10.sup.5 -2.10 .times. 10.sup.7

Co 1.00 .times. 10.sup.6
 Ni 1.15 .times. 10.sup.6

The examples discussed above are cited to illustrate a particular embodiment of this invention. It is contemplated that the use of the invention may involve components having different forms and compositions. It is intended that the scope of the invention be defined by the claims appended hereto.

* * * * *



Hydrotalcite Coating Formation on Al-Cu-Mg Alloys from Oxidizing Bath Chemistries

W. Zhang and R. G. Buchheit
Fontana Corrosion Center
Department of Materials Science and Engineering,
The Ohio State University
Columbus, OH 43210

Abstract

In this study, we have examined the effects of bath oxidizing power on hydrotalcite coating formation and breakdown. Overall, results indicate that increasing the oxidizing power of the coating bath shortens the immersion time required to form highly corrosion resistant coatings. Hydrotalcite conversion coatings were formed on 2024-T3 (Al-4.4Cu-2.5Mg-0.6Mn) panels by immersion in alkaline lithium salt solutions containing either carbonate, nitrate, or nitrate plus persulfate additions. The resulting coating structure was characterized by scanning electron microscopy. Corrosion resistance was characterized by electrochemical impedance spectroscopy and salt spray exposure testing. When nitrate and persulfate oxidizers were present in the bath, coating formation time and hydrogen evolution were sharply reduced, while coating weight was increased indicating an overall increase in coating efficiency. A decrease in pinhole-type coating defects is attributed to early cessation of hydrogen evolution. Coatings with high corrosion resistance were formed in 6 minutes or less of simple immersion. Coatings formed in the presence of oxidizers were much more corrosion resistant than those formed in carbonate-only solutions. Coatings formed in nitrate-containing baths withstand 168 h of ASTM B117 salt spray exposure with little or no pitting. In EIS tests, coatings exhibit total impedances of 2 to 5 $M\Omega\cdot cm^2$ after 24 hours' exposure to aerated 0.5M NaCl solution. It has also been found that in EIS tests in chloride solution, the total impedance of coatings formed in oxidizing baths increases with increasing exposure time. This "healing" process is so far unique to hydrotalcite coatings formed in the presence of oxidizers and is thought to be associated with low temperature hydrothermal sealing of the coating.

KEY WORDS: hydrotalcite coatings, conversion coatings, 2024-T3, electrochemical impedance spectroscopy.

Introduction

Al-Cu-Mg alloys are widely used in aerospace and defense applications because of their high strength-to-density ratios and age hardening characteristics. These alloys are susceptible to localized corrosion in their normal service environments, and corrosion resistant coatings are required to control corrosion damage. When high corrosion resistance is required, chromate conversion coatings serve as a foundation layer for highly corrosion resistant paints and primers. Chromate conversion coatings are also used as "stand-alone" coatings where only a modest degree of corrosion protection is required. Chromate conversion coatings are very effective, but the primary ingredient in coating bath formulations, Cr^{6+} , is subject to restricted use due to its high toxicity and carcinogenic effects. Much effort has been devoted to the development of alternative coating systems that are environmentally benign, and many environmentally friendly coating systems are under development (1, 2, 3, 4).

We have been developing a system based on the spontaneous formation of lithium-aluminum-carbonate-hydroxide hydrate compounds (hydrotalcite) on Al alloys when they are contacted with alkaline Li salt solutions (5, 6, 7). During immersion of Al or Al alloys to such solutions, a polycrystalline barrier film mainly comprised of hydrotalcite-like compounds is formed on the alloy surface. Much of our work has focused on the characteristics and performance of coatings formed from solutions whose primary anionic constituent, other than hydroxyl, is carbonate. Coatings formed from these solutions

contain the carbonate variant of hydrotalcite known as hydrolithisite:

$\text{Li}_2[\text{Al}_2(\text{OH})_6]_2\cdot\text{CO}_3\cdot n\text{H}_2\text{O}$. Other anionic variants of this compound have been successfully formed as coatings using anions such as chloride, hydroxide, silicate, and sulfate.

A key strength of the hydrotalcite coating process is its simplicity. Coatings form spontaneously when a surface is contacted with a solution during immersion or spray application. However, for broad applicability, coating formation must occur in a few minutes and corrosion resistance and adhesion of subsequently applied coatings must be high. Results have shown that carbonate coatings impart a significant degree of corrosion resistance to 1XXX (commercially pure), 3XXX (Al-Mn), 5XXX (Al-Mg), and 6XXX (Al-Mg-Si) alloys. However, the carbonate coating has not performed nearly as well on 2XXX (Al-Cu-Mg) and 7XXX (Al-Zn-Mg-Cu) alloy classes from which many aerospace alloys derive. Gains in corrosion resistance for these alloys have been made with carbonate chemistries. In fact, some carbonate coatings were able to provide 168 hours of salt spray resistance on 2024-T3, however there gains were achieved primarily by increases in processing time that were judged to be too lengthy for many applications (8). In our efforts to remedy these shortcomings, we have found that the addition of oxidizing agents to coating baths confers significant benefits. Oxidizer additions of the proper type and in the proper amount significantly reducing coating time and increase corrosion resistance.

In this paper we report on the effects of nitrate, persulfate and hydrogen peroxide additions to coating formation, structure and performance. Several additional aspects including metal loss and hydrogen evolution during coating process, coating weights, coating morphology and coating corrosion resistance of the carbonate, nitrate and persulfate coatings are compared. The mechanism through which oxidizing power affects the coating corrosion resistance is also discussed.

Experimental Procedures

Materials. All coatings were prepared on substrate panels cut from 0.1 inch thick 2024-T3 (UNS A90924, Al-4.4Cu-2.5Mg-0.6Mn) sheet stock. The panels were cut into 4 x 5 inch in size. All the chemicals were ordered from commercial vendors and were of reagent grade.

Coating Methods. Samples were degreased in an alkaline sodium metasilicate/sodium carbonate solution and deoxidized in a nitric acid/sodium bromate deoxidizer. Samples were rinsed in overflowing distilled water in between each processing step. The details these processing steps are shown in Table 1.

Hydrotalcite coating formation was carried out at 90°C for varying lengths of time ranging from 2 to 10 minutes. After coating, samples were immersed in a magnesium acetate-based solution to reduce coating bloom and promote sealing of pores. Between each step the panels were rinsed in distilled water. The panels were then dried in air for at

least 24 hours before any measurement. The details of the coating process are also summarized in Table 1.

Coating Weight. The coating weight was measured in accordance with ASTM B767-87 using an analytical balance with 0.0001g resolution (9). Coated panels were first cleaned with alcohol, then blown dry with air and weighed. Coatings were then stripped, rinsed with water, rinsed with alcohol, blown dry, and weighed again. This process was repeated until a change in the rate of mass loss was detected. The total weight loss up to the point where mass loss rate changed was taken as the total coating weight.

Weight Loss of Substrate Metal during Coating. During coating formation some of the substrate metal is dissolved. To measure this mass loss samples were weighed before coating. After coating formation, the coating was stripped off and the sample was weighed again. The mass difference was taken as the metal weight loss that occurred during immersion in the coating bath.

Hydrogen Collection. During the coating process, hydrogen evolves from the panel surface. This hydrogen was collected using a gas trap. Hydrogen evolving from the panel surface ascended into the trap displacing solution. The hydrogen collected in the trap was extracted and measured using a calibrated syringe. It should be noted that the hydrogen volume was not necessarily measured under standard conditions, but measurements were made under identical conditions of temperature and pressure and were therefore comparable.

Scanning Electron Microscopy (SEM). The coating morphology was examined using a Philips XI-30FEG SEM operated at 10kV.

Electrochemical Impedance Spectroscopy (EIS). The corrosion resistance of the coating was evaluated using EIS. The coated panel was exposed to aerated 0.5 M NaCl solution for 24 hours, or longer, before EIS measurement. Samples were exposed using a flat cell with a 32cm² window for the coated surface. The data was collected using a PAR model 273A potentiostat and Solartron model 1250 frequency response analyzer. A sinusoidal 10mV voltage signal with frequencies ranging from 10000Hz to 0.001Hz was used as a perturbation. The measurement was controlled by Scribner Associates Zplot™ impedance software installed in a personal computer.

Impedance spectra were modeled using an equivalent circuit analysis and complex non-linear least squares fitting of the data to a suitable equivalent circuit. To model single time constant spectra, a modified Randles circuit was used in which the capacitor was replaced by a constant phase element. The numerical value of the resistance associated with charge transfer through the coated surface was used as a figure of merit to judge coating corrosion resistance. To model spectra with two time constants, a parallel resistor-CPE combination was nested in the modified Randles circuit. In this two resistances (excluding the solution resistance) were added and used as the figure of merit. For spectra with three time constants, the highest frequency time constant was not fitted and the spectra were analyzed using two time constant model.

Salt Spray Exposure Testing. Coating corrosion resistance was also assessed by salt spray exposure. Salt spray test was conducted in accordance with ASTM B117-97 (10).

Determination of Nitrite Concentration after Coating. In certain experiments, the nitrite concentration in the coating bath after coating was determined. These determinations were made according to the method specified in ASTM D3867-90 "Standard Test Methods for Nitrite-Nitrate in Water" (11). In this analysis, sulfanilamide and N-1- (naphthyl) ethylenediamine dihydrochloride were used as a coloring reagents to react with nitrite ion and induce a color change. Optical absorbance at 543 nm was measured using a spectrophotometer. The nitrite concentration was then determined by comparison to a calibration curve determined from standards.

Detection of Sulfate Formation in Persulfate Bath after Coating Process. To examine if persulfate in the coating bath is reduced to sulfate during coating process, 10ml solution was taken out from persulfate coating bath after coating process and mixed with 2ml 0.1M $\text{Ba}(\text{NO}_3)_2$ solution. If persulfate is reduced to sulfate white BaSO_4 precipitates will form. Thus the reduction of persulfate can be verified visually.

Experimental Results

Coating Corrosion Resistance. EIS measurements show that the coating corrosion resistance increases in the following order: carbonate coating < nitrate coating < nitrate + persulfate coating. Data for the three different coatings are shown in Nyquist and Bode

plots in Figure 1. These data were collected after the coatings were exposed to 0.5M NaCl solution for 168 hours under free corrosion conditions. The spectra yield depressed and sometimes asymmetric semicircular arcs indicative of localized corrosion, which occurs at the coating breakdown. The arcs for the nitrate and nitrate plus persulfate coatings are not fully resolved due to the large time constant, but the asymmetry in the arc for the carbonate coating indicates diffusion, probably associated with pitting. Equivalent circuit modeling showed that the corrosion resistance of carbonate coating nitrate coating and nitrate + persulfate coating was on the order of $0.3 \text{ M}\Omega\cdot\text{cm}^2$, $1.2 \text{ M}\Omega\cdot\text{cm}^2$ and $6 \text{ M}\Omega\cdot\text{cm}^2$, respectively. It is worth noting that the corrosion resistance of the nitrate and nitrate + persulfate coatings is comparable to that of chromate conversion coatings determined under identical experimental conditions (12).

Extended exposure in NaCl solutions. During exposure to aerated 0.5 M sodium chloride solutions, the impedance of hydrotalcite coatings formed in oxidizing bath chemistries is observed to increase with increasing exposure time. This phenomenon is illustrated in Figures 2 a and b, which are Nyquist and Bode plots of impedance data for 2024-T3 samples with hydrotalcite coatings formed in the nitrate plus persulfate coating bath. Over the course of 48 hours in the NaCl solution, there is a dramatic change in character from a charge transfer-like response after one hour of exposure to a strongly capacitive response after 48 hours. The frequency domain over which capacitive behavior is exhibited increases substantially indicating an increase in coating barrier properties that is consistent with low temperature hydrothermal sealing. In certain experiments, coating impedance has been observed to increase for periods as long as 100 hours. In long term

exposure experiments, once this sealing action has occurred, the impedance remains stable or decreases only slightly. A similar trend in EIS data has also been reported on chromate conversion coatings, though the origins of these trends are almost certainly different (13).

Coatings formed in the nitrate and nitrate/persulfate chemistries in Table 1 consistently demonstrate the healing response shown in Figure 2 during exposure to chloride solution. This is not the case with coatings formed in the carbonate chemistries. Figure 3a and 3b are Nyquist and Bode plots of a 2024-T3 coated in a carbonate-based bath. In this case the coating impedance decreases slightly over a 48-hour immersion period.

Salt Spray Test Results. In the salt spray test conducted according to ASTM B117-97, hydrotalcite coatings formed in nitrate bath by 10 min immersion passed the 168 hours test. However carbonate coatings formed under similar conditions failed the test.

Coating Morphology. Figures 4 a, b, and c are representative scanning electron micrographs of the coatings formed in carbonate, nitrate and nitrate/persulfate baths. In all cases, the coatings consist of compact masses of intersecting plate-shaped crystals. In the as-formed condition, crystals with edges pointing outward are prevalent. This occurs because crystal growth occurs at the edges, and crystal nuclei with edges pointed outward into solution can more easily contact reactant species in solution. Additionally, crystals with this orientation can grow without impinging on neighboring crystals.

These coatings were formed under similar conditions of immersion time, temperature and bath concentration. However, the series of micrographs in Figure 3 show that the size of the crystals increases from carbonate coatings to nitrate coatings, and from nitrate to nitrate/persulfate coatings. It is not yet precisely known what accounts for the increase in crystallite size, but it may reflect acceleration in coating growth rate with increasing bath oxidizing power.

Figure 5 shows the pinhole-type defects on coatings formed in different chemistries. The density of this type defect decreases with the introduction of oxidizing agents into coating bath, as illustrated in Figure 5.

Coating Weight. Figure 6 shows the variation in coating weight for 2024-T3 samples serially immersed in carbonate, nitrate and nitrate/persulfate coating baths. In this experiment, 8 “runs” of three panels each were run through the processing baths. Coating weights were determined gravimetrically for panels in run 1, 3 and 6. In general, the coating weight decreases with increasing coating run number. In early runs, coatings tend to be smutty, e.g., filled with non-protective compounds formed by dissolution of alloying elements. Coating weights are higher, but corrosion resistance is always observed to be inferior. Coatings formed in runs 4 and greater are dominated by hydrotalcite and have the highest corrosion resistances. The data in Figure 5 also show that coatings formed in nitrate and nitrate/persulfate baths are consistently heavier than their carbonate counterparts by a margin of 600 to 700 mg/ft². The nitrate and nitrate/persulfate coatings appear to be roughly equivalent in weight. Hydrotalcite

coatings are considerably heavier than chromate conversion coatings, which range from 15 to 200mg/ft² (14), but are similar in weight to anodized coatings, which range from 500 to 2000 mg/ft² (15).

Substrate weight loss. Alkaline hydrotalcite coating baths have pH values ranging from 10.5 to 13, which is strongly activating for Al alloys. Some amount of dissolution occurs during coating formation. Figure 7 shows the weight loss of panels in the three different coating solutions at 23° and 90°C. Results showed that the weight losses in nitrate and in nitrate/persulfate solution were higher than in carbonate solution, indicating that the nitrate and nitrate/persulfate solutions were more aggressive to aluminum. Elevating the temperature from 23° to 90°C increases the substrate weight loss by a factor of 2.0 to 2.5, depending on bath chemistry.

Coating Efficiency. If coating efficiency is defined as coating weight divided by metal weight loss, it can be found that the coating efficiency was increased in the presence of oxidizing agents. The coating efficiency as defined above for carbonate, nitrate and persulfate chemistries at 90°C are 0.09, 0.20 and 0.29, respectively. This indicates that at the same metal consumption, more coating forms in the presence of oxidizing agent.

Open Circuit Potential (OCP) vs. Time during Coating Formation. OCP was monitored during coating formation process. Typical OCP vs. time behavior in carbonate and nitrate chemistry was shown in Figure 8. The OCP in nitrate chemistry quickly reached a stable value in less than 100s while the OCP in carbonate chemistry did not

stabilize until 600s after immersed into solution. This indicates that Al alloys passivate faster in nitrate bath than in carbonate bath.

Hydrogen Evolution during Coating Formation. When the panels are immersed in coating baths hydrogen evolves from sample surface. Hydrogen evolving persistently from a fixed site on the alloy surface is believed to interfere with coating formation and produce local defects. In carbonate solution, hydrogen evolution is evident throughout the entire immersion period both at room temperature and high temperature. In the nitrate and the nitrate/persulfate baths hydrogen evolution is not visible at room temperature and only obvious for the first 2 minutes or so at high temperature.

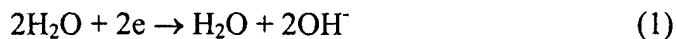
To compare the difference of hydrogen evolution in different coating solutions, the volume of the hydrogen evolved during coating process was measured at room temperature and 90°C. At room temperature, hydrogen evolved from alloy surface in carbonate solution is $1.8\text{cm}^3/\text{in}^2$. Since there is no hydrogen evolution in nitrate and nitrate + persulfate solutions at room temperature, the hydrogen evolutions for these two chemistries are 0. At 90°C, hydrogen volumes evolved from the alloy surface are $10\text{cm}^3/\text{in}^2$, $1\text{cm}^3/\text{in}^2$, and $0.1\text{cm}^3/\text{in}^2$ for carbonate bath, nitrate bath and nitrate plus persulfate bath, respectively. These data were shown in Figure 9. Overall the presence of oxidizers in the bath dramatically lowers hydrogen evolution rate.

Nitrite Concentration. Nitrate can be reduced by aluminum to nitrite (16). This reduction reaction may compete with hydrogen reduction occurring during coating

formation and suppress gas bubble formation. By suppressing bubble formation it may be possible to lower the number of coating defects. To determine if nitrate reduction was occurring, solution samples were extracted from the coating bath during a coating run. The samples were then examined for the presence of nitrite as described in the experimental procedures. Figure 10 shows the trend during the first four runs. The nitrite concentration, which is initially zero, increases to about 600 ppm after one coating run (three panels immersed for 10 minutes), and increased in a nearly linear fashion with successive runs.

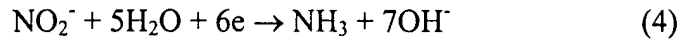
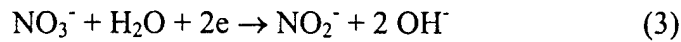
Discussion

The Effect of Bath Chemistries on Gas Evolution. Hydrotalcite coatings form on Al alloys under a range of conditions, but the structure, properties and performance of the coatings strongly depends on bath chemistry. In these experiments, the corrosion resistance of coatings was found to increase in the order of carbonate coating < nitrate coating < nitrate + persulfate coating. It is suggested that this effect is due primarily to the oxidizing power of the coating bath. In the carbonate solution, the cathodic reactions include water reduction and to a lesser extent oxygen reduction:



Since the amount of dissolved oxygen is limited, water reduction is effectively the only cathodic reaction and this reaction produces hydrogen gas. In the nitrate solution, the

nitrate ion can be reduced to nitrite. The following reduction reactions have been proposed to occur on Al in the presence of nitrate ions (16):



Evidence suggests that these reactions are occurring in nitrate coating baths. Chemical analysis confirms the presence of NO_2^- after coating, and coating baths develop the distinct odor of NH_3 with continued usage. These reduction reactions are kinetically facile and compete with water reduction. As a result, the hydrogen evolution in the nitrate bath was less pronounced than in carbonate bath. When $\text{S}_2\text{O}_8^{2-}$ is added to the nitrate solution, another cathodic reduction is introduced:



The presence of SO_4^{2-} has been verified by the formation of barium sulfate precipitate when barium nitrate was added to the coating bath after coating process. Persulfate reduction is also expected to compete with water reduction and reduces hydrogen evolution.

Hydrogen evolution during coating process is likely to be detrimental to the coating formation and protectiveness. Treverton et al. have suggested that hydrogen bubbles tend to prevent coating formation at the sites where persistent hydrogen evolution occurs (17). A model of hydrogen gas formation on aluminum surface proposed by Scamans et al. (18) can be adopted to explain why this might be so. In their model, molecular hydrogen forms at the interface between the oxide and aluminum. This process induces delamination at the metal-oxide interface and blistering is initiated. With time the blister

is pressurized by hydrogen because the compact layer cannot be penetrated by the gas molecules. When the pressure inside the blister is sufficiently high, the blister will burst, leaving a coating defect.

The inner layer of the hydrotalcite coating might suffer from blistering because of the hydrogen evolution. In carbonate bath chemistries, hydrogen evolution is vigorous through most of the coating process. This leaves little opportunity for the blisters that burst in later stages of the coating process to be healed. On the other hand, the hydrogen evolution in the nitrate and nitrate + persulfate chemistries is only vigorous in the beginning period of the coating process. Thus, the defects formed at early stages of coating process in these baths may have enough time to heal thereby reducing the density of defect sites in the coating. Since pitting corrosion may occur preferentially at these sites, lowering their density should result in an increase in corrosion resistance.

The Effect of Coating Bath Chemistries on Coating Healing. The healing behavior of hydrotalcite coatings formed in oxidizing bath chemistries can also be explained by considering the effect of oxidizers on gas evolution. The benefit of sealing hydrotalcite coatings in distilled water at elevated temperature has been reported previously (1). It is suggested that poorly crystallized AlOOH or $\text{Al}(\text{OH})_3$ forms in the interstitial spaces between talc crystals in the coating thereby increasing corrosion resistance. During the immersion of the coating in the 0.5 M NaCl solution, two competing processes occur: 1) corrosion attack by the chloride ion and, 2) sealing of the coating during which the barrier layer might be thickened or stabilized. These two processes have opposite effects on the

coating corrosion resistance as measured by EIS. In carbonate coatings the corrosion attack of chloride ion dominates the time-dependent EIS response because defects are so numerous. In nitrate and nitrate + persulfate coating, the sealing process is dominant in the initial period because there are comparatively fewer defects. As a result, the corrosion resistance increases with immersion time. Eventually, localized attack will set in and the coating impedance will decrease.

The Effect of Bath Chemistries on Coating Growth. The hydrotalcite coating formation on aluminum surface in the alkaline Li salt solution involves two simultaneous processes: 1) dissolution of aluminum and, 2) deposition of solid products on the aluminum surface. It has been reported that the addition of oxidizing agents in the phosphate conversion coating bath accelerates the rate of coating formation and makes the coating more dense (19). The oxidizing chemistries used in hydrotalcite coating formation may have similar effect. When the oxidizing species are used in the hydrotalcite coating bath, the aluminum dissolution and coating formation are accelerated and coating efficiency is also increased. This was evident in the metal loss and coating weight measurements. The open circuit potential (OCP) evolutions during coating formation in carbonate chemistry and nitrate chemistry also indicate the acceleration effect of oxidizing agents. The coatings formed in oxidizing chemistries were more developed, as shown by the morphologies. This may contribute to the increase in the coating corrosion resistance.

Summary

Hydrotalcite coatings formed in alkaline Li salts solution containing different anions demonstrate different levels of corrosion resistance. The coatings formed in carbonate, nitrate, and nitrate + persulfate solution have been studied. The corrosion resistance increases in the order carbonate coating < nitrate coating < nitrate + persulfate coating. This increase in corrosion resistance has been attributed to the increase in the oxidizing power of the solution. Coating efficiency is increased with increasing oxidizing power of coating bath. Hydrogen evolution during coating decreases dramatically with increasing oxidizing power and as a result causes fewer defects in the coating. The healing behavior of hydrotalcite coatings formed in oxidizing chemistries is explained in term of competition between chloride ion attack on coatings and sealing of the coatings. The accelerating effect of oxidizing species on coating formation also improves the coating performance by producing coatings with increased coating weight.

Acknowledgements

This project is sponsored by Defense Advanced Research Projects Agency under contract no. F49620-96-1-0305. The support of Valerie Laget and Hong Guan is appreciated.

References

1. M. Kendig and R. Buchheit, in: R. G. Buchheit, M. R. Jaworoski and P. D. Chalmer (eds), Surface Conversion of Al and Fe Alloys for Corrosion Resistance, NACE International, Houston, TX, 2000.
2. S. M. Cohen, Corrosion, 51(1), 71, 1995
3. R. L. Twite and G. P. Bierwagen, Progress in Organic Coatings, 33, 91, 1998
4. B. R. W. Hinton, Metal Finishing, 89(9), 55, and 89(10), 15, 1991
5. R. G. Buchheit, M. D. Bode, G. E. Stoner, Corrosion 50 (3), 205, 1994.
6. C. A. Drewien, M. O. Eatough, D.R. Tallant, C. R. Hills, and R. G. Buchheit, J. Mater. Res, Vol. 11, 1507, 1996.
7. R. G. Buchheit, C. A. Drewien, J. L. Finch, and G. E. Stoner, Corrosion/94, NACE, Paper 542, 1994.
8. R. G. Buchheit, paper No. 625, Corrosion/96, NACE International, Houston, TX 1996.
9. ASTM B767-87, " Standard Guide for Determining Mass Per Unit Area of Electrodeposited and Related Coatings by Gravimetric and Other Chemical Analysis Procedures" Philadelphia, PA: ASTM, 1987.
10. ASTM B117-97, " Standard Practice for Operating Salt Spray (Fog) Apparatus", Philadelphia, PA, ASTM, 1997
11. ASTM B3867-90, " Standard Test Methods for Nitrite-Nitrate in Water", Philadelphia, PA: ASTM, 1990.
12. X. Liu, Z. Xia , Fontana Corrosion Center, unpublished data, 1999.
13. G. S. Frankel, Mechanism of Al Alloy Corrosion and the Role of Chromate inhibitors, Second Annual Report, 1998.
14. K. A. Korinek, " Chromate Conversion Coatings" in Metals Handbook, Vol.13, ASM, Metals Park, OH, 1987
15. S. Wernick, R. Pinner and P. G. Sheasby, The Surface Treatment and Finishing of Aluminum and Its Alloys, Vol. 1, 5th ed., ASM International and Finishing Publications Ltd., 1987.
16. J. F. McIntyre, T. S. Dow, Corrosion 48(4), 309, 1992
17. J. A. Treverton, M. P. Amor and A. Bosland, Corrosion Science, 33, 1411, 1992
18. G. M. Scamans, A. S. Rehal, J. Mat. Science, 14, 2459, 1979
19. D. B. Freeman, Phosphating and Metal Pretreatment, Industrial Press Inc., New York, 1986.

Captions of Figures

- Figure 1(a). Nyquist plots of coatings formed in different chemistries after 168 hrs immersion in 0.5 M NaCl solution.
- Figure 1(b). Bode plots of coatings formed in different chemistries after 168 hrs immersion in 0.5 M NaCl solution.
- Figure 2 (a). Nyquist plots of a sulfate + persulfate coating obtained after different immersion time in 0.5 M NaCl solution.
- Figure 2 (b). Bode plots of a sulfate + persulfate coating obtained after different immersion time in 0.5 M NaCl solution.
- Figure 3 (a). Nyquist plots of a sulfate coating obtained after different immersion time in 0.5 M NaCl solution.
- Figure 3 (b). Bode plots of a sulfate coating obtained after different immersion time in 0.5 M NaCl solution.
- Figure 4. (a) SEM image of carbonate coatings.
- Figure 4. (b) SEM image of nitrate coatings.
- Figure 4. (c) SEM image of nitrate + persulfate coatings.
- Figure 5. (a) Defects in carbonate coatings.
- Figure 5. (b) Defects in nitrate coatings.
- Figure 5. (c) Defects in persulfate + nitrate coatings.
- Figure 6. Coating weights of three different coatings versus run number.
- Figure 7. Metal weight loss during coating process in different chemistries.
- Figure 8. Evolution of OCP during coating formation in different chemistries.
- Figure 9. Hydrogen evolution during coating process in different chemistries.
- Figure 10. Nitrite concentration increases with run number in nitrate chemistry.

Table

Table 1. Chemistry of the processing baths and processing parameters

Bath	Chemistry	Processing condition
Degreasing	Na_2SiO_3 , Na_2CO_3 -based	65°C, 2 min
Deoxidizing	HNO_3 , Sanchem 1000 (mainly NaBrO_3)	55°C, 3 min
Coating	Carbonate: LiCO_3 , Na_2CO_3 , LiOH , NaAlO_2 Nitrate: LiNO_3 , KNO_3 , LiOH , NaAlO_2 Persulfate: LiNO_3 , KNO_3 , LiOH , $\text{K}_2\text{S}_2\text{O}_8$, NaAlO_2	90°C, 5 min
Sealing	Clariant ES-1 (mainly Magnesium Acetate)	82°C, 15 min

Figures

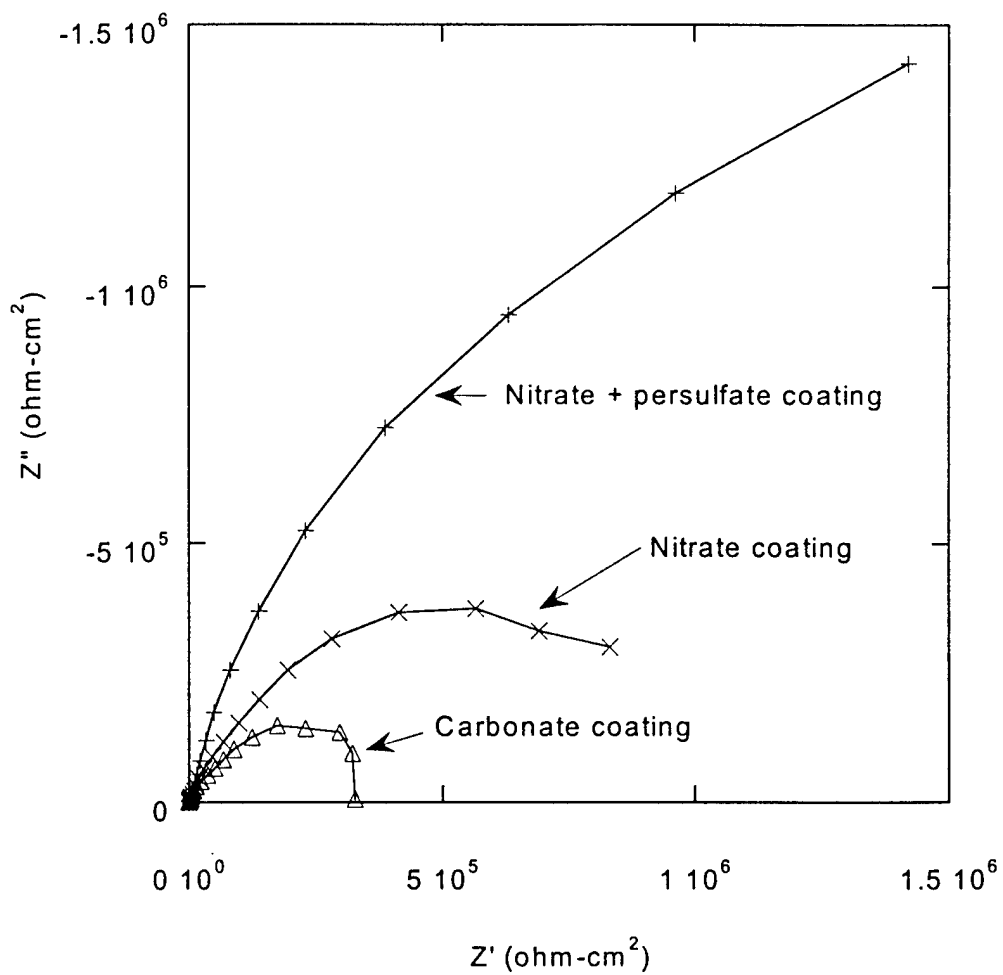


Figure 1(a). Nyquist plots of coatings formed in different chemistries after 168 hrs immersion in 0.5 M NaCl solution.

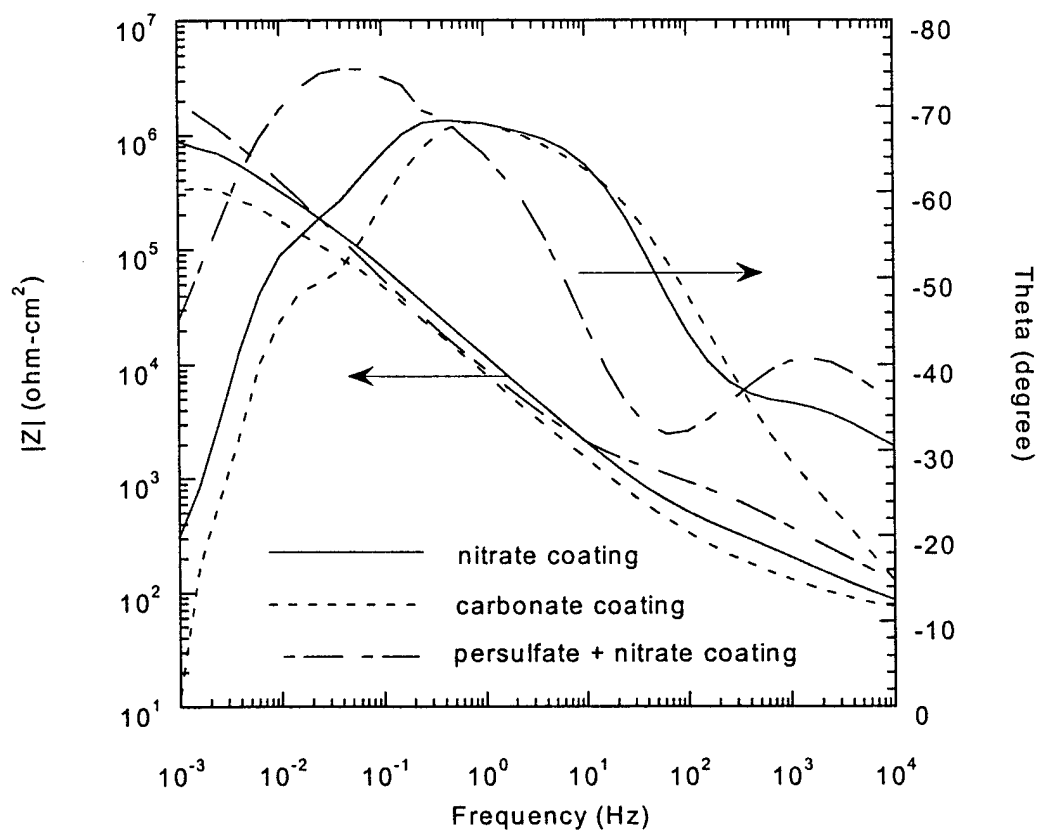


Figure 1(b). Bode plots of coatings formed in different chemistries after 168 hrs immersion in 0.5 M NaCl solution.

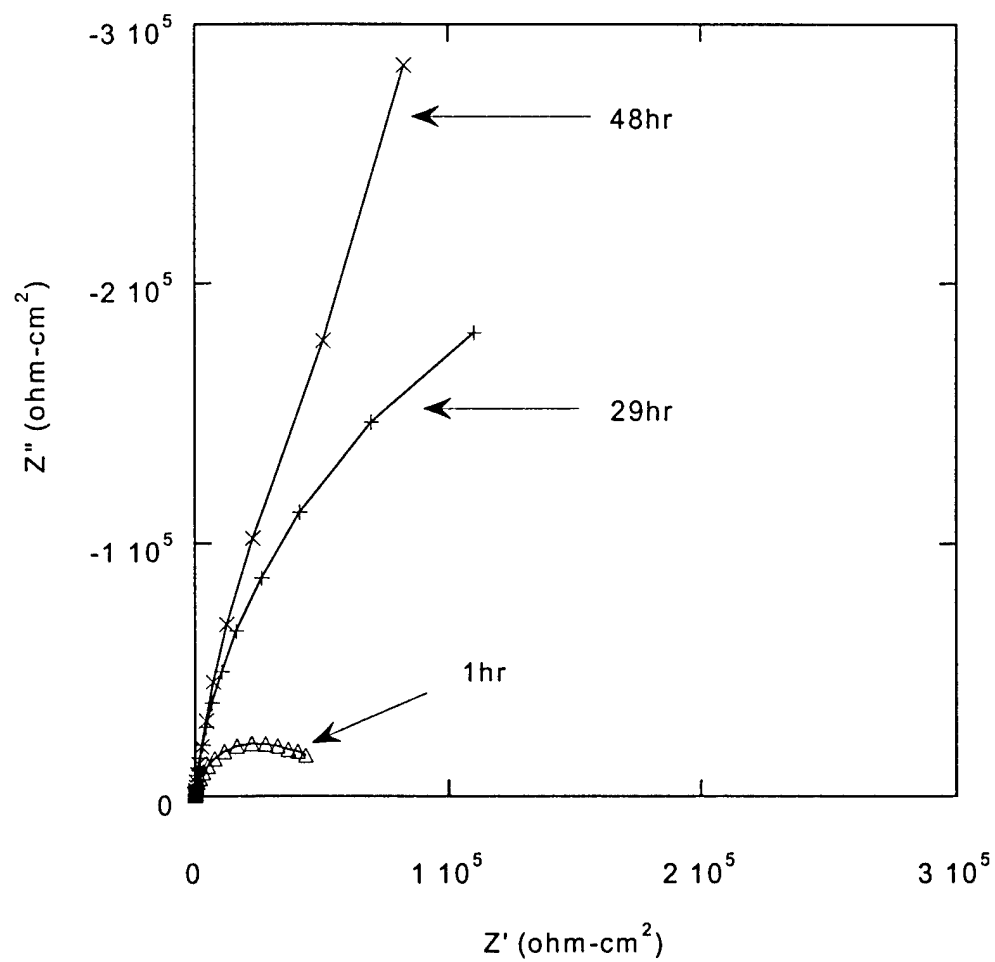


Figure 2 (a). Nyquist plots of a sulfate + persulfate coating obtained after different immersion time in 0.5 M NaCl solution.

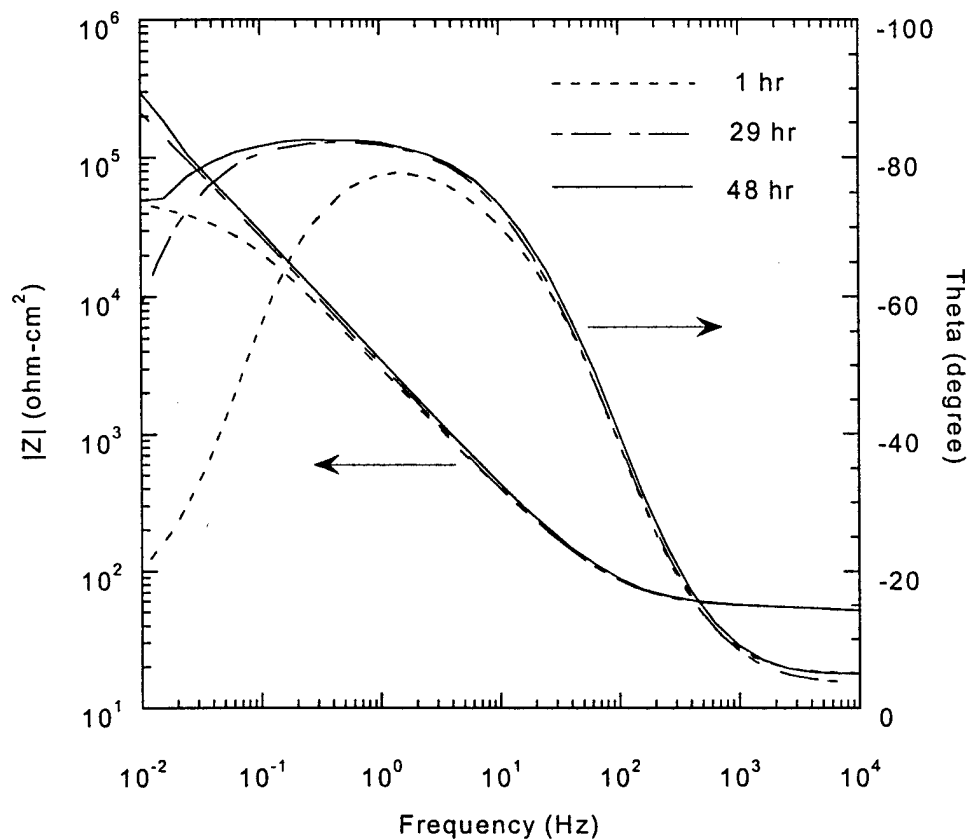


Figure 2 (b). Bode plots of a sulfate + persulfate coating obtained after different immersion time in 0.5 M NaCl solution.

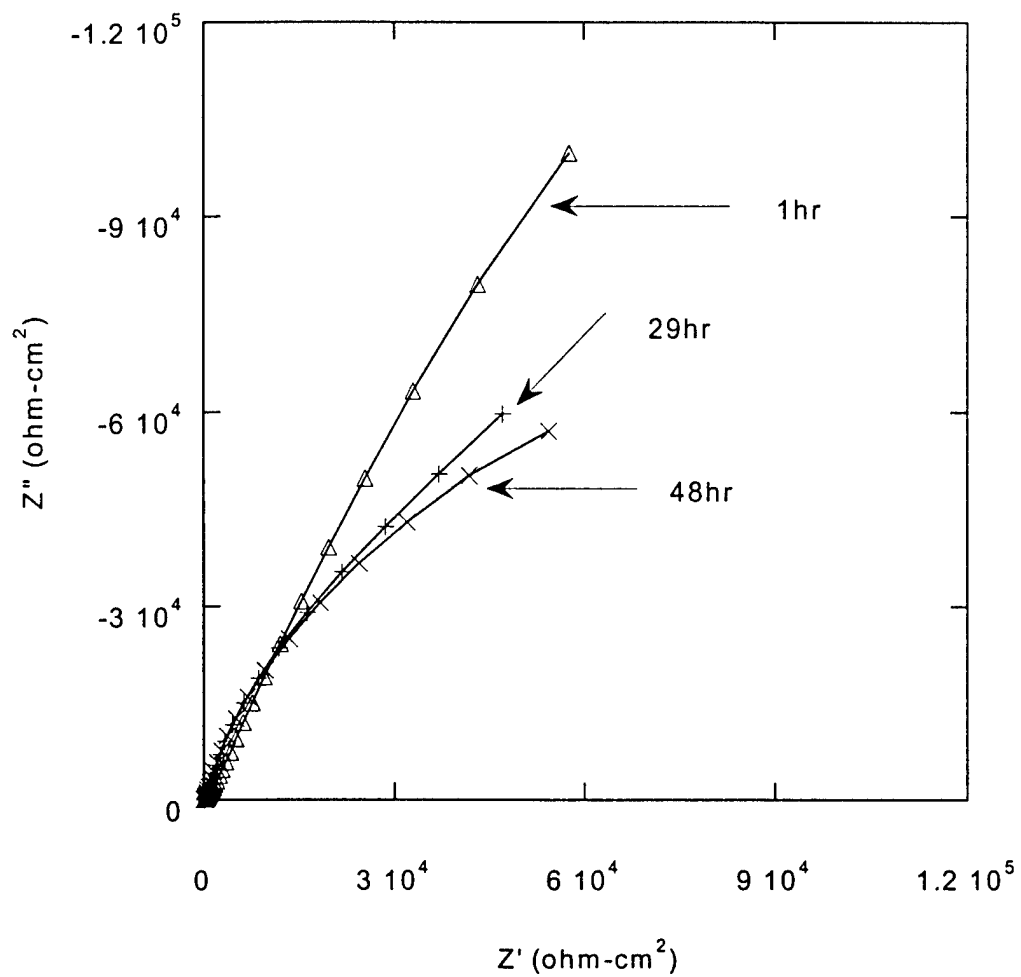


Figure 3 (a). Nyquist plots of a sulfate coating obtained after different immersion time in 0.5 M NaCl solution.

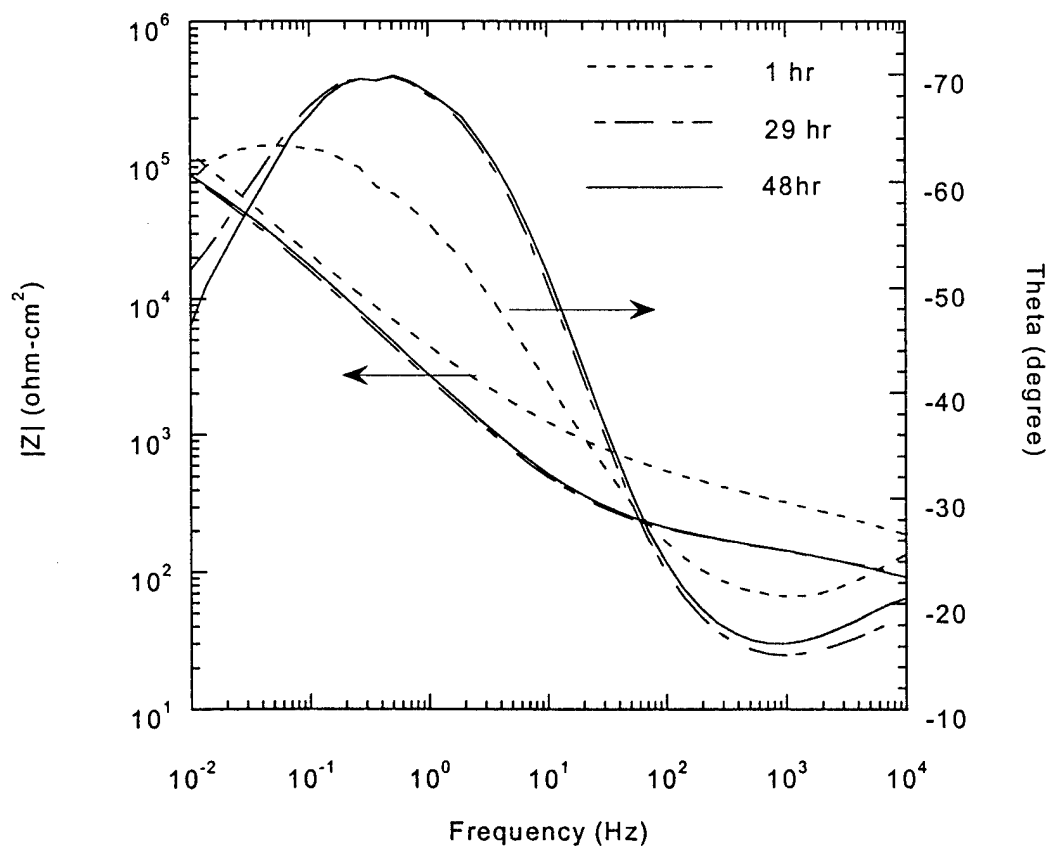
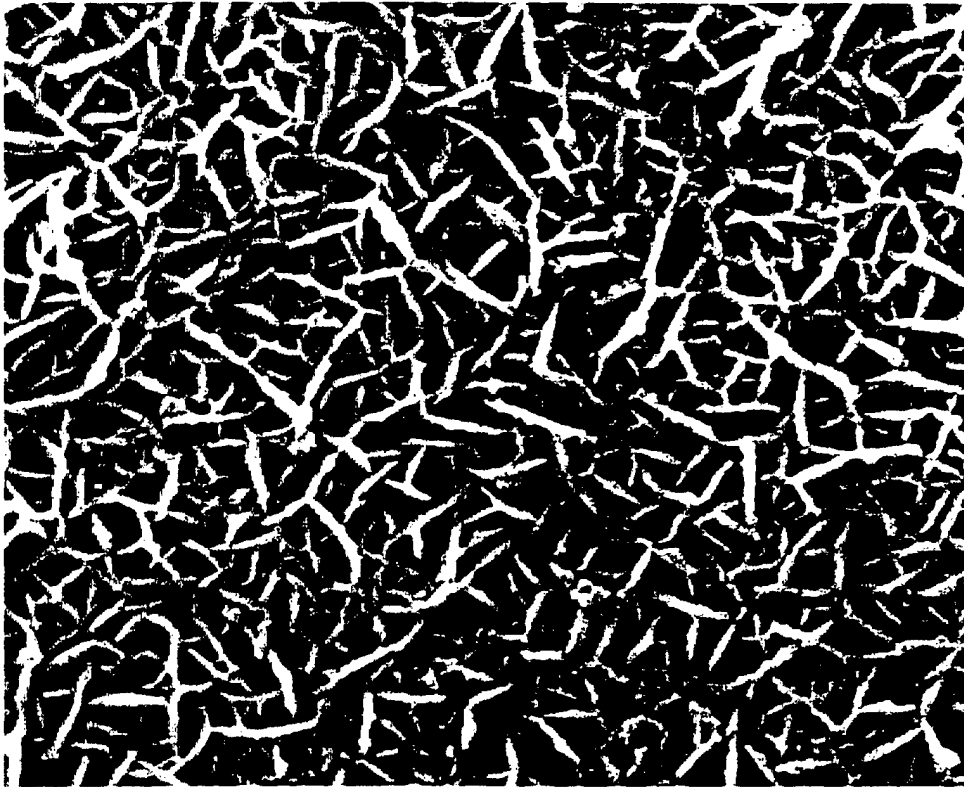


Figure 3 (b). Bode plots of a sulfate coating obtained after different immersion time in 0.5 M NaCl solution.



2 μm

Figure 4. (a) SEM image of carbonate coatings.



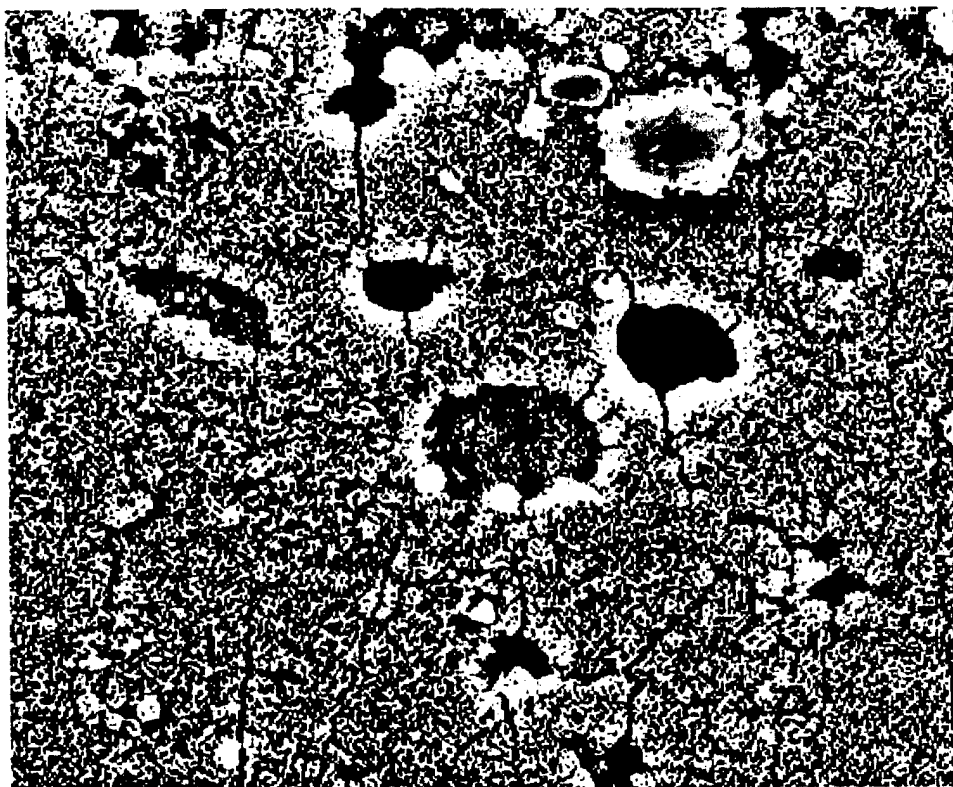
2 μm

Figure 4. (b) SEM image of nitrate coatings.



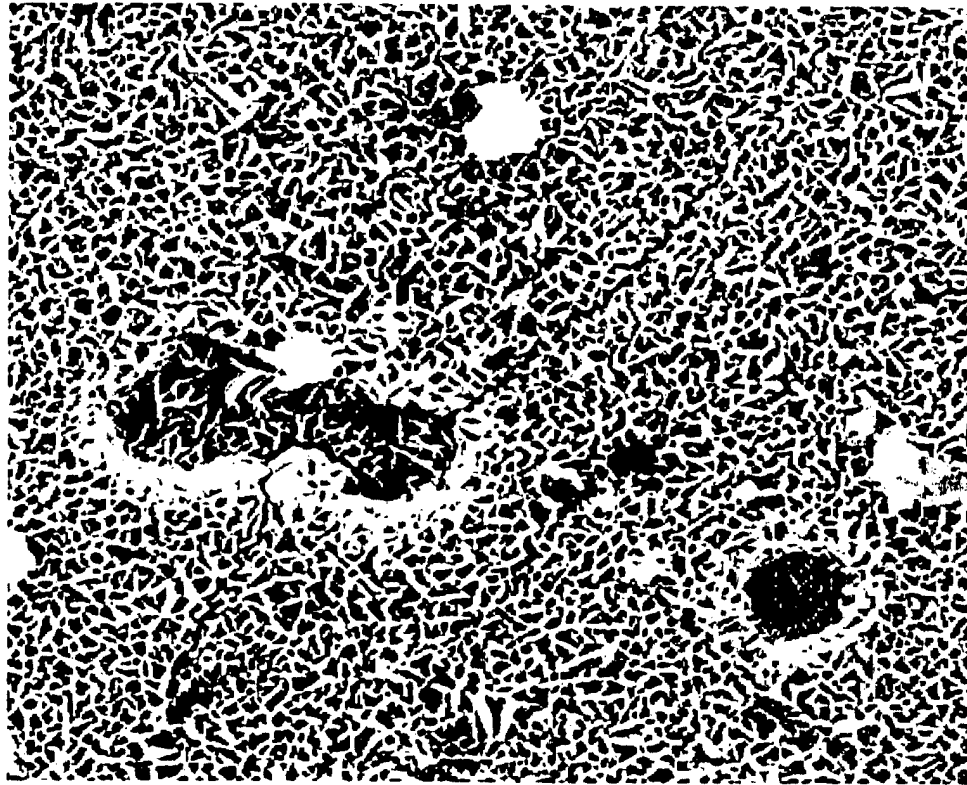
2 μm

Figure 4. (c) SEM image of nitrate + persulfate coatings.



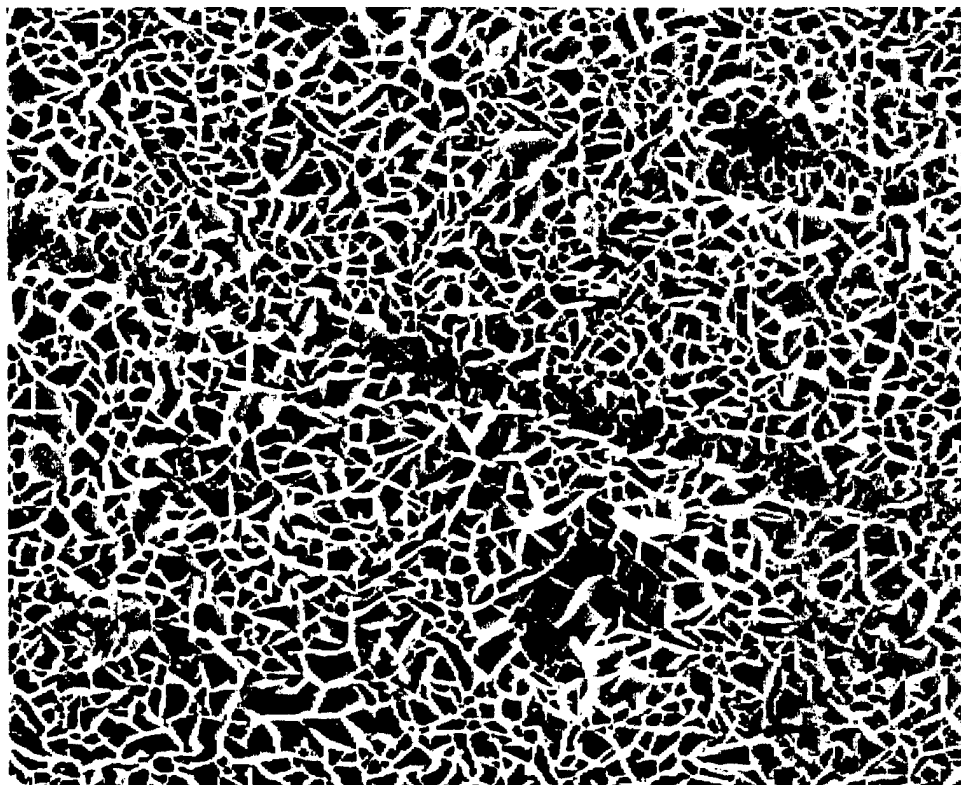
10 μ m

Figure 5. (a) Defects in carbonate coatings.



10 μ m

Figure 5. (b) Defects in nitrate coatings.



10 μ m

Figure 5. (c) Defects in persulfate + nitrate coatings.

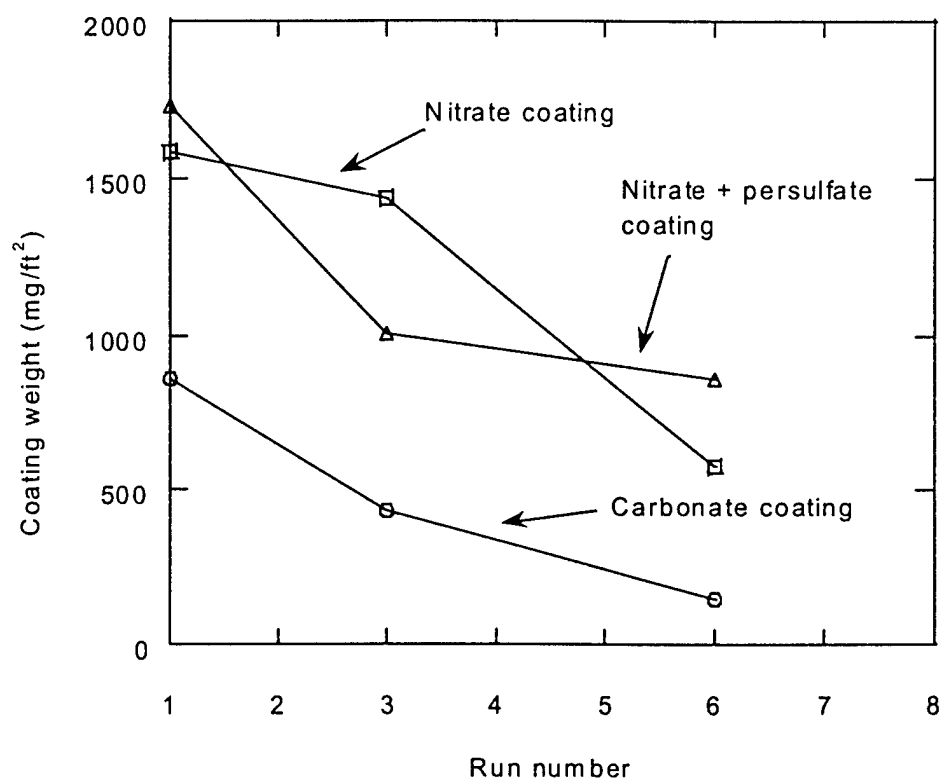


Figure 6. Coating weights of three different coatings versus run number.

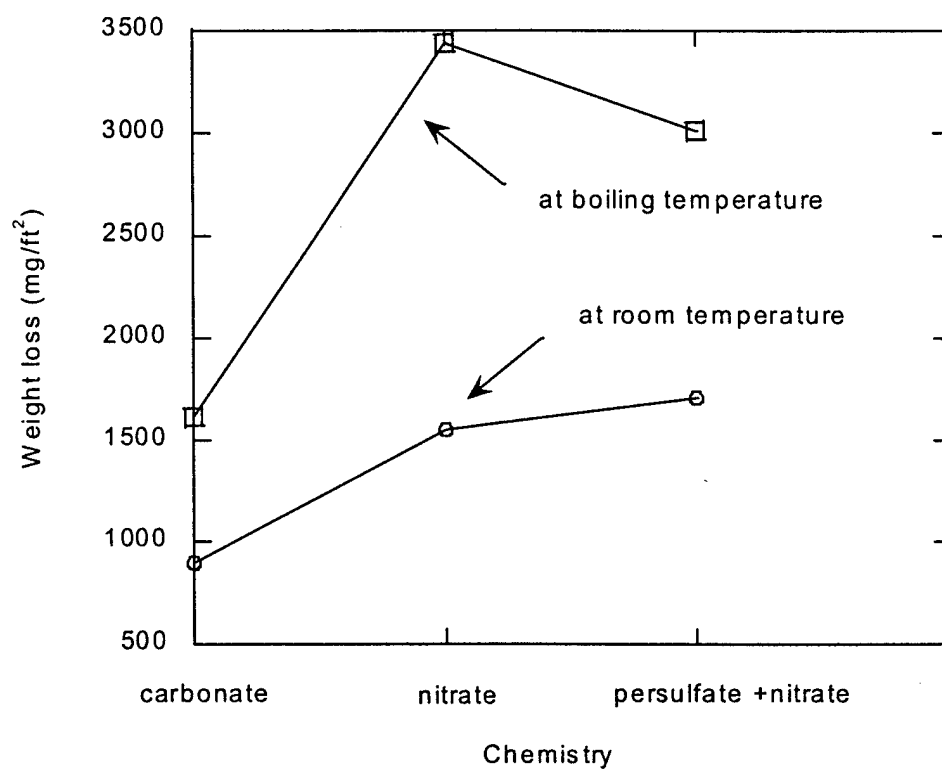


Figure 7. Metal weight loss during coating process in different chemistries.

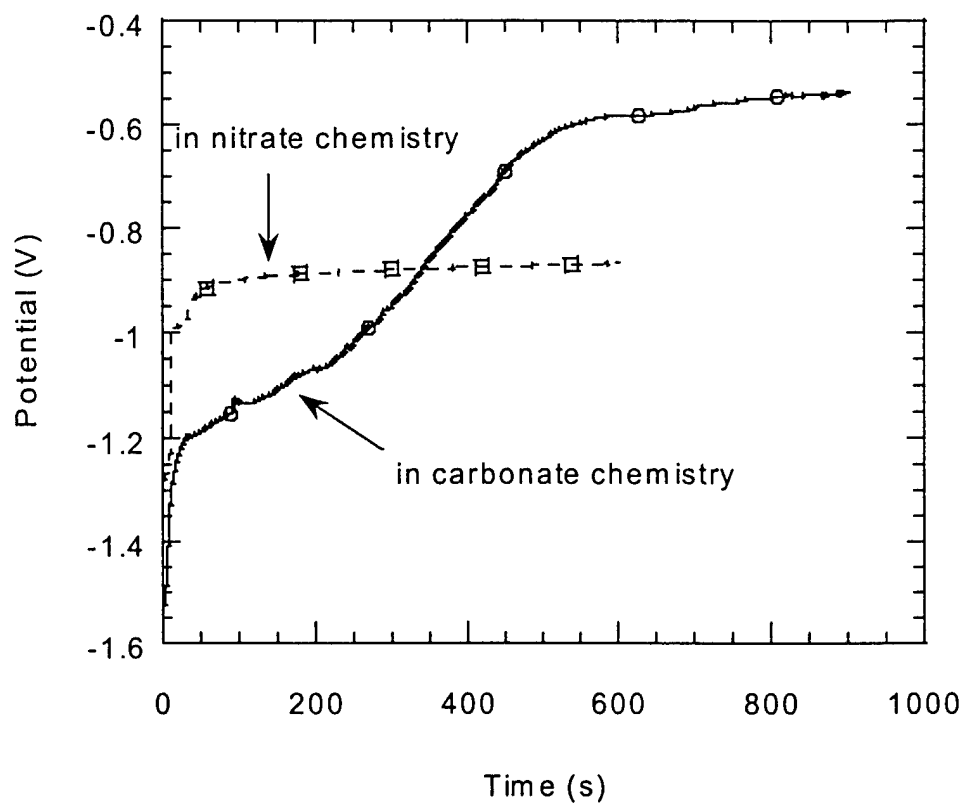


Figure 8. Evolution of OCP during coating formation in different chemistries.

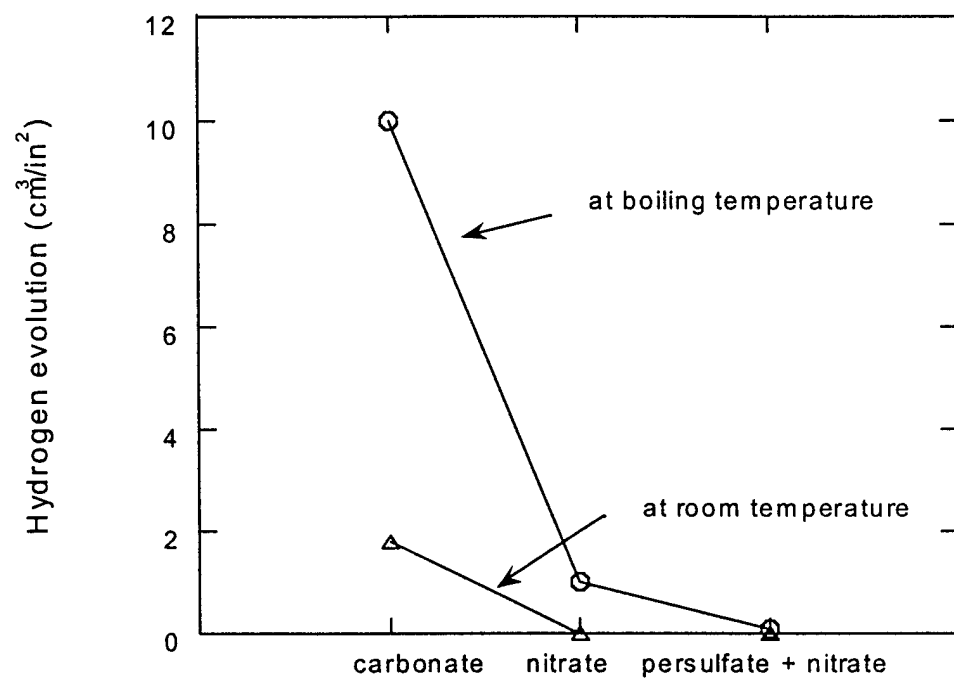


Figure 9. Hydrogen evolution during coating process in different chemistries.

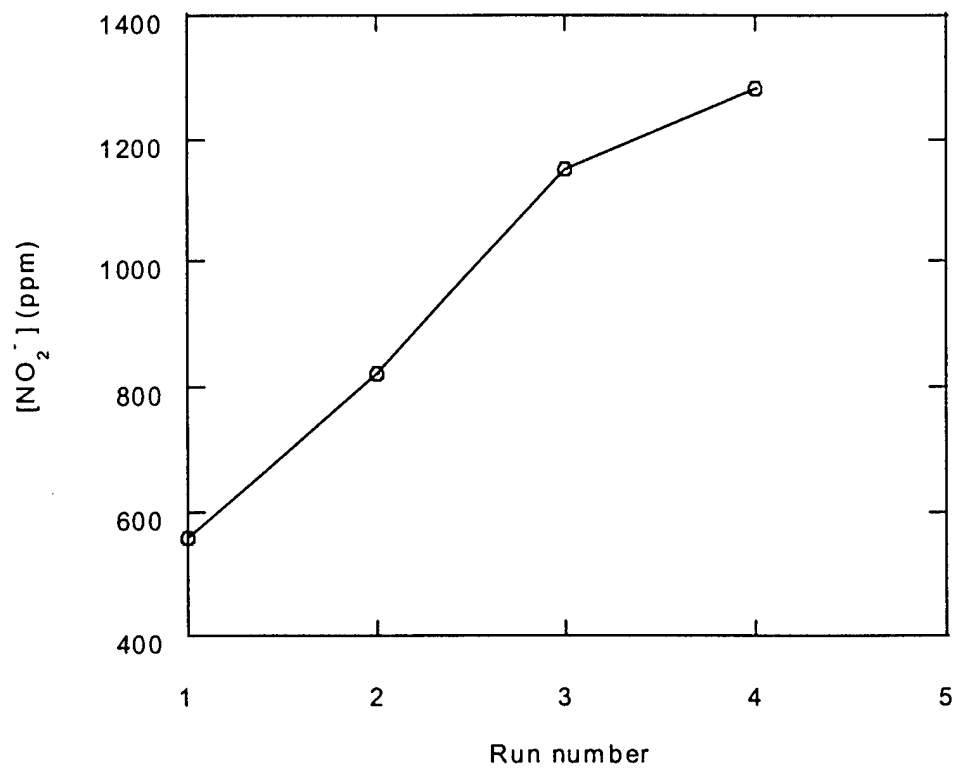


Figure 10. Nitrite concentration increases with run number in nitrate chemistry.

Submitted to *Corrosion Science* (in review)

Presented in the 198th Meeting of the ECS in Phoenix, Arizona. Symposium entitled: "Corrosion and Corrosion Prevention of Low Density Metals and Alloys".

**Development of Hydrotalcite as an Environmentally Benign Conversion Coating:
II. Effect of Bath Chemistry Evolution on Corrosion Resistance**

E.A. Pehovaz-Diez, R.B. Leggat, S.R. Taylor

Center for Electrochemical Science and Engineering
Department of Materials Science and Engineering
University of Virginia
Charlottesville, VA 22903

Abstract

Hydrotalcite-based conversion coatings (HT) are being developed as an environmentally benign alternative to chromate conversion coatings for aluminum aerospace alloys. HT films are formed by immersion of aluminum alloys in alkaline, lithium-salt solutions. An initial phase of this investigation used a fractional factorial design to examine processing variables that impact HT film quality. It has been observed that film quality diminishes with prolonged treatment of samples in a given bath. The present study was undertaken to analyze the effect of these bath chemistry changes on the corrosion resistance of the resulting HT films. Several HT bath parameters were monitored as a function of bath usage and correlated with corrosion resistance of the HT coated sample as determined by Electrochemical Impedance Spectroscopy. The concentrations of different bath ions were measured by Capillary Electrophoresis. In addition, the oxidizing power of the baths were monitored by measuring the open-circuit potential (OCP) of AA2024 panels and a platinum electrode while panels were being coated. Several correlations were observed. As the bath age increased, the corrosion resistance of the HT decreased, the OCP of the AA2024 and the Pt increased, the Al cation concentration and the ratio of nitrite to nitrate anions increased. Experiments were conducted to verify the observed changes as a function of time and bath use. This study has important implications for the development of an effective spray-applied chemistry. Understanding the time dependencies of bath chemistries used for immersion can optimize spray-application chemistries, which are not subject to the same flux of reactants.

Introduction

Hydrotalcite (HT) -based conversion coatings are an emerging environmentally compatible alternative to chromate conversion coatings for aluminum aerospace alloys. HT coatings are composed of hydrolithisite formed by exposure of the aluminum alloy to an alkaline lithium salt solution (e.g., lithium carbonate, lithium nitrate, lithium sulfate, etc.) (ref. Part I). There are numerous treatment parameters that must be considered (e.g., temperature, exposure time, pH, lithium ion concentration, oxoanion concentration, and post-treatment in a cerium solution). Part I of this series employed a fractional factorial design to determine which initial bath parameters were the most important in producing corrosion resistant coatings⁶. Several HT chemistry variants were examined and a lithium nitrate-based chemistry was chosen for further development. Using the optimized coating parameters, HT coatings with corrosion resistance comparable to CCC are attainable⁷.

It has been observed in preliminary experiments that the coating quality decreases with continued bath usage. Thus, once an optimal bath chemistry has been identified, it is important to be able to use a particular bath to produce HT coatings of consistent quality over time. Since the formation of HT coatings is an inherently dynamic process in which there is a continual generation and depletion of reacting species, it is believed that an understanding of bath chemistry changes as a function of time will provide insight into the causes of HT film variations. In the present study, the effect of bath chemistry evolution on corrosion resistance was investigated by correlation of ion concentration with the corrosion protection characteristics of HT coatings.

Given the possibility of spray application as an alternative to immersion coating, it was of interest to determine if previously unexplored factors associated with bath aging could be controlled to optimize corrosion performance.

Experimental

The evolution of a nitrate-based HT bath chemistry was monitored as a function of bath age and correlated with the corrosion resistance of the resulting coating. Initial investigations consisted of running several baths and removing samples for EIS and CE analysis as a function of bath age. Possible correlations between ion concentrations and corrosion resistance were tested by experiments designed to control the concentration of specific ion.

The initial composition of the bath was 0.3M lithium nitrate, 0.3M potassium nitrate, 0.1M lithium hydroxide, and 0.1M sodium aluminate at 95°C. After degreasing and deoxidization, the panels were coated by immersion in the alkaline lithium salt solution for five minutes. A solution that was continually used was designated a "bath", and each set of panels successively immersed was designated a "run". There were between five to sixteen runs per bath using five (5"x 4") panels / run. The bath volume was 3.5 L. Baths with greater run number were conducted to investigate the effect of extended bath use. An oxidizer, potassium persulfate, was added to some baths to observe the effect of increasing the bath's oxidizing power.

Aliquots were removed from the bath during each run for ionic analysis by Capillary Electrophoresis (CE). CE is a solution analysis technique that possesses high sensitivity and rapid, quantitative detection of ionic species and concentration that has been successfully employed in the field of corrosion science⁸. This technique involves

the separation of species by detecting differences in their ionic mobilities during migration due to an applied electric field. Separation is accomplished by applying high voltage from the injection side of the capillary to the collection side. Migration takes place through a fused silica capillary, and detection of the ions is achieved by ultraviolet absorbance⁹. The concentration of five cations (potassium K^+ , aluminum Al^{3+} , copper Cu^{2+} , sodium Na^+ , and lithium Li^+) and three anions (nitrate NO_3^- , nitrite NO_2^- , and carbonate CO_3^{2-}) were measured in addition to the pH.

The oxidizing power of all the baths was monitored by open circuit potential measurements of the aluminum panels being treated and also by a platinum electrode versus an SCE electrode held remotely via a salt bridge. After being removed from the bath, the panels were air-dried for 24 hours. The panels were then immersed in 0.5M NaCl for 24 hours prior to analysis by EIS. The corrosion resistance of the resulting HT film was measured using the R_{corr} parameter fit from EIS measurements. R_{corr} is the polarization resistance minus the diffusional impedance. This parameter has previously been used in the study of conversion coated aluminum alloys¹⁰.

Results and Discussion

Verification of technique

In order to determine the reliability of the CE procedure for determining the concentration of the different ionic species, an experiment was conducted in which coating baths were produced and left at room temperature without the introduction of aluminum panels for coating. Aliquots from the bath were removed at various times (0, 30, 120, 240, 480 minutes) and analyzed by CE. The calculated and measured concentrations are listed in Table 1. There was good agreement between calculated and measured concentrations for the potassium, aluminum, and nitrate ions. However, the agreement was not as good for the sodium and lithium. The measured lithium concentration was ca. 1.6X the calculated value, while the sodium was 7.5X the calculated value. This experiment was repeated for similar solutions made without sodium aluminate. Neither aluminum nor sodium was detected. Lithium was detected at a similarly elevated concentration relative to the calculated value. It is therefore believed that the elevated sodium is due to contamination in the sodium aluminate. The source of the extra lithium is unknown but may have resulted from reagent contamination. The coefficient of variance (standard deviation / average x 100) was less than 10 for all species except sodium and carbonate. In general, the carbonate concentration was observed to increase with time, which is attributable to the absorption of atmospheric carbon dioxide.

Different carrier electrolytes are used for anion and cation analysis depending on what ions are of interest. For accurate measurements, the samples under investigation should have a pH similar to the carrier electrolyte. The electrolyte most appropriate for measuring the cations of interest had a pH of 3. It was necessary to acidify the aliquots removed from the baths before CE analysis. It was therefore important to assure that the acidification of the aliquots did not alter the results. Using a standard bath solution, the nitrite and nitrate concentrations of three aliquots were analyzed using two electrolytes (one requiring acidification and the other not) that are appropriate for nitrite and nitrate. The results agreed remarkably well. The nitrate concentrations for the acidified and

alkaline aliquots were 20554 +/- 80 and 20504 +/- 74 ppm, respectively, while the nitrite concentration of the acidified and alkaline aliquots were 72 +/- 3 and 75 +/- 4 ppm, respectively. Based on these results, the methods used in measuring the ion concentration were believed to be reliable.

Observed Trends

The chemical and electrochemical parameters previously described were monitored as a function of bath age for several baths. The OCP of both the AA2024 panels and the platinum electrode was observed to increase with run number (Figure 2). The change in the OCP of Pt over the course of 16 runs was greater than the change in the OCP of the AA2024. The corrosion resistance was observed to decrease with run number (Figure 3). With the exception of Al^{3+} , none of the ion concentrations appeared to correlate with the corrosion resistance. Typical variations of the cation (copper, lithium, potassium, sodium) and anion (carbonate, nitrite, nitrate) concentrations as a function of run number for a single bath are shown in Figures 4 and 5, respectively. The aluminum concentration increased with bath age as expected due to continuous dissolution of the panels. The aluminum concentration for several baths is plotted versus run number in Figure 6.

Possible correlations between the corrosion resistance and the ratio of ion concentration were also examined. It was found that the ratio of the nitrite/ nitrate ion concentration increased with time and showed a promising correlation to coating performance (Figure 7). Thus, the observed correlations can be summarized as follows:

$$\uparrow \text{Run number} \propto \uparrow \text{OCP} \propto \downarrow R_{\text{corr}} \propto \uparrow [\text{Al}^{3+}] \propto \uparrow [\text{NO}_2^-/\text{NO}_3^-]$$

The increase in OCP with increasing bath age is counter-intuitive given the increasing nitrite/nitrate ratio. At this time no explanation for this apparent contradiction is forthcoming. The observation of the change in the OCP on the AA2024 and the platinum electrode indicates that the change is a function of the bath redox chemistry and is not restricted to changes in the alloy surface. It is tempting to suggest some role by copper liberated from the alloy, but copper concentrations measured as a function of bath age did not show any consistent trend as seen in Figure 4. As previously mentioned, the chemistry of hydrotalcite baths is dynamic due to the introduction of reactants by alloy dissolution and absorption of atmospheric CO_2 and depletion by precipitation of the HT.

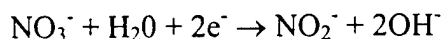
Verification of observed correlations

It was of interest to determine if the observed correlations were causal. The corrosion resistance and the nitrite / nitrate ratio were inversely correlated as seen in a plot of the two parameters as a function of run number (Figure 8). In order to verify this relation, several single run baths were prepared with different initial nitrite and nitrate concentrations. A nitrate chemistry was used for the baths and consisted of five different nitrite/nitrate ratios, 0:1, 1:2, 1:1, 2:1, 1:0, referred to as baths 1-5, respectively. CE was used to measure the actual nitrite/ nitrate ratio (Table 2). The corrosion resistance of the coatings produced in these baths was compared (Figure 9). The bath that was exclusively nitrate (bath 1) produced the coatings with the highest corrosion resistance, while the least corrosion resistant coatings were produced by the nitrite chemistry (bath 5).

Analysis of variance indicated that the Ht coatings produced from bath 1 and bath 2 were statistically equivalent and different from all other baths and that those produced from bath 3 and bath 5 were statistically similar baths. A relationship with bath 4 to the other baths could not be determined since its scatter was too great to distinguish it from the other baths.

Visual inspection revealed distinct differences in the coatings formed by the different baths. Coatings formed in baths 1 and 2 had an olive/gray coloring and a compact coating. The coatings for baths 3 and 5 had a dull silver coloring. The coatings produced from bath 4 had a black and smutty coating (i.e. flakes off when touched).

The effect of different bath components on the OCP was also investigated. The OCP of a platinum electrode and AA2024 panels was monitored for four baths that constitute serial addition of components of the nitrate chemistry. The compositions of the baths are listed in Table 3. The first bath consisted of solely of lithium hydroxide. The second bath consisted of the recipe for nitrate-based coating baths without aluminate. The third bath consisted of the standard nitrate-based solution. An oxidizer, potassium persulfate, was added to the standard nitrate chemistry in the fourth bath. The results for this experiment are shown in Figure 10. The OCP was observed to become more anodic as nitrate, aluminate, and persulfate were added. These confirmed that nitrate acts as an oxidizer in these baths by reduction to nitrite as shown in the following reaction



The reduction of nitrate to nitrite in the presence of aluminum alloys has been reported¹¹.

Although the correlation between corrosion resistance and the nitrite/nitrate ratio has been verified as causal, the relation between the nitrite/ nitrate ratio and the OCP remains unexplained. Nonetheless, this investigation of the effect of bath chemistry evolution has implications for optimization of coating processes. Spray-application is an acceptable, and often preferable, alternative to immersion application that is not subject to the flux of reactants associated with immersion baths. These results can be used for development of “one-use” spray applied chemistries.

Conclusions

- A correlation was observed during the evolution of a nitrate-based HT bath chemistry:

$$\uparrow \text{Run number} \propto \uparrow \text{OCP} \propto \downarrow R_{\text{corr}} \propto \uparrow [\text{Al}^{3+}] \propto \uparrow [\text{NO}_2^-/\text{NO}_3^-]$$
- The relationship between the nitrite / nitrate ratio and the corrosion resistance was verified as causal, however the counter-intuitive relationship between the nitrite/ nitrate ratio and the OCP remains unexplained.

Acknowledgements

This work is sponsored by DARPA (Contract # F49620-96-1-0305) under the direction of Dr. Stephen Wax and Maj. Paul Trulove (AFOSR).

References

1. R.G. Buchheit, M.D. Bode, and G.E. Stoner. *Corrosion*, **50**, 205 (1994).
2. C.J. Serna, J.L. Rendon, and J.E. Iglesias. *Clays and Clay Minerals*, **30**, 180 (1982).
3. G. Marcelin, *The Behavior of Interlayered Water in Open-Hydroxide Layered Lattices, Final Report to GRI*. Rpt. No. GRI92/0212, Gas Research Institute, Chicago, IL (1992).
4. R.G. Buchheit, M.A. Martinez, L.P. Montes, N.P. Cella, S.R. Taylor, and G.E. Stoner, Paper #216, Corrosion 1998. NACE, Houston Texas
5. R.G. Buchheit and M.A. Martinez, U.S. Patent 5,756,218: *Corrosion protective coating for metallic materials* (1998).
6. R. B. Leggat, N.P. Cella, C. Mastrangelo, R.G. Buchheit, S. R. Taylor, *JECS*, submitted.
7. R.G. Buchheit, S.B. Mamidipally, P. Schmutz, and H. Guan, Paper #103, Corrosion 2000. NACE, Houston Texas
8. R.G. Kelly, J. Yuan, C.M. Weyant, K.S. Lewis. *Journal of Chromatography A*, **834**, 433 (1999).
9. J. Krol, M. Benvenuti, and J. Romano, *Ion Analysis Methods for IC and CIA and Practical Aspects of Capillary Ion Analysis Theory*, Waters Corporation, Milford, MA. (1998)
10. R.G. Buchheit, M. Cunningham, H. Jensen, M.W. Kendig, and M.A. Martinez, *Corrosion* **54**, 61 (1998).
11. J. F. McIntyre and T.S. Dow. *Corrosion*, **48**, 309 (1992).

TABLES

Table 1.

	K^+	Al^{3+}	Na^+	Li^+	NO_2^-	NO_3^-	CO_3^{2-}
Calculated (ppm)	10,950	276	235	916	n/a	19,345	n/a
Measured Average (ppm)	12,529	288	1,760	1,429	104	19,253	1,843
Std. Dev.	141	14	176	57	7	274	214
Coeff. of Variance	1	5	10	4	7	1	12

Table 2.

Bath	NO₂⁻ / NO₃⁻ added	NO₂⁻ / NO₃⁻ measured
1	0:1	0.01
2	1:2	0.34
3	1:1	0.64
4	2:1	1.21
5	1:0	7.49

Table 3.

	Composition	pH	OCP Pt (mV_{SCE})	OCP 2024 (V_{SCE})
Bath 1	LiOH (4.2g/L)	11.6	-50	-1.42
Bath 2	Bath 1 + KNO ₃ (28.3g/L) + LiNO ₃ (2.2 g/L)	11.6	-890	-1.26
Bath 3	Bath 2 + Na ₂ Al ₂ O ₄ (600ppm)	11.7	-850	-1.22
Bath 4	Bath 3 + K ₂ S ₂ O ₈ (3.1g/L)	11.7	290	-1.04

Table and Figure Captions

Table 1. Calculated and measured ionic concentrations from nitrate-based HT chemistry at room temperature. Average values measured for five aliquots taken over eight hours.

Table 2. Ratio of nitrite-nitrate added to baths in order to evaluate effect of nitrite / nitrate ratio on corrosion resistance. Ratios based on bath additions and ratios measured by CE listed.

Table 3. Composition of baths in experiments to investigate effect of bath components on OCP of Pt electrode and AA2024 panels.

Figure 1. Atomic structure of hydrolithisite showing anion layer intercalated between lithium-aluminum hydroxide layers. (Reference 3)

Figure 2. OCP of platinum electrode (left axis, \square) and AA2024 (right axis, ∇) versus run number for single bath.

Figure 3. HT coating R_{corr} (left axis, \bullet) and AA2024 OCP (right axis, ∇) versus run number for single bath.

Figure 4. Cation concentrations (copper, lithium, potassium, and sodium) versus run number for single bath.

Figure 5. Anion concentrations (carbonate, nitrate, nitrite) versus run number for single bath.

Figure 6. Aluminum concentrations versus run number for several baths.

Figure 7. Ratio of Nitrite / Nitrate concentrations versus run number for several baths.

Figure 8. HT coating R_{corr} (left axis, \bullet) and [nitrite] / [nitrate] ratio (right axis, Δ) versus run number for single bath.

Figure 9. R_{corr} measured for HT coatings produced by single run baths of varying nitrite/nitrate concentrations.

Figure 10. Effect of bath components on AA2024 open circuit potential. Arrow indicates effect of nitrate.

Figures

Figure 1

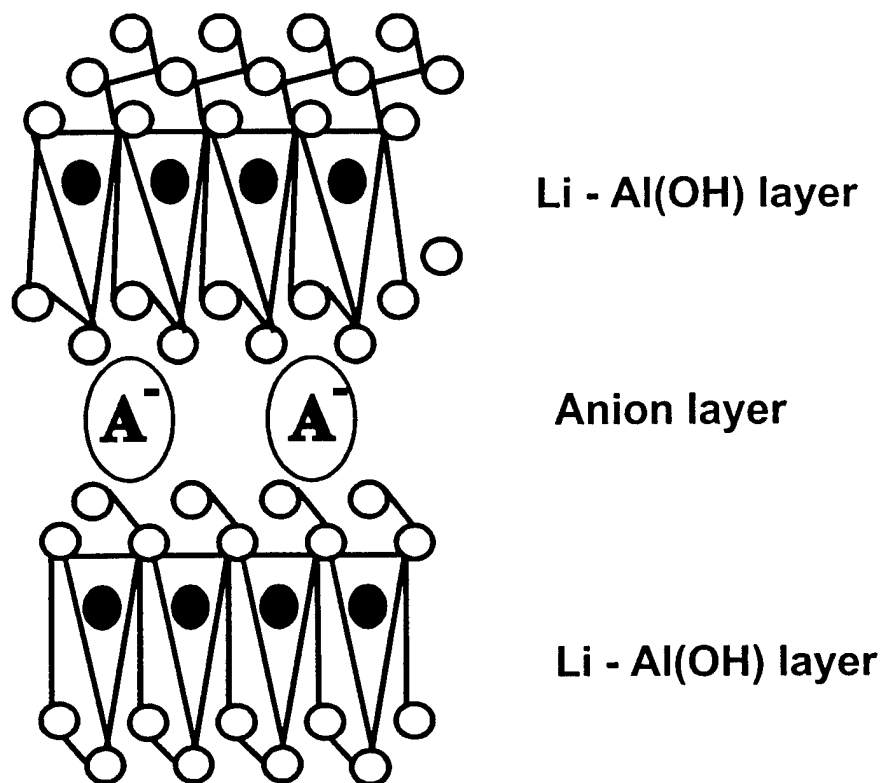


Figure 2

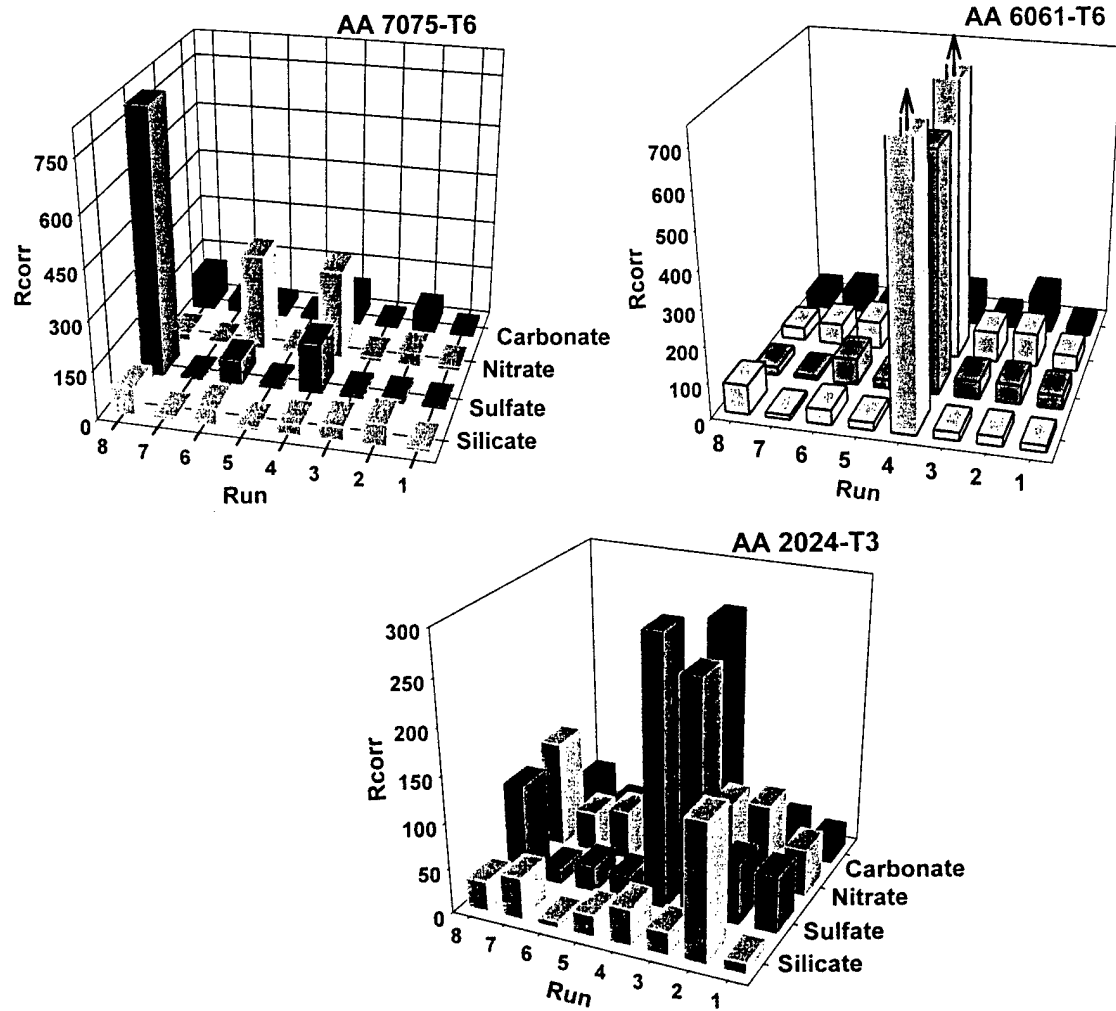
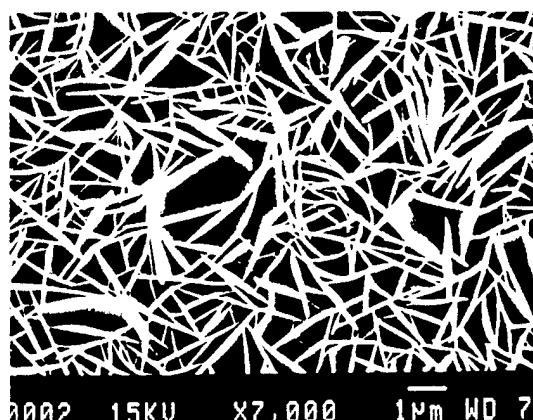
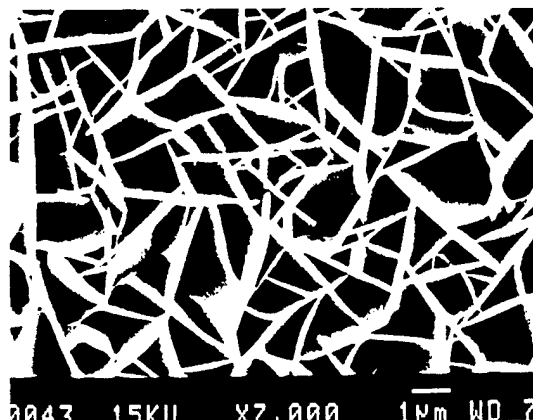


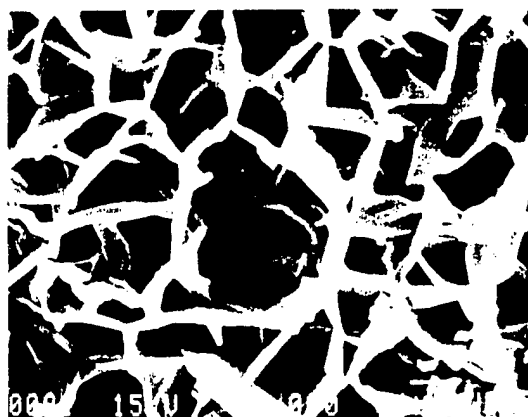
Figure 3



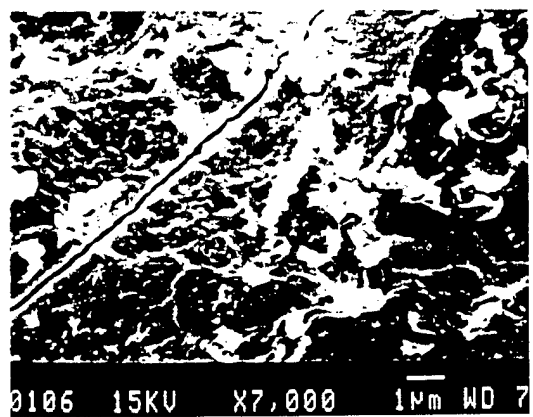
(a)



(b)



(c)



(d)

Figure 4.

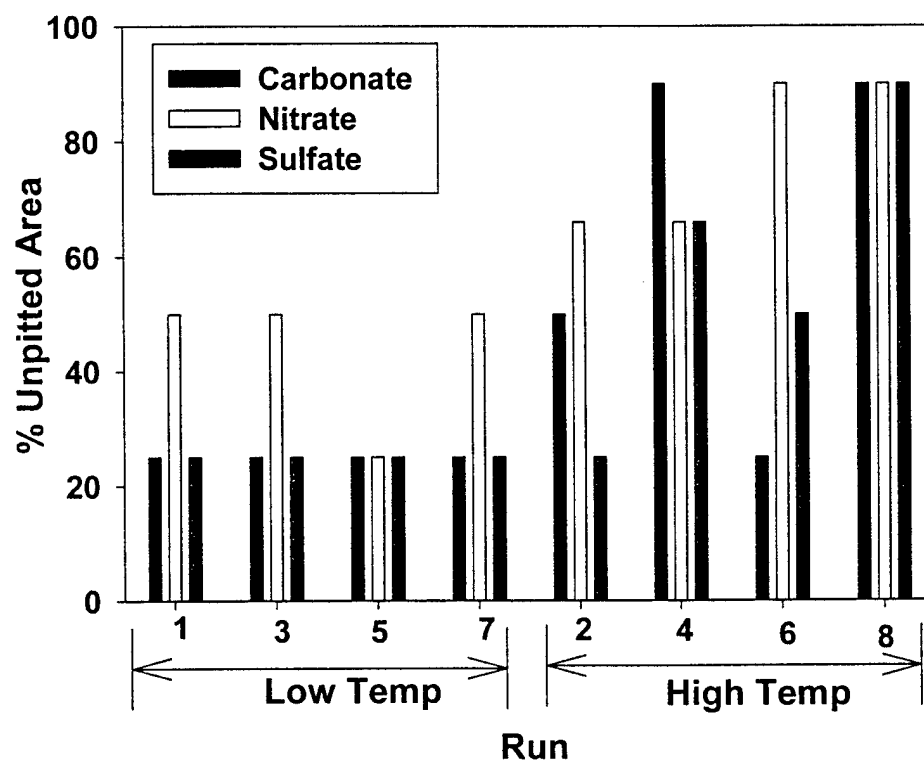


Figure 5.

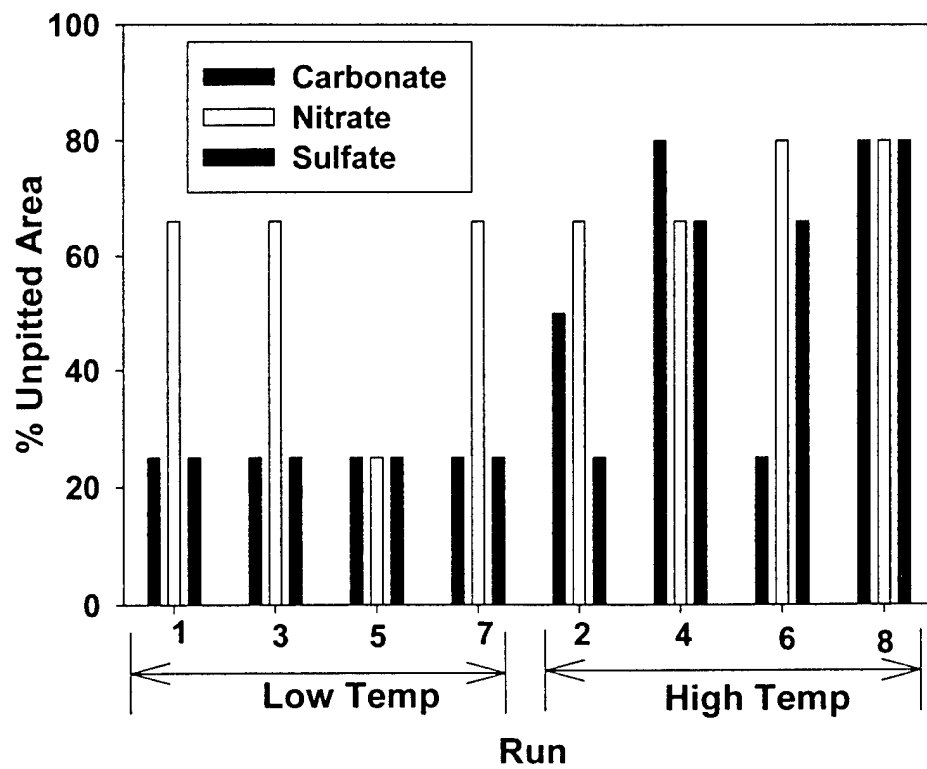
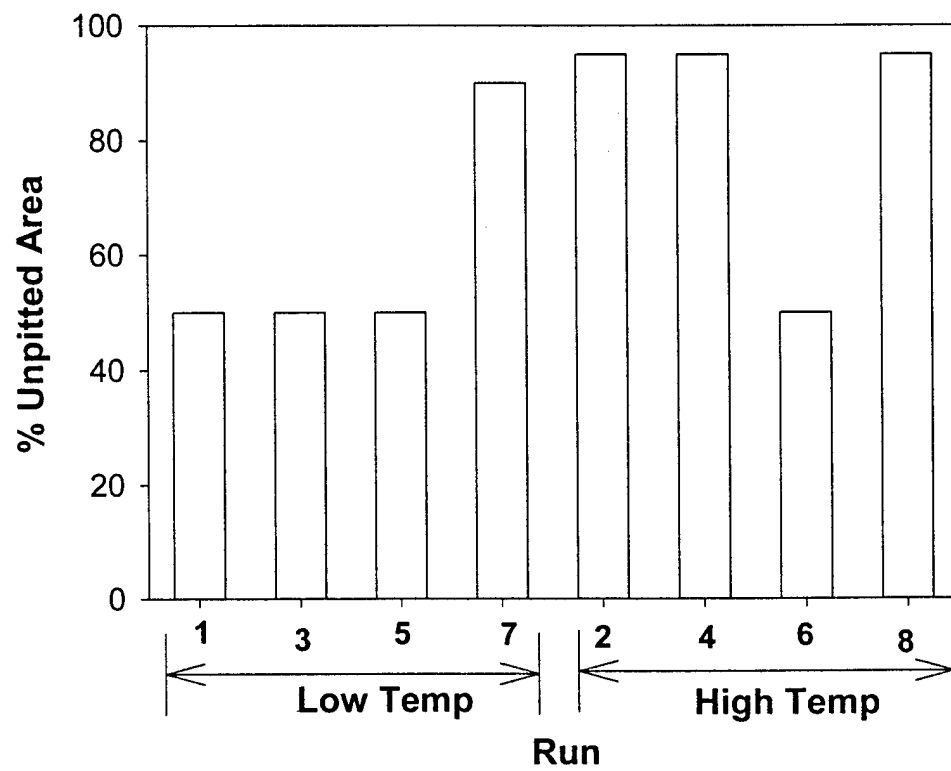


Figure 6.



Copper removal during formation of corrosion resistant alkaline oxide coatings on Al–Cu–Mg alloys

R. G. BUCHHEIT

Mechanical Metallurgy and Corrosion Department, Sandia National Laboratories, Albuquerque, New Mexico 87185, USA

Received 30 December 1996; revised 15 July 1997

The performance of corrosion resistant inorganic oxide coatings formed on Al–Cu–Mg alloys is often degraded by Cu enrichment that occurs during oxide formation. This is particularly true of coating processes conducted in basic solutions. A modification to an alkaline oxide coating process has been made that simultaneously eliminates Cu enrichment and forms a corrosion resistant coating. In this paper, the modified process is described and the resulting coating morphology, structure and composition are reported. Results from electrochemical and exposure corrosion tests show that useful gains in corrosion resistance are achieved. Cu removal during the modified process is rationalized using an argument based on the increase in Cu solubility that occurs in solutions with a pH greater than the solubility minimum for Cu (9.8), and the effect of Cu complexing by carbonate.

Keywords: copper, alloy, copper enrichment, copper removal

1. Introduction

Copper is an important alloying element in commercial aluminium alloys. Copper additions to aluminium, usually in combination with other elements, enable a desirable mix of mechanical properties to be developed through natural and artificial ageing practices. Up to 6.5 wt % Cu is added to wrought heat treatable alloys [1], and up to 14 wt % is added to cast alloys [2]. In binary alloys, the solid solubility of Cu varies from approximately 5.7 wt % at the solidus temperature to 0.05 wt % at room temperature [3]. Cu solubility is sometimes lowered when other alloying elements are present. As a result, much of the copper added to an alloy is segregated into second phase particles.

In many aqueous surface finishing procedures, the presence of Cu in aluminium is problematic. During finishing, the surfaces of work pieces become enriched with a variety of copper compounds, occasionally including metallic Cu, that are collectively referred to as 'smut'. Cu smut forms in etching alkaline degreasing solutions where Cu solubility is low [4]. Less frequently, it is observed to accumulate on surfaces during deoxidizing where aggressive chemical action intended to remove surface oxides attacks the underlying alloy substrate [5]. Metallic copper deposits form because the open circuit potential for the alloy substrate is negative to the reduction potential for Cu (how Cu is liberated from the alloy to begin with has not yet been explained for all relevant environments). Cu smut interferes with conversion coating formation [6], anodization [7] and with bonding of subsequently applied adhesives and paints [6, 8, 9]. It is also sus-

pected to contribute to increased susceptibility to corrosion during service due to galvanic coupling with Cu-rich surface regions.

In aqueous solutions it is thermodynamically possible to use chemical or electrochemical oxidation to remove Cu from aluminium alloy surfaces. It is also possible to use Cu complexing agents to supplement the efficacy of Cu removal by Cu oxidation. Several techniques have been explored experimentally with some success [10]. These techniques have been carried out in advance of conversion coating or anodizing. However, Cu enrichment can occur during the subsequent coating formation processes. It does not appear likely that Cu removal can be achieved after an anodized or conversion coated surface has been formed without degrading corrosion resistance.

A possible remedy to this dilemma is to simultaneously remove Cu while forming the corrosion resistant coating. This has been implemented in a modification to an alkaline oxide coating process that results in the formation of a corrosion resistant coating consisting predominantly of hydrotalcite, $\text{Li}_2[\text{Al}_2(\text{OH})_6]_2\text{CO}_3 \cdot 3\text{H}_2\text{O}$. These coatings are uniform and do not contain Cu in excess of the nominal Cu content of the alloy substrate. Coatings formed on 2024-T3 (Al–4.4Cu–2.5Mg–0.6Mn) using this method exhibit no pitting after 168 hours of salt spray exposure. This level of performance is comparable to that of corrosion resistant grade chromate conversion coatings.

In this paper the modified hydrotalcite coating process is described. The resulting coating morphology, structure and composition are reported for the original hydrotalcite coating process and for the

modified process. Results from electrochemical corrosion testing and standardized salt spray exposure corrosion testing are presented. Last, the phenomenon of Cu removal during coating formation is rationalized using data reported in the literature for Cu solubility and Cu complexing by carbonate.

2. Experimental procedures

2.1. Materials and surface preparation

Aluminium alloy samples 100 mm \times 125 mm \times 2 mm thick were prepared from 2024-T3 (Al-4.4Cu-2.5Mg-0.6Mn) sheet stock and were used for all experiments. In the T3 temper, the alloy is naturally aged for a minimum of 30 days. Copper is segregated into a variety of second phase particles and is also retained in solid solution.

Mill finish surfaces were prepared for coating by washing in an aqueous alkaline detergent solution to remove paint, grease and dirt. Samples were then immersed in a nonetching sodium silicate-sodium carbonate solution at 65°C for 2 min to remove any additional hydrocarbon contamination. Surface deoxidation was performed by immersion in a commercially available nitric acid-sodium bromate solution at 50°C for 2 min [11]. Hydrotalcite coating formation was conducted by immersing samples in a solution comprised of 7.2 g dm⁻³ lithium carbonate, Li₂CO₃, plus 0.4 g dm⁻³ sodium aluminate, NaAlO₂, pH 11.5 for 15 min. At this point, some of the panels were set aside and allowed to air dry in advance of further testing. The remaining samples were then immediately immersed in a solution containing 7.2 g dm⁻³ Li₂CO₃; 7.4 g dm⁻³ lithium hydroxide, LiOH; and 4 g dm⁻³ NaAlO₂ at 55°C for 180 min. This second solution had a pH of approximately 13.5. Samples were rinsed with flowing deionized water in between each processing solution. After processing, these samples were also allowed to dry in air at ambient temperatures. Samples exposed to the first solution only were prepared according to the original hydrotalcite formation process. Samples exposed to both solutions were prepared according to the modified process.

2.2. Characterization of surfaces

The morphology of sample surfaces was examined using scanning electron microscopy (SEM) carried out on an Amray 1645 scanning electron microscope. Grazing incidence angle X-ray diffraction (GIXRD) was used to identify compound present in surface films formed during exposure. Samples were examined using a Siemens D500 diffractometer at a grazing incidence angle of 4°. At this angle, the target sampling depth was approximately 1.0 μ m. Auger electron spectroscopy (AES) and ion etching were used to generate sputter depth composition profiles for elements of interest. AES was conducted using a Physical Electronics PHI 660 scanning auger microprobe.

Sputtering was conducted using a rastered 3 kV Xe⁺ ion beam. Individual element signals were corrected using the appropriate sensitivity factors to generate semiquantitative composition against depth profiles.

2.3. Corrosion testing of coated surfaces

The corrosion resistance of coated surfaces was evaluated using electrochemical impedance spectroscopy (EIS) and salt spray exposure testing. EIS was conducted on coated surfaces exposed to 0.5 M NaCl solution exposed to ambient laboratory air. Measurements were initiated after 24 \pm 1 h of exposure. Measurements were made using a three electrode arrangement (saturated calomel electrode as reference) in a flat cell that exposed 20 cm² of working electrode area. The cell was controlled using a Princeton Applied Research model 273 potentiostat and a Solartron 1255 frequency response analyser controlled by a commercially available software package [12]. EIS spectra were collected over a frequency domain ranging from 10 kHz to 10 mHz using a 10 mV amplitude sinusoidal voltage perturbation. Spectra were collected at a rate of 10 points per decade frequency. EIS data were fitted to an equivalent circuit model using a complex nonlinear least squares fitting routine to extract coating resistances and capacitances.

Salt spray testing was conducted for 168 h per ASTM B117 [13] which specifies exposure of coated panels at 35°C (95°F) to a fog generated by atomizing a 5% NaCl solution and injecting it into an enclosed exposure chamber. After exposure, samples were rinsed in deionized water and visually inspected for evidence of corrosion damage.

3. Results

3.1. Hydrotalcite coating

Degreasing and deoxidizing procedures were carried out prior to coating to remove organic debris and surface oxide films. Sample surfaces exhibited a dull metallic finish indicating very slight etching during deoxidation. Upon immersion in to the pH 11.5 Li-salt solution, vigorous hydrogen evolution occurred and a black to grey surface film developed. Hydrogen evolution ceased within 2 min of initial exposure although samples were immersed for a total of 15 min. A group of samples were removed and withheld from further processing and retained for surface analysis and corrosion testing, the remainder were further processed by exposure to the pH 13.5 Li-salt solution. Upon immersion in this solution, samples once again evolved hydrogen at a moderate to slow rate for a period of up to 5 min. The surface then changed colour from black or grey to green yellow and eventually cleared leaving a white translucent coating. The colour transformation was complete within 60 min although samples were immersed in this solution for a

total of 180 min. In all cases the coatings formed were thin and adherent to the alloy substrate.

3.2. Surface characterization

Surfaces of samples from each group were examined by SEM, grazing incidence X-ray diffraction (GI-XRD), and auger electron spectroscopy (AES). Figure 1 is a scanning electron micrograph of a 2024-T3 surface after exposure in the pH 11.5 Li-salt solution. The surface film is featureless except for cracks that probably formed as the film shrank during drying. Figure 2 shows the surface morphology after the additional 180 min exposure to the pH 13.5 Li-salt solution. In this case, the distinctive surface morphology associated with hydrotalcite coatings is observed [14]. The coating shown in Figure 2 is continuous across the surface and forms over Cu, Mg, and Fe-rich second phase particles present in the alloy. Figure 3 illustrates the continuity of the coating using a topology sensitive secondary electron imaging (SEI) mode. Figure 4 shows the same region imaged using a composition sensitive backscattered electron imaging (BEI) mode. This micrograph reveals the location of Cu and Fe-rich particles in the image frame of Figure 3. Comparison of Figs 3 and 4

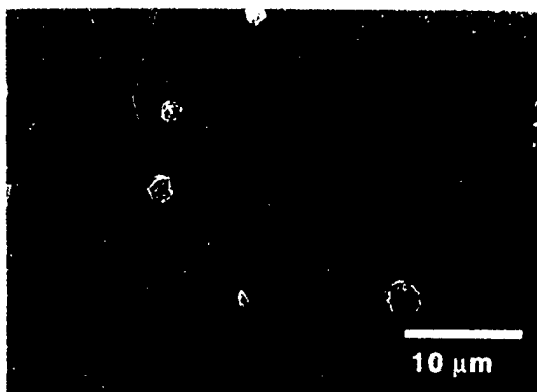


Fig. 1. SEM of a 2024-T3 surface after exposure to the pH 11.5 Li-salt solution for 15 min.

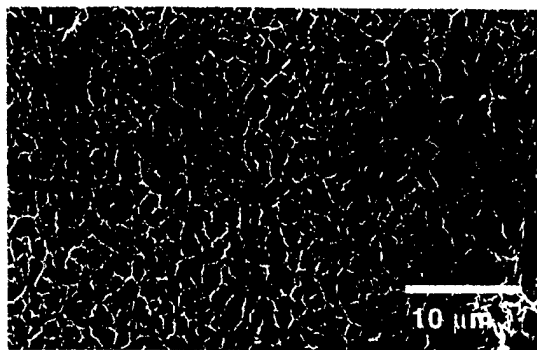


Fig. 2. SEM of a 2024-T3 surface after exposure to pH 11.5 Li-salt solution for 15 min followed by exposure to pH 13.5 Li-salt solution for 180 min.

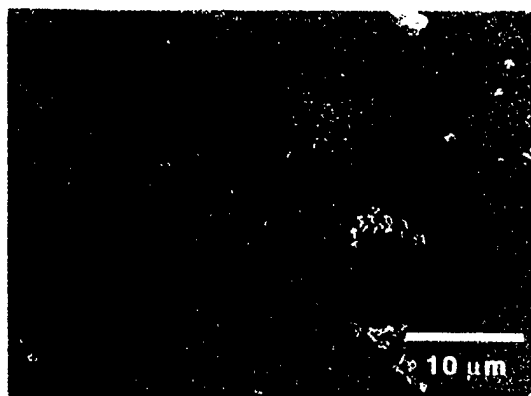


Fig. 3. SEI of 2024-T3 after exposure to pH 11.5 and 13.5 Li-salt solutions showing uniform coating coverage.

shows that the coating forms without interruption over the solute-rich second phase particles.

Figures 5 and 6 show oxygen, copper and aluminium sputter depth profiles for the surface of 2024-T3 with and without exposure to the pH 13.5 solution. Figure 5 shows the depth profiles for Al, O and Cu for a surface after exposure to the pH 11.5 solution. A Mg profile was also collected, but has been omitted for clarity. The surface film and substrate regions can be clearly distinguished by the sharp decrease in the oxygen signal and the corresponding increase in Al signal after 2000 s of sputtering time. The Cu profile exhibits a broad maximum with a peak concentration that is approximately four times the concentration present in the alloy substrate. As has been found in other studies, this maximum occurs near the oxide-metal interface [7]. It should be noted that there was also a maximum in the Mg profile at the same position noted for Cu. The level of peak Mg enrichment was also approximately four times that observed in the alloy substrate.

Figure 6 shows depth profiles after exposure to the pH 13.5 solution. As in Fig. 5, the oxide metal interface is reached after approximately 2000 s of sputtering indicating little or no net change in coating thickness during exposure to the pH 13.5 solution

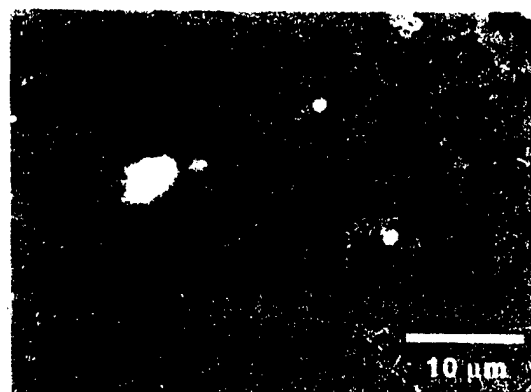


Fig. 4. BEI of the same region shown in Fig. 3 indicating the location of Cu, Fe, Mn-rich second phase particles (bright spots) covered by the coating.

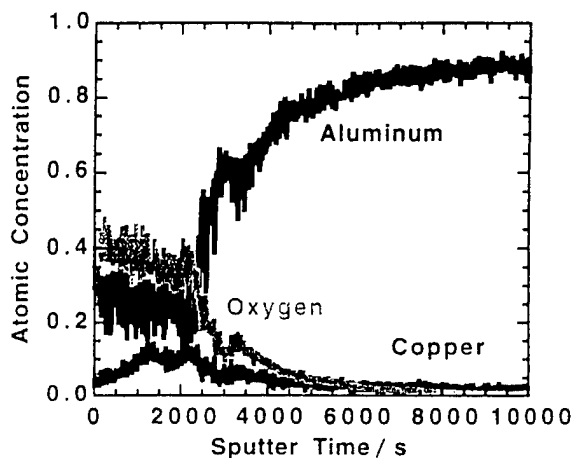


Fig. 5. Al, O and Cu sputter depth profiles from the surface film formed after exposure to the pH 11.5 solution.

assuming similar sputter rates for each oxide film. In this case, the maximum in the Cu concentration profile is absent showing that exposure to this solution removes Cu from the coating. The maximum in the Mg concentration profile detected after pH 11.5 exposure was also eliminated.

Figure 7 shows GIXRD patterns for 2024-T3 surfaces with and without exposure to the pH 13.5 Li-salt solution. The lower pattern is from the surface exposed to the pH 11.5 solution. This pattern contains the major reflections for aluminium from the underlying substrate (at 38° and $44^\circ 2\theta$) and for $\text{Al}(\text{OH})_3$ as bayerite which is present in the surface coating. The pattern also contains reflections near $30^\circ 2\theta$ that could not be conclusively indexed. The upper GIXRD pattern is from a surface after exposure to the pH 11.5 solution and the pH 13.5 solution. Aluminium and bayerite reflections are again observed. Additional reflections due to hydrotalcite are observed. The unindexed reflections near 30° in the lower pattern are now absent suggesting that they were associated with a Cu or Mg-containing com-

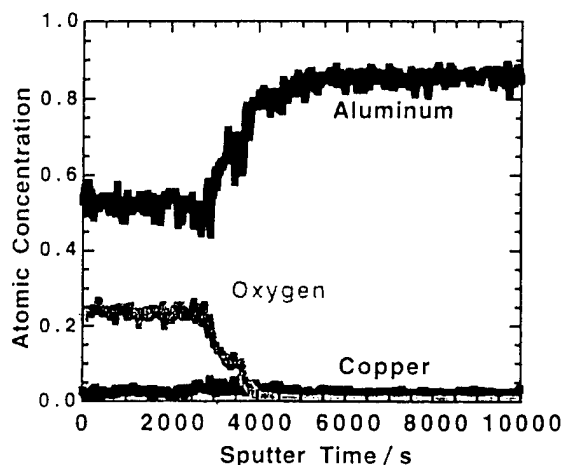


Fig. 6. Al, O, and Cu sputter depth profiles from the surface film formed after exposure to the pH 11.5 and 13.5 Li-salt solutions.

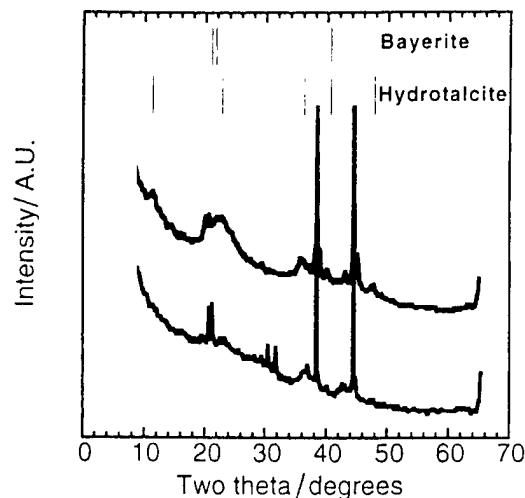


Fig. 7. GIXRD patterns from surfaces of 2024-T3 exposed to pH 11.5 solution (lower) and both the pH 11.5 and 13.5 solutions (upper). Uppermost hashes indicate locations of major bayerite and hydrotalcite reflections.

pound that was removed during exposure to the pH 13.5 solution.

Coating thicknesses were not directly measured in these experiments. However, based on prior work, it is known that the hydrotalcite films formed on 99% pure Al in a pH 13.5 solution are 3 to $5\ \mu\text{m}$ thick [4]. These thicknesses are appropriate estimates for the coatings formed in these experiments.

3.3. Corrosion resistance

In both electrochemical and salt spray exposure corrosion testing, the results of which are described below, corrosion resistance increased in the order: uncoated < coated in pH 11.5 solution \ll coated in pH 11.5 and 13.5 solutions. The corrosion resistance of the samples treated in both solutions was great enough that no pitting was observed after 168 h of salt spray exposure. Bare surfaces and surfaces coated in the pH 11.5 solution were heavily corroded and were virtually indistinguishable after salt spray testing.

Figure 8 shows impedance data in Bode magnitude and Bode phase angle plot formats for 2024-T3 surfaces in the three conditions of interest. On a qualitative basis, these spectra can be interpreted using an equivalent circuit (EC) model proposed for damaged porous aluminium oxide surfaces [15–17]. The model accounts for contributions to the spectra from the oxide covered surface and from damage due to pitting in the experimentally accessible portions of the frequency domain.

The selection of the EC model used to fit the EIS data is based in part on the structure of the hydrotalcite coating shown in Fig. 9. This figure shows a cross section of the coating in which the substrate, a dense inner layer, and a porous outer layer can be identified. Figure 10 is an idealized physical representation of the coating showing the two layers of the coating. The model accounts for the

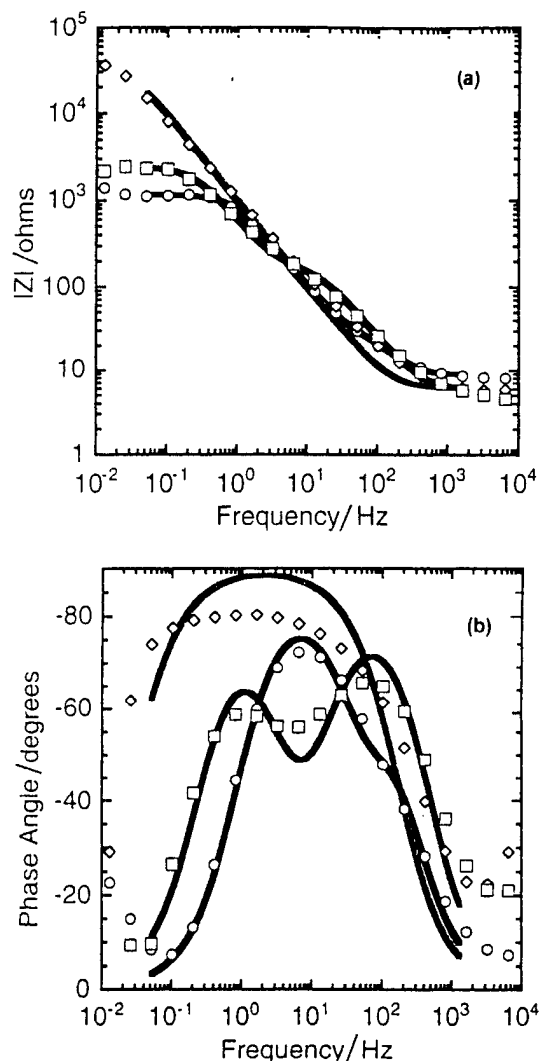


Fig. 8. Bode magnitude (a) and phase angle (b) plots for 2024-T3 surfaces in the three conditions of interest after 24 h of exposure to 0.5 M NaCl. Markers represent EIS data, lines represent the CNLS fit. Key: (O) bare, (◇) pH 11.5 and 13.5, (□) pH 11.5.

presence of pits for situations when damage has occurred. Figure 11 shows an EC model constructed using discrete circuit elements derived from the physical model of Fig. 10.



Fig. 9. TEM cross section of the hydrotalcite coating showing two distinguishable layers in the coating.

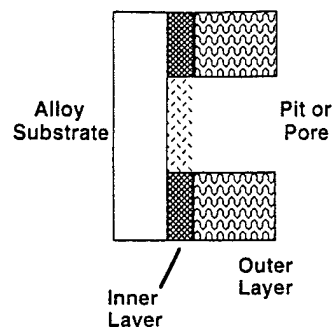


Fig. 10. Idealized physical model of the coating.

In this model, F represents the area fraction of the surface that is pitted. R_{sol} is the solution resistance. R_1 and C_1 , and R_2 and C_2 represent resistances and capacitances associated with the two layers of the coating. R_{pit} is a resistance due to the pit solution and R_{corr} and C_{corr} describe the faradaic reactions occurring within the pit. The use of this specific model and the appropriateness of discrete or distributed circuit elements is still the subject of some debate. However, this model is judged to be suitable for the purposes of evaluating relative differences in corrosion resistance among the samples studied here.

In Figure 8 the experimentally determined EIS data are indicated with symbols. The continuous lines indicate the CNLS fit from the EC model. In the Bode magnitude plot, the bare 2024-T3 sample and the one exposed to the pH 11.5 solution exhibit well defined d.c. limits between 1 and $2 \times 10^3 \Omega$. The plot for the sample exposed to the pH 11.5 and 13.5 solutions exhibits a far more capacitive response and does not reach a well defined d.c. limit at 10^{-2} Hz. In the context of the damage porous aluminium oxide EC model, this response is consistent with a significant amount of damage by pitting for the bare and pH 11.5 samples and little pitting damage for the pH 11.5 and 13.5 sample. Visual observation after testing confirmed this to be the case. The 2024-T3 sample exposed to the pH 11.5 solution exhibits a slightly greater d.c. limit than the bare sample. This response indicates marginally better corrosion resistance compared to bare surfaces. Visual examination

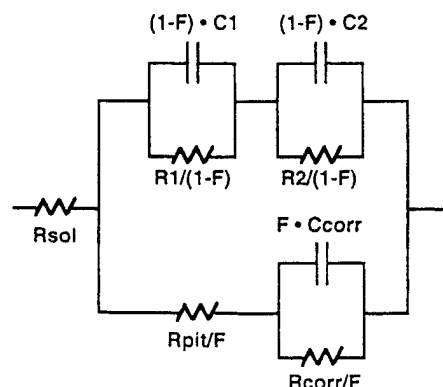


Fig. 11. Generalized equivalent circuit model used to fit EIS data.

showed that this surface was pitted after testing, but suffered noticeably less damage than the bare surface.

Examination of the phase angle plot in Fig. 8 shows that the bare 2024-T3 sample exhibits a single time constant likely due to pitting. In contrast, the sample exposed to the pH 11.5 solution exhibits two discrete time constants, one due to pitting, the other is likely due to the incompletely protective coating. The sample exposed to the pH 11.5 and 13.5 solutions exhibits a broad, somewhat lossy capacitive region.

Values for the circuit elements defined in the EC model are shown in Table 1. The parameters in Table 1 have been normalized by electrode area (20 cm^2), not by fractional area pitted which varied from sample to sample and was not measured. For a surface with a fractional pitted area, F , the elements are solution resistance (R_{sol}), pit electrolyte resistance (R_{pit}/F), pit corrosion resistance (R_{corr}/F), pit capacitance (FC_{corr}). The latter two elements were taken as the primary figures of merit for determining coating corrosion resistance. An explicit accounting of a duplex coating was made by using the two parallel R-C nets comprised of $R_1/(1-F)$, $(1-F)C_1$, $R_2/(1-F)$, and $(1-F)C_2$. However, these elements were not assigned to specific layers of the coating and, as shown in the Table, each element was not always required for a CNLS fit.

The R_{corr}/F value of $3.4 \times 10^4 \Omega \text{ cm}^2$ and FC_{corr} value of $3.9 \times 10^{-4} \text{ F cm}^{-2}$ are consistent with pitting corrosion of bare 2024-T3 exposed to an aerated chloride solution. The increase in R_{corr}/F and decrease in FC_{corr} shown in Table 1 indicate a slight decrease in pitting corrosion for the sample exposed to the pH 11.5 solution. However, the sample exposed to both the pH 11.5 and 13.5 solutions exhibits an R_{corr}/F value of $3.4 \times 10^6 \Omega \text{ cm}^2$ indicating high corrosion resistance.

4. Discussion

4.1. Origin of copper

In 2024-T3 copper is dissolved in solid solution in the matrix phase of the alloy and is concentrated in to a variety of second phase particles. Predominant particles include $(\text{Al,Cu})_6(\text{Mn,Fe,Cu})$, $\text{Al}_7\text{Cu}_2\text{Fe}$, $(\text{Al,Cu})_6\text{Mn}$, and Al_2CuMg [18]. During surface finishing in extremely alkaline or acid solutions, Cu surface enrichment likely occurs by particle dissolu-

tion and dealloying and possible dealloying of the matrix phase. Details of how Cu is extracted and redistributed from noble second phase particles across the surface have not been fully explained, but the phenomenological evidence indicates that the process does occur [19, 20].

Among these second phase particles listed, the Al_2CuMg type should be singled out, because it may contribute significantly to Cu enrichment at surfaces. These particles form during solidification and never fully redissolved in any subsequent thermomechanical processing. Al_2CuMg has been observed to make up 60% of the population of second phase particles 0.5 to $10\text{ }\mu\text{m}$ diameter range [20]. Electrochemical characterization experiments with the compound synthesized in bulk form suggest that it can be electrochemically active with respect to the surrounding microstructure [21].

4.2. Copper removal by alkaline carbonate solutions

In terms of corrosion resistance, the primary beneficial effect is derived by exposure to the pH 13.5 solution, but sequential exposure to both solutions must be used to avoid inferior performance. In the pH 11.5 solution, surface oxide formation is rapid and little substrate etching occurs. This coating offers little corrosion resistance, but does suppress etching that would otherwise occur during exposure to the pH 13.5 solution. In this second solution, improved corrosion resistance is developed. Cu is removed from the surface, and the oxide layer is converted to a more protective hydrotalcite coating.

Two factors appear to contribute to the removal of Cu observed during exposure to the pH 13.5 solution. These are: (i) the increased Cu solubility and (ii) the formation of stable cupric carbonate complex that shifts the Cu reduction potential to values more negative than the open circuit potential for the alloy.

Figure 12 shows the total Cu solubility as a function of solution pH [22]. Copper exhibits a solubility minimum at pH 9.8 to 10 where $\log[\text{Cu}^{2+}] = -9.48$. For coating solutions in the pH 11.0 to 11.5 range, which is the pH of the first coating bath, the total Cu solubility remains less than 10^{-8} M . Formation of a Cu-rich oxide layer on the alloy surface is not an unexpected phenomenon. However, beyond the solubility minimum, total Cu species solubility increases with increasing pH. At pH 13.5 the Cu solubility increases approximately four orders of magnitude to $2 \times 10^{-4}\text{ M}$.

Table 1. Summary of values obtained from CNLS fitting of EIS spectra

Sample	R_{sol} Ω	R_{pit}/F $\Omega \text{ cm}^2$	R_{corr}/F $\Omega \text{ cm}^2$	FC_{corr} F cm^{-2}	$R_1/(1-F)$ $\Omega \text{ cm}^2$	$(1-F)C_1$ F cm^{-2}	$R_2/(1-F)$ $\Omega \text{ cm}^2$	$(1-F)C_2$ F cm^{-2}
Bare	8.2	0.9×10^3	3.4×10^4	3.9×10^{-4}	7.4×10^4	3.9×10^{-6}	—	—
pH 11.5	5.9	—	1.2×10^5	1.4×10^{-5}	7.7×10^4	2.2×10^{-6}	3.5×10^3	1.5×10^{-6}
pH 11.5 and 13.5	6.1	—	3.4×10^6	4.7×10^{-6}	9.9×10^5	4.2×10^{-6}	—	—

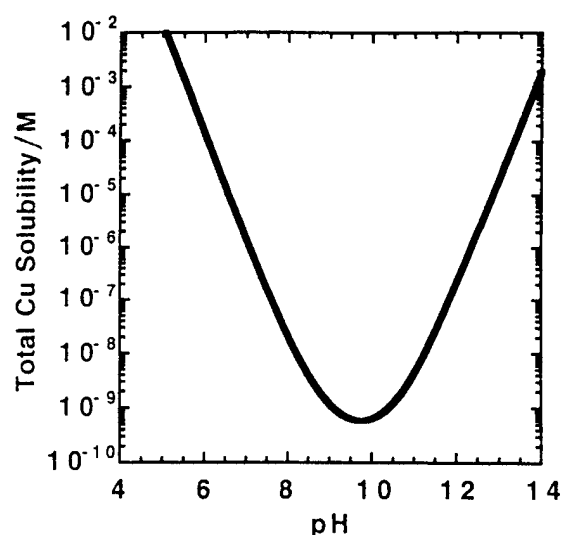
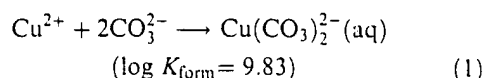


Fig. 12. Total equilibrium Cu solubility as a function of pH computed assuming a CuO-saturated solution and speciation of Cu^{2+} among dominant soluble hydrolysis products [23].

In the carbonate solutions used here, there is an added contribution to Cu solubility by formation of a stable cupric carbonate complex, $\text{Cu}(\text{CO}_3)_2^{2-}$. This complex forms according to the following reaction [23]:



where K_{form} is the formation constant for the complex. The formation of $\text{Cu}(\text{CO}_3)_2^{2-}$ increases the ability of these solutions to dissolve and retain Cu from coated surfaces by an additional three orders of magnitude. The magnitude of this effect is estimated by calculating the solubility limit for $\text{Cu}(\text{CO}_3)_2^{2-}$ in equilibrium with malachite, $\text{Cu}(\text{OH})_2(\text{CO}_3)$, which is a likely Cu compound in the oxide film formed in the pH 11.5 solution [23]:

$$[\text{Cu}(\text{CO}_3)_2^{2-}] = K_{\text{form}} \times K_s \times K_{a1} \times K_{a2} = 0.5 \text{ M} \quad (2)$$

where K_{form} is the formation constant from Equation 1, K_s is the solubility product for malachite ($\log K_s = 6.49$), K_{a1} and K_{a2} are the acid dissociation constants for bicarbonate and carbonate ($\log K_{a1} = -6.37$, $\log K_{a2} = -10.25$).

Redeposition of Cu^{2+} in solution onto the alloy surface is possible but may be restricted in the pH 13.5 solution since the Cu reduction potential is shifted to a value that is equal to or more negative than the measured open circuit potential for the alloy. At pH 13.5 the Cu/Cu(OH)₂ reduction potential is given as follows [4]:

$$E_{\text{Cu/Cu(OH)}_2} = 0.609 - 0.0591 \text{ pH} = -0.189 \text{ V}_{\text{SHE}} \text{ or } -0.430 \text{ V}_{\text{SCE}} \quad (3)$$

The reduction potential is shifted in the negative direction due to $\text{Cu}(\text{CO}_3)_2^{2-}$ formation by an amount V given by

$$V = 2.303 (RT/nF) \log K_{\text{form}} = -0.291 \text{ V} \quad (4)$$

where the gas constant R is $8.31 \text{ J K}^{-1} \text{ mol}^{-1}$, T is 298 K, n is 2 equiv. mol^{-1} , and Faraday's constant is $96500 \text{ C equiv}^{-1}$. The corrected Cu/Cu(OH)₂ reduction potential becomes $-0.721 \text{ V}_{\text{SCE}}$ which is negative to the typical open circuit potential for oxide covered 2024-T3 (-0.700 to $-0.500 \text{ V}_{\text{SCE}}$) [5].

5. Summary

A two stage hydrotalcite coating process involving exposure to a pH 11.5 Li-salt solution followed by exposure to a pH 13.5 solution produces corrosion resistant hydrotalcite films on Al-Cu-Mg alloys. These films are free from Cu in excess of the concentration present in the alloy. Oxide films formed using this method exhibit total impedances greater than $10^6 \Omega \text{ cm}^2$ after 24 h exposure to aerated 0.5 M NaCl and withstand 168 h of salt spray exposure without pitting. Cu appears to accumulate in oxide films formed during exposure to pH 11.5 Li-salt solutions, but is subsequently removed when samples are exposed to a pH 13.5 solution due to increased Cu solubility and complexing by carbonate.

Acknowledgements

This work was performed at Sandia National Laboratories sponsored by the US Department of Energy under contract no. DE-AC04-94AL85000. M. Martinez, W. Buttry, B. McKenzie are thanked for their assistance in sample preparation and analysis.

References

- [1] J. E. Hatch (Ed.), 'Aluminum: Properties and Physical Metallurgy', ASM, Metals Park, OH (1984) p. 321.
- [2] L. F. Modolfo (Ed.), *ibid.*, p. 693.
- [3] *Idem, ibid.*, p. 254.
- [4] M. Pourbaix, 'Atlas of Electrochemical Equilibria in Aqueous Solutions', NACE, Houston, TX (1974) p. 389.
- [5] C. A. Drewien and R. G. Buchheit, paper 622, Corrosion '94, NACE, Houston, TX (1994).
- [6] N. Fin, H. Dodink, A. E. Yaniv and L. Drori, *Appl. Surf. Sci.* **28** (1987) 11.
- [7] J. S. Solomon and N. T. McDevitt, *Thin Solid Films* **84** (1981) 155.
- [8] A. V. Pocius, T. H. Wilson, Jr., S. H. Lundquist and S. Sugii, in 'Progress in Advanced Materials and Processes: Durability, Reliability and Quality Control' (edited by G. Bartelds and R. J. Schekelmann), Elsevier Science, Amsterdam (1985) 71.
- [9] T. S. Sun, J. M. Chen and J. D. Venables, *Appl. Surf. Sci.* **1** (1978) 202.
- [10] F. Mansfeld and L. Kwiatowski, 'Surface Treatment of High-Cu Aluminum Alloys', University of S. California, Interim Report (1992).
- [11] Sanchem 1000, Sanchem, Inc., Chicago, IL.
- [12] ZPlot for Windows™, Scribner Associates, Charlottesville, VA.
- [13] ASTM B117, Standard Method of Salt Spray (Fog) Testing, v. 3.02, 'Annual Book of ASTM Standards', American Society for Testing and Materials, Philadelphia, PA (1993) 19.
- [14] R. G. Buchheit, M. D. Bode and G. E. Stoner, *Corrosion* **50** (1994) 205.

-
- [15] J. Hitzig, K. Juttner and W. J. Lorenz, *J. Electrochem. Soc.* **133** (1986) 887.
- [16] F. Mansfeld and M. W. Kendig, *ibid.*, **135** (1988) 828.
- [17] F. Mansfeld, S. Lin, S. Kim and H. Shih, *Electrochim. Acta* **34** (1989) 1123.
- [18] G. Phragmen, *J. Inst. Metals* **77** (1950) 459.
- [19] B. Mazurkiewicz and A. Piotrowski, *Corros. Sci.* **23** (1983) 697.
- [20] R. G. Buchheit, R. P. Grant, P. F. Hlava, B. A. McKenzie and G. L. Zender, *J. Electrochem. Soc.* **144** (1997) 2621.
- [21] K. Urushino and K. Sugimoto, *Corros. Sci.* **19** (1979) 225.
- [22] C. F. Baes, Jr. and R. E. Mesmer, 'Hydrolysis of Cations', R. E. Krieger Publishing, Malabar, FL (1986) 268.
- [23] P. Schindler, M. Reinert and H. Gamjager, *Helv. Chim. Acta* **51** (1968) 1845.

Surface Conversion of Aluminum and Ferrous Alloys for Corrosion Resistance, Proceedings of CORROSION/2000, R.G. Buchheit, M.R. Jaworoski, P.D. Chalmer, Eds., Houston TX (2000), p. 67-92.

Active Corrosion Protection in Chromate and Chromate-Free Conversion Coatings

R.G. Buchheit, S.B. Mamidipally, P.Schmutz, H. Guan
Fontana Corrosion Center
Department of Materials Science
Ohio State University
Columbus, Ohio 43210

ABSTRACT

Chromate conversion coatings are noted for their ability to self-heal if damaged by mechanical or chemical action provided the damage is not too severe. Self-healing, or active corrosion protection (ACP), involves release of chromate from the coating, its transport through solution, and its action at the site of damage; namely pits. A simple exposure cell, named the "simulated scratch cell", was recently devised by Zhao and co-workers to reproducibly examine chromate conversion coatings for evidence of these elements. This cell consists of two aluminum alloys surfaces, one coated and one bare, separated by a few millimeters of an aggressive solution. If a coating exhibits ACP, the inhibiting agent will be released into solution, interact with the bare surface, and stifle corrosion. Each of these elements can be readily tested by standard laboratory methods. Given these testable elements for ACP, and methods of examining for them, several chromate-free conversion coatings were studied for evidence of ACP. Candidate coatings were formed on AA 2024-T3 substrates by modifying, hydrotalcite coatings with Ce and Mn oxides. The key to imparting ACP in these coating systems is the use of Ce and Mn, which can exist as either a soluble high oxidation state oxide, or an insoluble lower oxidation state oxide depending on local oxidizing conditions and pH. Results of experiments based on the simulated scratch cell show that when high oxidation state oxides are introduced to hydrotalcite, they can be dissolved by a contacting solution, transported to defect sites on bare aluminum samples where they are reduced and precipitated elsewhere to inhibit further corrosion. These experiments show that self-healing is possible with conversion coatings other than those based on chromates.

INTRODUCTION

Chromate conversion coatings have been a mainstay in the repertoire surface finishing technologies for aluminum, zinc, ferrous alloys, cadmium, and other alloys for over 50 years. These coatings provide good resistance against atmospheric corrosion, and are excellent bases for primers and paints. Chromate conversion coatings are

distinguished by the ease with which they are applied, their applicability to a wide range of metals and alloys, and in many cases, their ability to resist corrosion by virtue of a built-in inhibitor reservoir that can provide additional corrosion protection beyond the barrier protection afforded by a thickened oxide layer.

Built-in, or "active" corrosion protection is distinguished from "passive" corrosion protection, which is due to a thickened barrier oxide film on a metal surface. Active corrosion protection (ACP) by conversion coatings is less important when the coating is used as base for paints and primers that are good barriers and contain soluble chromate inhibitors themselves. However, in situations where the conversion coating is the primary barrier against corrosion, ACP is critical. This allows the component surface to withstand minor mechanical and chemical damage during service without continued, detailed maintenance.

As is now well documented, chromium is being eliminated as an ingredient in metal finishing operations due to its poisonous effects on people and the environment. Over the past 15 years, a vigorous effort to minimize chromium release into the environment has developed. Part of this activity has focussed on development of chromate-free conversion coating technologies. In the case of aluminum alloys, the search for a suitable replacement has been complicated by the stringent performance requirements imposed in industrial and military specifications. A plethora of chromate-free technologies has emerged. Some of these coating are used on a commercial basis. However, none are used as widely, or as comfortably, as chromate conversion coatings. Arguably, part of the reason for lack of widespread implementation is that few if any of the chromate-free conversion coatings exhibits active corrosion protection, otherwise known as "self-healing".

ACTIVE CORROSION PROTECTION AND CHROMATE CONVERSION COATINGS

According to the most current views, chromate conversion coatings are a mixture of hydrated amorphous Cr(III)-Cr(VI) oxide (1), hydrated aluminum oxide, ferri/ferrocyanides (1,2,3), and small to moderate quantities of alloying elements from the substrate and minor ingredients added to commercial formulations. Coating thicknesses range from 50 nm to 2-3 μm , depending on bath chemistry and contact time. The total amount of Cr(VI) has been estimated to range anywhere from 6 to 50% (4,5,6). In freshly formed coatings a substantial fraction is reversibly bound in the mixed oxide, and may be leached when solution contacts the coating. With time, the leachable fraction of chromate decreases. Beyond their leachable chromate component, these coatings are largely insoluble and provide barrier protection of the underlying aluminum substrate.

There is both indirect and direct evidence supporting the idea that leached Cr(VI) results in dynamic repair by interaction with incipient defects in the coating. Figures 1a

and b show the accumulation of pitting damage as a function of exposure time for chromate and chromate-free conversion coatings due to salt spray testing (7). Results from chromate-free coatings are collected in Figure 1a, and results from chromate conversion coatings are collected in Figure 1b. In these figures, the smaller the pitting resistance index (PRI), the greater the accumulation of pitting damage. A comparison of the data in these figures shows two distinct behaviors. In Figure 1a, the PRI for many of the chromate-free coatings is high initially, and remains high for times as long as 200 hours. However, once pitting damage is initiated, it accumulates very rapidly. Correspondingly, the PRI drops off precipitously. This behavior appears to be characteristic of barrier protection. An intact barrier film is capable of resisting attack initially, but once the barrier is breached exposing bare metal, corrosion damage accumulates quickly.

A different behavior is exhibited by chromate conversion coatings. Figure 1b shows the PRI for several different commercial chromate conversion coatings. In this case, the PRI begins and remains high for over 1000 hours of exposure. Pitting does occur, as indicated by the slight decrease in PRI, but no precipitous decrease occurs indicating the rapid accumulation of damage. This behavior is attributed to active corrosion protection. Chromate leaches from the coating and acts at incipient pits prohibiting their propagation.

Clearly, the interpretation offered above for the data in Figure 1 is debatable. However, recent experiments provide a far more definitive indication of active corrosion protection. To test for ACP, Zhao et al., devised a special cell consisting of a chromate conversion coated surface and an opposing, uncoated alloy surface separated by a 1.8 mm thick O-ring (8). The space inside the O-ring and between the opposing surfaces was filled with 0.1 M NaCl. Any chromate detected on the bare surface after exposure in this cell would presumably originate from the CCC, migrate through solution and deposit on the bare surface. This simple approach, termed a "simulated scratch cell", enables rigorous examination of the requisite elements of active corrosion protection in a manner that is reproducible from experiment to experiment.

Zhao made polarization resistance measurements of initially bare surfaces after various lengths of exposure time in the simulated scratch cell. Polarization resistances increased from about $10^4 \Omega \text{ cm}^2$ to $10^6 \Omega \text{ cm}^2$ after 48 hours of exposure. In control experiments, where two uncoated surfaces were used to construct the cell, the polarization resistance decreased slightly over the same exposure interval. Raman spectroscopy of the initially bare surface after 48 hours showed clear evidence for the formation of solid compound in and around small pits that was spectroscopically similar to a chromate conversion coating. Solid chromium oxide deposition on the unpitted surface was not detected, but was probably present at concentrations below the detection limit of the instrumentation. In parallel experiments, Raman spectroscopy of a solution droplet in contact with a freshly formed CCC showed that 30 to 40 ppm chromate

Surface Conversion of Aluminum and Ferrous Alloys for Corrosion Resistance, Proceedings of CORROSION/2000, R.G. Buchheit, M.R. Jaworoski, P.D. Chalmer, Eds., Houston TX (2000), p. 67-92.

accumulated in after about 48 hours. On a CCC aged in air for 10 days, chromate only accumulated to a level of about 10 to 20 ppm.

All together, these results demonstrate that chromate is released from a CCC, which is then transported through solution to act a local sites of corrosion damage to slow the accumulation of damage. On the basis of this experiment, it is possible to establish several distinct testable elements of ACP. They are:

- 1) the inhibitor can be released into a contacting solution
- 2) the inhibitor can be transported through solution
- 3) the inhibitor acts on exposed metal to suppress further corrosion.

With these testable criteria and the simulated scratch cell as a test vehicle, it is possible to rigorously examine chromate-free coatings for evidence of active corrosion protection.

CERIUM-BASED CONVERSION COATINGS

Background. In the mid-1980s Hinton and coworkers examined corrosion inhibition of high strength Al alloys by rare earth metal (REM) salts dissolved in aqueous solutions, and showed that these compounds were effective inhibitors for aluminum, ferrous and zinc alloys. This work has continued steadily over the years, but the essential elements of Ce corrosion inhibition were clearly established in earliest reports of this group (9). Early work showed that 100 to 1000 ppm additions of CeCl_3 to sodium chloride solutions suppressed corrosion of 7075-T6 in potentiodynamic polarization testing and in alternate immersion weight loss testing. Surface analysis showed incorporation of Ce into compact and protective surface films. Polarization tests showed inhibition of cathodic reaction kinetics, and, as is now less widely regarded, the anodic kinetics. Later work established that Ce films formed at local cathodic sites on the alloy surface stifled oxygen reduction thereby limiting corrosion damage (10,11). Film formation was proposed to occur when local cathodic activity increased the near-surface solution pH, which stimulated precipitation of Ce hydroxide. Perhaps most importantly, it was shown that a film with persistent corrosion resistance could be formed by exposure of alloy surface to a CeCl_3 solution. This result was the basis for conversion coating formulations based on the use of Ce salts (12).

It was later suggested that films grew by an island-growth mechanism (13). Films formed first at sites of local cathodic activity such as intermetallic particles and grain boundaries. Ce^{4+} oxides detected in the coating were thought to arise by oxidation of Ce^{3+} in oxygenated alkaline solutions. This was later confirmed by x-ray absorption near edge structure (XANES) measurements (14). It was also shown that corrosion resistant Ce coatings could be formed on Al alloys by immersion in aqueous CeCl_3 solutions either at the open circuit potential, or under cathodic polarization. Coatings were also formed by contacting surface with $\text{Ce}(\text{NO}_3)_3$ dissolved in butoxyethanol (15). As in earlier

experiments, corrosion resistance appeared to be due to suppressed reduction reaction kinetics and, or for long coating formation times, suppression of the anodic kinetics and elevation in the pitting potential. Additionally, other cations were shown to inhibit reduction reaction kinetics and improve corrosion resistance by forming thin surface films. The best inhibitors included Ni^{2+} , Pr^{3+} , Nd^{3+} , and Ce^{3+} (16). Further studies indicated that cerium salts could be used to inhibit corrosion of zinc and steel substrates (17). It was also found that several different Ce salts provided effective corrosion inhibition (18).

The lingering problem for Ce-based passivation was the long time required for the protective film to form; up to one week in most cases. The Hinton group learned that the kinetics of Ce deposition were substantially increased by using Ce^{4+} solutions (12). Highly corrosion resistant films could be formed by contacting Al alloy surfaces with a slightly acidic 1000 – 10000 ppm CeCl_3 solution containing several weight percent hydrogen peroxide. The peroxide oxidized Ce^{3+} to Ce^{4+} in solution. Mixed Ce^{3+} - Ce^{4+} coatings formed in 6 to 10 of minutes on a range of alloys. The coatings possessed outstanding corrosion resistance in both electrochemical and exposure (salt spray) testing.

In the late 1980s, Mansfeld began to study the effectiveness of Ce-based passivation on Al alloys and Al-based metal matrix composites by electrochemical impedance spectroscopy (19). Results showed that the corrosion resistance of 6061-T6, 7075-T6, Al-SiC, and Al-graphite metal matrix composites in aerated 0.5M NaCl were greatly improved by pre-exposure to 1000 ppm CeCl_3 solutions for one week. Shih and Mansfeld monitored the EIS response of 6061-T6 and 7075-T6 aluminum alloys with and without passivation in a variety of rare earth metal salt solutions to confirm the earlier results of Hinton, which indicated long-term, low temperature exposure to these solutions promoted corrosion resistance (20).

Mansfeld combined elements from this work with ideas developed from studies of highly corrosion resistant supersaturated non-equilibrium Al-transition metal alloys (21,22) to develop a Ce-Mo surface modification process. In this three-step process, degreased and deoxidized Al alloy surfaces were first immersed in 10 mM $\text{Ce}(\text{NO}_3)_3$ at 100°C, then immersed in 10 mM CeCl_3 also at 100°C, and finally were potentiostatically polarized at +0.5 V_{sce} in deaerated 0.1M Na_2MoO_4 . Al alloys surfaces treated in this manner resisted pitting in aerated 0.5M NaCl solutions for 60 days.

Independent characterization of these coatings produced on 2024-T3 and 6061-T6 were carried out (23). The coating was analyzed after each stage in the process and the evolution in coating chemistry and thickness was determined. Results showed that the coating consisted primarily of hydrated aluminum oxide with Ce was detected on and near cathodic intermetallic compounds such as $\text{Al}_7\text{Cu}_2\text{Fe}$ in 2024 and $\text{Al}_{12}\text{Si}(\text{Fe}, \text{Mn}, \text{Cr})$ in 6061-T6. Ce was not associated with active intermetallics like Al_2CuMg . Rather, these intermetallics were dissolved during the anodic polarization in the molybdate solution, leaving Mo-rich pits. In general more Ce was detected in coatings on 2024-T3, than on

6061-T6. This work plainly showed the importance of alloy chemistry and microstructure in Ce-Mo coating formation. In terms of coating chemistry, Ce was detected in trivalent and tetravalent oxidation states, while Mo was detected only in its hexavalent form. It was argued that Mo^{6+} in the coating provided self-healing, by reduction to Mo^{4+} , however no Mo^{4+} was detected. XANES measurements of Ce-Mo coatings after exposure to 0.5M NaCl for 30 days suggests that Mo^{6+} is leached into solution and does not participate in self-healing (24).

Noting that the Ce-Mo surface modification process thickened the oxide film and imparted Ce and Mo into it, Kendig sought to determine how critical a role Ce and Mo played in determining the overall corrosion resistance (25). To isolate the role of these heavy metals, Kendig formed coatings using a Ce and Mo-free process consisting of 4h immersion in boiling 30 mM NaNO_3 followed by 2 polarization at 0.5 V_{sc} in 0.1M borate solution. Coatings containing only Ce or Mo were also made to isolate effects due to the presence of either Ce or Mo in the film. The corrosion resistance of these coatings were compared to that of coatings formed by Ce-Mo surface modification. Corrosion resistance during immersion in aerated 0.5 M NaCl solution was measured using EIS for exposure times up to two weeks. The data were analyzed by equivalent circuit analysis and the pitting resistance, R_{pit} , was used a figure of merit to estimate relative corrosion resistances. The pitting resistance of the coatings decreased in the order:

$$\text{Ce-Mo} > \text{Mo-only} > \text{Ce Only} > \text{Ce-Mo-free}.$$

The results suggested that Ce and Mo, in fact, played a synergistic role in providing corrosion resistance. According to Kendig's interpretation of the results, Ce forms insoluble oxides that reinforce the hydrated aluminum oxide film and the oxidizing Mo species plays the role of active inhibitor. This latter comment is significant in that it is perhaps the first referral to and recognition of "active corrosion protection" in a Cr-free conversion coating system. Whether ACP actually occurs as described earlier is an open question.

This fundamental work, which has evolved over the past 15 years, has spawned a considerable amount of technological innovation in corrosion inhibition. Rare earth metal (REM) salts are used as corrosion inhibitors added to metals as alloying elements (26, 27), imparted into conversion and anodized coatings (28), and used as soluble corrosion inhibitors (29). A number of recent patents have been issued that describe the use of cerium as a primary or supplemental ingredient in corrosion resistant coating formulations. These coating processes can be classified as follows:

1) *Ce-sealed hydrothermal films*. In these processes, thickened films are formed by hydrothermal treatment and then sealed in a Ce^{3+} or Ce^{4+} solution. Examples include Ce-sealed boehmite coatings formed by elevated temperature in water (30), or

triethanolamine solutions (31). Hydrotalcite coatings may also be sealed by contact with Ce solutions as will be described later (32).

2) *Surface Modification*. In these processes, a potential is applied to the surface to induce deposition of Ce from solution. This can be accomplished by cathodic polarization, which develops alkaline conditions at the electrode surface and induces Ce precipitation (11). As described above, Mansfeld uses slight anodic polarization to stimulate interaction of Mo with thickened hydrothermal layers sealed with Ce (33).

3) *Cerating*. These processes are analogs to Hinton's immersion-based approach to developing REM coatings. Surfaces are contacted with a slightly acidic solution containing soluble Ce^{3+} or Ce^{4+} as the primary film-forming agent (34).

Active Corrosion Protection from Ce-modified Hydrotalcite. Cerium occurs in a moderately soluble +4 oxidation state and a comparatively insoluble +3 oxidation state. If a tetravalent oxide were to be introduced into a thickened barrier layer on aluminum, it might be possible to replicate active corrosion protection. Consider a scenario where a solution contacts a Ce^{4+} -bearing coating. Under these conditions, soluble Ce^{4+} would be released. If the Ce^{4+} ions encountered the reducing conditions associated with bare metal exposed through a coating defect, reduction to Ce^{3+} and precipitation would ensue. Precipitation of a hydrated Ce oxide at the defect might then stifle further corrosion.

To test whether this hypothesized self-healing scenario is plausible, a series of experiments were carried out based on the methods of Zhao et al. (8). As described earlier, Zhao devised a simulated scratch cell (SSC) to test for ACP in chromate conversion coatings. Modifications made to Zhao's design are shown schematically in Figure 2. In the present experiment, one 2024-T3 surface is coated with Ce-modified hydrotalcite, the other bare 2024-T3. In these experiments, each surface was 5.1 cm^2 . The surfaces are separated by a 5 mm gap that was filled with a 0.5M NaCl solution. In this arrangement, the bare surface is examined for evidence of healing by release of Ce^{4+} from the Ce-modified hydrotalcite coating on the opposing surface.

For this experiment, Ce-modified hydrotalcite coatings were produced by a two step process. First, hydrotalcite was formed on degreased and deoxidized 2024-T3 (Al-4.4Cu-1.5Mg-0.6Mn) by contact for 10 minutes with a pH 12 bath containing LiNO_3 , KNO_3 , LiOH , and NaAlO_2 held at 98°C . The hydrotalcite coated surfaces were then immediately immersed in a room temperature solution containing 10g/L $\text{Ce}(\text{NO}_3)_3$ plus 30% H_2O_2 to induce precipitation of an adherent deposit of Ce^{4+} hydrated oxide on the alkaline hydrotalcite. Coatings were rinsed and air dried for 24 hours before any further use. Ce-modified hydrotalcite coatings have been made that will pass 168h of ASTM B117 salt fog exposure on 2024-T3. However, the coatings produced in this study were not that corrosion resistant. Figure 3 is a Nyquist plot showing the corrosion resistance of Ce-modified hydrotalcite coatings, La-modified hydrotalcite (described below), chromate conversion coatings and hydrotalcite sealed with magnesium acetate. The coatings used

in this study exhibited coating resistances, R_c , of about $10^5 \text{ ohm}\cdot\text{cm}^2$, which is about an order of magnitude less than a typical chromate conversion coating, and is an order of magnitude less than is exhibited by coatings that normally pass a salt spray test (35).

This simulated scratch cell is the primary vehicle used to test for elements of ACP. Aliquots of the gap solution were periodically extracted and examined for evidence of soluble Ce. After exposure, the cell was disassembled and the bare side was examined for the presence and distribution of Ce oxides. Corrosion resistance measurements were made of the bare side to determine if its corrosion resistance had increased signaling healing. Additionally, the corrosion resistance of the coated side was examined to determine if Ce release had caused a decrease in its corrosion resistance.

Ultraviolet (UV) absorbance measurements were used to detect Ce released into the gap solution during simulated scratch experiments. UV absorbance is sensitive to Ce concentrations as low as 10^{-5}M (Figure 4). It can distinguish between Ce^{3+} and Ce^{4+} at concentrations as low as 10^{-3}M (Figure 5). Figure 6 shows UV absorbance peak heights from aliquots of solution extracted from the simulated scratch cell for times ranging from 4 to 48 hours. The fact that Ce is detected confirms that Ce can be released from Ce-modified hydrotalcite into solution. The absorbance peak heights range from 0.5 to 0.9, which correspond to soluble Ce concentrations of about 3×10^{-4} to $3\times 10^{-3}\text{M}$ or 40 to 400 ppm. Inhibition of the bare surface in the cell is expected under these conditions considering that Hinton reports that 10 ppm CeCl_3 in 0.1 M NaCl is sufficient to reduce the corrosion rate of 7075-T6 (9).

To assess changes in corrosion resistance to the bare side sample of the cell that might indicate healing, the cell was disassembled after 48h of exposure and the bare side impedance was measured in aerated 0.05M NaCl. Figure 7 shows the coating corrosion resistance, R_c , determined by complex non-linear least squares fitting of EIS data to a simplified Randles circuit model. R_c data are plotted as a function of exposure time in the 0.05 M NaCl test solution. For comparison, R_c data are shown for a bare 2024-T3 surface exposed to another, identical bare surface for 48 h in the cell, and a polished 2024-T3 surface exposed only to the 0.05 M NaCl solution. The curves represent averages of three replicate runs; error bars have been omitted for clarity. Inspection of the data shows that the surface exposed in the simulated scratch cell with the Ce-modified hydrotalcite exhibits R_c values that are nearly an order of magnitude greater than that of a surface exposed only to another bare surface. This result suggests that the bare surface in the SSC has been protected from corrosion by release of Ce from the Ce-modified hydrotalcite coating.

Scanning electron microscopy (SEM) and Auger electron spectroscopy (AES) were used to characterize the deposition and distribution of Ce on the bare side of the cell. Figure 8 shows a secondary electron image of a bare surface exposed to Ce-modified hydrotalcite for 24 h in the cell. Polishing marks are clearly visible in this image, but superimposed on those marks is a cracked surface film with locally heavier deposits. The

figure indicates two areas where AES analysis was conducted. Area 1 is on a Cu-rich second phase and Area 2 on the matrix phase. Figure 9 shows AES spectrum of the Ce MNN and Cu LMM transitions for both of the analysis areas. Ce is detected on the second phase particle, but is absent on the matrix phase. This observation is consistent with Ce oxide deposition on Al alloys as it has come to be understood (18). Ce deposits initially and preferentially and on noble, Cu-rich intermetallic particles since they are sites that support reduction reactions, develop local alkalinity, and induce Ce precipitation (10,11).

In order to retain ACP for extended periods of time, it is necessary that the Ce^{4+} introduced into the coating be stable. Results show that Ce in hydrotalcite coatings tends to remain or oxidize to Ce^{4+} in the presence of atmospheric oxygen, condensed moisture, and the prevailing alkaline conditions associated with hydrotalcites. This Ce^{4+} is easily liberated to provide inhibiting action at defects elsewhere in the coating. Figure 10 shows x-ray photoelectron spectroscopy (XPS) data from Ce^{3+} - and Ce^{4+} -modified hydrotalcite coatings both before and after 168 hours of ASTM B117 salt fog exposure. Coatings modified by immersion in a $\text{Ce}(\text{NO}_3)_3$ solution produce coatings with Ce predominantly in a +3 oxidation state. Coatings modified by immersion in a $\text{Ce}(\text{NO}_3)_3$ solution plus H_2O_2 contain Ce predominantly in a +4 oxidation state. These spectra are shown in the uppermost (Ce^{3+}) and lowermost (Ce^{4+}) plots in Figure 10. The spectra from Ce in a +4 oxidation state are readily distinguished from those due to Ce in a +3 state by the intense Ce satellite at 918.5 eV and intense features due to peak splitting in the $\text{Ce}3d_{5/2}$ (885eV) and $\text{Ce}3d_{3/2}$ (902eV) (36). XPS data collected from Ce^{3+} - and Ce^{4+} -modified hydrotalcite coatings after salt fog exposure are remarkably similar and exhibit peak splitting characteristic of Ce^{4+} . This observation is in agreement with Davenport et al. who used x-ray absorption near edge spectroscopy to show that Ce^{3+} converted to Ce^{4+} in Ce-bearing coatings applied to Al-Mg alloys upon exposure to aerated chloride solutions (14). More importantly, this observation indicates that the Ce^{4+} in hydrotalcite coatings will be stabilized by the oxidizing power of natural environments until reducing conditions associated with the exposure of the aluminum substrate in defects is encountered. At those locations Ce^{4+} will be reduced and precipitated to inhibit corrosion.

Lanthanum-modified hydrotalcite. To check that ACP in Ce-modified hydrotalcite was not an artifact of the simulated scratch cell method, a series of experiments was carried out using lanthanum-modified hydrotalcite coatings. Lanthanum is an REM adjacent to Ce on the Periodic Table. Like Ce, its trivalent oxide is insoluble under alkaline conditions. However, La differs from Ce in that it does not form a soluble tetravalent oxide. Hence, La-modified hydrotalcite coatings are not expected to exhibit characteristics of ACP.

La-modified hydrotalcite coatings were formed using procedures identical to those used to form a Ce-modified coatings. La was introduced into the coating by immersion for 1 minute in a 10 g/L $\text{La}(\text{NO}_3)_3$ solution. The corrosion resistance of La-

modified coatings was about 10^5 ohm-cm^2 in EIS testing after 24 hour exposure to 0.5 M NaCl, which is similar to that of Ce-modified coatings.

Simulated scratch cell experiments were then conducted with La-modified coatings. Solution extracted from the cell was analyzed by inductively-coupled plasma atomic emission spectroscopy (ICP-AES) rather than by UV absorbance since La does not absorb at UV wavelengths. La was not detected in concentrations greater than 10^{-6}M for any exposure time between 4 and 48 hours. By comparison, Ce was detected in concentrations greater than $3 \times 10^{-4}\text{M}$. As expected, Auger analysis was not able to detect La bare side of the SSC after 48 hours of exposure. Accordingly, no increase in the corrosion resistance of the bare surface was recorded.

The behavior of Ce-modified hydrotalcite in simulated scratch cell exposure is consistent with the key elements of ACP suggested by the study of Zhao, et al. (8). In these experiments, Ce deposits preferentially on Cu-rich intermetallic particles on the bare surface representing the scratch. The interaction of Ce with corroding Al surfaces may be different that of chromates, but is certainly consistent with the evolution of Ce conversion coatings reported by Hinton and others. Additionally, the absence of indications for ACP from La-modified hydrotalcite strongly suggest that ACP is not an artifact induced by the simulated scratch cell experiment.

MANGANESE-BASED CONVERSION COATINGS

Manganese. In many respects, manganese is chemically similar to chromium. Conversion coatings based on Mn chemistries are therefore a logical approach to the chromate-free conversion coating replacement problem. One of the best known surface conversion technologies that has evolved is based on permanganate sealing of hydrothermally grown aluminum oxide films (37, 38, 39). In this process Al alloys surfaces are immersed in boiling distilled water or steam for times ranging from tens of seconds to 5 minutes. This produces a 300 to 500nm thick hydrated aluminum oxide film, which is further thickened by immersion in an Al salt solution for at least one minute. This surface is then immersed in a permanganate solution resulting in the deposition of reduced Mn oxides in the coating. A further sealing step is required to achieve corrosion resistance on unpainted 2XXX aluminum alloys.

Unpainted permanganate conversion coatings have been observed to withstand 336 hours of ASTM B117 salt fog exposure without significant corrosion. When the permanganate-based process is used as a paint base, filiform corrosion resistance of polyurethane powder coated 6XXX and 3XXX alloys is comparable to when chromate conversion coatings are similarly used. While the performance characteristics of permanganate coatings appear favorable, they have not yet been widely implemented.

Active corrosion protection from manganese-modified hydrotalcite. Manganese is especially interesting in conversion coating schemes because of its soluble high oxidation state oxoanion (MnO_4^-), and insoluble lower oxidation states (Mn^{4+} , Mn^{+3} , Mn^{+2}). As stated earlier, the existence of two oxidation states in the active agent appears to be important for ACP. It is also possible to modify hydrotalcites with permanganate using methods similar to those described with Ce and La. For these reasons, the behavior of Mn-modified hydrotalcite coatings has been examined using the simulated scratch cell.

Mn-modified hydrotalcite coatings were formed on 2024-T3 panels surfaces by first washing, degreasing and deoxidizing surfaces. The samples were then coated by a 4 minute immersion in a hydrotalcite coating bath consisting of LiNO_3 , KNO_3 , LiOH , and NaAlO_2 . After a thin "primer" HT coating was formed, the samples were immersed for 2 minutes in a bath of similar composition, but with a small potassium permanganate addition. As a last step, the samples were sealed in a Mg acetate-based sealing bath. All baths were held at temperatures ranging from 60° to 85°C . The coated samples were dried in air for at least 24 hrs before any further testing or examination.

The Mn-modified hydrotalcite coatings produced by this process were light gold in color. Examination of the coatings by scanning electron microscopy (SEM) showed no obvious morphology change associated with the modification by permanganate. Figure 11 shows the typical morphology of the coating.

Figure 12 shows variation in the corrosion resistance of permanganate-modified hydrotalcite coating and chromate conversion coating during exposure to aerated 0.5 M NaCl solution. The hydrotalcite coating impedance increases with immersion time in the 0.5 M NaCl solution for the first 30 hours or so, then decreases and attains a stable value around $2 \times 10^6 \Omega \cdot \text{cm}^2$. That is on the same order of magnitude with chromate conversion coating and 1000-fold higher than that of unprotected AA2024-T3. This value of corrosion resistance for 2024-T3 indicates that a passing result in a 168 hour salt spray test can be expected (36). In fact, salt spray exposure of permanganate-modified hydrotalcite coated 2024-T3 produces little to no pitting after 168 hours of exposure. Figure 13 shows photographs of 2024-T3 with a permanganate modified hydrotalcite coating, a chromate conversion coating and no coating after 168 hours of exposure.

Permanganate-modified hydrotalcite coatings were examined for evidence of ACP using the simulated scratch cell. Significant modifications in cell design and electrolyte chemistry were made after the experiments with Ce-modified hydrotalcite. In the present experiments, the cell was modified to permit in situ measurements as shown in Figure 14. In the modified cell, a bare 2024-T3 panel was fixed on the top of AA2024-T3 panel with a Mn-modified hydrotalcite coating using four plastic screws. A 5mm gap was created between the two panels by a rubber o-ring. The o-ring had a 40mm diameter and a 5mm thickness, thus the volume between the two samples were approximately 5ml. A platinum mesh was inserted into the small chamber through the rubber o-ring. A small hole was made on the top panel to fill 0.1 M NaCl solution and to accommodate a saturated calomel reference electrode (SCE).

Exposures were carried out for periods up to 460 hours. The untreated AA2024-T3 exposed to the Mn-modified hydrotalcite coating was tested using EIS conducted *in situ*. Similar experiments were carried out in cells constructed with a chromate conversion coated surface, and a surface without a coating present (both samples untreated). Figures 15 and 16 show results of *in situ* measurements of total impedance (R_{corr}) and total capacitance for the bare surfaces in each of the three types of cells as a function of exposure time. Measurements were carried out in triplicate.

The data from the control samples are indicative of stable localized corrosion, which was preceded by an induction period of about 100 hours. The total impedance for these samples remained stable at an average value of about $200 \text{ k}\Omega\cdot\text{cm}^2$ up to about 100 hours. Over the same time period, the capacitance was stable at a value of about $15 \text{ }\mu\text{F}/\text{cm}^2$. After 100 hours, there was a sharp decrease in the total impedance, which fell to about $20 \text{ k}\Omega\cdot\text{cm}^2$ by the end of the experiment. At the same point in the experiment, there was a sharp increase in the capacitance, which achieved a final value of nearly $80 \text{ }\mu\text{F}/\text{cm}^2$. This signaled the onset of stable localized corrosion. The occurrence of an induction time was probably due to the fact that the cell quickly became deaerated causing the corrosion potential to drop below the critical pitting potential. After the experiment, the exposed surfaces exhibited a greenish tint, with occasional black and gray staining. A uniform distribution of small pits were observed across all surfaces exposed in these cells.

Compared to the response of the control cells, the impedance data collected from the alloy surfaces exposed to the chromate conversion coating show evidence of inhibition. The total impedance value is about $100 \text{ k}\Omega\cdot\text{cm}^2$ initially and remained steady for the first 100 hours or so of exposure. Thereafter it climbed steadily to a final value of about $400 \text{ k}\Omega\cdot\text{cm}^2$. The capacitance data did not change significantly during this experiment, with the possible exception of a transient increase between 100 and 150 hours. Overall, the indication is that significant pitting did not develop on the bare surface during the test. After the exposure, these surfaces were mostly lustrous with only slight and occasional staining. On one sample no pits were visible by the unaided eye. On the other two, several small pits were visible.

The response of the surfaces exposed to the Mn-modified hydrotalcite coatings falls between the responses of the control cells and the cells with chromate coatings. The total impedance decreased slightly during the first 100 hours, although there was no significant increase in capacitance. At 100 hours there is a sharp increase in total resistance and capacitance. At the end of the experiment, the total resistance was equivalent to the initial impedance. Unlike the response in the control cells, the capacitance increase stabilized within about 30 hours and did not increase further for the duration of the experiment. Visual examination of these surfaces after the experiment showed that a uniform golden-brown deposit covered the surface. Some darker stains and

occasional pits were observed. These pits were fewer in number than those on the control samples, and one of the samples had no visible pitting.

In each of the three different types of cells, changes in behavior were detected after about 100 hours of exposure. In the control cells the change in the trends of total resistance and capacitance have been ascribed to the onset of stable pitting. The fact that evidence of inhibiting action by chromate and permanganate is also observed at about this time suggests the possibility that these inhibitors act to slow pit propagation, and may not play a strong role in suppressing pit initiation.

Analysis of the solution from permanganate-modified hydrotalcite simulated scratch cells has not yet been conducted. However, after exposure in the cell to the permanganate-modified hydrotalcite, the bare surface contained only several small pits, and were covered by a thin brown film suggesting transport on Mn species through solution and deposition in the form of a manganese oxide. Detailed surface analysis has not yet been conducted, but initial surveys by energy dispersive spectroscopy suggest that the Mn level of the surfaces is elevated after exposure in the simulated scratch cell.

SUMMARY

One of the distinguishing characteristics of chromate conversion coatings is their ability to self-heal if damaged by modest mechanical or chemical attack. This characteristic has been the subject of much discussion in the absence of a rigorous method for studying it. However, the recently devised simulated scratch cell enables the phenomenon to be examined in a much more deterministic fashion. Self-healing or as has been referred to here, ACP, can be broken down into several testable characteristics. They are: 1) that the coating contains a reservoir of an inhibiting agent that is stable until needed, 2) the inhibitor can be released into a contacting solution, 3) the inhibitor can be transported through solution, 4) the inhibitor acts on exposed metal to suppress further corrosion. Given these distinct characteristics, and a method of testing for them, it is possible to examine chromate-free conversion coatings for evidence of ACP. Results show that Ce-modified and Mn(permanganate)-modified hydrotalcite coatings exhibit signs of ACP. These characteristics arise due to the fact that the metals are introduced into the hydrotalcite as soluble high oxidation state hydrated oxides, but have insoluble lower oxidation state forms. When solution contacts these oxides, they dissolve and migrate through solution and are reduced when they contact the exposed Al surface elsewhere. Since these species are much less soluble in reduced form, they then precipitate on the bare surface and slow corrosion by stifling cathodic and possibly anodic kinetics. Similar experiments conducted with La-modified hydrotalcite do not show evidence of ACP.

La exists only in a low solubility trivalent form. Once it is introduced to the hydrotalcite coating, it is not released and cannot participate in the subsequent events that lead to Ce-like ACP.

ACKNOWLEDGEMENTS

The authors would like to acknowledge the financial support of the U.S. Department of Energy, Sandia National Laboratories, DARPA and SERDP. The authors would also like to thank M. Martinez, L. Montes, W. Buttry, and W. Zhang for various technical contributions.

REFERENCES

- 1) L. Xia, R. L. McCreery, J. Electrochem. Soc. (1999).
- 2) N. J. Newhard, Metal Finishing, 49, 66 (1972).
- 3) P. L. Hagans, C.M. Haas, Surface and Interf. Anal., 21, 65 (1994).
- 4) A. E. Hughes, R. J. Taylor, B. R. W. Hinton, Surface and Interf. Anal., 25, 223 (1997).
- 5) M. Koudlekova, J. Electrochem. Soc., 124, 1165 (1977).
- 6) A. J. Davenport, H. S. Isaacs, Corrosion Sci., 31, 105 (1990).
- 7) National Center for Manufacturing Sciences, "Alternatives to Chromium for Metal Finishing," NCMS Report 0273RE95, Ann Arbor, MI (1995).
- 8) J. Zhao, G. S. Frankel, R. L. McCreery, J. Electrochem. Soc., 145, 2258 (1998).
- 9) B. R. W. Hinton, D. R. Arnott, N. E. Ryan, Metals Forum, 7, 211 (1984).
- 10) A. J. Aldykewicz, Jr., H.S. Isaacs, A.J. Davenport, J. Electrochem. Soc., 142, 3342 (1995).
- 11) A. J. Aldykewicz, Jr., H.S. Isaacs, A.J. Davenport, J. Electrochem. Soc., 143, 147 (1996).
- 12) B. R. W. Hinton, L. Wilson, "Effect of Cerous Chloride Concentration on Corrosion Rate", Australian patent, PCT/AU88/00060.
- 13) D. R. Arnott, N. E. Ryan, B. R. W. Hinton, B. A. Sexton, A. E. Hughes, Applications of Surface Science 22/23, 236 (1985).
- 14) A. J. Davenport, H. S. Isaacs, M. W. Kendig, Corrosion Sci., 32, 653 (1991).
- 15) B. R. W. Hinton, D. R. Hinton, N. E. Ryan, Mater. Forum, 9, 162 (1986).
- 16) D. R. Arnott, B. R. W. Hinton, N. E. Ryan, Materials Perf., Aug., p. 42 (1987).
- 17) B. R. W. Hinton, D. R. Arnott, Microstructural Science, 17, 311 (1989).
- 18) B. R. W. Hinton, J. of Alloys and Compounds, 180, 15 (1992).
- 19) F. Mansfeld, S. Lin, S. Kim, H. Shih, Electrochim. Acta, 34, 1123 (1989), and F. Mansfeld, S. Lin, S. Kim, H. Shih, Corrosion, 45, 615 (1989).
- 20) H. Shih, F. Mansfeld, "Passivation in Rare Earth Metal Chlorides—A New Conversion Coating Process for Aluminum Alloys", p. 180, New Methods for Corrosion Testing of Aluminum Alloys, ASTM STP 1134, V. S. Argawala, G. M. Ugiansky, Eds., American Society for Testing and Materials, Philadelphia (1992).
- 21) B. A. Shaw, G. D. Davis, T. L. Fritz, K. A. Oliver, J. Electrochem. Soc., 137, 359 (1990).
- 22) W. C. Moshier, G. D. Davis, G. O. Cote, J. Electrochem. Soc., 133, 1063 (1990).

- 23) A. E. Hughes, J. D. Gorman, P. J. K. Patterson, Corrosion Science, 38, 1957 (1996), and J. D. Gorman, S. T. Johnson, P. N. Johnston, P. J. K. Paterson, A. E. Hughes, Corrosion Science, 38, 1977 (1996).
- 24) J. Wan, G. E. Thompson, K. Q. Lu, C. J. E. Smith, J. Phys. IV France, 7, c2, 1182 (1997).
- 25) M. Kendig, C. Thomas, J. Electrochem. Soc., 139, L103 (1992).
- 26) R. N. Singh, N. Verma, W. R. Singh, Corrosion, 45, 222 (1989).
- 27) A. C. Crossland, G. E. Thompson, P. Skeldon, G. C. Wood, C. J. E. Smith, H. Habazaki, K. Shimizu, Corrosion Sci., 40, 871 (1998).
- 28) F. Mansfeld, C. Chen, C. B. Breslin, D. Dull, J. Electrochem. Soc., 145, 2792 (1998).
- 29) F. M. Seon, J. Less Common Metals, 148, 73 (1989).
- 30) A. Kindler, U.S. Patent 5,192,374, March (1993).
- 31) R. Rungta, U.S. Patent 5,362,335, November (1993).
- 32) R. G. Buchheit, M. A. Martinez, U.S. Patent 5,756,218, May (1998).
- 33) F. B. Mansfeld, H. Shih, Y. Wang, U.S. Patent 5,194,138, March (1993).
- 34) S. Ikeda, U.S. Patent 4,992,115, February (1991), R. N. Miller, U.S. Patent 5,356,492, October (1994).
- 35) R. G. Buchheit, M. Cunningham, H. Jensen, M. W. Kendig, M. A. Martinez, Corrosion, 54, 61 (1998).
- 36) G. Praline, B. E. Koel, R. L. Hance, H-I. Lee, J. M. White, J. of Electron Spectroscopy and Related Phenomena, 21, 17 (1980).
- 37) J. W. Bibber, Metal Finishing, Dec., 46 (1993).
- 38) J. W. Bibber, Metal Finishing, April, 28 (1998).
- 39) J. W. Bibber, Corrosion Reviews, 15, 3/4, 303 (1997).

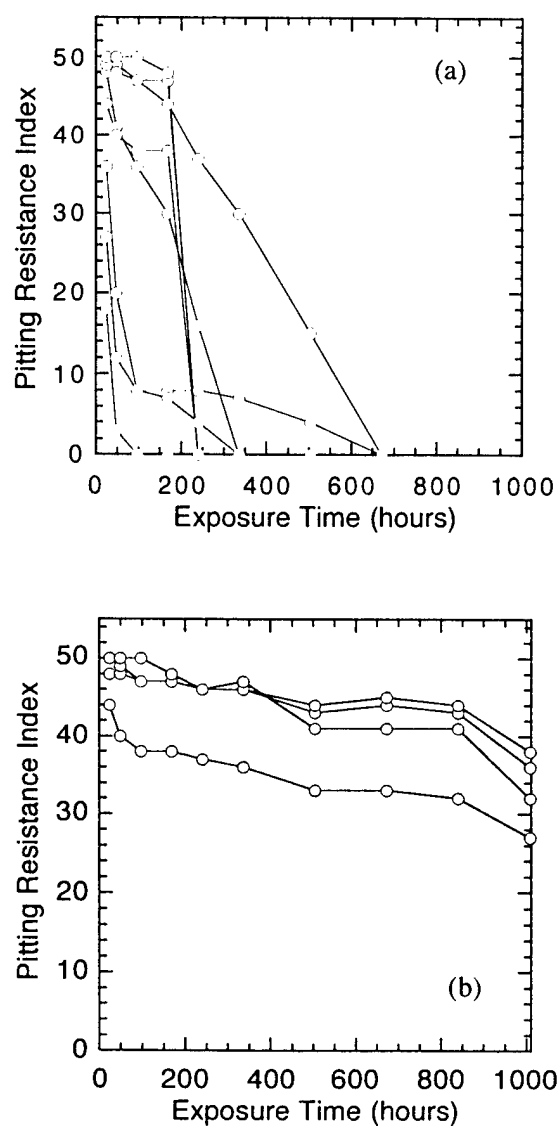


Figure 1. Accumulation of pitting damage versus exposure time for (a) chromate-free, and (b) chromate conversion coating on 7075-T6 after ASTM B117 salt spray exposure testing. Larger pitting resistance indices correspond to a lower incidence of pitting.

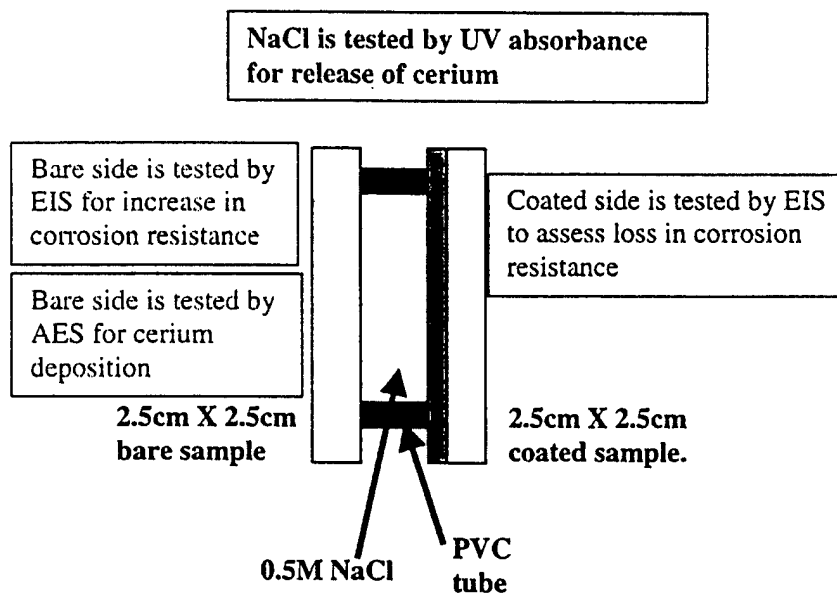


Figure 2. Simulated scratch cell used for the Ce- and La-modified hydrotalcite ACP experiments

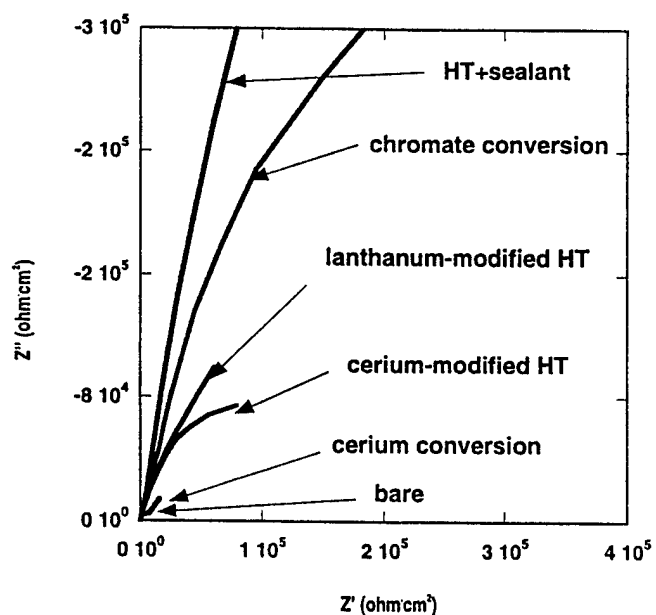


Figure 3. Nyquist plots of Ce- and La- modified hydrotalcite coatings and chromate conversion coatings exposed to aerated 0.5 NaCl for 24 h.

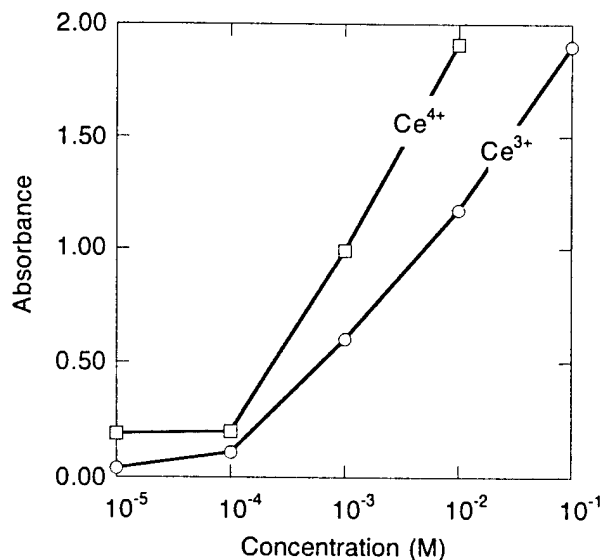


Figure 4. Absorbance versus Ce³⁺ and Ce⁴⁺ concentration.

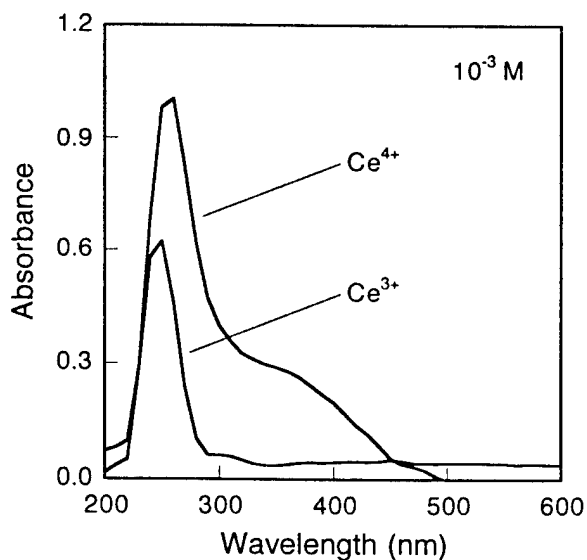


Figure 5. Absorbance spectra for Ce³⁺ (Ce(NO₃)₃), and Ce⁴⁺ (Ce(NO₃)₃ + H₂O₂) in aqueous solution illustrating the differences in peak shape that can be used to distinguish these species at higher concentrations.

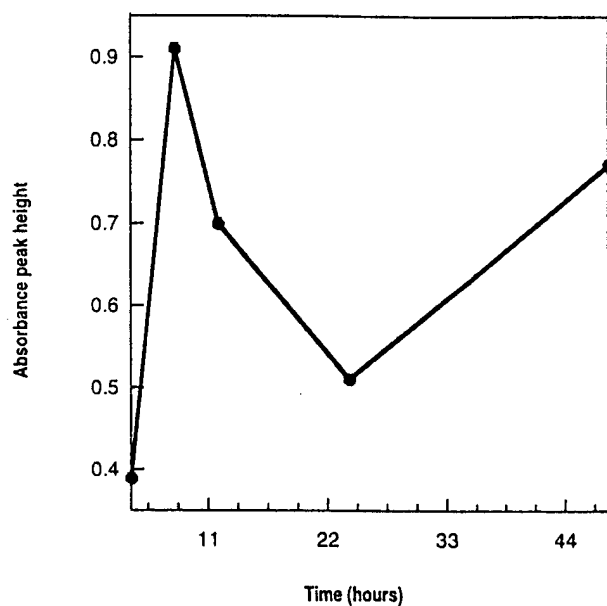


Figure 6. UV absorbance peak height from solution samples extracted from the simulated scratch cell after various exposure times. A 0.5 M NaCl solution was introduced into a cell in which bare 2024-T3 was exposed to Ce-modified hydrotalcite coated 2024-T3.

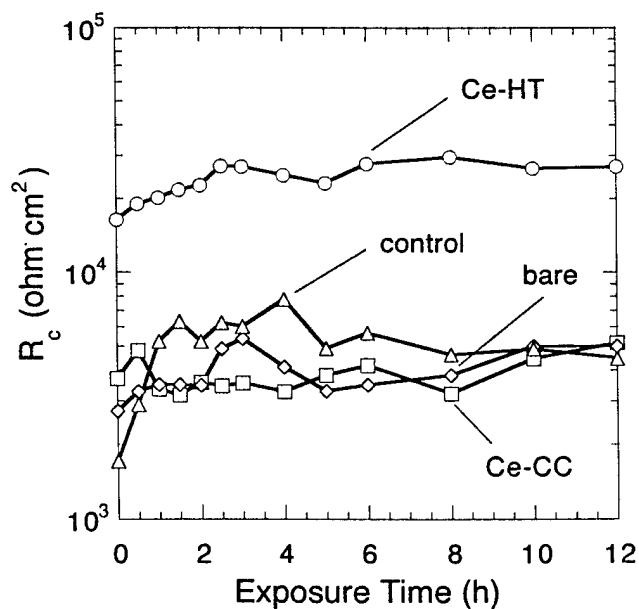


Figure 7. R_c determined by EIS after exposure to aerated 0.05 M NaCl for times up to 12 hours for 2024-T3 surfaces exposed in the simulated scratch cell with various other 2024-T3 samples: Ce-HT, Ce-modified hydrotalcite coated; Ce-CC, cerium conversion coated; bare, uncoated 2024-T3; control, 2024-T3 exposed only to 0.05M NaCl for the times indicated in the figure.

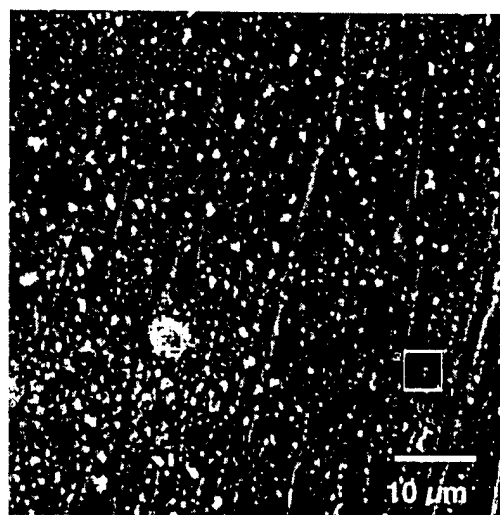


Figure 8. Backscatter scanning electron micrograph of a 2024-T3 surface exposed in the simulated scratch cell for 48 hours to 0.5 M NaCl. The other surface exposed in the cell was Ce-modified hydrotalcite. Two analysis regions are indicated. Region 1 is on a deposit located over a Cu-rich particle. Region 2 is on the matrix phase.

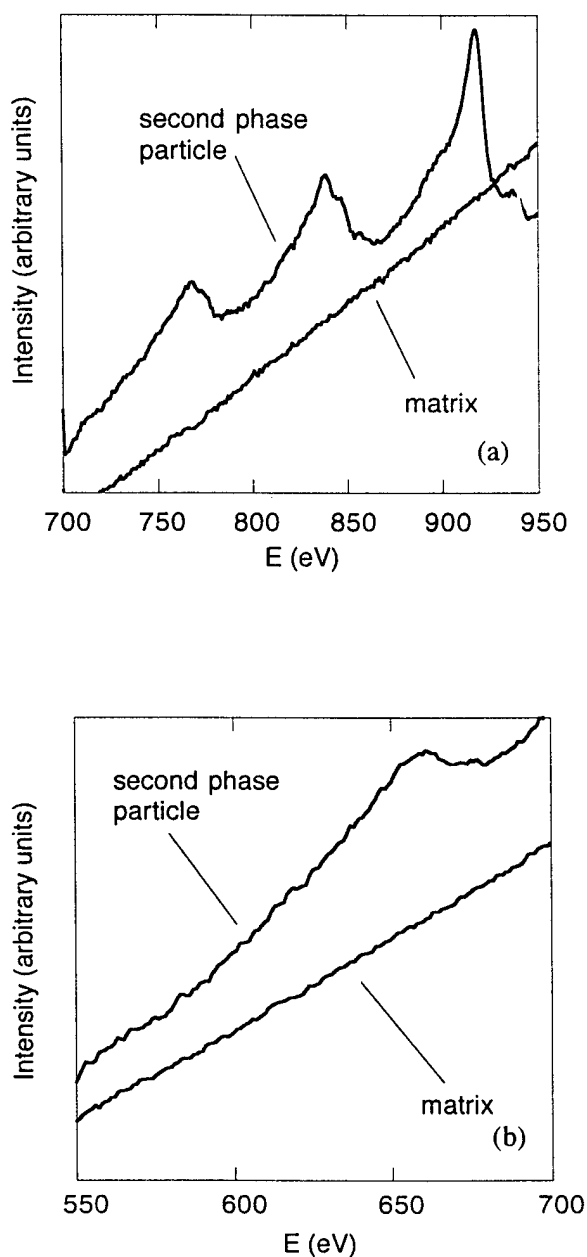


Figure 9. Auger spectra of the (a) Cu LMM and (b) Ce MNN Auger transition from a Cu-rich particle and the matrix phase on a bare 2024-T3 surface in the simulated scratch cell. The other surface was Ce-modified hydrotalcite and the cell contained a solution of 0.5 M NaCl.

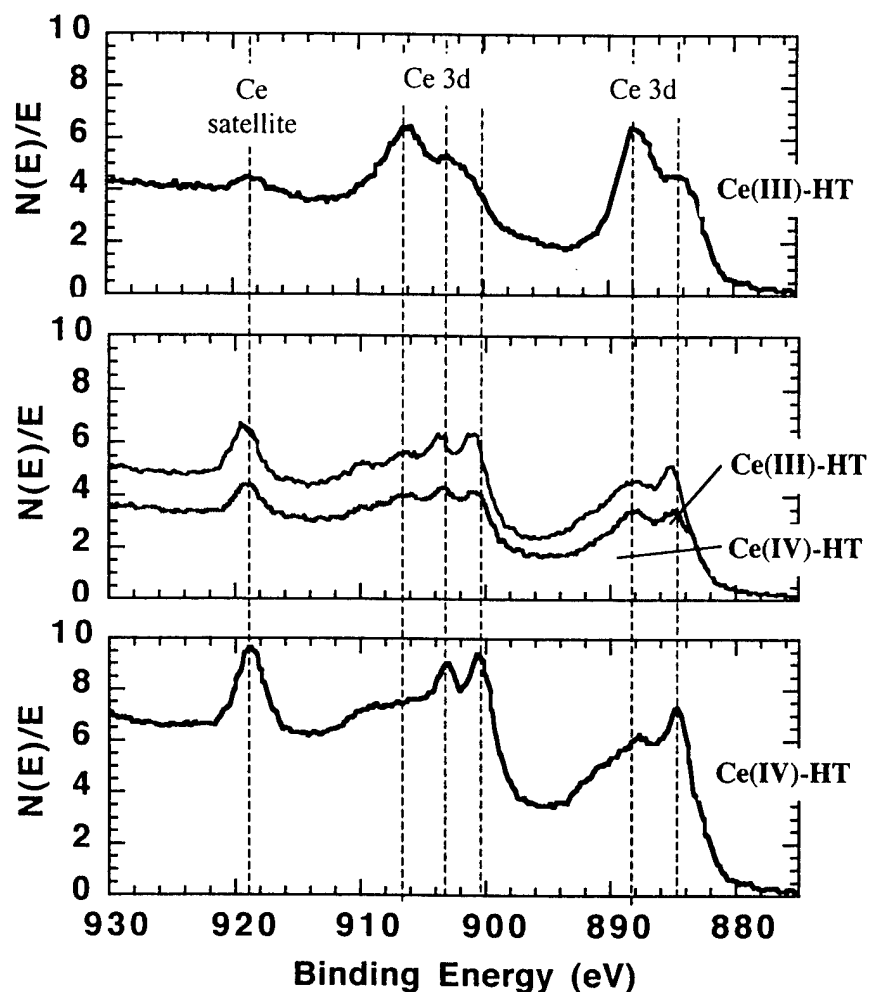


Figure 10. XPS data on Ce(III)- and Ce(IV)- modified hydrotalcite coated 2024-T3. The topmost figure shows the spectrum for Ce(IV)-modified hydrotalcite, while the bottommost figure shows the spectrum from Ce(III)-modified hydrotalcite. Coatings of each type were subjected to salt spray exposure for 168 hours and the post exposure spectra for each coating is shown in the middle figure.

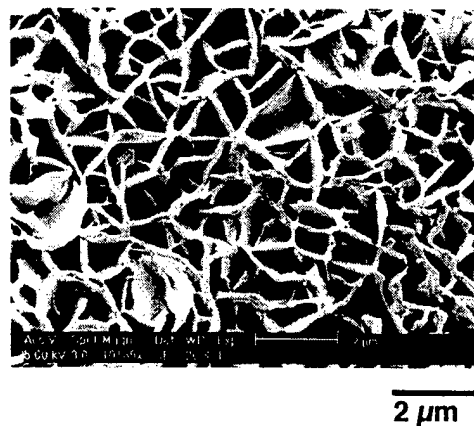


Figure 11. Scanning electron micrograph of the permanganate-modified hydrotalcite coating.

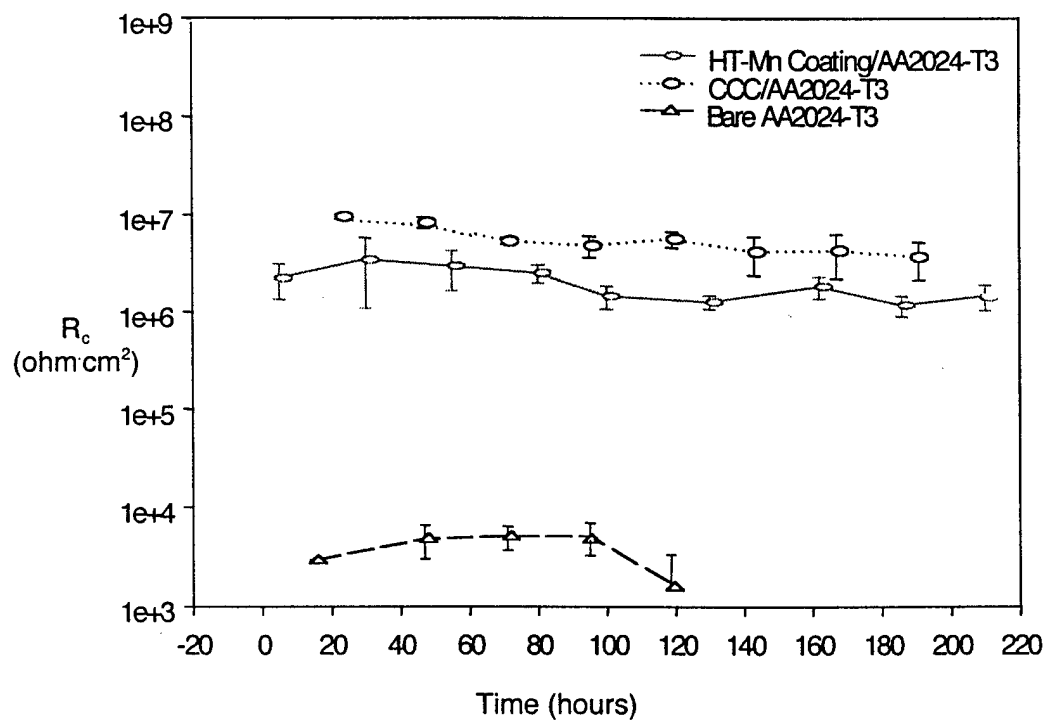


Figure 12. Coating resistance, determined by EIS, versus time for permanganate-modified hydrotalcite (HT-Mn), and a chromate conversion coatings (CCC) exposed to aerated 0.5 M NaCl solution.

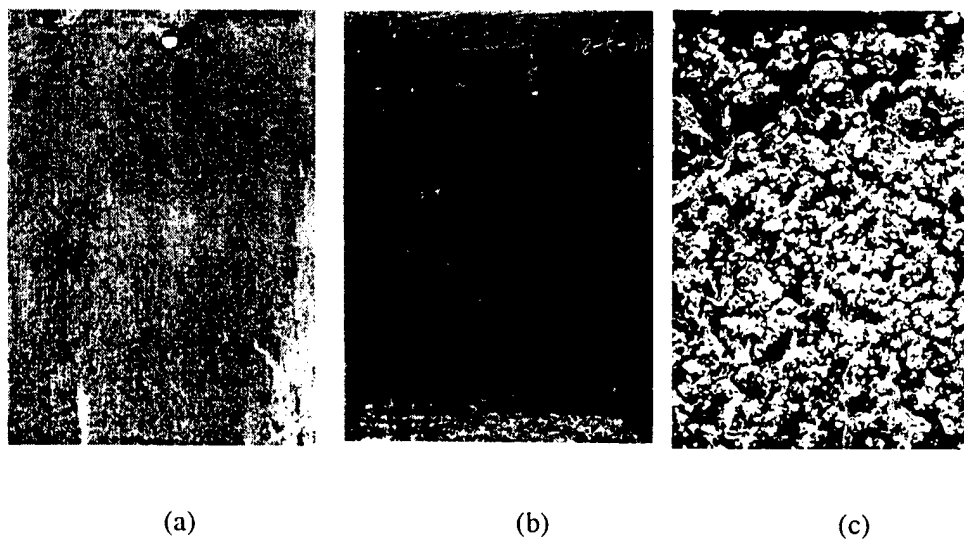
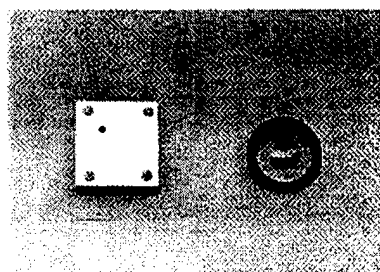
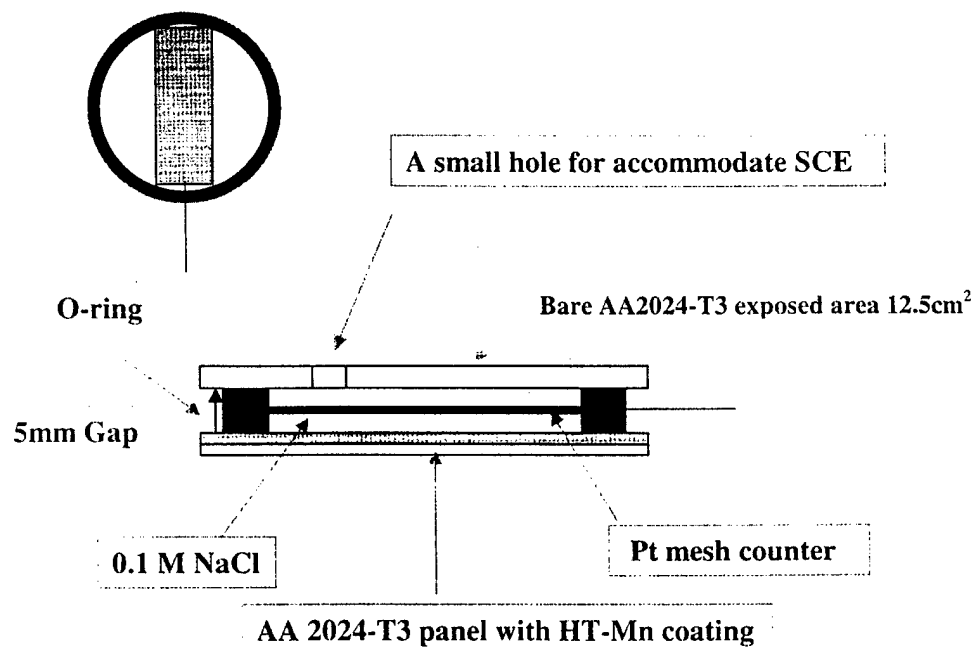


Figure 13. alloys 2024-T3 panels after 168 hours of ASTM B117 salt fog exposure; (a) permanganate-modified hydrotalcite, (b) chromate conversion coated, (c) no coating. Samples are 4 inches x 6 inches.



-Sample Exposed Area 12.5 cm²
 -5 mm Distance between panels
 -5 ml 0.1 M NaCl filled

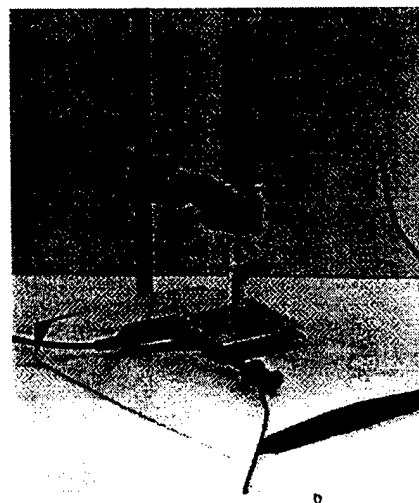


Figure 14. Schematic illustrations and photographs showing the simulated scratch cell modified for in situ measurement of ACP.

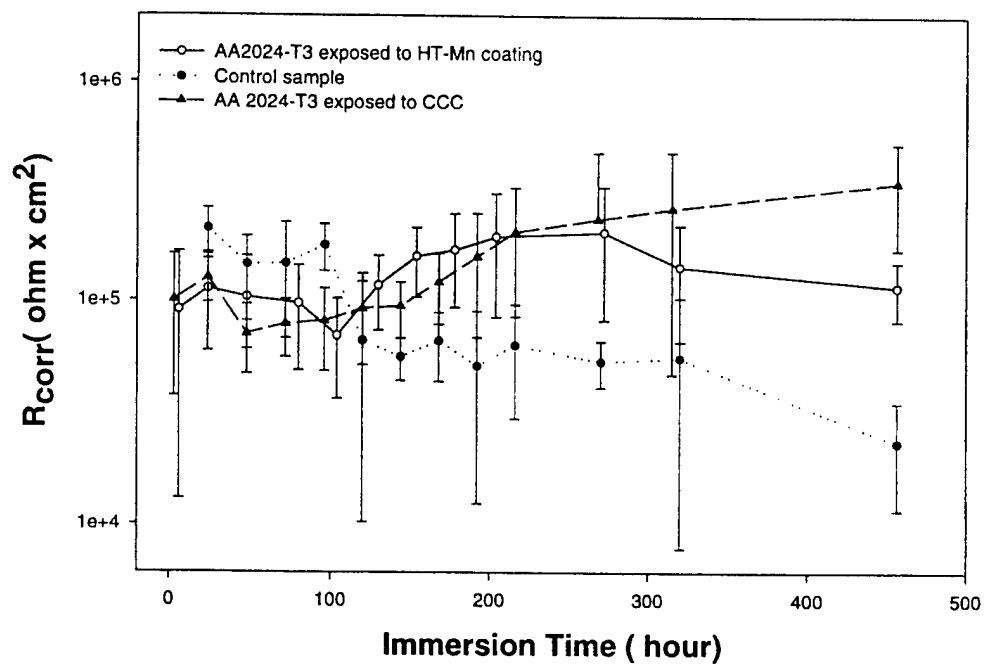


Figure 15. Corrosion resistance of bare 2024-T3 exposed to different conversion coatings in the modified simulated scratch cell. R_{corr} was determined from EIS measurements. In the control experiment, two uncoated 2024-T3 samples were used in the cell.

Accepted for publication in Corrosion June 2001

Active Corrosion Protection in Ce-modified Hydrotalcite Conversion Coatings

R.G. Buchheit, ¹S.B. Mamidipally, ²P.Schmutz, H. Guan
Fontana Corrosion Center
Department of Materials Science
Ohio State University
Columbus, Ohio 43210

¹Currently: Ion-Bond, Inc
1064 Chicago Road
Troy, Michigan 48083

²Currently: ETH Zurich

Please direct all correspondence to:

R.G. Buchheit
Ohio State University
Dept. of Materials Science and Engineering
477 Watts Hall
2041 College Rd.
Columbus, OH 43210
Tel. (614) 292-6085
Fax. (614) 292-9857
Email: buchheit.8@osu.edu

ABSTRACT

Chromate conversion coatings are noteworthy because of their ability to self-heal if mechanical or chemical damage occurs, provided the damage is not too severe. Self-healing, or active corrosion protection (ACP), involves several discrete processes: release of chromate from the coating, its transport through solution, and its action at the site of damage; typically pits. A simple exposure cell, named the "simulated scratch cell", was recently devised by Zhao and co-workers to reproducibly examine chromate conversion coatings for evidence of these processes. This cell consists of two aluminum alloy surfaces, one coated and one bare, separated by a gap several millimeters in width filled with an aggressive solution. If a coating exhibits ACP, the inhibiting agent will be released into solution, interact with the bare surface, and stifle corrosion. Each of these processes can be readily tested and examined standard laboratory and analytical methods. These techniques were used to study a Ce-bearing conversion coatings for evidence of ACP. Candidate coatings were formed on AA 2024-T3 substrates by modifying hydrotalcite coatings with Ce^{4+} compounds. Results of experiments conducted with the simulated scratch cell show that when Ce^{4+} is introduced into hydrotalcite, a classic ACP response is observed. Specifically, tetravalent Ce compounds in the coating are dissolved by an attacking solution, transported to active defect sites on bare aluminum surfaces, then reduced and precipitated to inhibit further corrosion. This paper reviews certain aspects of ACP in chromate conversion coatings, summarizes prior studies on Ce-containing conversion coatings, and presents details of new experiments, which show that self-healing is possible in Ce-bearing coatings.

Keywords: chromate-free coatings. chromate coatings, self-healing, active corrosion protection.

INTRODUCTION

Chromate conversion coatings are an important part of surface finishing processes for many alloys including aluminum, zinc, steels, and cadmium. These coatings provide good resistance against atmospheric corrosion, and are excellent bases for primers and paints.

Chromate conversion coatings are distinguished by the ease with which they are applied, their applicability to a wide range of metals and alloys, and in many cases, their ability to improve the substrate corrosion resistance by virtue of a built-in inhibitor reservoir. This inhibitor reservoir provides additional corrosion protection beyond the barrier protection afforded by a thickened oxide layer.

This built-in, or "active" corrosion protection (ACP) is distinct from "passive" corrosion protection that is often produced by a barrier oxide film on a metal surface. ACP by conversion coatings is less important when the coating is used as a base for paints and primers that are good barriers and contain soluble chromate inhibitors themselves. However, in situations where the conversion coating is the primary barrier against corrosion, ACP is critical. This allows a surface to retain corrosion resistance after minor mechanical and chemical damage has breached the oxide film.

As is now well documented, chromium is being eliminated as a constituent in metal finishing operations due to its poisonous effects on people and the environment. Over the past 15 years, a vigorous effort to minimize chromium release into the environment has developed. Part of this activity has focussed on development of chromate-free conversion coating technologies. In the case of aluminum alloys, the search for a suitable replacement has been complicated by the stringent performance requirements imposed by industrial and military specifications.

Nonetheless, a plethora of chromate-free technologies has emerged. Some of these coatings are used on a commercial basis, but none are used as widely, or as comfortably, as chromate conversion coatings. Arguably, part of the reason for lack or widespread implementation is that

few if any of the chromate-free conversion coatings exhibits (ACP), otherwise known as "self-healing".

In this paper we review certain aspects related to the phenomenology of active corrosion protection by chromate conversion coatings and present a summary of the research on the use of Ce as a constituent for conversion coatings on aluminum. We also present results from recent experiments, which show that it is possible to make Ce-bearing conversion coatings using simple coating methods that demonstrate characteristics of self-healing.

ACTIVE CORROSION PROTECTION AND CHROMATE CONVERSION COATINGS

According to the most current views, accelerated chromate conversion coatings are a mixture of hydrated amorphous Cr(III)-Cr(VI) oxide (1), hydrated aluminum oxide, ferri/ferrocyanides (1,2,3), small to moderate quantities of alloying elements from the substrate, and minor ingredients present in commercial formulations. Coating thicknesses range from 50 nm to 2-3 μm , depending on bath chemistry and contact time. The total amount of Cr(VI) has been estimated to range anywhere from 6 to 50% of the total coating chromium content (4,5,6). In freshly formed coatings, a substantial fraction is reversibly bound in the mixed oxide, and may be leached when solution contacts the coating. With time, the leachable fraction of chromate decreases. Beyond their leachable chromate component, these coatings are largely insoluble and provide physical barrier protection of the underlying aluminum substrate.

There is both indirect and direct evidence supporting the idea that leached Cr(VI) results in dynamic repair by interaction with incipient defects in the coating. Figures 1a and b show the accumulation of pitting damage as a function of exposure time for chromate and chromate-free conversion coatings due to salt spray testing (7). Results from chromate-free coatings are collected in Figure 1a, and results from chromate conversion coatings are collected in Figure 1b. In these figures, the smaller the pitting resistance index (PRI), the greater the accumulation of pitting damage. A comparison of the data in these figures shows two distinct behaviors. In Figure

1a, the PRI for many of the chromate-free coatings is high initially, and remains high for times as long as 200 hours. However, once pitting damage is initiated, it accumulates very rapidly. Correspondingly, the PRI drops off precipitously. This behavior appears to be characteristic of barrier protection. An intact barrier film is capable of resisting attack initially, but once the barrier is breached exposing bare metal, corrosion damage accumulates quickly.

A different behavior is exhibited by chromate conversion coatings (CCCs). Figure 1b shows the PRI for several different commercial CCCs. Very early in the exposure period, Cr and Cr-free coatings are indistinguishable on the basis of their PRI. For chromate coatings though, the PRI begins and remains high for over 1000 hours. Pitting does occur, as indicated by the slight decrease in PRI, but no precipitous decrease occurs indicating the rapid accumulation of damage. This behavior is attributed to active corrosion protection. Chromate leaches from the coating and acts at incipient pits prohibiting their propagation.

The data in Figure 1 show the superiority of CCCs, but whether the effect is due to self-healing is debatable. Recent experiments provide a far more definitive indication of active corrosion protection. To test for ACP, Zhao et al. devised a simple cell consisting of a chromate conversion coated surface and an opposing, uncoated alloy surface separated by a 1.8 mm thick O-ring (8). The space inside the O-ring and between the opposing surfaces was filled with 0.1 M NaCl. Any chromate detected on the bare surface after exposure in this cell must have originated from the CCC, migrated through solution and deposited on the bare surface. This simple device, termed a "simulated scratch cell", enabled rigorous examination of the discrete processes involved in active corrosion protection in a manner that was reproducible from experiment to experiment.

Zhao made polarization resistance measurements of initially bare surfaces after various lengths of exposure time in the simulated scratch cell. Polarization resistances increased from about $10^4 \Omega \text{cm}^2$ to $10^6 \Omega \text{cm}^2$ after 48 hours of exposure. In control experiments, where two uncoated surfaces were used to construct the cell, the polarization resistance decreased slightly

over the same exposure interval. Raman spectroscopy of the initially bare surface after 48 hours showed clear evidence for the formation of a solid compound in and around small pits that was spectroscopically similar to a chromate conversion coating. Solid chromium oxide deposition on the unpitted surface was not detected, but was probably present at concentrations below the detection limit of the instrumentation. In parallel experiments, Raman spectroscopy of a solution droplet in contact with a freshly formed CCC showed that 30 to 40 ppm chromate accumulated in about 48 hours. On a CCC aged in air for 10 days, chromate only accumulated to a level of about 10 to 20 ppm.

Altogether, these results demonstrate that chromate is released from a CCC, which is then transported through solution to act at pits to slow their growth perhaps by adsorbing to and stabilizing hydrous aluminum corrosion product in the pit. On the basis of this experiment, it is possible to establish several distinct, testable elements of ACP. They are:

- 1) release of the inhibitor from the coating into a contacting solution
- 2) transport of the inhibitor through solution
- 3) suppression of corrosion by action of the inhibitor.

With these testable criteria and the simulated scratch cell as a test vehicle, it is possible to examine chromate-free coatings for evidence of active corrosion protection.

CERIUM-BASED CONVERSION COATINGS

In the mid-1980s, Hinton and coworkers examined corrosion inhibition of high strength Al alloys by rare earth metal (REM) salts dissolved in aqueous solutions, and showed that these compounds were effective inhibitors for aluminum, ferrous and zinc alloys. This work has continued steadily over the years, but the essential elements of Ce corrosion inhibition were clearly established in earliest reports from this group (9). Studies showed that 100 to 1000 ppm additions of CeCl_3 to sodium chloride solutions suppressed corrosion of 7075-T6 in potentiodynamic polarization testing and in alternate immersion weight loss testing. Surface

analysis showed incorporation of Ce into compact and protective surface films. Polarization tests showed inhibition of cathodic reaction kinetics, and, as is now less widely regarded, the anodic kinetics. Later work by Aldykewicz, et al. shed more light on cathodic inhibition showing that Ce films formed at local cathodic sites on the alloy surface stifled oxygen reduction thereby limiting corrosion damage (10,11). Film formation was proposed to occur when local cathodic activity increased the near-surface solution pH, which stimulated precipitation of Ce hydroxide. Perhaps most importantly, it was shown that a film with persistent corrosion resistance could be formed by exposure of alloy surface to a CeCl_3 solution. Ultimately, this phenomenon was the basis for the conversion coating formulations developed Hinton based on the use of Ce salts (12).

Arnott, et al. showed that Ce films formation occurred by an island-growth mechanism (13). Films formed first at sites of local cathodic activity such as intermetallic particles and grain boundaries. Ce^{4+} oxides detected in the coating were thought to arise by oxidation of Ce^{3+} in oxygenated alkaline solutions. Davenport, et al. later confirmed this speculation by x-ray absorption near edge structure (XANES) measurements (14). It was also shown that corrosion resistant Ce coatings could be formed on Al alloys by immersion in aqueous CeCl_3 solutions either at the open circuit potential, or under cathodic polarization. Coatings were also formed by exposing surfaces to $\text{Ce}(\text{NO}_3)_3$ dissolved in butoxyethanol (15). As in earlier experiments, corrosion resistance appeared to be due to suppression of the reduction reaction kinetics and, or for long coating formation times, suppression of the anodic kinetics and elevation of the pitting potential. Additionally, other cations were shown to inhibit reduction reaction kinetics and improve corrosion resistance by forming thin surface films. The best non-cerium inhibitors included Ni^{2+} , Pr^{3+} , Nd^{3+} (16). Further studies indicated that cerium salts could be used to inhibit corrosion of zinc and steel substrates (17). It was also found that several different Ce salts provided effective corrosion inhibition (18).

The lingering problem for implementing immersion-based Ce passivation processes was the long time required for the protective film to form; up to one week in most cases. The Hinton

group learned that the kinetics of Ce deposition were substantially increased by using Ce^{4+} solutions (12). Highly corrosion resistant films could be formed by contacting Al alloy surfaces with a slightly acidic 1000 – 10000 ppm CeCl_3 solution containing several weight percent hydrogen peroxide, where the peroxide oxidized Ce^{3+} to Ce^{4+} in solution. Mixed Ce^{3+} - Ce^{4+} coatings were formed in 6 to 10 of minutes on a range of alloys. These coatings possessed outstanding corrosion resistance in both electrochemical and exposure (salt spray) testing.

In the late 1980s, Mansfeld began to study the effectiveness of Ce-based passivation on Al alloys and Al-based metal matrix composites by electrochemical impedance spectroscopy (19). Results showed that the corrosion resistance of 6061-T6, 7075-T6, Al-SiC, and Al-graphite metal matrix composites in aerated 0.5M NaCl were greatly improved by pre-exposure to 1000 ppm CeCl_3 solutions for one week. Shih and Mansfeld monitored the EIS response of 6061-T6 and 7075-T6 aluminum alloys with and without passivation in a variety of rare earth metal salt solutions to confirm the earlier results of Hinton (20).

Mansfeld combined elements from his earlier work with ideas developed from studies of highly corrosion resistant supersaturated non-equilibrium Al-transition metal alloys (21,22) to develop a Ce-Mo surface modification process. In this three-step process, degreased and deoxidized Al alloy surfaces were first immersed in 10 mM $\text{Ce}(\text{NO}_3)_3$ at 100°C , then immersed in 10 mM CeCl_3 also at 100°C , and finally were potentiostatically polarized at $+0.5 \text{ V}_{\text{sce}}$ in deaerated 0.1M Na_2MoO_4 . Al alloys surfaces treated in this manner resisted pitting in aerated 0.5M NaCl solutions for 60 days.

Independent characterization of the Ce-Mo coatings produced on 2024-T3 and 6061-T6 were carried out (23). The coating was analyzed after each stage in the process and the evolution in coating chemistry and thickness was determined. Results showed that the coating consisted primarily of hydrated aluminum oxide with Ce deposited on and near cathodic intermetallic compounds such as $\text{Al}_7\text{Cu}_2\text{Fe}$ in 2024 and $\text{Al}_{12}\text{Si}(\text{Fe}, \text{Mn}, \text{Cr})$ in 6061-T6. Ce was not associated with active intermetallics like Al_2CuMg . Rather, these intermetallics were dissolved during the

anodic polarization in the molybdate solution, leaving Mo-rich pits. In general, more Ce was detected in coatings on 2024-T3, than on 6061-T6. This work plainly showed the importance of alloy chemistry and microstructure in Ce-Mo coating formation. In terms of coating chemistry, Ce was detected in trivalent and tetravalent oxidation states, while Mo was detected only in its hexavalent form. It was argued that Mo^{6+} in the coating provided self-healing, by reduction to Mo^{4+} , however no Mo^{4+} was ever detected. XANES measurements of Ce-Mo coatings after exposure to 0.5M NaCl for 30 days suggests that Mo^{6+} is leached into solution and does not participate in self-healing (24).

Noting that the Ce-Mo surface modification process thickened the oxide film *and* imparted Ce and Mo into it, Kendig sought to determine how critical a role Ce and Mo played in determining the overall corrosion resistance (25). To isolate the role of these heavy metals, Kendig formed coatings using a Ce and Mo-free process consisting of 4h immersion in boiling 30 mM NaNO_3 followed by 2 polarization at 0.5 V_{sc} in 0.1M borate solution. Coatings containing only Ce or Mo were also made to isolate effects due to the presence of either Ce or Mo in the film. The corrosion resistances of these coatings were compared to that of coatings formed by Ce-Mo surface modification. Corrosion resistance during immersion in aerated 0.5 M NaCl solution was measured using EIS for exposure times up to two weeks. The data were analyzed by equivalent circuit analysis and the pitting resistance, R_{pit} , was used a figure of merit to estimate relative corrosion resistances. The pitting resistance of the coatings decreased in the order:

$$\text{Ce-Mo} > \text{Mo-only} > \text{Ce Only} > \text{Ce-Mo-free}.$$

The results suggested that Ce and Mo, in fact, played a synergistic role in providing corrosion resistance. According to Kendig's interpretation of the results, Ce forms insoluble oxides that reinforce the hydrated aluminum oxide film and the oxidizing Mo species plays the role of active inhibitor. The comments focussing on the role of Mo in corrosion protection by this

coating are significant in that they are perhaps the first referral to and recognition of the possibility “active corrosion protection” in a Cr-free conversion coating system. Whether ACP actually occurs as described earlier is an open question.

This fundamental work, which has evolved over the past 15 years, has begun to impact coating technology and industrial metal finishing. REM salts are used as corrosion inhibitors added to metals as alloying elements (26, 27), imparted into conversion and anodized coatings (28), and used as soluble corrosion inhibitors (29). A number of recent patents have been issued that describe the use of cerium as a primary or supplemental ingredient in corrosion resistant coating formulations. These coating processes can be classified as follows:

1) *Ce-sealed hydrothermal films*. In these processes, thickened films are formed by hydrothermal treatment and then sealed in a Ce^{3+} or Ce^{4+} solution. Examples include Ce-sealed boehmite coatings formed by elevated temperature in water (30), or triethanolamine solutions (31).

Hydrotalcite coatings may also be sealed by contact with Ce solutions as will be described later (32).

2) *Surface Modification*. In these processes, a potential is applied to the surface to induce deposition of Ce from solution. This can be accomplished by cathodic polarization, which develops alkaline conditions at the electrode surface and induces Ce precipitation (11). As described above, Mansfeld uses slight anodic polarization to stimulate interaction of Mo with thickened hydrothermal layers sealed with Ce (33).

3) *Cerating*. These processes are analogs to Hinton’s immersion-based approach to developing REM coatings. Surfaces are contacted with a slightly acidic solution containing soluble Ce^{3+} or Ce^{4+} as the primary film-forming agent (34).

ACTIVE CORROSION PROTECTION BY CE

The literature over the past 20 years clearly demonstrates the excellent corrosion protection by inorganic Ce coatings. We note that Cerium exhibits a moderately soluble +4 oxidation state and a comparatively insoluble +3 oxidation state. The relevant solubility curves are shown in Figure 2. We hypothesize that if a tetravalent oxide were to be introduced into a thickened barrier layer on aluminum, it might be possible to replicate active corrosion protection. When a solution contacts a Ce^{4+} -bearing coating, soluble Ce^{4+} may be released due to its high solubility. If the Ce^{4+} ions encounter reducing conditions like those associated with bare metal exposed through a coating defect, reduction to Ce^{3+} and precipitation would ensue. Precipitation of a hydrated Ce oxide at the defect might then stifle further corrosion. To test this hypothesis, a series of experiments were carried out based on the methods of Zhao et al. (8).

EXPERIMENTAL PROCEDURES

Materials and surface preparation. Coatings were formed on 4"x5" x 0.080" thick 2024-T3 (Al-4.5Cu-1.5Mg-0.6Mn) and 6061-T6 (Al-1.0Si-0.6Mg-0.3Cu) sheet stock. Prior to coating all samples were washed with an alkaline detergent, degreased in a sodium silicate/sodium carbonate solution, then deoxidized in a nitric acid/sodium bromate-based solution. Panels were rinsed in overflowing deionized water in between each step. Hydrotalcite coatings were formed by immersion in a bath containing a mixture of lithium, potassium and sodium salts. Coated surfaces were rinsed in a pore sealing magnesium acetate solution, then immediately immersed in either a cerium or lanthanum solution. Coatings were rinsed and air-dried for 24 hours before any further use. The compositions, temperature, immersion time for all of the steps are shown in Table I.

The simulated scratch cell. As described earlier, Zhao devised a simulated scratch cell to test for ACP in chromate conversion coatings (8). Modifications made to Zhao's design are shown schematically in Figure 3. In the present experiment, one 2024-T3 surface is coated with Ce-

modified hydrotalcite, the other bare 2024-T3 or 6061-T6. In these experiments, each surface was 5.1 cm^2 . The surfaces are separated by a 5 mm gap that was filled with a 0.5M NaCl solution. In this arrangement, the bare surface is examined for evidence of healing by release of Ce^{4+} from the Ce-modified hydrotalcite coating on the opposing surface.

Characterization techniques. Ultraviolet (UV) optical absorbance spectroscopy was used to characterize Ce in solution. A UV spectrometer with a Xe light source was used to pass light through solutions that had been contacted with Ce-modified HT coatings, or contained direct additions of $\text{Ce}(\text{NO}_3)_3$. Solution absorbance was analyzed for wavelengths ranging from 100 to 600 nm. Inductively coupled plasma-atomic emission spectroscopy (ICP-AES) was used to analyze for La release into solution because dissolved La is not a UV absorber.

The simulated scratch cell was the primary vehicle used to test for elements of ACP. Aliquots of the gap solution were periodically extracted and examined for evidence of soluble Ce. After exposure, the cell was disassembled and the bare side was examined for the presence and distribution of Ce oxides. Corrosion resistance measurements were made of the bare side to determine if its corrosion resistance had increased signaling healing. Additionally, the corrosion resistance of the coated side was examined to determine if Ce release had caused a decrease in its corrosion resistance.

To establish the sensitivity of the UV absorption technique, measurements were made on $\text{Ce}(\text{NO}_3)_3$ solutions with and without H_2O_2 additions (to oxidize Ce^{3+} to Ce^{4+}). Figure 4 shows representative absorption spectra from 10^{-3}M $\text{Ce}(\text{NO}_3)_3$ and $\text{Ce}(\text{NO}_3)_3 + \text{H}_2\text{O}_2$ solutions. Absorption peak height was used as the parameter to assess Ce concentration in the simulated scratch experiments. Due to the shoulder in the Ce(IV) spectra at longer wavelengths it is possible to distinguish Ce^{3+} from Ce^{4+} at concentrations as low as 10^{-3}M . Additional measurements with standard solutions showed that Ce concentrations as low as 10^{-5}M could be detected (Figure 5).

Scanning electron microscopy (SEM) and Auger electron spectroscopy (AES) were used to characterize surface morphologies and surface chemistries. AES measurements were made with a PHI 680 Auger spectrometer equipped with a field emission gun. The operating beam conditions were 10keV, 1nA, or 1.8KeV, 1nA depending on which spectral regions were being investigated. Areas of interest were identified by secondary electron imaging. For depth profiling, a 1 keV/0.5mA Argon ion beam was used. The sputter rate was 2.85 nm/min for SiO₂. Quantitative AES results were determined from derivative spectra using elemental sensitivity factors. Auger transitions from the relevant elements is given in Table II.

Electrochemical impedance spectroscopy (EIS) was used to measure the corrosion resistance of the various coatings and uncoated surfaces. Impedance spectra were collected from 10kHz to 10mHz sampling at 7 points per decade frequency. Typically spectra were collected after a surface had been in contact with 0.5M NaCl solution for 24 hours. The spectra were fit to a simple, single time constant equivalent circuit model to extract a resistance parameter that was used as a figure of merit to judge coating corrosion resistance (35).

RESULTS AND DISCUSSION

Corrosion resistance of Ce-modified hydrotalcite coatings. Ce-modified hydrotalcite (Ce-HT) coatings have been made that will pass 168h of ASTM B117 salt fog exposure on 2024-T3. However, the coatings produced in this study were not that corrosion resistant. Figure 6 is a Nyquist plot showing the corrosion resistance of Ce-modified hydrotalcite coatings, La-modified hydrotalcite (described below), chromate conversion coatings and hydrotalcite sealed with magnesium acetate. The coatings used in this study exhibited coating resistances, R_c , of about 10^5 ohm·cm², which is about an order of magnitude less than a typical chromate conversion coating, and is an order of magnitude less than is exhibited by any coatings that normally pass a salt spray test (35).

Ce release in the simulated scratch cell. Ultraviolet (UV) absorbance measurements were used to detect Ce released into the gap solution during simulated scratch experiments. Figure 7 shows UV absorbance peak heights from aliquots of solution extracted from the simulated scratch cell for times ranging from 4 to 48 hours. The fact that Ce is detected confirms that Ce can be released from Ce-modified hydrotalcite into solution. The absorbance peak heights ranged from 0.5 to 0.9, which correspond to soluble Ce concentrations of about 3×10^{-4} to 3×10^{-3} M, or 40 to 400 ppm. Inhibition of the bare surface in the cell is expected under these conditions considering that Hinton reports that 10 ppm CeCl_3 in 0.1 M NaCl is sufficient to reduce the corrosion rate of 7075-T6 (9).

Corrosion resistance of the simulated defect. To assess changes in corrosion resistance to the bare side sample of the cell that might indicate healing, the cell was disassembled after 48h of exposure and the bare side impedance was measured in aerated 0.05M NaCl. Figure 8 shows the coating corrosion resistance, R_c , determined by complex non-linear least squares fitting of EIS data to the simplified Randles circuit model. R_c data are plotted as a function of exposure time in the 0.05 M NaCl test solution, which was used to enhance sensitivity of the measurement. For comparison, R_c data are shown for a bare 2024-T3 surface exposed to another, identical bare surface for 48 h in the cell, and a polished 2024-T3 surface exposed only to the 0.05 M NaCl solution. The curves represent averages of three replicate runs; error bars have been omitted for clarity. Inspection of the data shows that the surface exposed in the simulated scratch cell with the Ce-modified hydrotalcite exhibits R_c values that are nearly an order of magnitude greater than that of a surface exposed only to another bare surface. This result suggests that the bare surface in the simulated scratch cell has, in fact, been protected from corrosion by release of Ce from the Ce-modified hydrotalcite coating.

Interaction of Ce with 6061-T6 and 2024-T3 surfaces. Figure 9 shows a secondary electron image of 6061-T6 surface exposed to Ce-modified hydrotalcite for 24 h in the cell. Polishing

marks are clearly visible in this image, but superimposed on those marks is a cracked surface film with locally heavier deposits. The figure indicates two areas where AES analysis was conducted. Area 1 is on a Cu-rich second phase, and Area 2 on the matrix phase. Figure 10 shows AES spectrum of the Ce MNN and Cu LMM transitions for both of the analysis areas. Ce is detected on the second phase particle, but is absent on the matrix phase. This observation is consistent with descriptions of Ce oxide deposition on Al alloys from solution (18). Ce deposits initially and preferentially and on noble, Cu-rich intermetallic particles because they are sites that support reduction reactions, develop local alkalinity, and induce Ce precipitation (10,11).

Figure 11 shows a scanning electron micrograph of a polished 2024-T3 surface that was in contact with 0.5 M NaCl plus 10^{-3} M $\text{Ce}(\text{NO}_3)_3$ solution for 48h. Figure 12 shows the Ce LMM and Ce NOO Auger transitions taken from various locations on the matrix phase and on the second phase particles. Although there is no obvious Ce deposit in this case, the intensity of the Auger transitions indicates that Ce interacts much more vigorously with particles than the matrix phase under these exposure conditions.

Sputtering experiments indicate that Ce does not interact as strongly with S phase particles and the matrix phase as with $\text{Al}_6(\text{Cu,Fe,Mn})$. Figure 13 shows several colonies of particles on a polished 2024-T3 section that was exposed under the same conditions as for Fig. 11. These colonies include the Al_2CuMg and $\text{Al}_6(\text{Cu,Mn,Fe})$ particle types. On the basis of the intensity of the Ce LMM Auger transition shown in Figure 14, Ce has deposited on all of the phases (Fig. 14a). However, after sputtering through 5 nm of the surface, the intensity of the Ce LMM peak strongly diminishes in the matrix phase measurements and the peak is absent on Al_2CuMg phase (Fig. 14b). In comparison, the peak remains strong in measurements made on the $\text{Al}_6(\text{Cu,Mn,Fe})$ particles. This suggests that the Ce deposition is greater on $\text{Al}_6(\text{Cu,Mn,Fe})$ than on other phases in the alloy, and is consistent with the idea that Ce deposition occurs preferentially and most strongly on cathodic sites on the alloy surface.

Ce inhibitor stability. Results show that Ce in hydrotalcite coatings tends to remain or oxidize to Ce^{4+} in the presence of atmospheric oxygen, condensed moisture, and the prevailing alkaline conditions associated with hydrotalcites. In order to retain ACP for extended periods of time, it is necessary that the Ce^{4+} introduced into the coating, or produced in situ be stable. This Ce^{4+} is easily liberated to provide inhibiting action at defects elsewhere in the coating. Figure 15 shows x-ray photoelectron spectroscopy (XPS) data from Ce^{3+} - and Ce^{4+} -modified hydrotalcite coatings both before and after 168 hours of ASTM B117 salt fog exposure. Coatings modified by immersion in a $\text{Ce}(\text{NO}_3)_3$ solution (no H_2O_2) produce coatings with Ce predominantly in a +3 oxidation state. Coatings modified by immersion in a $\text{Ce}(\text{NO}_3)_3$ solution plus H_2O_2 contain Ce predominantly in a +4 oxidation state. These spectra are shown in the uppermost (Ce^{4+}) and lowermost (Ce^{3+}) plots in Figure 15. The spectra from Ce in a +4 oxidation state are readily distinguished from those due to Ce in a +3 state by the intense Ce satellite at 918.5 eV and intense features due to peak splitting in the $\text{Ce}3d_{5/2}$ (885eV) and $\text{Ce}3d_{3/2}$ (902eV) (36). XPS data collected from Ce^{3+} - and Ce^{4+} -modified hydrotalcite coatings after salt fog exposure are remarkably similar and exhibit peak splitting characteristic of Ce^{4+} (center figure). This observation is in agreement with Davenport et al. who used x-ray absorption near edge spectroscopy to show that Ce^{3+} converted to Ce^{4+} in Ce-bearing coatings applied to Al-Mg alloys upon exposure to aerated chloride solutions (14). More importantly, this observation indicates that the Ce^{4+} in hydrotalcite coatings will be stabilized by the oxidizing power of natural environments until reducing conditions associated with the exposure of the aluminum substrate in defects are encountered. At those locations Ce^{4+} will be reduced and precipitated to inhibit corrosion.

Figure 16 illustrates how the Ce^{4+} stability might be preserved, and how the Ce reservoir might operate. When solution contacts the coating, tetravalent Ce oxides are dissolved (I to II). When Ce in solution comes in contact with a defect, the reducing nature of the bare Al would act to reduce Ce^{4+} to Ce^{3+} (II to III), with an attendant decrease in Ce solubility. As a result,

precipitation of a trivalent Ce oxide would be expected to occur (III to IV). Precipitation would be enhanced by local alkalinity that is thought to exist near Cu-rich second phase particles in Al-Cu-Mg alloys. This precipitation process stifles corrosion. If portions of the reprecipitated Ce are not in direct contact with the reducing Al substrate, it is possible under continued or renewed solution contact for Ce^{3+} oxides to be oxidized and redissolved by an oxygenated solution (IV to II). This would have the effect renewing the inhibitor cycle. While operation of this cycle has not yet been demonstrated to preserve corrosion resistance The XPS data in Figure 15 clearly indicate that the $\text{Ce}^{3+}/\text{Ce}^{4+}$ redox reaction is dynamic, and facile in both directions.

Lanthanum-modified hydrotalcite. To check that ACP in Ce-modified hydrotalcite was not an artifact of the simulated scratch cell method, a series of experiments was carried out using lanthanum-modified hydrotalcite coatings. Lanthanum is a rare earth element adjacent to Ce on the Periodic Table with some similar chemical characteristics. Like Ce, its trivalent oxide is insoluble under alkaline conditions. However, La differs from Ce in that it does not form a soluble tetravalent oxide. Hence, La-modified hydrotalcite coatings are not expected to exhibit characteristics of ACP.

La-modified hydrotalcite coatings were formed using procedures identical to those used to form Ce-modified coatings. La was introduced into the coating by immersion for 1 minute in a 10 g/L $\text{La}(\text{NO}_3)_3$ solution. The corrosion resistance of La-modified coatings was about 10^5 ohm-cm^2 in EIS testing after 24 hour exposure to 0.5 M NaCl, which is similar to that of Ce-modified coatings.

Simulated scratch cell experiments were then conducted with La-modified coatings. Solution extracted from the cell was analyzed by inductively-coupled plasma atomic emission spectroscopy (ICP-AES) rather than by UV absorbance because La does not absorb at UV wavelengths. La was not detected in concentrations greater than 10^{-6}M for any exposure time between 4 and 48 hours. By comparison, Ce was detected in concentrations greater than 3×10^{-4}

M. As expected, Auger analysis was not able to detect La bare side of the simulated scratch cell after 48 hours of exposure. Additionally, no increase in the corrosion resistance of the bare surface was recorded.

SUMMARY

One of the distinguishing characteristics of chromate conversion coatings is an ability to self-heal if damaged by modest mechanical or chemical attack. This characteristic has been the subject of significant study and subsequent discussion driven somewhat by the absence of any methods to perform mechanistic investigations. However, the recently devised simulated scratch cell enables a more deterministic examination of this phenomenon. Self-healing or as has been referred to here, ACP, can be broken down into several testable characteristics that include: 1) release of the inhibitor into a contacting solution, 2) transport of the inhibitor through solution, 3) suppression of corrosion on a bare metal surface by inhibitor released from the coating. Given these distinct characteristics, and a characterization methodology Ce-modified hydrotalcite conversion coatings were examined for evidence of ACP. Results show that these coatings do indeed show ACP behavior probably because Ce is introduced into the hydrotalcite as a soluble high oxidation state species. When solution contacts the coating, tetravalent Ce compounds dissolve and Ce^{4+} ions migrate through solution, and are reduced and precipitated as low solubility Ce^{3+} compounds at exposed Al surface sites. Since Ce is much less soluble in reduced form, it then precipitates on the bare surfaces and slows corrosion by stifling cathodic and possibly anodic kinetics. Similar experiments conducted with La-modified hydrotalcite do not show evidence of ACP. La exists only in a low solubility trivalent form. Once it is introduced to the hydrotalcite coating, it is not released and cannot participate in the subsequent events that lead to Ce-like ACP.

ACKNOWLEDGEMENTS

The authors would like to acknowledge the financial support of the U.S. Department of Energy, Sandia National Laboratories, DARPA and SERDP. The authors would also like to thank M. Martinez, L. Montes, W. Buttry, and W. Zhang for various technical contributions. The authors would like to thank J. Braithwaite for helpful suggestions on the manuscript.

REFERENCES

- 1) L. Xia, R. L. McCreery, J. Electrochem. Soc. (1999).
- 2) N. J. Newhard, Metal Finishing, 49, 66 (1972).
- 3) P. L. Hagans, C.M. Haas, Surface and Interf. Anal., 21, 65 (1994).
- 4) A. E. Hughes, R. J. Taylor, B. R. W. Hinton, Surface and Interf. Anal., 25, 223 (1997).
- 5) M. Koudlekova, J. Electrochem. Soc., 124, 1165 (1977).
- 6) A. J. Davenport, H. S. Isaacs, Corrosion Sci., 31, 105 (1990).
- 7) National Center for Manufacturing Sciences, "Alternatives to Chromium for Metal Finishing," NCMS Report 0273RE95, Ann Arbor, MI (1995).
- 8) J. Zhao, G. S. Frankel, R. L. McCreery, J. Electrochem. Soc., 145, 2258 (1998).
- 9) B. R. W. Hinton, D. R. Arnott, N. E. Ryan, Metals Forum, 7, 211 (1984).
- 10) A. J. Aldykewicz, Jr., H.S. Isaacs, A.J. Davenport, J. Electrochem. Soc., 142, 3342 (1995).
- 11) A. J. Aldykewicz, Jr., H.S. Isaacs, A.J. Davenport, J. Electrochem. Soc., 143, 147 (1996).
- 12) B. R. W. Hinton, L. Wilson, "Effect of Cerous Chloride Concentration on Corrosion Rate", Australian patent, PCT/AU88/00060.
- 13) D. R. Arnott, N. E. Ryan, B. R. W. Hinton, B. A. Sexton, A. E. Hughes, Applications of Surface Science 22/23, 236 (1985).
- 14) A. J. Davenport, H. S. Isaacs, M. W. Kendig, Corrosion Sci., 32, 653 (1991).
- 15) B. R. W. Hinton, D. R. Hinton, N. E. Ryan, Mater. Forum, 9, 162 (1986).
- 16) D. R. Arnott, B. R. W. Hinton, N. E. Ryan, Materials Perf., Aug., p. 42 (1987).
- 17) B. R. W. Hinton, D. R. Arnott, Microstructural Science, 17, 311 (1989).
- 18) B. R. W. Hinton, J. of Alloys and Compounds, 180, 15 (1992).
- 19) F. Mansfeld, S. Lin, S. Kim, H. Shih, Electrochim. Acta, 34, 1123 (1989), and F. Mansfeld, S. Lin, S. Kim, H. Shih, Corrosion, 45, 615 (1989).
- 20) H. Shih, F. Mansfeld, "Passivation in Rare Earth Metal Chlorides—A New Conversion Coating Process for Aluminum Alloys", p. 180, New Methods for Corrosion Testing of Aluminum Alloys, ASTM STP 1134, V. S. Argawala, G. M. Ugiansky, Eds., American Society for Testing and Materials, Philadelphia (1992).
- 21) B. A. Shaw, G. D. Davis, T. L. Fritz, K. A. Oliver, J. Electrochem. Soc., 137, 359 (1990).
- 22) W. C. Moshier, G. D. Davis, G. O. Cote, J. Electrochem. Soc., 133, 1063 (1990).

- 23) A. E. Hughes, J. D. Gorman, P. J. K. Patterson, Corrosion Science, 38, 1957 (1996), and J. D. Gorman, S. T. Johnson, P. N. Johnston, P. J. K. Paterson, A. E. Hughes, Corrosion Science, 38, 1977 (1996).
- 24) J. Wan, G. E. Thompson, K. Q. Lu, C. J. E. Smith, J. Phys. IV France, 7, c2, 1182 (1997).
- 25) M. Kendig, C. Thomas, J. Electrochem. Soc., 139, L103 (1992).
- 26) R. N. Singh, N. Verma, W. R. Singh, Corrosion, 45, 222 (1989).
- 27) A. C. Crossland, G. E. Thompson, P. Skeldon, G. C. Wood, C. J. E. Smith, H. Habazaki, K. Shimizu, Corrosion Sci., 40, 871 (1998).
- 28) F. Mansfeld, C. Chen, C. B. Breslin, D. Dull, J. Electrochem. Soc., 145, 2792 (1998).
- 29) F. M. Seon, J. Less Common Metals, 148, 73 (1989).
- 30) A. Kindler, U. S. Patent 5,192,374, March (1993).
- 31) R. Rungta, U. S. Patent 5,362,355, November (1993).
- 32) R. G. Buchheit, M. A. Martinez, U.S. Patent 5,756,218, May (1998).
- 33) F. B. Mansfeld, H. Shih, Y. Wang, U. S. Patent 5,194,138, March (1993).
- 34) S. Ikeda, U. S. Patent 4,992,115, February (1991); R. N. Miller, U. S. Patent 5,356,492, October (1994).
- 35) R. G. Buchheit, M. Cunningham, H. Jensen, M. W. Kendig, M. A. Martinez, Corrosion, 54, 61 (1998).
- 36) G. Praline, B. E. Koel, R. L. Hance, H.-I. Lee, J. M. White, J. of Electron Spectroscopy and Related Phenomena, 21, 17 (1980).

Table I. Bath chemistries used to prepare coatings used in this study.

Bath	Bath Chemistry	Temp. (°C)/pH	Time (min.)
Degrease	32 g/L Na ₂ SiO ₃ 48 g/L Na ₂ CO ₃	65/10	2
Deoxidize	30 g/L Sanchem1000TM 72 mL/L conc. HNO ₃	55/2	3
Hydrotalcite Coat	28.3 g/L KNO ₃ 6.9g/L LiNO ₃ 2.4g/L LiOH 0.06g/L NaAlO ₂ (Mg Acetate Rinse)	98/12	10
Ce Modify	10 g/L Ce(NO ₃) ₃ 3 mL/L 30 vol% H ₂ O ₂	23/3	1
La Modify	10g/L LaNO ₃	23/5	1

Table II. Characteristic Energies of Auger transitions for important elements.

Element	Characteristic Energy	Auger Transition
Cu	922	LMM
Mg	1188	KLL
Fe	705	LMM
Mn	592	LMM
Al	1396	KLL
Ce	670	LMM
Ce	80	NOO
La	634	LMM
Cl	184	LMM
O	510	KLL

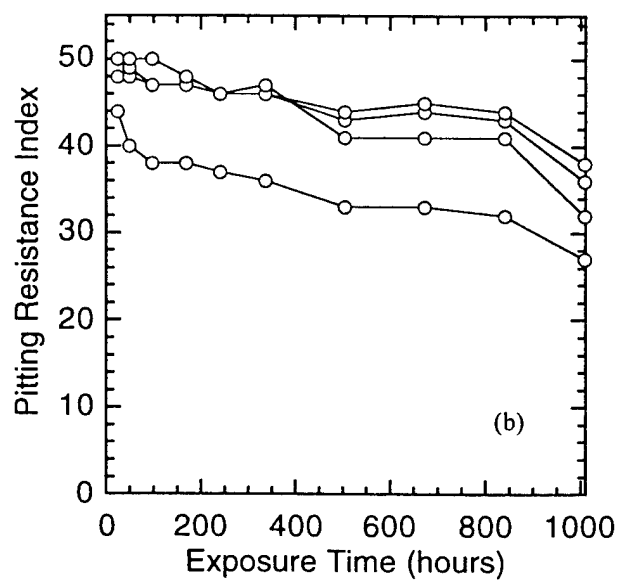
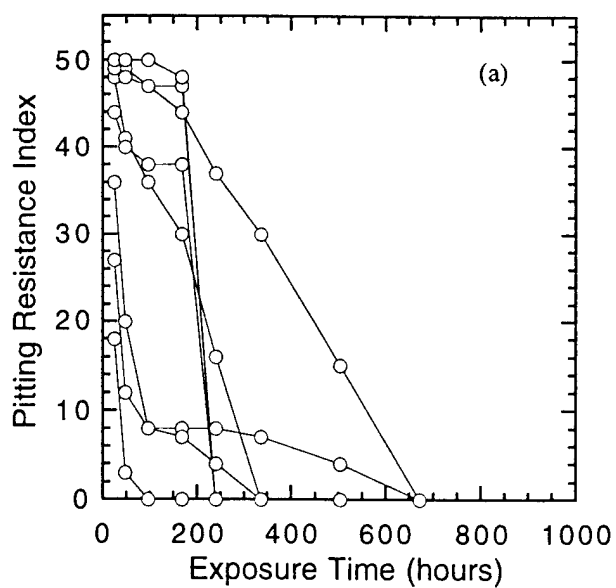


Figure 1. Accumulation of pitting damage versus exposure time for (a) chromate-free, and (b) chromate conversion coating on 7075-T6 after ASTM B117 salt spray exposure testing. Larger pitting resistance indices correspond to a lower incidence of pitting.

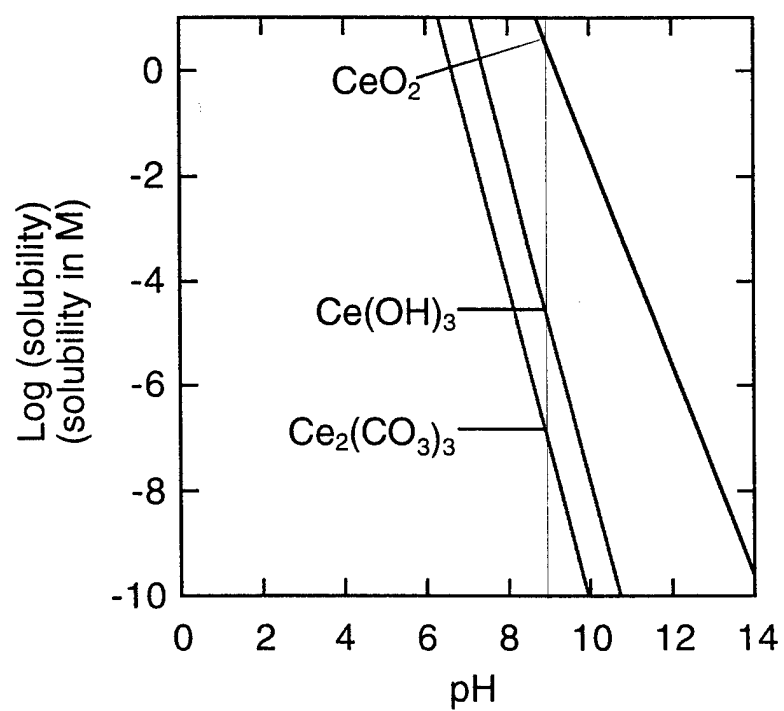


Figure 2. Solubility curves for Ce^{3+} and Ce^{4+} compounds illustrating the difference in solubility associated with the change in Ce oxidation state.

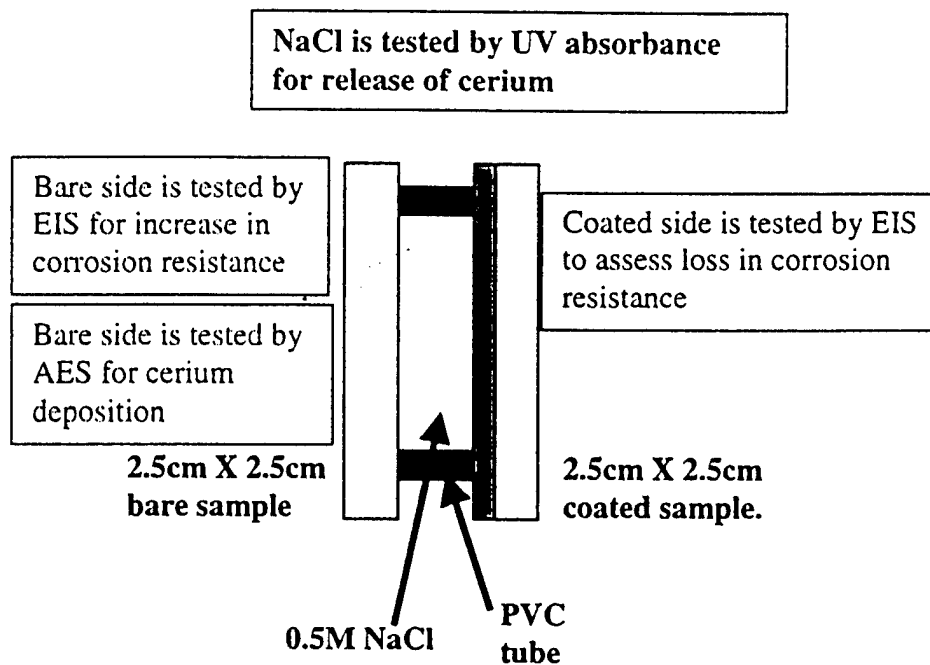


Figure 3. Simulated scratch cell used for the Ce- and La-modified hydroxylapatite ACP experiments.

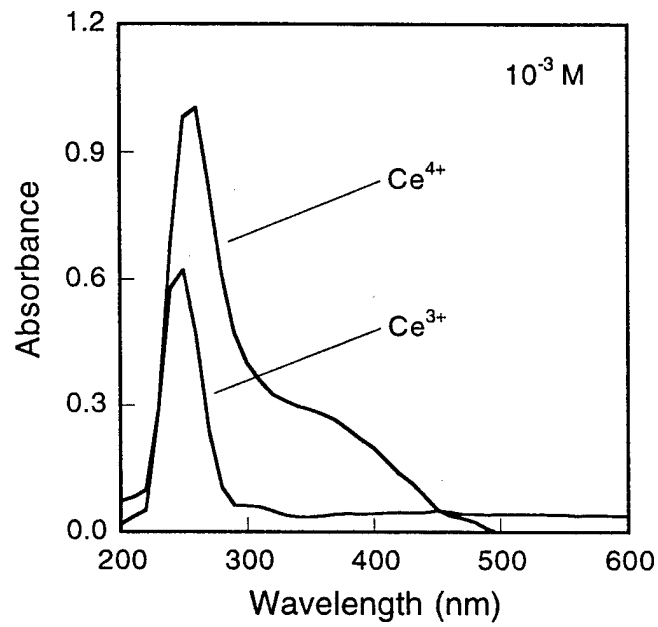


Figure 4. Absorbance spectra for Ce^{3+} ($\text{Ce}(\text{NO}_3)_3$), and Ce^{4+} ($\text{Ce}(\text{NO}_3)_3 + \text{H}_2\text{O}_2$) in aqueous solution illustrating the differences in peak shape that can be used to distinguish these species at higher concentrations.

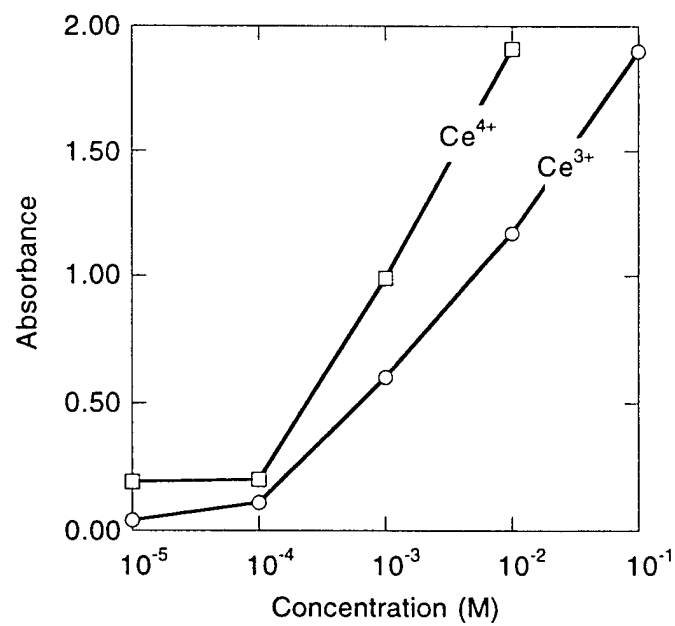


Figure 5. UV absorbance versus Ce³⁺ and Ce⁴⁺ concentration.

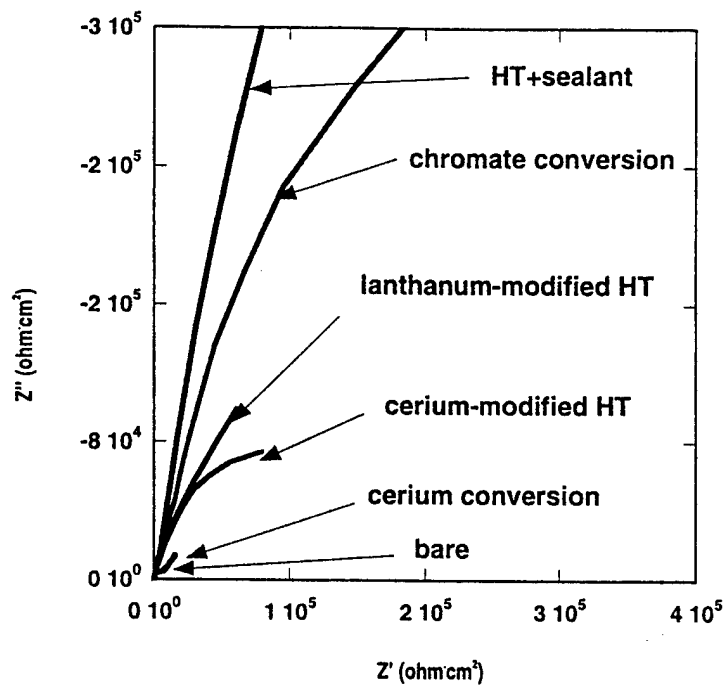


Figure 6. Nyquist plots of Ce- and La- modified hydrotalcite coatings and chromate conversion coatings exposed to aerated 0.5 NaCl for 24 h.

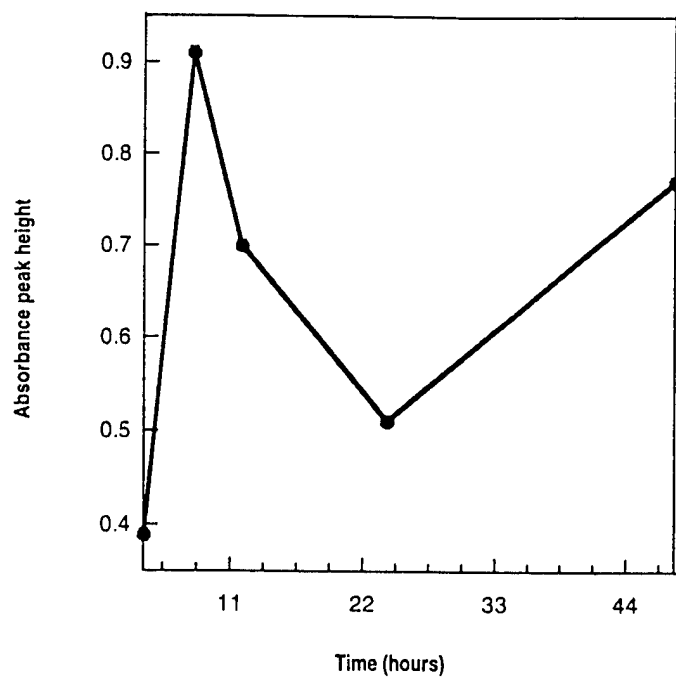


Figure 7. UV absorbance peak height from solution samples extracted from the simulated scratch cell after various exposure times. A 0.5 M NaCl solution was introduced into a cell in which bare 2024-T3 was exposed to Ce-modified hydrotalcite coated 2024-T3.

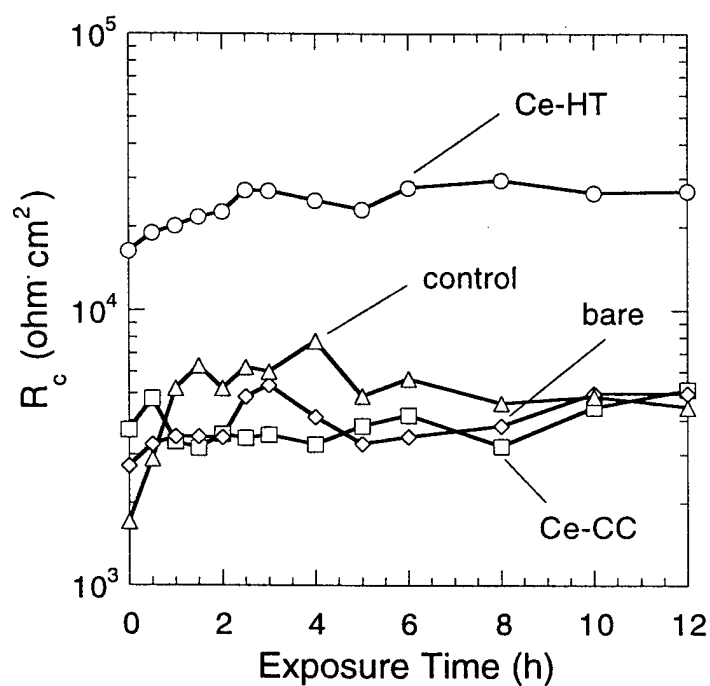


Figure 8. R_c determined by EIS after exposure to aerated 0.05 M NaCl for times up to 12 hours for 2024-T3. Surfaces were exposed in the simulated scratch cell with various other 2024-T3 surfaces as indicated. These included: Ce-HT, Ce-modified hydrotalcite coated; Ce-CC, cerium conversion coated; bare, uncoated 2024-T3; control, 2024-T3 exposed only to 0.05M NaCl.



Figure 9. Backscatter scanning electron micrograph of a 6061-T6 surface exposed in the simulated scratch cell for 48 hours to 0.5 M NaCl. The other surface exposed in the cell was Ce-modified hydrotalcite. Two analysis regions are indicated. Region 1 is on a deposit located over a Cu-rich particle. Region 2 is on the matrix phase.

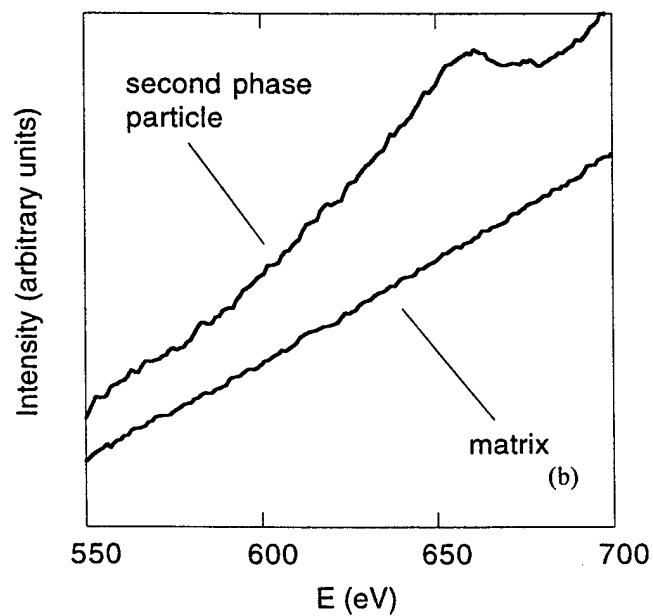
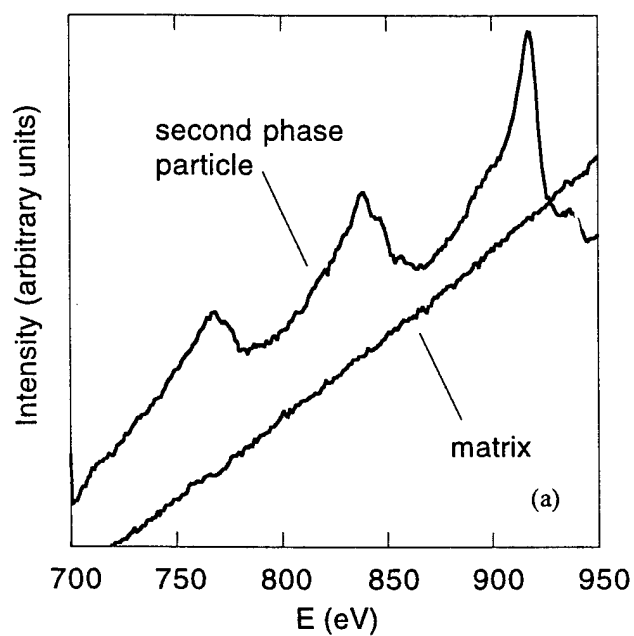


Figure 10. Auger spectra of the (a) Cu LMM and (b) Ce MNN Auger transition from a Cu-rich particle and the matrix phase on a bare 2024-T3 surface in the simulated scratch cell. The other surface was Ce-modified hydrotalcite and the cell contained a solution of 0.5 M NaCl.

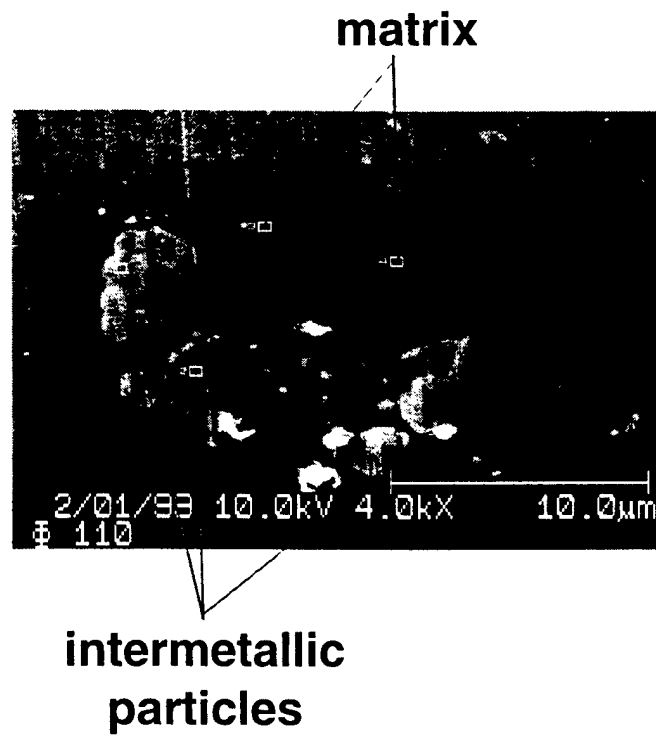


Figure 11. Scanning electron micrograph of a colony of particles on polished 2024-T3 exposed to 0.5M NaCl plus 10^{-3} M $\text{Ce}(\text{NO}_3)_3$ for 48 hours.

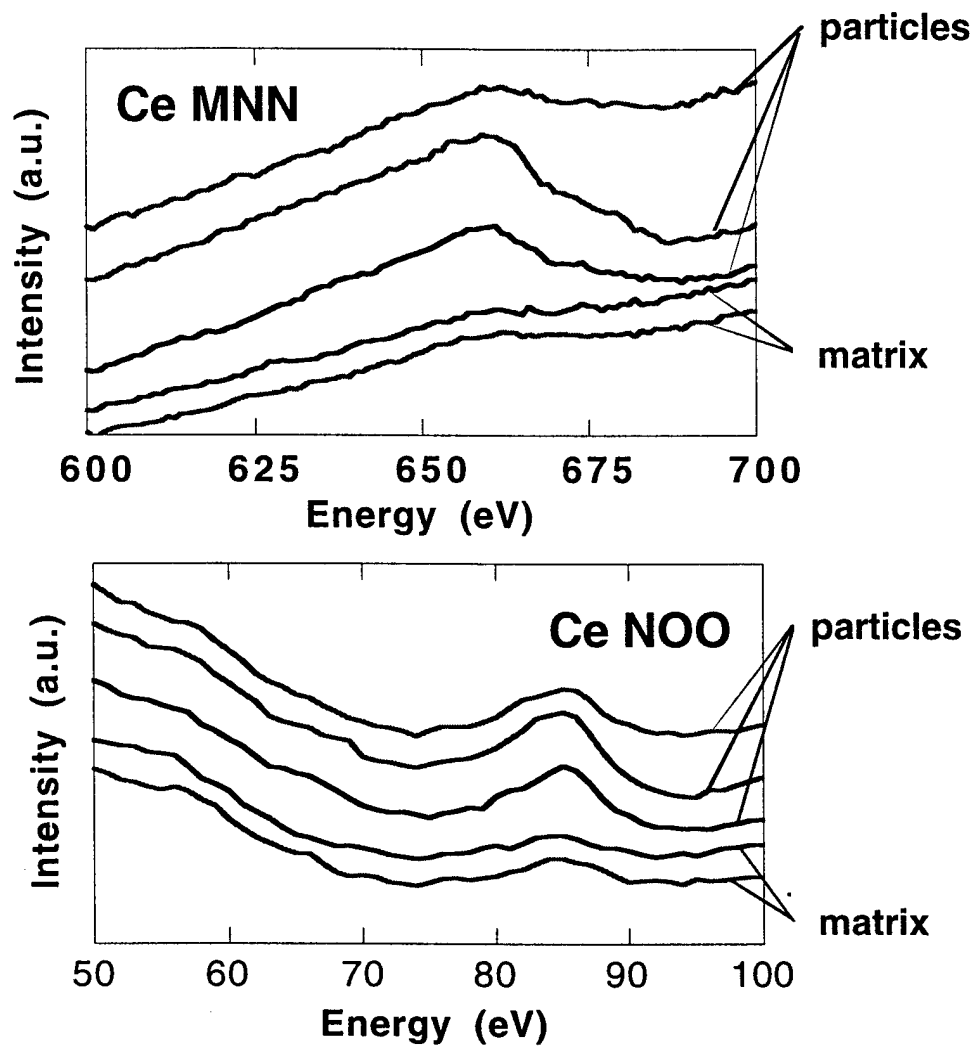


Figure 12. AES profiles in the Ce LMM and Ce NOO Auger transition regions. Intensity of the Auger transitions indicates that Ce interacts preferentially with intermetallic particles.

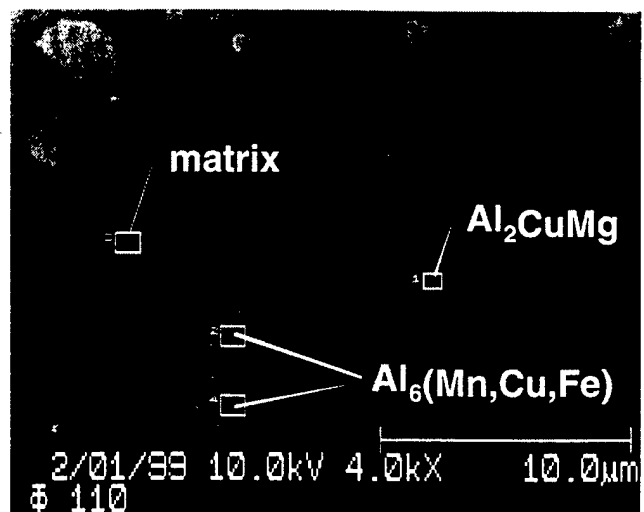


Figure 13. Scanning electron micrograph showing colonies of particles in 2024-T3 exposed to 10^{-3} M $\text{Ce}(\text{NO}_3)_3$ for 48 hours.

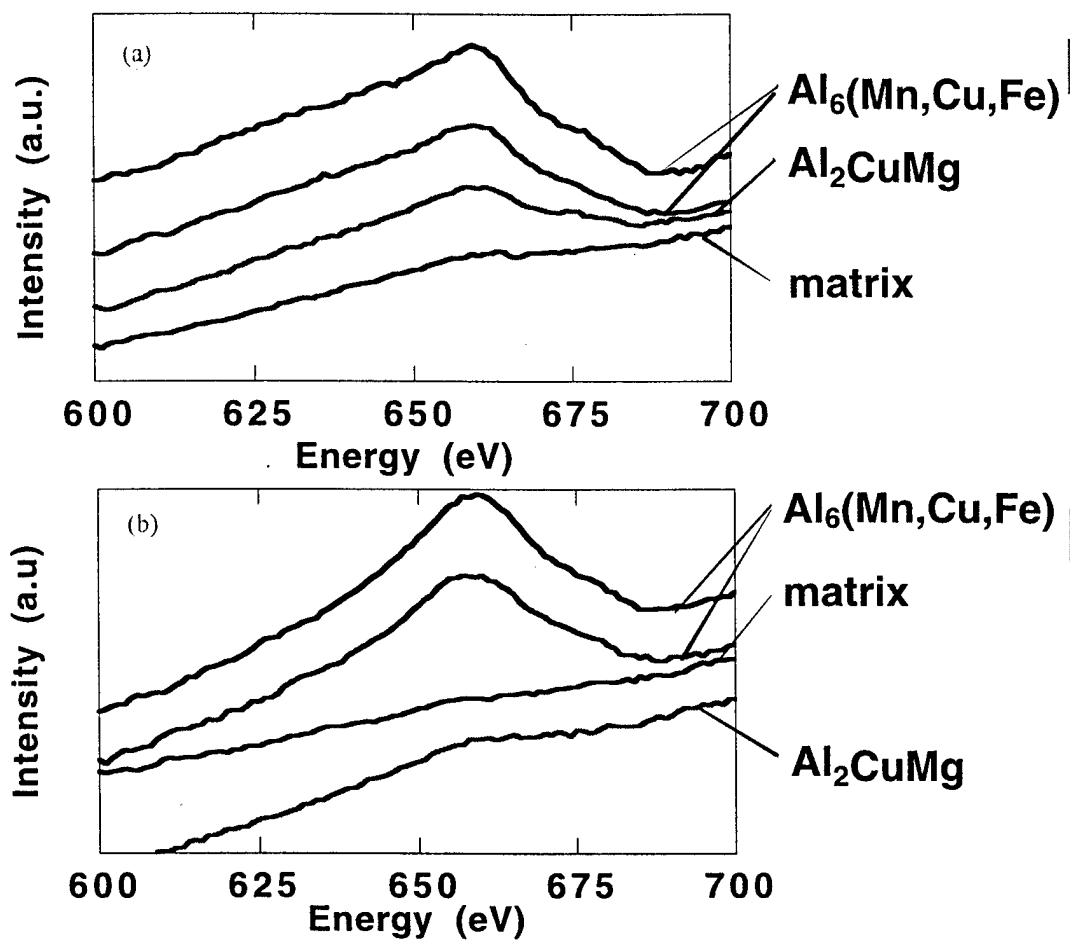


Figure 14. Composition depth profiles for Ce at the LMM Auger transition (a) before sputter etching, (b) after sputtering 5 nm of surface material. Ce is removed from the matrix phase and Al_2CuMg particles, but not $\text{Al}_6(\text{Cu,Mn,Fe})$.

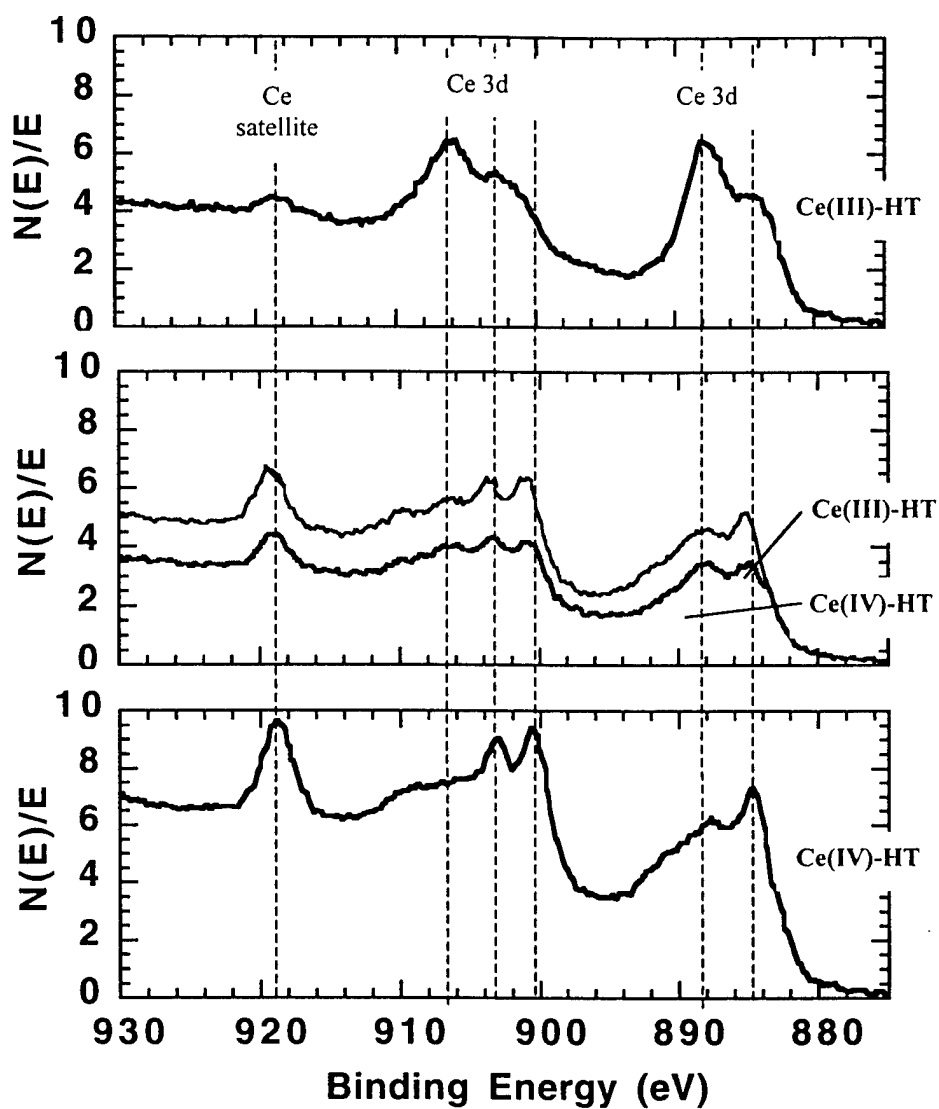


Figure 15. XPS data on Ce(III)- and Ce(IV)- modified hydrotalcite coated 2024-T3. The topmost figure shows the spectrum for Ce(III)-modified hydrotalcite, while the bottommost figure shows the spectrum from Ce(IV)-modified hydrotalcite. Coatings of each type were subjected to salt spray exposure for 168 hours and the post exposure spectra for each coating is shown in the middle figure.

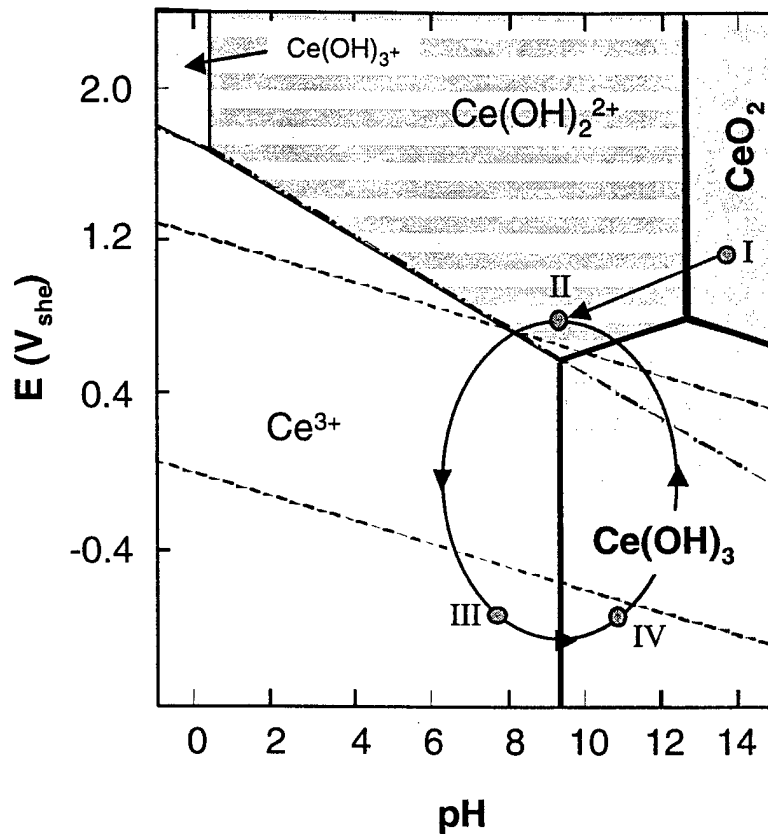


Figure 16. Pourbaix diagram for Ce illustrating regeneration of the Ce(IV) inhibitor reservoir. I-II: dissolution of Ce oxides. II-III: reduction of soluble Ce(IV) by bare Al at defects, III-IV: precipitation of Ce(III) at alkaline local cathodes, IV-II: re-oxidation of Ce not in direct contact with Al by dissolved oxygen in solution.

Submitted to *Colloids and Surfaces A: Physiochemical and Engineering Aspects* (in review)

**Adhesion of Epoxy to Hydrotalcite Conversion Coatings:
I. Correlation with Wettability and Electrokinetic Measurements**

R.B. Leggat, S.A. Taylor, S.R. Taylor*

University of Virginia
Department of Materials Science and Engineering
Charlottesville, VA 22904

* Corresponding author
804-982-5788 phone
804-982-5799 fax
srt6p@virginia.edu

Abstract

Hydrotalcite (HT) based conversion coatings are being developed as an environmentally benign alternative to chromate conversion coatings. This examination investigates the relationship between the interlayer oxoanion in the HT structure and surface chemistry, and their subsequent effect on adhesion of organic coatings. The interlayer ions examined included nitrate, carbonate, persulfate. Dry and wet-state adhesion of 25-75 μm thick epoxy films were measured by the pull-off tensile strength. The results were compared to surface energy and isoelectric point measurements using the rising height method and electrophoresis of HT powders, respectively. The Lifshitz-van der Waal (LVW) /Lewis acid-base approach was employed for analysis of contact angle data. It was observed that the HTs having increased LVW bonding had better wet state adhesion, while a reciprocal relationship was seen between dry state adhesion and the isoelectric point. The correlations with the dry and wet state adhesion are interpreted as indicating that dry state adhesion is optimized by minimizing unfavorable polar interactions between the basic epoxy and HT interfaces. Wet state adhesion, where polar interactions are disrupted, is dictated by non-polar bonding.

Keywords

Adhesion, Contact Angle, Conversion Coatings, Electrokinetic, Hydrotalcite

INTRODUCTION

Hydrotalcite-based (HT) conversion coatings are being developed as an environmentally benign alternative to chromate conversion coatings (CCCs) copper-bearing aluminum alloys [1]. The conversion coating provides some enhancement to the corrosion resistance of the substrate but functions predominantly to increase the adhesion of the subsequent organic layers. CCCs provide excellent corrosion resistance and adhesion, however, the known health and environmental hazards associated with chromates require significant expenditures in their handling and disposal [2]. There is thus an incentive to develop non-toxic replacements that provide the same level of performance as CCC [3].

Hydrotalcite is $\text{Mg}_6\text{Al}_2(\text{OH})_{16}\text{CO}_3 \cdot 4\text{H}_2\text{O}$ and is part of a larger class of intercalation compounds of aluminum hydroxide [4]. The term "Hydrotalcite" will be used herein to refer to all hydrotalcite-like compounds. It is the lithium variant of the aforementioned compound that has been developed as a conversion coating [5]. A coating based on the compound $\text{Li}_2[\text{Al}_2(\text{OH})_6]_2 \cdot \text{XO}_n \cdot n\text{H}_2\text{O}$, where XO_n is an oxoanion, is formed on aluminum alloys by exposure to alkaline lithium salt solutions. The macroscopic structure consists of blade-like crystals, (ca. $0.1\mu\text{m}$ wide and several μm long) as seen in Figure 1, similar to that observed for zinc phosphated steel. The atomic structure consists of oxoanions intercalated between layers of lithium-aluminum hydroxide [6].

There are a number of processing options by which the physical and chemical properties of HT coatings can be engineered. When the coating is formed by exposure to an alkaline lithium salt bath in the coating step, a number of different lithium salts can be used to vary the oxoanion. In addition, there are a number of post-treatments available such as transition metal sealing and hydrothermal reversion [7,8]. Previous efforts have focused on the development of bath chemistries that optimize the stand-alone corrosion resistance of the conversion coating on an aerospace alloy (AA2024-T3) [9]. However, in practice, HT conversion coatings will have to perform as part of a coating system that consists of the conversion coating in addition to several organic layers. Adhesion between HT conversion coatings and subsequent organic layers is therefore

relevant to the acceptance of these conversion coatings into commercial practice.

Adhesion across an interface occurs by physical and chemical bond formation. Chemical bonding involves covalent bond formation between the substrate and the adhesive, while physical bonding can involve mechanical interlocking or adsorption due to dispersive or donor-acceptor interactions [10]. Ideally, it would be desirable to know the relative contribution of these factors to the total adhesion. In this series of papers, the adhesion interactions between HT and an epoxy primer are investigated. The present investigation examines the effect of different interlayer oxoanions on the wetting and electrokinetic properties and their subsequent impact on practical adhesion. The use of surfactant treatments to improve adhesion will be examined in the second paper of this series.

BACKGROUND

Combination of the Young-Dupre and Girifalco-Good equations yields an equation that relates the contact angle between a liquid and a solid to their surface tensions:

$$\gamma_{LV} \cos \theta = 2(\gamma_S \gamma_L)^{1/2} \quad (1)$$

where γ is the surface energy, the subscripts L, S, and V are for the liquid, solid and vapor phases and θ is the contact angle[11]. Van Oss, Chaudury, and Good (VOCG) proposed that the surface energy can be separated into electrodynamic and electron acceptor-donor contributions according to the following expression:

$$\gamma = \gamma^{LVW} + \gamma^{AB} \quad (2)$$

where LVW is the Liftshitz-van der Waal component and AB is the Lewis acid-base component. The Lewis-acid base component accounts for the electron-donor (base) and electron acceptor interactions and is represented by a non-additive relation:

$$\gamma^{AB} = 2(\gamma^+ \gamma^-)^{1/2} \quad (3)$$

where γ^+ , γ^- are the acid and base contributions, respectively. Equation (1) can be rewritten to include equations (2) and (3) to yield:

$$(\gamma_S^{LVW} \gamma_L^{LVW})^{1/2} + (\gamma_S^+ \gamma_L^-)^{1/2} + (\gamma_L^+ \gamma_S^-)^{1/2} = 1/2 (1 + \cos \theta)^{1/2} \quad (4)$$

In order to determine the three unknown parameters, γ_S^{LVW} , γ_S^+ and γ_S^- , the contact angles of three known probe liquids on the unknown solid are needed [12]. The γ_S parameters can be determined by simultaneous solution of equation (4) for the three probe liquids (L1, L2, L3) in its matrix form (Equation 5):

$$\begin{bmatrix} \gamma_{L1}^{LVW} & \gamma_{L1}^- & \gamma_{L1}^+ \\ \gamma_{L2}^{LVW} & \gamma_{L2}^- & \gamma_{L2}^+ \\ \gamma_{L3}^{LVW} & \gamma_{L3}^- & \gamma_{L3}^+ \end{bmatrix}^{1/2} \begin{bmatrix} \gamma_S^{LVW} \\ \gamma_S^+ \\ \gamma_S^- \end{bmatrix}^{1/2} = \frac{1}{2} \begin{bmatrix} \gamma_{L1}(1 + \cos \theta_1) \\ \gamma_{L2}(1 + \cos \theta_2) \\ \gamma_{L3}(1 + \cos \theta_3) \end{bmatrix} \quad (5)$$

Some concern about the validity of the VOGC approach has been expressed. Among the critics of the method are Neumann and Kwok, who state that the VOGC method yields inconsistent γ_S components from contact angle data [13-15]. They argue that regardless of the γ_{Liquid} parameter set used, the approach itself is flawed and advocate the use of an equation-of-state approach. Others contend that the VOGC approach is conceptually sound, but that the mathematical formalism is not sufficient [16].

Different sets of probe liquid surface tension parameters have been suggested to address the apparent deficiencies of the VOGC method. Della Volpe and Siboni (DVS) enumerate these problems as [17,18]:

- (i) the systematic assignment of basic character to solids;
- (ii) the strong dependence of the solid surface tension components on the choice of probe liquids; and,
- (iii) the appearance of negative values for the solution of the roots of surface tension components.

DVS state that problem (i) is due to the arbitrary assignment of $\alpha = 1$ for water (where $\alpha = \gamma^+/\gamma^-$), which is the reference for assigning all other probe liquid values. Based on the solvchromatic acid-base scale, water is considered to be more acidic than basic [17]. Empirically derived values for α have been

suggested in two separate publications by DVS. In the original publication, a value of $\alpha = 6.5$ is calculated from experimental data on fourteen different polymers using ten probe liquids [18]. In a more recent publication, a best-fit approach was used to find a revised $\alpha = 4.35$ [19].

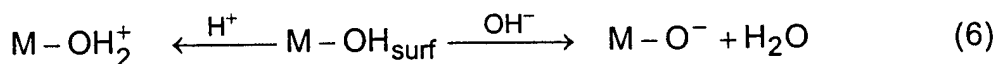
Van Oss *et al.* state that the predominance of electron-donicity (γ^-) in solids is the result of the prevalence of atmospheric oxygen and thus the presence of common minerals as oxide and hydroxides [20]. Furthermore, they contend that positive sites on a surface can result from a residual polar liquid (e.g. water) and not from inherent electron-accepting character of the solid.

The proper selection of probe liquids can minimize the impact of problems (ii) and (iii). Holländer recommends maximizing the difference in the ratios of γ^+/γ^- for two polar liquids used along with a non-polar liquid [21]. DVS have shown that the selection of probe liquids can be based on a mathematical parameter, the condition number (κ) for the matrix containing the surface tension parameters of the probe liquids. κ is an indication of the stability of a system having the form $[A]x = [B]$, such as equation (5). A large κ indicates an “ill-conditioned” system in which small perturbations in $[A]$ or $[B]$ result in large errors in the solution of x . Conversely, a small κ indicates a “well-conditioned” system [22]. The use of diiodomethane, water and a second polar liquid such as ethylene glycol, formamide, or glycerol generally provides a well-conditioned system.[23]

Diiodomethane is frequently included as a probe liquid because it is considered completely nonpolar (i.e. no γ^{AB} contribution). However, the existence of a small, but non-negligible γ^+ for diiodomethane is suggested based on its interfacial tension with water. A value of 0.72 mN/m for the γ^+ of diiodomethane is reported [24]. The effect of neglecting γ^+ for diiodomethane would result in an overestimation of γ^{LVW} by 15% and underestimation of γ^- by up to 100% [25]. It should be stated that interfacial tension is considered a poor method for calculating γ^+ for partially polar liquids because of reorientation of surface polar groups at the interface. Calculations based on the solubility of diiodomethane in water yield a more reasonable γ^+ value of ca. 0.01mN/m [26].

Given the lack of confidence in the acid and base components calculated using the VOEG approach, additional methods to evaluate the acid-base character is warranted. There are a number of techniques, in addition to contact angle measurements, by which the acid-base character can be assessed. These include calorimetry, XPS and IR spectral shifts, and inverse gas chromatography [27-29]. Electrokinetic measurements, which are particularly well-suited for irregularly shaped samples such as powders, offer another method of determining acid-base properties [30].

Hydroxyl groups terminate the surface of a metal oxide. Depending on the metal, the oxide can be characterized as acidic or basic [31]. In high pH solutions, the hydroxyl is deprotonated, while at low pH the hydroxyl is protonated:



The pH at which both reactions are equal and the net surface charge is zero is the pH of zero charge (pH_{ZC})[32]. Potentiometric titration can be used to measure the pH_{ZC}. Alternately, electrokinetic measurements can be used to measure the iso-electric point (IEP) which is the pH at which the zeta potential (ζ) changes sign. The IEP and pH_{ZC} are often erroneously used interchangeably. Only in the absence of specific adsorption are they equivalent. A high IEP indicates basic oxides, while a low IEP indicates acidic oxides. ζ is the potential at the hydrodynamically affixed shear plane which can be approximated as the outer Helmholtz plane of the double layer. ζ can be calculated from electrophoresis measurements in which the electrophoretic mobility (μ) of a particle in solution under an applied voltage is measured. The Smoluchowski equation relates ζ to μ for $(a/x_{\text{DL}}) \gg 1$:

$$\zeta = \mu\eta/\epsilon\epsilon_0 \quad (7)$$

where η is the solution viscosity, ϵ = solution dielectric constant, ϵ_0 = permittivity of free space, a is the particle radius, and x_{DL} is the double layer thickness [33].

The IEP has been related to the electron donicity of solids in organic solvents by Labib and Williams [34]. In a subsequent paper, the electron donicity scale was related to the aqueous pH scale [35]. Wu, et al. have found an indirect but significant linkage between γ - and ζ for inorganic particles in aqueous electrolytes [36].

EXPERIMENTAL METHODS

Preparation of Samples

Samples for adhesion testing

HT coatings were applied to 4"x5" aluminum alloy panels for adhesion testing. The alloy used was AA2024-T3 (Al-4Cu-1.5Mg). Three HT chemistries with varying interlayer oxoanions were examined: nitrate (NO_3), carbonate (CO_3), and persulfate + nitrate (S_2O_8). After initial degreasing and deoxidation, the panels were immersed in the HT coating baths. The compositions and treatment times of the different coating baths are listed in Table 1. The HT coating thickness was typically five μm . In addition, degreased AA2024 and CCC were included as a blank and control, respectively.

A two-component neat epoxy resin was spin-cast onto the panels for subsequent adhesion testing. The epoxy consisted of a BPA-epichlorohydrin resin (Araldite GY 6010, Ciba) with a cycloaliphatic amine hardener (HY 2964, Ciba). The epoxy viscosity was controlled during casting with a two-part solvent (50:50 toluene/butanol). The epoxy coatings attained a 25-75 μm dry film thickness.

Samples for wettability and electrokinetic experiments

Due to the complications introduced by surface roughness and porosity in wetting measurements of solids, wettability and electrokinetic experiments were performed using particles with surfaces chemically identical to the conversion coatings. After production of the panels for the adhesion tests, the coating baths

were allowed to cool to induce precipitation. The HT powders were collected, rinsed in deionized water, and oven dried at 100°C for 12 hours. The samples were ground by mortar and pestle then sifted through a 63 µm sieve prior to testing. Powders representative of the CCC were produced by coating 99.5% pure aluminum powders (17-23 µm, Alfa Aesar) in the same bath used for the adhesion samples. Degreased aluminum powders were used as a blank.

Adhesion Measurements

Practical adhesion was assessed by the pull-off tensile strength (POTS) obtained using a Gardner model P2A Pneumatic Adhesion Tensile Test Instrument (PATI). Testing was conducted according to ASTM D4541. A pull-off stub (1.265 cm² dia.) was attached to the epoxy coating using a high strength adhesive. The tensile force necessary to remove the epoxy from the substrate was used to calculate the POTS.

A series of samples were exposed to deionized water for 24 hours prior to adhesion testing to acquire wet-state POTS. After removal of the sample from the water, the panel was wiped dry and the pull-off stub was attached to the epoxy coating with a cyanoacrylate ester. The POTS was determined within 30 minutes of removal from water. A minimum of 16 samples was tested for each treatment in both the dry and wet states.

Contact Angle Measurements

A Krüss K121 Tensiometer was used to measure the contact angle of liquids on HT powders by the rising height method similar to the thin layer wicking method of van Oss, *et al.* [37]. In the rising height method, the powders are packed into a cylinder that is suspended from a microbalance. Probe liquids are allowed to wick through the packed column as the change in mass is recorded. The contact angle (θ) of the liquid on the powders is given by the Washburn equation (shown in its most useful form) as follows:

$$\cos \theta = \frac{m^2}{t} \frac{\eta}{\rho^2 \gamma c} \quad (8)$$

where t = time, m = mass of the wicked liquid, η = viscosity of the liquid, ρ = density of the liquid, γ = surface tension of the liquid; c = material constant [38].

The value of the c -constant is dependent on the sample and the sample holder. This value is determined by a preliminary measurement with a totally wetting liquid such as hexane. With the assumption that the contact angle is 0° in this case, the cosine of θ becomes 1 and equation (8) can be used to calculate c . Given the value of c , the contact angle for non-wetting liquids can be calculated. Diiodomethane, ethylene glycol, formamide, and water were used as probe liquids.

The solid surface tension of the powders was calculated from the contact angle data using the VOG approach. The surface tension parameters for the probe liquids were those used by van Oss[39]. The γ_S^{LVW} parameter was calculated from the diiodomethane data using equation (4) solved for non-polar liquids:

$$\gamma_S^{LVW} = \gamma_L \frac{(1 + \cos \theta)^2}{4} \quad (9)$$

The γ_{S+} and γ_{S-} parameters were calculated using equation 5. Two solutions were determined using water as one of the probe liquids and ethylene glycol or formamide as the second. The effect of the different γ_L parameter sets on γ_S was also evaluated.

Electrokinetic Measurements

The IEP was determined from micro-electrophoretic measurements of ζ as a function of pH. The electrophoretic mobility was measured for dilute powder suspensions (100 ppm powder in 1mM KCl) using a Zeta-Reader Mark 21 electrophorometer. The NO_3 , CO_3 , and S_2O_8 HT powders were evaluated. The pH was adjusted by titration of the suspension with 50mM NaOH and measured with a pH meter accurate to 0.01. ζ was calculated using the Smoluchowski

equation (Equation 7). The validity of this equation for the particular particle size and electrolyte was checked by verifying that $a / x_{DL} \gg 1$.

The pHZC was determined by potentiometric titration (PT) curves for the CCC and NO₃ HT powders using a Metrohm 726 auto-titrator. Solutions of 1g/L HT or CCC powder in 1mM NaNO₃ were maintained at 25°C \pm 1°C and purged with N₂. The acidic and basic curves were obtained by titration with 0.1M HNO₃ and 0.1 NaOH, respectively. The surface charge (σ) is given by the equation:

$$\sigma = F(\Gamma_{H^+} - \Gamma_{OH^-}) \quad (10)$$

where F is Faraday's constant and Γ is the surface concentration = [mol m⁻²]. In addition to the pH-titration volume curves, the specific surface area (SSA) is needed for calculation of σ .

The SSA of the NO₃ HT powder was determined by BET-N₂ gas adsorption using a Micrometrics Accelerated Surface Area and Porosimetry System. The powder was oven dried at 200°C for 1 hour prior to introduction into the vacuum chamber of the measurement system. The samples were then degassed for 24 hours before testing. BET was used to calculate the roughness of conversion coated panels in a similar manner. Specially designed AA2024 samples (apparent surface area = 1.5x10⁻³ m²) were coated with CCC, CO₃ HT, and NO₃ HT. The average measured surface area was used to calculate a roughness factor (R), which is the ratio of the measured surface area to the apparent surface area.

RESULTS AND DISCUSSION

Practical Adhesion

The dry and wet adhesion results are summarized in Table 2. Although there was significant scatter in the measured POTS values as seen in Table 2, a distribution of values is generally observed in pull-off tests [40]. Additionally, it must be remembered that failure can occur within either of the coating layers (conversion or organic coating) or any of the interfaces. Failure was generally

observed to initiate within the conversion coating and propagate at the interface between the epoxy and the conversion coating.

The CCC samples had the highest wet and dry POTS values. The HT conversion coated panels had POTS values that fell between those measured for the CCC and the degreased (not conversion coated) panels. Tukey's multiple comparison procedure was used in the analysis of variance (ANOVA) to determine which treatments had significantly different means [41]. The rankings for the dry POTS at 95% confidence was:

$$\text{CCC} > \text{CO}_3 = \text{NO}_3 > \text{Degreased} = \text{S}_2\text{O}_8$$

The wet POTS values were lower than the dry POTS values for all treatments. ANOVA indicated that the treatment rankings for wet-state POTS at 95% confidence were:

$$\text{CCC} > \text{CO}_3 > \text{S}_2\text{O}_8 = \text{NO}_3 > \text{degreased}$$

The rankings were similar between the dry and wet POTS with the exception of the S_2O_8 HT, which ranked higher in the wet POTS relative to the dry POTS.

The roughness factor (R) calculated from BET measurements is included in Table 2. The conversion coatings are rougher than the degreased sample. Although the difference in roughness between the CCC and the HT conversion coatings is statistically significant, it is a matter of degree and not magnitude. In fact, the HT conversion coatings are rougher than the CCC indicating that the difference in adhesion is not simply due to increased surface roughness.

Wetting characteristics of the HT by the epoxy were examined by Scanning Electron Microscopy of a pull-off stub after testing a NO_3 HT sample. A schematic is included to show the sample orientation along with the secondary electron micrograph in Figure 2. Bare HT blades are visible (high contrast areas), indicating incomplete wetting by the epoxy. Alternatively, the bare blades may be the result of HT pull-out during testing similar to that observed in composite testing. Either interpretation leads to the conclusion that there is poor surface chemistry interaction between the HT and the epoxy.

It was believed that the re-entrant angles provided by the surface morphology of the HT would provide increased practical adhesion by mechanical

anchoring of the cured epoxy. It is hypothesized that this mechanical adhesion is not realized due to poor surface chemistry interactions between the epoxy and HT. Wetting experiments offer insight into the surface characteristics of the HT conversion coatings.

Wetting of Conversion Coating Powders

The change in mass measured by the wicking of deionized water through the packed powders is shown in Figure 3. Equation (8) is rearranged so that $\text{mass}^2 \cdot \text{c}^{-1}$ is plotted versus time to separate the probe liquid variables in equation (11):

$$\frac{m^2}{c} * t = \cos \theta \left(\frac{\eta}{\rho^2 \gamma} \right) \quad (11)$$

In this form the slope in the linear region of Figure 2 is equal to the cosine of the contact angle multiplied by a constant. The fit slope was used to calculate the contact angles for the various powders shown in Table 3. Complete wetting is indicated by a contact angle of zero.

Prior to calculation of the γ_s parameters from the contact angle data, it was necessary to evaluate the effect of the different γ_L parameters on the solution of γ_s parameters. McCafferty and Wightman have calculated κ for several combinations of probe liquids using the parameters of VOGG[ref. 12] and DVS [ref.18], [42]. κ values for the parameter set of DVS[ref. 19] are also included with McCafferty's values in Table 5. In addition, κ for [2x2] matrices of two polar liquids in which γ_s^{LVW} was independently calculated are included.

The κ for the γ_L parameter sets that are considered ill-conditioned are italicized. The well-conditioned parameter sets were used in the calculation of the γ_s components for the NO_3 -HT powders. Two methods of solving for the γ_s parameters were examined. In the [3x3] solution, all three γ_s components are solved simultaneously using the parameters of all three probe liquids and the corresponding contact angles. In the [2x2], γ_s^{LVW} is first solved independently

using the diiodomethane data. The acid and base components of γ_s are then simultaneously solved using two polar probe liquids and their contact angles. As seen in Table 6, both methods yielded the same results.

When γ^+ for diiodomethane was changed to 0.72 mN/m as suggested by Tretinnikov, γ_s^{LVW} and γ_s^{total} decreased relative to the values calculated for the assumption of diiodomethane being totally nonpolar [25]. The change in the acid and base components depended on the combination of probe liquids. The change in γ^- was insignificant, however the change in γ^+ was significant.

Comparing the results from the VOGC, DVS (97), and DVS (00) parameter sets, γ_s^{total} and γ_s^{LVW} are similar as expected. The γ_L values for diiodomethane and the γ^{total} for all the probe liquids are the same in all three parameter sets. The two sets of values proposed by DVS (1997&2000) yielded similar results. However, when compared with the VOGC set, γ^+ was higher and γ^- was lower as expected.

The values calculated using the combination of diiodomethane, formamide, and ethylene glycol and their respective parameters from DVS (00) were instructive. The results are similar to those generated by the other liquid combinations when the probe liquid parameters of DVS are used. This combination of probe liquids was previously excluded due to the ill-conditioning of the matrices when the values of VOGC or DVS (97) were used. This supports the importance of probe liquid selection in calculating the surface tension components.

The γ_s parameters were calculated for the conversion coating powders using the VOGC parameter set with the assumption that diiodomethane is totally nonpolar. Separate solutions for combinations of diiodomethane, water, and formamide or ethylene glycol are listed in Table 7. The γ^{LVW} and γ^{total} values calculated for the degreased aluminum powder are similar to those obtained by McCafferty for plasma cleaned aluminum ($\gamma^{LVW} = 46.7$, $\gamma^{total} = 57.4$ mN/m) [42]. The acid and base components do not agree as closely; however, the relative magnitude of each is similar. The parameters for the conversion coating powders

indicate that they are all predominantly dispersive with a largely basic contribution to the polar component. Li, et al. had similar conclusions for Mg-Al hydrotalcites, which are Lewis bases [43]. Interestingly, it was found that variation of the surface tension components is a function of the interlayer anion. This is in agreement with the large γ - observed in the current study for the combination of water, diiodomethane and formamide. No variation was seen for the combination of water, diiodomethane and ethylene glycol.

The γ^{total} values calculated for the two different probe liquid combinations (water, diiodomethane and formamide or ethylene glycol) can be considered as a range. Formamide is a basic liquid (pH = 9.9) and ethylene glycol is an acidic liquid (pH = 5.0). Other researchers have found that the γ^{total} values calculated using these two probe liquid combinations represented the extrema for a range of values calculated using different probe liquid combinations [44].

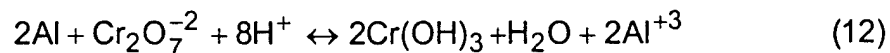
It was of interest to compare the γ_s components with the adhesion measurements. The wet POTS correlated well with γ^{total} . This finding was expected. With decreased wetting ($\gamma_s < \gamma_L$), there would be less interfacial contact area and void formation. These voids act as stress points for failure initiation and allow for accumulation of moisture at the interface. The wet POTS also correlated with γ^{LVW} as shown in Figure 4. This is in agreement with previous findings that the greater the proportion of dispersive bonding, the better the wet adhesion performance [45,46]. These results are logical since polar bonding increases the likelihood of water uptake and bond disruption. No correlation was observed between the adhesion performance (dry or wet) and the acid and base components of the conversion coatings.

Electrokinetic Measurements

The ζ as a function of pH is shown for the HT powders in Figure 5. The IEP was determined by a fit of the form $\zeta = \zeta_0 - a \cdot \exp(\text{pH})$ for each powder. The S_2O_8 HT has the most basic IEP (11.6+/- 0.2), while the NO_3 (11.3+/- 0.1) and CO_3 HT (11.1+/-0.2) are slightly less basic. These results support the general conclusion from the contact angle measurements that the HT powders have

strongly basic polar components. While measuring the electrophoretic mobility, some of the particles were observed to move in the direction opposite the majority of the particles, indicating that they had a net charge opposite that of the majority. This was interpreted as a result of the presence of discrete site of both positive and negative charge. Additionally, the intercalated structure allows for both positive and negative charge depending on what the terminating external layer. The reported ζ was that observed for the majority of the particles.

Electrophoretic measurement of ζ was not possible for the CCC powder, because the particles settled rapidly from suspension. The IEP of oxide-covered chromium has been measured previously by contact angle titration to be 5.2-5.3 [47]. CCC is certainly more complex than chromium oxide. In the presence of an activator such as fluoride, CCC is formed by the reaction of aluminum with dichromate [48]:



The degree of hydration and speciation of the cations in the CCC film varies with conditions; however, it is reported to be structurally similar to Cr-mixed oxides [49]. The corrosion resistance of CCC is attributed to the leachability of chromate from the film [50,51]. It would be expected that the presence of the Cr cations in solution would affect the IEP. Kendig, et al. reported that 10mM oxo-Cr(VI) decreased the IEP of anodized aluminum from 10.5 to 8.2 [52]. Therefore, it is reasonable to assume that the CCC has an IEP significantly less basic than that observed for the HT powders.

An alternative approach was used. Contact angles for buffered, aqueous solutions of different pH on CCC powders were measured by the rising height method to determine the IEP. The contact angle should go through a maximum at the IEP [47]. A plot of measured contact angle versus pH is shown in Figure 6. The data was fit to a parabolic curve that displayed a maximum, and thus the IEP, at pH=8.2 which agrees with Kendig's findings.

The IEP for the HT powders was compared to the dry POTS as shown in Figure 7. A value of 8.2 is included for the IEP of CCC as a reference. Increased dry POTS was observed for decreasing IEP. This correlation can be explained when one considers that amine-cured epoxy behaves as a Lewis base [53]. Thus, the strongly basic character of the HT conversion coatings results in unfavorable acid-base interactions with the epoxy. As the basicity decreases (IEP decreases), these interactions become less repulsive. Other researchers have reported a relation between ζ and adhesion for polymers, composites and organic coatings on steel [54-57].

Potentiometric titration was used to examine the ionizable surface species on NO_3 HT and CCC powders. The pH versus titrated volume is shown in Figure 8 for NO_3 HT and CCC powders in 1mM NaNO_3 . Two trials were run for the basic titration of the NO_3 HT powders. The plot for the CCC coincides with that observed for the electrolyte blank indicating that the pHZC for CCC is similar to the equivalence point of the electrolyte. The surface charge on the HT powder was calculated from the PT curve as seen in Figure 9. The surface charge remained positive until high pH as was observed in the ζ measurements. The pHZC was ca. 11.0, which is in reasonable agreement with the previously determined IEP of 11.3. Figure 9 is specific to 1mM NaNO_3 . Determination of the absolute pHZC would require additional measurements in different electrolytes.

BET analysis indicated that the SSA of the NO_3 HT powders was $10.8 \pm 1.1 \text{ m}^2/\text{g}$. These values are intermediate to the ranges reported in the literature for Mg-Al- CO_3 HT by Miyata ($15\text{-}85 \text{ m}^2/\text{g}$) and Li *et al.* ($3.7\text{-}3.9 \text{ m}^2/\text{g}$) [58,43].

Summary

The effect of varying the interlayer oxoanion in HT coatings on dry and wet state POTS of epoxy was examined. The wet-state adhesion rankings correlated with the γ_s^{total} and γ_s^{LVW} , while the dry state rankings were inversely related to the IEP. The dry state adhesion is controlled by repulsive interactions between the basic conversion coatings and the epoxy. In the wet state, polar interactions are disrupted by the presence of water, and dispersive (LVW) interactions dominate.

The results indicate that increased epoxy adhesion can be achieved by modification of the wettability or electrostatic characteristics of the HT coatings. This will be examined in the second paper of this series.

ACKNOWLEDGEMENTS

This work was supported by DARPA (Contract #49620-1-0305) under direction of Dr. Stephen Wax and Lt. Col. Paul Trulove (AFSOR). The use of the facilities of the Particle Science and Technology Center (Univ. Florida) is greatly appreciated. The authors gratefully acknowledge the BET measurements of B. Hostika (Univ. Virginia).

REFERENCES

- [1] R.G. Buchheit, M.D. Bode, G.E. Stoner, *Corrosion*, 50 (1994) 205.
- [2] C.J. Carpenter, *Plating and Surface Finishing*, 77 (1990) 35.
- [3] A. Nylund, *Aluminum Transactions*, 2 (2000) 121.
- [4] V.P. Isupov, *J. Structural Chemistry*, 40 (1999) 672.
- [5] R.G. Buchheit, M.D. Bode, G.E. Stoner, *Corrosion*, 50 (1994) 205.
- [6] C.J. Serna, J.L. Rendon, J.E. Iglesias, *Clays and Clay Minerals*, 30 (1982) 180.
- [7] R.G. Buchheit, M.A. Martinez, L.P. Montes, N.P. Cella, S.R. Taylor, G.E. Stoner, Paper No. 216, *Corrosion 98*, San Diego, 22-27 March, NACE, Houston, 1998.
- [8] R.G. Buchheit, S.B. Mamidipally, P. Schmutz, H. Guan in *Research Topical Symposium, Corrosion 2000*, Orlando, 26-30 March 2000, NACE, Houston, 2000.
- [9] R.B. Leggat, E.A. Pehovaz-Diez, N.P. Cella and S.R. Taylor in B.A. Shaw, R.G. Buchheit, J.P. Moran (Eds.), *Corrosion and Corrosion Prevention of Low Density Metals and Alloys*, 197th Meeting of the Electrochemical Society, Toronto, 14-18 May 2000, ECS, Pennington, 2001, p.124.
- [10] J.A. Baghdachi, *J. Coat. Technol.*, 69 (1997) 8.
- [11] A.W. Adamson, *A.P. Gast Physical Chemistry of Surfaces*, John Wiley & Sons, New York, 1997.
- [12] C.J. Van Oss, M.K. Chaudhury, R.J. Good, *Chem. Rev.* 88 (1988) 927.
- [13] D.Y. Kwok, D. Li, A.W. Neumann, *Langmuir*, 10 (1994) 1323.
- [14] D.Y. Kwok, Y. Lee, A.W. Neumann, *Langmuir*, 14 (1998) 2548.
- [15] D.Y. Kwok, *Colloids and Surface A*, 156 (1999) 191.
- [16] M. Greiveldinger, M.E.R. Shanahan, *J. Colloid Interface Sci.*, 215 (1999), 170.
- [17] V. Gutmann, *Electrochimica Acta*, 21 (1976) 661.
- [18] C. Della Volpe, S. Siboni, *J. Colloid Interface Sci.*, 195 (1997) 121.
- [19] C. Della Volpe, S. Siboni, *J. Adhesion Sci. Technol.*, 14 (2000) 235.
- [20] C.J. Van Oss, R.F. Giese, W. Wu *J. Adhesion*, 63 (1997), 71.
- [21] A. Holländer, *J. Colloid Interface Sci.*, 169 (1995) 493.
- [22] C.H. Edwards, D.E. Penney, *Elementary Linear Algebra*, Prentice-Hall, Englewood Cliffs, 1988.

- [23] R.J. Good, J. Adhesion Sci. Technol., 6 (1992) 1269.
- [24] B. Janczuk, W. Wojcik, A. Zdiennicka, J. Colloid Interface Sci, 157 (1993) 384.
- [25] O. N. Tretinnikov, J. Colloid Interface Sci., 229 (2000) 644.
- [26] C.J. Van Oss, W.Wu, A. Docoslis, R.F.Giese, Colloids and Surfaces B, 20 (2001) 87.
- [27] T.B. Loyd, Colloids and Surfaces A, 93 (1994) 25.
- [28] W.M Mullins, B.L. Averbach, Surface Science, 206 (1988) 41.
- [29] W.M Mullins, B.L. Averbach, *ibid*, 206 (1988) 52.
- [30] D. Fairhurst, V. Ribitsch, in T. Provder (Ed.), Particle Size Distribution II, ACS Symp. Series No. 472, ACS, Washington, DC, 1991, 337.
- [31] J.C. Bolger, in K.L. Mittal (Ed.), Adhesion Aspects of Polymeric Coatings, Plenum Press, New York, 1983, 3.
- [32] G.A. Parks, Chem. Rev., 65 (1965) 177.
- [33] R.J. Hunter, Zeta Potential in Colloid Science, Academic Press, London, 1989.
- [34] M.E. Labib, R. Williams, J. Colloid Interface Sci., 97 (1984) 356.
- [35] M.E. Labib, R. Williams, Colloid & Polymer Sci., 264 (1986) 533.
- [36] W. Wu, R.F. Giese, C. J. Van Oss, Colloids and Surfaces A, 89 (1994) 241.
- [37] C.J. Van Oss, R.F. Giese, Z. Li, K. Murphy, J. Norris, M.K. Chaudhury, R.J. Good, J. Adhesion Sci. Technol., 6 (1992) 413.
- [38] E.W. Washburn, Phys. Rev., 17 (1921) 273.
- [39] C.J. Van Oss, Interfacial Forces in Aqueous Media, Marcel Dekker, 1994.
- [40] J. Sickfeld, in K.L.Mittal (Ed.), Adhesion Aspects of Polymeric Coatings, Plenum Press, New York, 1983, 543.
- [41] J.L. Devore, Probability and Statistics for Engineering and the Sciences, 5th ed., Duxbury, Pacific Grove, 2000.
- [42] E. McCafferty, J.P. Wightman, J. Adhesion Sci. Technol., 13 (1999) 1415.
- [43] Z. Li, R.F. Giese, C.J. van Oss, Langmuir, 10 (1994) 330.
- [44] M. Gindl, G. Sinn, W. Gindl, A. Reiterer, S. Tschegg, Colloids and Surfaces A: Physiochem. Eng. Aspects, 181 (2001) 279.
- [45] J.C. Bolger, *Soc. Plast. Engr., Tec. Pap.*, 12 (1967) 15.
- [46] S.R. Taylor, G.L. Cahen, G.E. Stoner, J. Electrochem. Soc., 135 (1988), 2943.
- [47] E.McCafferty, J.P. Wightman, J. Colloid Interface Sci., 194 (1997) 344.
- [48] M.W. Kendig, A.J. Davanport, H.S. Isaacs, Corrosion Science, 34 (1993) 41.
- [49] L. Xia, R.L. McCreery, J. Electrochem. Soc., 145 (1998) 3083.
- [50] G.O. Ilevbare, J.R. Scully, J. Yuan, R.G. Kelly, Corrosion, 56 (2000) 227.
- [51] J. Zhao, G. Frankel, R.L. McCreery, J. Electrochem. Soc., 145 (1998) 2258.
- [52] M. Kendig, R. Addison, S. Jeanjaquet, J. Electrochem. Soc., 146 (1999) 4419.
- [53] F.M. Fowkes, in Encyclopedia of Polymer Science and Engineering, supplemental volume, John Wiley & Sons, New York, 1989, Acid-Base Interactions Chapter.
- [54] H.-J. Jacobasch, K. Grundke, S. Schneider, F. Simon, J. Adhesion, 48 (1995) 57.

- [55] H.-T. Chiu, J.-H. Wang, *Polymer Composites*, 19 (1998) 347.
- [56] A. Bismarck, D. Richter, C. Wuertz, J. Springer, *Colloids and Surfaces A*, 159 (1999) 341.
- [57] M. Kendig, *Corrosion*, 48 (1992) 218.
- [58] S. Miyata, *Clays and Clay Minerals*, 28 (1980) 50.

TABLES

Table 1. Conversion coating bath composition, time, and temperature

Abbrev. Name	Time (min)	Temp (°C)	Composition
Degreased	-	-	Degreased AA2024-T3 as blank
CCC*	5	40	0.025M Na ₂ Cr ₂ O ₇ , 0.024M NaF, 0.015M K ₃ Fe[CN] ₆ , and HNO ₃ added to a pH=2.
CO ₃ HT	5	95	0.07 M Na ₂ CO ₃ , 0.015M Li ₂ CO ₃ , 0.1M LiOH·H ₂ O, 600 ppm Al ₂ O ₃ ·Na ₂ O
NO ₃ HT	5	95	0.3M KNO ₃ , 0.03M LiNO ₃ , 0.1M LiOH·H ₂ O, 600 ppm Al ₂ O ₃ ·Na ₂ O
S ₂ O ₈ HT	5	95	NO3 recipe + 0.01M K ₂ S ₂ O ₈

* in house recipe, after Ilevbare, et al. [50]

Table 2. Dry and wet pull-off tensile strength (POTS) of epoxy from conversion coatings. Roughness factor from BET measurements included.

Treatment	Dry POTS (MPa)		Wet POTS (MPa)		R
	Mean	Std. Dev.	Mean	Std. Dev.	
Degreased	4.04	1.66	1.28	0.59	60+/-4
CCC	6.8	1.08	3.66	1.18	107+/-40
CO ₃	5.35	1.34	2.47	0.99	173+/-33
NO ₃	4.98	1.39	2.2	0.65	181+/-73
S ₂ O ₈	3.91	1.92	2.32	0.38	

* R = measured surface area/ apparent area

Table 3. Contact angle of probe liquids on powders measured by rising height method.

	CH ₂ I ₂	H ₂ O	FA	EG
Degreased	0	40.2	46.1	5.3
CCC	0	40.3	9.3	0
CO ₃	41.6	65.8	40.9	56.5
NO ₃	67.8	73.7	64.7	71.7
S ₂ O ₈	51.2	71	56.4	66.5

CH₂I₂= diiodomethane, FA= formamide, EG= ethylene glycol.

Table 4. Surface tension parameters for probe liquids proposed by van Oss and Della Volpe & Siboni [18,19,39].

	VOCG $\alpha = 1$			DV(1997) $\alpha = 6.5$			DV(2000) $\alpha = 4.35$			
	γ^{LVW}	γ^-	γ^+	γ^{LVW}	γ^-	γ^+	γ^{LVW}	γ^-	γ^+	γ^{tot}
H ₂ O	21.8	25.5	25.5	21.8	10	65	26.2	11.2	48.5	72.8
CH ₂ I ₂	50.8	0	0	50.8	0	0	50.8	0	0	50.8
FA	39	39.6	2.28	35.6	65.7	1.95	35.5	11.3	11.3	58
EG	29	47	1.92	31.4	42.5	1.58	33.9	51.6	0.97	48

$\alpha = \gamma^+/\gamma^-$ for water. CH₂I₂= diiodomethane, FA= formamide, EG= ethylene glycol.

Table 5. Condition numbers for the liquid surface tension component Matrix using the parameters proposed by van Oss et al. and Della Volpe. Calculated using the [3x3] and [2x2] matrix solutions.

	VOCG	DV (1997)	DV (2000)
DI-WA-FA	6.8	4.0	17.4
DI-WA-EG	6.7	4.8	4.3
DI-FA-EG	123.9	221.5	9.3
2x2 WA-FA	4.7	2.1	8.8
2x2 WA-EG	4.4	2.2	2.3
2x2 FA-EG	66.4	128.0	8.8

Table 6. Surface tension parameters calculated for NO₃ HT using different probe liquid parameters.

	DII γ^+	[nxn]	Liq 1	Liq 2	Liq 3	γ^{LVW}	γ^+	γ^-	γ^{total}
VOCG	0.000	2x2	DII	WA	FA	24.1	0.6	15.4	30.2
	0.000	3x3	DII	WA	FA	24.1	0.6	15.4	30.2
	0.000	2x2	DII	WA	EG	24.1	0.1	24.5	26.5
	0.000	3x3	DII	WA	EG	24.1	0.1	24.5	26.5
	0.720	3x3	DII	WA	FA	19.8	1.5	15.1	29.4
	0.720	3x3	DII	WA	EG	18.5	0.04	25.6	20.5
DV(97)	0.000	3x3	DII	WA	FA	24.1	1.1	6.4	29.5
	0.000	3x3	DII	WA	EG	24.1	0.01	8.5	24.4
DV(00)	0.000	2x2	DII	WA	FA	24.1	1.0	6.8	29.4
	0.000	3x3	DII	WA	EG	24.1	0.01	9.6	24.2
	0.000	3x3	DII	FA	EG	24.1	0.01	13.8	24.8

Table 7. Surface tension parameters calculated for powder samples using probe liquid parameters of van Oss [37]. Separate solutions are shown for combinations of diiodomethane, water, and formamide or ethylene glycol

Sample	Liq 3	γ^{LW}	γ^+	γ^-	γ^{total}
CCC	FA	50.8	0.7	28.1	59.4
	EG	50.8	0.1	34.8	53.4
CO ₃	FA	38.8	1.3	10.7	46.2
	EG	38.8	0.2	23.4	43.1
S ₂ O ₈	FA	33.6	0.3	13.5	37.5
	EG	33.6	0.4	23.3	39.8
NO ₃	FA	24.1	0.6	15.4	30.2
	EG	24.1	0.1	24.5	26.5
Al	FA	50.8	1.0	50.4	64.6
	EG	50.8	0.04	35.2	53.1

FIGURES

Figure 1.

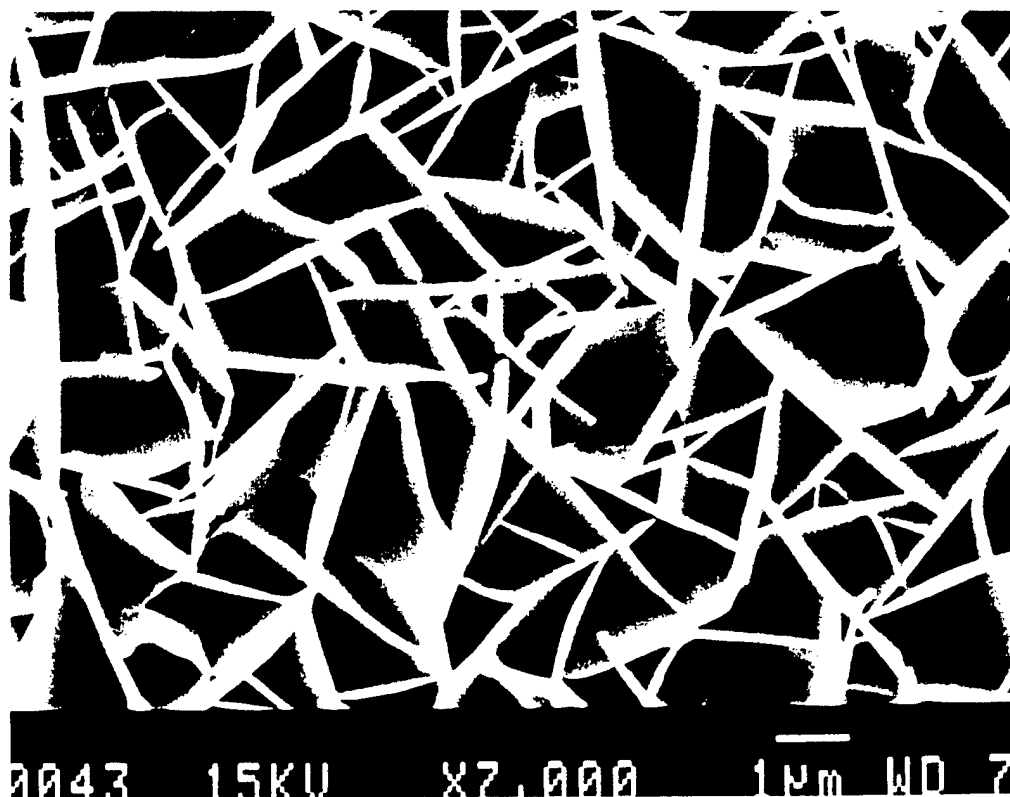


Figure 2

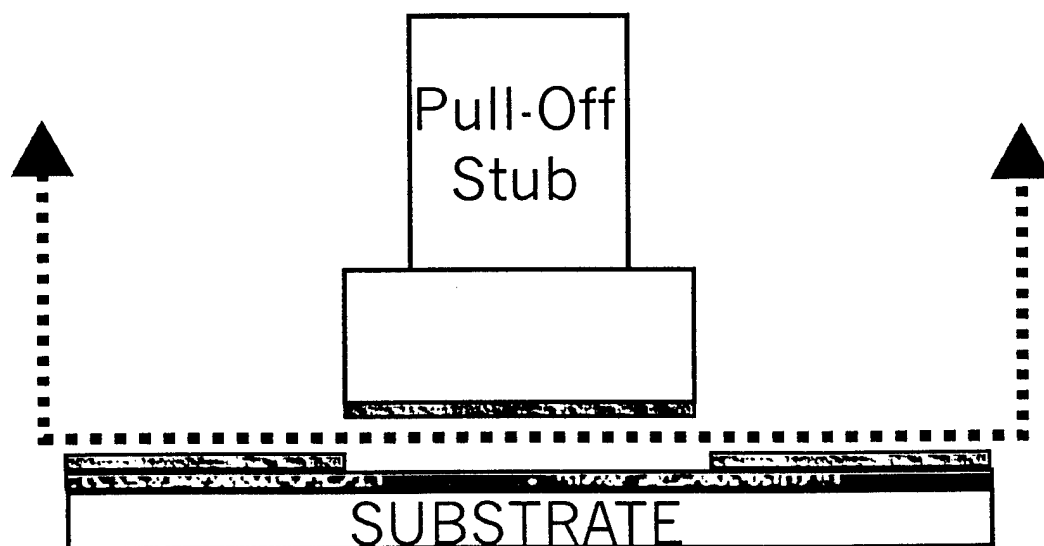
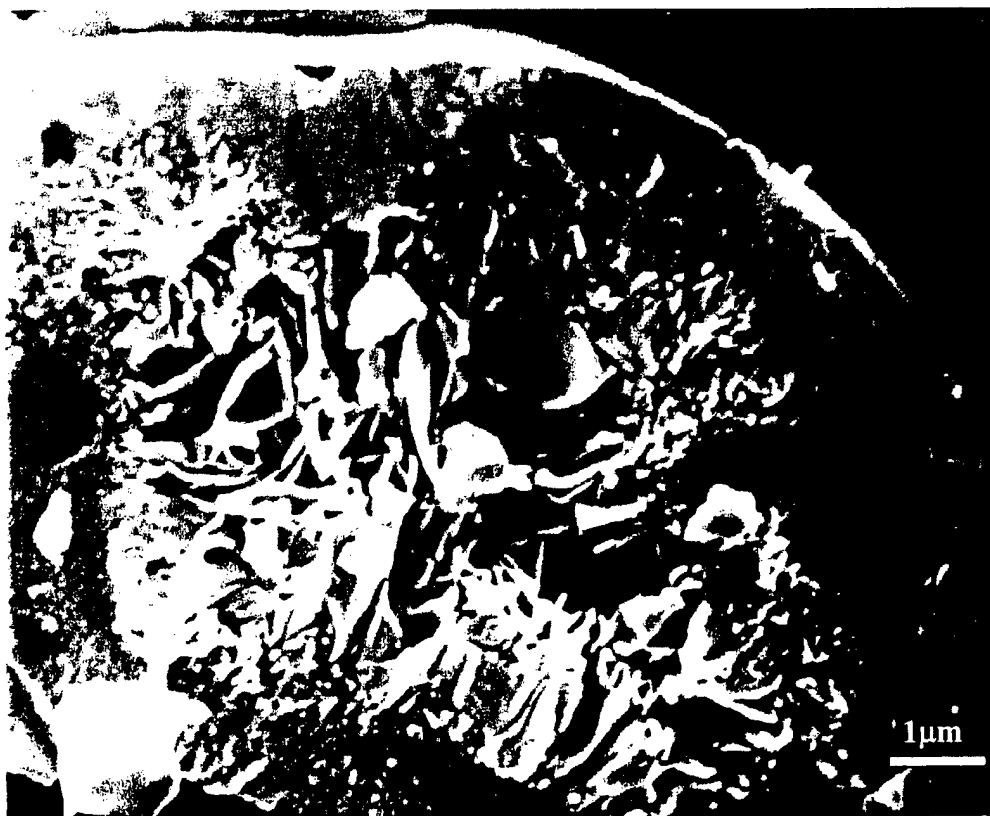


Figure 3

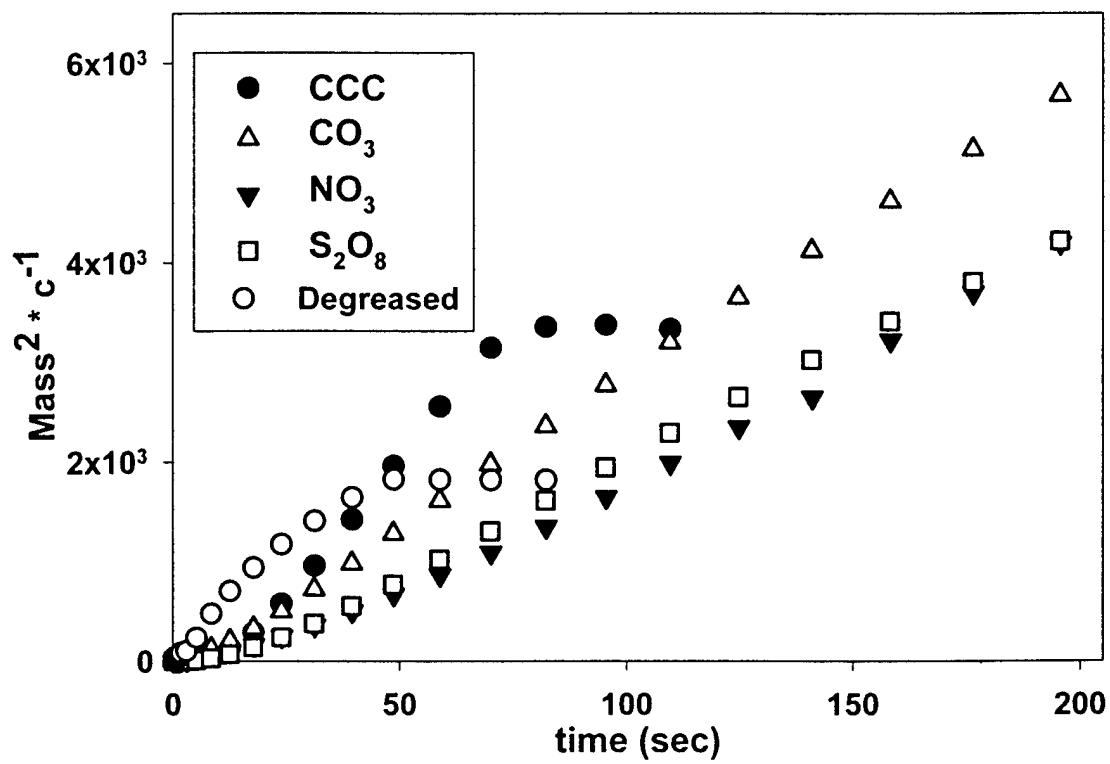


Figure 4

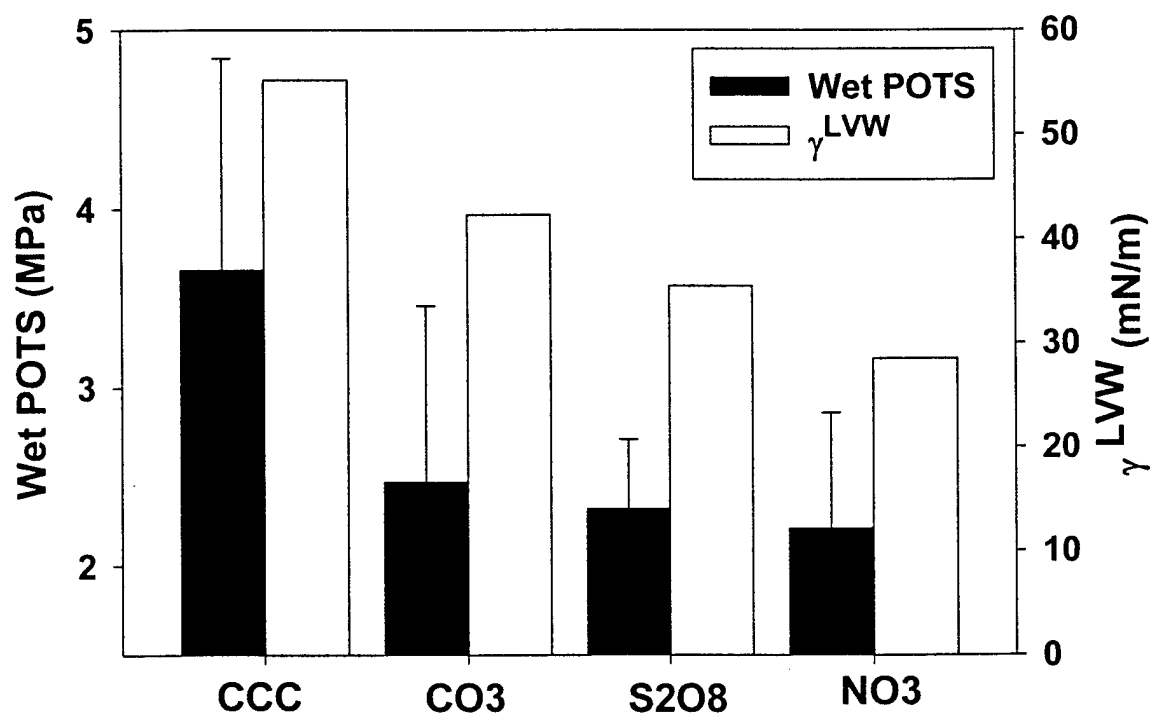


Figure 5

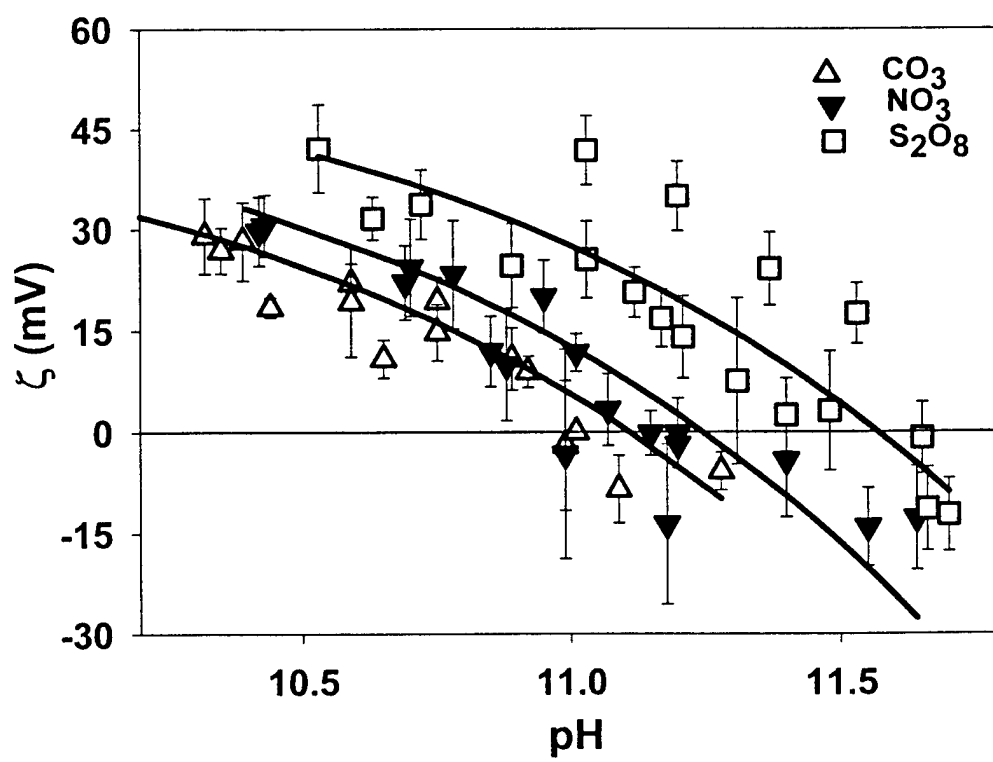


Figure 6

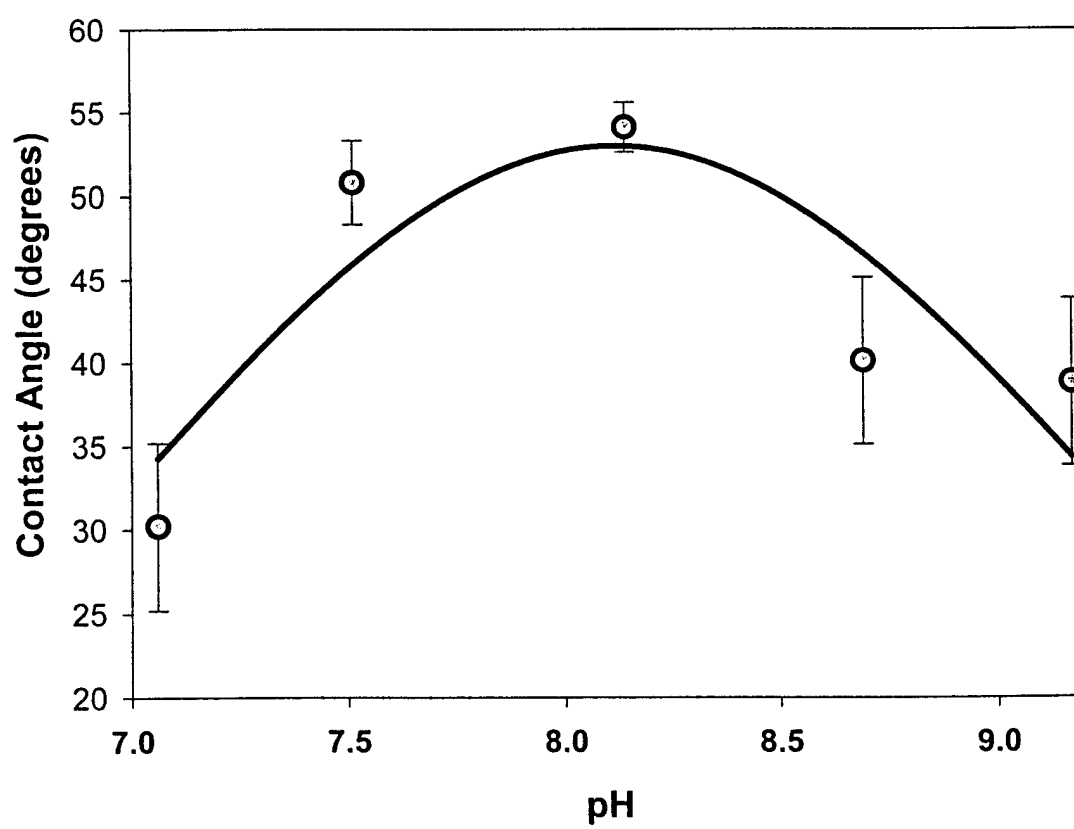
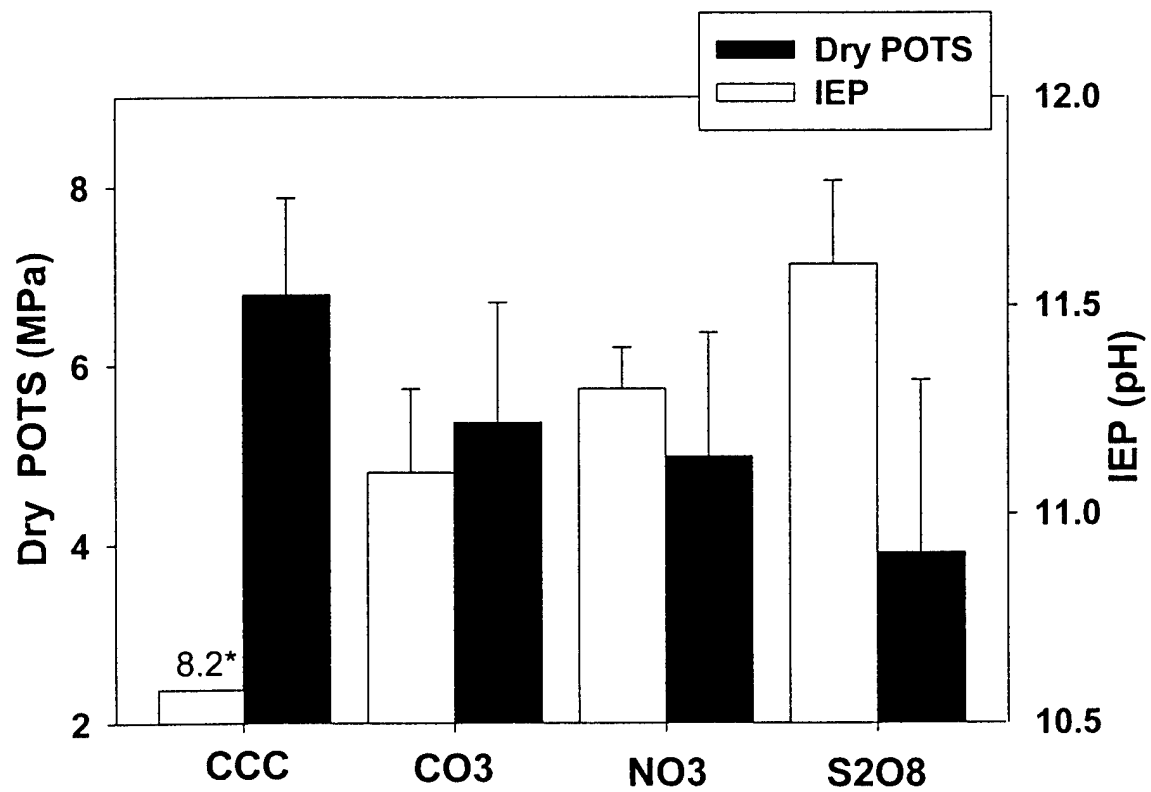


Figure 7.



* IEP of 8.2 based on contact angle measurements of buffered solutions on CCC powder included as reference.

Figure 8

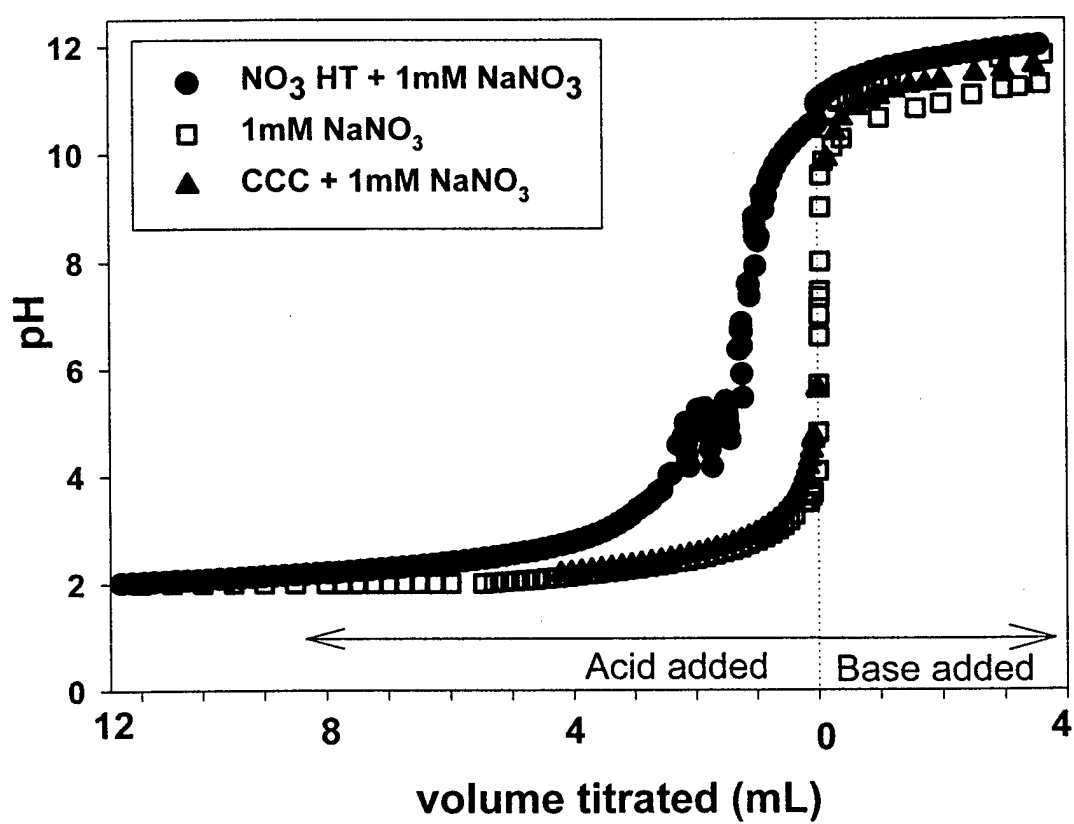


Figure 9

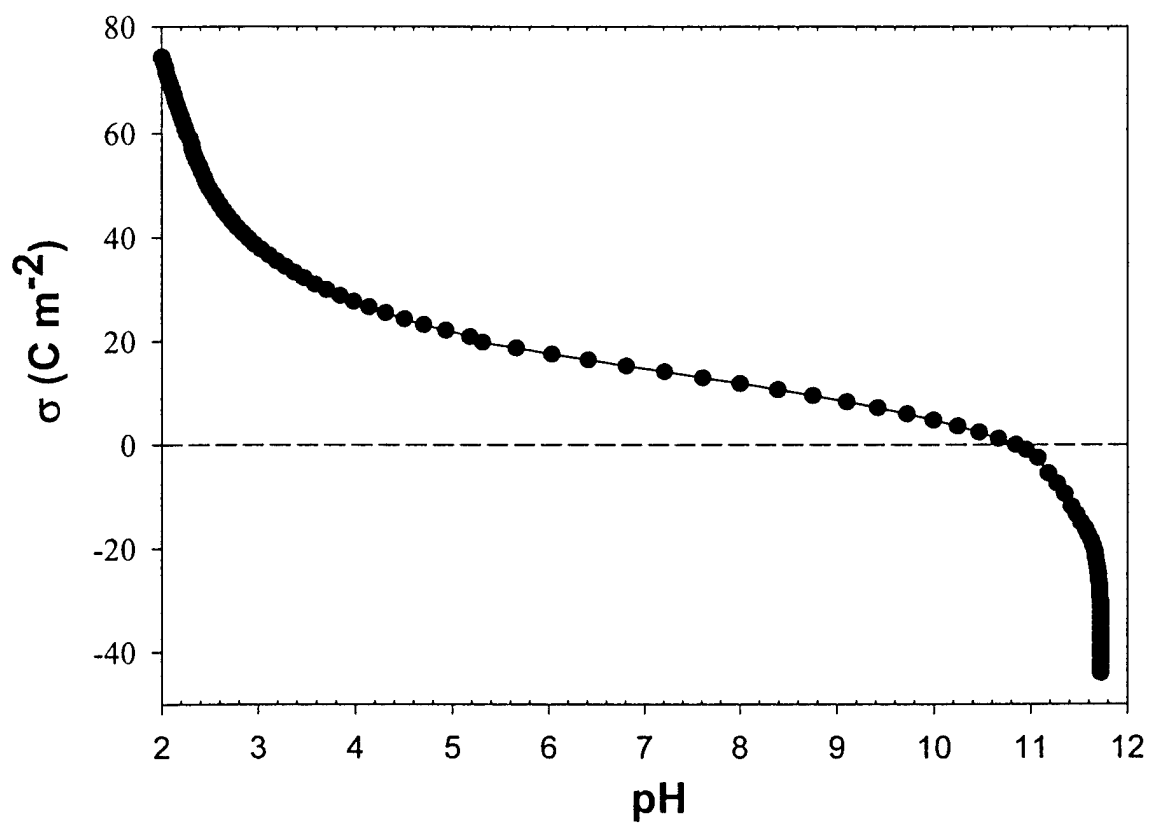


FIGURE CAPTIONS

Figure 1. SEI SEM micrograph showing blade-like structure typical of Hydrotalcite morphology. NO₃ HT shown here.

Figure 2. SEI SEM micrograph of pull-off stub after testing NO₃ HT showing poor adhesion between epoxy and HT. Schematic shows orientation of sample.

Figure 3. Wettability of water on CCC, CO₃-HT, NO₃-HT, and S₂O₈-HT conversion coating powders. Greater slope in linear region indicates lower contact angle (greater wettability).

Figure 4. Wet POTS (left axis, black bars) and γ^{LVW} (left axis, white bars) for CCC, CO₃-HT, NO₃-HT, and S₂O₈-HT conversion coatings.

Figure 5. ζ vs. pH for CO₃, NO₃, and S₂O₈ HT powders. Data fit to line of the form $\zeta = \zeta_0 - a \cdot \exp(\text{pH})$. IEP indicated by ζ sign change.

Figure 6. Contact angle of buffered solution on CCC powder versus pH. IEP indicated by contact angle maximum.

Figure 7. Dry POTS (left axis, black bars) and IEP (right axis, white bars) for CCC, CO₃-HT, NO₃-HT, and S₂O₈-HT conversion coatings.

Figure 8. Potentiometric titration for NO₃ HT and CCC in 1mM NaNO₃ using 0.1M NaOH and 0.1M HNO₃.

Figure 9. Surface charge (σ) vs pH for NO₃ HT calculated from data in Figure 8.

Submitted to *Colloids and Surfaces A: Physicochemical and Engineering Aspects* (in review)

**Adhesion of Epoxy to Hydrotalcite Conversion Coatings:
II. Surface Modification with Ionic Surfactants**

R.B. Leggat, S.A. Taylor, S.R. Taylor*

University of Virginia
Department of Materials Science and Engineering
Charlottesville VA 22904

* Corresponding author
804-982-5788 phone
804-982-5799 fax
srt6p@virginia.edu

Abstract

Hydrotalcites (HT) are a naturally occurring compound being developed as an environmentally benign conversion coatings for aluminum aerospace alloys . A successful conversion coating should provide corrosion resistance and act as a base for adhesion with subsequent organic layers. In the first paper of this series, the effect of interlayer cation substitution on the adhesion of epoxy primer was investigated. Interfacial tension and electrostatic interactions were found to influence adhesion between epoxy and conversion coatings. It was believed that increased adhesion could be attained by modification of these properties.

This investigation examines the effect of ionic surfactants on the corrosion resistance and epoxy adhesion for HT-based conversion coatings. Post-treatment of a NO_3 -HT conversion coating with a trialkyl ammonium surfactant (Adogen) increased the pull-off tensile strength (POTS) of an epoxy coating by 55%. However, treatment with a linear anionic surfactant, sodium lauryl sulfate (SLS); a linear cationic surfactant, cetyltrimethylammonium bromide (CTAB); or a divalent cation (Ca^{++}) had no effect on the epoxy POTS.

Electrophoresis and the rising height method were employed to investigate the effect of the Adogen on electrostatic interactions and interfacial tension, respectively. Adogen decreased the isoelectric point of NO_3 -HT powders from 11.3 to 10.5. This was attributed to a shift in the Outer Helmholtz Plane by the Adogen. A model epoxy molecule, N-methylethanolamine (NMEA), was used for contact angle measurements on conversion coating powders by the rising height method. The contact angle data was found to correlate with the epoxy dry adhesion rankings reported in Part 1 of this series. Adogen adsorption on NO_3 -HT powders decreased the NMEA contact angle from 67.9° to 24.1° . FTIR spectroscopy did not indicate primary bonding between NO_3 -HT and Adogen nor with NMEA. The improvement of epoxy adhesion on NO_3 -HT by Adogen is believed to be due to the increased wettability of the HT.

Keywords:

Adhesion, Electrostatics, Hydrotalcite Conversion Coatings, Interfacial Tension, Surfactants

INTRODUCTION

The first paper of this series related the adhesion of an epoxy primer to hydrotalcite (HT) based conversion coatings to the surface chemistry of the conversion coatings. The dry adhesion had a reciprocal relation to the zeta potential (ζ) of the HT, while the wet adhesion was correlated to the total solid surface tension (γ_s) and the dispersive component (γ^{LVW}) of the HT surface tension. It was believed that despite the possibility of extensive mechanical anchoring available through the HT surface morphology, the dry adhesion was limited by unfavorable polar interactions. In the wet-state, dispersive interactions dominate because polar interactions are disrupted by the presence of water. Furthermore, these results suggested that the adhesion of the epoxy to the HT conversion coatings could be improved by modification of interfacial tension and/or electrostatic interactions.

A number of mechanisms have been proposed for adhesion between a polymer and a metal substrate including: mechanical interlocking, adsorption, and electronic interactions [1-3].

Increased surface roughness and porosity can provide increased adhesion by self-anchoring of the polymer within asperities. However, incomplete wetting of the surface can result in loss of adhesion by increased stress and moisture accumulation at voids.

The adsorption theory for adhesion includes primary (covalent) and secondary (dispersion, dipole, and hydrogen) bond interactions between the adhesive and adherend. The contribution of secondary forces in adhesion has received much attention especially in the development of combining rules for calculating the surface free energy of solids from contact angle measurements [4-7]. The most recent of these separates the surface free energy (γ_s) into electrodynamic and Lewis acid-base contributions:

$$\gamma_s = \gamma^{LVW} + \gamma^{AB} \quad [1]$$

where γ^{LW} is the Liftshitz-van der Waal (dispersive + dipole) contribution and γ^{AB} is the acid-base contribution[8]. The γ^{AB} term is the root product of the acid-base energy components according to equation (2):

$$\gamma^{AB} = 2 \sqrt{(\gamma^+ \gamma^-)} \quad [2]$$

where γ^+ is the Lewis electron acceptor (acid) component and γ^- is the Lewis electron donor (base) component.

In the electronic theory of adhesion the electrostatic attraction or repulsion between to charged surfaces can be related to the related to the zeta potential (ζ). The adhesion of polymers [9], composites [10,11], and organic coatings have been related to ζ [12].

Adsorption of surfactants at the solid-liquid interface affects the surface charge and acid-base (hydrogen-bonding) character [13]. Surfactants are commonly included in paint formulations to decrease the surface tension of the paint and increase wetting of the substrate[14]. In a previous study addition of a large molecular weight organic cation to a polymer solution with a negative ζ inhibited displacement of the polymer by water at potentials below the potential of zero charge [12]. This study suggested that modification of the ζ by adsorbed molecules could improve adhesion.

In the present study, the effect of ionic surfactant adsorption on epoxy adhesion to HT conversion coatings was examined. Contact angle measurements of a model epoxy molecule on HT conversion coating powders were used to investigate the effect of surfactants on the epoxy-HT interfacial tension, i.e. wettability. Fourier Transform Infrared (FTIR) spectroscopy and electrophoresis were used to examine the role of covalent and electrostatic interactions, respectively. In addition, Electrochemical Impedance Spectroscopy (EIS) was used to evaluate the impact of ionic surfactants on the corrosion resistance of HT based conversion coatings.

For the sake of clarity, discussion of terminology is warranted. The pH at which the net surface charge is zero is the pH of zero charge (pHZC). Electrostatic properties are often assessed by electrokinetic methods in which the potential at the hydrodynamically affixed plane (ζ) is measured for a solid in a

liquid where one of the phases is stationary and the other is moving [15]. The isoelectric point (IEP), is the pH at which ζ changes signs. Only in the absence of specific adsorption, where ions can overcome their sphere of solvation, are the IEP and pHZC equivalent. The IEP is further complicated for oxides where interfacial tension contributions are present because pH effects the degree of dissociation of charged species as well as electron donating or accepting groups[16].

EXPERIMENTAL METHODS

Sample Preparation

AA2024 (Al-4Cu-1.5Mg) panels were coated with a nitrate-based hydrotalcite coating ($\text{NO}_3\text{-HT}$). After processing the panels, HT powders were precipitated from the coating baths, collected, rinsed in distilled water and oven dried at 100°C for 12 hours.

A series of $\text{NO}_3\text{-HT}$ panels were spin coated with a BPA-epichlorohydrin based epoxy hardened with a cycloaliphatic amine. A two-part solvent (50:50 toluene: butanol) was used at 4-weight % to control the resin viscosity.

Although the nitrate-base hydrotalcite was the conversion coating primarily used in this study, other conversion coating powders (including carbonate (CO_3) and persulfate (S_2O_8) hydrotalcites and chromate conversion coatings (CCC)) were used. Details of their preparation are included in the first paper of this series. Many of the techniques utilized in this study are described in the previous paper and the references therein.

Surfactant Studies

Surfactant was applied to the panels and powders by immersion in surfactant solutions. Adogen 464 (Adogen, Aldrich), methyl trialkyl ($\text{C}_8\text{-C}_{10}$) ammonium chloride was used as a cationic surfactant, and sodium lauryl sulfate (SLS, Fisher) was used as an anionic surfactant. The surface tension was

measured as a function of concentration for the surfactant solutions as shown in Figure 1 by the Wilhelmy plate method using a Kruss K12 tensiometer [17]. The critical micelle concentration (CMC) was determined by the change in slope a plot of surface tension as a function of surfactant concentration. The surfactants were applied to the panel samples as a post-treatment by immersion immediately after the coating bath. The surfactant adsorbed HT powders were prepared by mixing in surfactant solutions, decanting the solution, rinsing the powders with deionized water and drying over desiccant at room temperature for 12 hours. Regardless of the method of application, the surfactant concentrations (2.2×10^{-4} M Adogen and 3.5×10^{-4} M SLS) were chosen to be below their respective CMC (ca. 10% of the CMC).

The effect of the surfactants on the corrosion resistance and adhesion properties of the HT coating was evaluated. Electrochemical Impedance Spectroscopy (EIS) was run after 24 hours exposure to 0.5 M NaCl using a Solarton 1250 Frequency Response Analyzer and a Perkin Elmer 273A potentiostat. A parameter indicative of corrosion resistance, R_{corr} , was fit from the spectra using a complex non-linear least squares fitting program (Zview, Scribner Assoc.). R_{corr} is the polarization resistance minus the diffusional impedance and has been used previously in the study of conversion coatings [18]. Similar experiments were conducted using 99.9% pure copper substrates. Rather than using the surfactants as a post-treatment, the surfactants were added directly to electrolyte during the EIS measurements. The panels were exposed for 24 hours to 0.5M NaCl containing either 2.2×10^{-4} M Adogen or 3.5×10^{-4} M SLS. Blank samples were also included without surfactant addition.

Practical adhesion was measured by the pull-off tensile strength (POTS) of an epoxy coating from the panels in accordance with ASTM Method D4541. In addition to the dry-state adhesion, the wet-state adhesion was measured after 24 hours exposure to deionized water. NO_3 -HT panels that had received Adogen or SLS post-treatments were evaluated. In a separate experiment, a series of NO_3 -HT panels received post-treatments with either 5×10^{-4} M cetyltrimethylammonium bromide (CTAB) or 0.05M $\text{Ca}(\text{NO}_3)_2$.

Electrophoresis was used to evaluate the effect of the Adogen 464 on the ζ of NO₃-HT. The electrophoretic mobility was measured for dilute powder suspensions (100 ppm in 1mM KCl) of NO₃ HT with and without adsorbed cationic surfactant. The Smoluchowski equation was used to calculate the ζ from the electrophoretic mobility (μ) as a function of pH:

$$\zeta = \mu\eta/\epsilon\epsilon_0 \quad (3)$$

where η is the solution viscosity, ϵ = solution dielectric constant, and ϵ_0 = permittivity of free space. [15].

A BioRad FTS 6000 Spectrometer was used to collect FTIR spectra. A liquid cell with a 25 μ m path length between KBr windows was used for the neat Adogen spectra. The spectra for NO₃-HT powder was collected using pressed pellets of the powder mixed with KBr. The HT powder was manually ground in ethanol in order to prevent scattering by particles of dimensions similar to the wavelength of the incident beam [19]. The samples for which Adogen was adsorbed onto NO₃ HT were produced by allowing small volumes of Adogen to dry onto the HT powders in a desiccated chamber before pressing the KBr pellet. Molecular vibrations were assigned to peaks in the spectra and verified using web based software [20,21].

Model Epoxy Molecule Studies

The wetting of a model epoxy molecule, N-methylethanolamine (NMEA, TCI) on conversion coating powders was measured using the rising height method. The powders examined included hydrotalcite powders with different interlayer oxoanions (carbonate (CO₃) nitrate (NO₃) and persulfate (S₂O₈)) and chromate conversion coated aluminum powder (CCC). NO₃ HT powders with adsorbed Adogen were examined as well. The NMEA parameters (surface tension, viscosity, and density) used to calculate the contact angles from the rising height data are listed in Table 1.

Curing of the epoxy used in the adhesion studies was monitored as a function of time by FTIR. A thin layer of the epoxy resin + hardener mixture was applied to a KBr pellet. The FTIR spectra for the NO₃ HT powder with and without

the epoxy model molecule were also recorded. The NMEA was allowed to dry onto the ground HT powder before pressing into a KBr pellet.

The Wilhelmy plate method was used to measure the surface tensions of NMEA and the epoxy at 5, 15 and 30 minutes after mixing the resin and hardener.

Desorption of the Adogen from HT powders was examined by measuring the surface tension of water and NMEA after exposure to NO_3 -HT powders adsorbed with Adogen. The Adogen adsorbed NO_3 -HT powders were prepared as previously discussed. The surface tension of water and NMEA were measured by the Wilhelmy plate method. The HT powder was added at 0.5 weight % and stirred for 5 minutes. After allowing the powder to settle for 30 minutes, the surface tension was measured again. Control measurements were recorded for water and NMEA with 1-volume % Adogen or 0.5 weight % NO_3 HT powder.

RESULTS AND DISCUSSION

Surfactant Studies

The effect of ionic surfactants on the corrosion resistance and the adhesion properties of the NO_3 HT was examined. The R_{corr} values for the different surfactant treatments are shown in Figure 2. Tukey's method was employed in the analysis of variance [22]. The R_{corr} values were greater for the SLS treatment than for the control that had a higher R_{corr} than the Adogen treatment.

The R_{corr} results were interpreted in terms of the surface charge model of pitting. This model, also referred to as the pH of zero charge model, relates the pitting potential to the pH of zero charge (pHZC) based on the adsorption of chloride at the oxide/solution interface [23-25]. At solution pH greater than the pHZC, oxides acquire a negative charge by deprotonation of the surface hydroxyls. Chloride anions are electrostatically repelled from the surface. Conversely, at solution pH less than the pHZC, the oxide acquires a positive charge and chloride is attracted to the surface to induce pitting.

By modification of the surface charge, surfactants change the free energy of adsorption for chloride anions. Adsorption of the anionic SLS would decrease the negative surface charge of the HT surface and decrease the electrostatic attraction of the chloride anion. The adsorption of the cationic Adogen should increase the adsorption of the chloride ion.

This interpretation is supported by the R_{corr} values of copper in the presence of SLS and Adogen shown in Table 2. The R_{corr} values in 0.5 M NaCl were increased by the Adogen relative to the control. The R_{corr} values in the presence of SLS were equivalent to those observed for the control. The pHZC for copper is 5.0 [26]. At the neutral pH of 0.5 M NaCl, copper is negatively charged and the cationic Adogen is attracted to the surface. The efficacy of surfactants as corrosion inhibitors is dependent on the solution pH and metal pHZC. For example, other authors have found SLS to be an inhibitor for copper [27] and aluminum [28] at pH values below their respective pHZC where copper is positively charged and the SLS is attracted to the surface.

The practical adhesion results are shown in Figure 3. The wet and dry POTS values for the Adogen treated surface were statistically higher than that observed for the SLS treated surface and the control, which were statistically equivalent. These results were counter-intuitive. In the previous study, the dry POTS was found to increase with decreasing IEP. Based on electrostatic arguments, the adsorption of the cationic Adogen would be expected to increase the IEP and thus decrease the dry POTS. It was suspected that the hydrocarbon chains of the Adogen might account for the increased adhesion rather than the cationic head group.

The effect of the cationic head group on the dry POTS was explored by post-treatments of the NO_3 HT conversion coated panels with a single chained cationic surfactant, CTAB, or a divalent metal cation, Ca^{++} . There was no significant change in the dry POTS for either the CTAB or Ca^{++} relative to the control as shown in Table 3. This supports the conclusion that the trialkyl structure of Adogen is important to its effect on the adhesion of epoxy to NO_3 HT coatings.

An issue raised by the dry POTS results for the Adogen, CTAB, and Ca^{++} results is the likelihood of co-ion surfactant adsorption. There are many examples of co-ion surfactant adsorption in the literature including adsorption of: oleate (anionic) on hematite [29]; SLS on polystyrene latex [30]; and SLS on polycarbonate [31,32].

In addition to electrostatic contributions, the free energy of adsorption for a surfactant at the water-oxide interface is controlled by the hydrophobic interaction between the surfactant tail and water according to equation (4):

$$\Delta G_{\text{ads}} = zF\Psi_{\delta} + N\Phi \quad (4)$$

where z is the charge of the surfactant polar head group, F is Faradays constant (23,060 kcal/ equiv. V), Ψ_{δ} is the potential at the Stern layer, N is the number of carbon atoms in the surfactant hydrocarbon chain and Φ is the free energy decrease upon removal of 1 mole of CH_2 groups from solution (0.6 Kcal / mole) [33].

It is unlikely that Ca^{++} was adsorbed on the HT surface, due to the HT $\zeta \cong 50\text{-}60$ mV at neutral pH as reported in Part I of this series. As the hydrocarbon chain of the surfactant increases in length, adsorption becomes more likely. The hydrophobic driving force for adsorption is greater than the electrostatic repulsion for hydrocarbon chains with greater than two CH_2 groups. The Adogen molecule has three $\text{C}_8\text{-C}_{10}$ chains and CTAB has one C_{15} chain.

Because the improvement of adhesion was practically of interest, further study was limited to the Adogen treated surfaces. It should be noted that extensive work on the adsorption of SLS on a Mg-Al-CO_3 HT-like compound has been conducted by Pavan and co-workers [34,35]. Electrokinetic and wettability studies were employed in the examination of the Adogen effect on electrostatic interactions and interfacial tension.

The IEP of NO_3 HT powders with and without adsorbed Adogen were determined from ζ vs pH curves shown in Figure 4. Data was fit to an equation of the form $\zeta = \zeta_0 - a \cdot \exp(\text{pH})$. The fit parameters are shown in Table 4. It can be seen from the data that the IEP of the NO_3 HT decreased from 11.3 ± 0.1 to 10.5

± 0.2 mN/m in the presence of Adogen. These results are counter-intuitive as the adsorption of a cationic surfactant, such as Adogen, on a surface with positive charge would have been expected to increase the ζ .

A possible explanation for the observed decrease in ζ is a shift in the outer Helmholtz plane (OHP) due to the presence of the adsorbed Adogen. The OHP is a plane within of the double layer, which is the interfacial region where the electrostatic potential (Ψ) differs from the bulk. The Graham model of the double layer, describes three regions, the inner Helmholtz plane (IHP), the OHP, and the diffuse layer [36]. The IHP passes through the center of specifically adsorbed ions; the OHP is the plane passing through the center of solvated, non-specifically adsorbed ions. Ψ varies linearly through the IHP and OHP. In the diffuse layer, which begins at the OHP, Ψ varies exponentially due to Brownian disordering of the ions. In the absence of specifically adsorbing anions there is no IHP as shown in the left schematic of Figure 5. Assuming for the sake of discussion that ζ is equal to Ψ at the OHP, the adsorption of Adogen at the HT surface can account for the observed decrease in ζ as seen in the right side of Figure 5. The most favorable orientation for adsorption of the Adogen is with its hydrocarbons on the surface and the polar head pointing into solution. The IHP will now pass through the center of the polar head group and the OHP will be further from the surface. The decrease in ζ is indicated in the schematic. This model of ζ variation due to OHP shift has been invoked to account for the decrease of ζ due to the adsorption of a non-ionic surfactant [37]. Inherent to the application of this model to the current study is the assumption that the decrease in Ψ with distance is not compensated for by the charge of the Adogen ammonium head group. Alternatively, the cross sectional area of the Adogen may shield positive sites on the surface.

Primary bonding between Adogen and the NO_3 HT surface was investigated by FTIR spectroscopy. The spectra for the NO_3 HT powders, neat Adogen and Adogen adsorbed onto NO_3 HT are shown in Figure 6. There are three major regions in the spectrum for the NO_3 HT powder: $3700\text{-}3200\text{ cm}^{-1} =$

O-H (hydroxyl, water of hydration, and interlayer water); 1300-1350 = NO_3 oxoanions; 1000-600 = Al-OH, Li-OH [38,39]. The peaks in the Adogen adsorbed NO_3 HT spectrum are assigned in Table 5. Comparison with the Adogen and NO_3 HT spectra indicates that there is no primary bonding occurring between the Adogen and the NO_3 HT powder. All the peaks in the Adogen adsorbed NO_3 HT spectrum are equivalent and of equal intensity to the spectra of the individual components.

Model Epoxy Molecule Studies

It was of interest to determine the extent of primary and secondary bonding between epoxy and HT coating. NMEA was used as a model epoxy molecule for wetting and FTIR studies on conversion coating powders. Aside from the fact that cured epoxy would destroy the sample holder, the viscosity of epoxy made it impractical to use in powder wetting studies. NMEA was originally used for XPS studies with characterizing the interaction of epoxy with aluminum, titanium and copper surface [40]. The basis for using NMEA as an epoxy model molecule is its similar functionality as partially cured epoxy as seen in Figure 7. NMEA was characterized by surface tension measurements and FTIR spectroscopy to validate its use as an epoxy model in this study.

The surface tension of the NMEA was 34.2 mN/m as measured by the Wilhelmy method which is in good agreement with the value of 34.6 estimated by Yaws [41]. The surface tension of the coating epoxy was measured as a function of cure time and compared to the NMEA as seen in Table 6. The surface tension of the epoxy-hardener resin was measured to be 37.6 mN/m at 5 minutes after mixing. After 15 minutes the surface tension had increased to 39.0 mN/m. Evaporation of solvent would contribute to the increased surface tension with time. Gelling of the resin after 30 minutes prevented measurement at longer times. Thus, the NMEA has a surface tension that is reasonably similar to the epoxy resin-hardener during curing.

The FTIR spectra for the epoxy-hardener resin were recorded as a function of cure time at room temperature. The FTIR spectrum for the NMEA is

included along with the epoxy spectrum at 3 hours cure time in Figure 8. The spectra for the NMEA and epoxy at 3 hours have similar features, which are assigned to specific vibrations in Table 7. There are many groups that are common to both spectra including H-bonding vibrations for hydroxyl and amine groups and the C-H stretches and bends. The presence of oxirane rings and aromatic groups accounts for the majority of the vibrations unique to the epoxy spectrum. Based on the surface tension measurements and FTIR spectra, NMEA was determined to be an adequate model molecule for partially-cured epoxy.

Primary bonding between NO₃ HT and NMEA was investigated by FTIR spectroscopy as shown in Figure 9. The spectrum for NMEA and NO₃ HT together is dominated by the NO₃ HT powder. The peak at 1115 cm⁻¹(C-N) present in the NO₃ HT + NMEA spectrum is absent in the NO₃ HT spectrum, however, it is present in the NMEA spectrum. The fact that there are no peaks in the NO₃ HT + NMEA spectrum that can not be accounted for by the NO₃ HT and NMEA spectra suggests that strong chemical bonding does not occur between NO₃ HT and NMEA. Thus, it can be inferred that chemical bonding does not occur between NO₃ HT and epoxy.

The contact angle of NMEA on the different conversion coating powders was measured using the rising height method. In order to separate the particle dependent variables from the rising liquid variables, the results are plotted as (mass gain)² / packing constant versus time as seen in Figure 10. The slope of the lines is related to the contact angles, with the steeper slopes indicating lower contact angles. The contact angles for NMEA on the various powders are listed in Table 8. The contact angles correlate with the total surface tension of the conversion coatings (γ_s^{total}) and the dry POTS rankings discussed in Part I of this series. The presence of the Adogen decreased contact angle from 67.9 to 24.1°. The Adogen apparently increased the wettability of the NO₃ HT by NMEA.

Experiments were performed to determine if Adogen was desorbing from the HT powder. This was done by measuring the surface tension of water and NMEA after exposure to Adogen-adsorbed HT. As seen in Table 9, the surface tension of water was dramatically affected by the Adogen-adsorbed HT

suggesting that the Adogen did desorb in the presence of water. Even after 30 minutes the solution was still turbid due to powder in suspension. It is possible that the Adogen acted as a dispersing agent for the NO_3 HT powder. The effect of the Adogen adsorbed NO_3 HT was less pronounced for the NMEA surface tension.

Separate measurements were conducted to determine the independent effects of the Adogen and the HT powders on the surface tension of water and NMEA. As expected, the addition of Adogen decreased the surface tension of water, however, the NO_3 HT powder alone did not affect the surface tension. Neither the Adogen nor NO_3 HT powder alone affected the NMEA suggesting that the change in the surface tension of water was due to the dispersed HT powder. The desorption experiments do not definitively exclude the possibility of Adogen desorption in NMEA, however they do indicate that a change in the NMEA surface tension is not the reason for the increased wettability. The benefit of the surfactant is in its use as a post-treatment and not as an additive in the epoxy formulation.

The effect of the Adogen on the epoxy/ NO_3 HT interfacial tension is believed to be the reason for the increased epoxy POTS. The fact that NMEA is water-soluble suggests that the Adogen makes the NO_3 HT surface more hydrophilic. This conclusion can not be substantiated by contact angle measurements due to desorption of Adogen in water.

Summary

- Post-treatment of NO_3 HT conversion coatings with a trialkyl ammonium surfactant (Adogen) was found to increase the practical adhesion to epoxy, while a linear anionic surfactant (SLS) was found to have no effect.
- Post-treatment with a linear cationic surfactant (CTAB) or a divalent cation (Ca^{++}) had no effect on the practical adhesion between epoxy and NO_3 HT conversion coatings. Thus, indicating that the trialkyl structure of Adogen was important in its effect.

- Electrokinetic measurements indicated that the IEP of NO₃ HT was decreased by Adogen, which was attributed to a shift in the OHP.
- Adogen post-treatment decreased the corrosion resistance of NO₃ HT conversion coatings, while R_{corr} was increased by SLS post treatment.
- The wettability of an epoxy model molecule (NMEA) on conversion coating powders correlated with the epoxy dry adhesion reported in Part I of this study.
- FTIR spectroscopy indicated that primary bonding was not occurring between the NO₃ HT and the Adogen nor between NO₃ HT and NMEA.
- Adogen adsorption on NO₃ HT decreased the NMEA contact angle from 67.9° to 24.1 indicating that the improved adhesion was due to increased wettability.

ACKNOWLEDGEMENTS

This work was supported by DARPA (Contract #49620-1-0305) under direction of Dr. Stephen Wax and Lt. Col. Paul Trulove (AFSOR). The use of the facilities of the Particle Science and Technology Center (UFL) is greatly appreciated.

REFERENCES

- [1] A.J. Kinloch, J. Mater. Sci., 15 (1980) 2141.
- [2] G. Fourche, Polym. Eng. Sci., 35 (1995) 957.
- [3] J.A. Baghdachi, J. Coatings Technol., 69 (1997) 8.
- [4] F.M. Fowkes, Ind. Eng. Chem., 56 (1964) 40.
- [5] D.K. Owens, R.C. Wendt, J. Appl. Polym. Sci., 13 (1969) 1741.
- [6] D. H. Kaelble, J. Adhesion, 2 (1970) 66.
- [7] S. Wu, *ibid* (1973) 39.
- [8] C.J. Van Oss, M.K. Chaudhury, R.J. Good, Chem. Rev. 88 (1988) 927.
- [9] H.-J. Jacobasch, K. Grundke, S. Schneider, F. Simon, J. Adhesion, 48 (1995) 57.
- [10] H.-T. Chiu, J.-H. Wang, Polymer Composites, 19 (1998) 347.
- [11] A. Bismarck, D. Richter, C. Wuertz, J. Springer, Colloids Surf Physicochem. Eng. Aspects, 159 (1999) 341.
- [12] M. Kendig, Corrosion, 48 (1992) 218.
- [13] M.J. Rosen, Surfactants and Interfacial Phenomenon, 2nd ed., John Wiley & Sons, New York, 1989.
- [14] C.H. Hare, Protective Coatings: Fundamentals of Chemistry and Composition, Technology Publishing Co., Pittsburgh, 1994.
- [15] R.J. Hunter, Zeta Potential in Colloid Science, Academic Press, London, 1989.
- [16] C.J. Van Oss, Interfacial Forces in Aqueous Media, Marcel Dekker, New York, 1994
- [17] A.W. Adamson, A.P. Gast, Physical Chemistry of Surfaces, 6th ed., John Wiley & Sons, New York, 1997.
- [18] R.G. Buchheit, M. Cunningham, H. Jensen, M.W. Kendig, M.A. Martinez, Corrosion 54 (1998) 61.
- [19] R.J.P. Lyon, in J. Zussman (Ed.), Physical Methods in Determinative Mineralogy, Academic Press, London, 1967.
- [20] J. Gasteiger, Calculation and Visualization of IR and Raman Spectra, <http://www2.ccc.uni-erlangen.de>, (Jan. 16, 2001).
- [21] S. Thomas, IR Wizard, <http://www.chem.uni-potsdam.de/tools/>, (June 29, 2001).
- [22] J.L. Devore, Probability and Statistics for Engineering and the Sciences, 5th ed., Duxbury, Pacific Grove, 2000.
- [23] P.M. Natishan, E. McCafferty, G.K. Hubler, J. Electrochem. Soc., 133 (1986) 1061.
- [24] P.M. Natishan, E. McCafferty, G.K. Hubler, *ibid*, 135 (1988) 321.
- [25] E. McCafferty, *ibid*, 146 (1999) 2863.
- [26] R. Lindberg, G. Sundholm, J. Sjoblom, P. Ahonen, E.I. Kauppinen, J. Dispersion Sci. Technol., 20 (1999) 715.
- [27] R.F.V. Villamil, P. Corio, J.C. Rubim, S.M.L. Agostinho, J. Electroanal. Chem., 472 (1999) 112.
- [28] T. Zhao, G. Mu, Corros. Sci., 41 (1999) 1937.
- [29] J.B. Kayes, J. Colloid Interface Sci., 56 (1976) 426.

- [30] P.D. Bisio, J.G. Cartledge, W.H. Keesom, C.J. Radke, J. Colloid Interface Sci., 78 (1980) 225.
- [31] W.H. Keesom, R.L. Zelenka, C.J. Radke, J. Colloid Interface Sci., 125 (1988) 575.
- [32] P. Somasundaran, T.W. Healy, D.W. Fuerstenau, J. Phys. Chem. , 68 (1964) 3562.
- [33] D.W. Fuerstenau, in D.L. Johnson, P.N. Sen, Physics and Chemistry of Porous Media, American Institute of Physics, New York, 1984, 209.
- [34] P.C. Pavan, G.A. Gomes, J.B. Valim, Microporous and Mesoporous Materials, 21 (1998) 659.
- [35] P.C. Pavan, E.L. Crepaldi, G. A. Gomes, J. B. Valim, Colloids Surf. Physicochem. Eng. Aspects, 154 (1999), 399.
- [36] C.M.A. Brett, A.M.O. Brett, Electrochemistry: Principles, Methods and Applications, Oxford University Press, New York, 1993.
- [37] K.G. Mathai, R.H. Ottewill, Trans. Faraday Soc., 62 (1966) 750.
- [38] C.J. Serna, J.L. Rendon, J.E. Eglesias, Clays Clay Miner., 30 (1982) 180.
- [39] R.A. Nyquist, C.L. Putzig, M.A. Leugers, The Handbook of Infrared and Raman Spectra of Inorganic Compounds and Organic Salts, Academic Press, New York, 1979.
- [40] J. Marsh, L. Minel, M.G. Barthes-Labrousse, D. Gorse, Appl. Surf. Sci. 133 (1998) 270.
- [41] C.L Yaws, Chemical Properties Handbook: Physical, Thermodynamic, Environmental, Transport, Safety, and Health related Properties for Organic and Inorganic Chemicals, McGraw-Hill, New York, 1999.

Figure Captions

Figure 1. Surface Tension vs. Surfactant Concentration for Adogen and Sodium Lauryl Sulfate(SLS).

Figure 2. Effect of ionic surfactant post-treatment (Adogen and SLS) on corrosion resistance of NO₃ HT conversion coatings and adhesion with epoxy. R_{corr} fit from EIS data after 24h in 0.5 M NaCl right axis.

Figure 3. Effect of ionic surfactant post-treatment (Adogen and SLS) on epoxy adhesion. Wet and Dry pull-off tensile strength (POTS) .

Figure 4. NO₃ HT powder ζ vs. pH (100 ppm in 1mM KCl) with and without adsorbed Adogen. Data fit to curve of form $\zeta = \zeta_0 + a \cdot \exp(\text{pH})$. IEP is intercept at $\zeta = 0$.

Figure 5. Schematic of double layer. Left panel shows Outer Helmholtz Plane (OHP) through center of non-specifically adsorbed ions. Right panel shows shift of OHP due to adsorbed Adogen. Inner Helmholtz Plane (IHP) passes through center of Adogen ammonium ion. Resultant change in ζ indicated.

Figure 6. FTIR spectra for Adogen; Adogen adsorbed NO₃ HT; and NO₃ HT powder.

Figure 7. Schematic illustrating similarity between NMEA structure and partially cured epoxy resin + hardener after Marsh, et al. [41].

Figure 8. FTIR spectra for N-methylethanolamine (NMEA) and Epoxy at 3 hours cure.

Figure 9. FTIR spectra for N-methylethanolamine (NMEA); NO₃ HT powder + NMEA; and NO₃ HT powder.

Figure 10. Rising height method for N-methylethanolamine (NMEA) on conversion coating powders (CCC; NO₃⁻, CO₃⁻, S₂O₈⁻ HT; and Adogen adsorbed NO₃ HT).

Ordinate axis is $\text{mass}^2 \cdot \text{c}^{-1}$ to separate particle dependent variables.

Tables

Table 1. N-methylethanolamine parameters (density, viscosity, and surface tension) used in calculation of contact angle from rising height method data.

Density*	0.94	(g cm ⁻²)
Viscosity*	10.27	(cPoise)
Surface Tension*	34.57	(mNm ⁻²)

* manufacturer (TCI) info, ** [42]

Table 2. R_{corr} values fit from EIS spectra of 99.9% pure copper after 24h in 0.5M NaCl with either 2.2x10⁻⁴ M Adogen or 3.5x10⁻⁴ M SLS.

Treatment	R_{corr} (kΩ cm⁻¹)
Adogen	68.0 ± 6.4
SLS	7.9 ± 0.1
Control	10.2 ± 3.3

Table 3. Epoxy dry Pull-off tensile strength(POTS) on NO₃ HT treated with either 5x10⁻⁴ M CTAB or 0.05M Ca(NO₃)₂.

Treatment	POTS (MPa)
CTAB	4.78 ± 0.96
Ca(NO₃)₂	4.66 ± 1.09
Control	4.12 ± 1.84

Table 4. Fit of z vs pH data from NO₃ HT powders with and without adsorbed Adogen to a curve of the form $\zeta = \zeta_0 + a \cdot \exp(\text{pH})$.

Powder	ζ_0	a	IEP
NO₃ HT	57.5 ± 2.0	7.5x10 ⁻⁴ ± 1.0x10 ⁻⁴	11.3 ± 0.1
NO₃ HT + Adogen	70.3 ± 7.5	2.0x10 ⁻³ ± 0.3x10 ⁻³	10.5 ± 0.2

Table 5. Assignment of Adogen FTIR peaks.

wavenumber	Assignment
3450	O-H (h-bond)
2960	C-H (stretch)
2930, 2860	N-CH ₃ (stretch)
1640, 1390	N-O (nitrate)
1470	C-H (bend)
1120	C-N (bend)
620	C-Cl

Table 6. Surface tension of N-methylethanolamine and epoxy resin+ hardeners as a function of cure time.

Liquid	γ (mN/m)
NMEA	34.2
Epoxy t = 5 min	37.6
Epoxy t = 15 min	39
Epoxy t = 30 min	n/a gellation

Table 7. Comparison of FTIR peaks common and unique to N-methylethanolamine and epoxy resin+ hardner at 3 hours cure time.

	Common			
wavenumber range (cm-1)	3400-3300	3200-3000	3000-2700	1500-1400
assignment	O-H (h-bond)	N-H (stretch)	C-H (stretch)	C-H (bend)
	NMEA			
wavenumber	3150	1350	1145, 1175	1115
	O-H (h-bond)	O-H (bend)	C-OH (stretch)	C-N (bend)
	Epoxy			
wavenumber	3060	1610, 1580	1250	830
	oxirane-H, arom-H (stretch)	arom-NH (bend)	oxirane-H (bend)	neighbor arom. (out of plane)

Table 8. Contact angles of NMEA on conversion coating powders (CCC, NO₃-, CO₃-, S₂O₈- HT, and Adogen adsorbed NO₃ HT powders) calculated from rising height method data.

Powder	θ-NMEA
CCC	0°
CO ₃	57.7°
NO ₃	67.9°
S ₂ O ₈	77.1°
Adg-NO ₃	24.1°

Table 9. Surface tension of water and NMEA with addition of Adogen adsorbed NO₃ HT, NO₃ HT, and Adogen.

Composition	γ (mN/m)	
	Water	NMEA
pure	72.5	34.2
0.05 wt% Adg-NO ₃ HT	45.6	33
0.05 wt% NO ₃ HT	72.5	34.2
1 vol% Adogen	27.9	34.1

Figure 1.

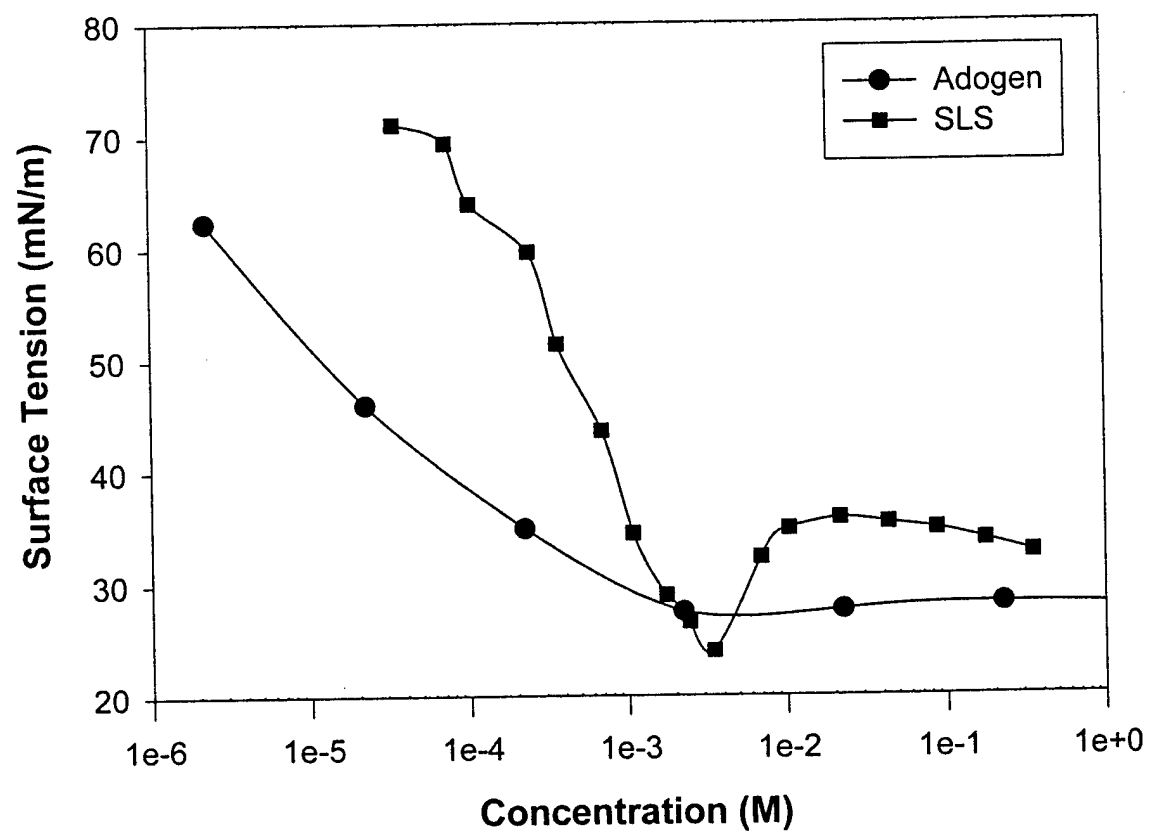


Figure 2.

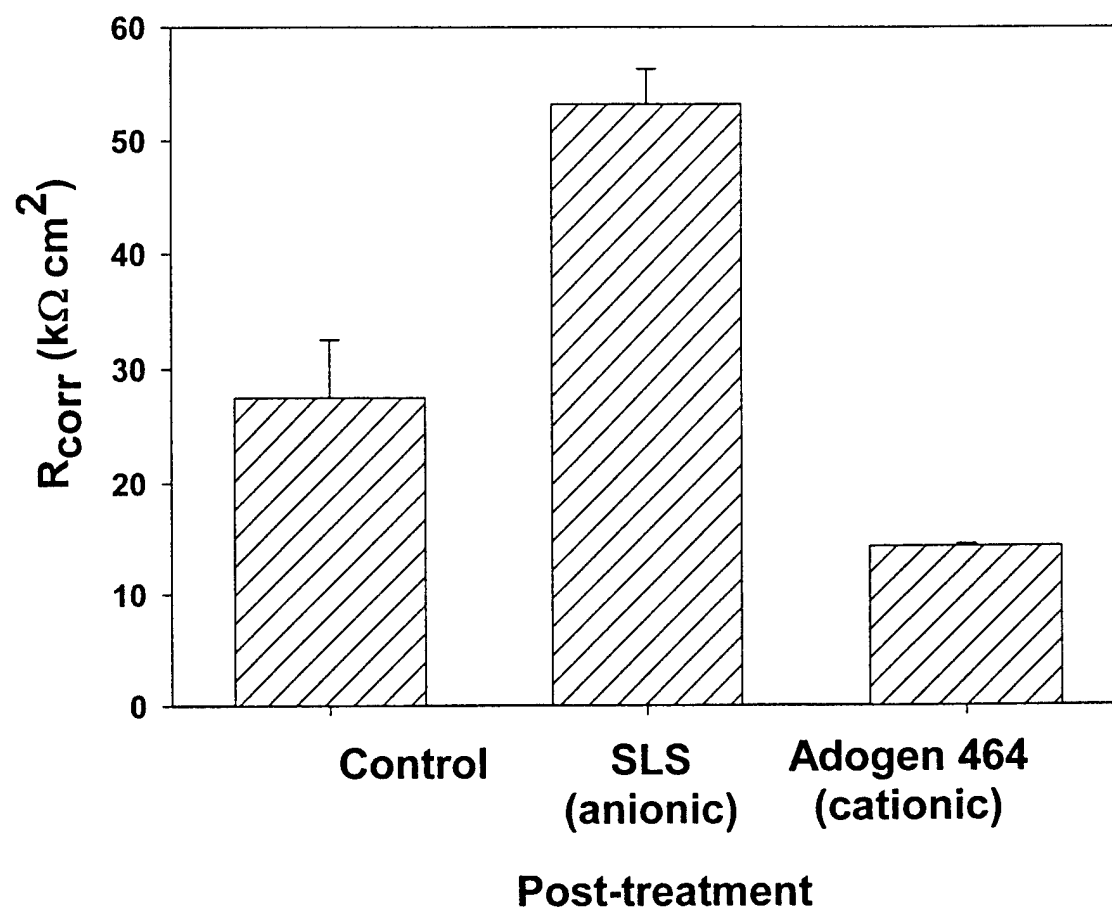


Figure 3.

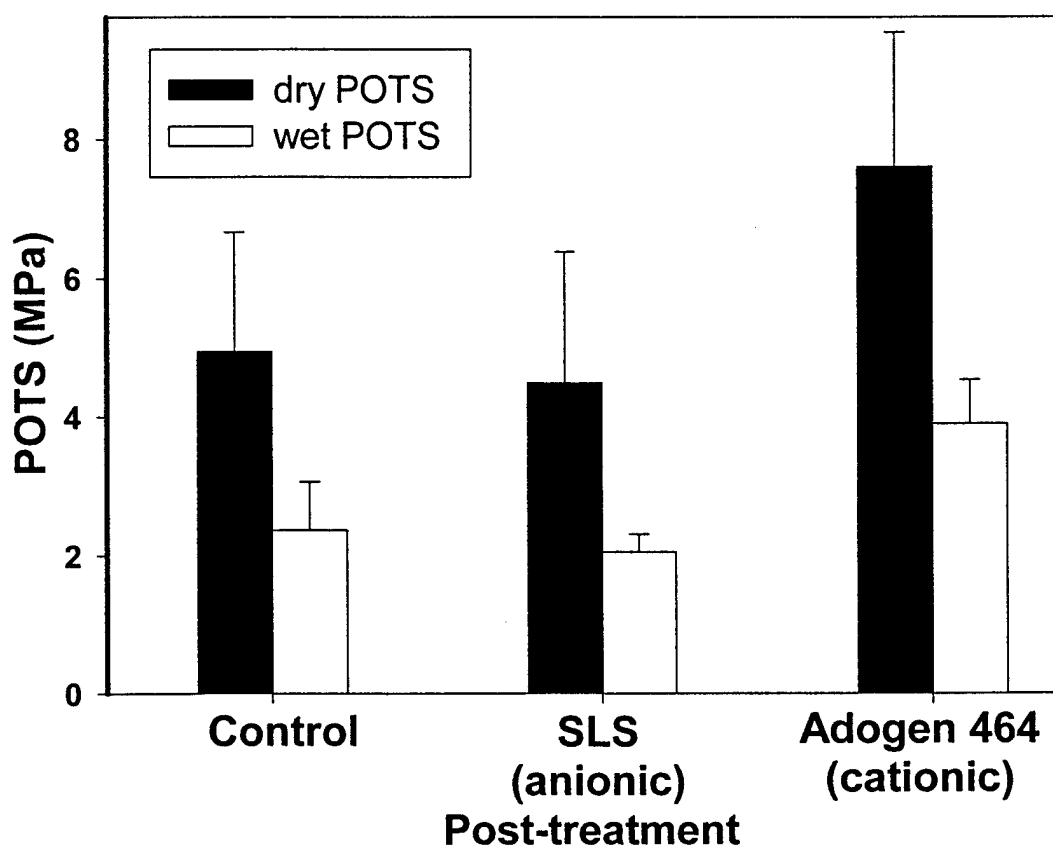


Figure 4.

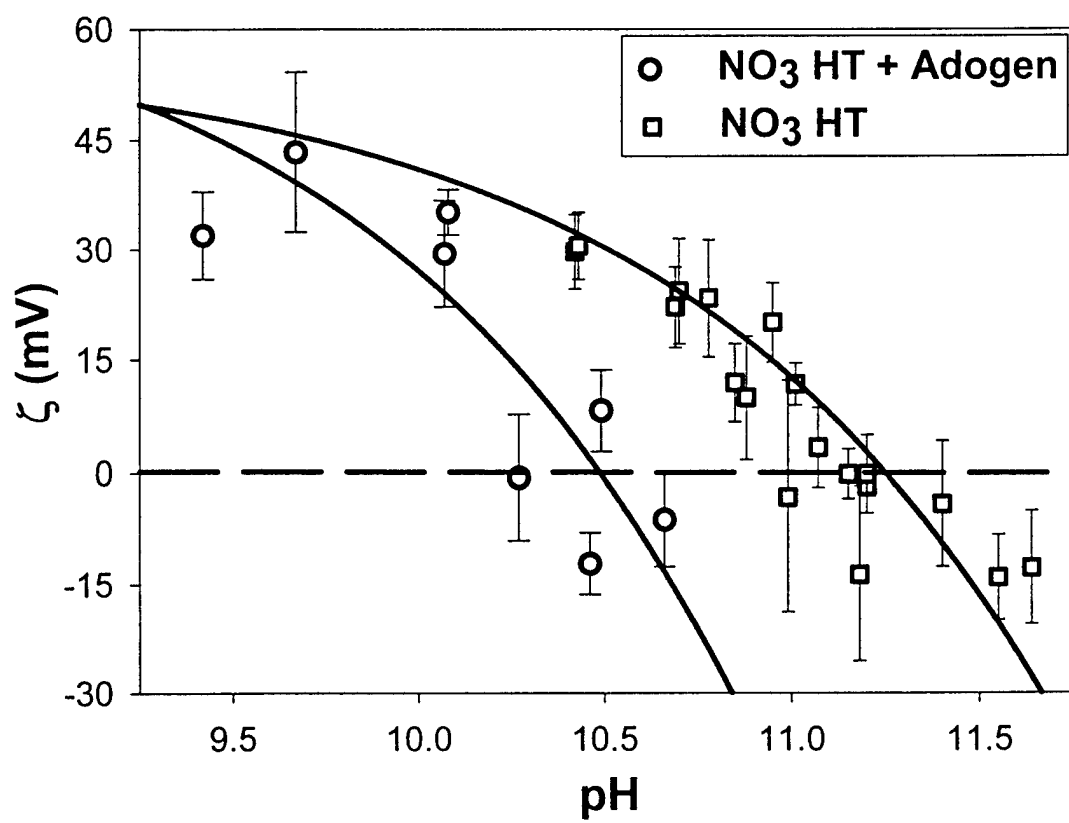


Figure 5.

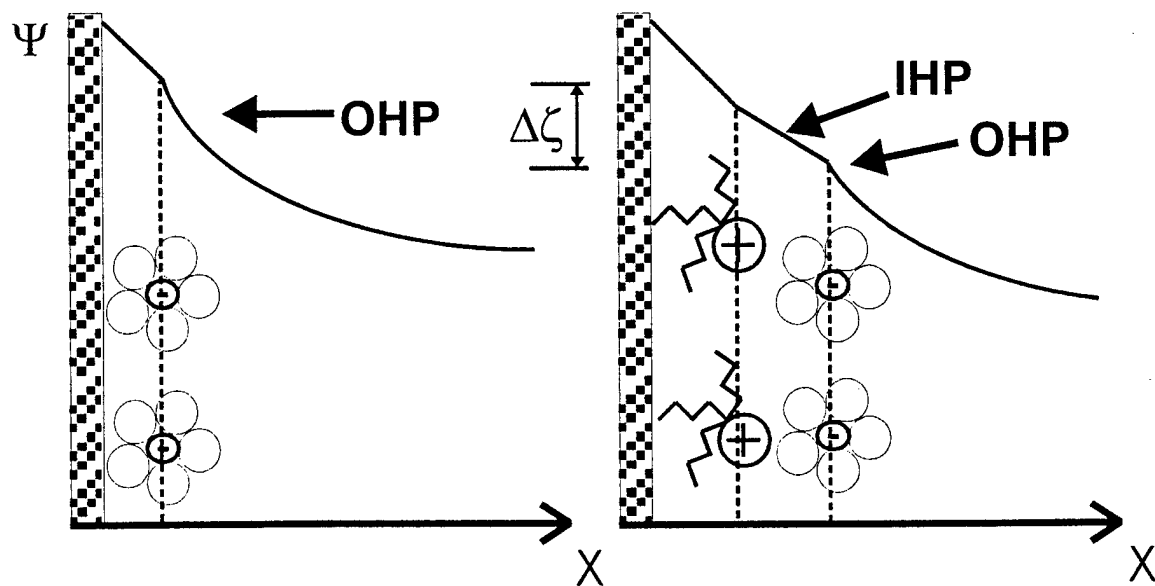


Figure 6.

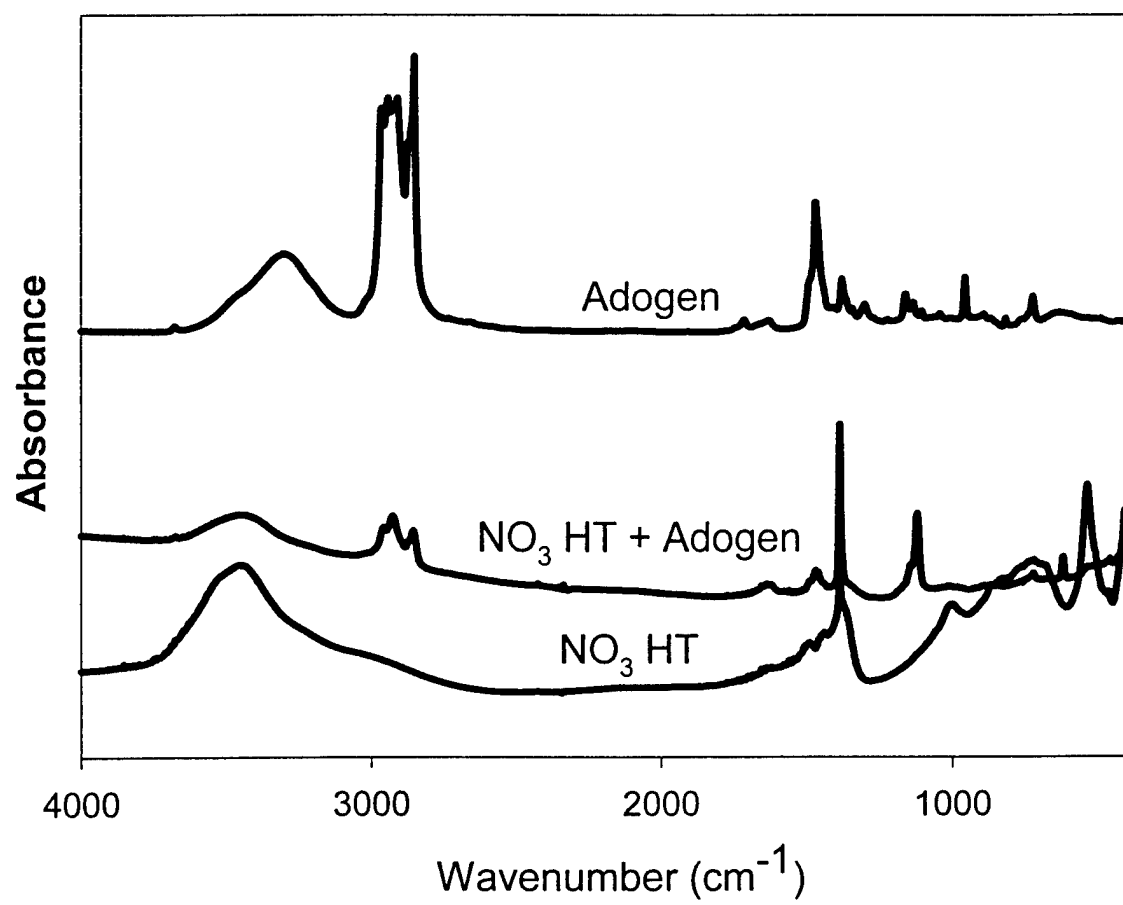
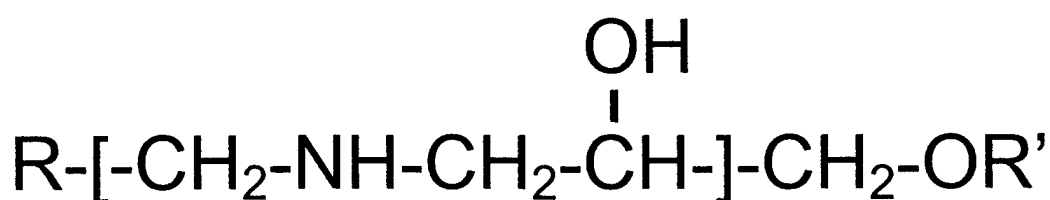
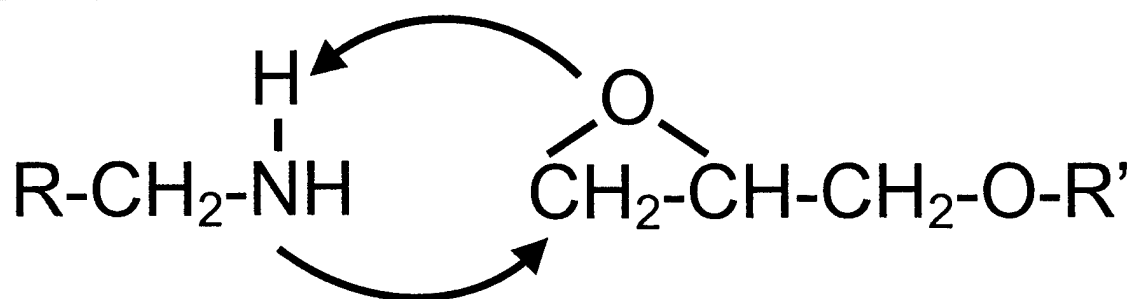


Figure 7

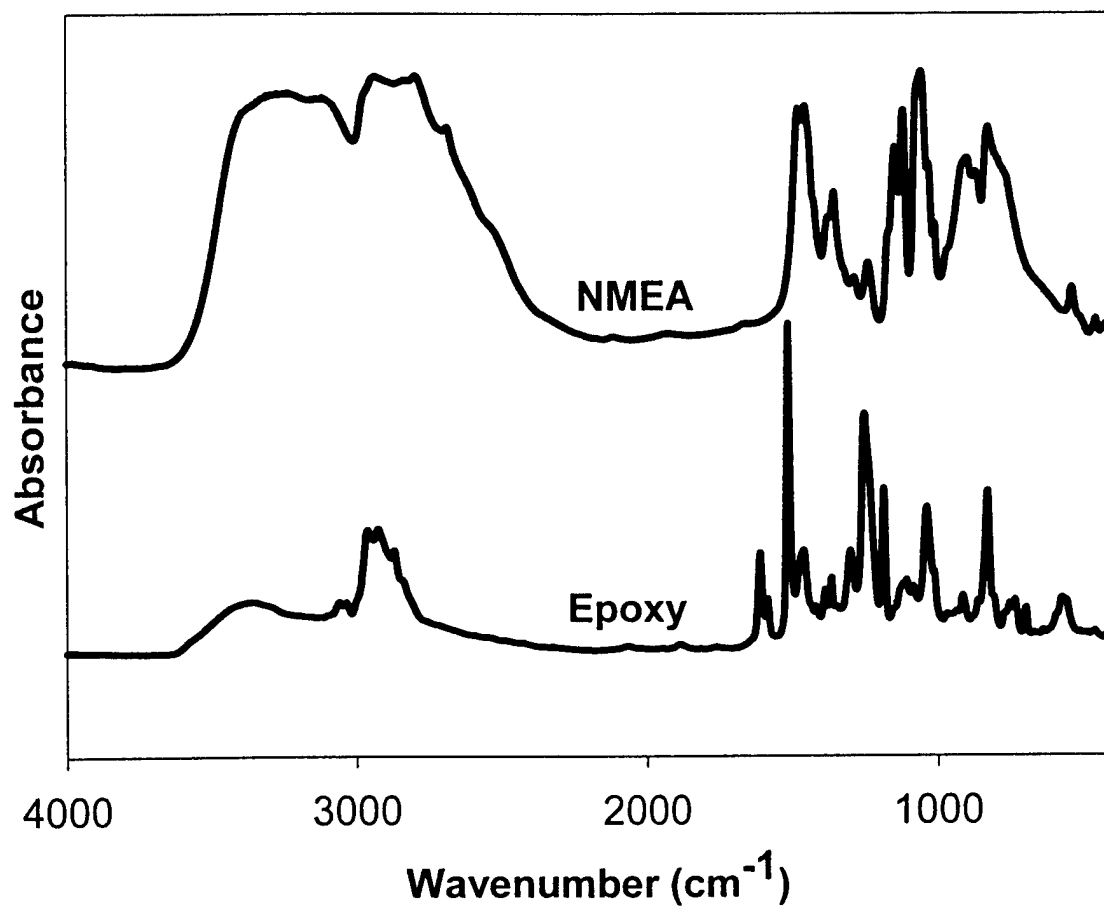
Amine Hardener + BPA based resin



N-methylethanolamine (NMEA)



Figure 8



Lithium-aluminum-carbonate-hydroxide hydrate coatings on aluminum alloys: Composition, structure, and processing bath chemistry

C. A. Drewien, M. O. Eatough, D. R. Tallant, C. R. Hills, and R. G. Buchheit

Materials and Process Sciences Center, Sandia National Laboratories, Albuquerque, New Mexico 87185

(Received 30 May 1995; accepted 18 January 1996)

A new corrosion resistant coating, being designed for possible replacement of chromate conversion coatings on aluminum alloys, was investigated for composition, structure, and solubility using a variety of techniques. The stoichiometry of the material, prepared by immersion of 1100 Al alloy into a lithium carbonate-lithium hydroxide solution, was approximately $\text{Li}_2\text{Al}_4\text{CO}_3(\text{OH})_{12} \cdot 3\text{H}_2\text{O}$. Processing time was shown to be dependent upon the bath pH, and consistent coating formation required supersaturation of the coating bath with aluminum. The exact crystal structure of this hydrotalcite material, hexagonal or monoclinic, was not determined. It was shown that both the bulk material and coatings with the same nominal composition and crystal structure could be formed by precipitation from an aluminum supersaturated solution of lithium carbonate.

I. INTRODUCTION

The aerospace and defense industries use aluminum alloys as the major component in a variety of parts, because aluminum alloys provide lightweight, easy fabrication, moderate strength and ductility, and nonrusting properties. In saline environments, pitting of aluminum and its alloys limits their usefulness. The application of a corrosion resistant chromate conversion coating, produced by immersing the cleaned metal into a solution containing sodium dichromate, increases the life of the metal on exposure to aggressive chloride environments. However, leaching of carcinogenic chromates into the environment during the lifetime of use of chromate-coated metals, worker exposure during processing, and coating bath chemicals disposal has led to the search for alternative coating systems to replace corrosion resistant chromate conversion coatings.

One possible replacement for chromate conversion coatings is based upon the novel use of lithium-aluminum-carbonate-hydroxide hydrate (hydrotalcite) as a corrosion resistant coating for aluminum alloys.¹ Hydrotalcite coatings impart corrosion resistance to the underlying aluminum substrate, and processing of the coatings, like chromate conversion coatings, is performed by simple immersion of the substrate into an aqueous solution.¹ These features make the lithium-aluminum-carbonate-hydroxide hydrate coating, hereafter referred to as a hydrotalcite coating, a very attractive candidate for replacement of chromate conversion coatings on aluminum alloys.

In order to recommend hydrotalcite coatings, the processing, composition, structure, and properties of the material must be understood. Recent literature²⁻⁵

addresses the structure and composition of hydrotalcites, because of the interest in utilizing hydrotalcites as catalysts, antacids, and absorbants. Hydrotalcite-manasseite is the generic mineral grouping for clays whose structural basis is positively charged brucite layers connected by hydrated anion layers. Naturally occurring rhombohedral hydrotalcite and hexagonal manasseite are rare, but many synthetic forms can be prepared by coprecipitation from alkaline solutions containing divalent and trivalent cations and anions such as sulfates, chlorides, carbonates, etc. The lithium-aluminum-anion-hydroxide version of hydrotalcite is a unique member of this group, because lithium is the only monovalent cation that is incorporated in hydrotalcites.

In this paper, processing of the lithium-aluminum-carbonate-hydroxide hydrate version of hydrotalcite and the composition and structure of this material as a coating and in bulk form are investigated using a variety of techniques.

II. PROCEDURE

Coating of many aluminum alloys with hydrotalcite is possible; in this study, only Al 1100, or commercially pure (~99%) aluminum, was used. The 1/4 in. thick sheet stock material was obtained in 4 × 5 in. sections. Samples were cleaned by abrading the surfaces in a solution of soap and water or by vapor degreasing with trichloroethane. An immersion in 65 °C sodium silicate-sodium carbonate solution removed organic and inorganic debris from the sample surfaces; the samples were rinsed and then de-oxidized in a room temperature nitric acid-1 M ammonium bifluoride bath. Samples were rinsed in de-ionized water and coated using a

15 min immersion in a room temperature bath of 0.1 M lithium carbonate solution whose pH was 11.15 or 12.05 \pm 0.5 (0.3 M lithium hydroxide addition).

Hydrotalcite powder was formed by precipitation from an aluminum saturated solution of 0.1 M lithium carbonate. Aluminum alloy panels were immersed into the room temperature solution; once hydrogen evolution ceased, new panels were introduced until a white precipitate was observed in the solution. The precipitate was filtered from solution, rinsed and filtered, and dried at room temperature. A Quanti-chrome Penta Pycnometer with helium gas was used to measure the density of the precipitated powder.

The Al and Li contents of the precipitate were analyzed by ICP-AES (inductively coupled plasma-atomic emission spectroscopy) using an ARL 3580. The coating composition was estimated from Secondary Ion Mass Spectrometer (SIMS) analysis obtained on a Cameca 4F. A primary beam voltage of 10 kV and a cesium source was used to sputter through the coating thickness at a rate of $2.25 \times 10^{-3} \mu\text{m/s}$. Negative ions were counted. Thermal gravimetric analysis followed by Fourier Transform Infrared Spectroscopy (TGA-FTIR) coupled with x-ray diffraction information was utilized to determine nominally the weight fractions of water and carbon dioxide in the precipitate. A PI Thermal Sciences Thermo-Gravimetric Analyzer coupled with a Biorad 40 Fourier Transform Infrared Spectrometer was used for this analysis. The heating rate was 15 $^{\circ}\text{C/min}$. The corresponding mass difference after water release at 177 and 275 $^{\circ}\text{C}$ and carbon dioxide release at 275, 532, and 632 $^{\circ}\text{C}$ allowed determination of water and carbon dioxide content of the precipitate through mass change.

For microstructural examination, samples were examined in a JEOL 6400 SEM operated at 15 kV. Transmission electron microscopy was performed on a JEOL 2000 FX operated at 200 kV. Cross-sectional

coating samples were prepared as described elsewhere.⁶ Selected area diffraction patterns (SADP) were obtained and indexed for phase identification.

Crystal structure and phase constitution of samples were investigated using a Siemens D500 powder diffractometer equipped with a receiving beam graphite crystal monochromator and a 2.2 kW long focused Cu x-ray tube. A step scan rate of 0.02° was employed.

Grazing incidence angle x-ray diffraction analysis proved to be a valuable method of obtaining information from the coating. A grazing angle of 0.2° provided a signal from about 1000 \AA into the sample. Appleman's refinement⁷ in the LSQ 90 software program of the Siemens Diffract 5000 system software was used to aid in crystal structure and lattice parameter determination.

Argon ion laser Raman spectroscopy was performed at an excitation wavelength of 514 nm using a triple spectrograph, a charge coupled detector, and a microscope attachment.

The solubility of the precipitate in hydrochloric acid solutions of pH = 1, 1.5, 2, and 4, and in sodium hydroxide solutions of pH = 10.79, 11.91, 12.68, and 13.31, were determined by introducing 1 g of precipitate to 100 mL of solution. The Al and Li content in solution after mixing was measured by ICP-AES and ICP-MS (mass spectroscopy) techniques.

III. RESULTS

A. Coating processing

The formation of hydrotalcite precipitate powder and coatings was performed by immersion of Al 1100 coupons into 0.1 M lithium carbonate coating bath, whereupon vigorous hydrogen evolution from the coupon surface was observed. Coatings of consistent thickness and appearance were obtained only after the coating bath was aged. To investigate the aging phenomenon, the aluminum concentration of the bath and the time until hydrogen evolution ceased was monitored for each subsequent sample. Starting with a solution of lithium carbonate, coupons of dimension 4×5 in. were immersed one at a time into the bath. When hydrogen evolution ceased, the sample was removed from the coating bath, and a 5 mL sample of the bath was obtained for bath analysis. Then another coupon was introduced to the bath, and the procedure was repeated.

The time until hydrogen evolution ceased is plotted per sample in Fig. 1, along with the aluminum concentration measured when the sample was removed from the bath. Time of hydrogen evolution per sample remained relatively constant after approximately seven samples, but the overall time involved to age the baths increased with increased solution pH. Aging of the bath was more rapid for a coating bath containing only lithium carbonate (pH = 11) as compared to a

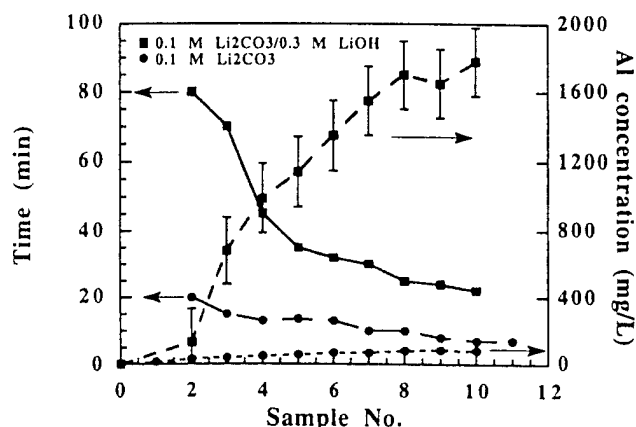


FIG. 1. Coating bath aluminum concentration and time until hydrogen evolution ceased per sample introduced to lithium carbonate baths of pH = 11.15 and 12.05.

bath whose pH was adjusted with lithium hydroxide to $\text{pH} \approx 12.6$. Figure 1 shows that the coating bath containing lithium hydroxide additions required more than three times longer or about 20 times the aluminum concentration to age than the lower pH bath.

The variation in appearance of the coatings with aging of the bath for both bath compositions can be seen by comparing the micrographs in Fig. 2. The platelet precipitates are seen immediately in the first coating from the lower pH bath [Fig. 2(a)] while no platelets are observed in the first coating from the higher pH bath [Fig. 2(d)]. Comparing Figs. 2(a)–2(c) with 2(d)–2(f), denser coatings developed faster in low pH solutions.

Aging of the bath did not entail a change in pH; pH values for the fresh bath and the aged bath differed by less than 0.03. Carbonate depletion by hydrotalcite formation was unmonitored; the solution was exposed to air and contained 0.1 M carbonate. Aging of the bath was necessary to raise the aluminum concentra-

tion of the bath to a value close to the solubility limit for $\text{Al}(\text{OH})_3$ (bayerite or gibbsite) in alkaline solutions (Fig. 3). Evidently, this assured the formation and growth of hydrotalcite by precipitation or nucleation and growth on the coupon surface. At $\text{pH} = 11$, the amount of dissolved aluminum ions in equilibrium with bayerite is 27 mg/L or $\log(\text{Al}^{3+}) = -3$. In contrast, the concentration measured when bath aging was complete was 80 mg/L [$\log(\text{Al}^{3+}) = -2.53$]. The logarithm of the concentration of aluminum dissolved in a basic solution of pH 12 is -1.8 , as shown in Fig. 3. The value obtained from the aged coating solution ($\text{pH} = 12.06$) was -1.2 . It is not clear whether bayerite formation precedes or supports the formation of hydrotalcite or if the kinetics and equilibria solely support formation of hydrotalcite over aluminum hydroxides. Continued use of the coating bath or allowing the bath to sit undisturbed led to precipitation of hydrotalcite. The concentration of aluminum left in solution after complete precipita-

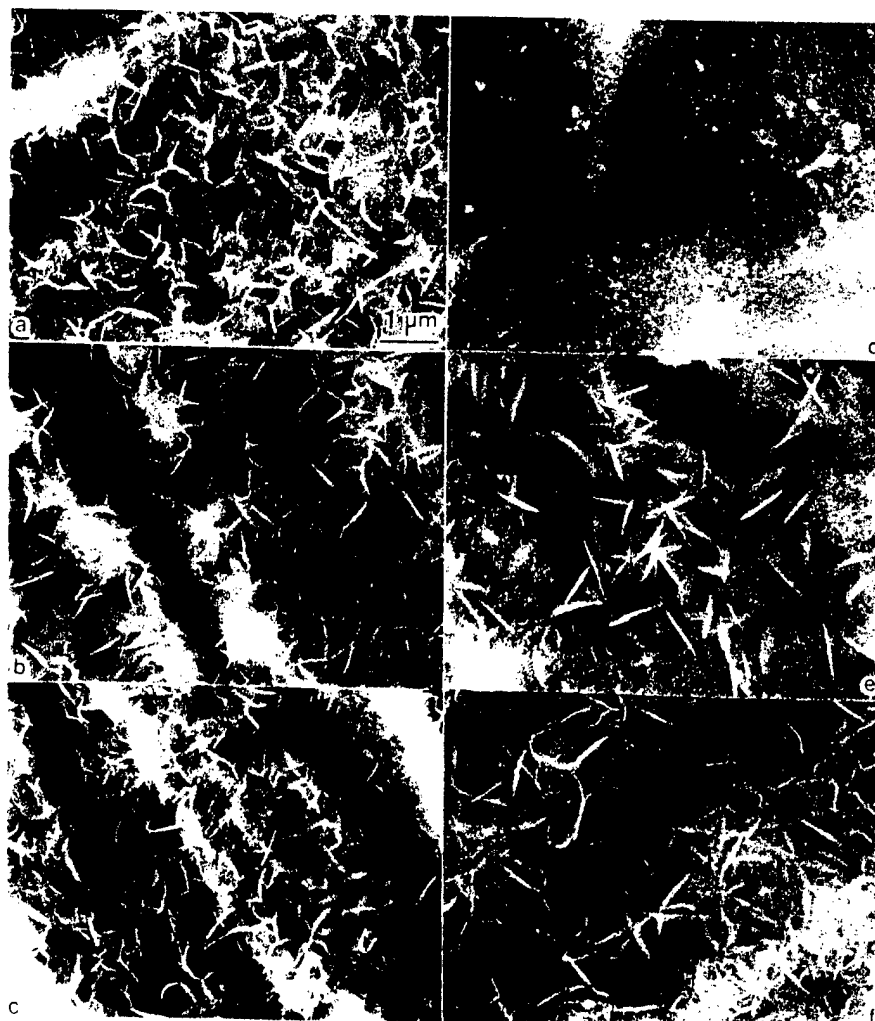


FIG. 1. SEM images showing coating coverage of aluminum surface for 1st, 2nd, and last samples introduced to coatings baths of pH 11.0 (a,b,c) and 12.05 (d,e,f).

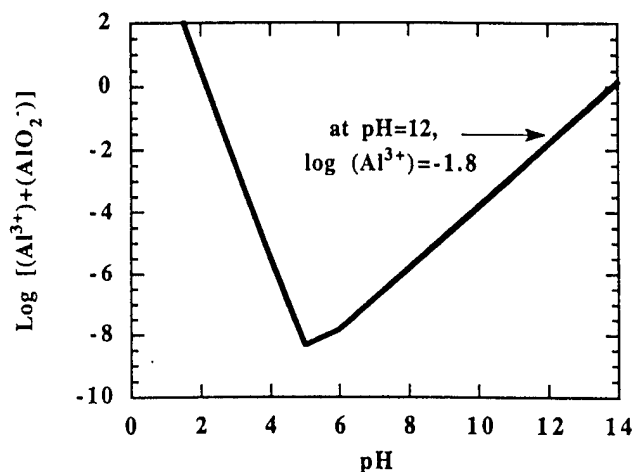


FIG. 3. Aluminum ion concentration in solution versus pH due to dissolution of bayerite.⁸

tion of hydrotalcite from an aged 0.1 M Li_2CO_3 bath was 8×10^{-6} M [$\log(\text{Al}^{3+}) = -5.09$], which is less than the value necessary to precipitate bayerite or gibbsite in alkaline solutions of pH = 11. Analysis of the precipitate yielded 100% hydrotalcite.

To confirm that precipitation of hydrotalcite from an aluminum supersaturated solution of lithium carbonate occurred, 100 ppm sodium aluminate was added to the bath of pH near 11. Precipitation of hydrotalcite occurred. Aging of the bath by additions of sodium aluminate can be easily performed to establish reproducible coating solutions and to reduce time involved in preparing the bath.

B. Composition

The hydrotalcite precipitate, formed in a room temperature aged solution of 0.1 M lithium carbonate, was filtered, rinsed, and dried into powder form. Wet chemistry analysis revealed that the aluminum to lithium molar ratio was 1.8 ± 0.12 , which is similar to that of the hydrotalcite compound $\text{Li}_2\text{Al}_4\text{CO}_3(\text{OH})_{12} \cdot 3\text{H}_2\text{O}$. The carbonate content and water content of the powder were determined from TGA-FTIR analysis; three molecules of interlayer water and about one molecule of carbon dioxide exist in the structure. The hydroxide content was not established.

Coating compositions could not be accurately determined; however, dynamic scanning ion microscopy was used to monitor the composition profile through the coating. The composition profile, shown in Fig. 4, reveals nearly constant levels of aluminum, lithium, hydrogen, carbon, and oxygen through the major part of the coating. Closer inspection of the interface region showed that a carbon-poor region existed (not shown here).

Since the composition of the coating was not precisely determined from the SIMS data (sensitivity factors

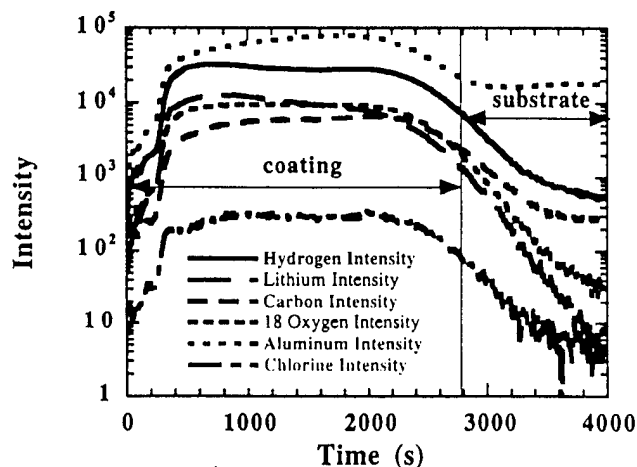


FIG. 4. SIMS profile for hydrotalcite coating on Al 1100 substrate.

for elements in the hydrotalcite matrix are unknown), Raman spectroscopy was used to show that bonding was similar in the coating and the hydrotalcite precipitate powder. Argon ion laser Raman spectra, obtained from the precipitate powder and on the coated sheet metal, are shown in Fig. 5. The coatings have a Raman spectra similar to the spectra obtained from the powder. The bands for carbonate appear at 1060 cm^{-1} , and absorption bands for both stretching and deformation vibrations of aluminum oxide are present in the $600\text{--}900 \text{ cm}^{-1}$ region. Similar results for the chloride version of this material, contaminated with trace amounts of carbonate, were reported by Dutta and Puri.⁹ The coatings also gave rise to a strong band at 517 cm^{-1} , which is believed to correspond to nanocrystalline silicon on the aluminum surface. Silicon is a trace constituent in 1100 Al alloys, and the cleaning solution contains a silicate. Note that this band is not present in the spectra from hydrotalcite powder.

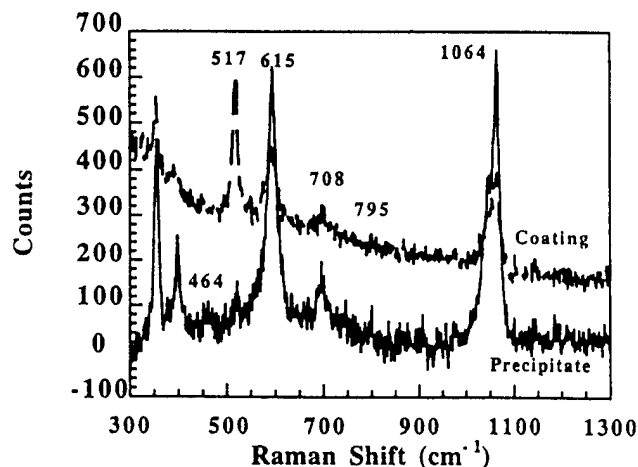


FIG. 5. Raman spectra from hydrotalcite precipitate and coating.

TABLE I. Solubility of hydrotalcite in room temperature hydrochloric acid and sodium hydroxide solutions.

pH	Al (mg/L)	% Al dissolved	Li (mg/L)	% Li dissolved
1.00	1276 \pm 9%	50	237 \pm 10%	100
1.51	<10	n/d	132	25
2.02	<10	n/d	76	5
3.98	<10	n/d	16	0.5
10.79	2 \pm 10%	0.1	3	9
11.91	22 \pm 10%	1	3	9
12.68	77 \pm 10%	3	5	16.5
13.31	220 \pm 10%	9	12	37

C. Solubility

The amount of hydrotalcite powder dissolved in 100 mL of hydrochloric acid or sodium hydroxide of various pH values is reported in Table I. The average value of three measurements is given with the range reported as error. The concentration has been converted to percentage of species dissolved into solution; it is apparent that lithium preferentially dissolves from the material. The useful pH ranges for hydrotalcite in hydrochloric acid solutions are at pH values greater than 3 and less than 11.

D. Crystal structure

X-ray diffraction analysis indicated that the precipitate powder and the coatings on the sheet metal contained hydrotalcite, whose lattice parameters were similar to those for the lithium-aluminum-carbonate-hydroxide hydrate version of hydrotalcite. The x-ray diffraction profile from the precipitated hydrotalcite is shown in Fig. 6. The interplanar spacings obtained from the precipitate and from grazing incidence angle x-ray diffraction analysis of the coated metal sheet are listed in Table II, along with observed intensities from the hydrotalcite powder and

lattice parameters obtained in this investigation and from reports in the literature. The peaks of the x-ray pattern may be indexed for both hexagonal and monoclinic structures; the lattice parameters and Miller indices for the observed interplanar spacings are shown in Table II for both crystal structures.

X-ray diffraction analysis using a slow scan step did not show conclusively whether the structure was hexagonal or monoclinic. Both crystal structures can be indexed with equal accuracy; no absence or presence of peaks specific to only one of the crystal structures was observed. A slight distortion of a hexagonal crystal could place it into the monoclinic class. Therefore, lattice parameters for both crystal systems are reported in Table II. The agreement with values reported by other investigators is best for the hexagonal system.

The measured density of the hydrotalcite powder was 2.05 ± 0.07 g/cm³, which is within the range of the value reported by Devyatkina *et al.*,³ who reported 2.03 ± 0.07 g/cm³ for a lithium-aluminum-carbonate-hydroxide hydrate containing 0.9 moles of CO₂. Using the experimentally determined density and lattice parameters, the unit cell would contain about 1.5 or 2 molecules of Li₂Al₄CO₃(OH)₁₂ · 3H₂O for a hexagonal and monoclinic structure, respectively.

E. Microstructure

A comparison of the microstructure of the hydrotalcite powder and the coated 1100 Al substrate can be made from the SEM images shown in Figs. 7(a) and 7(b). On the coating surface, crystals with an average size of 2–3 μ m are observed. The TEM image in Fig. 8(a) shows crystals with the same dimensions terminating at the coating/substrate surface. Below this layer is a narrow region of finely or poorly crystalline material. The selected area diffraction patterns for the two layers of the coating are shown in Figs. 8(b) and 8(c). Qualitative energy dispersive spectroscopy showed the inner region to be carbon-poor by comparison to the outer region of the two-layered coating. This suggests that the inner layer may be an aluminum or lithium-aluminum

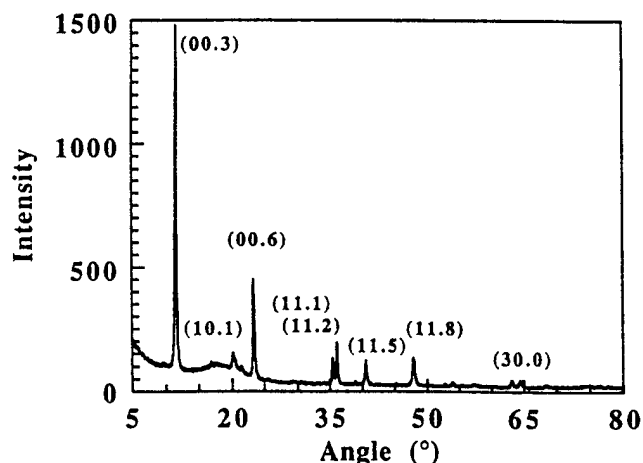


FIG. 6. X-ray diffraction profile of lithium-aluminum-carbonate-hydroxide hydrate.

TABLE II. Interplanar spacings, peak intensities, Miller indices, and lattice parameters for hydrotalcite.

<i>d</i> -spacing (Å) from precipitate	<i>d</i> -spacing (Å) from coating	Relative intensity from precipitate	Hexagonal unit cell Miller indices	Monoclinic unit cell Miller indices
7.622	7.595	100	003	002
3.806	3.792	24	006	004
2.530		10	111	-214
2.489	2.476	14	112	310
2.231	2.248	5	113	-123
2.222	2.222	7	115	304
2.210	2.213	3	200	123
2.025	2.023	2	10(10)	402
1.902		11	118	-321
1.471	1.457	3	300	330
Lattice parameters (this study)			$a = 5.099 \pm 0.001 \text{ Å}$ $c = 22.85 \pm 0.01 \text{ Å}$	$a = 8.520 \pm 0.002 \text{ Å}$ $b = 5.163 \pm 0.01 \text{ Å}$ $c = 15.24 \pm 0.08 \text{ Å}$ $\beta = 92.76^\circ \pm 0.6$
Lattice parameters (the literature)			$a = 5.095 \text{ Å}$ $c = 22.793 \text{ Å}^3$ $a = 5.32 \text{ Å}$ $c = 15.24 \text{ Å}^2$	$a = 8.68 \text{ Å}$ $b = 5.07 \text{ Å}$ $c = 15.12 \text{ Å}$ $\beta = 92.56^\circ$

oxide/hydroxide phase. This observation could indicate that formation of bayerite (or some lithium-aluminum hydroxide) precedes the formation of hydrotalcite.



FIG. 7. Comparison of the microstructure of the (a) hydrotalcite powder and (b) the coated 1100 Al substrate.

IV. DISCUSSION

The supersaturation by aluminum of an alkaline solution of lithium carbonate leads to precipitation of lithium-aluminum-carbonate-hydroxide hydrate, in a bulk form or as a coating on aluminum or its alloys. The material formed contained a ratio of Al/Li of 1.8, three molecules of water of hydration, and approximately one molecule of carbon dioxide. The approximate chemical composition of the material could be $\text{Li}_2\text{Al}_4\text{CO}_3(\text{OH})_{12} \cdot 3\text{H}_2\text{O}$. The excess lithium may be due to lithium carbonate, but its presence was not detected using XRD. Hydrotalcite with varied concentrations of carbonate can be synthesized³;



FIG. 8. (a) TEM image showing crystals with the same dimensions terminating at the coating/substrate surface. (b, c) Selected area diffraction patterns for the two layers of the coating.

however, the high concentration of carbonate in solution appeared to favor the formation of hydrotalcite with a carbonate stoichiometry very near 1. The solution analysis also suggested that the chemical equilibria favored hydrotalcite precipitation over bayerite or gibbsite (or aluminum hydroxides), because the aluminum concentration remaining in solution after precipitation of hydrotalcite was less than the equilibrium amount to precipitate bayerite or gibbsite. Neither bayerite nor gibbsite were detected in the x-ray diffraction pattern of the hydrotalcite precipitate. However, as determined using cross-sectional analytical techniques, a carbon-poor inner layer exists in the coatings. Lithium-aluminum-hydroxide hydrate has an x-ray diffraction profile very similar to that of hydrotalcite; its presence in either the coating or the powder may not be easily detected, particularly if the grain size is very small, as indicated by electron diffraction.

V. CONCLUSIONS

The structure and composition of lithium-aluminum-carbonate-hydroxide hydrate, formed as a bulk material or as a coating on aluminum alloys through precipitation from an alkaline solution of lithium carbonate, were analyzed, and an understanding of the bath chemistry to allow coating formation on aluminum alloys has been presented. The bulk material closely approximated the known compound, $\text{Li}_2\text{Al}_4\text{CO}_3(\text{OH})_{12} \cdot 3\text{H}_2\text{O}$. X-ray diffraction and density data indicated that 1.5 or 2 molecules of the compound existed within the hexagonal or monoclinic unit cell, respectively; however, the exact symmetry of the crystal has not been resolved. The experimentally determined lattice parameter values were in excellent agreement with reported values in the literature

for a hexagonal structure. From the x-ray diffraction patterns, Raman spectroscopy, morphology, and compositional analysis, the coating formed on Al 1100 appears to be consistent with a hydrotalcite structure.

ACKNOWLEDGMENTS

The authors appreciate the help of and would like to thank M. Bode, J. Finch, T. Neil, G. Nelson, M. Gonzales, J. Bullen, J. Michael, K. Alam, P. Puissant, B. Chambers, G. Zender, J. Schoeder, J. Bando, J. Barrera, D. Strall, T. Crenshaw, J. Reich, and R. Simpson for their technical support as concerns this work. This work was performed at Sandia National Laboratories, which is operated for the U.S. Department of Energy under Contract No. DE-AC04-94AL85000.

REFERENCES

1. R. G. Buchheit, M. Bode, and G. E. Stoner, *Corrosion* **50** (3), 205 (1994).
2. C. J. Serna, J. L. Rendon, and J. E. Iglesias, *Clay and Clay Minerals* **30** (3), 180–184 (1982).
3. E. T. Devyatkina, N. P. Kotsupalo, N. P. Tomilov, and A. S. Berger, *Russ. J. of Inorg. Chem.* **28** (6), 801 (1983).
4. I. Sissoko, E. T. Iyagba, R. Sahai, and P. Biloen, *J. Solid State Chem.* **60**, 283–288 (1985).
5. A. R. Poeppelmeier and S.-J. Hwu, *Inorg. Chem.* **20** (20), 3297–3302 (1987).
6. C. A. Drewien, C. R. Hills, and R. G. Buchheit, in *Proc. 51st Annual Meeting of the Microscopy Society of America* (Microscopy Society of America, San Francisco, CA, 1993), pp. 850–851.
7. D. Appleman, N.T.I.S. Doc. No. PB-216188 (1973).
8. M. Pourbaix, *Atlas of Electrochemical Equilibria in Aqueous Solutions*, 2nd ed. (National Association of Corrosion Engineers, Houston, TX, 1974), p. 174.
9. P. K. Dutta and M. Puri, *J. Phys. Chem.* **93**, 376–381 (1989).

Paper No.
740

CORROSION 98

RAPID ELECTROCHEMICAL CORROSION TESTING OF CHEMICALLY PASSIVATED ALUMINUM ALLOYS

R. G. Buchheit
The Ohio State University
Department of Materials Science and Engineering
Columbus, OH 43210

M. Cunningham, H. Jensen, M. W. Kendig
Rockwell Science Center
1049 Camino dos Rios
Thousand Oaks, CA 91360

M. A. Martinez
Sandia National Laboratories
P. O. Box 5800
Albuquerque, NM 87185

ABSTRACT

The corrosion resistance of 33 different conversion coatings applied to five different aluminum alloys was tested by salt spray exposure and electrochemical impedance spectroscopy (EIS). Results derived from the two tests were evaluated to determine if a relationship existed. Individual salt spray test panels, with an area of 30 in.², were visually inspected at regular intervals up to 168 hours of exposure. At each inspection interval, panels were assigned a pass rank if less than 5 pits were observed, or fail rank if more than 5 pits were observed. EIS data were analyzed using a simple equivalent circuit which yielded a "coating resistance", R_c , which was used as a figure of merit to assess coating performance. Examination of the data showed that both tests could be sensitive discriminators of corrosion protection, but that EIS was more discriminating in the extremes of coating performance. Analysis showed that the probability of achieving a passing salt spray result increased as R_c increased. In the regimes where both tests were sensitive, regression analysis showed that linear relationships could be constructed between the log of R_c and the probability of a coating meeting the pass/fail criterion in salt spray. Based on these relationships, threshold R_c values have been proposed to define the minimum value for which a given coating can be expected to attain a passing result in a 168 hour salt spray test. These values ranged from 2 to 5 x 10⁶ ohm•cm² for 356, 2024-T3 and 7075-T6, 1.5 x 10⁷ ohm•cm² for 7075-T6, and 2.3 x 10⁷ ohm•cm² for 3003.

Keywords: Salt spray testing, electrochemical impedance spectroscopy, corrosion test methods, conversion coatings, aluminum alloys, accelerated testing.

Copyright

©1998 by NACE International. Requests for permission to publish this manuscript in any form, in part or in whole must be made in writing to NACE International, Conferences Division, P.O. Box 218340, Houston, Texas 77218-8340. The material presented and the views expressed in this paper are solely those of the author(s) and are not necessarily endorsed by the Association. Printed in the U.S.A.

INTRODUCTION

The salt spray test, such as that defined by ASTM B117, is one of the most widely used proof tests for evaluating corrosion protection provided by organic and inorganic coatings on metals. The test offers many advantages including standardized protocols for conducting the exposure and evaluating the results, procedural simplicity, and the ability to discriminate. However, the test has been criticized for its lack of reproducibility from one test chamber to another, failure to predict service performance, and its inability to provide a quantitative measure of corrosion damage easily^{1,2}.

In recent years, impedance methods have been developed for measuring corrosion kinetics and studying corrosion mechanisms. Electrochemical impedance spectroscopy (EIS) has been used to evaluate the corrosion protection offered by organic^{3,4,5} and inorganic^{6,7} coatings. Corrosion testing using EIS provides a quantitative measure of corrosion protection in a way that salt spray testing cannot. But, EIS for testing corrosion resistant coatings has been criticized because it relies on expensive, sophisticated electronic equipment and generates results that require a significant amount of training to properly interpret.

Currently, both types of tests are used to evaluate corrosion resistant coatings. The corrosion resistance of conversion-type protective coatings is usually discussed in terms of results from one type of test or the other. Because of the disparate nature of the data generated, one obvious issue is whether a relationship exists between the results of salt spray exposure and EIS. The second issue is whether an EIS method can evaluate performance in a shorter amount of time and with greater sensitivity than salt spray testing. These issues have not been fully addressed by previous studies.

A recently completed study⁸ evaluating the performance of a variety of inorganic conversion-type coatings provided an opportunity to explore the relative merits of these two types of tests and to determine if the results might be related in some way. The study was aimed at evaluating progress towards developing a replacement for chromate conversion coatings for aluminum alloys. In this study, 33 different conversion coatings were applied to 5 different aluminum alloy substrates. Salt spray exposure testing was one of the performance evaluations conducted. Untested samples of each coating on each alloy type were subsequently made available for testing by EIS for the purpose of making a comparison to salt spray test results. EIS evaluations were typically performed in duplicate. Using this large sample population, the results of the two test procedures were compared, and a relationship was developed.

EXPERIMENTAL PROCEDURES

Materials. The aluminum alloy substrates used and their nominal chemical compositions are listed in Table 1. Test panels were obtained from commercial corrosion test sample suppliers. The 2024-T3, 6061-T6, and 7075-T6 panels were 3" x 10" x 0.025" (76 mm x 250 mm x 6.5 mm) thick. The 3003 panels measured 3" x 9" x 0.025" (76 mm x 230 mm x 6.5 mm) thick. All of these panels were prepared from single lots of commercial sheet stock. Alloy 356 is a casting alloy and cast panels measuring 4" x 6" x 0.125" (100 mm x 15 mm x 3.2 mm) thick were obtained. All test panels were supplied for conversion coating with a standard mill finish surface.

Thirty-three different chromate conversion and non-chromate conversion coatings were applied to the test panels of the alloy types listed above. The coatings were applied by the process vendors in the case of commercial products, or by the coating developers in the case of pre-commercial processes. Coatings were applied to all samples in the same process lots. The coatings and suppliers have been given

elsewhere⁸. Samples with obvious mechanical surface damage like scratches or scuffs were not included in either salt spray or electrochemical impedance testing.

Test methods. Salt spray testing was conducted as part of the prior study⁸, and results were made available for comparison to the EIS results generated in this work. Salt spray exposure was conducted according to ASTM B117, which specifies exposure in an enclosed chamber at 95° F (35° C) to a fog generated from a 5% NaCl solution. A total of five panels for each coating on each alloy were tested. The panels were inspected at periodic intervals and assigned a ranking based on visual appearance. The condition of the panels was compared against the MIL-C-5541E performance criterion which states that a single panel can have "no more than 5 isolated spots or pits, none larger than 0.031 in. (0.8 mm) in diameter"⁹. It is not always practical to measure pits during visual inspection. However it is accepted that a pit is counted only after it has produced a visible corrosion product stain or tail. This convention was used in the study reported in reference 8. Normally this criterion is applied after 168 hours of testing, but in this study it was applied after 24, 48, 96, and 168 hours of exposure. Based on this criterion, panels were assigned either a pass or fail rank at each inspection interval. This inspection method was used in an attempt to quantify corrosion damage by pitting that occurred during exposure.

MIL-C-5541E also specifies another failure condition, which is that "no more than 15 isolated spots or pits, none larger than 0.031 in. (0.8 mm) in diameter (can be present) on the combined surface area of all five specimen panels"⁹. This failure criterion was not applied to the treatment of the salt spray data in this study.

For EIS testing, coated panels were mounted in gasketed Plexiglas tubes exposing well-calibrated surface areas of either 20 or 24 cm². The cell comprised of the tube and the exposed panel contained 0.5 M NaCl. This cell also contained either Pt or Ni counter electrode and a saturated calomel reference electrode (SCE) in a Luggin tube. After 24±1 h exposure of the panel in this apparatus, the electrochemical impedance across the surface of the panel was measured at the open circuit potential. The impedance measurement was made as a function of frequency between 10 kHz and 10 mHz using a sinusoidal voltage modulation not in excess of 10 mV. At least seven points per decade frequency were collected. All measurements were made under ambient laboratory conditions (23±3°C). The experiments were conducted using a PAR 273 potentiostat with a Solartron 1255 frequency response analyzer. Two impedance spectra were collected from separate locations on each panel.

RESULTS AND DISCUSSION

Salt spray test results. Several attributes of the salt spray testing made the results especially suitable for a correlation study. First, panels always failed by pitting. Second, for each of the five alloys studied, a large sample population was available due to the number of coatings fielded. Five replicate panels were tested for each alloy-coating combination. Third, panels were evaluated at frequent intervals. Inspections were made periodically up to 1008 hours of exposure although only the data for 24, 48, 96, and 168 hours were used here. Thus, changes in pitting damage versus time could be evaluated. Finally, a wide range of coating performance was exhibited among the sample populations for each alloy. The broad range of performance was important for a statistically based development of the dependent variable used to describe the salt spray performance. The salt spray test results have been presented elsewhere¹⁰.

EIS results and data analysis. The circuit model shown in Figure 1 has been proposed by Mansfeld and coworkers^{6,7} to describe the electrochemical impedance for conversion coated (or chemically

passivated) aluminum. The model assumes an intact oxide film or coating having a specific resistance and capacitance, R_p and C_p respectively. As the coating degrades with exposure to the environment, a fraction, F , of the sample area is covered by pits. This results in a parallel conduction path capable of short circuiting the coating impedance represented by R_p and C_p . For most cases, the model in Figure 1 may be approximated by the model shown in Figure 2 at low or intermediate frequencies where:

$$C = C_p(1-F) + C_{pit}(F) \quad (\text{eq. 1})$$

and

$$1/R_c = (1-F)/R_p + F/R_{pit} \quad (\text{eq. 2}).$$

Since R_p is extremely high, on the order of 100 to 1000 $M\Omega\text{cm}^2$, and R_{pit} is on the order of 100 to 1000 Ωcm^2 , the following approximation can be made:

$$1/R_c \sim F/R_{pit} \quad (\text{eq. 3}).$$

The quantity R_c may be considered to be an apparent integrated pitting resistance. The use of the term " R_c " is intended to indicate that it is a composite quantity representative of the coating performance, and to distinguish it from R_p and R_{pit} which have formal definitions in equivalent circuit analysis of EIS data. With these approximations, the impedance can be approximated by the model of Figure 2. The overall expression for the complex impedance becomes:

$$Z(\omega) = R_s + R_c/(1+(j\omega\tau)) \quad (\text{eq. 4})$$

where R_s is the solution resistance, $\tau = R_c C$ (a time constant), ω is the angular frequency in rad/s, and $j^2 = -1$. Since the pitting process tends to be very heterogeneous, a distribution of time constants for this simple model must be invoked. This requires a non-unity exponential, n ($0 < n < 1$), in the term $(j\omega\tau)$. Hence equation 4 becomes:

$$Z(\omega) = R_s + R_c/(1+(j\omega\tau)^n) \quad (\text{eq. 5}).$$

Strictly speaking, the capacitance in Figure 2 is not a true capacitance giving a $1/\omega$ frequency response for its impedance, but rather it is an element whose admittance equals $Y(j\omega)^n$ where Y is the magnitude of the reactance, and n is a constant between 0 and 1. The apparent capacitance, C may be calculated according to the equation:

$$C = Y^{1/n} R_c^{(1-n)/n} \quad (\text{eq. 6}).$$

While the above interpretation of n may be debated, the data for the observed samples between 1 Hz and 1 kHz fit the above equation. In many cases, data from a broader range of frequencies also fit eq. 6. However, two situations were encountered that complicated fitting. The first case occurred where thick "paint-like" coatings were applied. In this case, R_s equaled the sum of the coating resistance and the ohmic resistance of the solution giving rise to an additional time constant at higher frequencies. The second case occurred in samples where the pitting rate was so high that the impedance of the element W (the Warburg impedance) of the Mansfeld model became significant with respect to R_c . These problematic cases were rare and usually occurred with one or two coatings per alloy substrate type.

It is maintained that the simplest model is the best when evaluating impedance spectra. Furthermore, a simple approach is essential if many spectra are to be analyzed with a minimum of effort. It is not clear that much more is learned by a more detailed analysis particularly in light of sample to sample variations. Hence, a modification to the model shown in Figure 2 has to fit all the data collected, recognizing that in some cases parts of the spectra have been ignored.

The results from complex nonlinear least squares (CNLS) fitting of the impedance data to eq. 5, and determination of apparent capacitance using eq. 6 have been presented elsewhere¹⁰.

A relationship between EIS and salt spray test results. Attempts were made to relate the various parameters derived from CNLS fitting of EIS data to the occurrence of a passing salt spray result or to the probability of achieving a passing result. Parameters examined included the coating resistance, R_c , the apparent capacitance, C , which exhibits characteristic changes as pitting damage increases¹¹, the time constant, τ ($\tau = R_c * C$), and $R_c * \tau$. The only sensible relationship obtained was between R_c and the probability of passing the salt spray test. This relationship was developed using the Mean Rank Method¹². This is one of several similar graphical analysis methods developed to analyze accelerated life test data. Examples showing use of these methods to treat data from localized corrosion phenomena have been given by Shibata¹³ and Williams¹⁴ who correlated the probability of pitting of stainless steels in potentiostatic and potentiodynamic polarization testing to various factors including alloy composition and surface roughness.

In the present analysis, probabilistic relationships between EIS and salt spray results were developed separately for each alloy. The R_c value from EIS was treated as the random variable, and the frequency with which coated panels met the MIL-C-5541E pass criterion was used to develop a relative dependent variable. As a guide, the results from the exercises used to develop the dependent variable are presented in Table 3 using a portion of the data set for coatings applied to 2024-T3.

To begin, a passing frequency (PF) was assigned to a given coating with a given R_c . The PF was the number of panels in a group of five replicates that achieved a passing rank per the MIL-C-5541E criterion. Next, (R_c , PF) pairs were arranged by increasing R_c as shown in the first and second columns of Table 2. The running sum of the PF was then computed. This quantity was termed the cumulative passing frequency (CPF) and is shown in the third column of Table 2. The values of the passing frequency were then ranked with the first occurrence of passing assigned a value of "1". Each increment in the CPF earned an increment in rank. In this analysis, a mean rank representing the relative dependent variable (CPF) is paired with the random variable, R_c . The mean rank is simply:

$$m = \frac{\sum \text{ranks}}{\text{observed frequency}} = \frac{\text{rank}_{\max} - \text{rank}_{\min}}{2} \quad (\text{eq. 7}).$$

Mean ranks associated with R_c values are shown in the fifth column of Table 2. The probability of observing a passing salt spray result is then given by¹²:

$$P = \frac{m}{n + 1} \quad (\text{eq. 8})$$

where n is the total sample size (total CPF for the sample population in this case). The probabilities are shown in columns 6 and 7 and are the relative dependent parameters that describe salt spray performance of the conversion coatings. These data were used to construct plots of passing probability versus R_c for individual alloy substrates as shown in Figures 3 through 7. In these plots the ordinate label "cumulative passing frequency" is used to denote that the dependent variable is a relative parameter calculated based on

the cumulation of data from the entire set. Four data sets are shown in each plot; one for each inspection interval. The CPF is the probability of finding a panel with 5 or less pits.

These plots graphically illustrate the relationship between the 24 hour EIS results and salt spray results for specific inspection intervals. Both tests discriminate corrosion performance for certain portions of each coating population suggesting that a correlation of results is possible in this range. However, among the poorer coating performances, EIS is more sensitive than salt spray. For each alloy, except 6061-T6, a significant number of the least corrosion resistant coatings exhibit a 0% CPF, indicating that all such panels failed the salt spray test within 24 h. In some cases, like 2024-T3 and 7075-T6, these data are distributed along the R_c axis indicating that there is a variation in corrosion resistance detectable by EIS. This shows that for coatings with low corrosion resistances, EIS can provide a more sensitive measure of corrosion resistance than salt spray testing.

In an analogous way, EIS is more discriminating than salt spray for highly corrosion resistant coatings. The sensitivity limit for R_c is determined by the minimum current resolution of the potentiostat used for EIS testing. The equipment and procedures used in this study enabled discriminating measurements of coatings with impedances of 1 to 5×10^8 to $\text{ohm}\cdot\text{cm}^2$. In salt spray testing, after the exposure is completed, it is not possible to discriminate the performance among panels that did not fail. One solution is to expose panels until all are failed; however, this can be time-consuming. For example, the salt spray test described in reference 8 was run for 1008 hours (41 days), and some of the coatings did not fail even after this length of time.

The issue of sensitivity between these two types of corrosion tests is potentially significant for coating process development. Salt spray testing may indicate the benefit of a process change that induces a large improvement in corrosion resistance of a single coating, or reveal gross differences in the corrosion resistance of different coatings. But it may not be capable of resolving smaller, but important differences in corrosion resistance. An example of this situation is found in the data for 2024-T3 in Figure 4 where EIS test results show a wide range of corrosion resistance in coatings with R_c values from 10^4 to 5×10^5 $\text{ohm}\cdot\text{cm}^2$. The equivalent salt spray results show equal levels of corrosion resistance among these coatings.

Regression analysis shows that a linear relationship exists between CPF and $\log R_c$ when portions of the data sets where the salt spray test is not sufficiently sensitive are neglected (e.g. when failure occurs in less than 24 hours, or when no corrosion is observed within 168 hours). It is possible to perform regression analysis in a way that includes these extreme portions of the $\log R_c$ -CPF data sets, but this was not done for two reasons. First, in the extremes of the data sets, the CPF is either 0% or very nearly 100%. Therefore above or below certain $\log R_c$ values, the expected CPF can be determined by simple inspection. Second, an accurate fit of the entire data set should yield a nearly identical functional dependence of CPF on $\log R_c$ in the region where the present analysis was conducted.

Table 3 summarizes regression models developed for each alloy, the data range for which the analysis was conducted, the correlation coefficients and the coefficient of determination. The coefficient of determination is simply the square of the correlation coefficient. Both are presented here since the correlation coefficient is a measure of the linear association between CPF and $\log R_c$, while the coefficient of determination indicates that fraction of the variability in CPR data is explained by a linear relationship to $\log R_c$ ¹⁵.

The adequacy of the regression models was further assessed by examining the CPF residuals. Normal probability plots of CPF residuals were constructed. For each alloy the residuals fell approximately along a straight line with correlation coefficients ranging from 0.94 for 2024-T3 CPF data to 0.99 for 3003 CPF data. This result confirms that there are no serious inadequacies in the regression models.

It is interesting to note that the slope parameter for the 2024-T3 CPF regression model is more than twice that of any other alloys tested. It is generally accepted that 2024-T3 is a very corrosion prone alloy that is difficult to conversion coat successfully¹⁶. The form of the CPR-log R_c relationship is more nearly that of a "threshold" than for any other alloy. Conversion coatings fail by pitting that is almost always initiated at second phase particles in the alloy substrate. The fact that the transition in behavior occurs so sharply is consistent with the notion that passivation of a single specific site largely determines success or failure for a conversion coating on 2024-T3. Inspection of Figure 4 suggests that this threshold in conversion coating protection occurs at an R_c value of 1 - 2 M Ω -cm² as determined by the EIS test methods used in this study.

The results of the regression analysis allow estimation of a threshold R_c value from EIS above which a given coating can be expected to generate a passing 168 hour salt spray result according to the 5 pit per panel MIL-C-5541E criterion. A passing probability greater than 80% applied to a set of 5 panels indicates that on average more than 4 of the 5 panels would be expected to meet the 5 pit per panel criterion. Given the methodology used to calculate CPF values, if more than 4 of 5 panels meet the criterion, then all 5 are likely to meet it. Even though this rationalization is somewhat arbitrary, it is proposed that the R_c value corresponding to an 80% CPF (R_{80}) defines the minimum value for which a passing salt spray result should be regularly expected. Table 4 summarizes the R_{80} values computed using the regression parameters in Table 3. The table shows R_{80} values determined from the regression parameters and the points where the 80% CPF threshold intercepts a 95% prediction interval. This interval defines where 95% of any future CPF data will fall for a given value of R_c , assuming that future CPF data will be normally distributed about a mean determined by the current results. The 95% prediction intervals for the cumulative passing frequency, CPF_{0.95}, were computed according to the following expression¹⁷:

$$CPF_0 = \hat{CPF}_0 \pm t_{0.95, n-2} \sqrt{\hat{\sigma}_{CPF}^2 \left[1 + \frac{1}{n} + \frac{(\log R_{c_0} - \overline{\log R_c})^2}{\sum_{i=1}^n (\log R_{c_i} - \overline{\log R_c})^2} \right]} \quad (\text{eq. 9})$$

where

$$\hat{\sigma}_{CPF}^2 = \frac{\sum_{i=1}^n (CPF_i - \hat{CPF}_i)^2}{n - 2} \quad (\text{eq. 10}).$$

In these equations, n is the number of (R_c , CPF) observations, CPF_0 is a given cumulative passing frequency, CPF_i is the i th cumulative passing frequency observation, \hat{CPF} is a cumulative passing frequency computed from a regression model, R_{c_0} is the R_c corresponding to CPF_0 and $\overline{R_c}$ is the average R_c for a set of R_c observations.

R_{80} values for 356, 2024-T3 and 6061-T6 determined using regression parameters are all approximately 2 to $5 \times 10^6 \text{ ohm}\cdot\text{cm}^2$, which has already been suggested as a threshold value for achieving a passing salt spray result¹⁸. The remaining two alloys, 7075-T6 and 3003 exhibit R_{80} values of 1.5×10^7 and $2.3 \times 10^7 \text{ ohm}\cdot\text{cm}^2$ respectively. The large value for 3003 is somewhat surprising because this alloy has good intrinsic corrosion resistance and is considered to be easy to conversion coat. It is possible that the higher threshold values for these two alloys suggest that the key initiation sites that lead to pitting are either relatively scarce (low number density), or only become passivated when most of the remainder of the surface is passivated.

Application of the relationships to new data. Coating resistance and salt spray results from conversion coatings outside the population used to develop the CPF-log R_c relationship development were examined to determine if they conformed to the linear CPF-log R_c relationship. The results were also examined to determine the adequacy of the R_{80} threshold for achieving a passing salt spray result. Figure 8 is a plot showing the fraction of panels passing a 168 hour salt spray test per MIL-C-5541E plotted as a function of a normalized R_c parameter. The R_c data were normalized by subtracting the coating resistance corresponding to 0% CPF (from Table 3) and dividing that quantity by the difference of the coating resistance at 100% CPF and 0% CPF. This normalization procedure enabled results from different alloy substrates (with different slope parameters and intercepts) to be plotted on the same set of axes.

The data in Figure 8 are from chromate and non-chromate conversion coatings on cast 356, 2024-T3, 6061-T6, and 7075-T6. The solid line is the response predicted on the basis of a linear CPF-log R_c relationship. Overall, the experimental data follow the linear relationship, but with a large amount of scatter. Some of conversion coatings exhibit coating resistances less than R_{80} , but passed salt spray. Interestingly, these were all chromate conversion coatings. Other coatings exhibited a passing fraction of 0% but had coating resistances that were distinguishable by EIS. This occurs because EIS can resolve subtle differences in coating corrosion resistance that salt spray testing cannot. When counting statistics were good (e.g. 28 samples of hydrotalcite coated 6061-T6) the observed passing fraction agrees well with the passing fraction predicted by the CPF-log R_c relationship. In all cases in Figure 8, coatings that yielded R_c values in excess of R_{80} yielded a passing salt spray result. This suggests that the R_{80} threshold is a good estimator of when a passing salt spray result can be expected.

SUMMARY

Salt spray and EIS data have been obtained from the same large set of Al alloy panels with inorganic corrosion resistant coatings. EIS data, collected after a 24 hour exposure to 0.5 M NaCl solution, were subjected to CNLS fitting to a generalized equivalent circuit model from which a "coating resistance", R_c , was extracted. R_c is taken as a measure of the resistance to pitting damage. A relative dependent parameter was developed from the occurrence of passing performances among sets of coated panels of a given alloy type in salt spray testing. This parameter was termed the cumulative passing frequency of CPF. The CPF is a measure of the probability of achieving a passing a salt spray test result according to the 5 pit per panel criterion established in MIL-C-5541E. A comparison of the results showed an overlap in the range of sensitivity of the tests. This was observed when the salt spray test was conducted according to ASTM B117 and the MIL-C-5541E 5 pit per 30 in.² panel failure criterion was applied after 168 hours of exposure, and the EIS test was conducted after 24 ± 1 hours of exposure to aerated 0.5 M NaCl solution. EIS testing was more sensitive than salt spray when the inspection interval was greater than 24 hours. The CPF exhibited a linear dependence on log R_c in the range where salt spray was sensitive. Based on this relationships, threshold R_c values were determined and are proposed to define the minimum performance in the EIS test for which a passing result in a 168 hour salt spray

exposure can be expected. These threshold values were approximately 2 to 5×10^6 ohm \cdot cm² for 356, 2024-T3 and 6061-T6; 1.5×10^7 ohm \cdot cm² for 7075-T6; and 2.3×10^7 ohm \cdot cm² for 3003.

ACKNOWLEDGMENTS

The authors are indebted to Paul Chalmer, the National Center for Manufacturing Sciences and the Alternatives to Chromium for Metal Finishing project steering group for making available test samples and salt spray data. The authors would especially like to acknowledge Norm Carlson and Texas Instruments who conducted the salt spray exposure tests and J. Braithwaite for helpful discussions on treatment of the data. The assistance of C. Cooper, S. Anderson with various experimental details is also gratefully acknowledged.

Sandia is a multiprogram laboratory operated by Sandia corporation, a Lockheed Martin Company, for the United States Department of Energy under Contract DE-AC04-94AL85000.

REFERENCES

1. F. Altmayer, Plating and Surf. Finishing, 72 (1985):p. 36.
2. B.R. Appleman, J. Coat. Tech., 62 (1990):p. 57.
3. F. Mansfeld, C.H. Tsai, Corrosion, 47 (1991):p. 958.
4. J. Titz, G.H. Wagner, H. Spahn, M. Ebert, K. Juttner, W.J. Lorenz, Corrosion, 46 (1990): p. 221.
5. J.N. Murray, H.P. Hack, Corrosion, 47 (1990):p. 480.
6. F. Mansfeld, S. Lin, S. Kim, H. Shih, J. Electrochem. Soc., 137 (1990): p. 78.
7. F. Mansfeld, H. Shih, J. Electrochem. Soc., 133 (1988): p. 1171.
8. "Alternatives to Chromium for Metal Finishing", Final Report 0273RE95, National Center for Manufacturing Sciences, Ann Arbor MI (1995).
9. Military Specification MIL-C-5541E, "Chemical Conversion Coatings on Aluminum and Aluminum Alloys", Systems Engineering and Standardization Department, Naval Air Engineering Center, Lakehurst, NJ, (revised November, 1990).
10. R.G. Buchheit, M. Cunningham, H. Jensen, M.W. Kendig, M.A. Martinez, Corrosion, accepted for publication, April (1997).
11. F. Mansfeld, S. Lin, S. Kim, H. Shih, Electrochim. Acta, 24, 1123 (1989).
12. see for example: D.M. Himmelblau, Process Analysis by Statistical Methods, John Wiley and Sons, Inc., New York (1970): p. 27, or W. Nelson, Accelerated Testing Statistical Models, Test Plans, and Data Analyses, John Wiley and Sons, Inc., New York (1990): p. 115.
13. T. Shibata, T. Takeyama, Corrosion, 33, 243 (1977).
14. D.E. Williams, C. Westcott, Metallic Corrosion, v.4, NRC of Canada, Toronto (1984): p. 390.

15. D.C. Montgomery, G.C. Runger, Applied Statistics and Probability for Engineers, John Wiley & Sons, Inc., New York (1994): p. 517.
16. J.E. Hatch, ed., Aluminum: Properties and Physical Metallurgy, ASM, Metals Park, OH, (1984): p. 242.
17. D.C. Montgomery, G.C. Runger, Applied Statistics and Probability for Engineers, John Wiley & Sons, Inc., New York (1994): p. 501.
18. M. W. Kendig, S. Jeanjaquet and M. Cunningham, "Replacement for Chromate Conversion Coating and Anodization", Final Report, to Rockwell International Space Systems Division and the South Coast Air Quality Management District, September 1993.

Table 1. Nominal compositions of the aluminum alloys used in this study.

Alloy	Alloying Element (w/o)					
	Cu	Mg	Zn	Si	Mn	Cr
356	---	0.35	---	7.0	---	---
2024-T3	4.4	1.5	---	---	0.6	---
3003	0.12	---	---	---	1.2	---
6061-T6	0.3	1.0	---	0.6	---	0.2
7075-T6	1.6	2.5	5.6	---	---	0.23

Table 2. A tabular example which illustrates the development of the relative dependent variable according to the mean rank method using a portion of the EIS-salt spray data from 2024-T3 substrates.

$\log R_c$ (R_c in Ω - cm^2)	Passing Frequency	Cumulative Passing Frequency	Ranks	Mean Rank (m)	$m/(n+1)$	$m/(n+1)$ $\times 100$
4.74	0	0	0	0	0/29	0
5.05	0	0	0	0	0/29	0
5.48	0	0	0	0	0/29	0
5.64	1	1	1	0.5	0.5/29	2
5.77	5	6	2-6	4	4/29	14
5.88	3	9	7-9	8	8/29	28
5.96	0	9	9-9	9	9/29	31
5.97	5	14	10-14	12	12/29	41
5.98	5	19	15-19	17	17/29	59
6.16	4	23	20-23	21.5	21.5/29	74
6.39	0	23	23-23	23	23/29	79
6.45	0	23	23-23	23	23/29	79
8.20	5	28	24-28	26	26/29	90

Table 3. Linear regression models for CPF as a function of R_c .

Alloy	Regression Model for CPF	Data Range Used for Model (ohm·cm ²)	Correlation Coefficient	Coefficient of Determination
356	$-114 + 29.1\log R_c$	Greater than 5×10^3	0.98	0.95
2024-T3	$-535 + 96.5\log R_c$	$3 \times 10^5 - 3 \times 10^6$	0.95	0.91
3003	$-210 + 39.4\log R_c$	$2 \times 10^5 - 6 \times 10^7$	0.98	0.97
6061-T6	$-191 + 41.5\log R_c$	Up to 5×10^6	0.99	0.98
7075-T6	$-196 + 38.4\log R_c$	$1 \times 10^5 - 4 \times 10^7$	0.96	0.92

Table 4. R_{80} values computed using the regression models in Table 3.

Alloy	80% CPF Threshold from Regression Models (ohm·cm ²)	95% Prediction Interval at the R_{80} Threshold (ohm·cm ²)
356	4.6×10^6	$1.5 \times 10^6 < R_{80} < 1.5 \times 10^7$
2024-T3	2.4×10^6	$1.4 \times 10^6 < R_{80} < 4.1 \times 10^6$
3003	2.3×10^7	$1.1 \times 10^7 < R_{80} < 4.8 \times 10^7$
6061-T6	3.4×10^6	$2.0 \times 10^6 < R_{80} < 6.7 \times 10^6$
7075-T6	1.5×10^7	$3.6 \times 10^6 < R_{80} < 3.9 \times 10^7$

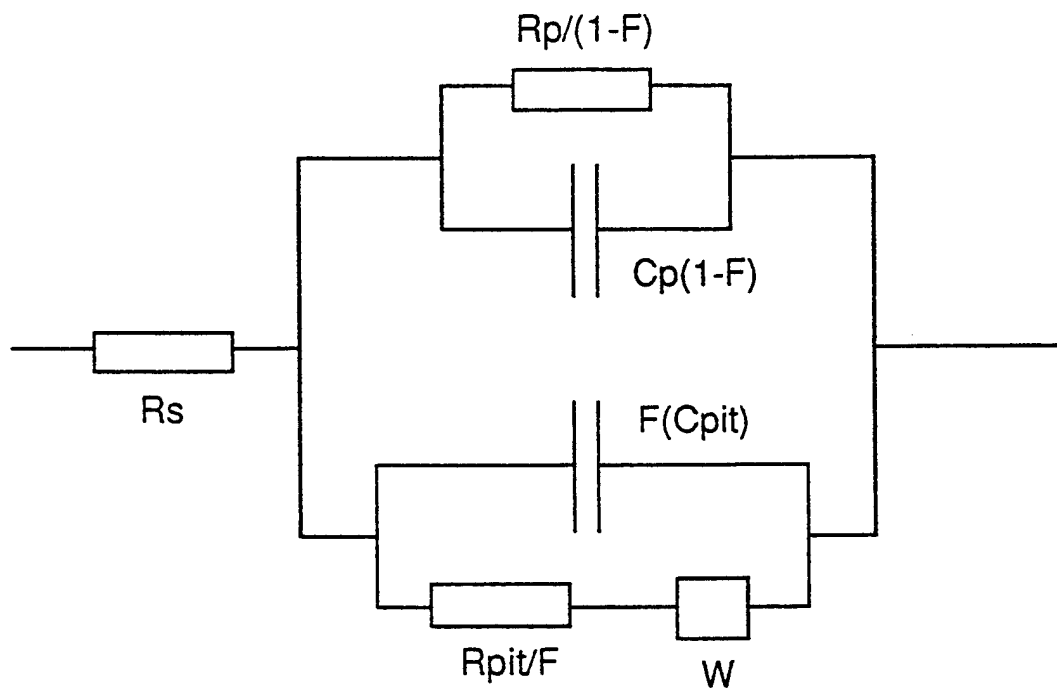


Figure 1. Model for the coating impedance on chemically passivated aluminum alloys^{6,7}.

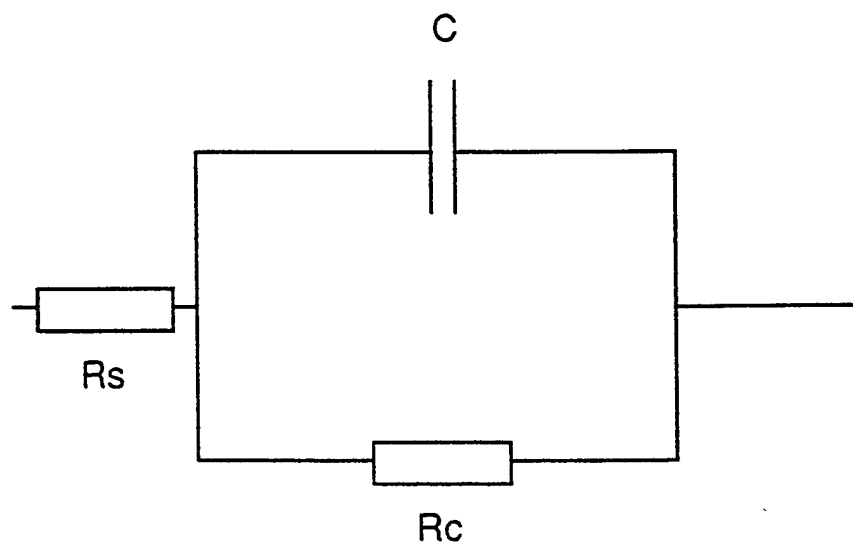


Figure 2. Simplified circuit resulting with certain assumptions.

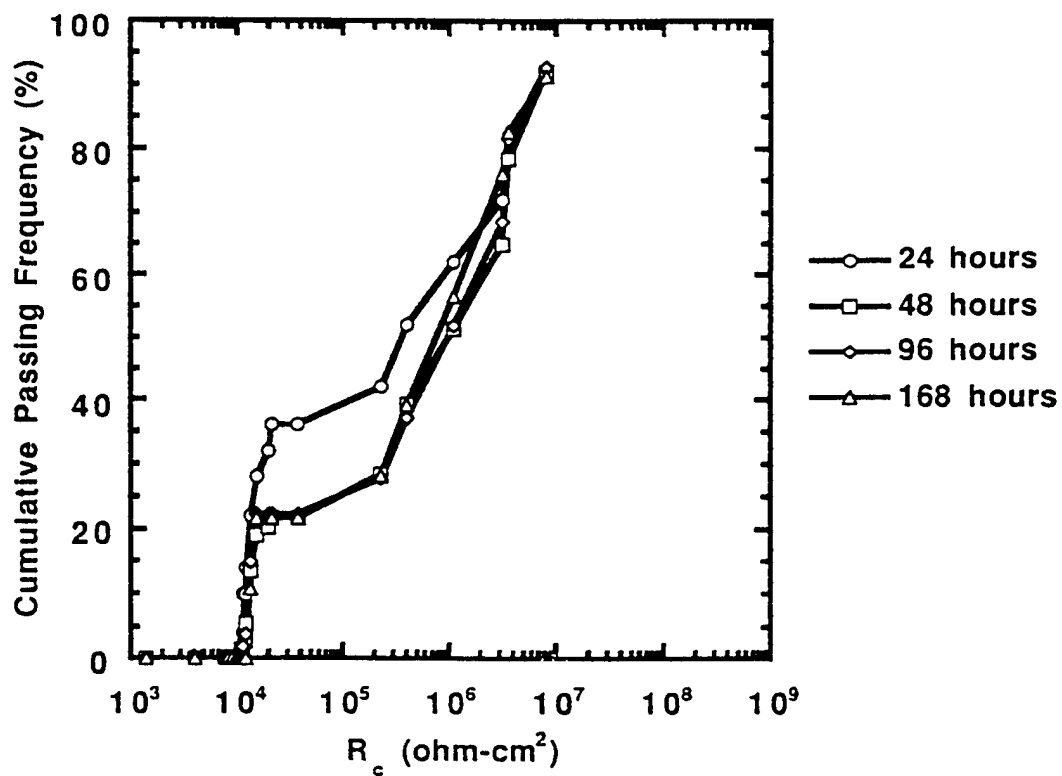


Figure 3. Cumulative passing frequency plot for 356.

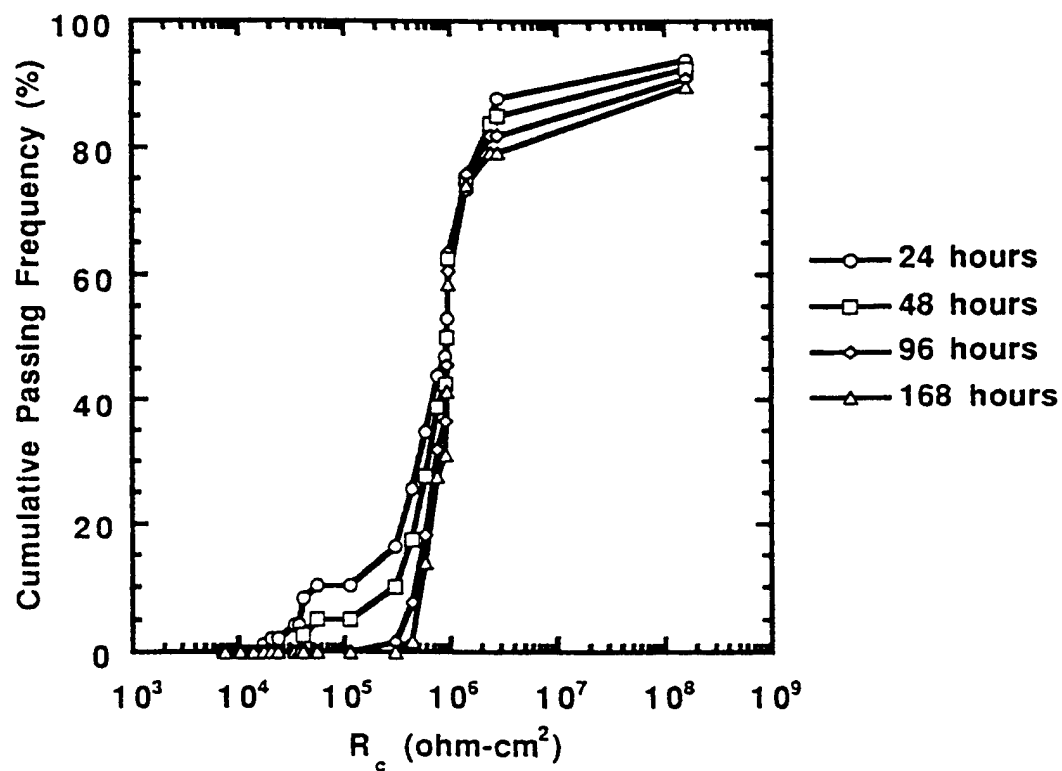


Figure 4. Cumulative passing frequency plot for 2024-T3.

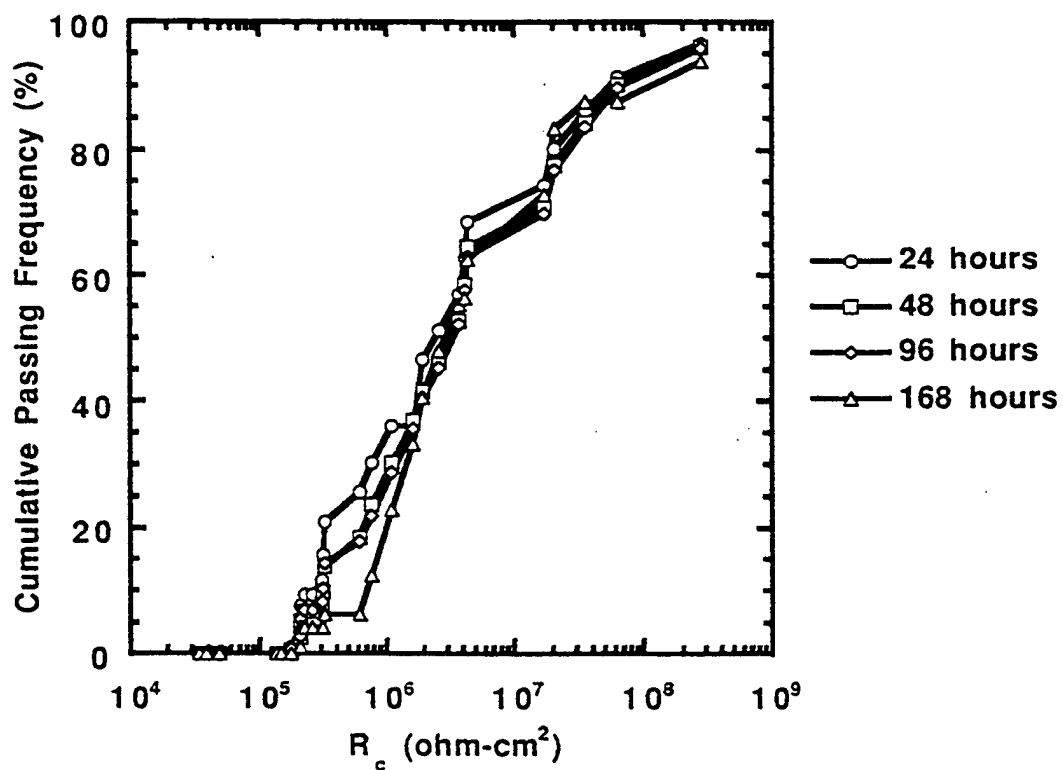


Figure 5. Cumulative passing frequency plot for 3003.

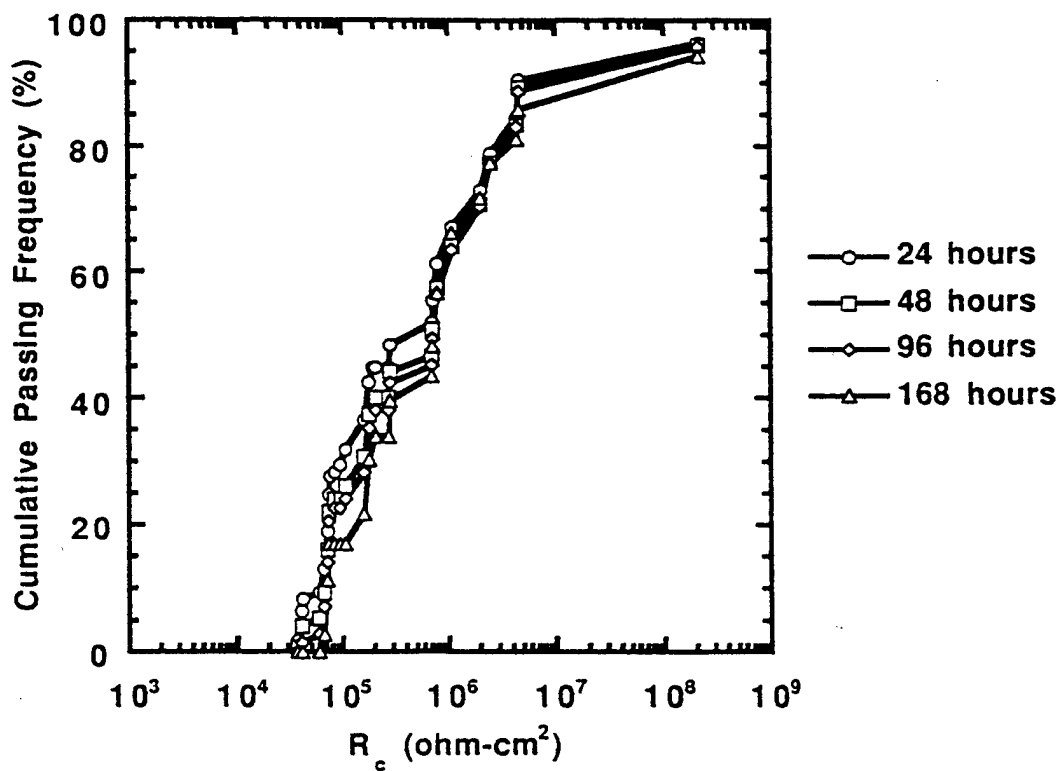


Figure 6. Cumulative passing frequency plot for 6061-T6.

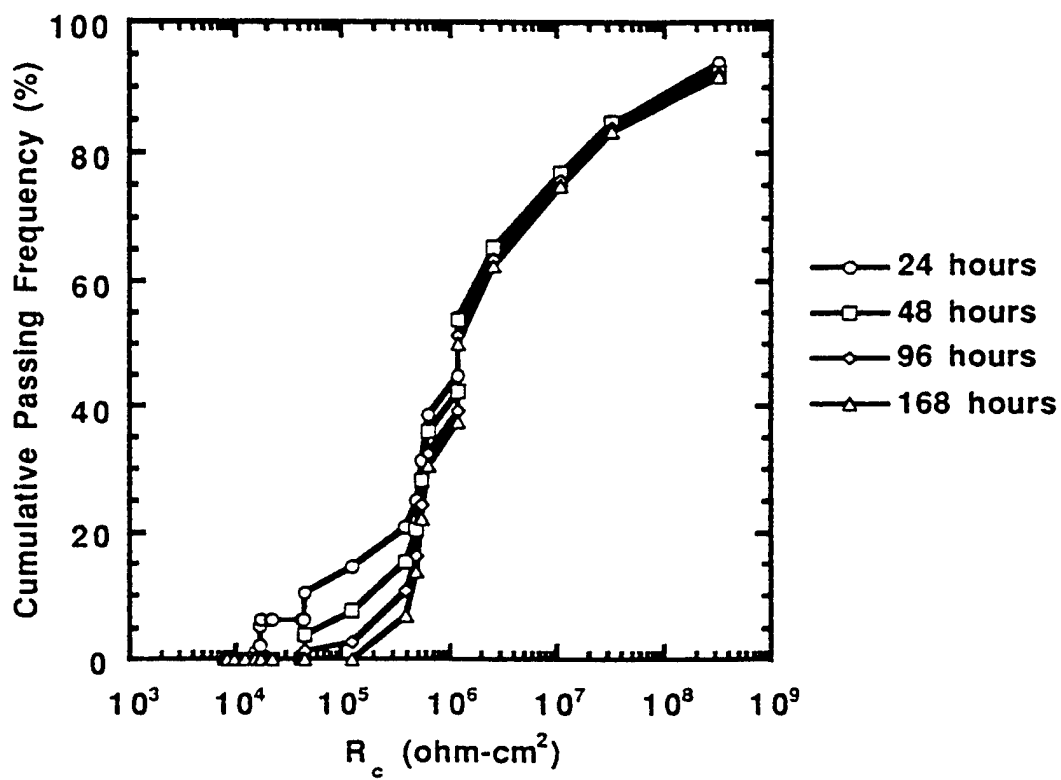
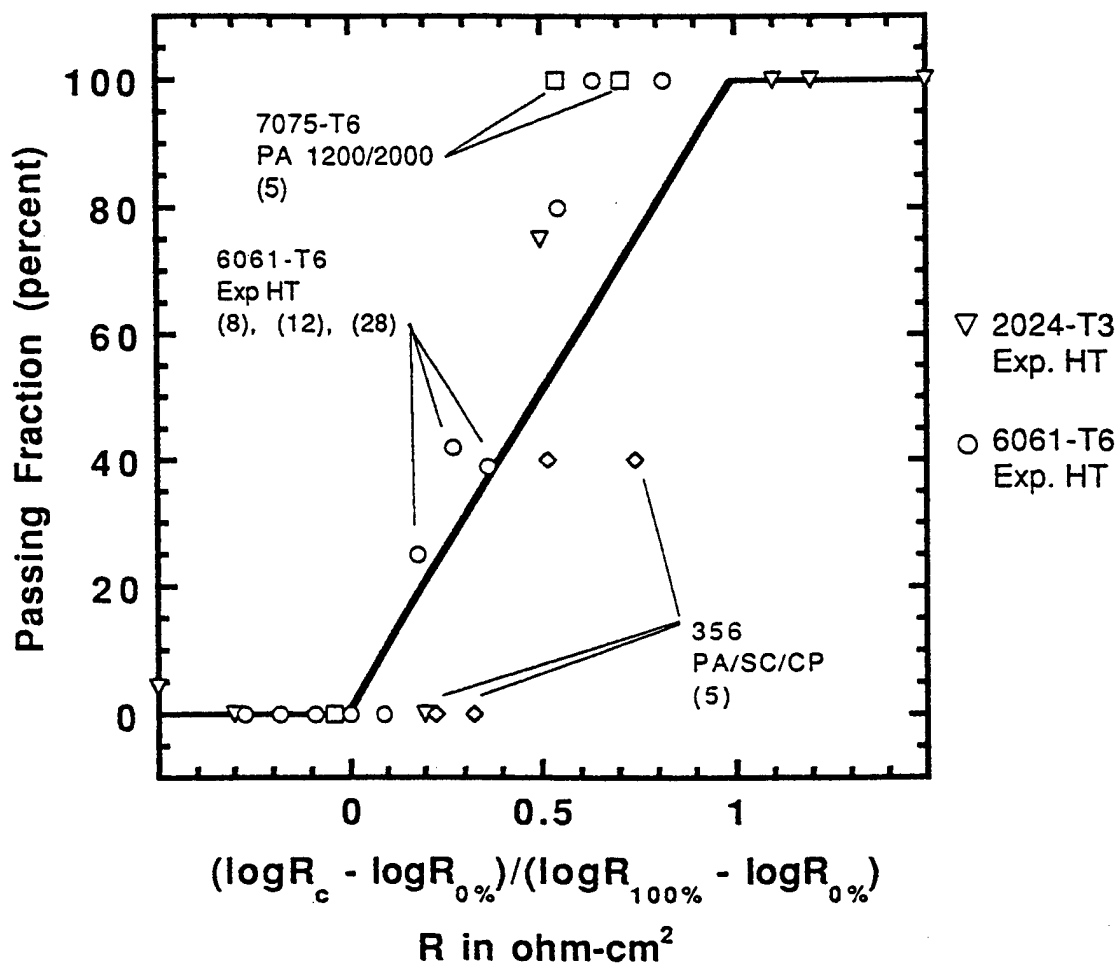


Figure 7. Cumulative passing frequency plot for 7075-T6.



Legend

○	7075-T6	commercial chromate
m	6061-T6	experimental hydrotalcite
▽	2024-T3	experimental hydrotalcite
◇	cast 356	commercial permanganate commercial cobalt/amine commercial organo-Ti/Zr

Figure 8. Passing frequency versus normalized R_c values for conversion coatings not used in developing the Log R_c -CPF relationships.

US PATENT & TRADEMARK OFFICE

PATENT FULL TEXT AND IMAGE DATABASE

[Home](#)[Boolean](#)[Manual](#)[Number](#)[Help](#)[Hit List](#)[Bottom](#)[View Shopping Cart](#)[Add to Shopping Cart](#)[Images](#)

(1 of 1)

United States Patent

RE35,576

Buchheit, Jr., et al.

July 29, 1997

Method for increasing the corrosion resistance of aluminum and aluminum alloys

Abstract

Aluminum and aluminum alloys are protected from corrosion by immersion in an alkaline lithium or alkaline magnesium salt solution. Immersion in the salt solution causes the formation of a protective film on the surface of the aluminum or aluminum alloy which includes hydrotalcite compounds. A post film formation heat treatment significantly improves the corrosion resistance of the protective film.

Inventors: **Buchheit, Jr.; Rudolph G.** (Albuquerque, NM); **Stoner; Glenn E.** (Charlottesville, VA)Assignee: **Center for Innovative Technology** (Herndon, VA)Appl. No.: **534929**Filed: **September 28, 1995****Related U.S. Patent Documents**

Reissue of:	Patent No.:	Issued:	Appl. No.:	Filed:
	05266356	Nov 30, 1993	723445	Jun 21, 1991

Current U.S. Class:

427/372.2; 427/435; 427/443.2

Intern'l Class:

B05D 003/02

Field of Search:

427/372.2,435,443.2

References Cited [Referenced By]**U.S. Patent Documents**

Patent No.	Date	Inventor(s)	Class
3973998	Aug., 1976	Datta et al.	148/6.
4004951	Jan., 1977	Dorsey, Jr.	148/6.
4054466	Oct., 1977	King et al.	148/6.
4063969	Dec., 1977	Howell, Jr.	148/6.
4319924	Mar., 1982	Collins, Jr. et al.	106/14.

Foreign Patent Documents

Patent No.	Date	Inventor(s)
53-35899	Mar., 1974	JP.
54-148141	Nov., 1979	JP.

Other References

Abstract from Dialog File 33: Aluminum Industry Abstract Patent No. Japanese J7 7026,211 (16 Feb. 1973) Journal Announcement: 7801.

Isobe, y. et al., "Chemical Conversion Treatment of Aluminum Alloys with the Mixed Solution of MgSO₄ and NaHCO₃", Boshoku Gijutsu (Corrosion Engineering), 38, pp. 161-166 (1989) (including English Translation) (no month avail.).

Tanaka, S., et al., "Chemical Treatment of Aluminum Alloys with the Mixed Solution of LiNO₃ and NaHCO₃", Boshoku Gijutsu (Corrosion Engineering) 39, pp. 425-431, Aug. 15, 1990 (and English Translation).

Mushiro, M., et al., "Studies on Aluminum Oxide Film Formed in Alkaline Baths Containing Nitrates, Part 1", Metal Finishing Society of Japan, 23, pp. 370-374 (1972) (no month avail.).

Uchiyama, T., "Recent studies on chemical oxide coatings of aluminum," Japan Institute of Light Metals (Kei-Kimzoku), 32, pp. 202-210 (1982) (no month avail.).

Uchimaya, T., "A Study on Chemical Conversion Coatings Formed on Aluminum in Boiling Sea Water," Metal Finishing Society of Japan (Kinzoku Hyomen Gijutsu), 37, pp. 178-183 (1986). (No month avail.).

Primary Examiner: Pianalto; Bernard

Attorney, Agent or Firm: Fitzpatrick, Cella, Harper & Scinto

Claims

Having thus described our invention, what we claim as new and desire to secure by Letters Patent is as follows:

1. A method for providing an aluminum alloy containing lithium with a surface coating that protects against corrosion, comprising the steps of immersing a substrate comprised of an aluminum alloy that contains 0.5 to 10 weight percent lithium in an alkaline salt solution having a pH of at least 8 and a concentration ranging from 0.01M to 1.0M wherein an anion

of said salt in said alkaline salt solution is capable of forming a salt with said lithium in said aluminum alloy, and drying a film formed on said substrate after said step of immersing.

- 2. A method as recited in claim 1 wherein said anion of said salt in said alkaline salt solution is selected from the group consisting of CO.sub.3.sup.2-, SO.sub.4.sup.2-, Cl.sup.-, Br.sup.-, and OH.sup.-.
- 3. A method as recited in claim 2 wherein said step of immersing is performed when said alkaline salt solution has a temperature ranging from 25.degree. C. to 30.degree. C.
- 4. A method as recited in claim 1 further comprising the step of heating said film formed on said substrate.
- 5. A method as recited in claim 4 wherein said step of heating is performed at approximately 150.degree. C. for approximately four hours.

6. A method of protecting aluminum and aluminum alloys against corrosion comprising the step of immersing an aluminum or aluminum alloy in an aqueous solution consisting ofladd.essentially of .laddend.a lithium salt .ladd.to form a corrosion resistant coating.laddend. .ladd.7. A method of protecting aluminum and aluminum alloys against corrosion comprising the step of immersing an aluminum or aluminum alloy in an aqueous solution which is free of a quantity of tannin sufficient to form a corrosion resistant coating, comprising a lithium salt to form a corrosion resistant coating. .laddend.ladd.8. A method of protecting aluminum and aluminum alloys against corrosion comprising the step of immersing an aluminum or aluminum alloy in an alkaline aqueous solution consisting essentially of a lithium salt to form a corrosion resistant coating. .laddend.ladd.9. A method as recited in claims 6, 7 or 8 wherein the pH is greater than 9.laddend.ladd.10. A method as recited claims 6, 7 or 8 where the pH is 10 or greater. .laddend.ladd.11. A method as recited in claims 6, 7 or 8 wherein the lithium salt is LiCl, LiOH, LiBr, Li.sub.2 CO.sub.3 or Li.sub.2 SO.sub.4. .laddend.ladd.12. A method as recited in claims 6, 7 or 8 wherein the concentration of the lithium salt ranges from 0.01 to 0.6 molar. .laddend.ladd.13. A method as recited in claims 6, 7 or 8 wherein said concentration of the lithium salt ranges from 0.05 molar to 0.1 molar. .laddend.ladd.14. A method as recited in claims 6, 7 or 8 wherein said immersing step is performed when the lithium salt solution has a temperature ranging from 25.degree. C. to 30.degree. C. .laddend.ladd.15. A method as recited in claims 6, 7 or 8 further comprising the step of heating the coating formed on the aluminum or aluminum alloy to improve the corrosion resistance of the coating. .laddend.ladd.16. A method as recited in claim 15 wherein said heating step is performed at approximately 150.degree. C. for approximately 4 hours. .laddend.ladd.17. A method of protecting aluminum and aluminum alloys against corrosion by forming a hydrotalcite coating on a surface of an aluminum or aluminum alloy substrate by immersing said substrate in a solution consisting essentially of a lithium salt solution having a pH which allows hydrotalcite formation, for a length of time sufficient to allow a degree of hydrotalcite formation which provides corrosion resistance for the substrate. .laddend.ladd.18. A method as recited in claim 17 wherein said pH is greater than 10. .laddend.ladd.19. A method as recited in claim 17 wherein said length of time is on the order of minutes. .laddend.ladd.20. A method as recited in claim 17 wherein said alkaline metal salt is a lithium salt selected from the group consisting of LiCl, LiOH, LiBr, Li.sub.2 CO.sub.3 or Li.sub.2 SO.sub.4. .laddend.ladd.21. A method as recited in claim 17 wherein said step of immersing is performed at approximately room temperature.laddend.ladd.22. A method as recited in claim 17 further comprising the step of heating the hydrotalcite coating subsequent to formation to improve the corrosion resistance of the coating. .laddend.

Description

BACKGROUND OF THE INVENTION

1. Field of the Invention

The present invention is generally related to forming protective coatings on aluminum and aluminum alloys which will increase corrosion resistance by using chemicals that pose a relatively small environmental hazard and have a small toxic effect.

2. Description of the Prior Art

Metal surfaces are often protected from corrosion by the application of a barrier coating. A first category of barrier coatings are anodic oxides, and these types of coatings are usually formed by an electrochemical means known as "anodizing" during immersion in an inorganic acid like H.sub.2 SO.sub.4 or H.sub.3 PO.sub.4. Anodic oxides have a wide range of thicknesses and porosities. Porous coatings can be "sealed" in steam, boiling water or various salt solutions. A second category of barrier coatings are ceramic coatings, and these type of coatings are usually special cements applied to a metal to prevent corrosion. A common example of a ceramic coating is porcelain enamel. A third category of coatings are molecular barrier coatings, and these types of coatings are formed by the addition of organic molecules to solution. Effective inhibitors are transported to the metal-solution interface and have a reactive group attached to a hydrocarbon. The reactive group interacts with the metal surface while the hydrocarbon group is exposed to the environment. As the molecules form the molecular barrier coating, corrosion reactions are slowed. A fourth category of barrier coatings are organic coatings, and these types of coatings are generally intended to simply prevent interaction of an aggressive environment with the metal surface. Organic coatings are the most widely used barrier coatings for metals and paint is a typical example of an organic coating. A fifth category of barrier coatings are conversion coatings, and these types of coatings are made by a process which "converts" some of the base metal into the protective oxide coating. Chromate and phosphate conversion coatings are the two most common types of conversion coatings currently used.

Chromate and phosphate conversion coatings can be formed by chemical and electrochemical treatment of a metallic component during immersion in a solution containing hexavalent chromium (Cr.sup.+6), phosphorus as a phosphate anion, and usually other components. Literally hundreds of subtly different, proprietary chromate conversion coating formulas exist. For aluminum and aluminum alloys, the primary active ingredient in the bath is usually a chromate, dichromate (CrO.sub.4.sup.2- or Cr.sub.2 O.sub.7.sup.2-), or phosphate (PO.sub.4.sup.3-). The pH of the solutions is usually in the range of 1.3 to 2.5, but a few alkaline bath formulas are known. The process results in the formation of a protective, amorphous coating comprised of oxides of the substrate, complex chromium or phosphorus compounds, and other components of the processing solution. Only a small number of coatings and chromating processes have been characterized by surface analysis techniques. But in coating systems that have been studied, the following compounds have been reported: substrate oxides and hydroxides such as Al.sub.2 O.sub.3 and Al(OH).sub.3, chromium oxides and hydroxides such as Cr.sub.2 O.sub.3, CrOOH, Cr(OH).sub.3, and Cr.sub.2 O.sub.3 .multidot.xH.sub.2 O, and phosphates such as AlPO.sub.4. These coatings enhance corrosion resistance of bare and painted surfaces, improve adhesion of paint, or other organic finishes, or provide the surface with a decorative finish.

Chromate conversion coatings are applied by contacting the processed surfaces with a sequence of solutions. The basic processing sequence typically consists of the following six steps: cleaning the metal surface, rinsing, creating the conversion coating on the metal surface, rinsing, post treatment rinsing, and drying. The cleaning, rinsing, and drying steps are fairly standard procedures throughout the industry. The chief variant among the processes used is the composition of the chromate conversion solution. The compositions of these solutions depends on the metal to be treated and the specific requirements of the final product. The chief disadvantage of chromate conversion coating processes is that they involve the use of environmentally hazardous and toxic substances. It is expected that the use of substances like chromates will soon be regulated under stringent guidelines.

Because of the environmental problems with chromates, much work has been done to develop protective coatings which do not employ such compounds. For example, U.S. Pat. No. 4,004,951 to Dorsey discloses applying a hydrophobic coating on an aluminum surface by treatment with a long chain carboxylic acid and an equivalent alkali metal salt of the carboxylic acid, U.S. Pat. No. 4,054,466 to King et al. discloses a process for the treatment aluminum in which vegetable tannin is applied to the surface of the aluminum, and U.S. Pat. No. 4,063,969 to Howell et al. discloses treating aluminum with a combination of tannin and lithium hydroxide. In each of the above patents, the primary protective ingredient is the complex organic compound, the treatment solution is applied at slightly elevated temperatures (90.degree.-125.degree. F.), and the treatment solution is kept at a mid-level pH (4-8 in King and Howell, and 8-10 in Dorsey). Csanady et al., in Corrosion Science, 24, 3, 237-48 (1984) showed that alkali and alkali earth metals stimulated Al(OH).sub.3 growth on aluminum alloys. However, Csanady et al. report that the incorporation of Li.sup.+ or Mg.sup.+ into a growing oxide film degrades corrosion resistance.

SUMMARY OF THE INVENTION

It is therefore an object of the present invention to provide an improved process for forming a protective coating on aluminum and aluminum alloys which is environmentally sound, utilizes low-cost chemical ingredients, and is procedurally similar to existing coating processes.

It is another object of the present invention to use alkali metal salts, such as Li.sub.2 CO.sub.3, Li.sub.2 SO.sub.4, LiCl, LiOH, and LiBr, and alkaline earth metal salts, such as MgCl.sub.2, MgBr.sub.2, and MgCO.sub.3, in a treatment solution having an elevated pH to provide a protective coating on aluminum.

It is yet another object of the present invention to use aqueous alkaline salts to treat aluminum alloys containing lithium to produce a protective coating on the aluminum alloy.

According to the invention, aluminum alloys have been found to exhibit increased corrosion resistance after exposure to aqueous alkaline (pH ranging from 8-13) solutions of lithium salts. Because lithium salts are similar in character to magnesium salts, similar results are likely to be achieved for solutions containing a magnesium cation. Upon immersion in the alkaline bath, a specific chemical composition containing aluminum, lithium (or magnesium) and the salt anion is formed as a protective film on the aluminum surface. Formation of the protective film readily occurs at room temperature. Heating the aluminum substrate after film formation may liberate water and volatile anions bound in the chemical structure of the film. Aluminum alloys which contain lithium or magnesium and magnesium based alloys only need to be treated with an alkaline salt solution to form the protective aluminum-lithium-anion film or aluminum-magnesium-anion film. Lithium and magnesium salts are ubiquitous, low cost compounds which are not hazardous to the environment and, therefore, the inventive process has significant advantages over the use of chromate conversion coatings.

DETAILED DESCRIPTION OF THE PREFERRED EMBODIMENTS OF THE INVENTION

Corrosion resistant films can be formed on aluminum and aluminum alloy components using a multi-step process involving immersion in an alkaline lithium salt bath. Corrosion resistance may be enhanced by a subsequent heat treatment and room temperature aging process. Components to be coated are first degreased using hexane or some other suitable degreasing agent. Then, the components are cleaned in an alkaline bath. The residue from the cleaning process is removed in a deoxidizing acid bath. The components are then immediately immersed in an alkaline lithium salt solution. For example, the solution may be 0.01 to 0.6 M Li.sub.2 CO.sub.3 (the upper solubility limit). The best results have been achieved with alkaline lithium salt solutions with concentrations ranging from 0.05 to 0.1 M. The pH of the solution must be greater than 8 and is most preferably between 11 and 12. The components remain in the alkaline lithium salt bath for approximately 5 to 60 minutes (or longer for thicker coatings). The salt bath may be maintained at room temperature (e.g., 25.degree. -30.degree. C.) during immersion. The components are then removed and dried. The components may then be heat treated and aged. For example, heating in air at 150.degree. C. and aging for seven days at room temperature yields desirable results. Coatings formed by this process are thin and translucent. The appearance of these coatings is similar to that produced by some traditional conversion coating and the corrosion resistance is comparable to some chromate conversion coatings in accelerated testing.

The compounds formed on the aluminum surface during immersion in the salt solution have a structure comprised of layers of hydroxide ions separated by alternating layers of metal (Al and Li (or Mg)) cations and anions of the salt. The compounds belong to a class of clays known as hydrotalcites. The hydrotalcite compounds in the surface film can, without further processing, impart corrosion resistance to the aluminum. However, the protective properties of the film may degrade in acid and neutral solutions. Therefore, a post film formation heat treatment has been found to be beneficial in improving corrosion resistance. Heat treatment is believed to liberate water and volatile anions bound in the hydrotalcite structure to create more corrosion resistant film which is less susceptible to degradation. Titanium salts, hydrofluoric acid, phosphoric acid, and sodium hydroxide may be added to the alkaline lithium salt solution to improve the characteristics of the resulting corrosion resistant film; however, such additions are not required.

Hydrotalcite compounds are detectable on aluminum and aluminum alloys after immersion in solutions with a pH as low as 8. However, increasing amounts of the hydrotalcite compounds result when the solution has a higher pH. Increased corrosion resistance has been observed in the presence of several lithium salt solutions including LiCl, LiOH, LiBr, Li.sub.2 CO.sub.3, and Li.sub.2 SO.sub.4. Other lithium salts should also be suitable for hydrotalcite compound formation. Hydrotalcite films are formed in solution at room temperature. Increasing the lithium salt solution temperature causes volatile species like carbonates and sulfates to escape solution as carbon dioxide and sulfur dioxide, thereby inhibiting hydrotalcite formation. Aluminum alloys which contain lithium at a level ranging from 0.5 to 10 weight percent would only need to be exposed to aqueous alkaline salts having anions such as CO.sub.3.sup.2-, SO.sub.4.sup.2-, Cl.sup.-, Br.sup.-, and OH.sup.-, or the like, since the lithium in the alloy surface could react with the immersion solution. The immersion time required to form the hydrotalcite compounds in the protective film depends on the alloy type, salt concentration, salt type, and bath pH.

Corrosion performance of the coatings made by the inventive process have been compared to conventional coatings. Accelerated tests were performed using electrochemical impedance spectroscopy (EIS) in aerated 0.5 M NaCl solution. In these tests, the polarization resistance, R_p , is determined and provides a measure of the corrosion resistance. In general, larger values of R_p indicate better corrosion resistance. Corrosion performance coatings is tracked as a function of time to determine how long a coating will offer the necessary level of protection. Moreover, the time at which a coating no longer often a threshold level of corrosion protection is a useful way of the ranking the effectiveness of different coating processes. A drawback to evaluating coating corrosion performance in actual service environments is that testing times can be exceedingly long. An ideal test environment is one that is severe enough to keep testing times down, but maintains enough sensitivity to distinguish among different levels of coating performance and induces damage by the same mechanisms that are expected to operate under service conditions. EIS testing in 0.5 M NaCl solution satisfies these criteria (e.g., film breakdown can be detected in reasonable periods of time, the performance of various coatings can be distinguished, the performance of coatings on various alloys can be distinguished, and the damage mechanisms are followed since chloride ion instigates film failure in service environments).

In the EIS tests, five panels were prepared from commercial sheet stock. The sheet stock used was alloy 1100, which has a composition of 99.5% Al with the remainder being iron, silicon and copper and is commercially available from Kaiser Aluminum and Chemical Corporation. The test panels were cut from the sheet stock and mechanically polished with successively finer SiC paper ending with a 600 grit final polish. The panels were then decreased by immersing them in 1,1,1 trichloroethane at 70.degree. C. and deoxidized in an ammonium bifluoride (75 g/l)/concentrated nitric acid bath for ten minutes. The panels were then rinsed in a 10 mega-Ohm distilled water cascade for five minutes. The panels were then subjected to immediate immersion procedures for film formation. The first panel had a film formed by immersion in 0.6M Li.sub.2 CO.sub.3 at pH 11.2 for one hour at room temperature. After removing the panel from the immersion bath, it was cascade rinsed in distilled water and allowed to dry in ambient air. The panel was aged seven days in a desiccator at room temperature prior to EIS testing. The second panel had a film formed by the same process as the first panel, but, it was additionally subjected to a heat treatment step of 150.degree. C. for four hours. The third panel had a film formed by the Parker-Amchem Alodine 1200 process. The film is a mixture of hydrated aluminum oxide Cr.sub.6+ and various chromium oxides, the relative proportions of which can vary widely. The fourth panel was given a chromate conversion coating treatment of fifteen minutes in 1.0M Na.sub.2 CrO.sub.4 at pH 8.5. The fifth panel acted as a control and did not have a protective film formed thereon.

Table 1 shows the polarization resistance measurements for the five panels after three hours exposure to 0.5M NaCl.

TABLE 1

Alloy 1100 Type of Coating	R_p (ohms-cm.sup.2)
(1) Lithium Carbonate	1.5*10.sup.4
(2) Lithium Carbonate + Heat	1.5*10.sup.5
(3) Alodine 1200	2.5*10.sup.4
(4) Chromate	1.5*10.sup.5
(5) No Coating	1.0*10.sup.3

As can be seen from Table 1, the polarization resistance (R_p) measurements were as good or better than that measured for the standard alodine coating and the chromate coating. Table 1 also shows that the post film formation heat treatment resulted in improving the corrosion resistance by an order of magnitude. Similar improved corrosion resistance results were obtained with other aluminum alloys.

It has also been determined that under constant immersion conditions in NaCl at the free corrosion potential, the coating polarization resistance increases. Table 2 presents the measured polarization resistance of lithium carbonate coated and heat treated aluminum alloy 1100 versus time in aerated 0.5M NaCl solution at pH 5.5.

TABLE 2

Immersion Time (hours)	R_p (ohms-cm.sup.2)
0	2.0*10.sup.5
20	1.5*10.sup.5
43	2.0*10.sup.5
67	6.0*10.sup.5
91	3.0*10.sup.3
115	7.0*10.sup.3
240	5.0*10.sup.5

The increase with time in the immersion bath indicates that barrier properties may be maintained for extended exposure periods under less severe service conditions. The anticipated service conditions are atmospheric exposure 0-100% relative humidity and/or under organic and polymeric paints and coatings.

Another electrochemical method for evaluating corrosion performance is known as anodic potentiodynamic polarization testing. Typical parameters obtained from such testing that are commonly used to characterize corrosion behavior are the corrosion potential ($E_{\text{sub.corr}}$), the breakaway potential ($E_{\text{sub.br}}$), and the passive current density ($i_{\text{sub.pass}}$). Lower corrosion potentials usually correspond with lower corrosion resistance. The breakaway potential is the potential at which the surface film no longer offers significant protection from corrosion; therefore, higher breakaway potentials correspond with more corrosion resistance. The passive current density is a direct measure of the corrosion rate in the potential range where the surface film is stable. Lower passive current densities correspond with better corrosion resistance.

Tables 3 and 4 show the anodic polarization data summary for 99.999% aluminum in deaerated 0.6M salt solutions at a pH ranging from 6 to 7 and at a pH ranging from 10 to 10.5, respectively.

TABLE 3

pH = 6-7		
	LiCl	NaCl
$E_{\text{sub.coff}}$ (V.sub.sce)	-1.020	-0.940
$E_{\text{sub.br}}$ (V.sub.sce)	-0.640	-0.660
$i_{\text{sub.pass}}$ (A/cm.sup.2)	7.0×10^{-7}	4.0×10^{-7}

TABLE 4

pH = 10-10.5		
	LiCl	NaCl
$E_{\text{sub.COFF}}$ (V.sub.sce)	-1.500	-1.750
$E_{\text{sub.br}}$ (V.sub.sce)	-0.600	-0.650
$i_{\text{sub.pass}}$ (A/cm.sup.2)	1.5×10^{-6}	7.0×10^{-5}

In Table 3, the polarization curve parameters are similar for LiCl and NaCl which would indicate no special passivating effects due to the presence of lithium in a neutral solution. However, the results in Table 4 show that the more alkaline lithium containing solution increases the breakaway potential by 0.050 Volts and the passive current density is reduced by an order of magnitude compared to the similar sodium containing solution.

Table 5 summarizes anodic polarization data obtained for 99.999% aluminum in various other lithium salt solutions.

TABLE 5

0.1M Li.sub.2 SO.sub.4			
0.1M LiBr 0.1M LiOH			
	pH 11.0	pH 11.0	pH 10.5
$E_{\text{sub.COFF}}$ (V.sub.sce)	-1.850	-1.750	-1.800
$E_{\text{sub.br}}$ (V.sub.sce)	-0.420	-0.040	-0.420
$i_{\text{sub.pass}}$ (A/cm.sup.2)	2.5×10^{-5}	9.0×10^{-6}	1.0×10^{-6}

In each case, the measured $E_{\text{sub.br}}$ and/or $i_{\text{sub.pass}}$ parameters indicate a beneficial passivating effect. Hence, a wide variety of lithium salts can be used in immersion solutions to create a corrosion resistant film on aluminum and aluminum alloys.

To determine whether aluminum-lithium alloys could be passivated by exposure to an alkaline solution (e.g., non-lithium containing since lithium is present in the alloy), 99.999% Al and an Al-3 weight percent Li alloy (Al-3Li) were immersed in 0.6M NaCl at pH 5.5 and pH 10 prior to anodic potentiodynamic polarization testing. Tables 6 and 7 present the anodic polarization data summaries for 99.999% Al in deaerated 0.6M NaCl solution and for a solution heat treated and quenched Al-3Li in deaerated 0.6M NaCl solution, respectively.

TABLE 6

99.999% Al in Deaerated 0.6M NaCl Solution		
	pH 5.5	pH 10
$E_{\text{sub.COFF}}$ (V.sub.sce)	-0.985	-1.340
$E_{\text{sub.br}}$ (V.sub.sce)	-0.725	-0.725
$i_{\text{sub.pass}}$ (A/cm.sup.2)	1.0×10^{-7}	3.0×10^{-7}

TABLE 7

Solution Heat Treated and Quenched Al-3Li in Deaerated 0.6M NaCl Solution		
	pH 5.5	pH 10
$E_{\text{sub.COFF}}$ (V.sub.sce)	-0.965	-1.080
$E_{\text{sub.br}}$ (V.sub.sce)	-0.640	-0.575

i.sub.pass (A/cm.sup.2)
2.1*10.sup.-6
2.0*10.sup.-7

With reference to Table 6, the corrosion potential for 99.999% pure aluminum decreases by nearly 0.400V, and neither E.sub.br nor i.sub.pass are significantly changed. This indicates that no benefit was obtained by treating the pure aluminum with the alkaline solution. However, with reference to Table 7, the Al-3Li treated with the alkaline NaCl solution had an E.sub.br which increased by 0.065 V and an i.sub.pass which was reduced by a factor of 10. These results indicate that corrosion resistance of the aluminum-lithium alloy was significantly increased by pretreatment with the alkaline salt.

In general, the first element in a group in the Periodic Table exhibits properties which deviate from the trends of its group. Commonly the physical and chemical behavior of the first element in the group is more like the elements in the next group (see Bodie et al., Concepts and Models of Inorganic Chemistry, 2nd, John Wiley & sons, Inc. New York, 1983). Physical chemists have described this phenomena as "diagonal relationships", referring to the fact that the element is similar in behavior to an element diagonally positioned to it on the Periodic Table. Lithium, being the first element in Group IA behaves more like Group IIA magnesium than other Group IA elements, like sodium and potassium. Diagonal relationships are evident when comparing physical properties like solubility. For example, fluorides, carbonates and phosphates of Mg and Li are only moderately soluble, while the same Na and K compounds are highly soluble.

There are several physical and chemical characteristics shared by lithium and magnesium which would suggest that magnesium salts could be used to protect aluminum and aluminum alloys in the same manner shown above for lithium salts. For instance, lithium and magnesium compounds have unusually high lattice energies resulting in relatively good chemical stability. The hydrolysis behavior of lithium and magnesium are also similar (see Baes et al., Hydrolysis of Cations, Robert E. Krieger Publishing Co., Malabar, FL, 1986). Lithium is the only Group IA ion to hydrolyze appreciably, but does so only in extremely alkaline solutions. Magnesium also hydrolyzes, but does not do so appreciably before the precipitation of brucite (Mg(OH).sub.2). In the bath solutions discussed above in conjunction with the present invention, lithium exists mainly as Li.sup.+ and is believed to be imbibed into Al(OH).sub.3 to form a hydrotalcite-like structure. Similarly, magnesium in the bath solution would exist primarily as Mg.sup.2+ and would also be easily imbibed. The radii of the two ions is nearly identical (e.g., 0.086 nm for Li.sup.+ and 0.090 nm for Mg.sup.2+) so these cations could occupy the same sites in the cation layer of the hydrotalcite structure without significantly altering the structure. In fact, the naturally occurring variant of hydrotalcite, Mg[Al.sub.2(OH).sub.6].sub.2.multidot.CO.sub.3.nH.sub.2O contains magnesium (see Miyata, Clay Minerals, 23, 369-375, 1975).

While the invention has been described in terms of its preferred embodiments, those skilled in the art will recognize that the invention can be practiced with modification within the spirit and scope of the appended claims.

* * * * *

Images

View Shopping Cart

Add to Shopping Cart

Hit List

Top

Home

Boolean

Manual

Number

Help

Paper No.
212

CORROSION 98

INORGANIC CR-FREE CONVERSION COATINGS FOR HIGH CORROSION RESISTANCE AND LOW ELECTRICAL CONTACT RESISTANCE

R.G. Buchheit
The Ohio State University
Department of Materials Science and Engineering
Columbus, Ohio 43210

M.A. Martinez, L.P. Montes
Sandia National Laboratories
P.O. Box 5800
Albuquerque, New Mexico 87185

N. Cella, G.E. Stoner, S.R. Taylor
University of Virginia
Department of Materials Science and Engineering
Charlottesville, Virginia 22903

ABSTRACT

Many military applications require that conversion coatings for aluminum alloys provide high corrosion resistance while retaining low electrical contact resistance. In this paper, the performance requirements for Class 1A and Class 3 conversion coatings established in Military Specifications MIL-C-81706 and MIL-C-5541E are summarized. The corrosion resistance and electrical contact resistance of actual Class 1A and Class 3 coatings are presented. Results show that the required levels of performance are usually achieved on wrought alloys, but not on cast alloys. The corrosion resistance and electrical contact resistance of Cr-free conversion coatings has also been examined. Results indicate that the required performance levels are rarely achieved on any type of alloy substrate. Last, corrosion and electrical properties of coatings formed using methods based on low-toxicity alkaline oxide coatings procedures are described. Results from initial attempts to produce highly corrosion resistant coatings with low electrical resistance are presented.

Keywords: Conversion coatings, Cr-free conversion coatings, electrochemical impedance spectroscopy, salt spray exposure, electrical contact resistance.

INTRODUCTION

In many industrial applications, chromate conversion coatings are applied to aluminum alloys to promote corrosion resistance and to promote paint adhesion. In military applications, chromate conversion coatings are often required to provide high corrosion resistance while retaining low electrical contact resistance. Low electrical contact resistance is required ensure that mating surfaces are at the same potential

Copyright

©1998 by NACE International. Requests for permission to publish this manuscript in any form, in part or in whole must be made in writing to NACE International, Conferences Division, P.O. Box 218340, Houston, Texas 77218-8340. The material presented and the views expressed in this paper are solely those of the author(s) and are not necessarily endorsed by the Association. Printed in the U.S.A.

(usually ground), or to ensure information surety by screening external electrical noise. Generic examples of components requiring high corrosion resistance and low electrical contact resistance are: electrical power connectors, data transmission connectors, connector land areas, chassis for circuit boards, and mating surfaces for housings and casings. These parts are normally subject to exposures ranging from marine-atmospheric involving intermittent condensation, to inert gas. Corrosion protection is normally supplied to aluminum surfaces to avoid forming loose corrosion product that may interfere with system operation. Conversion coating performance requirements vary from application to application, but coatings are normally supplied in accordance with MIL-C-5541E "Chemical Conversion Coatings on Aluminum and Aluminum Alloys", and MIL-C-81706 "Chemical Conversion Materials for Coating Aluminum and Aluminum Alloys". These specifications establish acceptable materials for preparing coatings, and minimum performance levels for corrosion resistance and electrical contact resistance for chromate conversion coatings in proof testing.

The performance levels established in these specifications can also be used as the basis for proof testing to judge the adequacy of Cr-free conversion coatings for military applications. This paper summarizes the performance requirements in the Military Specifications and presents corrosion resistance and electrical contact resistance properties of commercial chromate conversion coating. Corrosion resistance and electrical contact resistance of commercial and developmental Cr-free conversion coatings is also presented. Results show that few of the Cr-free coatings meet the specified performance levels, and few give the mix of properties that chromate coatings provide. Early results from a work to specifically intended to devise corrosion resistant Cr-free conversion coatings with low electrical contact resistance are also presented.

EXPERIMENTAL PROCEDURES

Materials. Aluminum alloys 356 (Al-7.0Si), 2024-T3 (Al-4.5Cu-1.5Mg-0.6Mn), 6061-T6 (Al-1.0Mg-0.6Si), and 7075-T6 (Al-5.6Zn-2.5Mg-1.5Cu) were used as substrates on which various conversion coatings were applied. The 2024-T3, 6061-T6 and 7075-T6 samples were cut into 4 x 5 in. panels from 0.080 in. thick sheet stock with an ASTM B209 mill finish surface. The 356 samples were cast panels measuring 4 x 6 x 0.125 in. No special surface treatment was conducted other than alkaline degreasing, acid deoxidizing, and conversion coating.

Coatings. Commercial and developmental Cr-free conversion coatings were applied to alloy substrates by three coating chemical vendors. These vendors were selected on performance in the NCMS Chrome Alternatives Study which surveyed the corrosion, paint adhesion, and electrical contact resistance properties of approximately 30 chromate free conversion coatings for aluminum alloys (1). The vendors were instructed to supply coatings that conformed with MIL-C-5541E class 3 performance definitions (coatings applied for corrosion resistance where low electrical contact resistance is required). The vendors were then allowed to select the specific coating system from their suite of products. The only constraints placed on the processing were that the coating was to be predominantly inorganic, and free of intentionally introduced chromium compounds. Table 1 lists the generic characteristics of the coatings supplied.

Chromate conversion coatings were also prepared on alloy substrates to serve as controls. The control coatings were also applied to conform with the MIL-C-5541E Class 3 definition.

Corrosion Testing. Corrosion resistance was tested using electrochemical impedance spectroscopy and salt spray exposure. Salt spray testing was conducted according to ASTM B117. Results were evaluated

according to the MIL-C-5541E 5 pit-per-panel pass/fail criterion. Panels were visually inspected at periodic intervals for exposure times up to 336 hours (14 days).

EIS spectra were collected from a 20 cm² area of conversion coated surface that had been exposed to aerated 0.5 M NaCl solution for 24±1 hours. Spectra were collected from 10 kHz to 10 mHz at a sampling at a rate of 7 points per decade frequency using a 10 mV sinusoidal voltage perturbation. The EIS measurement was conducted at the open circuit potential of the sample. Two experiments were conducted for each sample.

The EIS data were analyzed using a simplified equivalent circuit model proposed to account for corrosion damage occurring on chemically passivated aluminum alloys surfaces (2). From this analysis a coating resistance, R_c , and coating capacitance, C_c , were extracted. The R_c value was used as the figure of merit to assess the level of corrosion protection offered by the conversion coating.

Electrical Contact Resistance Testing. Electrical contact resistance measurements were performed by pressing a flat, polished 1.0 in.² copper platen on the coated aluminum surface under a 200 lb. load. Resistance was measured with a meter accurate to 10 μ ohms. Four to ten measurements were made per sample. The number of measurements made depended on available sample area (3,4).

RESULTS AND DISCUSSION

Performance requirements established in MIL-C-81706 and MIL-C-5541E. MIL-C-81706 "Chemical Conversion Materials for Coating Aluminum and Aluminum Alloys", and MIL-C-5541E "Chemical Conversion Coatings on Aluminum and Aluminum Alloys" define performance levels, processing methods, and chromate chemicals acceptable for military applications. These specifications are also widely used, in whole or in part, in establishing requirements for many non-military applications. The main performance attributes defined in these specifications are corrosion resistance, paint adhesion and electrical contact resistance.

MIL-C-81706 defines two classes of coatings which are distinguished by the main coating performance attributes. Class 1A coatings are intended for maximum protection against corrosion in situations where the conversion coated surface is either painted or unpainted. Class 3 coatings are intended for use where corrosion protection and low electrical contact resistance are required. For chromate conversion coatings the primary difference in Class 1A and Class 3 coatings is thickness. Class 3 coatings are typically thinner (20-40 mg/ft.²) than the more corrosion resistant Class 1A coatings (20 - 90 mg/ft.²) (5).

MIL-C-81706 also defines two performance levels for these coatings. Higher performance is required for "qualification", and lower performance is acceptable for "quality conformance". Coatings must meet the qualification requirements in order to be placed on the MIL-C-81706 Qualified Products List. The quality conformance requirements are typically those used for lot inspection and quality control. These requirements are found in the specification and are summarized in Table 2.

The performance requirements in MIL-C-5541E are less stringent than those in MIL-C-81706. To obtain a pass ranking for corrosion resistance according to the MIL-C-81706 specification all panels (5 total panels, 150 in.²) "shall show no evidence of corrosion whatever when compared to unexposed panels with the naked eye except in those areas within 1/4 inch from the edges (etc.)" when subjected to salt spray exposure testing. To obtain a pass ranking per MIL-C-5541E, a single panel can have "no more

than 5 isolated spots or pits none larger than 0.031 inches in diameter after salt spray exposure testing". Additionally, "no more than 15 isolated spots or pits, none larger than 0.031 inches in diameter, (shall be present) on the combined surface area of all 5 specimen panels". As a rule, a pit is countable if it leaves a visible corrosion product stain or "tail" on the panel surface.

MIL-C-5541E defines performance criteria for process control (quality control) and for lot acceptance. These performance requirements are summarized in Table 3. The lot acceptance criteria are essentially visual inspection of as-coated surfaces to insure that conversion coated surfaces are uniform and flaw-free.

MIL-C-81706 directs that electrical contact resistance measurements be made on coated alloy surfaces with a contact area of 1 square inch and load of 200 pounds. The average contact resistance shall be less than 5 milliohms per square inch for as-coated surfaces, and less than 10 milliohms per square inch for panels exposed to ASTM B117 salt spray for 168 hours. Individual readings greater than 20% of the specified maximum are acceptable provided the overall average for the set of measurements is below the specified limit. For MIL-C-81706 Class 3 coatings qualification, measurements are to be made on 5 individual 6061-T6 panels. No electrical contact resistance measurements are required for quality conformance inspection. MIL-C-5541E does not specify performance requirements other than to indicate that the performance level is to suit the needs of the application for the procuring activity.

Corrosion resistance and electrical contact resistance of chromate conversion coatings. Table 4 summarizes corrosion resistance and electrical contact resistance data for Class 3 and Class 1A chromate conversion coatings applied to 6061-T6, 7075-T6, and 356. Class 3 coatings are replicate coatings applied by the same vendor. The Class 1A coatings were prepared by the same vendor, but were produced in different chromate bath chemistries. The table indicates whether a coating passed or failed a salt spray exposure test according to the MIL-C-5541E 5-pit-per-panel criterion. Pass and fail rankings were determined after 168 and 336 hours of exposure. Corrosion resistance was also determined by standardized EIS testing (2). Coating resistance, R_c , data are given for each alloy-coating combination. Last, a measure of coating electrical contact resistance is given. Contact resistances were determined according to the procedures described in MIL-C-5541E. No contact resistance data were collected from samples after exposure to salt spray.

For qualification and quality conformance testing, Class 3 coatings must be tested on 6061-T6 substrates only. The corrosion resistance requirement is that no corrosion occur after 168 hours of salt spray exposure and that a contact resistance of $5 \text{ m}\Omega/\text{in.}^2$ or less be exhibited. The data of Table 4 indicate that the Class 3 coatings examined in this study would meet the requirements. Standardized impedance measurements for corrosion resistance yielded coating resistance values of 0.2 and $1.0 \text{ M}\Omega/\text{cm}^2$ which are large for coatings of this type.

Performance on 7075-T6 substrates is not specified, but the data in Table 4 indicate that Class 3 coatings pass 168 hours of salt spray exposure and have contact resistances less than $5 \text{ m}\Omega/\text{in.}^2$. The Class 3 coating does not meet the corrosion or contact resistance requirements on 356 although the contact resistances are not far above the $5 \text{ m}\Omega/\text{in.}^2$ limit.

Class 1A coatings are intended for use in applications where maximum corrosion resistance is required. However in this study some class 1A coatings exhibited low electrical contact resistances on alloys other than 6061-T6.

Corrosion resistance and electrical contact resistance of commercially available Cr-free conversion coatings. Figure 1 is a plot of electrical contact resistance and corrosion resistance data from a broad range of chromate and non-chromate conversion coatings. In this plot, coating corrosion resistance is plotted on the abscissa as coating resistance, R_c , determined by EIS. Electrical contact resistance is plotted on the ordinate. Each data point represents an individual coating-alloy substrate combination. Commercial chromate conversion coatings are represented by closed data points. Chromate-free conversion coatings are represented by open data points. Data points in region 'A' represent coatings with corrosion resistances greater than $1 \text{ M}\Omega\text{-cm}^2$ and electrical contact resistances less than $5 \text{ m}\Omega/\text{in.}^2$. These coatings are likely to meet the performance requirements established in the military specifications. Data that fall in region 'B' exhibit coating resistances between 0.5 and $1.0 \text{ M}\Omega\text{-cm}^2$ in EIS testing and have contact resistances between 5 and $10 \text{ m}\Omega/\text{in.}^2$ in contact resistance tests. These coatings are considered to be marginal and may, in some cases, meet the performance requirements in the military specifications. Data that fall in region 'C' exhibit coating resistances less than $0.5 \text{ M}\Omega\text{-cm}^2$ and have electrical contact resistances greater than $10 \text{ m}\Omega/\text{in.}^2$. These coatings are considered to be unlikely to satisfy military specification performance requirements.

On the basis of these results three coating vendors were selected to provide coatings to meet the Class 3 coating requirements. The generic characteristics of the coating chemistry and processing were given in Table 1.

Corrosion resistance and electrical contact resistance data for the three coatings are summarized in Table 5. The data show that Cr-free conversion coating number 2 (based on Mn chemistry) meets the performance requirements for Class 3 coatings because it meets these requirements on 6061-T6 substrates. Coatings 2 and 3 meet the Class 3 requirements on 7075-T6, but none of the coatings meet the performance requirements on 356. It should be noted, in this study, none of the commercial chromate conversion meet the Class 3 requirements.

Corrosion resistance and electrical contact resistance of hydrotalcite coatings sealed with transition metal salt solutions. In prior work it was discovered that transition metal oxides rapidly precipitated from neutral solutions onto fresh hydrotalcite coatings [3]. This occurs because most transition metals have exceedingly low solubility in alkaline solutions. Fresh hydrotalcite coatings are moist and very alkaline. Contact with neutral transition metal salt solutions induces vigorous transition metal oxide precipitation on the hydrotalcite. A group of transition metal salts were selected to determine if corrosion resistance could be improved while retaining or imparting low electrical contact resistance. Transition metal oxides exhibit a wide range of electrical conductivities and a group of metal oxides were selected to span the range available. Figure 2 is a plot of electrical contact resistance determined according to MIL-C-5541E plotted versus the coating resistance, R_c , determined in the standard EIS test. In general, coatings with low electrical resistance also provided the lowest corrosion resistance. This behavior is consistent with the notion that conductive coatings permit reduction reactions to be supported at high enough rates to drive pitting corrosion. Insulating oxides like those associated with Fe, Ni, and Co suppress cathodic reactions lowering the driving force for pitting. Notable exceptions to this trend are Ce(IV) and Rh. These transition metal sealants have been selected for further study.

SUMMARY

In some applications, conversion coatings for Al alloys must provide high corrosion resistance and low electrical contact resistance. Achieving this mix is difficult because a conductive coating can facilitate galvanic corrosion action which lowers corrosion resistance. Nevertheless, traditional chromate conversion

coatings provide these attributes. A survey of Cr-free conversion coatings shows that very few provide a mix of high corrosion resistance and low electrical contact resistance that chromate conversion coatings do. This severely limits choices in procurement of Cr-free conversion coatings for military applications, and defines an area where development work could be focused. Last, Cr-free hydrotalcite coatings normally exhibit high electrical contact resistance. However, initial studies show that appropriate types of post treatment can increase corrosion resistance and decrease electrical contact resistance.

ACKNOWLEDGMENTS

Sandia is a multiprogram laboratory operated by Sandia Corporation, a Lockheed Martin Company, for the United States Department of Energy under contract DE-AC04-94AL85000.

REFERENCES

- 1.) Alternatives to Chromium for Metal Finishing, Final Report 0273RE95, NCMS Project No. 02-17-0403, National Center for Manufacturing Sciences, Ann Arbor, MI (1995).
- 2.) R.G. Buchheit, M. Cunningham, H. Jensen, M.W. Kendig, M.A. Martinez, "A Correlation Between Salt Spray and EIS Test Results for Conversion Coated Aluminum Alloys" Corrosion accepted for publication April, 1997.
- 3.) L.J. Bailin, P. Fitzpatrick, M.J. Joyce, "Evaluation of Unpainted Alodine Chromate Conversion Coatings for Corrosion Resistance and Electrical Conductivity", Lockheed Missiles&Space Co., Inc., Palo Alto, CA, LMSC-F035575 Rev. A, Appendix E, June, 1985.
- 4.) J. L. Finch, Procedure for Contact Electrical Resistance Measurements As Developed for Use at Sandia National Laboratories", SAND94-1108, June, 1994.
- 5) Coating, Chromate on Aluminum", Sandia Specification 9904151-02, August, 1989.

Table 1. Generic characteristics of Cr-free coatings examined for conformance with MIL-C-81706 Class 3 performance requirements.

Coating	Primary coating ingredients and processes
Commercial Cr-free 1	Non-electrolytic immersion in an acid solution containing Zr compounds and fluoride compounds. Elevated temperature post coating drying treatment used.
Commercial Cr-free 2	Non-electrolytic immersion in a solution containing Mn as the primary ingredient. Elevated temperatures used during processing.
Commercial Cr-free 3	Non-electrolytic immersion in a solution containing Co and amine compounds. Coated surfaces are then sealed in a solution containing W and V compounds.

Table 2. Summary of MIL-C-81706 performance requirements.

Corrosion Resistance Properties			
	Class	Alloy Substrates (number of panels)	Performance Requirement
For Qualification	1A	2024-T3 and 7075-T6 (5 ea.)	No evidence of corrosion after 336 hours of ASTM B117 Salt Spray Exposure
	3	6061-T6 (5)	No evidence of corrosion after 168 hours of ASTM B117 Salt Spray Exposure
For Quality Conformance Inspection	1A	2024-T3 (5)	No evidence of corrosion after 168 hours of ASTM B117 Salt Spray Exposure
	3	6061-T6 (3)	No evidence of corrosion after 168 hours of ASTM B117 Salt Spray Exposure
Electrical Contact Resistance			
For Qualification	3	6061-T6 (5)	Contact resistance less than 5 mΩ/in. ² prior to salt spray, and less than 10 mΩ/in. ² after 168 hours of salt spray exposure
For Quality Conformance Inspection	not required		

Table 3. Summary of the MIL-C-5541E process control performance requirements.

Property	Class	Alloy Substrates (number of panels)	Test	Performance Requirement
Corrosion Resistance	1A	2024-T3 (5)	Salt Spray Exposure per ASTM B117	< 5 pits per panel < 15 pits per 5 panels
	3	6061-T6 or 2024-T3 (5)	Salt Spray Exposure per ASTM B117	< 5 pits per panel < 15 pits per 5 panels
Electrical Contact Resistance	none			

Table 4. Summary of corrosion resistance and electrical contact resistance data for Class 1A and Class 3 chromate conversion coatings applied to various alloy substrates.

Corrosion Resistance					
Alloy and Coating Type		Salt Spray		Coating Resistance from EIS [†] log R _c (R _c in Ω-cm ²)	Electrical Contact Resistance ^{††} (mΩ/in ²)
		168h 336h			
6061-T6	Class 3	pass	pass	6.21	2.29
		pass	fail	5.34	2.4
	Class 1A	pass	fail	6.66	0.40±0.2
		pass	pass	6.04	0.61±0.2
		pass	pass	5.90	0.48±0.2
		pass	pass	5.45	1.06±0.3
7075-T6	Class 3	pass	fail	6.74	1.05
		pass	fail	6.71	0.52
	Class 1A	pass	pass	7.05	19.7±6
		pass	pass	6.08	31.2±14
		pass	pass	6.08	73.0±25
		pass	fail	5.59	2.22±3.1
356	Class 3	fail	fail	6.37	9.38
		fail	fail	6.05	3.65
	Class 1A	pass	fail	5.36	1.31±1
		pass	fail	6.05	0.96±0.6
		pass	fail	6.56	4.39±2.5

[†] average of two measurements

^{††} values without uncertainties are single point measurements, values with uncertainties are averages of 8 measurements.

Table 5. Summary of corrosion resistance and electrical contact resistance data for Cr-free conversion coatings applied to 356, 6061-T6, and 7075-T6 substrates.

Alloy and Coating Type	Corrosion Resistance		Coating Resistance from EIS [†] log R _c (R _c in Ω-cm ²)	Electrical Contact Resistance ^{††} (mΩ/in ²)
	Salt Spray			
	168h 336h			
6061-T6				
Commercial Cr-free 1	fail	fail	4.53	1.95±1.9
Commercial Cr-free 2	pass	pass	5.46	0.23±0.1
Commercial Cr-free 3	fail	fail	4.91	2.02±1.0
7075-T6				
Commercial Cr-free 1	fail	fail	4.91	483±280
Commercial Cr-free 2	pass	pass	5.83	3.20±4.0
Commercial Cr-free 3	pass	pass	6.02	2.48±0.6
356				
Commercial Cr-free 1	fail	fail	4.53	3.11±1.2
Commercial Cr-free 2	fail	fail	5.46	1.10±1.0
Commercial Cr-free 3	fail	fail	4.91	0.80±0.3

[†] average of two measurements

^{††} averages of 8 measurements.

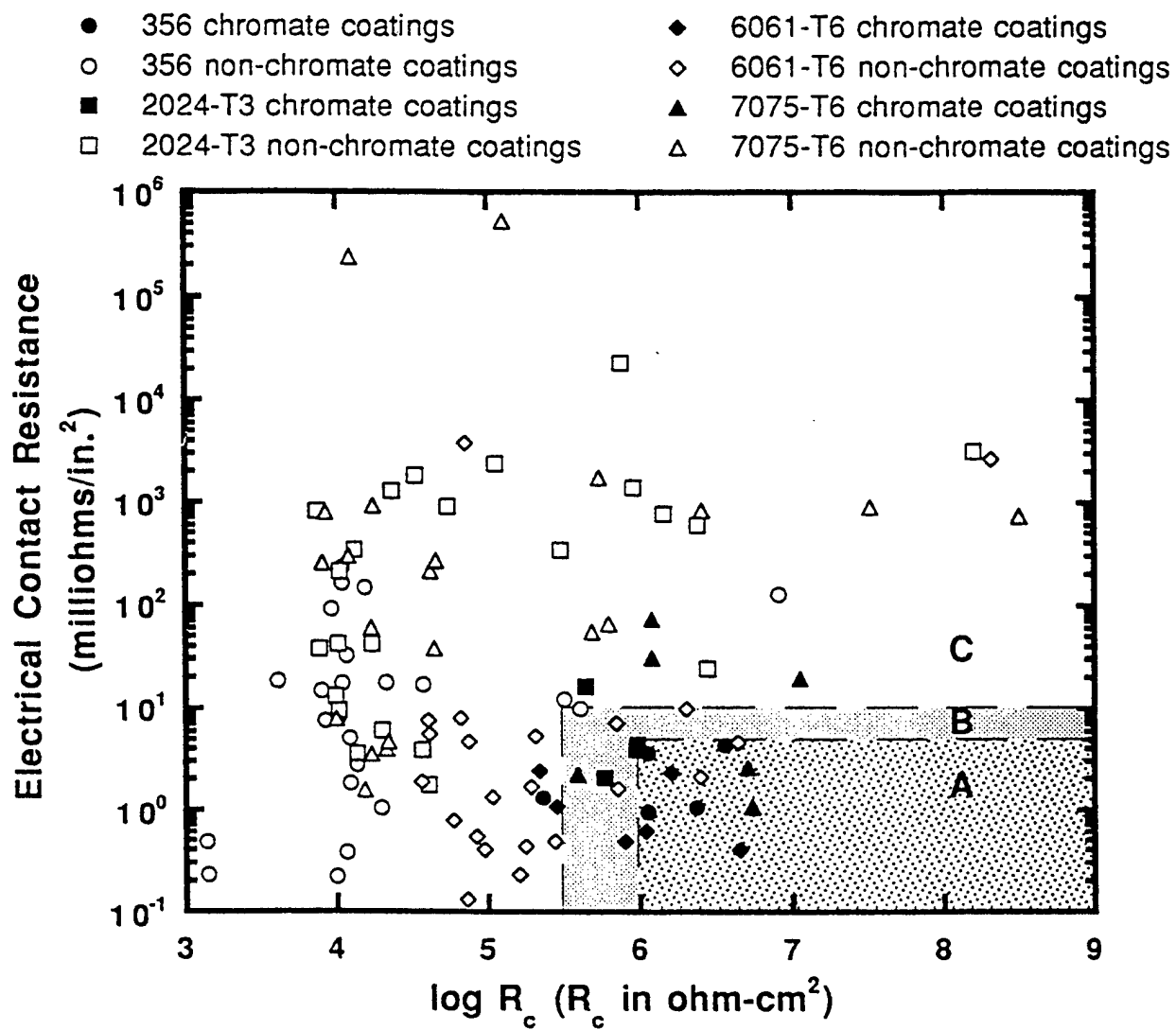


Figure 1. Electrical contact resistance and coating corrosion resistance determined by EIS for chromate and chromate-free conversion coatings applied to a variety of Al alloy substrates.

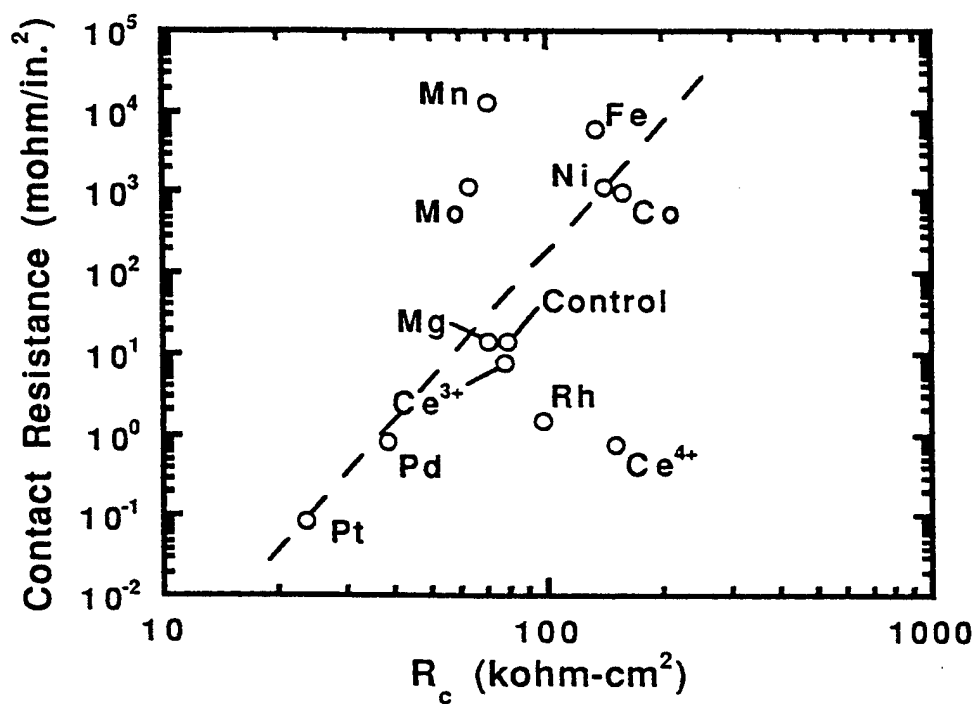


Figure 2. Plot of electrical contact resistance determined according to MIL-C-5541E versus coating resistance, R_c , for transition metal sealed hydrotalcite coatings.

Submitted to *Corrosion* (in press)

**Corrosion Performance of Field Applied
Chromate Conversion Coatings**

R.B. Leggat *, S.R. Taylor *, W. Zhang **, R.G. Buchheit **

* Center for Electrochemical Science and Engineering
University of Virginia
Charlottesville, VA 22903

** Fontana Corrosion Center
The Ohio State University
Columbus, OH 43210

Abstract

Alternative conversion coatings designed to replace chromate conversion coatings (CCCs) are typically compared to laboratory prepared CCCs with regards to stand-alone corrosion performance. This study seeks to determine the stand-alone corrosion resistance of field-applied CCCs in order to establish a more realistic benchmark for new non-chromate conversion coatings. Salt spray exposure, wet tape adhesion tests and measurement of electrical contact resistance were performed according to the military specifications that govern what conversion coatings are accepted for use by DOD facilities. In addition, other analytical techniques such as electrochemical impedance spectroscopy and auger electron spectroscopy depth profiling were employed.

In an initial study, all of the field-applied coatings on AA2024, AA6061 and AA7075 displayed significant pitting after 168 hours salt spray exposure. Additionally, attention in pre-cleaning the surface prior to coating was found to increase CCC corrosion resistance.

Based on the results of the field-applied coatings, a second phase of investigation was initiated to examine the effects of coating time and application method (spray versus immersion) on the corrosion resistance and paint adhesion. This study was conducted using facilities designed to simulate conditions in an aircraft maintenance depot. It was found that spray and immersion application produced coatings with equivalent performance. Regardless of application method, five-minutes of continuous exposure to solution was required to obtain adequate coating weight.

The results of this study suggest that a review of the relevant military specifications is merited so that emerging, environmentally benign conversion coatings can be evaluated against an appropriate metric.

Key Words: adhesion, aluminum aerospace alloys, chromate conversion coating, corrosion resistance, electrical contact resistance, military specifications, salt spray.

Introduction

Conversion coatings are applied to metals in order to increase corrosion resistance and increase adhesion of subsequently applied organic coatings. A conversion coating is the result of two chemical reactions: dissolution of the native surface oxide and formation of a more corrosion resistant, inorganic compound of the original metal¹.

Chromate conversion coatings (CCCs) are the most common conversion coatings applied to aluminum aerospace alloys. Although CCCs provide excellent corrosion resistance and adhesion, many of the chemicals used in the processing are under strict regulation due to their toxicity. Epidemiological studies have established the carcinogenicity of hexavalent chromium^{2,3}. The worker health and safety risks of using chromate-based conversion coatings are compounded by effluent disposal costs⁴. Thus, the health risks and cost of producing chromate conversion coatings has driven the development of non-toxic, environmentally benign alternatives, which have recently been reviewed by Nylund⁵.

Presently CCCs remain an essential component in effective corrosion protection systems on aluminum alloys for military applications. In order for candidate non-chromate conversion coatings to gain attention as viable candidates for use by the Department of Defense, they must meet the requirements of two military specifications: (1) MIL-C-81706, "Chemical Conversion Coatings for Coating Aluminum and Aluminum Alloys", and (2) MIL-C-5541, "Chemical Conversion Coatings on Aluminum and Aluminum Alloys".

The two aforementioned specifications both govern the same systems (i.e. chromate conversion coatings on aluminum) but have important differences with regards to whether it is the process or the end product that is monitored. MIL-C-81706 is a "materials" specification and defines the characteristics of the conversion coating chemistry including appearance and properties of the applied coating. This specification differentiates two classes of coatings, 1A and 3, depending on the intended purpose of the coating. Class 1A coatings are used when maximum corrosion protection is needed, while Class 3 coatings are used when corrosion protection and low electrical contact resistance are needed. In addition, MIL-C-81706 specifies two levels of performance for qualification and quality conformance. In order to be placed on the Qualified Products List (QPL) associated with MIL-C-81706 (QPL-81706), a product must perform at the qualification level. The quality conformance requirements are used mainly for quality control and lot inspection. On the other hand, MIL-C-5541 is a "process" specification and defines the characteristics of a coating applied in a production environment. This specification defines the requirements for monitoring the processes used in coating production and is independent of the materials that are used. A "process" specification is typically used when the properties of the end product are not easily measured. The process is controlled assuming that the product will be within specification as long as the process is within its parameters.

Under the military specifications, corrosion performance of conversion coated aluminum is assessed by exposure to five percent salt spray according to ASTM B117⁶. The corrosion resistance requirements are more rigorous for MIL-C-81706 than MIL-C-5541. In order to meet MIL-C-81706 requirements, no evidence of corrosion with the exception of $\frac{1}{4}$ " of the edge is allowed after exposure of five panels for a specified time.

The required exposure time varies depending on the alloy and coating class as shown in Table 1. Under MIL-C-5541, a single panel can have no more than 5 pits and no more than a total of 15 pits for five panels in order to meet the requirement.

In addition to corrosion resistance, these two military specifications also mandate adhesion performance, electrical contact resistance and coating weight. Adhesion of an epoxy primer and topcoat to the conversion coating is satisfactory for both military specifications when no intercoat separation is observed after wet tape testing per Method 6301 of Federal Test Method Standard Number 141⁷. Electrical contact resistance of less than 5 m Ω cm⁻² for as coated surfaces and less than 10 m Ω cm⁻² post salt spray exposure are required by MIL-C-81706. A coating weight of at least 40 mg / ft² is required by MIL-C-81706 for Class 1 coatings.

These stringent military specifications, although initially developed for CCCs, are presently used as the benchmark for new non-chromate conversion coatings. The corrosion resistance, paint adhesion, and electrical contact resistance of twenty-nine chromate-free conversion coatings on test panels of five aluminum alloys were evaluated using military specifications in a study by the National Center for Manufacturing Sciences⁸. In this study, the coatings were applied by immersion in each of the respective manufacturer's laboratories. In a similar study on vendor-prepared, spray-applied coatings by the Air Force Research Laboratory, ten conversion coating systems were evaluated⁹. These studies indicate that while progress has been made in the area of alternative conversion coatings, they do not compare well to CCCs when tested according to these military specifications.

The common understanding of the structure, chemistry, and performance of CCC has been developed through examination of coatings applied by immersion processing normally under ideal or near ideal conditions. However, it is likely that coatings applied during normal aircraft depot maintenance are considerably different. These coatings are applied by spraying using contact times that are relatively short. Thus, the goal of this study is to characterize coatings formed using flightline (or field) application methods.

This study consisted of two related investigations. The first was conducted at an Air Logistic Center (ALC), which are the actual facilities used when a plane is brought in for scheduled maintenance. The results from the initial investigation prompted a second investigation, in which samples were prepared by the Coatings Technology Integration Office (CTIO) of the Air Force Research Labs using specially designed laboratories to simulate the environmental conditions of the different ALCs that support the fleet. The follow-up study was conducted at this facility in an attempt to reproduce the conditions of initial study at the ALC depot.

Experimental

Air Logistic Center Applied Coatings.

CCCs were formed on 4"x5" coupons of three different alloys: 2024-T3 (UNS 92024, Al-4.4Cu-1.5Mg- 0.6Mn), 6061-T6 (UNS 96061, Al-1.0Mg- 0.6Si), and 7075-T6 (UNS 97075, Al-5.6Zn-2.5Mg-1.6Cu). The as-received samples were initially subjected to a deoxidizing pretreatment using a phosphoric acid/nitric acid solution. The deoxidizing solution was spray-applied and permitted to contact the samples for a total of five minutes prior to rinsing with tap water. The samples were then conversion coated by

spray application using Turco Alumigold B*, which is a MIL-C-81706 qualified product. The conversion coating solution was in contact with the panels for five minutes, then the samples were rinsed and allowed to dry.

A second batch of panels was then prepared using the same general procedures as just described. However, these panels were manually abraded with non-metallic ScotchBrite* pads while in contact with the deoxidizing solution for twelve minutes.

After drying overnight, selected panels were primed and topcoated, again using standard ALC procedures and materials. The spray-applied primer was a two part, high solids epoxy with a maximum of 340 g/L volatile organic content. After drying, a high solids polyurethane topcoat was spray applied.

The panels were subsequently tested as standalone CCCs, and as candidate coating systems (CCC + primer + topcoat). In addition to the testing required by the military specifications, other analytical methods were employed. The weight of the CCC was measured according to MIL-C-81706. The panels were weighed, stripped in nitric acid, and re-weighed to determine coating weight. Powder scraped from the CCC panels was analyzed by X-ray diffraction (XRD). The surface of the CCC panels were inspected by scanning electron microscopy (SEM). The electric contact resistance was measured using a 1-in² copper contacting electrode under a load of 200 lbs per MIL-C-81706. Compositional depth analysis was performed using Auger electron spectroscopy (AES). A 3keV Ar⁺ ion beam was used for sputtering. The 66, 210, and 229 eV peaks were monitored for aluminum, oxygen, and chromium.

The corrosion resistance of the panels receiving the CCC treatment alone was assessed by electrochemical impedance spectroscopy (EIS) and salt spray. EIS was performed after 24 hours exposure to 0.5M NaCl. A metric indicative of corrosion resistance, R_{corr} , was fit from the spectra using a non-linear least squares program. The R_{corr} is the polarization resistance minus diffusional impedance and has previously been used in the analysis of conversion coated aluminum alloys¹⁰. Salt spray exposure was done according to ASTM method B117. The coatings were ranked by time to failure. Visual detection of 5 or more pits per panel constituted a failure.

Testing of primed samples was done according to MIL-PRF-85285 "Performance Specification Primer Coatings: Epoxy, High-Solids" because any conversion coating would be expected to eventually perform as part of a coating system that would include a primer coat. Adhesion was tested by the wet tape test according to ASTM D3359 Test B¹¹. This method conforms to the military specifications with the exception of a cross-hatch cut of the paint rather than an X-cut. This modification was used because it is more quantitative. The coated sample is exposed to distilled water for 24 hours prior to introduction of the lattice cuts through the film to the substrate. Pressure sensitive tape is laid across the lattice and then removed. The samples are ranked from 0-5 by comparison with descriptions and images. A ranking of 5 is given for a sample displaying no paint removal and a ranking of 0 is given for 65 percent or greater paint removal as seen in Table 2.

Lab Simulated Coatings

* Trade name

* Trade name

Based on the results of the ALC-prepared samples, a follow-up study was designed to examine the effect of chromate conversion coating time and the effect of application method. The study was limited to aluminum alloy 2024-T3. The panels were manually abraded prior to degreasing for 20 minutes at 100°F. Panels were then deoxidized for 2 minutes in 18% phosphoric acid at room temperature. Both immersion and constant overflow spray of Alumigold B were used for application of the CCC. Exposure times of 2, 5, and 9 minutes were used. The coating solution had been made three days prior. The coating times were chosen to assure that a coating weight of 40 mg/ft² was achieved based on calibration experiments made at the time of the solution preparation. During spray application, the panels were held in racks at 45° with a constant overflow of solution. After drying overnight, selected panels were primed using a two-part, high solids epoxy. In addition, a fraction of the primed panels were topcoated with high solids polyurethane.

The testing was similar to that done for the initial study. Some of the testing performed in the initial study was limited to the samples with nine-minute exposure times as seen in Table 3. In addition to the wet tape test, the pull-off tensile strength of the epoxy primer was tested according to ASTM method D4541 using a Type IV self-alignment adhesion tester¹².

Panels receiving the CCC, primer, and topcoat were scribed and exposed to salt spray according to ASTM B117. The exposure time was 2,000 hours. MIL-PRF-85285 requires that “the primer coating, with and without a topcoat, shall not exhibit blistering, lifting of either coating, nor substrate corrosion”. Filiform testing, also required by MIL-PRF-85285, was not performed.

Results and Discussion

Air Logistic Center Applied Coatings

As can be seen in the EIS test results shown in Table 4, the samples that were abraded prior to conversion coating had higher average R_{corr} values for all three alloys. Previous studies of conversion coated aluminum alloys have proposed a correlation between the R_{corr} parameter and salt spray performance¹⁰. Based on the results of this earlier study, conversion coatings on AA2024 and AA6061 with R_{corr} values greater than $2 \times 10^6 \Omega\text{cm}^2$ are expected to pass 168 hours of salt spray exposure, while an R_{corr} value of at least $1.5 \times 10^7 \Omega\text{cm}^2$ is required for coatings on AA7075. Using these proposed threshold values, only the abraded AA6061 coatings were expected to pass 168 hours salt spray.

Regardless of pretreatment, little or no weight change was detected after stripping the CCC, indicating that the coatings were very thin. On the basis of coating weight, these coatings would qualify as Class 3 because their weight was less than 40 mg/ft². Class 1A films, used for maximum corrosion resistance, require 40 mg/ft². Therefore, based on film weight alone, these coatings were not expected to survive 168 hours salt spray. Even though the weights of the ALC-applied CCCs were very low, the contact resistance of the films was higher than that specified for a Class 3 coating. The electrical contact resistance for the coatings on AA2024, AA6061, and AA7075 were 9, 12, and 12 mΩin⁻², respectively. The military specifications require an electrical contact resistance of no more than 5-mΩin⁻².

The salt spray performance is shown as fraction failed per observation time in Table 5. Only the abraded AA6061 coatings passed the 168 salt spray exposure required for quality conformance by MIL-C-81706. This was predicted by the R_{corr} values obtained from the EIS testing. As previously mentioned, the R_{corr} threshold proposed for predicting salt spray performance of AA7075 is higher, therefore the AA7075 coating was not expected to pass.

The rankings from the wet tape test are shown in Table 6. MIL-C-5541 specifies no separation. Coatings receiving a rank of 4 or 5 were considered to have passed. It can be seen that the ALC-applied CCCs were able to provide passing adhesion results for the majority of samples. Pretreatment (*i.e.*, abraded vs. non-abraded) or alloy type did not effect the adhesion results.

XRD indicated that the CCC was amorphous regardless of alloy or pretreatment. No other compounds were detected. The peaks seen in the XRD spectra are from aluminum metal that was removed with the conversion coating by the scraping process (Figure 1). The SEM image shown in Figure 2 reveals that the surface of the coating is rough and apparently inhomogeneous. This appearance is typical of CCCs whether they are applied in the field or in the lab^{13,14}.

The AES depth profiles shown in Figure 3 varied considerably among the different alloys for the panels receiving no pretreatment. On the other hand, the depth profiles of the conversion coating on abraded panels were much more consistent for the different alloys. The coating non-uniformity on the panels that received no pretreatment is evident in the photograph shown in Figure 4.

Based upon the results of this study, none of the field-applied (ALC-applied) coatings would have qualified as a Class 1A coating. For these coatings, it can be seen that pretreatment by abrasion during the deoxidation process made a significant improvement in the conversion coating performance. The difference between abraded and non-abraded samples is likely due to the tenacious rolling oils present on as-received sheet stock. It should be noted that MIL-C-5541 does require that the base metal be cleaned such that a "water break-free surface" is obtained.

Lab Simulated Coatings

A follow-up study was designed to address issues raised by the ALC study. A study by the Air Force Research Laboratory had suggested that 2 minutes of constant overflow during spray application was necessary to obtain sufficient coating weight⁹. In addition, the effect of the application method (spray vs. immersion) was of interest.

Coating weight measurements were made for all coating times (2, 5, and 9 minutes) and for both application methods (spray and immersion). Based on the coating weights shown in Table 7, the required 40 mg/ft² was achievable only for the five and nine minute exposure times for both application methods. The values listed for the spray application are based on a coating area of 0.28 ft² (2 sides x 4" x 5" x .007 ft²/in²). This area is artificially high because only one side was directly sprayed although both sides were in contact with the solution to some degree. Therefore, the calculated weights for the spray-applied coatings are believed to be artificially low. Based on the requirement of 40 mg/ft² for Class 1A coatings, the coatings with five and nine-minute exposure times are expected to pass 168 hours salt spray.

The R_{corr} values fit from the EIS measurements were $3.3 \times 10^6 \pm 2.5 \times 10^6$ and $2.9 \times 10^6 \pm 2.8 \times 10^6 \Omega\text{-cm}^2$ for the nine-minute exposure times of the immersion and spray applied coatings, respectively. Based on the previously discussed threshold R_{corr} value of $2 \times 10^6 \Omega\text{-cm}^2$ for coatings on AA2024, these coatings were expected to pass the 168h salt spray exposure. It should be noted that while the range of R_{corr} values observed for the immersion and spray applied coatings was large (8.8×10^5 to 8.4×10^6 and 2.8×10^5 to $1.1 \times 10^7 \Omega\text{-cm}^2$ for the immersion and spray applied coatings, respectively), it is typical of the scatter observed for barrier property measurements of inorganic or organic coatings. The arithmetic mean of 8 samples per treatment was used in this study for comparison with a previously determined R_{corr} critical threshold value, which had been determined by Buchheit, et al. using the mean rank method for an 80% cumulative passing frequency. As previously stated, the EIS testing was limited to the nine-minute application times to minimize the size of the experimental matrix.

The salt spray results are reported in Table 8 as fraction failed per observation time. The samples were left in the salt spray chamber for 1,000. Only 168 hours is required for quality conformance and 336 hours for qualification of coatings on AA2024. A majority of the five and nine-minute coatings survived 336 hours. The spray-applied coating performed better than immersion-applied coatings. At each observation time, a greater fraction of the spray applied coatings survived than the immersion applied coatings for the same coating time. Note that none of the two-minute immersed samples passed 168 hours of salt spray, while none of the two-minute spray-applied coatings could survive 336 hours of salt spray.

Adhesion was measured by the wet tape test and by measuring the pull-off-tensile-strength. The results of the adhesion testing, shown in Table 9, indicate that the adhesion measured by the wet tape test was comparable regardless of coating time or application method. The additional adhesion tests (pull-off-tensile-strength) verified that the adhesion was statistically equivalent for all treatments.

The scribed, primed and topcoated panels were evaluated after 2,000 hours exposure to salt spray. No blistering or lifting of the topcoat or primer was observed for any of the nine-minute spray or immersion applied panels. However, corrosion was observed on two of the four immersion applied panels. Therefore two of the four 9-minute immersion applied panels failed the salt spray exposure, but all of the spray applied panels passed.

The better salt spray performance of the spray-applied coatings (both stand-alone and painted) was unexpected. This may be attributable to bath chemistry changes with time for the immersion coatings. Spray applied coatings are formed by a constant chemistry that is continually refreshed, while immersion techniques form coatings in a bath that will change with time. The effect of bath chemistry evolution on the corrosion performance of a non-chromate conversion coating has recently been reported in which coating quality was found to decrease with bath age¹⁵. Another factor is that the immersion coatings were at constant elevated temperature, while no temperature control was provided for the spray application. It should be stated that the sprayed solution was at elevated temperature but cooling certainly occurred once in contact with the panels. The effect of cooling during spraying has not been investigated.

In light of this, coating systems should be viewed as an interdependent entity in which the performance of the whole is more than the simple sum of its individual

components, i.e., conversion coating, primer coat, and topcoat. A case in point is the present investigation of CCCs. Although the field applied CCCs did not pass the military specifications for stand alone corrosion protection, these same CCCs perform quite well when used in the field within a complete coating system. The antithesis may also be true, in that a new alternative conversion coating may perform well as a stand alone corrosion protection material, but not possess the requisite interfacial chemistry to function within a complete coating system. This has been observed in testing within these laboratories and will be reported in a subsequent paper. The results of this study strongly suggest the need to use a total system test approach to qualify alternative conversion coatings when incorporated into a complete coating system. The ideas presented here will possibly make pre-screening of conversion coatings a more cumbersome process, but additional research is being conducted to better understand the interfacial properties that control substrate-coating interactions.

Conclusions

There were several significant results in this study of field applied and lab applied coatings. The salt spray performance was predicted by EIS and coating weight. The prediction of salt spray performance based on threshold R_{corr} values was supported by these results. The adhesion required by military specification was obtained regardless of alloy type, pretreatment, application method (spray or immersion), or coating time. At least five-minutes of continuous exposure during coating was needed to obtain adequate coating weight for both application methods. In the lab-simulated study, the spray-applied coatings were slightly better than the immersion applied.

The present military specifications for conversion coatings require a level of performance that not even field-applied chromate conversion coatings can meet. Yet we know from experience, that field-applied CCCs provide an excellent substrate for coating, and that the coatings on these same field-applied CCCs **do** pass military specifications **for a coating system** (i.e., conversion coating, primer, and topcoat). Thus, present military specifications may set unreasonable requirements for emerging environmentally benign conversion coatings that would eventually be used within a coating system, and may screen out very adequate conversion coating materials.

References

- 1 "Metals Handbook" Vol. 5 Surface Cleaning, Finishing, and Coating. 9th edition, 457 (1982).
- 2 "Rankings of Pollutants with Respect to Hazard to Human Health". Environmental Protection Agency Report # EPA-450/3-92-010 (1994).
- 3 H.J. Gibb, *Plating and Surface Finishing* **86**, 19 (1999).
- 4 C.J. Carpenter *Plating and Surface Finishing* **77**, 35 (1990).
- 5 A. Nylund, *Aluminum Transactions*, **2**, 121 (2000)
- 6 ASTM Method B117 "Standard Test Method of Salt Spray (Fog) Testing. ASTM, Philadelphia, PA (1999).
- 7 Federal Test Standard Number 141, Method 6301.1 "Adhesion (Wet) Tape Test" (1965).

- 8 "Alternatives to Chromium for Metal Finishing". National Center for Manufacturing Sciences, Report 0273RE95. Ann Arbor, MI (1995).
- 9 S. Susta, Science Applications International Corp. (Personal communication)
- 10 R.G. Buchheit, M. Cunningham, H. Jensen, M.W. Kendig, and M.A. Martinez, *Corrosion* **54**, 61 (1998).
- 11 ASTM Method D3359 "Standard Test Methods for Measuring Adhesion by Tape Test". ASTM, Philadelphia, PA (1995).
- 12 ASTM Method D4541 "Standard Test Method for Pull-off Strength of Coatings using Portable Adhesion Testers" ASTM, Philadelphia, PA (1995).
- 13 J.A. Treverton, M.P. Amor, A. Bosland, *Corrosion Science*, **33**, 1411 (1992)
- 14 A.E. Hughes, R.J. Taylor, B.R.W. Hinton, *Surface and Interface Analysis*, **25**, 223 (1997).
- 15 R.B. Leggat, E.A. Pehovaz-Diez, N.P. Cella, S.R. Taylor, in *Corrosion and Corrosion Prevention of Low Density Metals and Alloys*, ed. B.A. Shaw, R.G. Buchheit, J.P. Moran (Pennington, NJ: ECS, 2001), p.124.

Acknowledgements

This work was sponsored by DARPA (Contract #F49620-1-0305) under direction of Dr. Stephen Wax and Maj. Paul Trulove (AFOSR). The assistance of Maj. Barnard Ghim and Steve Finely of CTIO are greatly appreciated. Discussions with Dr. Stefan Susta of SAIC were helpful in conducting this study.

Captions for Tables and Figures

Table 1. Corrosion Resistance Requirements of MIL-C-81706.

Table 2. Ranking of tape test samples according to ASTM D3359. Reprinted, with permission. Copyright ASTM.

Table 3. Testing done on lab-simulated coatings. Matrix identical for spray and immersion applied coatings.

Table 4. EIS results for ALC applied coatings on AA2024, AA6061, and AA7075. R_{corr} fit from spectra for both pretreatments.

Table 5. Fraction of ALC coatings that failed per observation time in salt spray. MIL-C-81706 requires 168h for quality conformance on alloys.

Table 6. Adhesion Testing of primed and topcoated, ALC applied coatings by wet tape test. Ranked according to ASTM D3359 on a scale of 5-0 with 5 being the best and 0 being the worst. Pass or fail according to MIL-C-5541 based on ranking of 4 or 5 considered passing.

Table 7. Coating weights for all times of spray and immersion application. Samples produced in lab simulating depot conditions.

Table 8. Fraction of coatings that failed per observation time in salt spray. MIL-C-81706 requires 168h for quality conformance and 336 for qualification on AA2024. Samples produced in lab simulating depot conditions.

Table 9. Adhesion Testing of primed coatings produced in lab simulating depot conditions by wet tape test and pull-off tensile strength. Pass or fail of tape test according to MIL-C-5541 based on ranking of 4 or 5 considered passing.

Figure 1. X-Ray diffraction spectrum for CCC scraped from ALC applied coatings. Peaks in spectrum from aluminum removed from panel during scraping.

Figure 2. SEM image of ALC applied CCC. Sample abraded prior to coating.

Figure 3. Auger electron spectroscopy depth profiles for ALC applied coatings. Spectra for coatings on AA2024, AA6061, AA7075 with both pretreatments shown.

Concentrations of oxygen (∇), aluminum ($\#$), and chromium (Φ) plotted as atomic fraction.

Figure 4. Photograph showing non-uniformity of CCC on samples receiving no pretreatment.

Tables

Table 1.

Corrosion Resistance Properties	Treatment-Class	Aluminum Alloys Treated With Film Forming Materials	Exposure to 5% Salt Spray - Hours
For Qualification	1A 3	2024-T3, 7075-T6 6061-T6	336 168
For Quality Conformance Inspection	1A 3	2024-T3 6061-T6	168 168

Class 1A - For maximum protection against corrosion,
Class 3 - For protection against corrosion where low
electrical (contact) resistance needed.

Table 2.

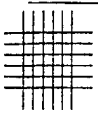
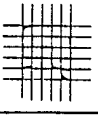
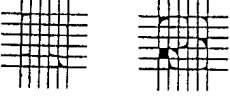
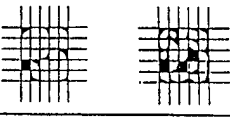
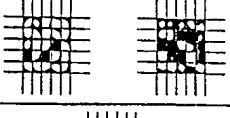
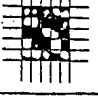
<u>Rank</u>	<u>%Removed</u>	<u>Example</u>
5B	0%	
4B	<5%	
3B	5-15%	
2B	15-35%	
1B	35-65%	
0B	>65%	

Table 3.

CCC Alone	2 minutes	5 minutes	9 minutes
Coating Weight	X	X	X
EIS			X
Salt Spray Exposure	X	X	X
CCC + Primer			
Pull-Off Tensile Strength	X	X	X
Wet Tape Test	X	X	X
CCC+ Primer + Topcoat			
Salt Spray Exposure			X

Table 4.

Pretreatment 1 (As-received)	
	R_{corr} ($\text{k}\Omega\text{cm}^2$)
AA2024	11.1 +/- 1.7
AA6061	323.8 +/- 316.5
AA7075	18.3 +/- 3.6
Pretreatment 2 (Abraded)	
	R_{corr} ($\text{k}\Omega\text{cm}^2$)
AA2024	25.7 +/- 19.5
AA6061	1997.5 +/- 1657.9
AA7075	4863.2 +/- 2357.4

Table 5.

Pretreatment 1 (As-received)				
	24 hours	48 hours	66 hours	168 hours
AA2024	5/5			
AA6061	3/5	4/5	5/5	
AA7075	0/5	1/5	5/5	
Pretreatment 2 (Abraded)				
	24 hours	48 hours	66 hours	168 hours
AA2024	5/5			
AA6061	0/5	0/5	0/5	0/5
AA7075	5/5			

Table 6.

Pretreatment 1 (As-received)		
	D3359 ranks	MIL-SPEC
AA2024	3B, 4B, 5B	2 / 3 pass
AA6061	2B, 4B, 5B	2 / 3 pass
AA7075	4B, 5B, 5B	3 / 3 pass
Pretreatment 2 (Abraded)		
	D3359 ranks	MIL-SPEC
AA2024	4B, 4B, 5B	3 / 3 pass
AA6061	4B, 4B, 4B	3 / 3 pass
AA7075	3B, 5B, 5B	2 / 3 pass

Table 7.

Immersion	Coating Weight (mg/ft²)
2 minute	23.9 +/- 5.4
5 minute	41.2 +/- 4.5
9 minute	48.8 +/- 3.6
Spray	
2 minute	N/A
5 minute	36.3 +/- 1.5*
9 minute	37.5 +/- 12.8*

* Coating on both sides of 4"x5" panel assumed

Table 8.

	168 h	336 h	504 h	672 h	1,000+ h
Immersion Application					
2 minute	4/4				
5 minute	0/4	1/4	3/4	3/4	4/4
9 minute	0/4	0/4	2/4	3/4	4/4
Spray Application					
2 minute	1/4	4/4			
5 minute	0/4	0/4	0/4	1/4	4/4
9 minute	0/4	0/4	1/4	1/4	4/4

Table 9.

Immersion	POTS (psi)	Tape Test	MIL-Spec
2 minute	995 +/- 142	4B, 5B	2/2 pass
5 minute	1046 +/- 182	5B, 5B	2/2 pass
9 minute	964 +/- 166	5B, 5B	2/2 pass
Spray			
2 minute	973 +/- 139	4B,5B	2/2 pass
5 minute	1036 +/- 143	4B,5B	2/2 pass
9 minute	900 +/- 154	4B,5B	2/2 pass

Figure 1.

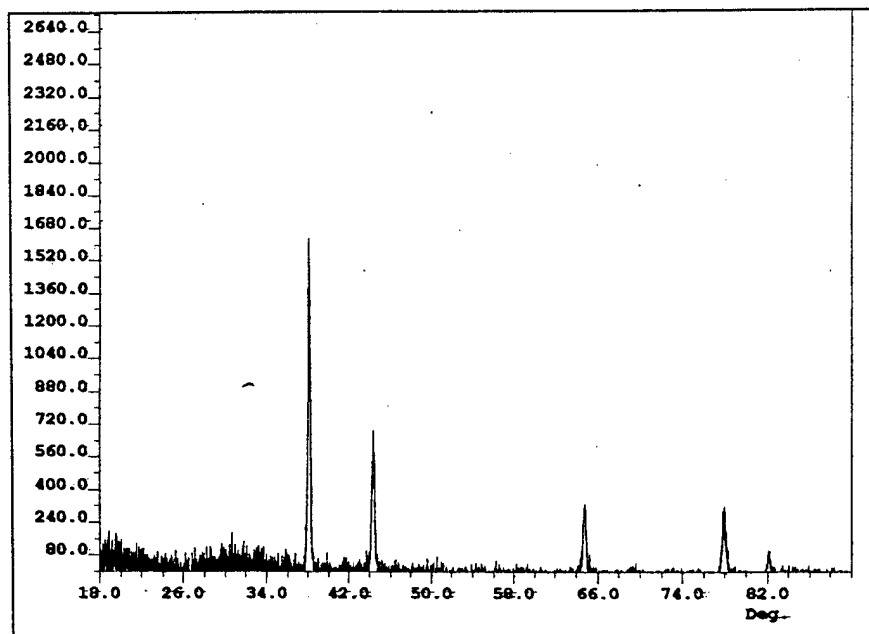


Figure 2.



Figure 3.

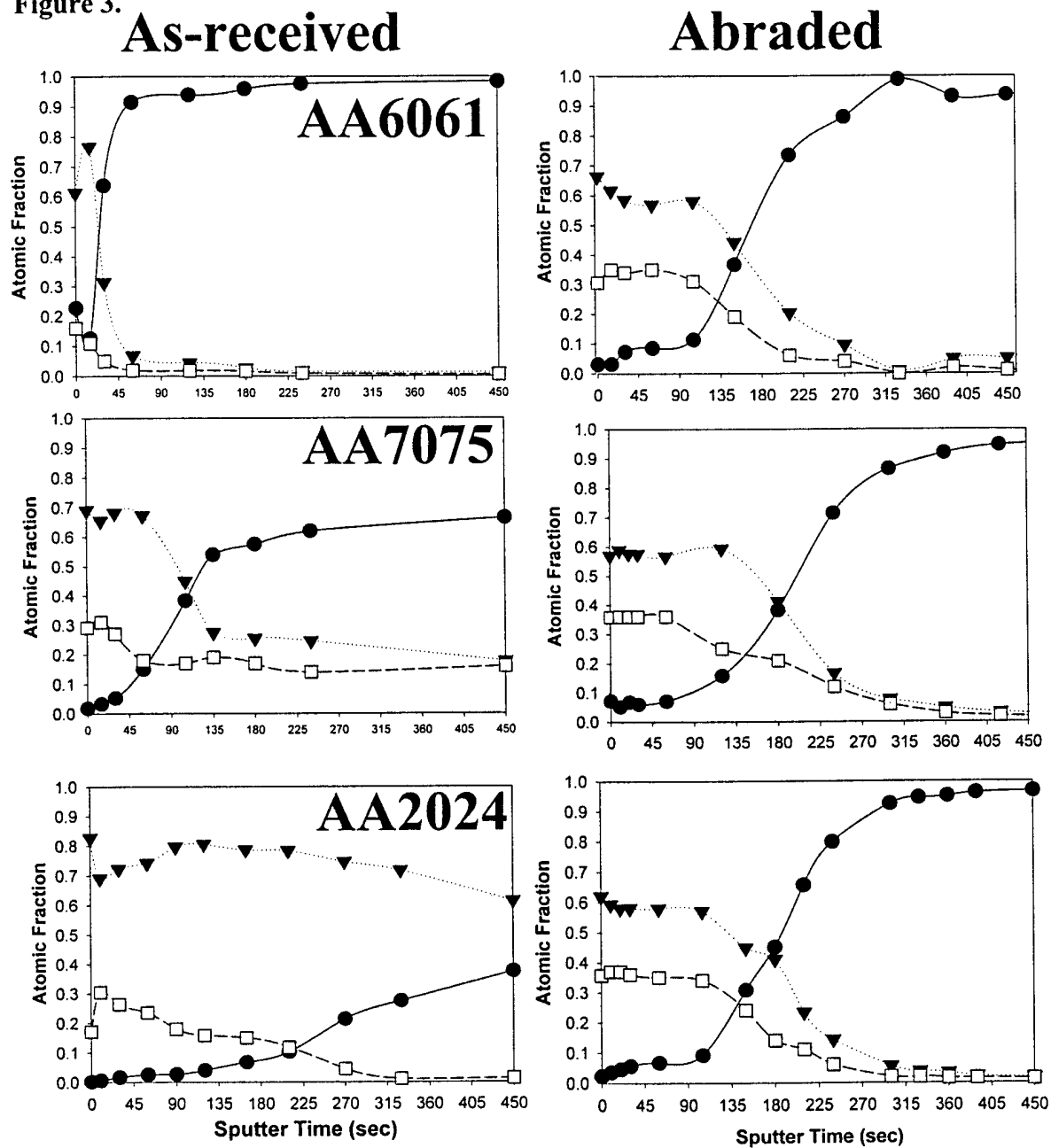
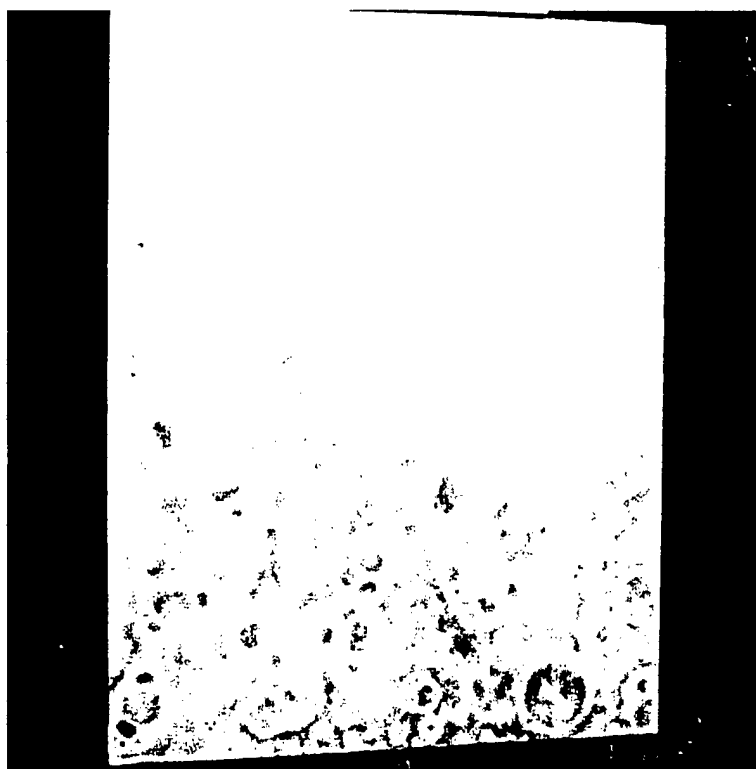


Figure 4.



Submitted to *Corrosion* (in press)

Performance of Hydrotalcite Conversion Treatments on AA2024-T3 When Used within a Coating System

R. B. Leggat*, W. Zhang**, R.G. Buchheit**, S. R. Taylor*

* Department of Materials Science and Engineering
University of Virginia
Charlottesville, VA 22904

** Department of Materials Science and Engineering
The Ohio State University
Columbus, OH 43210

ABSTRACT

Hydrotalcite (HT) conversion coatings are a possible alternative to chromate conversion coatings for the pretreatment of aluminum aerospace alloys, but must meet several criteria for acceptance. Relevant to acceptance are the abilities of these coatings to provide: stand alone corrosion protection, suitable adhesion with subsequent organic layers, and overall corrosion protection when used within a coating system. This study examines the salt spray performance of nine different HT treatments on AA2024 as stand alone conversion coatings and as a substrate for an epoxy primer. In addition, the adhesion of epoxy to the HT and the corrosion characteristics of HT coatings as assessed by electrochemical impedance spectroscopy were determined. Salt spray testing was done under the pertinent military specifications and used chromate conversion coatings (CCC) as the benchmark. Two epoxy primers were evaluated: one with a chromate inhibitor (Class-C) and one with a non-chromate inhibitor (Class-N). The standalone HT treatments did not perform as well as the CCC but showed favorable performance relative to bare AA2024. In the primed samples, the CCC and bare AA2024 performed better than the HT coated samples. Current HT coating chemistries have been optimized for stand-alone corrosion resistance. A correlation between stand alone salt spray performance and EIS response was observed. The standalone corrosion resistance or epoxy adhesion could not explain the salt spray performance of the epoxy-primed samples, supporting the need for total system testing approach in coating development.

Keywords: AA 2024, adhesion, conversion coatings, EIS, salt spray.

INTRODUCTION

Conversion coatings are commonly applied to aluminum alloys to increase corrosion resistance and to provide increased adhesion of subsequent organic layers¹. Currently, chromate-based conversion coatings (CCC) are used and are a key component in the performance of aerospace coating systems. Although they provide excellent adhesion and corrosion performance, chromates are hazardous materials that require significant expenditure in waste processing².

Conversion coatings based on a naturally occurring compound, hydrotalcite (HT), are being developed as an alternative to chromate-based conversion coatings³. Hydrotalcite is formed on aluminum alloys by exposure to alkaline lithium salt solutions. The compound formed consists of aluminum/lithium-hydroxide layers intercalated by anions from the lithium salt. The physical and chemical properties of HT-based coatings can be controlled by selection of this interlayer anion, as well as by numerous post-coating treatments^{4,5}, thus providing a large array of treatment options in the discovery of an optimal conversion coating procedure.

Previous research has focused on the optimization of standalone corrosion resistance of HT-based coatings on an aerospace alloy (AA2024-T3)⁶. However, in order for candidate conversion coating chemistries to ultimately be used by certain customers, e.g., department of defense (DOD) facilities, they must conform to military specifications. One such specification is MIL-C-81706 "Chemical Conversion Materials for Coating Aluminum and Aluminum Alloys"⁷, which is a materials specification that defines the characteristics of the conversion coating chemistry including appearance and properties of the applied coating. Another specification that also covers conversion coatings on aluminum alloys, MIL-C-5541E "Chemical Conversion Coatings on Aluminum and Aluminum Alloys"⁸, is a process specification that defines the characteristics of a coating applied in a production environment. MIL-C-5541E controls the qualification of candidate systems and is therefore the specification relevant to the present study.

Given that a conversion coating will be used as part of a coating system consisting of a conversion coating, a primer, and one or more topcoats, testing of candidate conversion coatings should also include samples coated with at least a primer coat. The military specification that controls epoxy primers is MIL-PRF-23377G "Performance Specification Primer Coatings: Epoxy, High Solids"⁹. Any conversion coating that causes a previously qualified primer to fail the tests specified by MIL-PRF-23377G will not be used, even if the conversion coating itself qualified under MIL- C-5541E.

Salt spray exposure is the method specified for the assessment of corrosion resistance for both MIL-C-81706 and MIL-PRF-85582C. Although there is considerable criticism of method reliability and relevance to service performance, salt spray testing is recognized as the standard in many industries as well as the military¹⁰.

In the current study, the salt spray performance of HT coated, epoxy primed AA 2024-T3 is investigated. The primary goal was to determine the optimal treatment for service performance. The selection of treatments for evaluation was based on a number of considerations. During the coating step, chemistries including different lithium salts were used in order to incorporate various oxoanions (e.g., carbonate, nitrate, persulfate) into the HT structure. Some of the coated samples also received additional post-coating treatments such as a transition metal seal, hydrothermal reversion, or adsorption of a hydration inhibitor. Practicality was another factor in determining what treatments were analyzed. Elimination of potentially unnecessary processing steps (e.g., degreasing and/or deoxidizing) or energy intensive parameters (e.g., elevated temperature) would be of interest.

The flexibility of numerous treatment options available for HT processing is coupled to questions of product variation. Treatment variables that could be relevant include:

- Importance of degreasing and deoxidizing steps
- Effect of different anions in the HT interlayer
- Effect of different temperature / time combinations in processing

- Effect of post-coating treatments such as hydrothermal reversion or adsorption of a hydration inhibitor
- Effect of incorporating active corrosion protection.

Additional testing included electrochemical impedance spectroscopy (EIS) and adhesion testing. These tests were performed to determine the relative importance of stand alone corrosion resistance and coating adhesion in salt spray performance. Although the importance of adhesion in the corrosion resistance of painted substrates is debated^{11,12}, it is generally recognized that some degree of wet adhesion is necessary for adequate corrosion protection¹³.

EXPERIMENTAL METHODS

Application of Coatings

Various HT coating chemistries were applied to 4" x 5" AA2024-T3 (UNS 92024) panels. Prior to processing, the panels were scrubbed with non-metallic Scotchbrite[®] pads in Alconox[®] solution then rinsed in deionized water and air-dried. The majority of the HT coatings were applied using a conventional three-bath process consisting of degreasing, deoxidization, and coating. Bare AA2024-T3 was included as a blank, while CCC applied by an Alodine[®] process were used as a control. A total of nine different HT coatings were evaluated. These treatments and the corresponding abbreviation used hereafter are listed in Table 1.

A total of 15 panels were made for each treatment evaluated. Five of the panels were set aside for stand-alone salt spray testing. Three days after the conversion coatings were applied, the remaining panels were coated with a two-part, high solids epoxy primer. Half of the primed samples were coated with a chromated primer (Deft[®] 02-Y-40 Type 1, Class C per MIL-P-23377G), while the others received a primer with non-chromate inhibitors (Deft 02-W-38 Type 1, Class N). After drying, a high solids polyurethane topcoat (Deft 03-GY-321) was

* Trade name

applied. The top-coated and primed samples were allowed to dry for three weeks prior to salt spray exposure.

Salt Spray Exposure

The samples were exposed to 5-wt. % sodium chloride salt spray in accordance to ASTM B117 ¹³. Salt spray exposure was initiated ten days after the conversion coatings were applied. The stand-alone (unprimed) samples were exposed for 336 hours per MIL-C-81706 and visually inspected for signs of corrosion after 168 and 336 hours exposure. The panels were removed and washed before the final evaluation was made. MIL-C-81706 specifies that no corrosion whatsoever should be visible. For comparison, specimens were rated on a scale of 0 - 5, where 0 indicates no corrosion and 5 severe. Ranking was assign based on the appearance of all five replicates in aggregate.

The primed samples were exposed for 2,000 hours per MIL-PRF-85582C. According to the military specification, the primer "shall not exhibit blistering, lifting of either coating, nor substrate corrosion after exposure...". Again, a qualitative ranking was used for comparison. Three parameters were evaluated for each replicate: corrosion at the scribe, undercutting, and blistering. For corrosion, "0" indicates a bright, clean scribe; "1" indicates staining and possibly minor corrosion spots, but no build-up of corrosion product; 2 through 5 indicates the relative severity of corrosion product build-up, with 2 and 3 typically being limited to the scribe and 4 and 5 showing migration from the scribe. Undercutting indicates lifting, or loss of adhesion of the coating system at the scribe due to corrosion. Blistering indicates attack at the scribe only. The ranking for the undercutting and blistering were also ranked on a scale of 0-5 based on severity, where 0 indicates no change, 1- minor, 2- minor to moderate, 3- moderate, 4- major, and 5- severe.

Electrochemical Impedance Spectroscopy

AA2024-T3 panels were treated with selected chemistries listed in Table 1 and included AlO₂, CO₃, Hydro, MnO₄, NO₃-5-95, NO₃-PPA, and S₂O₈. Bare

AA2024-T3 was also tested as a blank. EIS data for the samples was collected after 24 hours exposure to 0.5M NaCl at room temperature and ambient aeration. A parameter indicative of the corrosion resistance of the coating, R_{corr} , was fit from the spectra using a complex non-linear least squares fitting program. R_{corr} is the polarization resistance minus the diffusional impedance and has been used successfully in previous studies of conversion coated aluminum alloys ¹⁴.

Adhesion Testing

Epoxy coatings were applied to panels treated with selected chemistries listed in Table 1 that included: AlO_2 , CO_3 , Hydro, MnO_4 , NO_3 -5-95, NO_3 -PPA, and S_2O_8 . Bare AA2024-T3 and CCC were also coated as a blank and control, respectively. The epoxy consisted of a BPA-epichlorohydrin resin with a polyamide hardener supplied by Ciba-Geigy, and is representative of the epoxy chemistry used in epoxy primers for aerospace applications. Spin casting was used to apply epoxy coatings 25-75 μm thick.

The practical adhesion was measured by the pull-off tensile strength (POTS) of the epoxy from the samples using a pneumatic adhesion tensile testing instrument (PATTI). The POTS tests were performed in accordance to ASTM method D4541 "Standard Test Method for Pull-Off Strength of Coatings Using Portable Adhesion Testers" using a Gardner model P2A PATTI.

In addition to measuring the dry adhesion, the wet state adhesion was measured after 24 hours exposure to deionized water. After aqueous exposure, the samples were wiped dry and the pull-off stubs were attached with cyanoacrylate adhesive. The adhesive was allowed to cure for 30 minutes prior to testing.

RESULTS AND DISCUSSION

The salt spray ranking of the unprimed and primed samples are listed in Table 2 and 3, respectively. Rankings of the damage parameters (corrosion, undercutting, and blistering) for the Class N (non-chromated) and C2

(chromated) primer-coated samples are graphically depicted in Figure 1 and 2, respectively.

Stand Alone Corrosion Protection

The most apparent result from the salt spray is that the chromate conversion coating performed better than the HT treatments for both the stand alone and primer coated samples. In the present study, the laboratory-applied CCC was the only unprimed treatment to pass the 336 hour requirement of MIL-C-81706. However, it should be pointed out that in a previous study of field-applied CCC¹⁵, the salt spray performance of the CCCs did not conform to the military specification, despite the proven service history of CCCs.

Six of the HT treatments ranked better than the bare AA2024-T3. Two of the treatments, MnO_4 and Hydro, received rankings of 2 followed by S_2O_8 and AlO_2 (ranking of 3) and NO_3 -5-95 and NO_3 -30-RT (ranking of 4). Based on prior studies, the MnO_4 and Hydro coatings would have been expected to display good stand-alone corrosion resistance. MnO_4 coatings have been shown to provide active corrosion protection¹⁶, while the hydrothermally treated HT reverts the HT a bayerite layer whose thickness is comparable to that of anodized coatings⁴.

The R_{corr} values fit from the EIS data for each treatment are included in Table 2. Threshold R_{corr} values have been proposed as indicators of the salt spray performance of conversion coated aluminum alloys¹⁴. Conversion coatings on AA2024-T3 with a R_{corr} value greater than 2×10^6 - $5 \times 10^6 \Omega\text{cm}^2$ would be expected to have five or less visible pits after 168 hours salt spray. The exposure time in the present study was greater (336 hours) and ranking employed an ordinal scale rather than pass/fail. Nonetheless, the R_{corr} values can be used as a qualitative indicator of salt spray performance. In fact, the stand-alone salt spray performance correlated reasonably well with the R_{corr} values. For the chromated control samples, values from the previously mentioned study were included for reference¹⁴.

Primed Samples

When Class-C (chromated) primers are used, the conversion coating seems to be unnecessary in terms of corrosion resistance. However this is not the case for non-chromated primers. In the presence of the Class-N primer (non-chromated), the bare AA2024-T3 samples performed only slightly worse than the CCC, and only one HT treatment (AlO_2) performed as well as the blank. Thus, eight of the nine HT conversion coatings tested here decrease the corrosion resistance when used within a coating system.

It should also be pointed out that chromate in both the conversion coating and primer greatly reduced the amount of blistering. However, the Class-N primer showed better undercutting resistance for 6 of the 11 treatments.

Looking at the results for the stand-alone conversion coatings and the primer-coated samples, the effects of the different treatments can be compared. The degreasing and deoxidizing steps decrease the corrosion resistance of the non-primed NO_3 -HT conversion coating. However, in the primer-coated samples, an equivalent corrosion resistance was seen regardless of the pretreatment steps. In addition, when the pretreatment was included, the two time-temperature combinations had the same corrosion resistance whether tested as stand alone or with primer coats. Varying the time and temperature of the coating step alters the coating thickness and morphology. The fact that the two time-temperature combinations produced coatings with similar corrosion resistance suggests that the coating morphology is not the determining factor in corrosion resistance. It is difficult to delineate the separate effects of time and temperature because neither was independently controlled. Practically, these results indicate that the cost associated with elevated temperature does not gain any improvement in corrosion performance.

Several post-coating treatments for HT were evaluated within the present study. The results of the unprimed MnO_4 and Hydro coatings have already been discussed. In general, none of post-treated HT conversion coatings performed well when used within a coating system. It was believed that the use of a hydration inhibitor, phenylphosphinic acid (PPA), as a post-coating would

increase the environmental durability of the conversion coating / primer interface. Not only did it decrease the performance when primed, it also decreased the corrosion resistance of the unprimed samples. In addition to adsorption, the PPA might have reacted with the HT by intercalation causing the observed decrease in corrosion resistance. Other researchers have reported intercalation of phenylphosphonic acid in hydrotalcite-like compounds by anion exchange¹⁷.

As a means of comparing the overall performance of the primed treatments, the corrosion, undercutting, and blistering parameters were summed for all five replicates. For the Class-N primer, the ranking is as follows:

$$\text{CCC} > \text{S}_2\text{O}_8 \geq \text{Bare} \geq \text{NO}_3\text{-5m-95} = \text{NO}_3\text{+PPA} > \text{Other treatments}$$

For the Class-C primer:

$$\text{CCC} > \text{Bare} > \text{NO}_3\text{-nopre} = \text{NO}_3\text{-30-RT} > \text{AlO}_2 > \text{Other treatments}$$

This is not intended as a rigorous analysis, but merely as a method to compare the treatments.

Adhesion

The dry and wet-state POTS results are shown in Table 4. Cumulative probability plots are useful for visualizing the POTS distributions and rankings for different treatments as seen in Figures 3 and 4 for the dry and wet states, respectively.

A one-way analysis of variance (ANOVA) was used to test for differences among the average POTS values. Tukey's method was used to compare each treatment with the others to see which were significantly different at a 95% confidence¹⁸. The fact that the population sizes and standard deviations were different among the treatments decreases the rigidity of the test, but a reasonable approximation is obtained. The comparison from Tukey's method can be interpreted by looking at what treatments significantly differ from one another.

The CCC POTS is significantly larger than all other treatments. Comparing the bare AA2024-T3 with the other treatments, the CO_3 , NO_3 , and MnO_4 POTS are all higher than the degreased AA2024-T3. The Hydro and S_2O_8 HT are equivalent to the bare AA2024-T3, while the AlO_2 HT was worse than the bare AA2024. The rankings are:

$$\text{CCC} > \text{CO}_3 \approx \text{NO}_3 \approx \text{MnO}_4 > \text{Hydro} \approx \text{bare AA2024} \approx \text{S}_2\text{O}_8 > \text{AlO}_2$$

Similar analysis was used for the wet POTS results. The most apparent result is the large decrease in the wet state POTS relative to the dry state. This was true for all treatments. Fischer's LSD Multiple Comparison Test indicated that the POTS for CCC and CO_3 are significantly larger than all other treatments. It is most likely that the POTS for CO_3 is not equivalent to CCC as evidenced by the difference in the median values shown in Figure 4. Comparing the bare AA2024-T3 with the other treatments, the POTS for S_2O_8 and NO_3 are higher than the bare AA2024. The POTS for MnO_4 , AlO_2 , and Hydro HT are all equivalent to the bare AA2024. The rankings are:

$$\text{CCC} > \text{CO}_3 > \text{S}_2\text{O}_8 \approx \text{NO}_3 > \text{MnO}_4 \approx \text{AlO}_2 \approx \text{Hydro} \approx \text{bare AA2024}$$

There is a factor not accounted for in the EIS or adhesion tests that could account for the difference in the corrosion performance observed for the stand alone and primed samples. The intercalation reaction by which the hydrotalcite is formed is reversible. As previously mentioned, the hydrotalcite will de-intercalate. This is not problematic in the absence of a primer. However, in the presence of a primer, the release of ions beneath the primer provides an osmotic gradient that further promotes water ingress. This mechanism can be viewed as an asset or a liability. If the hydrotalcite were engineered such that the interlayer oxoanion was a slowly leaching inhibitor, de-intercalation could provide a reservoir for active corrosion protection at the onset of water ingress.

Summary

No correlation was observed between the wet and dry POTS rankings and the salt spray performance of the primer coated samples. Adhesion issues will be examined in future publications. In addition, no correlation was observed between the primer-coated salt spray performance and the stand alone corrosion resistance whether gauged by EIS or salt spray.

This study has determined that the salt spray performance of the nine HT conversion coatings tested is not as good as CCC when implemented within a full coating system (i.e., conversion coating with a primer and top coat). In some cases, HT performs worse than a non-conversion coated but painted sample. Thus, present HT coating chemistries are better optimized for stand-alone corrosion resistance than for resistance within a coating system. The salt spray performance of a coating system cannot be predicted by simple addition of the independent performance of each component, which points to the need to test the coating component under development within a total coating system. Individual components of a coating system may perform well in isolation, yet their composite may behave in an unexpected manner.

CONCLUSIONS:

- ❖ Present hydrotalcite coating chemistries are optimized for stand-alone corrosion resistance.
- ❖ The hydrotalcite coating chemistries tested in the present study do not perform as well as chromate conversion coatings as a coating pretreatment (i.e. within a coating system).
- ❖ Neither the pre-treatment, incorporation of active corrosion protection, reversion, nor the hydration inhibitor improved performance of the painted samples.

- ❖ The salt spray performance of primed and conversion coated AA2024 does not correlate with the epoxy adhesion or stand alone corrosion resistance of the conversion coating.
- ❖ The need for an integrated approach in coatings development is reinforced.

Acknowledgements

This work was sponsored by DARPA (Contract #F49620-1-0305) under direction of Dr. Stephen Wax and Lt. Col. Paul Trulove (AFOSR). The assistance of Deb Peeler (AFRL), Ken Chitwood, Keith Clendenon, Dennis Huff, Scott Lanter, Andy Logue and Dick Tocci of UDRI in paint application and salt spray testing is greatly appreciated.

REFERENCES

1. Metals Handbook, Vol. 5: Surface Cleaning, Finishing, and Coating (ASM, Metals Park, 1982), p. 597.
2. C.J. Carpenter, Plating and Surface Finishing 77, 4 (1990): p. 35.
3. R.G. Buchheit, M.D. Bode, G.E. Stoner, Corrosion 50, 3 (1994): p. 205.
4. R.G. Buchheit, M.A. Martinez, L.P. Montes, N.P. Cella, S.R. Taylor, G.E. Stoner "Non-Electrolytic Formation of Al-Oxide Surface Layers by Reversion of Hydrotalcite", Corrosion/98, paper no. 216, (Houston, TX: NACE, 1998)
5. R.G. Buchheit, M.A. Martinez, L.P. Montes, N.P. Cella, S.R. Taylor, G.E. Stoner "Inorganic Cr-Free Conversion Coatings for High Corrosion Resistance and Low Electrical Contact Resistance", Corrosion/98, paper no. 212, (Houston, TX: NACE, 1998)
6. R. B. Leggat, E.A. Pehovaz-Diez, N.P. Cella, S.R. Taylor in Corrosion and Corrosion Prevention of Low Density Metals and Alloys, ed. B.A. Shaw, R.G. Buchheit, J.P. Moran, (ECS, Pennington, 2001), p. 124.
7. MIL-C-81706 "Military Specification Chemical Conversion Materials for Coating Aluminum and Aluminum Alloys"

8. MIL-C-5541E "Military Specification Chemical Conversion Coatings on Aluminum and Aluminum Alloys"
9. MIL-PRF-85582C "Performance Specification Primer Coatings : Epoxy, Waterborne"
10. B.R. Appleman, J. Coatings Technology 62, 787 (1990): p. 57.
11. P. Walker, JOCCA 68, 12 (1985): p. 319.
12. W. Funke, JOCCA 69, 3 (1986): p. 78.
13. R.A. Dickie, in Adhesion Aspects of Polymer Coatings, ed. K.L. Mittal. (Plenum Press, New York, 1983), p. 391.
14. R.G. Buchheit, M. Cunningham, H. Jensen, M.W. Kendig, and M.A. Martinez, Corrosion, 54, 1 (1998): p.61.
15. R.B. Leggat, S.R. Taylor, W. Zhang, R.G. Buchheit, Corrosion, 2001 (in review)
16. R.G. Buchheit, S.B. Mamidipally, P. Schmutz, and H.Guan "Active Corrosion Protection in Chromate and Chromate-Free Conversion Coatings", Corrosion 2000, paper no. 103, (Houston, TX: NACE, 2000)
17. F.M. Vichi, O.L. Alves, J. Mater. Chem. 7, 8 (1997): p. 1631.
18. J.L. Devore, Probability and Statistics for Engineering and the Science (Duxbury, Pacific Grove, 2000), p. 141.

Tables and Figure Captions

Table 1. HT conversion coating chemistries evaluated. Immersion time, temperature, and components of coating bath listed in addition to other processing variations.

Table 2. Stand alone corrosion resistance by salt spray and EIS. Rankings of unprimed treatments after 336 hours salt spray exposure. (0 indicates no corrosion- 5 indicated greatest severity of corrosion). Reported value average of five replicates. Rcorr values fit from EIS data after 24 hours exposure to 0.5M NaCl.

Table 3. Rankings of primed treatments after 2000 hours salt spray exposure. Three parameters evaluated for each replicate corrosion, undercutting, and blistering (left to right). 0 indicates lowest degree of severity- 5 greatest degree of severity. Class-N primer contains a non-chromate inhibitor. Class-C is a chromated primer.

Table 4. Dry and Wet POTS of epoxy from treated substrates. Arithmetic mean^x, standard deviation, and median values reported.

Figure 1. Rankings of degree of corrosion, undercutting, and blistering for treatments with primer containing non-chromate primer (Class-N). Bar indicates average value for 5 replicates.

Figure 2. Rankings of degree of corrosion, undercutting, and blistering for treatments with chromated primer (Class-C). Bar indicates average value for 5 replicates. No blistering observed for any treatment.

Figure 3. Dry POTS cumulative probability curves.

Figure 4. Wet POTS cumulative probability curves.

Table 1.

Abbrev. Name	Time (min)	Temp (oC)	Recipe
AlO ₂	5	95	NO ₃ -5m-95 coating followed by 15 min immersion in boiling 0.1M Al ₂ O ₃ ·Na ₂ O
Bare	-	-	Bare AA2024-T3 as blank
CCC	-	-	Alodine 1200S™ used a control.
CO ₃	5	95	0.07 M Na ₂ CO ₃ , 0.015M Li ₂ CO ₃ , 0.1M LiOH·H ₂ O, 600 ppm Al ₂ O ₃ ·Na ₂ O
Hydro	5	95	NO ₃ -5m-95 coating followed by 15 min immersion in boiling deionized H ₂ O
MnO ₄	5	95	NO ₃ -5m-95 coating followed by 5 min immersion in NO ₃ recipe + 0.01M MnO ₄ at 95oC
NO ₃ + PPA	5	95	NO ₃ -5m-95 coating followed by dip in 10 wt % phenylphosphinic acid (PPA) at RT
NO ₃ -30-RT	30	RT	0.3M KNO ₃ , 0.03 LiNO ₃ , 0.1M LiOH·H ₂ O, 600 ppm Al ₂ O ₃ ·Na ₂ O (NO ₃ recipe)
NO ₃ -5m-95	5	95	(NO ₃ recipe)
NO ₃ -nopre	5	95	NO ₃ recipe except no degreasing or deoxidizing steps
S ₂ O ₈	5	95	NO ₃ recipe + 0.01M K ₂ S ₂ O ₈

Table 2.

Specimen ID	Unprimed 336 hours	Rcorr (kΩ cm ²)
AlO ₂	3	26 ± 7
Bare	5	7 ± 1
CCC	0	944 ± 568*
CO ₃	5	16 ± 2
Hydro	2	285 ± 142
MnO ₄	2	250 ± 130
NO ₃ -PPA	5	11 ± 2
NO ₃ -30-RT	4	n/a
NO ₃ -5-95	4	26 ± 6
NO ₃ -nopre	5	n/a
S ₂ O ₈	3	96 ± 26

Table 3.

Specimen ID	Class N Primer 2000 hours	Class C Primer 2000 hours	Specimen ID	Class N Primer 2000 hours	Class C Primer 2000 hours
AlO ₂ (1)	2-4-2	1-1-0	NO ₃ -PPA (1)	3-2-2	2-5-0
AlO ₂ (2)	2-5-2	1-1-0	NO ₃ -PPA (2)	3-1-1	2-5-0
AlO ₂ (3)	2-5-0	1-2-0	NO ₃ -PPA (3)	3-1-0	2-5-0
AlO ₂ (4)	2-4-2	1-1-0	NO ₃ -PPA (4)	3-1-1	2-5-0
AlO ₂ (5)	2-4-2	2-1-0	NO ₃ -PPA (5)	3-1-1	2-5-0
Bare (1)	2-2-2	0-0-0	NO ₃ -30-RT (1)	3-1-3	1-0-0
Bare (2)	2-1-3	1-0-0	NO ₃ -30-RT (2)	3-0-4	2-0-0
Bare (3)	2-1-1	1-0-0	NO ₃ -30-RT (3)	3-1-5	2-0-0
Bare (4)	2-1-1	1-0-0	NO ₃ -30-RT (4)	3-1-5	1-0-0
Bare (5)	2-1-2	0-0-0	NO ₃ -30-RT (5)	3-0-4	1-0-0
CCC (1)	1-0-0	0-0-0	NO ₃ -5-95 (1)	3-1-1	1-1-0
CCC (2)	1-0-0	0-0-0	NO ₃ -5-95 (2)	3-1-1	1-4-0
CCC (3)	1-0-0	1-0-0	NO ₃ -5-95 (3)	3-1-0	2-3-0
CCC (4)	1-0-0	1-0-0	NO ₃ -5-95 (4)	3-2-1	1-3-0
CCC (5)	1-0-0	0-0-0	NO ₃ -5-95 (5)	3-2-1	2-4-0
CO ₃ (1)	3-1-5	2-3-0	NO ₃ -nopre (1)	3-1-3	2-0-0
CO ₃ (2)	3-0-5	2-2-0	NO ₃ -nopre (2)	3-0-2	1-0-0
CO ₃ (3)	3-0-5	2-2-0	NO ₃ -nopre (3)	3-0-3	1-0-0
CO ₃ (4)	3-0-5	2-3-0	NO ₃ -nopre (4)	3-0-3	1-0-0
CO ₃ (5)	3-1-5	2-3-0	NO ₃ -nopre (5)	3-0-3	2-0-0
Hydro (1)	3-1-2	1-2-0	S ₂ O ₈ (1)	3-1-0	1-4-0
Hydro (2)	3-1-1	1-2-0	S ₂ O ₈ (2)	3-1-0	1-4-0
Hydro (3)	3-2-2	1-2-0	S ₂ O ₈ (3)	3-1-1	1-4-0
Hydro (4)	3-3-1	1-2-0	S ₂ O ₈ (4)	3-1-1	1-3-0
Hydro (5)	3-2-3	1-3-0	S ₂ O ₈ (5)	3-1-0	1-3-0
MnO ₄ (1)	3-1-1	1-3-0			
MnO ₄ (2)	3-2-1	1-3-0			
MnO ₄ (3)	4-2-0	1-3-0			
MnO ₄ (4)	4-1-1	1-3-0			
MnO ₄ (5)	3-1-0	1-4-0			

Table 4.

Spec. ID	Dry POTS (MPa)			Wet POTS (MPa)		
	Mean	Std. Dev.	Median	Mean	Std. Dev.	Median
AlO₂	3.21	1.03	3.19	1.43	0.37	1.4
Bare	4.04	1.66	3.79	1.28	0.59	1.22
CCC	6.8	1.08	6.72	3.66	1.18	3.69
CO₃	5.35	1.34	5.31	2.47	0.99	2.4
Hydro	4.53	1.51	4.85	1.41	0.37	1.47
MnO₄	4.72	1.02	4.64	1.88	0.49	1.96
NO₃-5m-95	4.98	1.39	4.85	2.2	0.65	2.25
S₂O₈	3.91	1.92	4.29	2.32	0.38	2.39

Figure 1.

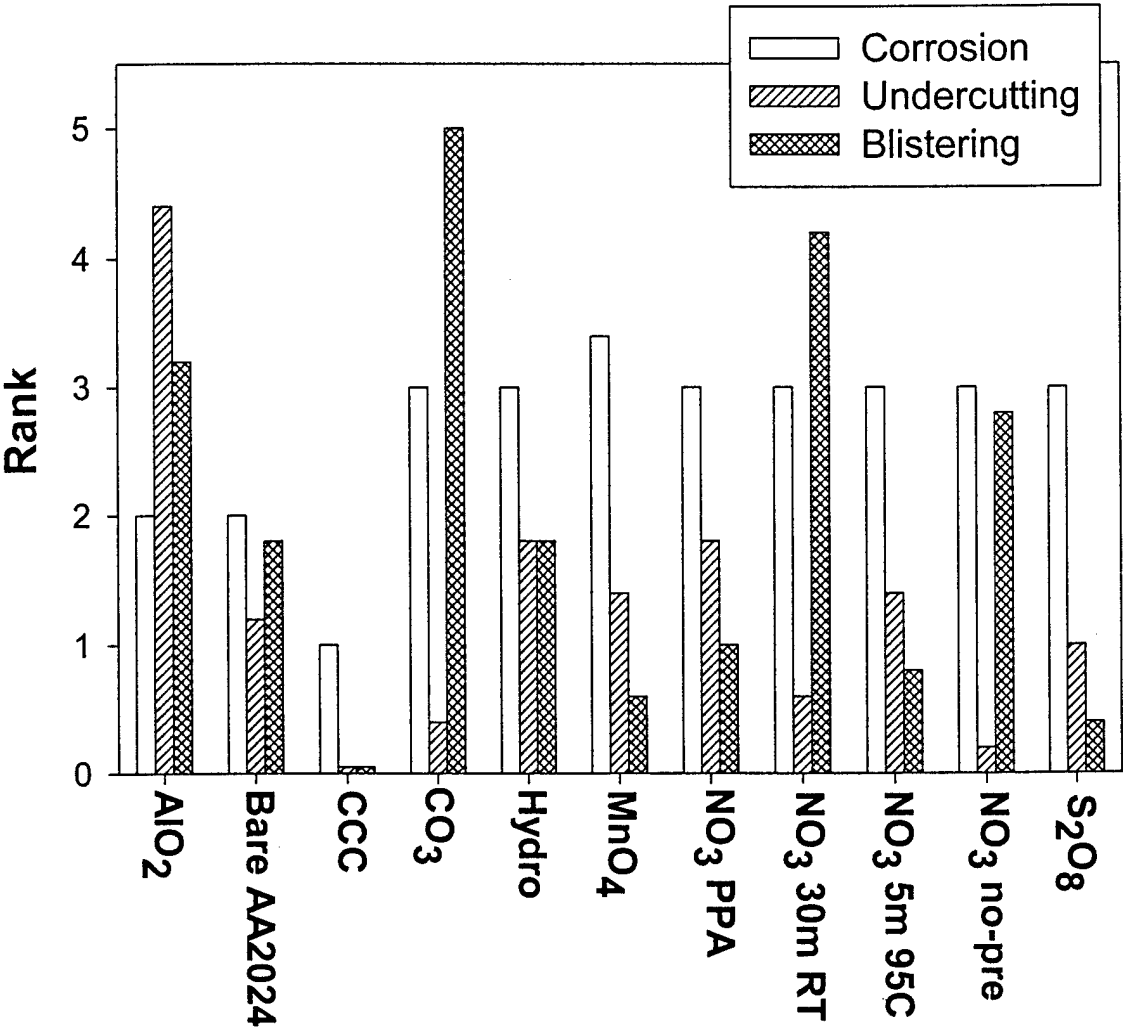


Figure 2.

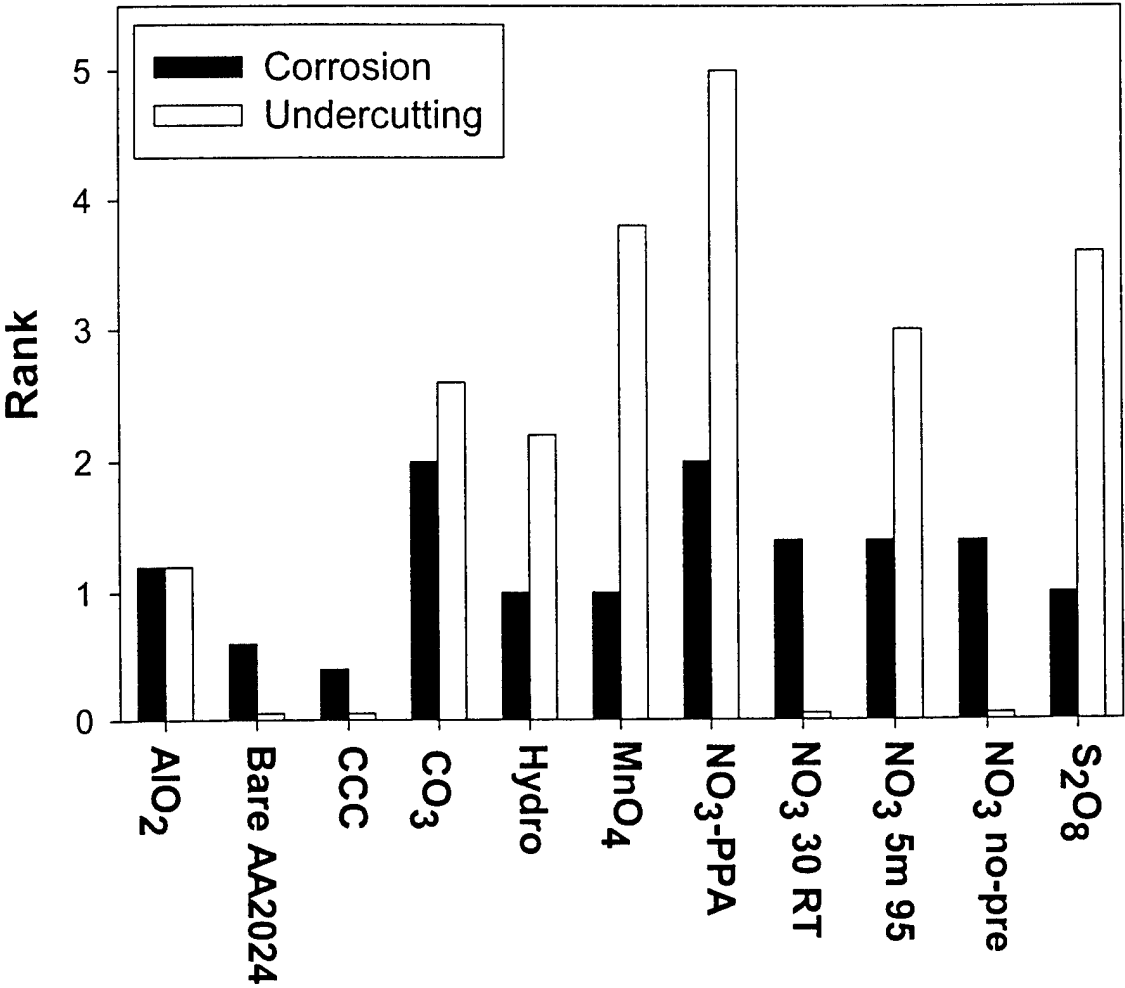


Figure 3

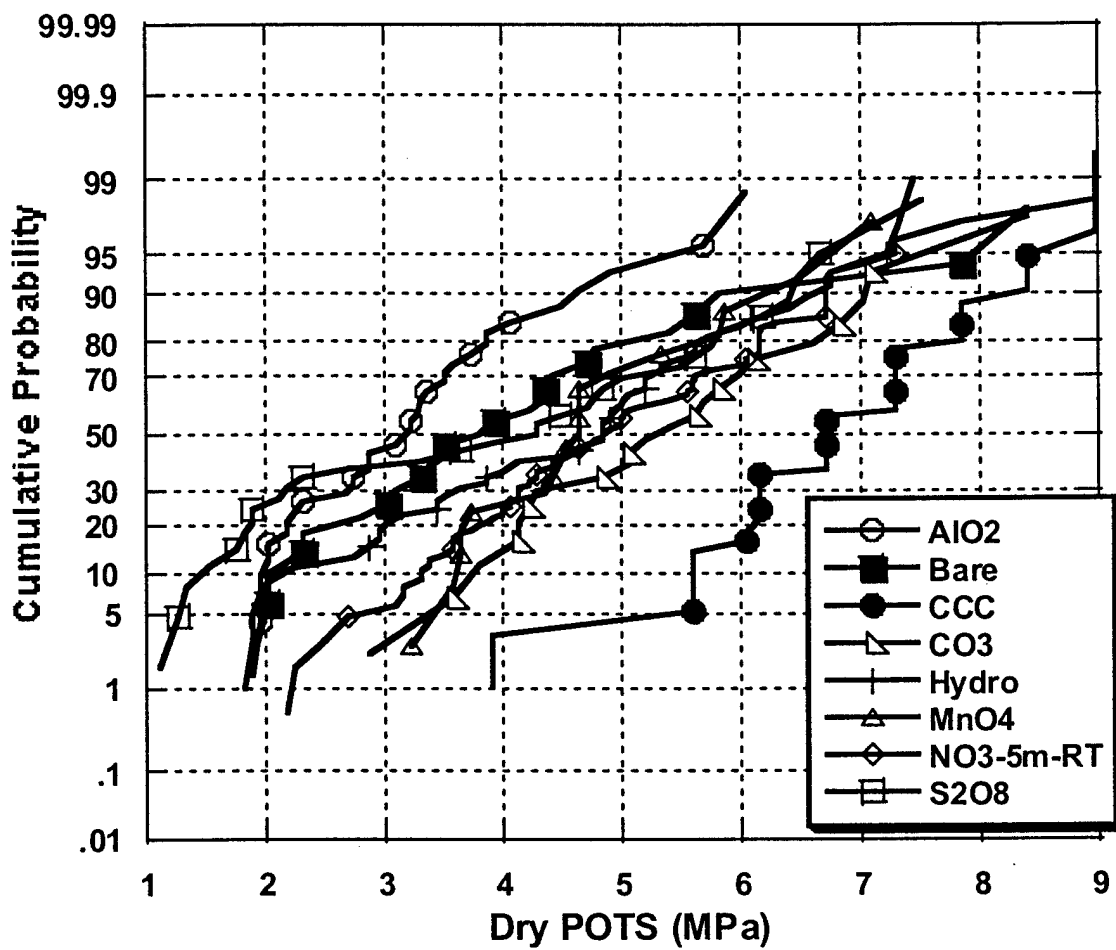


Figure 4

